SEA LEVEL VARIABILITY AND CHANGE

EDITED BY: Ivan D. Haigh, Marta Marcos, Sönke Dangendorf and Francisco Calafat

PUBLISHED IN: Frontiers in Marine Science

frontiers Research Topics

frontiers

ISSN 1664-8714
ISBN 978-2-88945-150-0
DOI 10.3389/978-2-88945-150-0

About Frontiers

Frontiers is more than just an open-access publisher of scholarly articles: it is a pioneering approach to the world of academia, radically improving the way scholarly research is managed. The grand vision of Frontiers is a world where all people have an equal opportunity to seek, share and generate knowledge. Frontiers provides immediate and permanent online open access to all its publications, but this alone is not enough to realize our grand goals.

Frontiers Journal Series

The Frontiers Journal Series is a multi-tier and interdisciplinary set of open-access, online journals, promising a paradigm shift from the current review, selection and dissemination processes in academic publishing. All Frontiers journals are driven by researchers for researchers; therefore, they constitute a service to the scholarly community. At the same time, the Frontiers Journal Series operates on a revolutionary invention, the tiered publishing system, initially addressing specific communities of scholars, and gradually climbing up to broader public understanding, thus serving the interests of the lay society, too.

Dedication to Quality

Each Frontiers article is a landmark of the highest quality, thanks to genuinely collaborative interactions between authors and review editors, who include some of the world's best academicians. Research must be certified by peers before entering a stream of knowledge that may eventually reach the public - and shape society; therefore, Frontiers only applies the most rigorous and unbiased reviews.
Frontiers revolutionizes research publishing by freely delivering the most outstanding research, evaluated with no bias from both the academic and social point of view.
By applying the most advanced information technologies, Frontiers is catapulting scholarly publishing into a new generation.

What are Frontiers Research Topics?

Frontiers Research Topics are very popular trademarks of the Frontiers Journals Series: they are collections of at least ten articles, all centered on a particular subject. With their unique mix of varied contributions from Original Research to Review Articles, Frontiers Research Topics unify the most influential researchers, the latest key findings and historical advances in a hot research area! Find out more on how to host your own Frontiers Research Topic or contribute to one as an author by contacting the Frontiers Editorial Office: **researchtopics@frontiersin.org**

SEA LEVEL VARIABILITY AND CHANGE

Topic Editors:
Ivan D. Haigh, University of Southampton, UK
Marta Marcos, Mediterranean Institute for Advanced Studies (CSIC), Spain
Sönke Dangendorf, University of Siegen, Germany
Francisco Calafat, National Oceanography Centre, UK

The city of Palma de Mallorca from Palma Bay
Image by Sönke Dangendorf

In June 2015 we held a workshop on the beautiful island of Mallorca, Spain with a focus on sea level variability and change. Over 120 sea level experts from around the world attended this workshop, from a range of different disciplines. The main aims of the workshop were to: 1.) Evaluate the current state-of-knowledge of sea level science; 2.) Identify gaps and unresolved questions in any aspect of sea level science; and 3.) Design future research to address these issue. All aspects of sea level changes were covered, from global to regional, observations and modelling, processes driving mean sea level changes and extremes, from the geological scale to the instrumental era and future projections and including impacts on the coastal zones. This E-Book presents papers that came out of that workshop. Overall, these papers illustrate the multi-disciplinary nature of sea level research, cross-cutting many fields of research including: oceanography, meteorology, geology, coastal morphodynamics, engineering and the social-economic aspects. Collectively, theses articles represent an interesting range of perspectives and original studies that contribute to understanding the dynamic nature of sea level and its impacts across a wide range of time and space scales. Enjoy reading them!

Citation: Haigh, I. D., Marcos, M., Dangendorf, S., Calafat, F., eds. (2017). Sea Level Variability and Change. Lausanne: Frontiers Media. doi: 10.3389/978-2-88945-150-0

Table of Contents

Chapter 6: Impacts of sea level change

frontiers in Marine Science

EDITORIAL
published: 22 February 2017
doi: 10.3389/fmars.2017.00046

Editorial: Sea Level Variability and Change

Ivan D. Haigh[1], Marta Marcos[2], Sönke Dangendorf[3] and Francisco Mir Calafat[4]*

[1] Ocean and Earth Sciences, National Oceanography Centre, University of Southampton, Southampton, UK, [2] Mediterranean Institute for Advanced Studies (CSIC), Esporles, Spain, [3] Department of Civil Engineering, Research Institute for Water and Environment, University of Siegen, Siegen, Germany, [4] National Oceanography Centre, Liverpool, UK

Keywords: sea level, coastal flooding, extreme events, tides, storm, storm surges, mean sea level

Editorial on the Research Topic

Sea Level Variability and Change

There is strong observational evidence that global mean sea levels are rising and there is great concern that the rate of rise will accelerate throughout the twenty-first century and beyond, significantly threatening coastal communities (Church et al., 2013; IPCC, 2014). With rapid population growth and accompanying infrastructure development at the coast, modern society has become increasingly vulnerable to even small changes in sea level. More than 600 million people currently live in coastal areas with an elevation less than 10 m above present-day mean sea level (McGranahan et al., 2007). An assessment of 136 of the world's largest port cities estimated that, by the 2070s, the population exposed to flooding risk may grow by more than a factor of three in these cities due to the combined effects of sea level rise, land subsidence, population growth, and urbanization, with asset exposure increasing to more than 10 times that of current levels (Hallegatte et al., 2013). Therefore, understanding future sea level rise and variability is an urgent issue of utmost importance.

The 12 articles in this Research Topic assess sea level change and variability on a range of different temporal (from minute to hundreds of years) and spatial (individual beach to global) scales.

The first contribution to this Research Topic considers tides, which dominate sea level variability in a large proportion of the world's oceans. In a perspective article, Medvedev et al. evaluate the nature of tides in three enclosed basins, namely the Baltic, Black, and Caspian seas. Oceanic tides penetrate only weakly, or not at all, into these enclosed basins and consequently direct forcing of tides dominates the variability. The authors use spectral analysis on long observation time series and find that the formation and predominance of diurnal or semidiurnal tides in these seas appears to depend on the frequency-selective properties of the respective basins.

The next four contributions deal with meteorological influences on sea level. Vilibić et al. focus on meteotsunamis, which are atmospherically generated long ocean waves in the tsunami frequency band. Understanding of meteotsunamis has advanced considerably during the last two decades and the authors identify key research gaps and discuss different approaches for developing meteotsunami warning systems. Pérez-Gómez et al. analyse the characteristics of two high frequency sea level events recorded in European Atlantic waters, using sea level, wave, atmospheric pressure and wind datasets. The first event was associated with possible wave-induced "seiches" that occurred along the North coast of Spain during the storms of January/February 2014 and the second was a series of small sea level oscillations detected after an earthquake in the mid-Atlantic in February 2015. They consider these events in regard to the limitations of automatic

OPEN ACCESS

Edited and reviewed by:
Isabel Iglesias, Interdisciplinary Centre of Marine and Environmental Research, Portugal

****Correspondence:***
Ivan D. Haigh
i.d.haigh@soton.ac.uk

Specialty section:
This article was submitted to Coastal Ocean Processes, a section of the journal Frontiers in Marine Science

Received: *14 December 2016*
Accepted: *09 February 2017*
Published: *22 February 2017*

Citation:
Haigh ID, Marcos M, Dangendorf S and Mir Calafat F (2017) Editorial: Sea Level Variability and Change. Front. Mar. Sci. 4:46. doi: 10.3389/fmars.2017.00046

algorithms for tsunami warning. Wadey et al. undertake a detail comparison of two key North Sea coastal flooding events that have occurred in the last 60 years. These events are the "Big Flood" of 31 January–1 February 1953 and the recent 5–6 December 2013 event. Using a range of oceanographic and meteorological datasets they: contrast the meteorological forcing; compare the high sea levels observed during both events; compare the coastal flooding and impact; and discuss the role of the improved flood defenses and storm surge forecasting since 1953. Using a set of 220 tide gauges, Mawdsley and Haigh investigate the temporal variations in storm surges around the world and the spatial coherence of its variability. They compare results derived from two parameters used to represent storm surge (skew surge and the more traditional, non-tidal residual) and compare inter-annual and multi-decadal variations in skew surge with fluctuations in regional climate indices. They find that using skew surge time-series improves estimation of long-term trends in storm surges, because phase offsets caused by time errors are not present in skew surge time-series.

Three contributions deal with longer-term changes in mean sea level. Hünicke and Zorita analyse mean sea level records in the Baltic and parts of the North Sea with the aim of detecting an acceleration of sea-level rise over the twentieth and twenty-first centuries associated with climate change. Comparing a range of statistical methods they find positive, but not statistically significant, acceleration in the Baltic Sea area since 1900. They highlight that the failure to detect a significant acceleration in sea level could be due to the still small magnitude of the acceleration paired with high inter-annual sea-level variability at the regional scale, rather than the absence of acceleration linked to climate change. Andersen and Piccioni present an updated and improved version of the Danish Technical University's Arctic Ocean altimetric sea level time-series and use it to assess trends in mean sea level in this region. They find a total sea level rise of 2.2 $\pm$ 1.1 mm/yr and a significant increase of 15 mm/yr in the Beaufort Sea, corresponding to changes in the Beaufort Gyre relating to wind driven phenomenon that leads to freshwater accumulation. Using individual contributors the authors were also able to assess and close the Arctic sea level trend budget over the period 2005–2015 within the error bars, for the first time. Using optimal estimation, Fu analyses statistical properties of decadal global mean sea level variability, which is of importance to understanding its longer-term evolution with climate change. He finds that the estimated standard error of the trend determined from the global mean sea level record from radar altimetry is about 0.3 mm/yr on decadal scales, which is comparable to the widely quoted 0.4 mm/yr systematic error and can therefore not be neglected in the error budget.

Another two contributions to this Research Topic are related to the interplay between changes in sea level and coastal morphology. Ulm et al. investigate the impact a loss of a Barrier island would have on water levels and waves along the coastline of Tampa Bay. Barrier Islands make up an eight of the world's coastlines and buffer the mainland coastal areas from storm surge and wave energy. Using a numerical model, they find that that loss of the Egmont Key Island at the entrance to Tampa Bay would result in significantly increased water level and wave heights in the Bay. Le Cozannet et al. consider the applicability of the widely-used Bruun rule in predicting shoreline retreat on sandy beaches with sea level rise. Considering probabilistic sea-level rise scenarios, they propagated these uncertainties through the sediment balance equation, that sums the Bruun effect with other drivers in an attempt to better understand where and when the Bruun rule can be (in)validated. Their results confirm that low-energy gently sloping beaches with little human impacts and small gradients in longshore drift and sheltered from storms are the most relevant to assess the validity of the Bruun rule in the sediment balance equation.

The final two contributions deal with impacts of sea level change on coastal communities. Sorensen et al. investigate couplings between sea state and flood hazard at present and in the future for the town of Thyboron in Denmark. Using a range of datasets and stakeholder interviews, their study includes a detailed analysis of change and variability in the groundwater table, precipitation, land motion, geotechnical ground properties, sewerage systems, and other infrastructure. They find that apart from obvious adverse effects from future storm surge events, knowledge about the coupled effects of the abovementioned parameters needs to be taken into account to reach optimal mitigation and adaptation measures. Wolff et al. assess sea-level rise related coastal flood impacts for Emilia-Romagna in Italy using the Dynamic Interactive Vulnerability Assessment (DIVA) modeling framework. Their results emphasize that the scale of assessment and resolution of the input data can have significant implications for the results of coastal flood impact assessments. They highlight that understanding and communicating these implications is essential for effectively supporting decision makers in developing long-term robust and flexible adaptation plans.

Overall, these papers illustrate the multi-disciplinary nature of sea level research, cross-cutting many fields of research including: oceanography, meteorology, geology, coastal morphodynamics, engineering, and the social-economic aspects. Collectively, the articles in this Research Topic represent an interesting range of perspectives and original studies that contribute to understanding the dynamic nature of sea level and its impacts across a wide range of time and space scales. Enjoy reading them!

AUTHOR CONTRIBUTIONS

IH, MM, SD, and FM co-wrote this editorial.

ACKNOWLEDGMENTS

We thank the authors of the papers included in this Research Topic for their excellent contributions.

REFERENCES

Church, J. A., Clark, P. U., Cazenave, A., Gregory, J. M., Jevrejeva, S., Levermann, A., et al. (2013). "Sea Level Change. Climate Change 2013: The Physical Science Basis," in *Contribution of Working Group I to the Fifth Assessment Report of the Intergovernmental Panel on Climate Change,* eds T. F. Stocker, D. Qin, G.-K. Plattner, M. Tignor, S. K. Allen, J. Boschung, A. Nauels, Y. Xia, V. Bex, and P. M. Midgley (Cambridge, UK; New York, NY: Cambridge University Press).

Hallegatte, S., Green, C., Nicholls, R. J., and Corfee-Morlot, J. (2013). Future flood losses in major coastal cities. *Nat. Clim. Change* 3, 802–806. doi: 10.1038/nclimate1979

IPCC (2014). "Climate Change 2014: "Synthesis Report," in *Contribution of Working Groups, I, II and III to the Fifth Assessment Report of the Intergovernmental Panel on Climate Change,* eds R. K. Pachauri and L. A. Meyer (Geneva: Core Writing Team; IPCC), 151.

McGranahan, G., Balk, D., and Anderson, B. (2007). The rising tide: assessing the risks of climate change and human settlements in low elevation coastal zones. *Environ. Urban. Copyr.* 19, 17–37. doi: 10.1177/0956247807076960

Conflict of Interest Statement: The authors declare that the research was conducted in the absence of any commercial or financial relationships that could be construed as a potential conflict of interest.

frontiers in Marine Science

PERSPECTIVE
published: 14 April 2016
doi: 10.3389/fmars.2016.00046

Tides in Three Enclosed Basins: The Baltic, Black, and Caspian Seas

Igor P. Medvedev[1,2]*, *Alexander B. Rabinovich*[1,3] *and Evgueni A. Kulikov*[1]

[1] *P. P. Shirshov Institute of Oceanology, Russian Academy of Sciences, Moscow, Russia,* [2] *Roshydromet, Fedorov Institute of Applied Geophysics, Moscow, Russia,* [3] *Department of Fisheries and Oceans, Institute of Ocean Sciences, Sidney, BC, Canada*

Tides are the main type of sea level variability in the world oceans. However, oceanic tides penetrate weakly, or do not penetrate at all, into enclosed basins such as the Baltic, Black, and Caspian seas. Consequently, only directly forced tides are formed in these basins. Long observation time series (up to 123 years in the Baltic Sea and 38 years in the Black and Caspian seas) at numerous stations were used to precisely estimate tidal constituents. High-resolution spectra revealed fine structure of discrete peaks at tidal frequencies. The diurnal radiational constituent S_1 (1 cpd), apparently associated with breeze winds, was found to play an important role in general tidal dynamics in these seas. Harmonic analysis of tides for individual yearly series with consecutive vector averaging over the entire observational period was applied to estimate mean amplitudes and phases of tidal constituents. Our findings indicate that the formation and predominance of diurnal or semidiurnal tides in these seas appears to depend on the frequency-selective properties of the basins. Thus, in the Baltic Sea with fundamental eigen period of about 27 h, diurnal tides dominate in the major eastern gulfs. In the Black Sea amplification of semidiurnal tides is observed in the northwestern part, and is likely associated with local resonance. The predominance of semidiurnal tides in the Caspian Sea has also probably a resonant nature. Maximum tidal heights estimated for a 100-year period are 23 cm in the Baltic Sea, 18 cm in the Black Sea and 21 cm in the southern Caspian Sea.

Keywords: tides, tide gauges, Baltic Sea, Black Sea, Caspian Sea, seiches, sea-level spectra

OPEN ACCESS

Edited by:
Francisco Mir Calafat, Natural Environment Research Council, UK

Reviewed by:
João Miguel Dias, University of Aveiro, Portugal
Xiangbo Feng, University of Reading, UK

***Correspondence:**
Igor P. Medvedev
medvedev@ocean.ru

Specialty section:
This article was submitted to Coastal Ocean Processes, a section of the journal Frontiers in Marine Science

Received: *01 December 2015*
Accepted: *23 March 2016*
Published: *14 April 2016*

Citation:
Medvedev IP, Rabinovich AB and Kulikov EA (2016) Tides in Three Enclosed Basins: The Baltic, Black, and Caspian Seas. Front. Mar. Sci. 3:46. doi: 10.3389/fmars.2016.00046

INTRODUCTION

Tides are the major type of sea level oscillations in the world oceans. Maximum amplitudes of tides are mainly observed in coastal waters of certain marginal seas. Into isolated inland seas, such as the Black, Caspian and Baltic seas, oceanic tides penetrate weakly, or do not penetrate at all. The Baltic Sea is a large enclosed shallow sea connected to the North Sea through the narrow and shallow Danish straits. The Black Sea has limited water exchange with the Mediterranean Sea through the Turkish Straits (the Bosporus, the Sea of Marmara, and the Dardanelles). Tides from neighboring basins have small influence on tidal oscillations in these seas. The Caspian Sea is the largest entirely enclosed inland body of water on the Earth; consequently, only directly forced tides are formed in this sea.

Despite their small amplitudes, tides in all these seas are scientifically interesting and important; their accurate assessment is crucial for the understanding of the overall dynamics of the respective basins. Tides produce regular periodic oscillations of sea level and currents; other processes superimpose the tidal background. The mechanism responsible for the formation of tides in these seas is in many ways similar to the mechanism of formation of eigen sea modes (seiches) and

storm surges, in particular, the destructive surges in the Gulf of Finland, the Baltic Sea (Kulikov and Medvedev, 2013).

Tidal oscillations in the Baltic Sea and in the Black Sea have been studied for over 100 years, but the nature of their anomalous features is still not sufficiently clear (Defant, 1961; Engel, 1974). Tides in the Caspian Sea have been examined very little and mainly as part of more general investigations of sea level oscillations in this basin (cf. German, 1970; Levyant et al., 1994). Studies of tides in these seas are based on relatively short series of tide gauge data ($\leq$1 year). The accuracy of these calculations is limited because of the small tidal signal in comparison with the background noise level (s/n ratio). Long time series of high-quality observations are necessary to precisely estimate tidal constituents in these seas.

Medvedev et al. (2013) used multi-year (5–31 years) hourly data-sets from 35 tide gauge stations to examine tidal oscillations in the Baltic Sea. High-resolution spectral analysis revealed fine structure of tidal harmonics exceeding the noise level. In the last three years, the authors were able to collect a large amount of additional tide gauge data for the Baltic Sea, allowing more detailed study. Furthermore, it became interesting to compare the tidal character and generation mechanism in the Baltic Sea with those in two other large European inland seas: the Black and Caspian. In the present study, we used long-term hourly observations from a great number of coastal tide gauges to accurately evaluate tides in these three seas and compare their principal features.

OBSERVATIONS

In the Baltic Sea we used data from 38 stations located along the coasts of Russia, Latvia, Lithuania, Estonia, Poland, Germany, Denmark, Sweden, and Finland. The mean duration of sea-level records in this sea was $\sim$17 years; the longest series of $>$100 years were at six Swedish stations. In the Black Sea we used sea level series from 23 stations on the Russian, Ukrainian and Georgian coasts. The maximum length of 38 years was at Tuapse (northeastern coast); the mean length of the series was 17 years. In the Caspian Sea observations from 11 stations on the coasts of Russia, Kazakhstan, Azerbaijan, and Turkmenia were used, with a maximum duration of 38 years at Makhachkala (northwestern coast) and a mean length of 11 years. The series of observations were carefully checked; shifts and spikes were eliminated, short gaps (shorter than 1 day) were interpolated.

TIDAL SPECTRA

To examine the spectral properties of sea level oscillations we used a procedure similar to that described by Thomson and Emery (2014). To improve the spectral estimates, we applied a Kaiser-Bessel (KB) spectral window with half-window overlaps prior to the Fourier transform. The length of the window was chosen to be 8192 h, yielding DOF (degrees of freedom) from 22 (Aladga) to 158 (Stockholm). The spectral resolution for all spectra was $\Delta f \approx 0.00293$ cycles per day (cpd).

Six selected spectra (two for each sea) are shown in **Figure 1A**. They are divided into two groups: "deep-sea," for stations located on deep-sea coasts of the corresponding basins (left), and "shallow-water," for shallow-water coasts (right). The spectra are "red," with spectral energy decreasing with increasing frequency as ω^{-2}, which is typical for the long wave spectra (cf. Rabinovich, 1993). The shape and depths of the sea determines the natural (eigen) frequencies of the basin. In particular, a wide spectral "hump" at frequencies 0.8–1.6 cpd in the sea-level spectrum at Kronstadt (the Gulf of Finland, eastern part of the Baltic Sea) appears to be associated with the fundamental eigen period of 27 h, dominant in this part of the Baltic Sea (Lisitzin, 1974; Jönsson et al., 2008; Kulikov and Medvedev, 2013).

The monotonic character of the continuum spectra is interrupted by prominent discrete peaks at tidal frequencies. These particular peaks are of primary interest for the present study. Four major tidal harmonics, are recognizable in most records: diurnal K_1 (period of 23.93 h) and O_1 (25.82 h), and semidiurnal M_2 (12.42 h), and S_2 (12.00 h). Although amplitudes of tidal constituents in isolated seas are small, because these oscillations are regular and deterministic, the respective spectral peaks are well-defined. In the Baltic Sea (everywhere, except the central part and the region of the Danish straits) diurnal peaks are predominant; in the Black and Caspian seas the semidiurnal tidal peaks prevail.

Multi-year series of tide gauge observations enabled us to provide the detailed tidal spectroscopy and to resolve individual tidal constituents. The high-resolution spectra can reveal specific properties of the tidal harmonics, which are unrecognizable in ordinary spectra. For the present analysis, we selected stations with the longest time series (the same as shown in **Figure 1A**) and used the following lengths for the Kaiser-Bessel spectral window: for Stockholm, Tuapse and Makhachkala, $N = 2^{17}$ h $= 131072$ h ≈ 5461 days ($\Delta f \approx 0.000183$ cpd); for Kronstadt and Odessa, $N = 2^{16}$ h $= 65536$ h ≈ 2731 days ($\Delta f \approx 0.000366$ cpd), and for Aladga, $N = 52584$ h ≈ 2191 days ($\Delta f \approx 0.000456$ cpd). The results are shown in **Figures 1B–D**.

The high-resolution spectral peaks corresponding to the major diurnal (Q_1, O_1, P_1, K_1, and S_1) and semidiurnal (N_2, M_2, S_2, and K_2) harmonics are clearly above the noise level and significantly exceed the 95% confidence spectral level. Even peaks related to some secondary constituents (e.g., $2N_2$, μ_2, and L_2) are seen in these spectra, despite their tiny amplitudes. What is especially important, these high-resolution spectra allowed us to resolve tidal harmonics from the same groups, in particular, P_1-S_1-K_1 and T_2-S_2-R_2-K_2. As a result, we could identify an interesting feature related to the solar harmonic S_1. The gravitational input at this frequency is negligible; this harmonic is associated with *radiational* forcing, i.e., with the cumulative effect of sea-breeze winds, atmospheric tides and diurnal air/sea water temperature changes (Zetler, 1971; Wunsch, 1972; Pugh, 1987). The frequency S_1 is located between the frequencies of gravitational harmonics K_1 and P_1 and it is indistinguishable in the conventional (low-resolution) spectra (**Figure 1A**). However, in the high-resolution spectra (**Figures 1B–D**) the S_1 peak is clearly seen.

In the Baltic and Black seas the magnitude of S_1 is roughly equal to P_1, while in the Caspian Sea it is sufficiently greater than O_1, P_1, and K_1. A substantial difference is evident in the

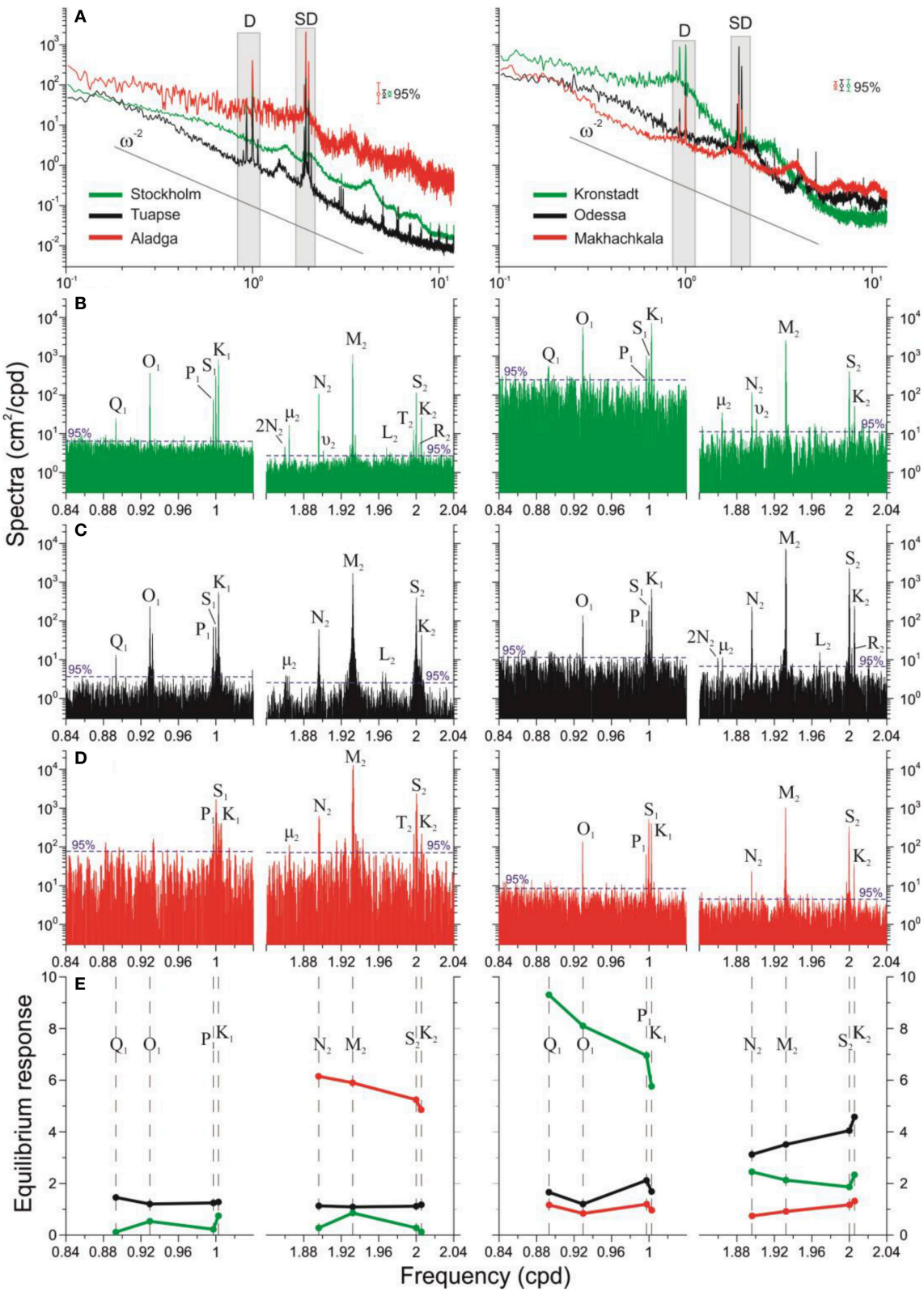

FIGURE 1 | Sea level spectra for six stations in the Baltic Sea (green), Black Sea (black), and Caspian Sea (red); the left column of plots is related to "deep-sea" stations, the right column to "shallow-water" stations. The stations are indicated in **Figure 2**. **(A)** Low-resolution spectra at six stations; the 95%

(Continued)

FIGURE 1 | Continued
confidence levels are shown, spectral power law ω^{-2} is denoted by a thin solid black line, shaded areas indicate diurnal (D) and semidiurnal (SD) tidal frequency bands shown in plots below. **(B)** High-resolution diurnal and semidiurnal spectra for Stockholm and Kronstadt, the Baltic Sea; main tidal peaks are indicated. **(C)** The same for Tuapse and Odessa, the Black Sea. **(D)** The same for Aladga and Makhachkala, the Caspian Sea. **(E)** The equilibrium response R_j, i.e., the ratio of observed and theoretical amplitudes of diurnal and semidiurnal tidal constituents for six selected "deep-sea" (left) and "shallow-water" (right) stations.

character of diurnal tides in the southern (deepest) part and other parts of the Caspian Sea. In particular, at Makhachkala (northwestern coast) S_1 is predominant, but other diurnal harmonics (K_1, O_1, and P_1) are prominent (**Figure 1D** right); the ratios between their amplitudes is close to theoretical for the tidal potential (e.g., Pugh, 1987). The diurnal tidal spectrum at Aladga (southern basin) is substantially different: the O_1 peak is absent, while the K_1 and P_1 peaks are nearly equal and considerably smaller than S_1 (**Figure 1D** left). A very similar effect was observed by Rabinovich and Medvedev (2015) for tidal oscillations in the Curonian Lagoon in the southeastern Baltic Sea: S_1 strongly dominates, diurnal O_1, and semidiurnal tidal harmonics are absent, while K_1 and P_1 are not related to the gravitational forcing, but to the seasonal modulation of the S_1 oscillations induced by sea-breeze winds and associated set-up and set-down motions in the lagoon. We may assume that likewise, the observed diurnal tides in the southern part of the Caspian Sea are more related to the radiational effects than to gravitational forcing. Although amplitudes of diurnal radiational tidal sea level oscillations are relatively small, associated currents in the surface layer can be significant (cf. Zaytsev et al., 2010). At the same time, semidiurnal tides in the southern Caspian Sea are "classical": major gravitational tidal peaks (M_2, N_2, and K_2) are evident and their relative magnitudes are in agreement with tidal theory. The S_2 tide is affected by radiational effects. We used the "credo of smoothness" (Zetler, 1971; Feng et al., 2015) to separate the gravitational and radiational components of S_2. In the Caspian and Baltic seas the mean ratio (radiational/gravitational) varies from 0.1 to 0.7, and in the Black Sea from 0.05 to 0.6. This is larger than the typical radiational contribution into S_2 of ∼16–17% (Zetler, 1971; Wunsch, 1972), probably because of weakness of gravitational tides in these seas.

In the Baltic Sea, despite their relatively small amplitude, not only major, but also several secondary harmonics are distinguishable in the spectra of Stockholm and Kronstadt (**Figure 1B**). In the Black Sea in addition to four major, a few secondary semidiurnal peaks are noticeable in the spectra of Tuapse and Odessa (**Figure 1C**).

To examine the generation properties of tides in various basins, we estimated the "equilibrium response":

$$R_j = H_j^{\mathrm{obs}}/H_j^{\mathrm{eq}} \quad (1)$$

i.e., the ratio of the observed amplitude of j-th harmonic (H_j^{obs}) and the theoretical amplitude of the equilibrium tide (H_j^{eq}) (Pugh and Woodworth, 2014). Such responses for major diurnal and semidiurnal constituents for the deeper parts of the Baltic and Black seas are very similar and small. The reason of small R_j for Stockholm is probably because this site is located near the M_2 and K_1 amphidromic points (cf. Medvedev et al., 2013). It is obvious that in both deep regions (central part of the Baltic Sea and eastern – Caucasian – part of the Black Sea) generation of tides has mainly non-resonant character. Diurnal and semidiurnal tides at other regions of the three seas have also non-resonant type of generation with R_j small and almost uniform (**Figure 1E**). There are, however, three important exceptions:

(1) Kronstadt, diurnal tides (**Figure 1E** right)
The anomalous amplitudes of diurnal tides in the Gulf of Finland are found to be due to resonance with the fundamental gulf mode with a period $T \approx 27$ h (Jönsson et al., 2008; Kulikov and Medvedev, 2013). The R_j for Kronstadt and other sites located in this gulf increases sharply with decreasing frequency, i.e., approaching the fundamental gulf period: from ∼6.0 for K_1 ($T_j = 23.93$ h) to 9.5 for Q_1 ($T_j = 26.87$ h). For semidiurnal tides R_j in this region is approximately four times smaller and consistent. The strong prevalence of diurnal tides in the Gulf of Finland compared to semidiurnal tides (**Figure 2**) appears to be related specifically to this resonant effect. Similar resonance response for semidiurnal tides was observed by Sutherland et al. (2005) for Juan de Fuca Strait and by Arbic et al. (2007) for Ungava Bay.

(2) Odessa, semidiurnal tides (**Figure 1E** right)
The equilibrium response for semidiurnal tides in the shallow northwestern part of the Black Sea is significantly greater than for diurnal tides and gradually increases with increasing frequency: from 3.0 for N_2 ($T_j = 12.66$ h) to 4.5 for K_2 ($T_j = 11.97$ h). Probably this is due to the influence of the first seiche mode of the Black Sea, estimated by Maramzin (1985) to be ∼9.5 h. This mode has maximum amplitudes specifically in the shallow northwestern part of the sea, in the vicinity of Odessa. In the background spectrum at Odessa, a "hump" with peak period of about 10 h is clearly seen (**Figure 1A** right).

(3) Aladga, semidiurnal tides (**Figure 1E** left)
As was indicated previously, gravitational diurnal tides are not observed in the southern basin of the Caspian Sea; that is why R_j for these tides is not shown for Aladga. However, semidiurnal tides are noticeable in this region (**Figure 1D** left) and the respective R_j are substantially larger than those for any other station shown in **Figure 1E**. The response increases with decreasing frequency (from 5.0 for K_2 to 6.5 for N_2). This appears to be related to the eigen mode with a period of about 14–15 h (Levyant et al., 1994).

In general, the results show that eigen modes of the corresponding basins appear to play an important role in formation of tides in the Baltic, Black, and Caspian seas. Also, the spectral analyses show the prevalence of tidal harmonics

in comparison to the background noise, enabling us to use harmonic analysis to directly calculate tides.

QUANTITATIVE AND SPATIAL CHARACTERISTICS OF TIDES

We used the least squares method of harmonic analysis to estimate mean tidal amplitudes and phases of 14 tidal constituents, including diurnal, semidiurnal and higher-frequency. The analysis was done based on yearly series of observations for 38, 23, and 11 stations in the Baltic, Black, and Caspian seas, respectively. The results of the calculations for individual years were vectorly averaged over the entire observational period.

The computed amplitudes and phases were used to predict tides for a 100-year period (2001–2100) to take into account the 18.6-year nodal tidal variations and evaluate the maximum tidal heights. We also estimated specific tidal characteristics. Amplitudes of the major diurnal and semidiurnal constituents were used to calculate "form factor" (Pugh, 1987), i.e., the type of tides:

$$F = \frac{H_{K_1} + H_{O_1}}{H_{M_2} + H_{S_2}}. \quad (2)$$

The "Energy factor" was estimated as the ratio of the cumulative energy of diurnal $\left(H^2_{Dj}\right)$ and semidiurnal $\left(H^2_{SDj}\right)$ harmonics:

$$E_f = \sum_j^{N_D} H^2_{Dj} / \sum_j^{N_{SD}} H^2_{SDj}. \quad (3)$$

Maximum tidal heights and the energy factor in the three seas are shown in **Figure 2**.

In the Baltic Sea the amplitudes of the diurnal constituents O_1 and K_1 are approximately equal; the greatest amplitudes are observed in the head of the Gulf of Finland (~3 cm in Kronstadt and Gorniy Institute) and in the Gulf of Riga (up to 1.8 cm). Diurnal tides prevail in the eastern part of this sea: F = 6–8 in

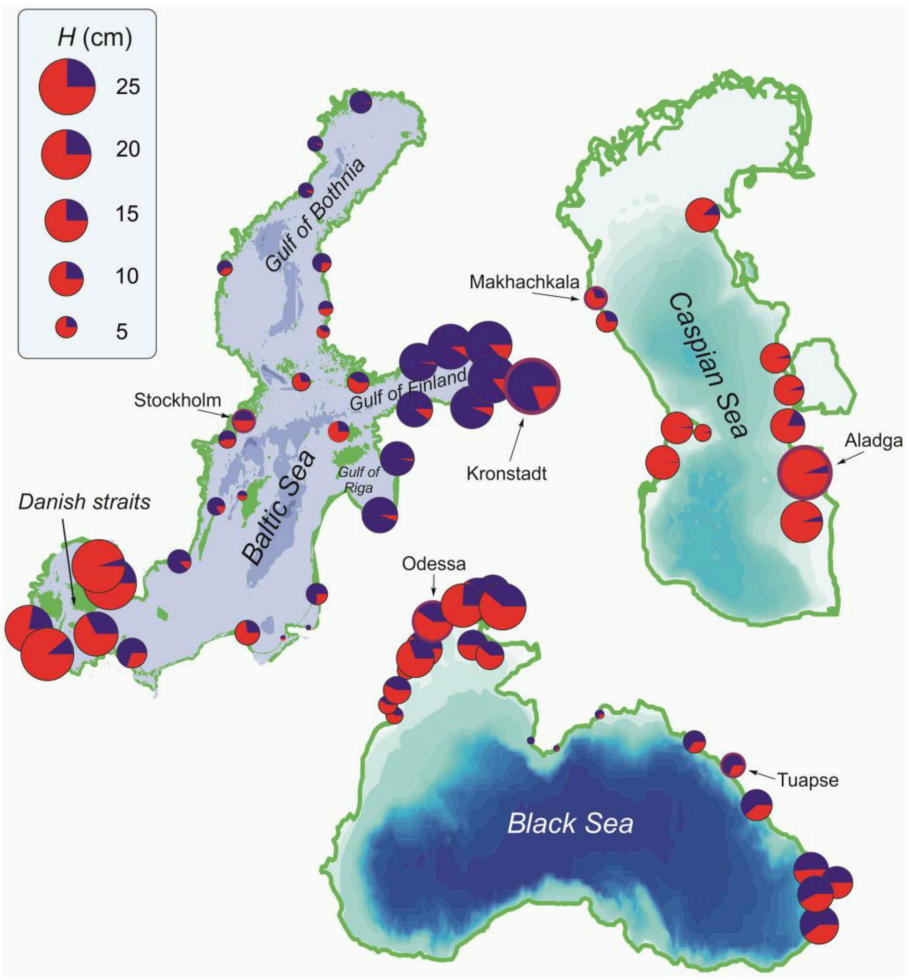

FIGURE 2 | Distribution of maximum tidal heights in the Baltic, Caspian, and Black seas evaluated for a 100-year period. The segment colors indicate relative contribution of diurnal (blue) and semidiurnal (red) energy into the total energy of the tidal oscillations.

the Gulf of Finland, 4.5–6 in the Gulf of Riga, and 5–8 in the Gulf of Bothnia. The minimum diurnal amplitudes of 0.4 cm are observed in the central part of the Baltic Sea, where the K_1 and O_1 amphidromic points are situated. The maximum amplitude of the main semidiurnal harmonic M_2 of about 6 cm is observed near the Danish straits, where the Baltic tides are influenced by semidiurnal tides arriving from the North Sea. The minimum M_2 amplitudes of 0.2 cm are observed in the Gulf of Bothnia. The maximum cumulative tidal heights of 23 cm in the Baltic Sea occur in Neva Bay, in the easternmost part of the Gulf of Finland, and near the Danish straits.

The semidiurnal tides predominate in the main part of the Black Sea (cf. Engel, 1974; Fomicheva et al., 1991). The M_2 amplitude in the northwestern part of the sea is 2.8–3 cm, the diurnal harmonics O_1 and K_1 have amplitudes of 1.3–1.7 cm, and $F = 0.3–1.0$. The relatively high diurnal amplitudes in the northwestern part of the Black Sea (**Figure 2**) are caused by the radiational harmonic S_1, which is up to 4 cm on this coast. The maximum tidal heights of 18 cm are observed in the northwestern part of the sea (Kherson and Nikolayev). In the Caspian Sea tides also are of semidiurnal type ($F = 0.2–0.9$). The highest amplitude of the M_2 harmonic is 5.4 cm at Aladga. The amplitudes of diurnal harmonics O_1 and K_1 in the Caspian Sea do not exceed 0.8–1 cm. The maximum evaluated tidal height in the Caspian Sea is 21 cm on the southeastern coast of the sea. (**Figure 2**).

CONCLUSIONS

Long multi-year series of hourly sea level observations were used to examine tides in three large enclosed basins: the Baltic, Black, and Caspian seas. Despite relatively small amplitudes, tides were found to be evident in the sea level spectra as discrete spectral peaks significantly exceeding the background noise level. This enabled us to evaluate tides based on both spectral and harmonic analysis.

Our findings indicate that the formation and predominance of diurnal or semidiurnal tides in these seas depends on the frequency-selective properties of the basins. Thus, in the Baltic Sea with fundamental eigen period of about 27 h, diurnal tides dominate in the major eastern gulfs. In the Black Sea, resonant amplification of semidiurnal tides appears to be observed in the northwestern part. The predominance of semidiurnal tides in the Caspian Sea also most likely has a resonant nature. The radiational tides associated with solar radiational forcing on the sea surface were found to play an important role in the general tidal regime in these three seas. Maximum tidal heights estimated for a 100-year period are 24 cm in the Baltic Sea, 18 cm in the Black Sea, and up to 21 cm in the southern part of the Caspian Sea.

The accurate assessment of tides is crucial for the understanding the overall dynamics of these three seas. Tides produce regular periodic oscillations of the sea level and currents, and influence the general motions in these basins. All the other processes superimpose tidal background.

AUTHOR CONTRIBUTIONS

IM coordinated the work on the manuscript, wrote the initial version of the manuscript and prepared the figures. AR revised the text and figures substantially, EK did a substantial polishing of text. All authors actively contributed to the development of the manuscript idea, to its writing and preparation of figures.

ACKNOWLEDGMENTS

We gratefully acknowledge Fred Stephenson (Institute of Ocean Sciences, Sidney, BC, Canada) for valuable comments and suggestions. This work was supported by the Russian Foundation for Basic Research (grants 15-05-05986 and 16-35-60071), the Russian Science Foundation (grant 14-50-00095) and funds of P.P. Shirshov Institute of Oceanology.

REFERENCES

Arbic, B. K., St-Laurent, P., Sutherland, G., and Garrett, C. (2007). On the resonance and influence of the tides in Ungava Bay and Hudson Strait. *Geophys. Res. Lett.* 34, L17606. doi: 10.1029/2007GL030845

Defant, A. (1961). *Physical Oceanography*, Vol. 2. Oxford: Pergamon Press.

Engel, M. (1974). Hydrodynamisch-numerische Ermittlung von Beweungsvorgängen im Schwarzen Meer. *Mitteilungen Inst. Meereskunde Univ. Hamburg.* 22, 1–71.

Feng, X., Tsimplis, M. N., and Woodworth, P. L. (2015). Nodal variations and long-term changes in the main tides on the coasts of China. *J. Geophys. Res. Oceans* 120, 1215–1232. doi: 10.1002/2014JC010312

Fomicheva, L. A., Rabinovich, A. B., and Demidov, A. N. (1991). "Sea level," in *Hydrometeorology and Chemistry of the USSR Seas, Vol. 4, The Black Sea*, eds A. I. Simonov and E. N. Altman (St. Petersburg, Russia: Gidrometeoizdat), 329–354.

German, V. Kh. (1970). Spectral analysis of sea level fluctuations in the Sea of Azov, Black and Caspian seas in the frequency range from one cycle per several hours to one cycle per several days. *Tr. GOIN.* 103, 52–73.

Jönsson, B., Döös, K., Nycander, J., and Lundberg, P. (2008). Standing waves in the Gulf of Finland and their relationship to the basin-wide Baltic seiches. *J. Geophys. Res.* 113, C03004. doi: 10.1029/2006jc003862

Kulikov, E. A., and Medvedev, I. P. (2013). Variability of the Baltic Sea level and floods in the Gulf of Finland. *Oceanology* 53, 145–151. doi: 10.1134/s0001437013020094

Levyant, A. S., Rabinovich, B. I., and Rabinovich, A. B. (1994). Computation of seiche oscillations in seas of arbitrary configuration (exemplified by the Caspian Sea). *Oceanology* 33, 588–598.

Lisitzin, E. (1974). *Sea Level Changes*. Amsterdam: Elsevier.

Maramzin, V. Ya. (1985). "Computation of seiche oscillations by the finite element method in basins of arbitrary shape," *in Theoretical and Experimental Investigations of Long Wave Processes*, eds V. M. Kaistrenko and A. B. Rabinovich (Vladivostok: Far Eastern Scientific Center, USSR Academy of Sciences), 104–114.

Medvedev, I. P., Rabinovich, A. B., and Kulikov, E. A. (2013). Tidal oscillations in the Baltic Sea. *Oceanology* 53, 526–538. doi: 10.1134/s0001437013050123

Pugh, D. T. (1987). *Tides, Surges and Mean Sea-Level*. Chichester: John Wiley.

Pugh, D., and Woodworth, P. (2014). *Sea-Level Science: Understanding Tides, Surges, Tsunamis and Mean Sea-Level Changes*. Cambridge: Cambridge University Press.

Rabinovich, A. B. (1993). *Long Ocean Gravity Waves: Trapping, Resonance and Leaking*. St. Petersburg, Russia: Gidrometeoizdat.

Rabinovich, A. B., and Medvedev, I. P. (2015). Radiational tides at the southeastern coast of the Baltic Sea. *Oceanology* 55, 319–326. doi: 10.1134/S0001437015030133

Sutherland, G., Garrett, C., and Foreman, M. (2005). Tidal resonance in Juan de Fuca Strait and the Strait of Georgia. *J. Phys. Oceanogr.* 35, 1279–1286. doi: 10.1175/JPO2738.1

Thomson, R. E., and Emery, W. J. (2014). *Data Analysis Methods in Physical Oceanography, Third and Revised Edition*. New York, NY: Elsevier.

Wunsch, C. (1972). Bermuda sea-level in relation to tides, weather and baroclinic fluctuations. *Rev. Geophys. Space Phys.* 10, 1–49. doi: 10.1029/RG010i001p00001

Zaytsev, O., Rabinovich, A. B., Thomson, R. E., and Silverberg, N. (2010). Intense diurnal surface currents in the Bay of La Paz, Mexico. *Cont. Shelf Res.* 30, 608–619. doi: 10.1016/j.csr.2009.05.003

Zetler, B. D. (1971). Radiational ocean tides along the coasts of the United States. *J. Phys. Oceanogr.* 1, 34–38.

Conflict of Interest Statement: The authors declare that the research was conducted in the absence of any commercial or financial relationships that could be construed as a potential conflict of interest.

frontiers in Marine Science

PERSPECTIVE
published: 03 May 2016
doi: 10.3389/fmars.2016.00057

Modern Approaches in Meteotsunami Research and Early Warning

Ivica Vilibić[1], Jadranka Šepić[1], Alexander B. Rabinovich[2,3] and Sebastian Monserrat[4]*

[1] Institute of Oceanography and Fisheries, Split, Croatia, [2] P.P. Shirshov Institute of Oceanology, Russian Academy of Sciences, Moscow, Russia, [3] Fisheries and Oceans Canada, Institute of Ocean Sciences, Sidney, BC, Canada, [4] Department of Physics, University of the Balearic Islands, Palma de Mallorca, Spain

The understanding of meteotsunamis—significant atmospherically generated long ocean waves in the tsunami frequency band—has advanced considerably during the last two decades. Scientists and specialists use near-field *in situ* data and remote observations, as well as atmospheric and ocean modeling, to study destructive events. The phenomenon has been reported and investigated worldwide, indicating its relevance as a marine natural hazard and demonstrating the urgent need for meteotsunami warning systems for certain countries. In this paper we summarize the present knowledge of the phenomenon, identify particular research gaps, and propose near-future critical components of meteotsunami research. We emphasize a potential concept of merging yet-to-be-developed meteotsunami warning systems and existing tsunami or multi-hazard early warning systems.

Keywords: meteotsunami, natural hazard, air-sea interaction, world oceans, research gaps, sea level measurements, early warning system

OPEN ACCESS

Edited by:
Ivan David Haigh,
University of Southampton, UK

Reviewed by:
Matthew John Eliot,
Damara WA Pty Ltd, Australia
Kevin James Horsburgh,
National Oceanography Centre, UK

****Correspondence:***
Ivica Vilibić
vilibic@izor.hr

Specialty section:
This article was submitted to Coastal Ocean Processes, a section of the journal Frontiers in Marine Science

Received: *23 October 2015*
Accepted: *11 April 2016*
Published: *03 May 2016*

Citation:
Vilibić I, Šepić J, Rabinovich AB and Monserrat S (2016) Modern Approaches in Meteotsunami Research and Early Warning. Front. Mar. Sci. 3:57. doi: 10.3389/fmars.2016.00057

INTRODUCTION

Nomitsu (1935) was first to write about "*tsunamis of atmospheric origin*" and to describe significant atmospherically induced tsunami-like oscillations observed in certain harbors and bays of the Japanese islands. Defant (1961) indicated that similar oscillations are also observed in some other regions of the world oceans and recommended the general term "*meteorological tsunami*" or "*meteotsunami*" for this type of phenomena. Rabinovich and Monserrat (1996, 1998) introduced this term to the tsunami community. The similarity of seismically generated tsunamis and meteotsunamis was obvious; also, it became clear that many "tsunamis of unknown origin" described in tsunami catalogs (e.g., Soloviev and Go, 1974; Lander et al., 1993) are, in fact, meteorological tsunamis. After an overview paper by Monserrat et al. (2006) the term "*meteotsunami*" became widely used and respective long oceanic waves began to be recognized as other natural hazards.

Meteotsunamis have the same temporal and spatial scales as ordinary tsunami waves and can affect coastal areas in a similar destructive way, but they are generated by traveling atmospheric disturbances, rather than by underwater earthquakes, landslides or volcanic eruptions (Monserrat et al., 2006). A specific property of meteotsunamis is that they are *phenomena of resonance*: intensive waves can be produced only through resonant transfer of energy from the atmosphere to the ocean via Proudman resonance (Proudman, 1929), $U = c$, or Greenspan resonance (Greenspan, 1956), $U = c_j$, where U is the speed of atmospheric disturbances,

$c = \sqrt{gh}$ is the long wave speed, c_j is the speed of one of the first modes of edge waves, h is the ocean depth and g is the gravitational acceleration. Normally, catastrophic meteotsunamis occur only in particular regions that have extensive shelf areas promoting these types of resonances, with depths ranging from 25 to 150 m, conducive for long wave speeds of 16 to 40 m/s. Specific local topographic features facilitating the substantial amplification of arriving waves are a V-shape for the external embayment opened toward the incoming long ocean waves and narrow-entrance internal bays/harbors with high Q-factor (Miles and Munk, 1961).

In certain harbors and bays of the world oceans, the phenomenon has been known for a long time and is called by local names: "*abiki*" in Japan, "*rissaga*" on the Balearic Islands, "*šćiga*" in the Adriatic Sea, "*marrobbio*" ("*marrubbio*") in Sicily, and "*milghuba*" in Malta (Monserrat et al., 2006; Rabinovich, 2009). The science of meteotsunamis has developed rapidly in the last two decades, documenting the phenomenon along the coasts of all continents except Antarctica (**Figure 1**). Much of this work has been consolidated in two special issues: Physics and Chemistry of the Earth (Rabinovich et al., 2009) and Natural Hazards[1] (Vilibić et al., 2014).

Meteotsunami research concentrates on several issues: (i) what processes and conditions in the atmosphere are responsible for the generation of meteotsunamis; (ii) how is the atmospheric energy transferred to the ocean waves, (iii) what types of resonant properties control the process; (iv) how does bathymetry affect the propagation and amplification of meteotsunami waves; and (v) what architecture and protocols should be used for timely and reliable detection of tsunamigenic atmospheric disturbances and early meteotsunami warning? The last question implies that the knowledge of the phenomenon is appropriate for real-time detection and prediction of meteotsunamis. It is also the ultimate question to be answered to mitigate damage caused by coastal flooding and/or strong currents.

The 1978 Vela Luka meteotsunami (Adriatic Sea, Croatia) caused a loss of $7 M (in 1978 prices), equal to ¼ of the annual income of the entire island of Korčula (Vučetić et al., 2009). The 2006 Balearic meteotsunami ("*rissaga*") sank or damaged several tens of boats and yachts in Ciutadella Harbor (Menorca Island, Spain) with a total cost of more than $30M euros (Monserrat et al., 2006). The 1954 Great Lakes meteotsunami (Ewing et al., 1954), the 1979 "*abiki*" in Nagasaki Bay (Hibiya and Kajiura, 1982), and several events observed at the UK coast (Haslett and Bryant, 2009; Tappin et al., 2013; Sibley et al., 2016) resulted in human casualties and severe destruction. Two recent examples came from Odessa (Ukraine, the northwestern Black Sea) and Fremantle Harbor (Western Australia). In Odessa on 27 June 2014 a meteotsunami devastated some beach areas and injured 6 people (Šepić et al., 2015a). In Fremantle on 17 August 2014 a ship broke a mooring line and hit a major railway bridge, causing it to be shut down for more than 2 weeks (Pattiaratchi and Wijeratne, 2015). An operational meteotsunami warning system and safety procedures at civil protection and coastal operations could significantly reduce the risk for human lives and mitigate the damage coming from destructive meteotsunami events (Golnaraghi, 2012). In some regions meteotsunami warning systems can be included into multi-hazard warning systems (MHWS), in particular, into the systems responsible for forecasting typhoons, hurricanes, and associated storm surges (cf. Pattiaratchi and Wijeratne, 2015).

RESEARCH GAPS AND PERSPECTIVES

Atmospherically-induced long waves in the open ocean have spatial and temporal scales similar to the mesoscale atmospheric disturbances which generate them. An individual tsunamigenic atmospheric disturbance has typical horizontal scales of 10-100 km and can propagate over 50-500 km (Belušić et al., 2007). Meteotsunami waves are commonly formed over extensive shelf areas where the speed of the atmospheric disturbance matches the long wave speed (Šepić et al., 2015b). Meteotsunamis propagating onshore from the open ocean actively accumulate energy and are further amplified approaching the coast due to the shoaling effect (cf. Lamb, 1932); focusing in some bays and inlets they can cause catastrophic effects (Šepić et al., 2015b). Because these phenomena are relatively small-scale, a full numerical reproduction of the respective tsunamigenic atmospheric disturbances and associated long ocean waves is still a challenge. The modeling problem can be broken into four components: atmospheric modeling, ocean modeling, coupled atmospheric-ocean modeling, and modeling of coastal inundation and damage.

Aside from the exact knowledge of the atmospheric physics responsible for the creation of tsunamigenic disturbances (duct waves, wave-CISK[2], storms, frontal passages, gales or squall lines, etc.; see Belušić et al., 2007; Tanaka, 2010), the source mechanism and generation of atmospheric gravity waves or other meteotsunami sources are still not properly reproduced by atmospheric models. Observations are typically inadequate to resolve the generation of atmospheric mesoscale structures and associated surface pressure disturbances. Numerical modeling of these structures is also a problem: a number of simulations may be needed for reasonable reproduction of the atmospheric conditions and traveling small-scale disturbances visible in surface air pressures or winds (Belušić et al., 2007). Similar initial atmospheric forcing—e.g., a train of atmospheric waves—traveling over a few hundred kilometres can produce completely different responses at a given "hot-spot," depending on the specific track: disturbances, approaching the site, can intensify and produce strong sea level response or weaken and produce negligible response (Šepić and Vilibić, 2011). Novel ensemble-based methods, like stochastic convection, can overcome these shortcomings (Teixeira and Reynolds, 2008).

A critical issue in tsunami modeling is the proper reproduction of the tsunami source (Satake and Fujii, 2014). This issue is partly overcome in meteotsunami studies by imposing an artificial atmospheric disturbance, which travels over a tsunamigenic region (Whitmore and Knight, 2014; Šepić et al.,

[1] It is also published as a book by Springer (Dordrecht, The Netherlands, 2014).

[2] Conditional Instability of the Second Kind.

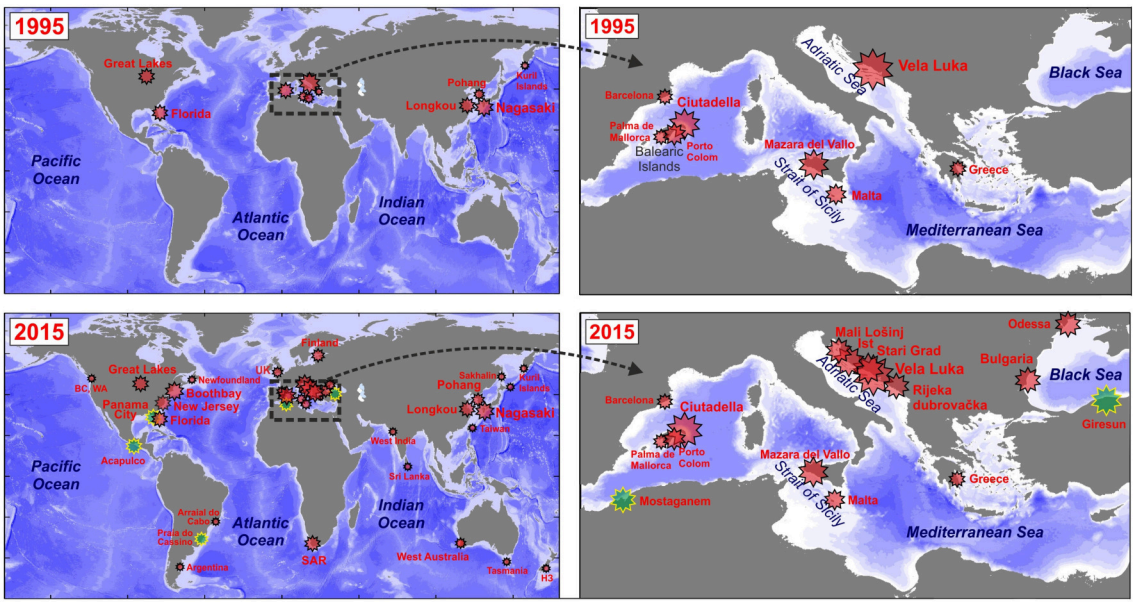

FIGURE 1 | Locations where meteotsunamis had been documented by the year 1995 (upper panels), and by the year 2015 (lower panels). Size of stars is proportional to intensity of the documented events. The information shown in the figure was constructed using the data presented by Rabinovich and Monserrat (1996), Monserrat et al. (2006), Rabinovich (2009), Šepić et al. (2015a), and Pattiaratchi and Wijeratne (2015). Green stars indicate locations where meteotsunami-like events occurred (Acapulco – 2 May 2015; Giresun – 24 September 2014; Mostaganem – 3 August 2007; Panama City – 28 March 2014; and Praia do Cassino – 9 February 2014) but still have not been proven by research studies.

2015b). Such an approach may be effective for the hazard risk assessments, which aim to estimate and map expected extreme meteotsunami wave heights, but is inappropriate for an operative real-time meteotsunami forecast. Altogether, the reproduction of meteotsunami sources is a challenge for atmospheric scientists modeling mesoscale processes, directing their research not just to a pure increase of the model resolution (that can be done with more powerful computers), but to preserve feasible physics at these spatial and temporal scales, and to create new parameterization schemes within models.

If the atmospheric forcing is known, the ocean modeling of meteotsunamis is straightforward, as physics of generated ocean waves is barotropic to first order. This enables us to use 2D models, similar to those applied for tsunami research (Monserrat et al., 2006). Another very important issue is bathymetry, that needs to be at high spatial resolution (∼10–50 m) and properly integrated into the model, especially in coastal areas and in areas of rapidly changing depth (shelf breaks, submarine channels, etc.) where meteotsunamis amplify and modify (Monserrat et al., 2006). This is particularly true for bays and harbors with large amplification factors, which are prone to frequent meteotsunami events. A small change in the model coastline or depths can result in significant changes in eigen frequencies of the respective basin and maximum estimated wave-heights (Vilibić et al., 2008).

The development of coupled atmospheric-oceanic models, which are required for accurate meteotsunami reproduction, is also important. At present, there are no reliable coupled models, since existing atmospheric models are not able to properly reproduce the evolution of traveling air pressure waves over water basins. An attempt to take into account the effect of such coupling has so far only been made by Renault et al. (2011) for the region of the Balearic Islands, however, simulated ocean wave heights at Ciutadella, the main Balearic meteotsunami "hot spot," were significantly underestimated. Therefore, this is a principal issue where substantial advancement is needed in the future.

Precise high-resolution capacities for continuous monitoring and detection of tsunamigenic disturbances and meteotsunami waves are of primary importance. Various observational networks are available for both atmospheric and oceanic measurements, but no standards for meteotsunami observations have yet been developed and therefore not a single network was adopted to properly capture meteotsunamis. Investigations of meteotsunamis are mainly based on standard meteorological and oceanographic networks, which mostly have insufficient accuracy and too coarse temporal resolution (e.g., 6-min NOAA CO-OPS air pressure network or 10-min regional meteo-ocean buoy network in the Gulf of Maine) and do not properly capture high-frequency processes at a minute timescale (Thomson et al., 2009; Šepić and Rabinovich, 2014). Some operational networks are more advanced: in particular, on the Balearic Islands (Marcos et al., 2009; Tintoré et al., 2013) and in the Adriatic Sea (Šepić and Vilibić, 2011), but they are either in the pilot-phase of development or not incorporated into a meteotsunami warning system. A decision on new standards based on 1 min or better time resolution and 1 Pa pressure measurements should be established for the regions affected by meteotsunamis. This is especially important for meteorological observations commonly following the standards

of the World Meteorological Organisation (WMO), in particular within the frame of Multi-Hazard Early Warning Systems (MHEWS; Golnaraghi, 2012).

Recently, 1-min resolution sea level observations around the world oceans became available through the IOC Sea Level Station Monitoring Facility service (http://www.ioc-sealevelmonitoring.org). These observations will definitely allow better assessment of high-frequency oscillations in many regions. The service has 100 data providers, indicating that the urgent need for high-resolution sea level monitoring, largely coming from the tsunami community, has finally pushed tide gauge observation standards to 1-min time resolution. However, spatial resolution of such a global network is insufficient for measurements of highly variable processes with scales of a few tens of kilometres or less.

Another important issue, to be potentially used in a meteotsunami warning system, is the obvious correlation of tsunamigenic atmospheric disturbances with specific weather conditions, at least in the Mediterranean region (Jansà et al., 2007) and Japan (Tanaka, 2010). These conditions are largely associated with the wave-ducting theory (Lindzen and Tung, 1976): a strong shear of unstable air masses in the mid-troposphere creates atmospheric disturbances which then propagate in the stable lower troposphere over long distances. High-resolution atmospheric and sea level data in the Mediterranean indicated a high correlation between meteotsunamis and synoptic patterns over the entire basin (Šepić et al., 2015b). It is quite possible that some other mechanisms might control meteotsunamigenic processes at other "hot spot areas." An illustrative example is the U.S. East Coast where meteotsunamis are often generated by hurricanes or large scale derecho systems (Wertman et al., 2014; Šepić and Rabinovich, 2014).

"Classical" sea level instruments and approaches might not be a solution for proper measurements of meteotsunami waves, as it is too costly to have a dense tide gauge network at meteotsunami hot spots. A densified network of cheap autonomous water level loggers might be a better choice, as it requires no maintenance and is easily deployed and recovered at piers, cliffs and the sea bottom. However, these water level data are not available in real time and may be used only for research purposes. Multi-hazard standard observatories, satellites mapping the spatial and temporal characteristics of tsunamigenic disturbances (Belušić and Strelec Mahović, 2009) and meteorological (Anderson et al., 2015) or high-frequency ocean radars (Lipa et al., 2014) for early detection of meteotsunami waves, may be other ways of collecting the data for real-time meteotsunami warning. Unfortunately, these observation systems are expensive, cannot cover all meteotsunami hot spots and their applicability for meteotsunami detection still needs to be quantified.

Most of the above research issues are still focused on reproduction of tsunamigenic atmospheric disturbances and associated oceanic waves. This respective knowledge is a prerequisite for building a meteotsunami warning system. However, there are other aspects relevant for creation of a system appropriate for *a priori* studies, in particular, for assessment of meteotsunami hazard, vulnerability and risk, including socio-economic effects (Geist et al., 2014).

In summary, the critical components of meteotsunami research that, in our opinion, need to be advanced for better understanding of the phenomenon and eventual creation of a reliable meteotsunami warning system are:

(i) Improvement of atmospheric models and of their high-resolution physics, resulting in reliable reproduction of tsunamigenic atmospheric disturbances;
(ii) Development of coupled atmosphere-ocean models to reproduce meteotsunami events;
(iii) Construction of high-resolution bathymetry grids for coastal regions and critical depth features (shelf breaks, canyons, shoals, sills, etc.);
(iv) Connection of intense high-frequency sea level oscillations with particular synoptic conditions and definition of site-dependant and region-dependant meteotsunami indices;
(v) Installation of meteorological radars for continuous monitoring of tsunamigenic atmospheric disturbances and elaboration of efficient detection algorithms to identify these disturbances;
(vi) Verification of new technological solutions and instrumentation for detection of spatial and temporal characteristics of tsunamigenic atmospheric disturbances and associated ocean waves, and their amplification approaching the coast;
(vii) Risk assessment of meteotsunamis and mitigation of their socio-economic impact.

TOWARD METEOTSUNAMI WARNING SYSTEMS

A meteotsunami warning system for particular hot-spot areas can be created based on the following four approaches: (i) identification of tsunamigenic atmospheric synoptic conditions; (ii) real-time detection of tsunamigenic atmospheric disturbances using a microbarograph network; (iii) measurement and tracking of high-frequency sea level oscillations by high-resolution digital tide gauges; and (iv) numerical simulation of meteotsunamis based on coupling of atmosphere-ocean numerical models.

The first approach is already operational on the Balearic Islands, where a meteotsunami forecast is given a few days ahead, but only at the qualitative level (Jansà et al., 2007). This forecast is based on identification of favorable synoptic conditions which include: (i) weak winds at the sea surface, (ii) an inflow of hot and dry air masses from Africa in the lower troposphere, overtopped by (iii) a strong mid-troposphere jet characterized by (iv) unstable conditions which favor the growth of mid and upper troposphere convective formations.

The second approach has been preliminary tested at a pilot microbarograph network in the Adriatic Sea (Šepić and Vilibić, 2011), and it is based on real-time detection of intense air pressure disturbances. The intensity is determined from 5-min air pressure segments. Parameters of the identified tsunamigenic disturbances are then automatically calculated. These parameters include disturbance intensity, rate of change and propagation direction and speed, which are then compared

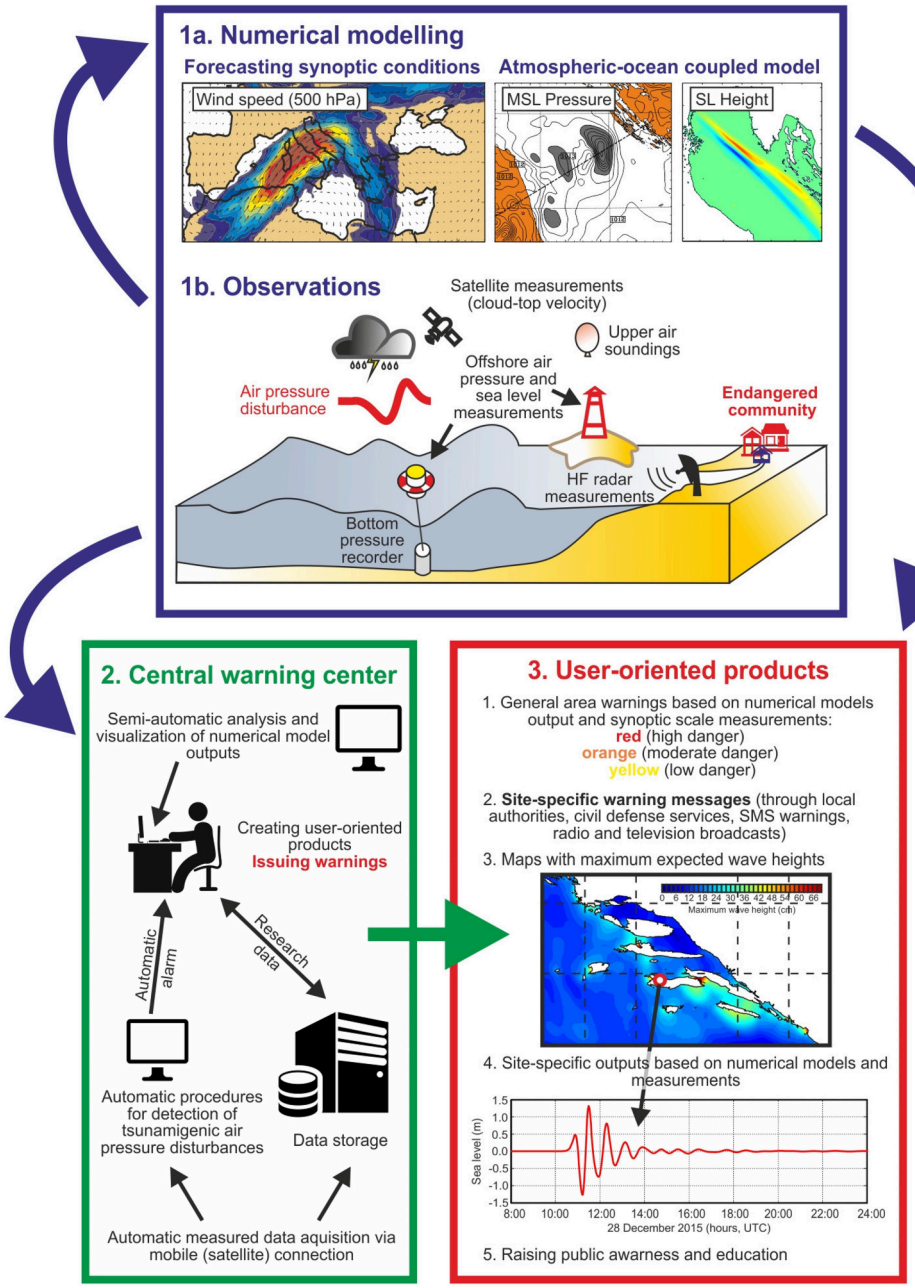

FIGURE 2 | The multilayer architecture of the proposed meteotsunami warning system, which includes observational and numerical modeling capacities, processing tools for detection of tsunamigenic conditions, and capacities for dissemination of the warning to civil authorities and the public.

with the prescribed values in the meteotsunami warning matrix estimated from historical meteotsunami events (Šepić and Vilibić, 2011). This is similar to a procedure that has been used for seismic tsunamis (Tinti et al., 2012). Such an approach can be used for an operative forecast of potentially destructive events an hour or less before their arrival at the coast.

The main idea of the third approach is sea level monitoring at a "*beacon*" station positioned off the hot-spot region, providing again approximately an hour of advance time for the most endangered locations (Marcos et al., 2009). This approach is also similar to the procedures developed for early tsunami warning, which is based on open-ocean tsunami detection systems (Mungov et al., 2013). However, since meteotsunamis

are generated over shelf areas or along coasts, the respective warning system should be based on measurements at available island stations, shelf buoys or coastal stations that are positioned along the wave path.

The fourth approach is operational within the BRIFS (Balearic Rissaga Forecasting System, www.socib.eu). Present coupled atmospheric-oceanic models are able to provide qualitative reproduction of meteotsunami waves, but still underestimate their amplitude and the potential for damage (Renault et al., 2011). This is because these models do not describe properly the evolution of tsunamigenic disturbances propagating onshore.

None of the above approaches can yet provide reliable early warning. A meteotsunami warning system should have identification-to-warning time on a minute scale, it has to be able to identify most potentially destructive events and to produce a minimum number of false warnings, following criteria developed for tsunami warning systems (Igarashi et al., 2011; Pararas-Carayannis, 2015). Therefore, the architecture of a meteotsunami warning system has to be based on a multilevel structure (**Figure 2**). Preconditioning (detection of tsunamigenic synoptic conditions), source detection (modeling and real-time tracking of atmospheric disturbances) and real-time numerical modeling of meteotsunami generation, propagation and transformation in the coastal zone should be part of an integrated system. Such a system needs to become a part of the general tsunami warning system, or of a broader MHEWS system, once it has advanced to the operative level of providing reliable disaster warnings. The system could be supplemented with additional procedures, including radar or satellite detection of tsunamigenic atmospheric disturbances (Belušić and Strelec Mahović, 2009; Anderson et al., 2015) and hazardous long ocean waves (Lipa et al., 2014). The warning system should also be site- or region-specific, as the phenomenon seems to have regionally dependant characteristics and on particular occasions can affect thousands of kilometres within a few days (Šepić et al., 2015a).

Constructing a meteotsunami warning system for any region should take into account the cost of such a system in comparison with the meteotsunami risk over a reasonable timescale. It is obvious that such a system is primarily important for "hot spots," i.e., for specific areas where destructive meteotsunamis can be expected. Active international cooperation and close coordination of efforts, exchange of ideas, knowledge, and approaches are crucial for successful investigation and mitigation of this natural hazard.

AUTHOR CONTRIBUTIONS

IV coordinated the work on the manuscript and wrote the initial version of the manuscript, JS prepared the figures and revised the text substantially, AR did a substantial polishing of text and figures, while all authors actively contributed to the development of the manuscript idea, to its writing and preparation of figures.

ACKNOWLEDGMENTS

We wish to thank Fred Stephenson of the Canadian Hydrographic Service, Institute of Ocean Sciences (Sidney, British Columbia) for editing the text and helpful advice. The work of IV and JS has been supported by the Croatian Science Foundation under the project MESSI (UKF Grant No. 25/15) and SCOOL (IP-2014-09-5747), and for AR by the Russian Science Foundation (grant 14-50-00095) and funds of IO RAS.

REFERENCES

Anderson, E. J., Bechle, A. J., Wu, C. H., Schwab, D. J., Mann, G. E., and Lombardy, K. A. (2015). Reconstruction of a meteotsunami in Lake Erie on May 27, 2012: roles of atmospheric conditions on hydrodynamic response in enclosed basins. *J. Geophys. Res.* 120, 8020–8038. doi: 10.1002/2015JC010883

Belušić, D., Grisogono, B., and Bencetić Klaić, Z. (2007). Atmospheric origin of the devastating coupled air-sea event in the east Adriatic. *J. Geophys. Res.* 112, D17111. doi: 10.1029/2006JD008204

Belušić, D., and Strelec Mahović, N. (2009). Detecting and following atmospheric disturbances with a potential to generate meteotsunamis in the Adriatic. *Phys. Chem. Earth* 34, 918–927. doi: 10.1016/j.pce.2009.08.009

Defant, A. (1961). *Physical Oceanography*. London: Pergamon Press.

Ewing, M., Press, F., and Donn, W. L. (1954). An explanation of the Lake Michigan wave of 26 June 1954. *Science* 120, 684–686. doi: 10.1126/science.120.3122.684

Geist, E. L., ten Brink, U. S., and Gove, M. (2014). A framework for the probabilistic analysis of meteotsunamis. *Nat. Hazards* 74, 123–142. doi: 10.1007/s11069-014-1294-1

Golnaraghi, M. (2012). *Institutional Partnerships in Multi-Hazard Early Warning Systems*. Heidelberg: Springer.

Greenspan, H. P. (1956). The generation of edge waves by moving pressure distributions. *J. Fluid Mech.* 1, 575–592. doi: 10.1017/S002211205600038X

Haslett, S. K., and Bryant, E. A. (2009). Meteorological tsunamis in Southern Britain: an historical review. *Geogr. Rev.* 99, 146–163. doi: 10.1111/j.1931-0846.2009.tb00424.x

Hibiya, T., and Kajiura, K. (1982). Origin of "abiki" phenomenon (kind of seiches) in Nagasaki Bay. *J. Oceanogr. Soc. Jap.* 38, 172–182. doi: 10.1007/BF02110288

Igarashi, Y., Kong, L., Yamamoto, M., and McCreery, C. S. (2011). Anatomy of historical tsunamis: lessons learned for tsunami warning. *Pure Appl. Geophys.* 168, 2043–2063. doi: 10.1007/s00024-011-0287-1

Jansà, A., Monserrat, S., and Gomis, D. (2007). The rissaga of 15 June 2006 in Ciutadella (Menorca), a meteorological tsunami. *Adv. Geosci.* 12, 1–4. doi: 10.5194/adgeo-12-1-2007

Lamb, H. (1932). *Hydrodynamics*. Cambridge: Cambridge University Press.

Lander, J. F., Lockridge, P. A., and Kozuch, M. J. (1993). *Tsunamis affecting the West Coast of the United States, 1806-1992*. Boulder: Colorado, National Geophysical Data Center, 242.

Lindzen, R. S., and Tung, K.-K. (1976). Banded convective activity and ducted gravity waves. *Mon. Wea. Rev.* 104, 1602–1617.

Lipa, B., Parikh, H., Barrick, D., Roarty, H., and Glenn, S. (2014). High-frequency radar observations of the June 2013 US East Coast meteotsunami. *Nat. Hazards* 74, 109–122. doi: 10.1007/s11069-013-0992-4

Marcos, M., Monserrat, S., Medina, R., Orfila, A., and Olabarrieta, M. (2009). External forcing of meteorological tsunamis at the coast of the Balearic Islands. *Phys. Chem. Earth* 34, 938–947. doi: 10.1016/j.pce.2009.10.001

Miles, J., and Munk, W. (1961). Harbor paradox, *J. Waterways Harbor Division* 87, 111–130.

Monserrat, S., Vilibić, I., and Rabinovich, A. B. (2006). Meteotsunamis: atmospherically induced destructive ocean waves in the tsunami frequency band. *Nat. Hazards Earth Syst. Sci.* 6, 1035–1051. doi: 10.5194/nhess-6-1035-2006

Mungov, G., Eblé, M., and Bouchard, R. (2013). DART® Tsunameter retrospective and real-time data: a reflection on 10 years of processing in support of tsunami research and operations. *Pure Appl. Geophys.* 170, 1369–1384. doi: 10.1007/s00024-012-0477-5

Nomitsu, T. (1935). A theory of tsunamis and seiches produced by wind and barometric gradient. *Mem. Coll. Sci. Imp. Univ. Kyoto A* 18, 201–214.

Pararas-Carayannis, G. (2015). Tsunami warning system in the Pacific: brief historical review of its establishment and institutional support. *Sci. Tsunami Hazards* 34, 101–139.

Pattiaratchi, C. B., and Wijeratne, E. M. S. (2015). Are meteotsunamis an underrated hazard? *Philos. Trans. R. Soc. A* 373, 20140377. doi: 10.1098/rsta.2014.0377

Proudman, J. (1929). The effects on the sea of changes in atmospheric pressure. *Geophys. Suppl. Mon. Notices R. Astr. Soc.* 2, 197–209. doi: 10.1111/j.1365-246X.1929.tb05408.x

Rabinovich, A. B. (2009). "Seiches and harbor oscillations," in *Handbook of Coastal and Ocean Engineering*, ed Y. C. Kim (Singapore: World Scientific Publishing Company), 193−236.

Rabinovich, A. B., and Monserrat, S. (1996). Meteorological tsunamis near the Balearic and Kuril Islands: descriptive and statistical analysis. *Nat. Hazards* 13, 55–90. doi: 10.1007/BF00156506

Rabinovich, A. B., and Monserrat, S. (1998). Generation of meteorological tsunamis (large amplitude seiches) near the Balearic and Kuril Islands. *Nat. Hazards* 18, 27–55. doi: 10.1023/A:1008096627047

Rabinovich, A. B., Vilibić, I., and Tinti, S. (2009). Meteorological tsunamis: atmospherically induced destructive ocean waves in the tsunami frequency band. *Phys. Chem. Earth* 34, 891–893. doi: 10.1016/j.pce.2009.10.006

Renault, L., Vizoso, G., Jansà, A., Wilkin, J., and Tintoré, J. (2011). Toward the predictability of meteotsunamis in the Balearic Sea using regional nested atmosphere and ocean models. *Geophys. Res. Lett.* 38, L10601. doi: 10.1029/2011gl047361

Satake, K., and Fujii, Y. (2014). Review: source models of the 2011 Tohoku Earthquake and long-term forecast of large earthquakes. *J. Disaster Res.* 9, 272–280. doi: 10.20965/jdr.2014.p0272

Šepić, J., and Rabinovich, A. B. (2014). Meteotsunami in the Great Lakes and on the Atlantic coast of the United States generated by the "derecho" of June 29–30, 2012. *Nat. Hazards* 74, 75–107. doi: 10.1007/s11069-014-1310-5

Šepić, J., Vilibić, I., and Fine, I. (2015b). Northern Adriatic meteorological tsunamis: assessment of their potential through ocean modeling experiments. *J. Geophys. Res.* 120, 2993–3010. doi: 10.1002/2015JC010795

Šepić, J., Vilibić, I., Rabinovich, A. B., and Monserrat, S. (2015a). Widespread tsunami-like waves of 23-27 June in the Mediterranean and Black Seas generated by high-altitude atmospheric forcing. *Sci. Rep.* 5, 11682. doi: 10.1002/2015JC010795

Šepić, J., and Vilibić, I. (2011). The development and implementation of a real-time meteotsunami warning network for the Adriatic Sea. *Nat. Hazards Earth Syst. Sci.* 11, 83–91. doi: 10.5194/nhess-11-83-2011

Sibley, A., Cox, D., Long, D., Tappin, D., and Horseburgh, K. (2016). Meteorologically generated tsunami-like waves in the North Sea on 1/2 July 2015 and 28 May 2008. *Weather* 71, 68–74. doi: 10.1002/wea.2696

Soloviev, S. L., and Go, C.h., N. (1974). *Catalogue of Tsunamis on the Western Shore of the Pacific Ocean*. Moscow: Nauka. [in Russian; English Translation: Canadian Transl. Fish. Aquatic Sci., No. 5078, Ottawa, 1984, 439].

Tanaka, K. (2010). Atmospheric pressure-wave bands around a cold front resulted in a meteotsunami in the East China Sea in February 2009. *Nat. Hazards Earth Syst. Sci.* 10, 2599–2610. doi: 10.5194/nhess-10-2599-2010

Tappin, D., Sibley, A., Horsburgh, K., Daubord, C., Cox, D., and Long, D. (2013). The English Channel tsunami of 27 June 2011 – a probable meteorological source. *Weather* 68, 144–152. doi: 10.1002/wea.2061

Teixeira, J., and Reynolds, C. A. (2008). Stochastic nature of physical parameterizations in ensemble prediction: a stochastic convection approach. *Mon. Wea. Rev.* 136, 483–496. doi: 10.1175/2007MWR1870.1

Thomson, R. E., Rabinovich, A. B., Fine, I. V., Sinnott, D. C., McCarthy, A., Sutherland, N. A. S., et al. (2009). Meteorological tsunamis on the coasts of British Columbia and Washington. *Phys. Chem. Earth* 34, 971–988. doi: 10.1016/j.pce.2009.10.003

Tinti, S., Graziani, L., Brizuela, B., Maramai, A., and Gallazzi, S. (2012). Applicability of the decision matrix of North Eastern Atlantic, Mediterranean and connected seas Tsunami Warning System to the Italian tsunamis. *Nat. Hazards Earth Syst. Sci.* 12, 843–857. doi: 10.5194/nhess-12-843-2012

Tintoré, J., Vizoso, G., Casas, B., Heslop, E., Pascual, A., Orfila, A., et al. (2013). SOCIB: The Balearic Islands Coastal Ocean Observing and Forecasting System responding to science, technology and society needs. *Mar. Technol. Soc. J.* 47, 101–117. doi: 10.4031/MTSJ.47.1.10

Vilibić, I., Monserrat, S., and Rabinovich, A. B. (2014). Meteorological tsunamis on the US East Coast and in other regions of the World Ocean. *Nat. Hazards* 74, 1–9. doi: 10.1007/s11069-014-1350-x

Vilibić, I., Monserrat, S., Rabinovich, A. B., and Mihanović, H. (2008). Numerical modelling of the destructive meteotsunami of 15 June 2006 on the coast of the Balearic Islands. *Pure Appl. Geophys.* 165, 2169–2195. doi: 10.1007/s00024-008-0426-5

Vučetić, T., Vilibić, I., Tinti, S., and Maramai, A. (2009). The Great Adriatic flood of 21 June 1978 revisited: an overview of the reports. *Phys. Chem. Earth* 34, 894–903. doi: 10.1016/j.pce.2009.08.005

Wertman, C. A., Yablonsky, R. M., Shen, Y., Merrill, J., Kincaid, C. R., and Pockalny, R. A. (2014). Mesoscale convective system surface pressure anomalies responsible for meteotsunamis along the US East Coast on June 13th, 2013. *Sci. Rep.* 4, 7143, doi: 10.1038/srep07143

Whitmore, P., and Knight, B. (2014). Meteotsunami forecasting: sensitivities demonstrated by the 2008 Boothbay, Maine, event. *Nat. Hazards* 74, 11–23. doi: 10.1007/s11069-014-1056-0

Conflict of Interest Statement: The authors declare that the research was conducted in the absence of any commercial or financial relationships that could be construed as a potential conflict of interest.

frontiers in Marine Science

ORIGINAL RESEARCH
published: 16 November 2016
doi: 10.3389/fmars.2016.00206

Lessons Derived from Two High-Frequency Sea Level Events in the Atlantic: Implications for Coastal Risk Analysis and Tsunami Detection

Begoña Pérez-Gómez[1], Fernando Manzano[1], Enrique Alvarez-Fanjul[1], Carlos González[2], Juan V. Cantavella[2] and François Schindelé[3]*

[1] Puertos del Estado, Madrid, Spain, [2] Instituto Geográfico Nacional, Madrid, Spain, [3] Commissariat á l'énergie Atomique et Aux Énergies Alternatives (CEA), Direction des Applications Militaires Ile-de-France (DAM, DIF), Arpajon, France

The upgrade and enhancement of sea level networks worldwide for integration in sea level hazard warning systems have significantly increased the possibilities for measuring and analyzing high frequency sea level oscillations, with typical periods ranging from a few minutes to a few hours. Many tide gauges now afford 1 min or more frequent sampling and have shown such events to be a common occurrence. Their origins and spatial distribution are diverse and must be well understood in order to correctly design and interpret, for example, the automatic detection algorithms used by tsunami warning centers. Two events recorded recently in European Atlantic waters are analyzed here: possible wave-induced "seiches" that occurred along the North coast of Spain during the storms of January and February of 2014, and small sea level oscillations detected after an earthquake in the mid-Atlantic the 13th of February of 2015. The former caused significant flooding in towns and villages and a huge increase in wave-induced coastal damage that was reported in the media for weeks. The latter was a smaller signal present in several tide gauges along the Atlantic coast that coincided with the occurrence of this earthquake, leading to a debate on the potential detection of a very small tsunami and how it might yield significant information for tsunami wave modelers and for the development of tsunami detection software. These kind of events inform us about the limitations of automatic algorithms for tsunami warning and help to improve the information provided to tsunami warning centers, whilst also emphasizing the importance of other forcings in generating extreme sea levels and their associated potential for causing damage to coastal infrastructure and flooding.

Keywords: sea level, warning, high frequency, detection, automatic algorithms, tsunami

OPEN ACCESS

Edited by:
Sönke Dangendorf, University of Siegen, Germany

Reviewed by:
Ivica Vilibic, Institute of Oceanography and Fisheries, Croatia
Sebastian Monserrat, University of the Balearic Islands, Spain

****Correspondence:***
Begoña Pérez-Gómez
bego@puertos.es

Specialty section:
This article was submitted to Coastal Ocean Processes, a section of the journal Frontiers in Marine Science

Received: *11 February 2016*
Accepted: *03 October 2016*
Published: *16 November 2016*

Citation:
Pérez-Gómez B, Manzano F, Alvarez-Fanjul E, González C, Cantavella JV and Schindelé F (2016) Lessons Derived from Two High-Frequency Sea Level Events in the Atlantic: Implications for Coastal Risk Analysis and Tsunami Detection. Front. Mar. Sci. 3:206. doi: 10.3389/fmars.2016.00206

INTRODUCTION

Sea level-related hazards have become an important concern in recent decades due partly to the impact of climate change on mean sea level rise and its potential for increasing the number of storm surge extreme events (Church et al., 2001; Woodworth and Blackman, 2002, 2004). Additionally, several catastrophic tsunamis have occurred since the beginning of this century, raising awareness of society to this risk. Since 2000 more than 380.000 people died during natural disasters related to coastal inundation or sudden sea level rise: Indian Ocean tsunami (2004), Chile tsunami (2010),

Japan tsunami (2011), Hurricane Katrina (US, 2005), Hurricane Sandy (US, 2012), Cyclon Nargis (Myanmar, 2012), etc., This terrible number of casualties demonstrates the great vulnerability of the coastal zone, which has seen a population increase of 35% since 1995 and is today inhabited by 23% of the world population.

For this reason, real, or near-real time sea level data are critical to the design of early sea level and tsunami warning systems. The latter are now being implemented in practically all the main basins, following the Indian Ocean tsunami in 2004 and according to the recommendations of the Intergovernmental Coordination Groups (ICG's) established by the UNESCO Intergovernmental Oceanographic Commission (IOC), such as the NEAMTWS (North East Atlantic, Mediterranean and Adjacent Seas Tsunami Warning System) ICG in Europe (IOC UNESCO, 2007). One of these recommendations is the need of sea level data with 1 min or less sampling and latency, which has motivated the upgrade of existing tide gauge networks around the world. To make best use of these data new software must be developed to automatically quality control and process data, to issue sea level alert messages, and to implement algorithms for automatic tsunami detection. Examples of the algorithms applied to offshore pressure data from DART buoys are described by Rabinovich et al. (2011) and Rabinovich and Eblé (2015), whilst other authors focus on the application of this kind of algorithm to coastal tide gauge data such as Beltrami et al. (2011), Bressan et al. (2013) and Pérez-Gómez et al. (2013).

Several years ago, Puertos del Estado (hereafter PdE) implemented such software for the Spanish REDMAR tide gauge network, in response to the small tsunami generated by the Algerian earthquake, in May 2003, in the Western Mediterranean (Alasset et al., 2006; Sahal et al., 2009; Vich and Monserrat, 2009; Vela et al., 2014). The objective was real time tsunami detection and the transmission of alert messages to the network and harbor operators during future events. Nowadays, due to the recent establishment of the National Tsunami Warning System in Spain, run by the National Geographic Institute (IGN: Instituto Geográfico Nacional) in collaboration with Spanish Civil Protection, real time sea level data and the mentioned alert messages from the REDMAR network are also received by the IGN. However, this algorithm for tsunami detection has also proven useful for identifying other more frequent high-frequency harbor oscillations such as "meteotsunamis" (related to atmospheric pressure) or infragravity waves (generated by wind waves), which present strong similarities to seismically generated tsunamis (same periods and physical properties), in such a way that it can be difficult to recognize one from another. Testing the software with data from a seismic tsunami is of course difficult because these are fortunately rare events in our region. For this reason, any high frequency sea level oscillations are helpful in assessing the skills of these algorithms.

Monserrat et al. (2006a) compared the characteristics of tsunamis and "meteotsunamis," a term suggested by different authors (Nomitsu, 1935; Defant, 1961; Rabinovich and Monserrat, 1996; Vilibić et al., 2005; Rabinovich, 2009) for those atmospherically generated sea level oscillations with periods of a few minutes to a few hours that may affect the coast at particular bays or harbors in the same way than a tsunami generated by an earthquake. Although less catastrophic than major seismic tsunamis (the spatial scale is smaller: local or regional), they are related to atmospheric forcing and mainly to moving pressure disturbances (atmospheric gravity waves, pressure jumps, frontal passages, or squalls). These events and their worldwide occurrence have been widely studied, described and acknowledged as potentially-hazardous sea level phenomena by many authors, aside from those already mentioned: (Orlić, 1980; Hibiya and Kajiura, 1982; Pattiaratchi and Wijeratne, 2015; Šepić et al., 2015a,b). In Spain, they are particularly common in the Balearic Islands, where they are named "rissagas" (Gomis et al., 1993; Jansà et al., 2007; Marcos et al., 2009), and on the Western Mediterranean Spanish coast. In fact, two special issues on "meteotsunamis" have been published: Physics and Chemistry of the Earth (Rabinovich et al., 2009) and Natural Hazards (Vilibić et al., 2014). Recent studies for the UK and North Sea coast have also been published by Tappin et al. (2013) and Sibley et al. (2016).

"Infragravity waves," a phenomenon first described in 1950 by Walter Munk (the name was coined by Kinsman in 1965, according to Pugh and Woodworth, 2014), are also high frequency sea level oscillations generated by non-linear interactions of swell waves arriving at the coastline during a storm (Munk, 1949, 1962). These waves, with shorter periods than meteotsunamis (between 30 s and 5 min), may sometimes also be amplified through resonance in bays and harbors (Longuet-Higgins and Stewart, 1962; Wu and Liu, 1990; Herbers et al., 1995). Such oscillations are common along the North coast of Spain. Infragravity waves have been reported to be responsible for flooding in other regions (Sheremet et al., 2014) due to their "tsunami-like" behavior and their contribution to increasing the coastal impact of wind waves.

The aim of this paper is to analyze and discuss the characteristics and possible physical sources of two events that occurred in the Atlantic recently: the sea level oscillations recorded along the North Spanish coast in January and February 2014 and the feasibility of a small tsunami being recorded after an earthquake in the Atlantic ridge the 13th of February 2015. Although in principle different in origin, their effects on sea level records from tide gauges are not that different and can be detected with the same algorithms developed for tsunami warning. Understanding the problems and limitations of existing algorithms in identifying and distinguishing different types of high-frequency phenomena is important for issuing appropriate alerts and is in fact the main objective of this paper. At the same time, as new tide gauge technology allows us to measure other sea level processes apart from the tide and storm surge contribution, the study extends our existing knowledge on the physical sources of these higher frequency oscillations and their associated coastal risks. Finally, the paper provides also an assessment of the response of the upgraded REDMAR network and PdE multi-parameter alert system during those dates.

The paper is structured as follows: after description of the data and methods, the results of the analysis of the two events are presented, followed by the discussion and conclusions on the main findings about these particular events and the consequences

for future detection and interpretation of sea level oscillations data.

DATA AND METHODS

The 1 min sampled sea level time series available today in the region are the main source of information used in the analysis of these two events, most of them from PdE REDMAR sea level network, composed of 37 tide gauge stations at the main harbors of Spain. Wind wave, atmospheric pressure and wind data from wave buoys deployed near the Spanish coast are also used to determine the influence of these parameters on the observed sea level oscillations. These buoys belong to PdE deep water buoy network (Álvarez-Fanjul et al., 2002), and are located at around 400 m depth and 10–20 miles away from the coast. Outputs from the wave and sea level forecasting systems of PdE (Álvarez-Fanjul et al., 2001; Gómez-Lahoz and Carretero-Albiach, 2005) were used to understand the physical conditions relating to wind waves, the tide and storm surges during the dates of the events. Estimated arrival times of tsunami wave propagation were computed by the Spanish Geographic Institute (IGN) for the earthquake of 13th February 2015 and used for the analysis of the sea level records in this study.

This work also takes advantage of some specific characteristics of the REDMAR tide gauge network: with a raw sampling interval of 2 Hz, this array of Miros radar sensors additionally provides wind wave parameters at the tide gauge site (significant wave height, maximum wave height, mean period, and peak period) with a sampling interval of 20 min. These local wind wave parameters are transmitted to PdE alongside the records of 1-min averaged sea level data. Furthermore, a decision was taken several years ago to upgrade the stations with atmospheric pressure and wind sensors with 1-min sampling resolution, to facilitate their future use in "meteotsunamis" alert systems—an important improvement that was recommended by the scientific community working on "meteotsunamis" (Vilibić et al., 2016). From the 37 stations in REDMAR, 17 already have these new meteorological sensors transmitting their data in real time to PdE system (13 of these were installed during the last year within the national project SAMOA: *Sistema de Apoyo Meteorológico y Oceanográfico a las Autoridades Portuarias:* System of Oceanographic and Meteorological Support to the Harbour Authorities). Unfortunately for the events analyzed here, 1-min atmospheric pressure was only available for the Vigo tide gauge, on the Galician coast.

Total 1-min sea level data from the REDMAR are automatically filtered before being passed through the tsunami detection algorithm and the multi-parameter alert system of waves, sea level, and high frequency oscillations (including tsunamis) implemented by PdE. A detailed description of this system can be found in Pérez-Gómez et al. (2013). The recent upgrade to 1-min sampling and transmission latency has led to a new strategy for sea level data quality control and processing in real-time, including its contribution to the mentioned alert system that sends an email to the network operators when one of the main parameters is over a predetermined threshold, with three levels of alert: 2: "warning" (yellow), 3: "risk" (orange) and 4: "danger" (red).

The algorithm for tsunami detection, an important element of the software, is based on: (1) the elimination of low frequency sea level oscillations (periods larger than 3 h such as the tide) by means of a FIR filter with a Kaiser window of 15 points, (2) the computation of the variance of the filtered signal in a moving window, and (3) its evaluation with respect to predefined thresholds for each harbor. The algorithm has been in operation since 2008, having been tested and validated using the tsunami of May 2003 in the Balearic Islands and other tsunamis in the Indian Ocean. The filtered signal and the alert "level" are stored in the PdE data bank. To date, the performance of the algorithm has been very good, which is in part due to the near-real time automatic quality control of sea level that is undertaken every 15 min. This quality control in real time is a complex task: a tide gauge malfunction will almost always generate an initial false alert when the first 1-min observation is received, and this is automatically canceled when detailed analysis and quality control running a few minutes later flags the suspect data. For this reason, the alerts are received solely by experienced operators at PdE and the IGN who make informed decisions based upon comparisons with other parameters and stations in the system (the IGN will only pay attention to these messages if an earthquake has been detected by their seismic network).

Data from non-REDMAR tide gauges were downloaded from the data portals of the IOC Sea Level Station Monitoring Facility (SLSMF: http://www.ioc-sealevelmonitoring.org/) or the IBIROOS *In-Situ* Tac (http://www.ibi-roos.eu/Access-to-data/The-IBI-Portal). As high-passed filtered data were not available from these sites, we applied the same filter used in REDMAR to the 1-min sea level data from other institutions.

In order to characterize the 1-min high-pass filtered oscillations in this study, we have implemented a scheme of data processing for a specific period, which consists of the following steps:

- Interpolation of short gaps (<4 min)
- Estimation of *seiche* wave amplitude and period by means of the zero-up crossing procedure
- Temporal evolution of the spectra: spectrogram

The zero-up crossing procedure is usually adopted for wind waves, where a wave is defined as the portion of a record between two successive zero-up crossings. This generates a reasonable estimate of the variation in amplitude of these sea level oscillations by computation of the significant wave height [H_s: mean of wave height (trough to crest) of the highest third of the waves] and maximum wave height (H_{max}) in the recorded burst. The algorithm is applied here to a moving window of 6 h (360 min) with an overlap of the last 20 min. From a mathematical point of view, this approach should be applied on stationary sea states. Since this may not be the case for these 1 min sea level data the significant wave height computed here is not perfectly equivalent to the one obtained for wind waves

and should be considered just an estimation of the oscillation amplitude ($H_s/2$ or $H_{max}/2$).

The spectrograms of the 1-min filtered signal were obtained by means of a fast Fourier transform applied to windows of around 8 h (512 points) or 1 day (1536 points) with an overlap of around 2 h (128 points).

In order to identify clearly the periods of the infragravity waves and the presence of wind waves or swell, we also performed spectral analysis of the 2 Hz data during the events at some of the stations. After applying a high-pass filter to eliminate periods larger than 45 min, the power spectral density is obtained by calculating the auto-covariance function smoothed with a Parzen lag window (Jenkins and Watts, 1968). In the future, additional data processing scripts will be needed to improve the characterization in near-real time of these high-frequency sea level oscillations from 2 Hz data, especially for those periods of the infragravity waves (30 s to 5 min), which are not well-resolved with 1 min sampling. To address this, we plan to analyze original 2 Hz raw data from the tide gauges in the REDMAR network, that are currently being transmitted hourly to PdE.

SEA LEVEL OSCILLATIONS ALONG THE SPANISH COAST DURING THE STORMS OF JANUARY–FEBRUARY 2014

From early January to end February 2014 the Northeast Atlantic suffered the impact of a sequence of unprecedented extreme storms characterized by huge wind waves and severe coastal flooding. These storms were caused by a powerful jet stream driving low pressure systems and associated winds and waves across the Atlantic. Apart from the great damage to the coastline recorded in other countries such as the UK (BBC, 2014), where storm surge magnitude is usually larger than in the Spanish coast, several coastal villages, beaches, and harbors of the North Spanish coastline were this time also inundated by the extreme waves, resulting in the destruction of maritime promenades and reaching houses at waterfront areas (**Figure 1**). These events had therefore a tremendous impact on the media (El País, 2014) that put the focus on the huge wind waves seen by the population and recorded in the open waters by PdE deep water buoy network (Álvarez-Fanjul et al., 2002).

The multi-parameter alert system worked well during these storms, providing red alerts (level 4) of wind waves, sea level and oscillations from all the existing buoys and tide gauges along the North Spanish coast, from Galicia to the Basque Country (see stations location in **Figure 2**). Significant wave heights and mean and peak periods at the buoys are displayed in **Figure 3**. Sea level oscillation warnings were also correctly issued, indicating that the tsunami detection algorithm was performing well. In the particular case of the storm of January 6th, we received additional red alerts of sea level oscillations from stations as far away as the Canary Islands.

Observational Data

As can be seen in **Figure 4** (left) the high-pass filtered 1-min time series from the tide gauges along the Spanish coast exhibit significant sea level oscillations simultaneously with this sequence of storms along almost all the coastline. A detailed study of the sea level data and a description of the atmospheric and oceanographic conditions during these days are presented below. The REDMAR tide gauges also provide information on wind waves recorded locally in the harbors and the significant wave heights (H_{m0}) from these are also displayed in **Figure 4** (right). We can see that during these storms there were also important wind waves (0.4–1 m height is considered important inside a harbor) even at the quays where the tide gauge station is located. These wind waves (mostly swell) are usually a problem for harbor operations and confirm the critical situation at the coast and harbors these days: the local wind waves along with sea level oscillations and their associated currents may increase the damage to infrastructures and the possibility of flooding.

These observed sea level oscillations are thought in principle to be "infragravity waves" generated by non-linear wave interactions of the incredibly high swell waves arriving at the coastline during these storms. The particularly long peak periods of the wind waves in open waters (**Figure 3**, right) make this

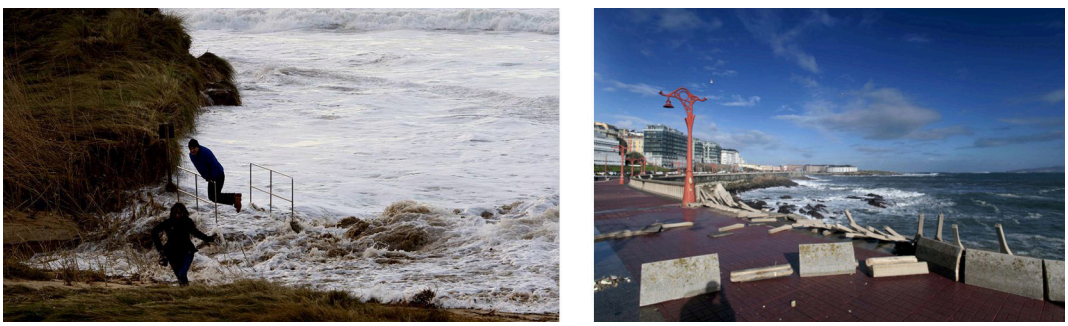

FIGURE 1 | Left: people running away from the waves at Esteiro beach (Xove, Lugo, Northern Galicia) during the storm of February 2nd 2014 (Nadja storm). Source: La Voz de Galicia, photographer: Pepa Losada: http://www.lavozdegalicia.es/album/galicia/2014/02/02/danos-temporal/0110139132886851159078 5.htm. **Right:** impact on Coruña maritime promenade after the same Nadja storm. Source: El Ideal Gallego: http://www.elidealgallego.com/album/coruna/efectos-temporal-coruna/20140202182014171505.html.

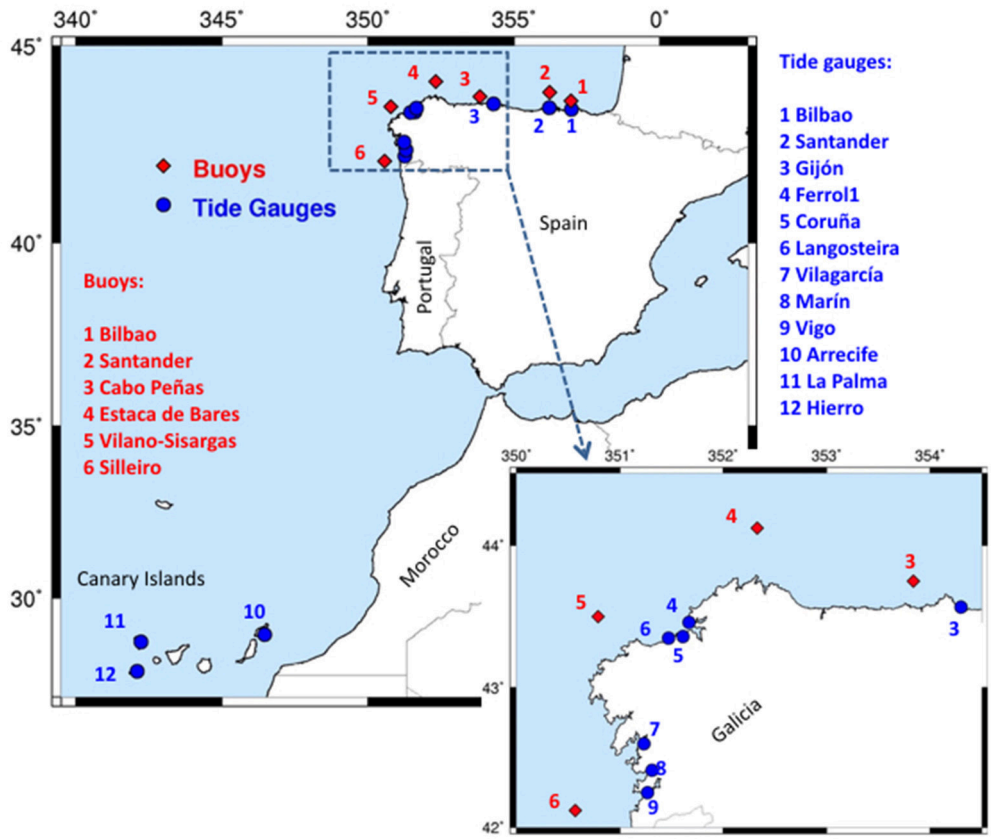

FIGURE 2 | Position of the REDMAR tide gauges and Deep Water buoys from Puertos del Estado. Santander buoy belongs to the Spanish Oceanographic Institute.

event special and interesting: peak periods of up to 22.3 s were recorded at Bilbao buoy the 6th of January. Spectral analysis of the sea level time series should provide information, however, on the possibility of a "meteotsunami" generation as well. It is interesting to note the spatial scale of these events, along hundreds of kilometers of coast.

The largest sea level oscillations are observed on January 6th and February 2nd, as well as the most extreme wind waves recorded by the deep water buoys. During the first one, maximum significant wave heights of 12.4 m and 12.0 m were recorded by Vilano-Sisargas and Estaca de Bares buoys respectively (PdE, 2014). On February 2nd, however, the latter recorded an even larger significant wave height: 12.8 m, very close to its historical record (12.9 m). Maximum wave heights may be estimated roughly by multiplying these values by 1.6, which would result in individual wind waves of 20 m or more in open waters. This was confirmed by the delayed data processing of raw data from Estaca de Bares buoy, where an individual freak wave of 29 m height was found, becoming the highest wave height ever measured along the Spanish coast (M.I. Ruiz, personal communication). An alert level "4" for wind waves was issued by PdE alert system. As already mentioned these waves presented as well extremely long periods with peak periods reaching 22.3 s (**Figure 3**, right); this was a very distinctive characteristic of these storms, possibly related to the excited frequencies on the sea level oscillations, as will be shown later.

On both dates we also received level "4" alerts for sea level oscillations from most of the tide gauges shown in **Figure 4**; however, total sea level alerts (highs and lows) did not exceed level "2" on January 6th, and level "3" around February 2nd. This difference is due to the more precise coincidence of the second storm with the spring tide (**Figure 5**). In fact, this spring tide played a key role in the flooding, overtopping of waves and extreme sea levels recorded during this storm. The astronomical tide was particularly large that day due to the coincidence of the new moon and the lunar perigee (January 30th), its proximity to the perihelion (January 4th) and to zero lunar declination (February 2nd). Coincidence of lunar perigee and zero lunar declination occurs only every 6 years (Pugh, 2004).

Origin of the Oscillations

High frequency sea level oscillations were the second important contributor to the total extreme sea levels on these days. It is necessary to determine, first, the origin of these oscillations: in the absence of an earthquake and the coincidence with such big waves the first impression is that they are infragravity waves, very common in the Spanish Atlantic harbors, as already mentioned; nevertheless, they might also be meteotsunamis like

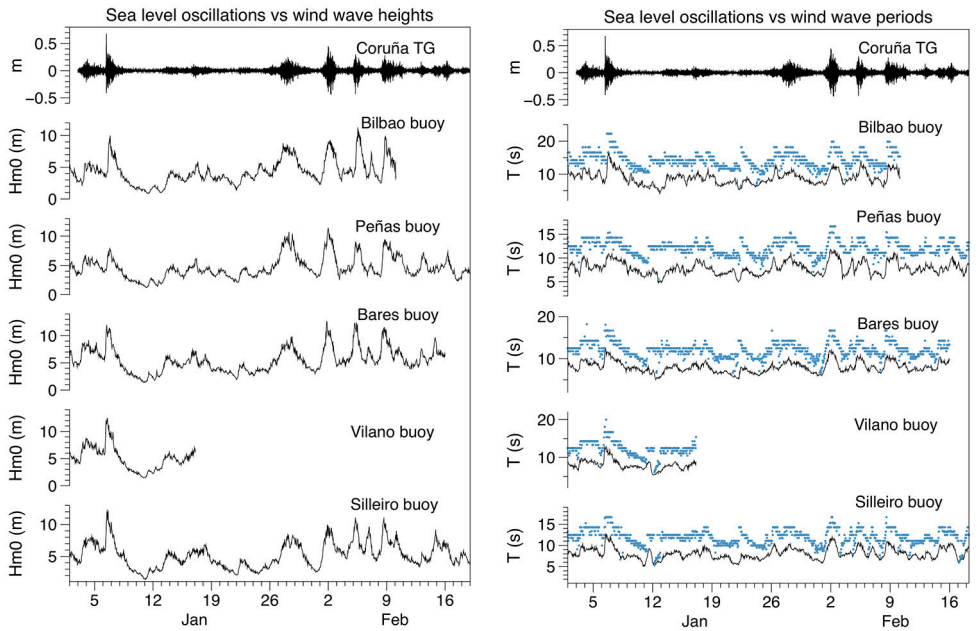

FIGURE 3 | Significant wave height H_{m0} (left) and periods (**right:** mean period T_m, black line, peak period T_p, blue dots) recorded in open waters by the PdE deep water buoys during the stormy period of January and February 2014. Sampling interval from the buoys is 1 h. Sea level oscillations (1 min high-pass filtered sea level) from Coruña tide gauge at the top of both plots for comparison: the larger oscillations occur during the extreme events of wind waves.

those described in Frère et al. (2014). That paper described a meteotsunami event which occurred on June 26–28, 2011 in this region and which was recorded by all the tide gauges presented here, as well as at other stations from Portugal to England. It is interesting to notice the differences with our case: first, weather conditions in June 2011 were rather calm (summer time): wind waves at Peñas buoy (near Gijón tide gauge) were just around 1 m height between the 26th and 28th of June 2011. This is a typical situation during meteotsunamis on the Mediterranean Spanish coast, which usually occur in summer (Tintoré et al., 1988; Gomis et al., 1993; Monserrat et al., 2006b; Marcos et al., 2009). Second, analysis of the atmospheric pressure data from buoys and tide gauges revealed for this event that the oscillations occur when the atmospheric pressure is at a relative low level. This does not seem to be exactly the situation in 2014: **Figure 6** shows that the larger sea level oscillations in our case are not exactly coincident with lower levels of pressure at the nearby deep water buoy. In fact, they seem to occur approximately 1 day later and coincide instead on February 2nd with a relatively higher value of pressure.

Nevertheless, a meteotsunami could still have been generated for example by a sudden change in atmospheric pressure. Detection of fast atmospheric pressure jumps is usually difficult from existing meteorological networks as the sampling of most of the stations is too infrequent (10 min to 1 h). This is the case for the buoys of PdE network but also for others as described in Frère et al. (2014). The sampling interval of these buoys is 1 h, far from the 1 min temporal resolution required for implementation of future meteotsunami warning systems. As mentioned in previous section the REDMAR tide gauge network already takes into account this requirement and several microbarographs are now in operation with 1-min sampling and a resolution of 0.1 HPa (the resolution at the buoys is 1 HPa). In 2014 one of these sensors was already functioning at Vigo harbor tide gauge. **Figure 7** (top) shows in detail the changes in atmospheric pressure recorded at this tide gauge on January 6th: although the resolution is clearly better than the one from the buoy (displayed also in the figure), it is difficult to conclude that there is a change capable of generating a meteotsunami. The relation of the oscillations with the sudden increase in wind waves is however more evident from middle and lower panels of **Figure 7**, which show the oscillations of sea level at Coruña plotted along with the wind waves significant wave height recorded by the nearest offshore buoy (Vilano) and by the tide gauge itself, respectively.

The amplitudes of these sea level oscillations (significant and maximum wave heights as explained in Section Data and Methods) are shown in the bottom panels of **Figure 8** for La Coruña and La Palma tide gauges. Notice the resemblance of the peaks with the ones in significant wave height of wind waves in **Figures 3**, **4**. This supports the idea of the swell wind waves being the forcing mechanism of these oscillations, which reach H_s and H_{max} of 0.5 and 0.9 m respectively in La Coruña, and of 0.3 and 0.5 m in La Palma, well far away from the center of the storms. **Figure 8** (top panels) displays as well the spectrogram or temporal evolution of the spectra of 1 min data for these two stations (1536 points window with 128 points overlap): an increase in the energy content at higher frequencies (2 min or 0.5 cpm to 7 min or 0.15 cpm) is observed when each event starts. These periods are very close to the range of frequencies of the infragravity waves (30 s–5 min).

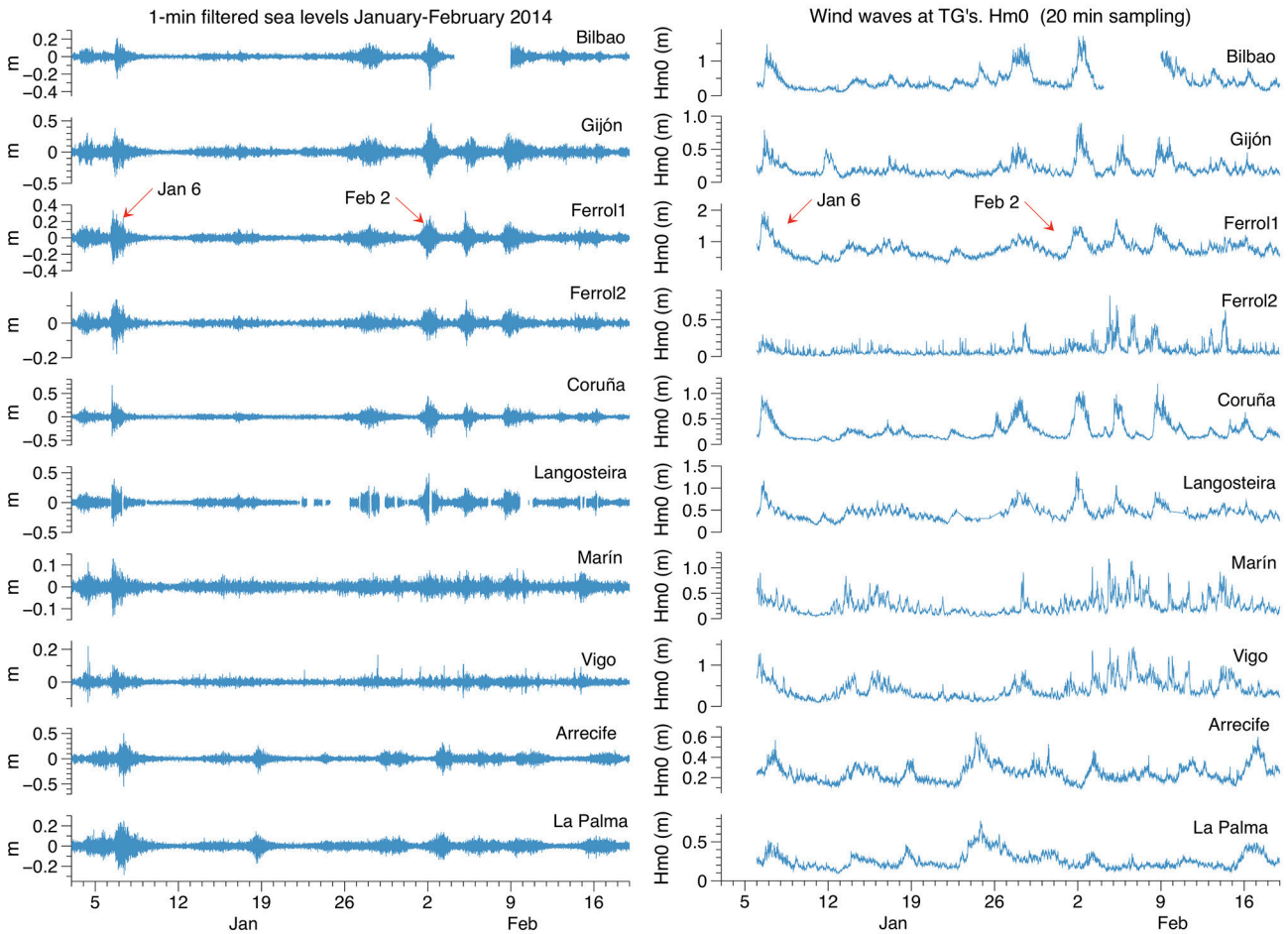

FIGURE 4 | Left: 1 min high-pass filtered sea level data from the REDMAR network during the stormy period January- February 2014, showing the occurrence of significant high-frequency sea level oscillations along the Spanish coast; **right:** significant wave height (H_{m0}) computed by these Miros tide gauges for the same period.

We cannot discard the possibility of one of these frequencies being related to the excitation of the natural eigen periods at some harbors. Left panels on **Figure 9** display for Coruña and La Palma tide gauges, the spectra for one specific day of 1 min data when maximum oscillations were recorded (red line) and the spectra for another day with no significant oscillations (blue line). The latter represent the spectral content of the background noise and therefore the natural frequencies or eigen periods of each location. A vertical logarithmic scale is used for an easier comparison of the two spectra. The frequency peaks on red and blue lines seem to be practically the same on both stations, what would confirm that we are observing an excitation of the natural eigen periods during the storm of January 6th, most evident at Coruña tide gauge.

Interestingly, **Figure 8** (upper panel) shows a permanent signal in the range of 19–25 min (0.05–0.04 cpm) in the Coruña time series. It seems the signal is present before and after the increase of the oscillations amplitude and is also clear in the background noise spectra of 1 min data in **Figure 9**. This signal is not present or is very small in La Palma tide gauge (Canary Islands), but it is close to one found for the event of June 2011, on almost all the stations (Frère et al., 2014); this would discard a local topographic feature being responsible for this frequency peak although Frère et al. did not find a clear explanation about their origin. A spectrogram of the 1-min atmospheric pressure from Vigo tide gauge (not shown) revealed that this was the only band of frequencies with significant variance in the high temporal resolution atmospheric pressure data for all these weeks.

As the periods excited during 2014 events are very close to the Nyquist frequency of 1 min data (2 min), spectral analysis of the original 2 Hz data was performed also for the Coruña and La Palma tide gauge records during the storm of January 6th (**Figure 9**, right panels). In this case we have used a window of 1 h of data with maximum amplitude of the oscillations. The background noise at very high frequencies was so small that its spectra is not shown in this case. These 2 Hz spectra allow a clear distinction between the frequencies of the infragravity waves we are discussing here and the wind-waves at the tide gauge locations: we can see for the latter that most of the energy is concentrated on the swell band, with peaks at 0.37 min (22.2 s)

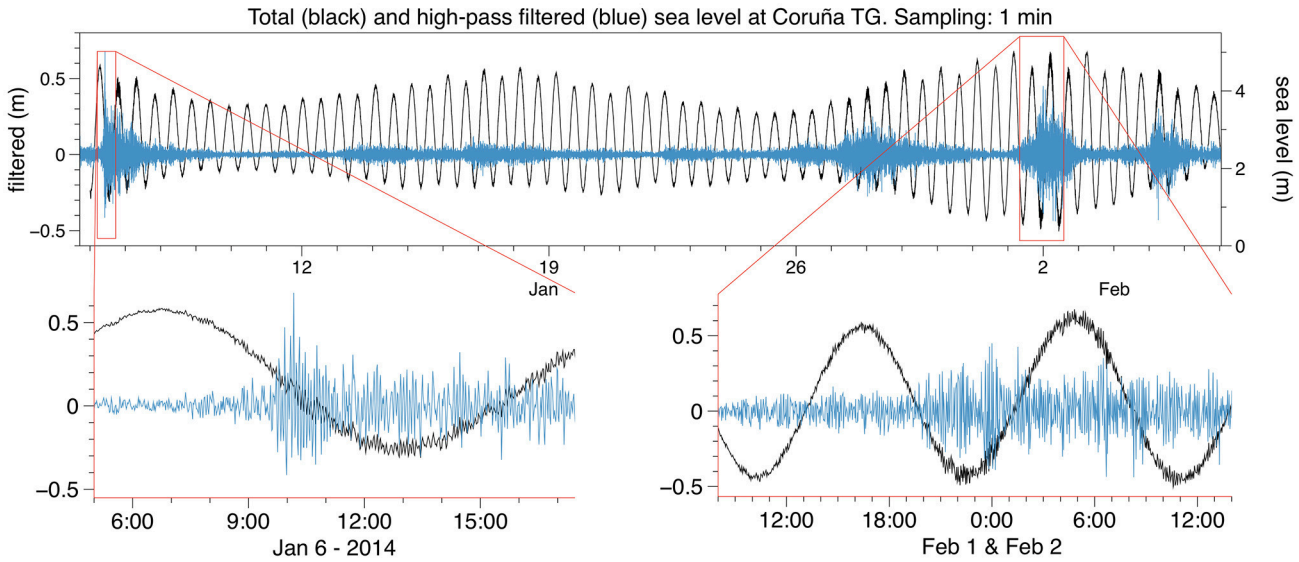

FIGURE 5 | Total sea level (black) and high-pass filtered signal (blue) recorded by Coruña tide gauge for January–February 2014; data sampling: 1 min. The two most extreme events (January 6th and February 2nd) are shown amplified below. The maximum amplitude of the oscillation does not occur during high-tide, especially on January 6th.

and 0.39 min (23.4 s) for Coruña and La Palma, respectively. These very long peak periods are also present for this event at the open waters buoys, as already mentioned. This would explain therefore that associated infragravity waves were generated at a low frequency range, 4–6 min, and that their wave peaks were much narrower than usual for this particular event. According to the 1-min spectra (**Figure 9**, left panels), these waves were then further amplified at the resonance eigen periods at Coruña and La Palma, 4.5 min and about 6 min, respectively, becoming a peculiar and interesting case of resonance amplification of infragravity waves.

Contribution to Extreme Sea Levels

A better understanding of the contribution of these oscillations to total sea level is possible from the data presented in **Table 1**. Column 2 shows the maximum sea levels recorded by the tide gauges of Bilbao, Santander, Gijón, and Coruña during the storm of February 2nd, when the coastal inundation affected a largest area of the coast. These extreme sea levels are derived from the total 1-min sea level data. Column 3 contains the height of the tide at that instant, computed with the harmonic constants derived from harmonic analysis of more than one year of hourly sea level data in each harbor. The magnitude of the storm surge forecasted by the Nivmar system in operation at PdE is presented in column 4 for the point closer to each tide gauge, and column 5 contains the contribution from the "seiche" oscillation, estimated as half the significant wave height H_s (of the "seiche") obtained in the way described in Section Data and Methods. The most important conclusion is that the extreme sea levels recorded during this event were significantly affected by these infragravity waves that had the same or even larger magnitude than the storm surge itself. In fact, the storm-surge component was rather moderate or small as was confirmed from analysis of the storm surge forecasted by the Nivmar system (the value forecasted for Coruña harbor was even negative). The addition of the values in columns 3, 4, and 5 is exactly the observed extreme value in column 2 for Santander and Gijón, and very close to it in Coruña and Bilbao (only 1 and 2 cm larger respectively).

The individual maximum wave heights (H_{max} of the "seiche") recorded during this event reached 0.56 m in Bilbao, 0.45 m in Santander, 0.77 m in Gijón and 0.83 m in Coruña. The extreme sea level could have been larger in fact in Bilbao and Santander, as this maximum amplitude of the oscillations took place a couple of hours after the high tide in these harbors.

According to **Table 1** we can see also that although the extreme high waters were below the historical record or maximum sea level recorded in each tide gauge since 1992, the 99.5 percentile of high waters was exceeded at all these harbors during this particular storm except at Coruña (precisely the one with a smallest storm surge component).

Therefore, the extreme sea level values recorded were in great part caused by the large spring tide added to a moderate or negligible storm surge, in combination with "seiches" of H_s reaching up to 0.5 m (0.25 m amplitude) in some cases. Since these oscillations are stochastic in nature, (and similar to wind waves in this sense) we need to take account of the probability of an individual maximum wave coinciding with the high tide.

SEA LEVEL DATA RECORDED AFTER THE ATLANTIC RIDGE EARTHQUAKE, FEBRUARY 13TH, 2015

An earthquake with magnitude Mw = 7.1 took place in the middle of the Atlantic ridge on February 13th, 2015 at 18:59:12 (UTC). The earthquake epicenter was located at 52.649°N,

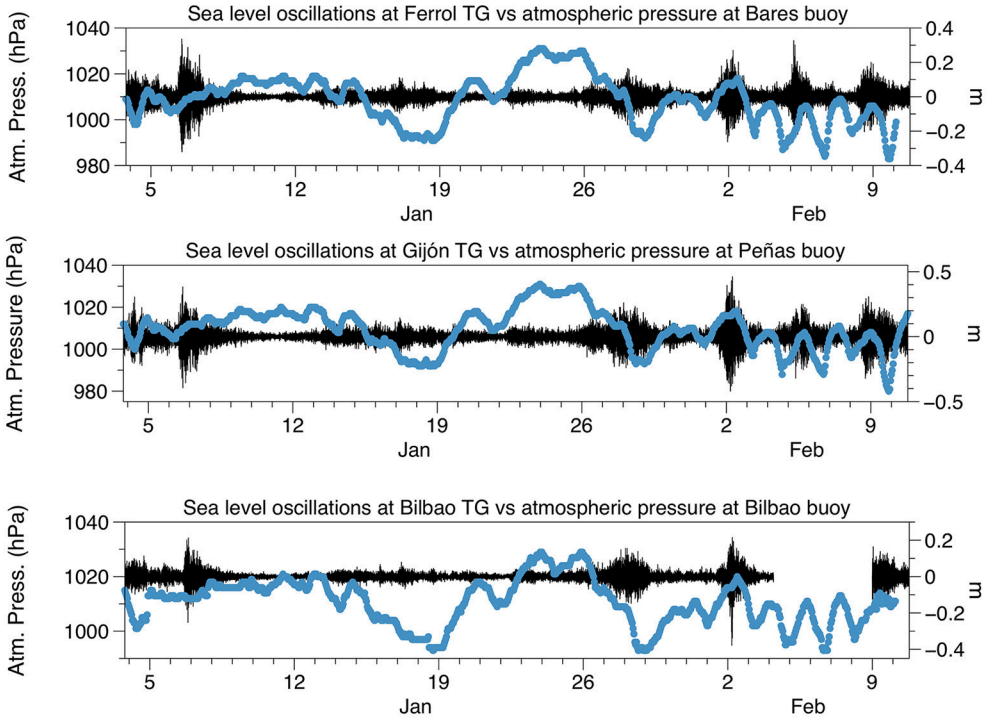

FIGURE 6 | Sea level oscillations at Ferrol, Gijón, and Bilbao tide gauges for January–February 2014 (black lines), and atmospheric pressure recorded by the nearest deep water buoy (blue lines: Bares, Peñas, and Bilbao, respectively). Data sampling for sea level oscillations is 1 min, data sampling for atmospheric pressure recorded by buoys is 1 h.

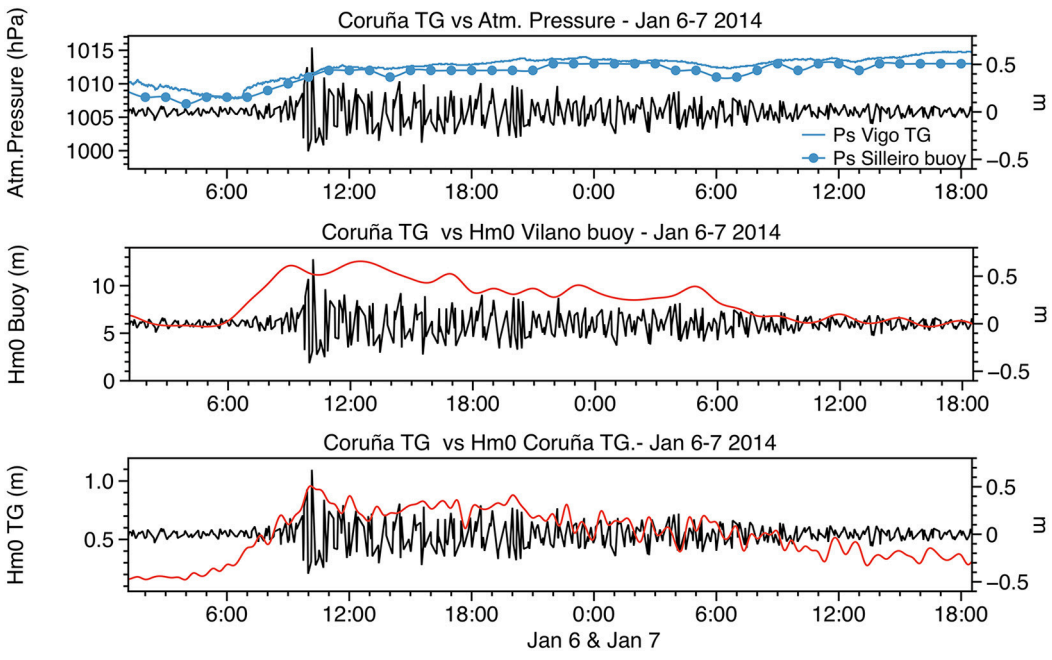

FIGURE 7 | Sea level oscillations on January 6th 2014 at Coruña harbor vs.: top: atmospheric pressure data from Silleiro buoy (hourly values, blue dotted line) and from Vigo tide gauge (1 min values, blue line); **middle:** significant wave height recorded by Vilano buoy (red line); **bottom:** significant wave height recorded by Coruña tide gauge itself (red line). There is not atmospheric pressure data available from the nearest buoy (Vilano).

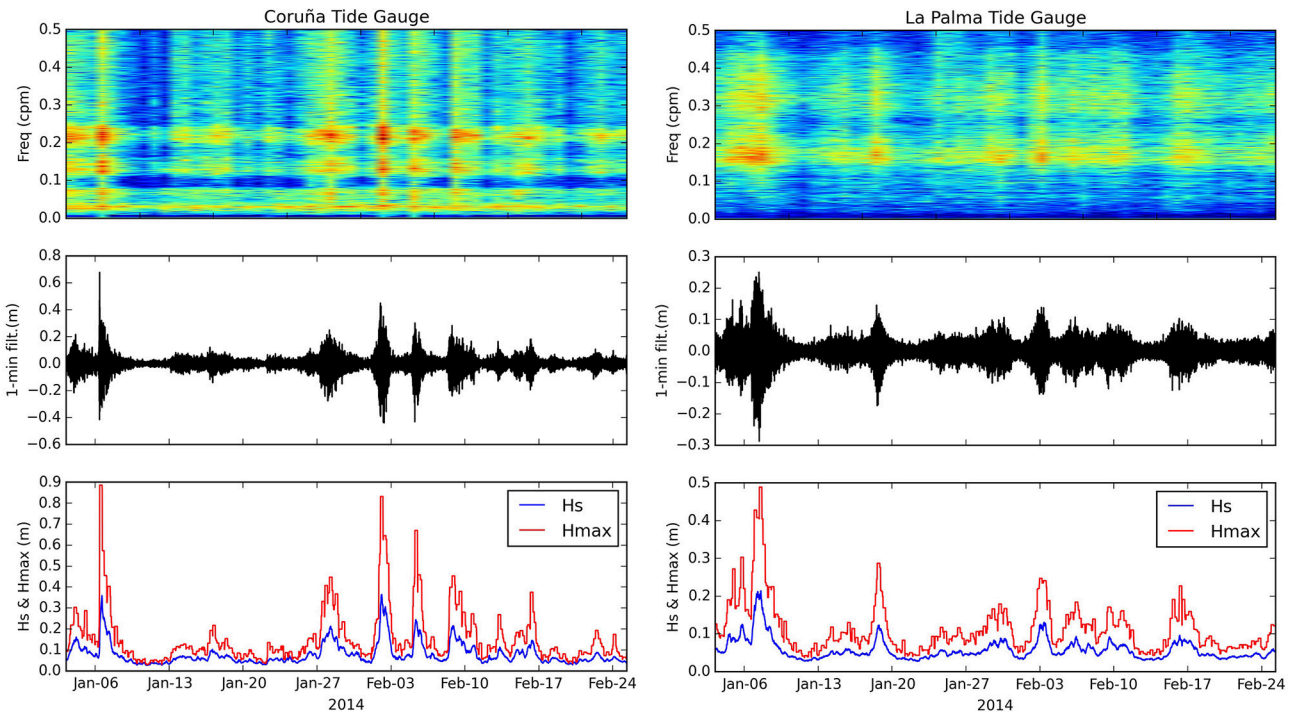

FIGURE 8 | Top: spectrogram of 1 min high-pass filtered sea level data at Coruña (left) and La Palma (right) tide gauges, showing the daily variation of the spectra along the stormy period January–February 2014. Applied to 1536 points windows with 128 points overlap (colors in variance units). The storms coincide with the increase of energy on higher frequencies of sea level (periods 2′–6′); **middle and bottom:** 1 min high-pass filtered time series and estimated "seiche" amplitudes (half the significant wave height H_s and maximum wave height H_{max}) at these stations during this period (zero-crossing procedure).

31.902°W, well within the Earthquake Source Zone monitored by the NEAMTWS Candidate Tsunami Service Providers (CTSP's). The exact position of the epicenter in this region determines the kind of message provided by the NEAMTWS CTSPs in the Atlantic; in this case it was in the region where messages must be issued for earthquakes with magnitude larger than 5.5.

In spite of the relatively high magnitude of the earthquake the focal mechanism was a strike-slip one in a transform fault (with centroid depth: 25.2 km, strike: 277, dip: 88, slip: −170, according to the Global Centroid Moment Tensor Catalog: Dziewonski et al., 1981; Ekström et al., 2012); a tsunami wave is not expected for this kind of earthquakes due to the lack of significant vertical movement of the ocean bottom. For this reason, NEAMTWS warning center provided just an information message for the region 12 min after the earthquake.

Interestingly, about 3 h after, a small increase of variability was observed in the 1-min filtered data from Langosteira tide gauge, a station located on the Northwest corner of the Spanish coast, at the external harbor of La Coruña (**Figure 1**). This signal could have been interpreted by mistake as the record of a small tsunami by a technician on duty on a tsunami warning center. In fact, this information was leaked out to press by an expert external to NEAMTWS and the National Tsunami Warning Center in Spain. The automatic algorithm for tsunami detection in PdE triggered an alert level "2" message for the station of Langosteira; the first alert was issued at 22:54:00 UTC, and several times thereafter until the morning of the 14th of February. It is important to stress that the thresholds of the algorithm are fixed according to the local variability of sea level at each harbor. As described in the previous section, oscillations similar to these ones are common along the North Spanish coast and are usually caused by wind waves in this region.

Looking for more tsunami signals after the earthquake of February 13th, 2015, a review was made through the IOC Sea Level Station Monitoring Facility (IOC/SLSMF) and other data portals such as the IBIROOS *In-Situ* Tac (that includes all *in-situ* marine observational platforms, including tide gauges, in the Atlantic European coast). A significant improvement on the availability of 1 min sea level time series during the last 10 years has been possible thanks to the new requirements established for tsunami warning: the percentage of tide gauges with 1 min sampling in this region has increased from 0% in 2006 to a 61% of the existing stations in 2015. As a result, records were available from the 50 locations shown in **Figure 10** (left), with stations from Iceland (Reykjavik) to Cape Verde (Palmeira), and a couple of stations in the Canadian coast. Other stations on the US coastline and Canada that did not appear to display any significant signal or that had less frequent data sampling were not included in this analysis. Similarly, French stations are not included here as CEA (France) advised that a significant signal was not detected along the French coast.

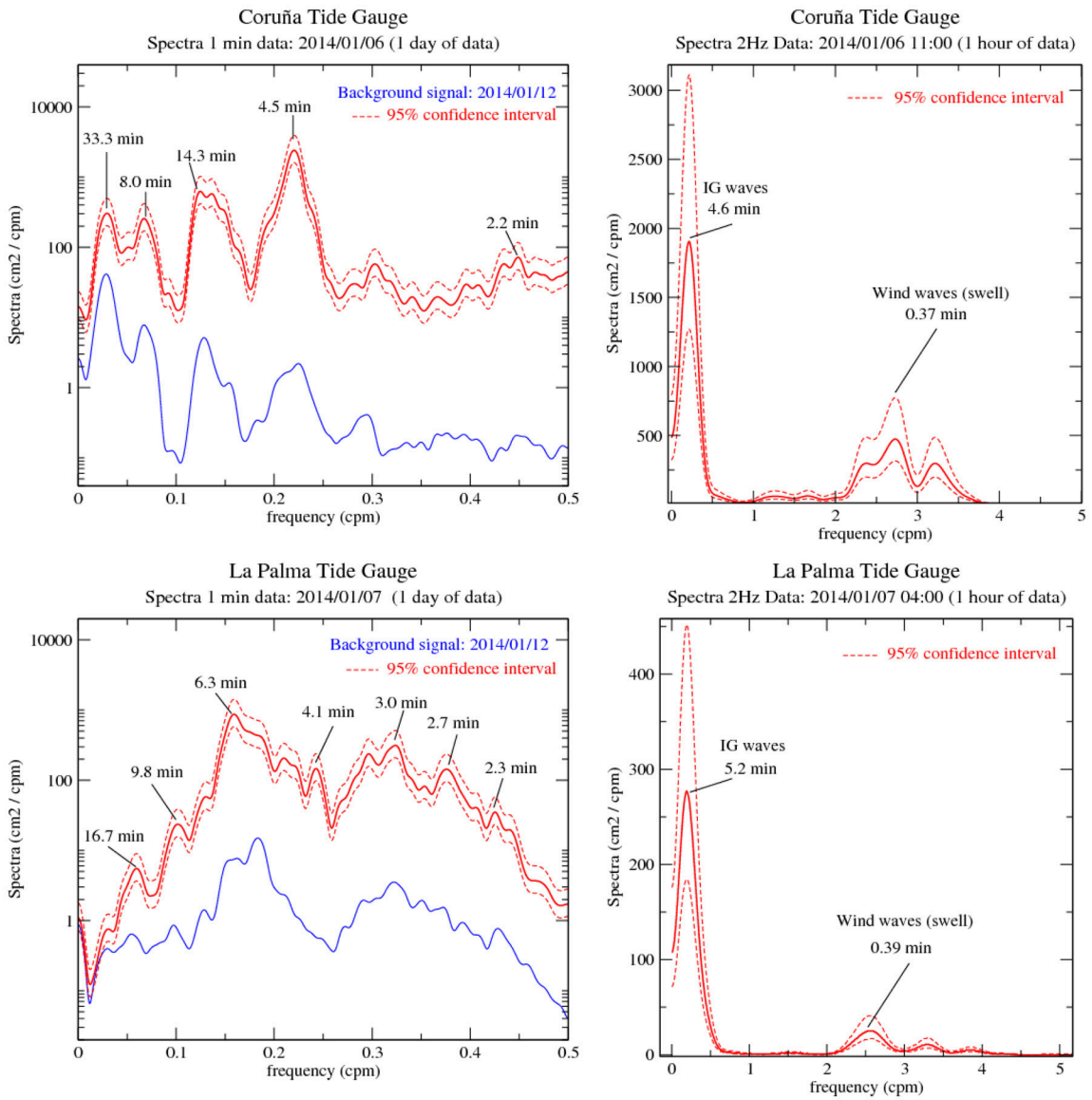

FIGURE 9 | Spectral analysis for Coruña and La Palma tide gauges, during the storm of January 6–7, 2014. Left: spectra applied to 1 day of 1-min data, **right:** spectra applied to 1 hour of 2 Hz data. The 1- min and 2 Hz data have been high-pass filtered (periods <3 h and periods <45 min respectively). Red lines: spectra for 1 day/hour of maximum sea level oscillations (and 95% confidence intervals). Spectra from the background signal was added to the 1-min spectra (blue line) and a logarithmic vertical scale used in this case for easier comparison of the peaks. Spectra method: auto-covariance function smoothed with a Parzen lag window (40 degrees of freedom). Swell waves and infragravity waves are observed in the 2 Hz spectra.

The filtered signal obtained from the rest of stations revealed different magnitudes of potentially normal variability at each harbor whilst those stations along the Iberian Peninsula North and North-West coasts displayed a possible earthquake-related signal. These stations were: Bilbao, Santander, Gijón, Coruña, Ferrol, and Langosteira, from the REDMAR network, and Peniche, Nazare, and Leixoes in the Portuguese coast, north of Lisbon. A possible signal could also be perceived at Reykjavik (Iceland) and Palmeira (Cape Vert). However, there were not significant oscillations in the filtered time series at the Canary Islands stations.

The arrival time of the potential tsunami wave was obtained by IGN for each tide gauge station from the numerical model TTT (Travel Time Software) SDK v3.3 (**Table 2**). The program calculates propagation velocities based on an input bathymetry grid and uses Huygens constructions to propagate the wave front from the epicenter to all nodes on the grid (Wessel, 2009). A map of this theoretical tsunami propagation time is shown in **Figure 10** (right), with contour lines of 1 h.

The 1-min filtered sea level time series are displayed in **Figure 11** for the subset of these 50 stations where a signal, however small, was found. The red line indicates the time

TABLE 1 | Column 2: extreme total sea levels (m) / time (hh:mm GMT) recorded the 2nd of February by the tide gauges of Bilbao, Santander, Gijón and Coruña (sampling interval: 1 min); columns 3–5: contribution of the tide, surge and high frequency oscillation (considered here as half the significant wave height), the two latter at 05:00 GMT; columns 6 and 7: 99.95 percentile, and maximum sea level of the historical record (1992 to present).

Station	Max/Time (1 min) (m)	Tide (m)	Surge (m) (Nivmar)	Seiche (m) (Hs/2)	Percentile 99.95 (m)	Historical record (m)
Bilbao	4.86/05:01	4.65	0.10	0.13	4.85	4.99
Santander	5.36/04:55	5.15	0.11	0.10	5.34	5.38
Gijón	5.30/04:35	4.96	0.09	0.25	5.23	5.40
Coruña	5.01/04:49	4.85	−0.08	0.25	5.10	5.30

Reference of heights: REDMAR datum for each station (more information on http://portus.puertos.es/Portus_RT/?locale = en).

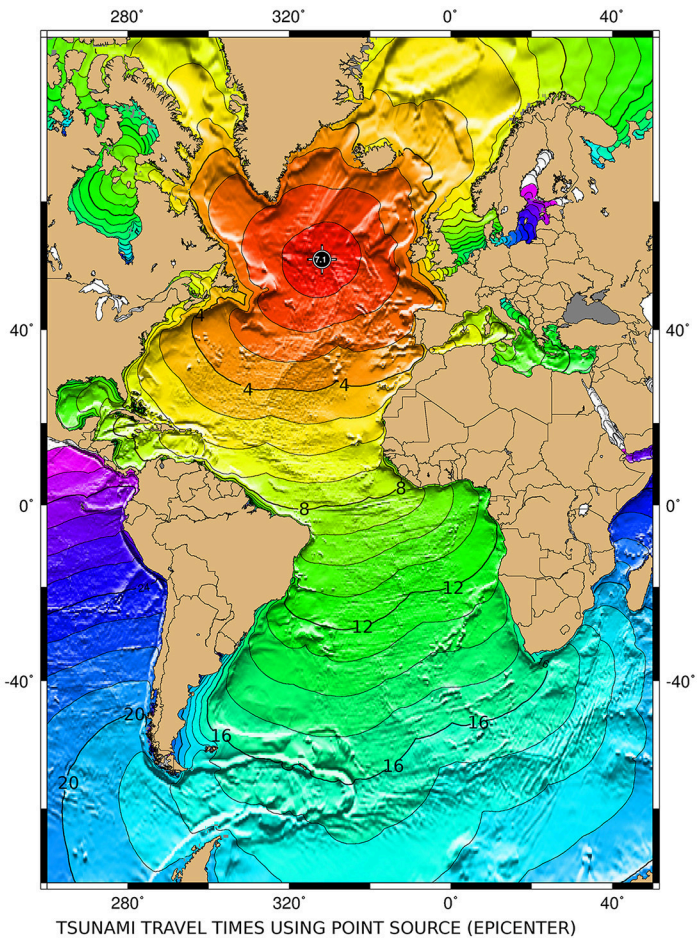

FIGURE 10 | Left: up to 50 tide gauges (red dots) with 1-min data were available during the 13th of February 2015 earthquake event. Only a subset of them presented a possible small signal; the most evident was observed in Langosteira tide gauge; **right:** tsunami propagation (1 h contour line) generated at the epicenter of the earthquake of 13th February 2015, 18:59:12 UTC, in the Atlantic ridge, as provided by the model TTT SDK v3.3.

of the earthquake. Expected arrival times from the numerical simulation presented in **Table 2** have been added by means of vertical black arrows.

These plots reveal, firstly, that there is no clear signal at most of the stations, if the times of earthquake and expected arrival of the wave are considered. The time series show a different behavior after the arrival time at all the stations except Palmeira, Ponta Delgada, and Reikjavik. In particular an increase of variability is observed immediately after or coincident with the arrival time only at Langosteira, Ferrol, Gijón, and Leixoes. Others show a signal several hours before or after the estimated arrival time.

It is difficult to determine clearly if a very small tsunami could have reached these tide gauges mainly for two reasons: (a) the uncertainty in the simulated arrival times could be large

TABLE 2 | Estimated arrival times of the first tsunami wave from numerical simulations of the earthquake of February 13th, 2015 in the Atlantic ridge.

Station	Tsunami arrival time	UT Time
Langosteira	3 h 01 m 56 s	22:01:08
Ferrol	3 h 05 m 25 s	22:04:37
Gijón	3 h 29 m 33 s	22:28:45
Bilbao	3 h 34 m 21 s	22:33:33
Santander	3 h 21 m 57 s	22:21:09
Reykjavik	3 h 42 m 08 s	22:41:20
Peniche	3 h 18 m 08 s	22:17:20
Nazare	3 h 20 m 26 s	22:19:38
Leixoes	3 h 28 m 29 s	22:27:41
Ponta Delgada	2 h 52 m 32 s	22:51:44
Palmeira	5 h 51 m 21 s	00:50:34 (14th)

Derived from IGN run of model TTT SDK v3.3.

for those points where local bathymetry is not well resolved, (b) the local variability of each harbor and their relation to other oceano-meteorological reasons such as meteotsunamis or wind-waves.

Analysis of Langosteira Tide Gauge

It is interesting that, by chance or not, the increase of variability at this station coincides rather clearly with the expected arrival time from the model in this case, and that there is not significant energy during the day or few hours before the event.

Langosteira and Gijón 1 min high-pass filtered signals are displayed in **Figure 12** along with their spectrogram and estimated amplitude. In this case the spectrogram was derived using a 512 points window (around 8 h) with a 128 points (2 h) overlap. It can be seen that the event recorded in Langosteira reflects not only a small increase of the magnitude of the signal, with waves reaching amplitudes of 10–15 cm, but also the appearance of higher frequency oscillations, with energy suddenly present at all the lower periods up to 2 or 2.5 min, as observed in the events of 2014 presented in previous section, along with the 15–25 min period signal already present before the event. Once again, it seems there is a kind of permanent background oscillation in this band of frequencies in this part of the Spanish coast, observed now also at Langosteira and Gijón tide gauges, similar to the one observed at Coruña during January–February 2014, and to the one found by Frère et al. (2014).

The daily spectra of 1-min data for 1 day before (12th of February) and 1 day after the event (15th of February) are displayed in **Figure 13** (left panel), in the same way described for **Figure 9** for January–February 2014. This figure confirms the previous statement that a signal with a period between 15 and 25 min is always present (peak on 17.2 min); the higher frequency oscillations (up to 2 min) are mostly excited during the event (red line). Notice the coincidence of this signal with the ones observed in previous section for Coruña tide gauge (nearby Langosteira). In that case the excitation of the lower periods seemed to be associated to the storms and huge wind waves; it could be the case also in this event.

In the right panel of **Figure 13** the spectral analysis of the 2 Hz data from Langosteira tide gauge is displayed (again in the same way as those in **Figure 9**). Here, the presence of a peak on the infragravity waves band is also clear, with a period of 1.9 min, clearly inside the infragravity frequency range. Wind waves swell are also present in this case with a peak period of 13.2 s (0.22 min), significantly lower, nevertheless, than in 2014 events, what would explain the lower period of this infragravity wave, most common according to the literature.

Although there were not extreme waves and storms during February 2015, their influence cannot be completely disregarded for Langosteira. **Figure 14** shows the increase in significant wave height (up to 6.5 m) and mean period of the wind waves recorded at the nearby buoy of Estaca de Bares (offshore, north of Langosteira), during the appearance of the oscillations in this station. Based on the experience of other events, therefore, this sudden change in amplitude and period of the wind waves would be most likely the origin of the oscillations (infragravity waves) observed in this tide gauge coincidentally when a potential small tsunami could have reached the station. The 1 min meteorological data recorded at Vigo tide gauge during the same period also simply reflect an increase in the wind velocity at that time (related to wind waves on the other hand); the atmospheric pressure data does not show any relevant feature before February 13th, confirming the origin of the observed sea level oscillations in Langosteira in the infragravity waves.

The discussion above illustrates how considering these kind of signals as a small tsunami useful for validation of tsunami modeling without more careful analysis can be dangerous, and how the analysis of other environmental variables, as well as a better knowledge of the local sea level variability in the station, and the local response to the different forcings, is needed.

DISCUSSION

Nowadays we are in a fortunate new position to improve our understanding of sea level oscillations at higher frequencies (periods of the order of minutes) thanks to significant changes in observational sea level networks. Detection of small tsunami signals at tide gauges is of great interest for assessing the skill of existing tsunami warning systems and for validation of tsunami propagation models, and this need is leading to the development of new methodologies of sea level data processing and automatic detection algorithms such as the ones described in this paper. However, the tsunami footprint on sea level records resembles other more frequent types of phenomena, already known and studied from an academic point of view, but not usually considered within sea level warning systems.

The analysis of the two events presented in this paper has provided several lessons. First of all, it reveals the importance of considering these oscillations for a more precise design of sea level alert systems. Although wave-setup is already considered of relevance for sea level forecasts and this may be solved by

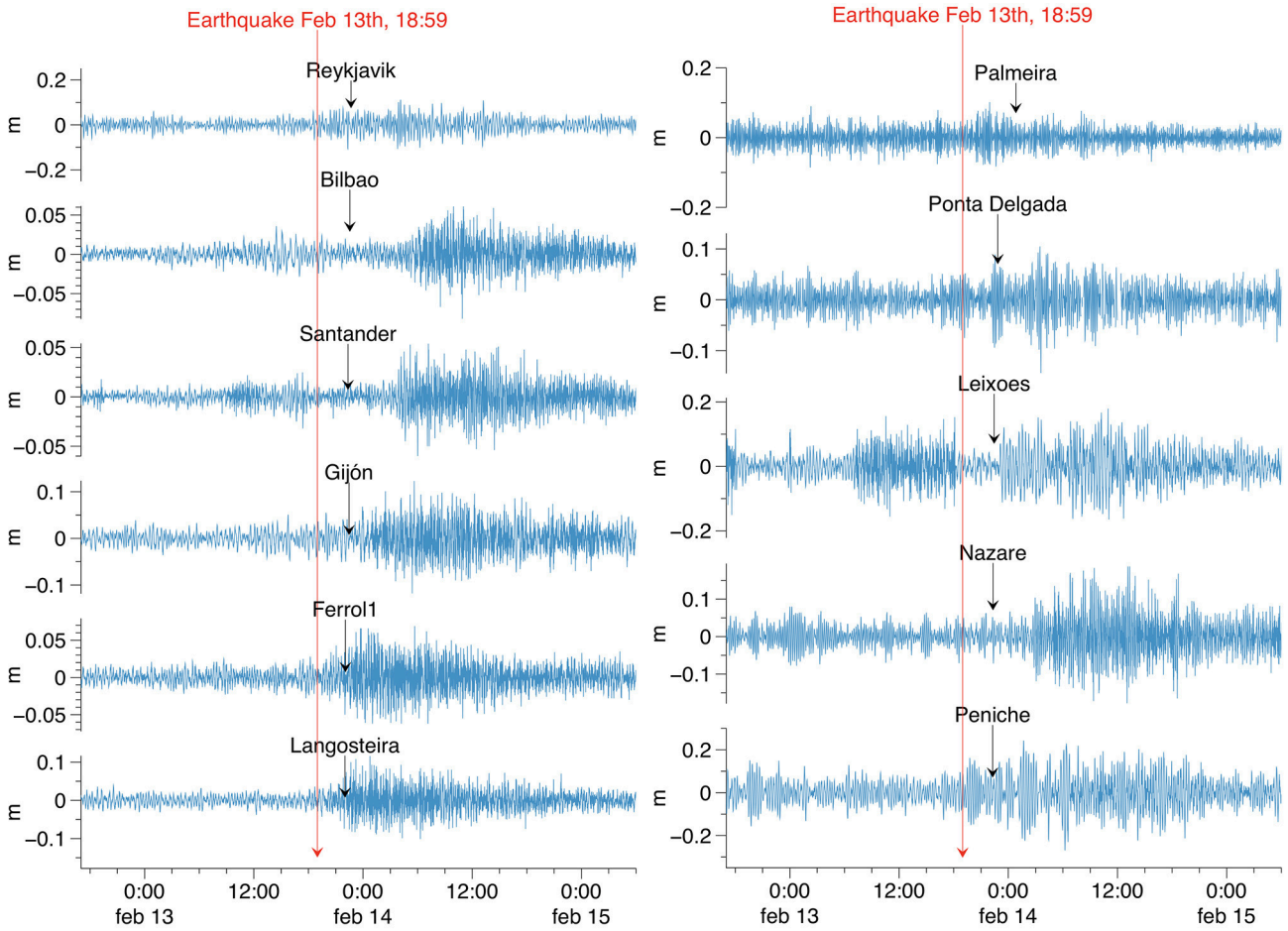

FIGURE 11 | 1 min high-pass filtered sea level time series from those stations on Figure 10 where a signal, even if small, might be present after the earthquake of February 13th 2015 showing the expected arrival times in Table 2, derived from the tsunami propagation model, at each tide gauge (black arrows). The earthquake time is indicated by the red arrow.

means of coupled wind-wave and storm surge models, additional sea level oscillations in the frequency of the "tsunami" signals should also be taken into account in the future. In the examples described in this paper the forcing of these oscillations seems to be mainly wind waves, but in other regions the forcing may be different (meteotsunamis such as the "rissaga" events in the Mediterranean Sea, for example). Case studies like this one will contribute to a better physical knowledge of all these phenomena.

Another important lesson from this study it that detection of small tsunamis from tide gauges is uncertain due to the inherent sea level variability caused by all these oceano-meteorological agents, but also due to errors in tsunami propagation models or problems in the data (transmission fails, spikes, etc). This leads to a continuous need for refinement of automatic algorithms based on the analysis of events like the ones described here.

The storms of January and February 2014 represent an example of real extreme events where both wind-waves and sea level, with their different components combined, and even without a significant storm surge, may cause severe damage and flooding in harbors and along the coastline. Therefore, future extreme analysis should consider this random process to determine maximum (and minimum) sea levels. The low sampling interval allows an adequate measurement of the effect of these oscillations in sea level records, which is the main reason for the upgrade of the tide gauge networks that in the past usually worked with 10 or 15 min sampling intervals at best. The sea level signals observed along the Spanish coast in January and February 2014 were not that different from the ones of a small tsunami.

The tsunami automatic detection algorithm in PdE performed perfectly well during these storms, providing red alerts for oscillations. The multi-parameter alert system provided as well red alerts for wind wave heights in open waters (although the most anomalous feature of these storms were the long peak periods), and yellow or orange alerts for total sea level. However, the sea level forecast did not reach the level of alert obtained from observations as it was based on just the forecast of the tide and the storm surge. This confirms the interest of the multi-hazard approach and the need for taking into account these physical phenomena in the future developments of the sea level forecasting system.

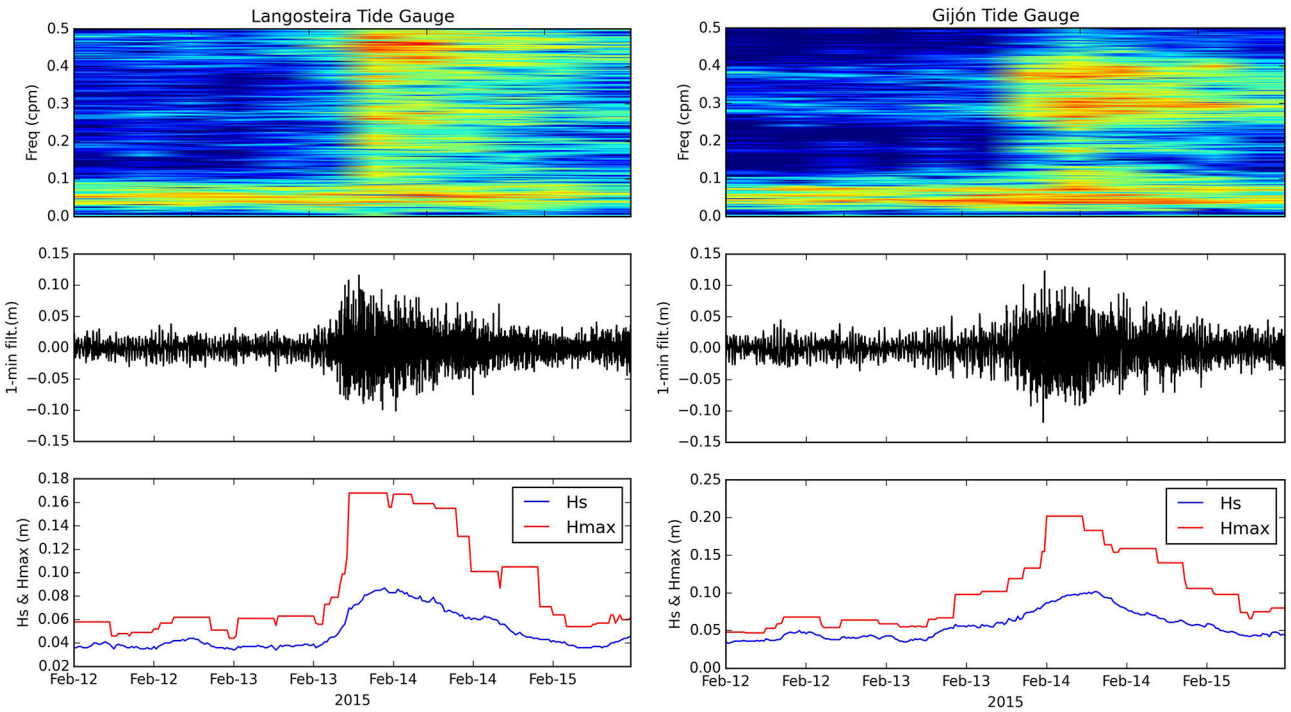

FIGURE 12 | Top: spectrogram of 1 min high-pass filtered sea level data at Langosteira (left) and Gijón (right) tide gauges, showing the temporal evolution of the spectra along February 12–15th 2015. Applied to 512 points windows with 128 points overlap (colors in variance units). A constant signal with periods in the range of 15–25 min is present before the event at both stations; new signals for lower periods (until 2 or 2.5 min) appear when the event starts; **middle and bottom:** 1 min high-pass filtered time series and corresponding estimated "seiche" amplitude (half the significant wave height H_s and the maximum wave height H_{max}) during this period (zero-crossing procedure).

Concerning the observational network, in this paper we present the development of a new procedure for characterization of these oscillations in terms of amplitude and period. Initially implemented for the 1 min data submitted in real time in PdE, and tested with success in these two examples, the procedure needs to be improved and adapted to automatic processing of the original 2 Hz raw data. This is important especially for the periods of the infragravity waves, very close to the Nyquist frequency of 1 min data, as we have seen here, and will become possible as the network communications and access to these data improve in the future. A prototype is in fact already in operation for one tide gauge from the REDMAR network.

The Atlantic Ridge earthquake on 13th February 2015 was not expected to generate a tsunami signal; however, the occurrence of small oscillations in the North and West coast of the Iberian Peninsula revealed the complexity of interpretation of tide gauge data and the need for analysis of sea level in combination with other environmental variables. Although the signal observed in a few tide gauges is coherent with the expected arrival time of a small tsunami, and the wind waves at that time were not extreme, a detailed analysis has shown that these oscillations could be most likely infragravity waves and not a tsunami signal (spectral analysis of the time series reveals similar behavior of this event and the previous one).

Although we point to the wind waves as the main mechanism of the oscillations observed in these two examples, we cannot discard completely the possibility of a combination of effects and the occurrence as well of a meteotsunami, especially during one of the events of 2014. Considerable research has been done about these oscillations associated with atmospheric pressure disturbances in the last decades; the availability of microbarographs like those already in operation in the REDMAR network is expected to be of help in the establishment of future meteotsunami warning systems. These data could be integrated into these systems as the sea level data are already included in the tsunami warning systems. Although ideally offshore bottom pressure sensors would be more useful in both cases, the reality is that nowadays the only data available in real time for most of the countries in Europe are provided by tide gauges at the harbors, so it makes sense that we should improve the tools to use these data in near-real time and to interpret them correctly. Future work should focus therefore on more detailed studies of the local response of small bays and harbors to all these external forcings. This local knowledge will allow the design of more reliable and refined alert systems. This is the objective of future projects in PdE, that is starting now to pay more attention to the tremendous amount of 2 Hz and 1 min data recorded inside the Spanish harbors.

Finally, tsunami warning centers should be aware of these limitations and the complexity of the sea level measurements: once again, multi-hazard experts, with a combined knowledge

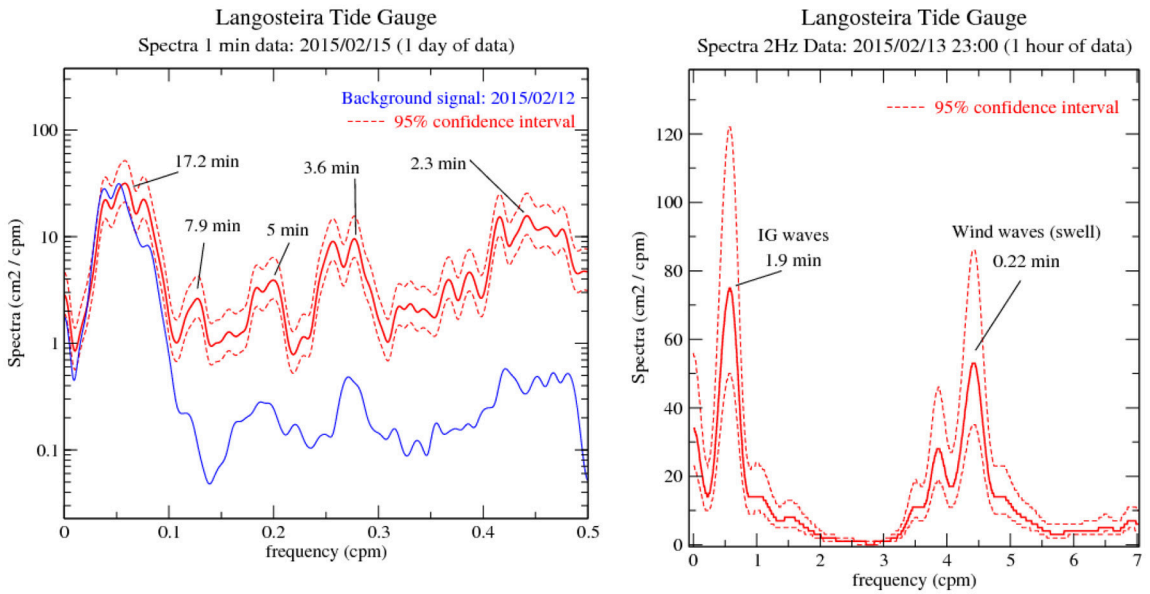

FIGURE 13 | Left: spectral analysis of 1 min **(left)** and 2 Hz **(right)** data for Langosteira tide gauge on February 13th 2015. The 1-min and 2 Hz data have been high-pass filtered (periods < 3 h and periods < 45 min respectively). Red lines: spectra for 1 day/hour of maximum sea level oscillations (and 95% confidence intervals). Spectra from the background signal was added to the 1-min spectra (blue line) and a logarithmic vertical scale used in this case for easier comparison of the peaks: the energy at higher frequencies (e.g., periods of 3.6 and 2.3 min) increase significantly during this event. The 2 Hz spectrum reveals the energy content on the infragravity waves (peak very close to the Nyquist frequency of 1 min data) and on the swell bands. Spectra method: auto-covariance function smoothed with a Parzen lag window (40 degrees of freedom).

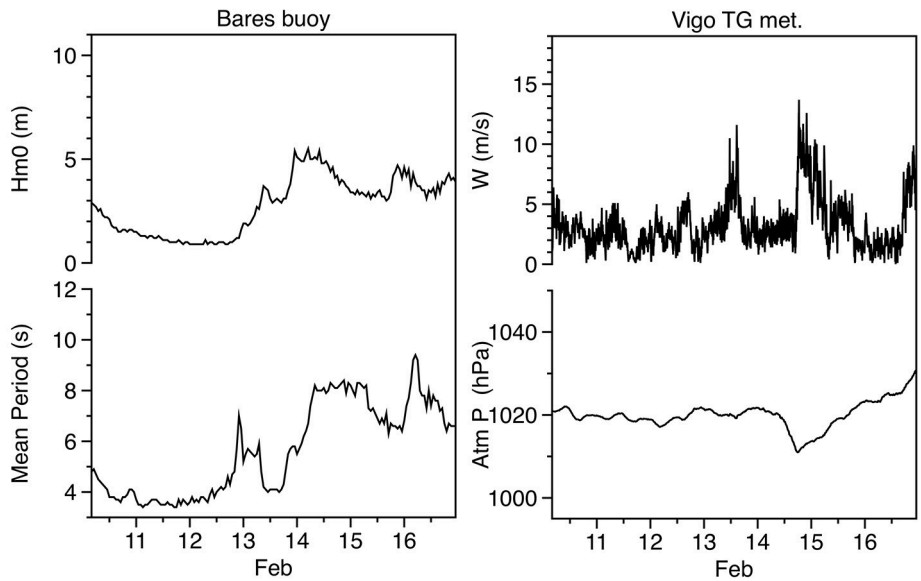

FIGURE 14 | Left: significant wave height (H_{m0}) and mean period (T_m) recorded by Bares open waters buoy during the oscillations event of February 2015; **right:** mean wind velocity and atmospheric pressure recorded by the meteorological sensors of Vigo tide gauge for the same period (1-min sampling resolution).

of tsunamis, oceanography and meteorology, and making use of information from the whole network of stations (and not relying just on local information) will ensure reliable interpretation of the detection networks and a better understanding of the sea level risks taking into account all the different phenomena and the catastrophic consequences that their superposition may generate.

AUTHOR CONTRIBUTIONS

BP: originator of the idea of the paper, manuscript writing; preparation of figures and tables, development of the algorithm for 1 min data processing, responsible of the sea level data processing in PdE including design of automatic quality control and alert issues. FM: implementation of an upgrade of the tsunami algorithm for tsunami detection in Java; generation of an offline Java script of this algorithm for easy application to the stations not included in the Portus system (Puertos del Estado). CG, JC, FS: tsunami wave arrival times at each station, description of the earthquake characteristics. EA: detailed review of the article, including re-writing of several sections and an improved description of the measurements during the storms of January–February 2014, with emphasis in the analysis of the storm surge, seiche and tide components.

FUNDING

PdE, Instituto Geográfico Nacional and CEA. SOPRANO project (Spanish national project: Plan Estatal de Investigación Científica y Técnica y de Innovación 2013–2016 (Convocatoria 2014), Ministerio de Economía y Competitividad).

ACKNOWLEDGMENTS

We wish to thank first all the operators and maintenance technicians of Puertos del Estado networks of tide gauges and buoys (Sidmar and Oceanor personnel, Marta de Alfonso and María Isabel Ruiz). We thank as well the Sea Level Station Monitoring Facility of the IOC (UNESCO), the IBIROOS *In-Situ* Tac and the different national operators for the provision of tide gauge data of non-Spanish stations for the event of February 13th 2015. The Tsunami Travel Time software (TTT SDK v 3.3) was developed by Dr. Paul Wessel (Geoware, http://www.geoware-online.com), and is used by the NOAA Pacific Tsunami Warning Center and licensed to NOAA/ITIC for redistribution. Finally, we would like to express our gratitude to Dr. Angela Hibert, who kindly accepted to read the manuscript and make suggestions to improve the English writing. This study has been performed in the framework of the Spanish funded project SOPRANO.

REFERENCES

Alasset, P.-J., Hébert, H., Maouche, S., Calbini, V., and Meghraoui, M. (2006). The tsunami induced by the 2003 Zemmouri earthquake (MW= 6.9, Algeria): modelling and results. *Geophys. J. Int.* 166, 213–226. doi: 10.1111/j.1365-246X.2006.02912.x

Álvarez-Fanjul, E., de Alfonso, M., Ruiz, M. I., Lopez, J. D., and Rodriguez, I. (2002). "Real time monitoring of Spanish coastal waters: the deep water network," *Proceedings of the Third International Conference on EuroGOOS* (Athens).

Álvarez-Fanjul, E., Pérez-Gómez, B., and Rodríguez, I. (2001). Nivmar: a storm surge forecasting system for Spanish waters. *Sci. Mar.* 65, 145–154. doi: 10.3989/scimar.2001.65s1145

BBC (2014). *UK Storms: Extreme Weather Caused Years of Erosion 21 February 2014. BBC News Magazine*. Available online at: http://www.bbc.com/news/uk-26277373 (Accessed February 2016).

Beltrami, G. M., Di Risio, M., and De Girolamo, P. (2011). "Chapter 27: Algorithms for automatic, real-time tsunami detection in sea level measurements," in *The Tsunami Threat-Research and Technology,* ed N.-A. Moerner (InTech), 549–573. doi: 10.5772/13908

Bressan, L., Zaniboni, F., and Tinti, S. (2013). Calibration of a real-time tsunami detection algorithm for sites with no instrumental tsunami records: application to coastal tide-gauge stations in eastern Sicily, Italy. *Nat. Hazards Earth Syst. Sci.* 13, 3129–3144. doi: 10.5194/nhess-13-3129-2013

Church, J. A., Gregory, J. M., Huybrechts, P., Kuhn, M., Lambeck, K., Nhuan, M. T., et al. (2001). "Changes in sea level," in *Climate Change: The Scientific Basis*, eds J. T. Houghton, Y. Ding, D. J. Griggs, M. Noquer, P. J. van der Linden, X. Dai, K. Maskell, and C. A. Johnson (New York, NY: Cambridge University Press), 639–694.

Defant, A. (1961). *Physical Oceanography*, *Vol. 2*. Oxford: Pergamon Press.

Dziewonski, A. M., Chou, T.-A., and Woodhouse, J. H. (1981). Determination of earthquake source parameters from waveform data for studies of global and regional seismicity. *J. Geophys. Res.* 86, 2825–2852. doi: 10.1029/JB086iB04p02825

Ekström, G., Nettles, M., and Dziewoński, A. M. (2012). The global CMT project 2004–2010: centroid-moment tensors for 13,017 earthquakes. *Phys. Earth Planet. Inter.* 200–201, 1–9. doi: 10.1016/j.pepi.2012.04.002

El País (2014). *El Temporal Provoca Olas Gigantes de Hasta 13 Metros de Altura en el Cantábrico.* 3 February 2014. Available online at: http://elpais.com/elpais/2014/02/03/actualidad/1391412691_659227.html

Frère, A., Daubord, C., Gailler, A., and Hèbert, H. (2014). Sea level surges of June 2011 in the NE Atlantic Ocean: observations and possible interpretation. *Nat. Hazards* 74, 179–196. doi: 10.1007/s11069-014-1103-x

Gómez-Lahoz, M., and Carretero-Albiach, J. C. (2005). Wave Forecasting at the Spanish Coasts. *J. Atmos. Ocean Sci.* 10, 389–405. doi: 10.1080/17417530601127522

Gomis, D., Monserrat, S., and Tintoré, J. (1993). Pressure-forced seiches of large amplitude in inlets of the Balearic Islands. *J. Geophys. Res.* 98, 14437–14445. doi: 10.1029/93JC00623

Herbers, T. H. C., Elgar, S., and Guza, R. T. (1995). Generation and propagation of infragravity waves. *J. Geophys. Res.* 100, 24863–24872. doi: 10.1029/95JC02680

Hibiya, T., and Kajiura, K. (1982). Origin of the Abiki phenomenon (a kind of seiche) in Nagasaki Bay. *J. Oceanogr. Soc. Jpn.* 38, 172–182. doi: 10.1007/BF02110288

IOC UNESCO (2007). North-East Atlantic, the Mediterranean and Connected Seas Tsunami Warning and Mitigation System, NEAMTWS, Implementation Plan. Technical report 73, Intergovernmental Oceanographic Commission.

Jansà, A., Monserrat, S., and Gomis, D. (2007). The rissaga of 15 June 2006 in Ciutadella (Menorca), a meteorological tsunami. *Adv. Geosci.* 12, 1–4. doi: 10.5194/adgeo-12-1-2007

Jenkins, G. M., and Watts, D. G. (1968). *Spectral Analysis and its Applications.* San Francisco, CA: Holden Day.

Longuet-Higgins, M. S., and Stewart, R. W. (1962). Radiation stress and mass transport in gravity waves, with application to "surf beats." *J. Fluid Mech.* 13, 481–504. doi: 10.1017/S0022112062000877

Marcos, M., Monserrat, S., Medina, R., Orfila, A., and Olabarrieta, M. (2009). External forcing of meteorological tsunamis at the coast of the Balearic Islands. *Phys. Chem. Earth* 34, 938–947. doi: 10.1016/j.pce.2009.10.001

Monserrat, S., Vilibić, I., and Rabinovich, A. B. (2006a). Meteorological tsunamis: Atmospherically induced destructive ocean waves in the tsunami frequency band. *Phys. Chem. Earth* 34, 1035–1051. doi: 10.5194/nhess-6-1035-2006

Monserrat, S., Gomis, D., Jansá, A., and Rabinovich, A. B. (2006b). Ciutadella harbour, Menorca, Spain, 15 June 2006 rissaga. *Tsunami Newsletter* 38, 5–7.

Munk, W. H. (1949). Surf beats. *Eos. Trans. Am. Geophys. Un.* 30, 849–859. doi: 10.1029/TR030i006p00849

Munk, W. H. (1962). *Long Waves, in The Sea*. New York, NY: J. Wiley.

Nomitsu, T. (1935). A theory of tsunamis and seiches produced by wind and barometric gradient. *Mem. Coll. Sci. Imp. Univ. Kyoto A* 18, 201–214.

Orlić, M. (1980). About a possible occurrence of the Proudman resonance in the Adriatic. *Thalassia Jugo-slavica* 16, 79–88.

Pattiaratchi, C. B., and Wijeratne, E. M. S. (2015). Are meteotsunamis an underrated hazard? *Philos. Trans. R. Soc. A* 373, 1–23. doi: 10.1098/rsta.2014.0377

PdE (2014). *Historical Information* Available online at: Puertos del Estado website: http://portus.puertos.es/Portus_RT/?locale=en (Accessed February 2016).

Pérez-Gómez, B., Alvarez-Fanjul, E., Pérez, S., de Alfonso, M., and Vela, J. (2013). Use of tide gauge data in operational oceanography and sea level hazard warning systems. *J. Oper. Oceanogr.* 6, 1–18. doi: 10.1080/1755876X.2013.11020147

Pugh, D. T. (2004). *Changing Sea Levels. Effects of Tides, Weather and Climate*. Cambridge, UK: Cambridge University Press.

Pugh, D. T., and Woodworth, P. L. (2014). *Sea Level Science: Understanding Tides, Surges, Tsunamis and Mean Sea Level Changes*. Cambridge, UK: Cambridge University Press.

Rabinovich, A. B. (2009). "Seiches and harbour oscillations," in *Handbook of Coastal and Ocean Engineering*, ed Y. C. Kim (Singapore: World Scientific Publishing Co), 193–236.

Rabinovich, A. B., and Eblé, M. C. (2015). Deep-ocean measurements of tsunami waves. *Pure Appl. Geophys.* 172, 3281–3312. doi: 10.1007/s00024-015-1058-1

Rabinovich, A. B., and Monserrat, S. (1996). Meteorological tsunamis near the Balearic and Kuril Islands: descriptive and statistical analysis. *Nat. Hazards* 13, 55–90. doi: 10.1007/BF00156506

Rabinovich, A. B., Stroker, K., Thomson, R., and Davis, E. (2011). DARTs and CORK in cascadia basin: high-resolution observations of the 2004 Sumatra tsunami in the northeast Pacific. *Geophys. Res. Lett.* 38, L08607. doi: 10.1029/2011gl047026

Rabinovich, A. B., Vilibić, I., and Tinti, S. (2009). Meteorological tsunamis: atmospherically induced destructive ocean waves in the tsunami frequency band. *Phys. Chem. Earth* 34, 891893. doi: 10.1016/j.pce.2009.10.006

Sahal, A., Roger, J., Allgeyer, S., Lemaire, B., Lavigne, F., Cedex, M., et al. (2009). The tsunami triggered by the 21 May 2003 Boumerdes-Zemmouri (Algeria) earthquake: field investigations on the French Mediterranean coast and tsunami modelling. *Nat. Hazards Earth Syst. Sci.* 9, 1823–1834. doi: 10.5194/nhess-9-1823-2009

Šepić, J., Vilibić, I., Lafon, A., Macheboeuf, L., and Ivanovic, Z. (2015b). High-frequency sea level 512 oscillations in the Mediterranean and their connection to synoptic patterns. *Prog. Oceanogr.* 137, 284–298. doi: 10.1016/j.pocean.2015.07.005

Šepić, J., Vilibić, I., Rabinovich, A. B., and Monserrat, S. (2015a). Widespread tsunami-like waves of 23-27 June in the Mediterranean and Black Seas generated by high-altitude atmospheric forcing. *Sci. Rep.* 5:11682. doi: 10.1038/srep11682

Sheremet, A. T., Staples, F., Ardhuin, S., and Suanez, Fichaut, B. (2014). Observations of large infragravity wave runup at Banneg Island, France. *Geophys. Res. Lett.* 41, 976–982. doi: 10.1002/2013GL058880

Sibley, A., Cox, D., Long, D., Tappin, D., and Horseburgh, K. (2016). Meteorologically generated tsunami-like waves in the North Sea on 1/2 July 2015 and 28 May 2008. *Weather* 71, 68–74. doi: 10.1002/wea.2696

Tappin, D., Sibley, A., Horsburgh, K., Daubord, C., Cox, D., and Long, D. (2013). The English channel tsunami of 27 June 2011 – a probable meteorological source. *Weather* 68, 144–152. doi: 10.1002/wea.2061

Tintoré, J., Gomis, D., Alonso, S., and Wang, D. P. (1988). A theoretical study of large sea level oscillations in the Western Mediterranean. *J. Geophys. Res.* 93, 10797–10803.

Vela, J., Pérez-Gómez, B., González, M., Otero, L., Olabarrieta, M., Canals, M., et al. (2014). Tsunami Resonance in Palma Bay and Harbor, Majorca Island, as Induced by the 2003 Western Mediterranean Earthquake. *J. Geol.* 122, 165–182. doi: 10.1086/675256

Vich, M. D. M., and Monserrat, S. (2009). Source spectrum for the Algerian tsunami of 21 May 2003 estimated from coastal tide gauge data. *Geophys. Res. Lett.* 36, 1–5. doi: 10.1029/2009GL039970

Vilibić, I., Domijan, N., and Cupić, S. (2005). Wind versus air pressure seiche triggering in the Middle Adriatic coastal waters. *J. Mar. Syst.* 57, 189–200. doi: 10.1016/j.jmarsys.2005.04.007

Vilibić, I., Monserrat, S., and Rabinovich, A. B. (2014). Meteorological tsunamis on the US East Coast and in other regions of the World Ocean. *Nat. Hazards* 74, 1–9. doi: 10.1007/s11069-014-1350-x

Vilibić, I., Sepić, J., Rabinovich, A. B., and Monserrat, S. (2016). Modern approaches in meteotsunami research and early warning. *Front. Mar. Sci.* 3:57. doi: 10.3389/fmars.2016.00057

Wessel, P. (2009). Analysis of observed and predicted tsunami travel times for the pacific and Indian Oceans. *Pure Appl. Geophys.* 166, 301–324. doi: 10.1007/s00024-008-0437-2

Woodworth, P. L., and Blackman, D. L. (2002). Changes in extreme high waters at Liverpool since 1768. *Int. J. Climatol.* 22, 697–714. doi: 10.1002/joc.761

Woodworth, P. L., and Blackman, D. L. (2004). Evidence for systematic changes in extreme high waters since the mid-1970s. *J. Clim.* 17, 1190–1197. doi: 10.1175/1520-0442(2004)017<1190:EFSCIE>2.0.CO;2

Wu, J. K., and Liu, P. L.-F. (1990). Harbour excitations by incident wave groups. *J. Fluid Mech.* 217, 595–613. doi: 10.1017/S0022112090000866

Conflict of Interest Statement: The authors declare that the research was conducted in the absence of any commercial or financial relationships that could be construed as a potential conflict of interest.

frontiers in Marine Science

ORIGINAL RESEARCH
published: 06 November 2015
doi: 10.3389/fmars.2015.00084

A comparison of the 31 January–1 February 1953 and 5–6 December 2013 coastal flood events around the UK

Matthew P. Wadey[1]*, *Ivan. D. Haigh*[1,2], *Robert J. Nicholls*[3], *Jennifer M. Brown*[4], *Kevin Horsburgh*[4], *Ben Carroll*[5], *Shari L. Gallop*[1,6], *Travis Mason*[7] and *Elizabeth Bradshaw*[8]

[1] Ocean and Earth Science, National Oceanography Centre, University of Southampton, Southampton, UK, [2] School of Civil, Environmental and Mining Engineering and the UWA Oceans Institute, The University of Western Australia, Crawley, WA, Australia, [3] Faculty of Engineering and the Environment, University of Southampton, Southampton, UK, [4] National Oceanography Centre, Liverpool, UK, [5] ABP Marine Environmental Research Ltd, Southampton, UK, [6] Department of Environmental Sciences, Macquarie University, North Ryde, NSW, Australia, [7] Channel Coastal Observatory, National Oceanography Centre, Southampton, UK, [8] British Oceanographic Data Centre, National Oceanography Centre, Liverpool, UK

OPEN ACCESS

Edited by:
Isabel Iglesias,
Centro Interdisciplinar De Investigação Marinha E Ambiental, Portugal

Reviewed by:
Antonio Olita,
National Research Council, Italy
Ivica Vilibic,
Institute of Oceanography and Fisheries, Croatia
Matthew Lewis,
Bangor University, UK

***Correspondence:**
Matthew P. Wadey
m.p.wadey@soton.ac.uk

Specialty section:
This article was submitted to Coastal Ocean Processes, a section of the journal Frontiers in Marine Science

Received: 28 May 2015
Accepted: 05 October 2015
Published: 06 November 2015

Citation:
Wadey MP, Haigh ID, Nicholls RJ, Brown JM, Horsburgh K, Carroll B, Gallop SL, Mason T and Bradshaw E (2015) A comparison of the 31 January–1 February 1953 and 5–6 December 2013 coastal flood events around the UK. Front. Mar. Sci. 2:84. doi: 10.3389/fmars.2015.00084

A North Sea storm surge during 31 January–1 February 1953 caused Northwest Europe's most severe coastal floods in living memory. This event killed more than 2000 people on the coasts of England, the Netherlands, and Belgium. In the UK, where this study focuses, this event was a pivotal influence for flood risk management. Subsequent progress included a national tide gauge network, a storm surge forecasting and warning service, and major defense upgrades such as the Thames Barrier. Almost 60-years later, on 5–6 December 2013 Storm "Xaver" generated a surge event of similar magnitude. This paper describes a detailed comparison of these two events in the UK in terms of: (1) the meteorological conditions; (2) the observed high sea levels; and (3) the coastal flooding and impacts. The 1953 storm had a more southerly track and generated bigger waves due to the north-northwesterly onshore winds off East Anglia. The 2013 storm had a more west-to-east path from the north Atlantic to Scandinavia. Consequently, the 1953 high waters were more extreme in the southern North Sea. However, the 2013 event coincided with larger astronomical tides, resulting in a larger spatial "footprint". The extreme sea levels impacted communities on the west, east, and south coasts, with 2800 properties flooded during the 2013 event, compared to 24,000 properties (mainly between the Humber and Thames) in 1953. The 1953 floods remain a benchmark in the UK as an event which included failed defenses, damaged property and infrastructure and loss of life. Measures taken after 1953 greatly reduced the consequences of the 5–6 December 2013 storm. Continued monitoring of extreme sea levels and their consequences is important to inform a realistic perspective on future planning and resilience.

Keywords: storm surge, coastal flooding, 1953 flood, 2013 Xaver storm, North Sea, extreme sea levels, return periods

INTRODUCTION

Many regions around the world have suffered terrible losses from extreme sea levels and coastal floods. The last decade has witnessed two of the most costly natural disasters in US history: Hurricane Katrina in 2005 (Jonkman et al., 2009) and Hurricane Sandy in 2012 (Blake et al., 2013). Coastal flooding from these two events caused >1000 deaths. In May 2008 Cyclone Nargis crossed southern Myanmar, which generated a 5m high storm surge inundating >50 km inland, killing 130,000 people (Fritz et al., 2009; Lin et al., 2009). In November 2013, Typhoon Haiyan impacted the central Philippines, leaving nearly 8000 people dead, missing, or injured, and more than 1.1 million houses damaged or destroyed with most of the impacts caused by the storm surge (LeComte, 2014). Over the coming century, sea level rise (SLR) will allow extreme sea level events to occur more frequently (Haigh et al., 2010; Wahl et al., 2011), a situation potentially worsened by rapid coastal development (e.g., Neumann et al., 2015; Stevens et al., 2015). Therefore, monitoring and understanding coastal flood events is important to provide a perspective on future planning and resilience.

Northern Europe has a long history of severe coastal flooding (c.f. Lamb, 1991). The North Sea region is notorious for storm surges and coastal floods, and is adjacent to many low-lying hinterlands which contain highly populated urban areas, infrastructure, and agricultural land. The shallow bathymetry and narrower shape of the basin further south, allows storms from the North Atlantic to pile water up against the southern coastlines. All eight countries that border the North Sea have experienced repeated human and agricultural losses from the sea (Gönnert et al., 2001; Plüß et al., 2001; De Kraker, 2006). Coastal floods are documented to have killed 100,000 people in the UK in 1099, with large events and death tolls also in 1212, 1421, and 1446, 1468, 1539, 1552, and 1570 (Gönnert et al., 2001). Since 1900, storm surge damage along the East Coast of the UK occurred in 1901, 1906, 1944, 1953, 1976, 1978, 1983, 1993 (ABI, 2006), and 2007 (Horsburgh et al., 2008). Central London was last flooded by a storm surge (exacerbated by heavy river flow) on 7 January 1928, when a 1.5 m surge propagated up the Thames River killing 14 people (BBC, 2014a).

In the UK, the most severe coastal flood in living memory occurred during 31 January-1 February 1953, which killed 307 people along the east coast of England, 1836 people in the Netherlands, and up to 40 in Belgium (RMS, 2003; Baxter, 2005; Gerritsen, 2005; McRobie et al., 2005). There were also >250 boating-related deaths (Kelman, 2009), including 19 in Scotland (Hickey, 2001) and 133 in the sinking of the Princess Victoria ferry in the Irish Sea. These figures exclude deaths in the aftermath related to illness and stress. This flood event reinforced changes to risk management, embodied by the Delta Works programme in the Netherlands and the Thames Barrier and associated defenses in the UK, which has been operational since 1982. These defenses, forecasting, warning systems, and evacuation plans have been tested by several storm surges since 1953 (see Appendix 1), most notably during 5–6 December 2013 when Storm "Xaver" (also called "Bodil" or "Sven" in Scandinavia) impacted coastlines in Ireland, Scotland, Wales, northwest England, the North Sea, and the English Channel. This brought intense media coverage and prompted comparisons with 31 January-1 February 1953. It has been widely referred to as the "biggest North Sea surge for 60 years" (e.g., Harwood, 2013; BBC, 2014b).

The aim of this paper is to compare the coastal flood events of 31 January-1 February 1953 with 5–6 December 2013, with a focus on the UK. The main objectives are first to contrast the meteorological forcing; second to compare the high sea levels observed during both events, contrasting the tidal, surge, and mean sea level (MSL) components that combined to generate high water levels; and third to compare the coastal flooding and impact, and discuss the role of the improved flood defenses and storm surge forecasting since 1953. Before the early 1990s, tide gauges (and a high quality sea level record) covered much less of the UK's coastline; hence part of the motivation of this paper was to gather data so that the 1953 floods could be sufficiently represented in a new UK database of coastal flood events described by Haigh et al. (2015). This follows a recent detailed assessment of water levels and geomorphological impacts in the North Sea during the December 2013 event by Spencer et al. (2015), reminiscent of Steers (1953)—which was a key publication following the 1953 event.

The structure of the paper is as follows: to next describe the data sources and the methodology, then the three objectives are addressed by comparison of the meteorological conditions, comparison of observed high waters, and comparison of coastal flooding and impacts, respectively. A discussion of the key findings, along with conclusions are given in the discussion and conclusions.

DATA AND METHODS

The first objective was to compare the meteorological conditions of both events. This was primarily assessed by using MSL pressure and wind fields from the twentieth century Reanalysis, Version 2 (Compo et al., 2011). These meteorological fields are available every 6 h and have a horizontal resolution of 2° and were downloaded from the reanalysis web page (http://www.esrl.noaa.gov/psd/data/gridded/data.20thC_ReanV2.html). An interactive MATLAB® interface was used, developed by Haigh et al. (2015), to digitize the track of each storm, starting from when the low-pressure systems developed, until when the storms dissipated or moved beyond latitude 20°E. Different disciplines capture storm tracks in different ways. For this analysis the storm tracks were captured by selecting the grid point of lowest atmospheric pressure at each 6-h time step (**Figures 1**, **2**). From the start to the end of the storm, we recorded the 6-hourly: (1) time; (2) latitude and (3) longitude of the minimum atmospheric pressure cell; and (4) the minimum mean sea level pressure.

To compare water levels during both events, the second objective, a variety of data sources were utilized. The main data source for the 5–6 December 2013 event were 15-minute sea level time series from 39 of the UK's national "Class A" tide gauge sites. This network is managed by the National Oceanography Centre (NOC) and is owned and funded by the Environment Agency (EA). Quality controlled data from this

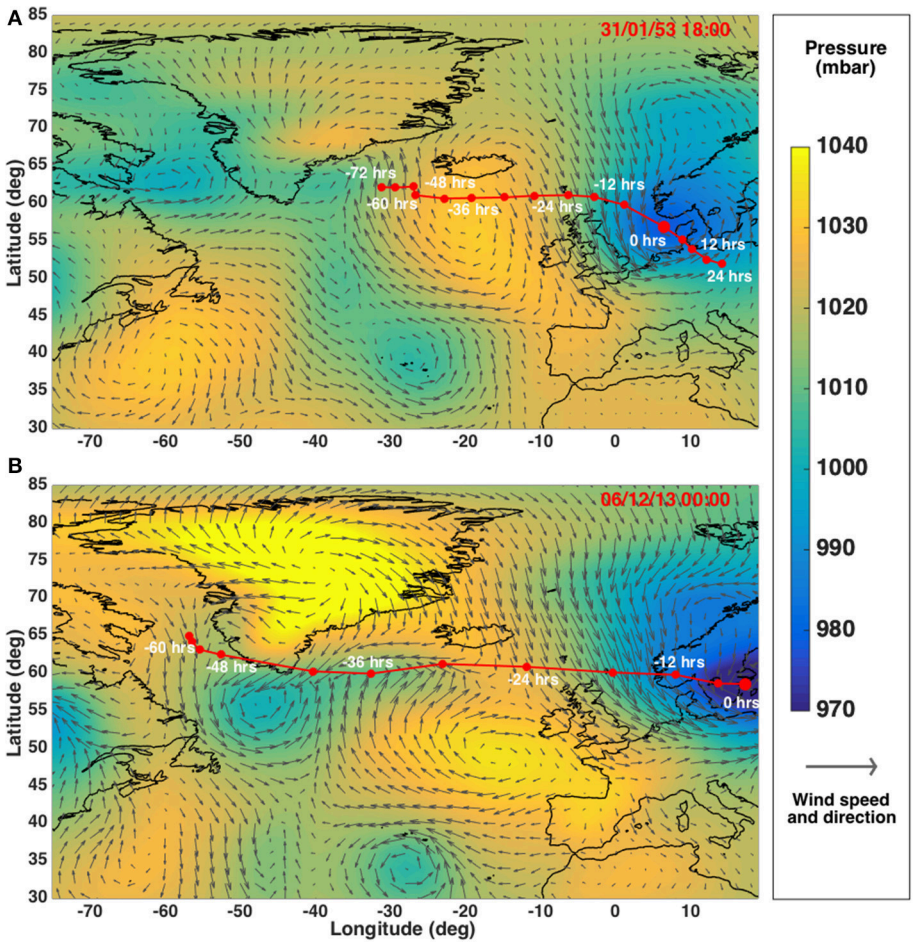

FIGURE 1 | (A) Synopses of storm track and wind-field for the 31 January–1 February 1953 storm, and **(B)** the 5–6 December 2013 storm.

network were downloaded from the British Oceanographic Data Centre (BODC; www.bodc.ac.uk). Time series from a further three east coast gauges (Scarborough, Herne Bay, and Deal Pier) and six south coast gauge sites (Arun, Sandown, Lymington, Swanage, West Bay Harbour, Teignmouth) were downloaded from the Channel Coastal Observatory (www.channelcoast.org). These record sea level every 10-minutes. Datasets from two additional tide gauges on the south coast (Southampton Dock Head and Calshot), and six on the northeast coast (Spurn Head, King George Dock, Grimsby, Blacktoft, Brough, South Ferriby) were obtained from Associated British Ports (ABP).

A direct comparison of 2013 water levels with the 1953 event is difficult due to a lack of 1953 data. In 1953 there was not a national tide gauge network, and high frequency time series of sea level were recorded on paper charts (many of which have been lost or not yet digitized) rather than digitally. In addition, several tide gauges failed during the storm. Only four national tide gauges (Newlyn, Immingham, North Shields, and Aberdeen) are available to directly compare between 1953 and 2013 (**Table 1**). Therefore, to compare sea levels during both events, data was gathered from several other sources (listed in **Table 2**) at multiple coastal locations (shown in **Figure 3**).

A well-known source of sea levels for the 1953 event is Rossiter (1954), who tabulated hourly time series over the 7-day period centered around 31 January 1953. This covered 15 UK gauges between Aberdeen and Newhaven, and single measurements at three other locations (Lowestoft, Great Yarmouth, and Southend). Single high water (HW) level values at many stations recorded during the 1953 event are also held by the EA and are available in reports accessible online (e.g., Johnson, 2014). In addition, a database of the annual highest observed sea levels around the coast of Great Britain was used, obtained from tide gauges and tide registers. This was collated by Graff and Blackman (1978), who expanded the earlier data collation of Suthons (1963) and Lennon (1963). This source is only used if other measurements are unavailable, and it is assumed that the 1953 maxima are likely to represent the 31 January-1 February event (on the east and southeastern coasts). Other sources have already compiled data of the 1953 event, including Steers et al. (1979), Flather (1984), RMS (2003), and Wolf and Flather (2005). Furthermore, Spencer et al. (2014, 2015) recently compiled sea

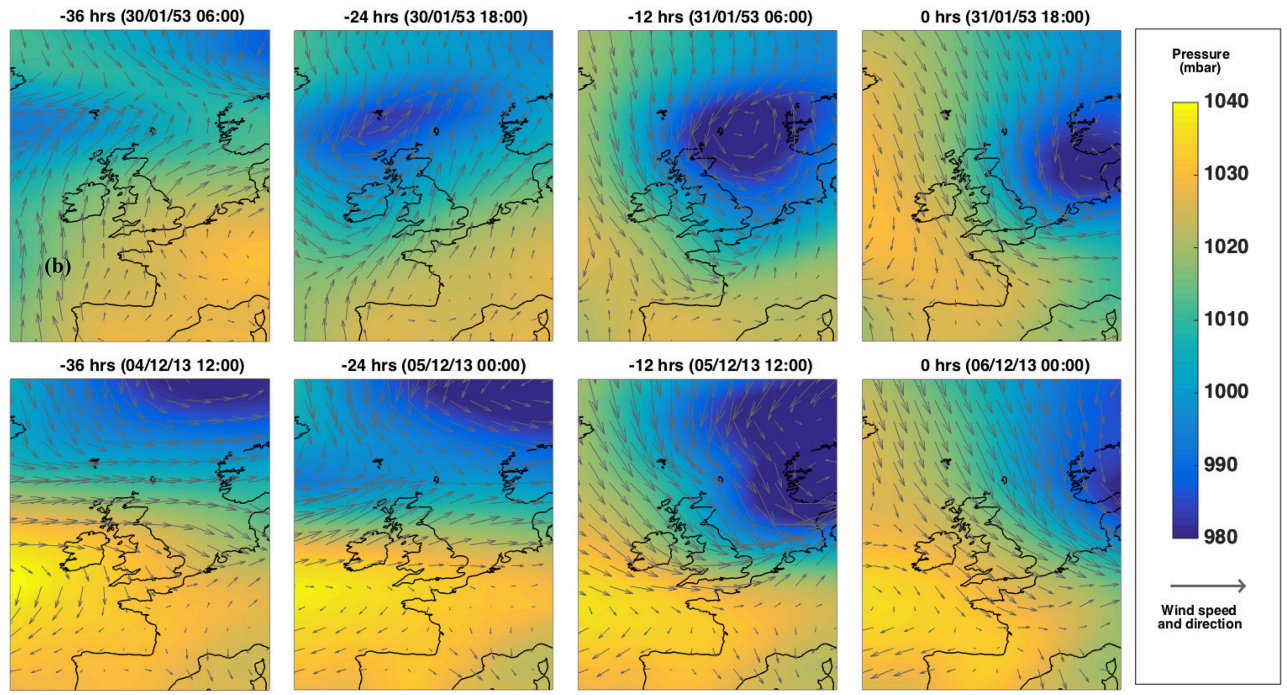

FIGURE 2 | Closer view of 12-hourly wind and pressure in the 1953 and 2013 events (0 h is nearest pressure-wind reading to the time of the largest return period HW of each event in the UK Class A tide gauge database).

TABLE 1 | Sites with tide gauge data from the BODC for 1953 and 2013.

Site	Time of HW	Peak observed HW (mCD)	MSL (30-day running mean) (mODN)	Tide (MSL removed) (m)	Skew surge (m)	NTR (m)	RP2008 (years)	RP (offset) (years)
Aberdeen	31/01/1953 14:00	4.79	–	–	–	–	<1	1
	05/12/2013 15:00	5.23	2.68	1.96	0.59	0.67	22	20
North Shields	31/01/1953 17:00	6.16		–	–	–	22	48
	05/12/2013 16:15	6.58	3.06	2.43	1.08	1.21	430	405
Immingham	31/01/1953 19:00	8.42	–	–	–	–	9	17
	05/12/2013 19:15	9.12	4.11	3.36	1.65	1.89	798	749
Newlyn	01/02/1953 06:00	5.29	3.04	2.10	0.15	0.32	<1	<1
	06/12/2013 06:45	5.83	3.26	2.59	0.07	0.12	<1	<1

These high water (HW) values are provided as their original chart datum (CD) values, and can be converted to ordnance datum using values provided at: http://www.ntslf.org/tides/datum. The non-tidal residual (NTR) is the maximum during the tidal cycle. Return period (RP) is provided for the year 2008 and offset for SLR. Tidal values are not provided where a comparable harmonic analysis was not possible (due to lack of data).

levels for the 2013 event, which are especially detailed in North Norfolk and Suffolk—we use 17 of these from Spencer et al. (2015) where corresponding values for 1953 are also provided.

This improved collation of sea level records for the 1953 event, highlights that some of the values quoted for the same sites (but from different sources) do not always agree. Examples include Great Yarmouth, where there are six mentions of HW, the maximum, and minimum varying by 0.02 m; whereas at North Shields the five sources vary by up to 0.43 m. The reason for the difference between values (taken from different sources) is not clear. Possible issues include datum conversion (e.g., from local chart to Ordnance Datum), rounding of decimals (e.g., from the datum conversion, or imperial to metric conversion), and error in interpretation of the original chart values. Where there is more than one value for any given site, it is stated (in **Table 2**) which value was selected for plotting (**Figures 4**, **5**). This is based upon judgment about the most likely value, although it cannot be conclusively stated whether the "chosen" HW value is correct (therefore it is important to list all sources). The four BODC (Source "A") values are considered the most reliable; otherwise the modal value (where more than two values were available) was used, and in some instances a mean value (e.g., at Sheerness). Where there are closely adjacent values in upper reaches of estuaries and rivers (e.g., the

TABLE 2 | High water (sea level) data for the 31 January–1 February 1953 and 5–6 December 2013 events.

Region	Site name	No. (Figure 1)	Chainage	Type	31 January-1 February 1953											5-6 December 2013				
					Time	A	B	C	D	E	F	Other	Chosen HW (mODN)	Return period (years)	Skew surge (m)	Time	HW (mODN)	Skew surge (m)	Return period (years)	Source
SW England	St Mary's	1	0	1												D2 06:45	2.96	−0.01	<1	A
	Newlyn	2	2	1	D2 06:00	2.24							2.24	<1	0.15	D2 06:45	2.78	0.07	<1	A
	Ilfracombe	3	252	1												D1 07:15 D2 08:00	4.96 4.88	0.00 0.08	<1 <1	A
	Hinkley	4	326	3												D1 08:15	6.65	0.13	<1	A
	Newport	5	398	3												D1 08:30	7.22	0.29	<1	A
	Mumbles	6	492	1												D1 07:45	5.00	0.04	<1	A
	Milford Haven	7	616	3												D1 07:30	3.78	0.00	<1	A
	Fishguard	8	714	3												D1 08:30	2.82	−0.02	<1	A
	Barmouth	9	832	3												D1 09:30	3.41	0.34	<1	A
	Holyhead	10	1014	1												D1 11:45	3.5	0.48	3	A
	Llandudno	11	1112	1												D1 12:00	5.06	0.67	15	A
	Liverpool	12	1168	3						5.32						D1 12:30	6.22	1.08	38	A
	Heysham	13	1250	1												D1 12:15	6.15	1.01	4	A
	Workington	14	1392	3												D1 12:30	4.77	0.07	<1	A

(Continued)

TABLE 2 | Continued

Region	Site name	No. (Figure 1)	Chainage	Type	31 January-1 February 1953											5-6 December 2013				
					Time	A	B	C	D	E	F	Other	Chosen HW (mODN)	Return period (years)	Skew surge (m)	Time	HW (mODN)	Skew surge (m)	Return period (years)	Source
	Port Erin	15	Isle of Man	1												D1 12:30	3.2	0.20	<1	A
NW Scotland	Portpatrick	16	1650	1												D1 13:00	2.48	0.04	<1	A
	Millport	17	1782	1												D1 14:30	1.88	−0.24	<1	A
	Tobermory	18	2320	1												D1 07:00	3.21	0.59	4	A
	Ullapool	19	2564	1												D1 07:15	3.5	0.56	9	A
Lewis	Stormoway	20	Island	1												D1 07:30	2.95	0.30	1	A
N Scotland	Kinlochbervie	21	2670	1												D1 08:15	3.22	0.34	1	A
Shetland	Lerwick	22	Island	1												D1 12:15	1.3	0.14	<1	A
North Sea Scotland	Wick	23	2870	3												D1 12:45	2.44	0.51	1	A
	Aberdeen	24	3224	3	D1 14:00	2.65	2.65			2.62			2.65	2	0.59	D1 15:00	2.98	0.69	20	A
	Methil	25	3390	1						3.61			3.61	27						
	Kirkcaldy	26	3402	1						3.22			3.22	1						
	Grangemouth	27	3414	3						3.73			3.73	57						
	Leith (Edinburgh)	28	3420	3			3.08			3.19			3.08	<1	0.78	D1 15:15	3.71	0.78	22	A
NE England	North Shields (R.Tyne Entr)	29	3624	3	D1 17:00	3.56	3.31	3.67	3.32	3.22			3.56	43	1.26	D1 16:15	3.98	1.08	429	A
	Hartlepool	30	3668	1			3.40						3.40	3						
	R.Tees Entr	31	3676	1			3.84						3.84	80						

(Continued)

TABLE 2 | Continued

Region	Site name	No. (Figure 1)	Chainage	Type	31 January-1 February 1953											5-6 December 2013				
					Time	A	B	C	D	E	F	Other	Chosen HW (mODN)	Return period (years)	Skew surge (m)	Time	HW (mODN)	Skew surge (m)	Return period (years)	Source
	Whitby	32	3718	2	D1 18:00			3.70					3.70	23		D1 17:15	4.32	1.26	588	A
	Scarborough	33	3752	1												D1 17:20	4.39	1.43	626	L
	Bridlington	34	3794	1												D1 17:45	4.56	1.76	824	C
	Spurn Head	35	3858	1												D1 18:30	5.03	1.68	1800	M
Humber Estuary	Hull	36	3886	3	D1 19:10		4.60	4.95					4.95	286		D1 19:15	5.81	1.93	1285	C
	King George Dock	37		3												D1 18:30	5.29	1.19		M
	Immingham	38		3		4.52	4.66		4.50	4.51		4.52 (G) 4.51 (H)	4.52	18	1.43	D1 19:15	5.22	1.66	798	A
	Goole	39		4						5.13	4.52				N/A	D1 19:45	6.04	1.37		C
	Blacktoft	40		4						4.91						D1 19:45	6.01	1.53		M
	Brough	41		4						4.86						D1 18:30	5.13			M
	St Andrews Dock	42		3						4.69										
	Humber Dock	43		3						4.82										
	South Ferriby	44		4					4.79							D1 18:30	4.64			M
	Grimsby	45	3896	3			4.42			4.41			4.41	21		D1 18:10	4.83	1.43		M
Lincolnshire, southwest Wash	Marsh Road Sluice	46	3994	4						5.11			5.11	N/A						

(Continued)

TABLE 2 | Continued

Region	Site name	No. (Figure 1)	Chainage	Type	31 January-1 February 1953										5-6 December 2013				
					Time	A	B	C	D	E	F	Other	Chosen HW (mODN)	Return period (years)	Skew surge (m)	Time	HW (mODN)	Skew surge (m)	Return period (years)	Source
	Haven Sluice, Boston	47		4						5.48			5.30	22						
	Boston	48		4							5.30						6.1	1.60	707	C
	Boston Dock	49		4					5.25											
	Boston Grand Sluice	50		4					5.40											
	Fosdyke	51		4					5.40											
	Lawyers Sluice	52	3996	4						5.36			5.36	N/A						
Cambridgeshire	Wisbech	53	4010	4					5.10				5.10	N/A						
Norfolk	King's Lynn	54	4018	4	D1 20:00		5.67		5.65	5.69	5.85	5.76 (H)	5.76	348	2.40	D1 20:00	6.05	2.05	800	C
	Thornham	55	4044	1							5.34–5.49		5.49	3793			5.64		4576	F
	Scolt Head	56	4052	1							5.37		5.37	1628			6.17		1513	F
	Burnham Overy Staithe	57	4056	1							5.49		5.49	2462			5.52		1736	F
	Wells-next-the-Sea	58	4062	1				5.13	5.13		5.13		5.13	537	2.70		5.31	2.26	692	F
	Stiffkey	59	4070	1							4.57		4.57	113			5.34		1331	F
	Blakeney	60	4074	1							4.27-6.07		6.07	1572			6.30		1876	F
	Cromer	61	4094	1												D1 19:15	3.76	1.08	20	A
	Great Yarmouth	62	4148	2	D1 22:04		3.29	3.28	3.28	3.29	3.30	3.28 (H)	3.30	200	2.68		3.32	2.19	146	C

(Continued)

TABLE 2 | Continued

Region	Site name	No. (Figure 1)	Chainage	Type	31 January-1 February 1953										5-6 December 2013				
					Time	A	B	C	D	E	F	Other	Chosen HW (mODN)	Return period (years)	Skew surge (m)	Time	HW (mODN)	Skew surge (m)	Return period (years)	Source
Suffolk	Lowestoft	63	4164	2	D1 22:19		3.44	3.35		3.35		3.44 (G) 3.35 (I) 4.61 (H) 4.81 (K)	3.44	499	2.41	D1 22:30	3.26	1.98	193	A
	Southwold (Harbour)	64	4182	1					3.50		3.50		3.50	962	2.50		2.76		39	F
	Aldeburgh (Slaughden)	65	4200	1					3.78		3.78		3.78	2837	2.5		3.17		164	F
	Felixstowe	66	4232	1				4.05					4.05	482	2.32					
Essex Thames	Harwich	67	4238	2				4.02		3.99	4.02	3.99 (I) 3.98 (H)	4.02	389		D2 02:00	3.45	1.30	29	C
	Holland-on-Sea/Holland Sluice	68	4258	1			4.02	4.05		4.07			4.05	218						
	Clacton-on-Sea	69	4262	1							4.10	4.15 (H)	4.10	228			3.76		29	C
	Colchester	70	4270	4						3.95			3.95	75						
	West Mersea Island	71		2							4.43		4.43	890			3.42–4.40		3–437	F
	Burham-on-Crouch	72	4302	3								4.50 (H)	4.50	299						
	Southend-on–Sea	73	4312	1			4.60	4.68 4.62		4.60	4.60		4.60	259	2.29	D2 00:45	4.10	1.10	17	C
	Tilbury	74	4314	3				4.85		4.90			4.90	741			4.20		24	C
	London Bridge	75		4			5.39						N/A	N/A						
	Victoria Dock	76		4						4.73										
	Tower Pier	77		4						5.41										

(Continued)

TABLE 2 | Continued

Region	Site name	No. (Figure 1)	Chainage	Type	31 January-1 February 1953										5-6 December 2013				
					Time	A	B	C	D	E	F	Other	Chosen HW (mODN)	Return period (years)	Skew surge (m)	Time	HW (mODN)	Skew surge (m)	Return period (years)	Source
Kent	Chatham	78	4318	3/4			4.79						4.79	518						
	Sheerness	79		2				4.90		4.69		4.67 (H) 4.70 (l)	4.74	429	2.16	D2 00:45	4.10	1.00	15	C
	Herne Bay	80	4346	1								4.65 (L)	4.65	1324	2.99	D2 01:30	4.10	1.50	39	L
	Deal Pier	81	4396	1												D2 01:00	4.40	1.52	79	L
	Dover	82	4412	1	D2 01:00		4.57			4.57			4.57	350	1.89	D2 00:45	4.78	1.39	720	A
English Channel	Rye	83	4468	3						4.66			4.66	34			5.10	1.00	1166	N
	Pevensey Bay	84	4500	1						3.90			3.90	<1			4.87	0.74	449	C
	Newhaven	85	4528	1			3.76			3.79			3.79	1	1.00	D2 01:15	4.27	0.81	42	A
	Shoreham	86	4550	3	D2 01:15											D2 01:15	4.03	0.58	18	C
	Arun Platform	87	4570	1												D2 01:20	3.83	0.78	75	L
	Portsmouth	88	4616	1						2.47			2.47	1	0.82	D2 01:00	2.83	0.69	11	A
	Sandown	89	Island	1												D2 02:10	2.86	0.76	49	L
	Southampton	90a	N/A	3								2.08(M)		<1	0.72	02:50	2.70	0.69	10	M
	Calshot	90	4632	2												D2 02:40	2.77	0.86	34	M
	Yarmouth	91	Island	2												D2 02:45	1.85	0.70	3	C
	Lymington	92	4652	2												D2 02:50	1.88	0.66	2	L
	Swanage Pier	93	4694	1												D2 02:30	1.18	0.61	<1	L

(Continued)

TABLE 2 | Continued

Region	Site name	No. (Figure 1)	Chainage	Type	31 January-1 February 1953											5-6 December 2013				
					Time	A	B	C	D	E	F	Other	Chosen HW (mODN)	Return period (years)	Skew surge (m)	Time	HW (mODN)	Skew surge (m)	Return period (years)	Source
	Weymouth	94	4736	1												D2 08:45	1.66	0.17	<1	A
	West Bay Harbour	95	4786	1												D2 08:45	2.38	0.15	1	L
	Teighnmouth	96	4844	3												D2 08:20	2.39	0.08	<1	L
	Plymouth	97	4950	2												D2 07:45	2.57	0.05	<1	A
	Jersey	98		1												D2 08:30	5.16	−0.22	<1	A
	Portrush	99		1												D1 08:00	1.76	0.53	N/A	A
	Belfast	100a								2.00										
	Bangor	100b		1												D1 12:00	1.91	0.13		A
	Dublin	101		1						4.86						D1 12:30	5.23	0.57		O

The sources, of which there are several for some locations in 1953, are labeled: A, BODC; B, Rossiter (1954); C, ©Environment Agency database; D, Steers et al. (1979); E, Graff and Blackman (1978); F, Spencer et al. (2015); G, Pye and Blott (2006); H, RMS (2003); I, Wolf and Flather (2005); J, Flather (1984); K, Zurich (2014); L, Channel Coastal Observatory; M, Associated British Ports (ABP); N, Rye Harbourmaster (www.ryeharbour.net); O, Marine Institute www.http://data.marine.ie/. All return periods are from the EA national study (McMillan et al., 2011) and are offset for sea level rise around the base year of 2008. Note the chainage is the reference distance along the coast in the EA study, and it is noted where locations are inland (i.e., on a tidal river—e.g., Boston), return periods in these locations should be treated with caution. Exposure type is categorized: 1–4 (1, open coast; 2, sheltered coast; 3, estuary; 4, river).

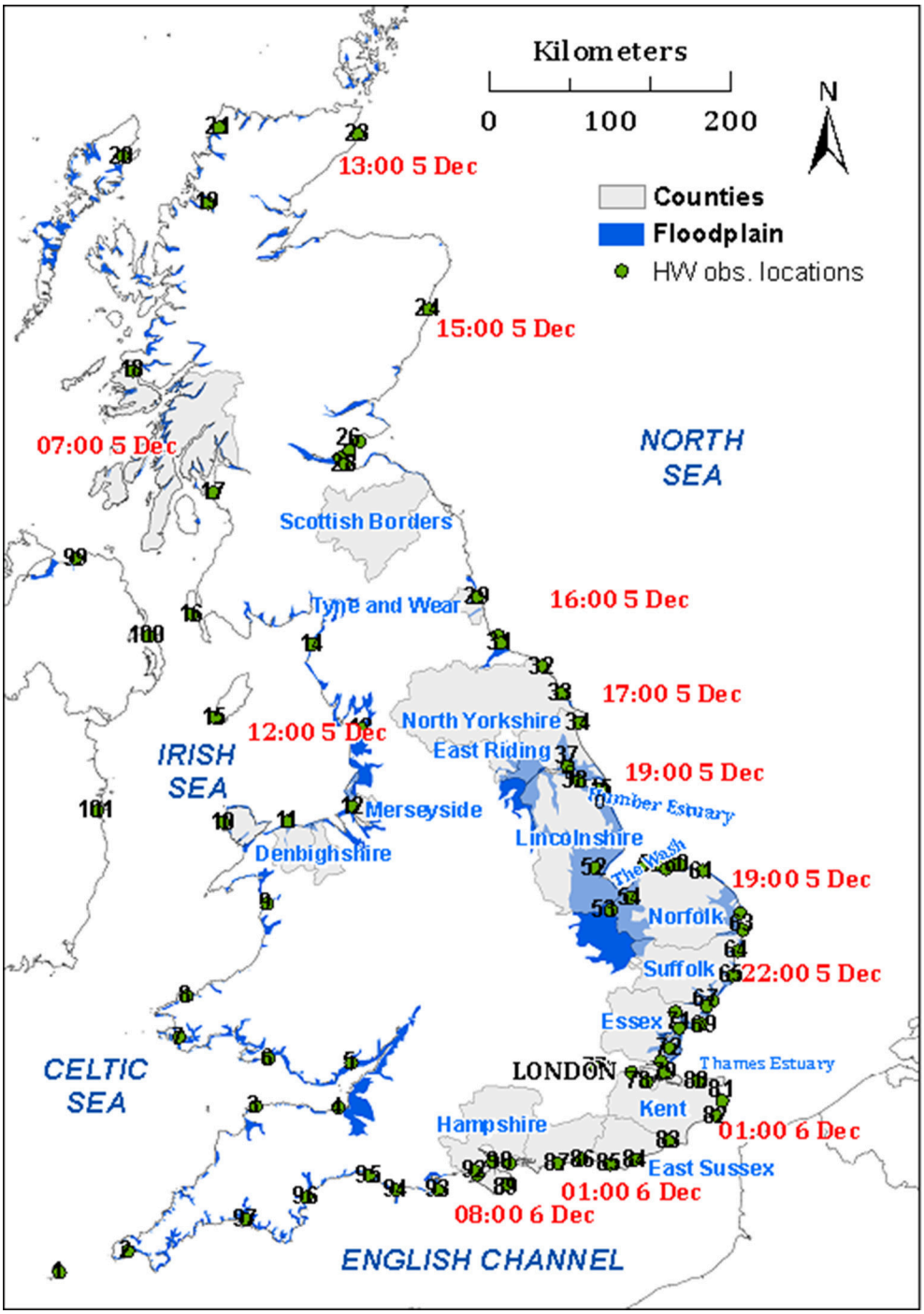

FIGURE 3 | Map of UK counties referred to throughout the paper. Also shown are the locations of HW recordings (refer to **Table 2** for site names and data sources), and timings of HW during 5–6 December 2013 (which were similar to the timing of the HWs of 31 January-1 February 1953). The background blue shaded area is land surface that is below a static extreme water level (approximately 1 in 200 years), and which without defenses is theoretically susceptible to coastal inundation.

Humber, Boston etc.), a single representative value for plotting (**Figures 4**, **5**) is applied.

Where high frequency time series longer than a month of data are available, sea levels were separated into the main component parts of tide, non-tidal residual (usually mostly surge) and MSL (Pugh, 1987); as described in Wadey et al. (2014). Where possible when comparing residuals we refer to the "skew surge," i.e., the peak observed HW minus the peak tidal HW (de Vries et al.,

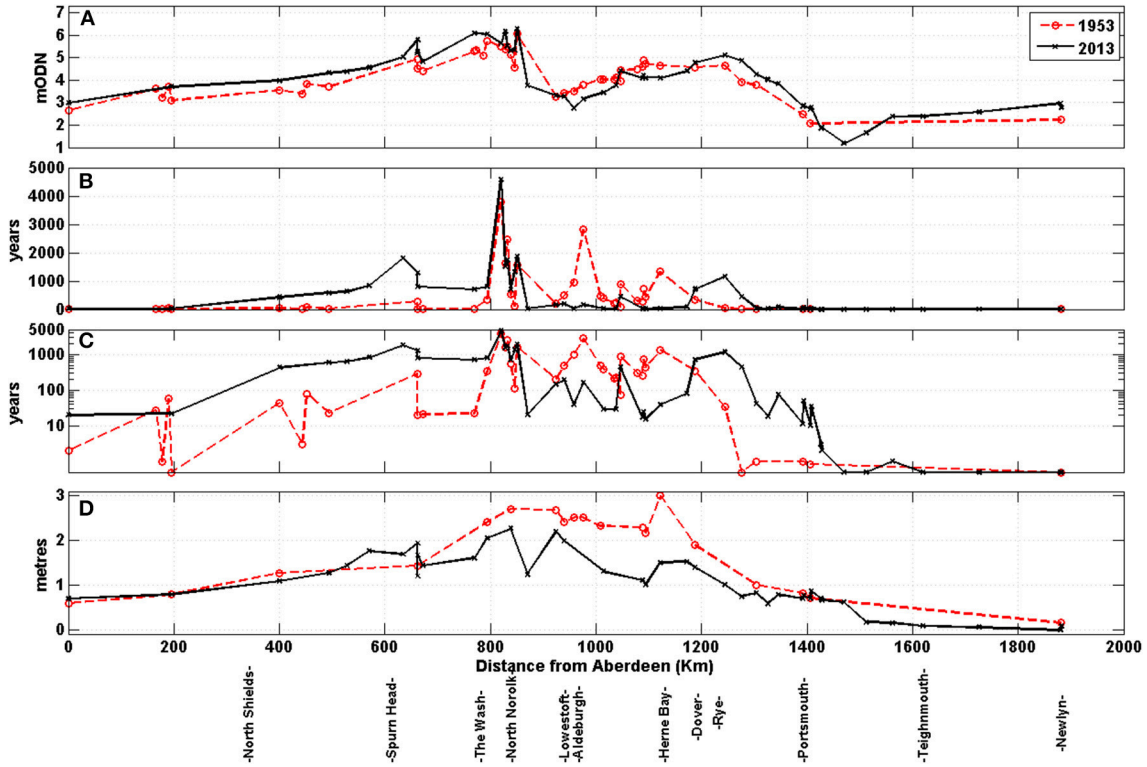

FIGURE 4 | Line plot to compare the: (A) observed high waters; (B) return periods on a non-logarithmic y-scale and (C) on a logarithmic y-scale; and (D) skew surges of the 1953 and 2013 events in the North Sea.

1995; Horsburgh and Wilson, 2007). For most of the 1953 HW recordings, there is not enough data available for a comparative tidal analysis. This is because the data is a single HW value, or in the case of Rossiter (1954), a 7-day time-series. Hence the focus here is on the high waters (HWs), although we assembled predicted tide and surge heights (quoted) from a range of existing sources to allow for a basic comparison of the contribution of the respective sea level components to the total HW levels. All time refers to Greenwich Mean Time (GMT), and (with the exception of **Table 1**) elevations are metres above Ordnance Datum Newlyn (mODN)—the UK's principle national elevation benchmark, which is approximately MSL at Newlyn Cornwall 1915–1921.

Each HW was assigned a return period value using the latest Environment Agency (EA) national extreme value statistics (McMillan et al., 2011; Batstone et al., 2013), which are relative to a baseline MSL (year 2008). The rate of mean SLR at the UK's longest tide gauge record at Newlyn, Cornwall (which traverses the years 1953 and 2013) has a linear rate of 1.81 mm/year (Wadey et al., 2014). This suggests that MSL in December 2013 was 0.11 m higher than it would have been in January 1953. Therefore, return periods are discussed with reference to both the EA's 2008 values and also to the offset sea level (to give a better indication of the return period water level in 1953). An improvement in future work would be to offset return periods in context with regionally variable SLR (e.g., due to vertical land movement, c.f. Shennan and Horton, 2002; Bradley et al., 2009). Caution is advised where we have associated the EA's open coast return period levels with HWs recorded in estuaries and rivers (particularly where highlighted by location type "4" in the fifth column of **Table 2**), since these were generated for open coast conditions.

It is emphasized that the scope of this paper is to provide only a basic synthesis of the impacts (for the third objective). For 1953, several key sources provided details of the impacts along the east coast, notably Steers (1953) who surveyed the damage and described meteorological conditions, flooding, and erosion impacts. Other detailed accounts of the human losses are provided by Pollard (1978) and Summers (1978) and in Essex (which was one of the worst-hit areas) by Grieve (1959). The human impact is also captured by Baxter (2005). Kelman (2009) provides possibly the most detailed itemization of the fatalities in the UK. In the case of the 2013 event, media reports, and literature continue to emerge about the 2013 event in the form of reports (e.g., ABPmer, 2014; EA, 2014a) and peer-reviewed research (Sibley et al., 2015; Spencer et al., 2015).

COMPARISON OF THE METEOROLOGICAL CONDITIONS

The first objective is to compare the meteorological forcing during both events. Both storms, as noted by Spencer et al. (2015), fit a "SE tracking" category, of the three types of North Sea

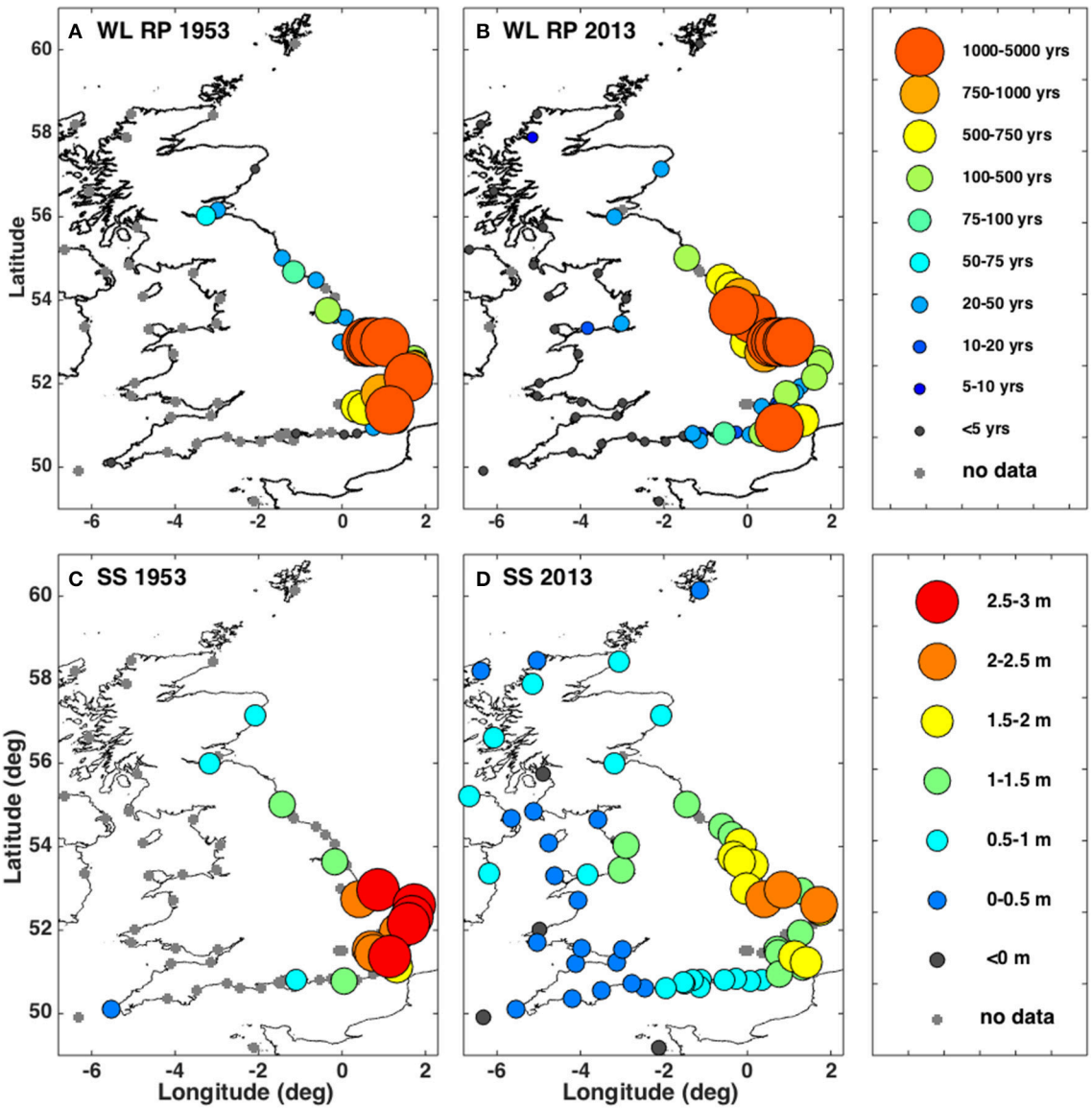

FIGURE 5 | Return periods of (A) 1953 and (B) 2013; and skew surge heights during (C) 1953 and (D) 2013 events. Note the return periods are offset for SLR in both events.

synoptic storm climatology defined by Muir Wood et al. (2005). Such storms are characterized by an intensifying circulation moving in a south-easterly direction around a high pressure system located to the west of Ireland, causing high winds over the western North Sea which later becomes directed southward. The rate of movement of the storm center is significant to the duration of the wind blowing over the sea surface, which is important for the growth of waves and surge: the development of the 2013 event was much quicker than the 1953 event (Sibley et al., 2015). The distinct characteristics of each storm affected the extremity of HWs, waves, and flooding observed in 1953 and 2013.

The 1953 storm developed to the southeast of Greenland on 28 January and moved eastwards, crossing Scotland to the north, before traveling in a south-eastward path across the North Sea and into Germany (**Figure 1A**). The track of the depression from the Atlantic over the north of Scotland into the North Sea, and the accompanying movement of the high-pressure system behind it, meant that powerful northerly winds swept down the eastern UK coast and the western part of the North Sea. The central pressure of the storm over the northern North Sea dropped to 964 mbars at 06:00–12:00 on 31 January (MetOffice, 2014a) (having been at 1004 mbar at 12:00 on 29 January) (Steers, 1953). At 18:00 on 31 January when the storm's effects at the coast were becoming apparent, very strong northerly winds were generated over the North Sea, attributable to interaction with the high pressure (anticyclone) to the west of the UK (**Figure 2A**). On 31 January 1953 at Costal Hill, Orkney, wind gusts of up to 110 knots [204 km h^{-1}] were recorded, and 60 knot [111 km h^{-1}]

wind speeds in Aberdeenshire (Wolf and Flather, 2005); whilst the highest recorded 10-min mean wind speed at Stonehaven, Scotland was 65 knots [120 km h^{-1}] from a northwest direction (Hickey, 2001).

In the 2013 event, Storm "Xaver" developed off the coast of Greenland on 4 December, enhanced by another low pressure system located over the Norwegian Sea (**Figure 1**). It progressively deepened as it tracked across the north of Scotland and Northern Europe on 4–5 December; and on 5 December the eastward track developed a south-easterly component as the system moved around the area of high pressure to the west of Ireland. The damaging effects of winds were notable from 08:00, 5 December in Scotland, blowing debris onto railway tracks and closing train services, and killing a lorry driver in West Lothian. High winds continued into the early afternoon, with incidences of wave overtopping (and localized flooding) on the west coast. On the east coast of England, maximum wind speeds were recorded during the afternoon to early evening—which, as described later, is significant with regard to the timing of the HWs. For example along the coast of Suffolk during the 2013 event, the maximum wind gusts (56 km h^{-1}) were reached before 18:00 on 5 December, about 4 h before HW—by which time the wind direction was also more north-easterly and slightly offshore (**Figure 2B**). On 5–6 December the storm moved across southern parts of Norway and Sweden (**Figure 1**); with the lowest area of central pressure of 960 mbar over the area of maximum intensity in the Baltic Sea, and as low as 959 mbar over southern Sweden (Mills et al., 2013). On 5 December 2013, wind had gusted widely at 60–70 knots [111–130 km h^{-1}] across Scotland, with Altnaharra (Sutherland) recording a gust of 81 knots [150 km h^{-1}]. The mountain station at Aonach Mor (at an elevation of 1130 m) recorded a gust of 123 knots [228 km h^{-1}]. Gusts also exceeded 60 knots [111 km h^{-1}] along North Sea and Irish Sea coasts and over 70 knots [130 km h^{-1}] in the Western Isles.

The maximum wind speeds recorded at weather stations in Scotland during the 1953 and 2013 storms were similar—both storms generated extreme peak wind speeds. However, as shown in **Figure 1A**, the passage of the 1953 storm track from Ireland into Europe was exceptionally slow taking 24 h to reach the coast off the Netherlands. The 2013 storm took approximately half this time to reach the same longitude. In regard to the 1953 event, Steers (1953) remarked that: *"the great damage to forests in north-eastern Scotland in itself implies something quite exceptional"* (similar damages were not reported for 2013). In the southern North Sea basin, compared to 2013, the 1953 wind speeds were stronger and more sustained across the North Sea during the 1953 event, hence increasing the wave heights and the likelihood of coincidence of the peak storm conditions with high tide. The 2013 storm track was similar to that of 1953 in its approach to northeast Scotland (**Figure 1**). However, the 1953 storm tracked southwards into the Netherlands, whereas the 2013 storm continued along a more eastward trajectory over Scandinavia. This meant that on the night of the 31 January 1953, the low pressure system and winds were more pronounced in the southern North Sea—strong winds (and waves) focused upon shorelines from Yorkshire to the Thames, close in time to the peak of the high water levels. The 1953 storm track allowed for a north-south elongated wind field over the North Sea, increasing wave fetch and surge generating winds. The 1953 storm center also moved relatively slowly toward the southern North Sea, steadily increasing the duration of northerly gales and worsening sea conditions that impacted N-NE facing coasts (Flather, 1984).

In summary, while there are similarities in weather conditions during both storms, there are also key differences, such as the more southerly track over the North Sea during 1953. Steers (1953) described the noon forecast issued on 31 January: *"All districts will have gale force winds, severe in many places, and squally showers, mainly of hail, or snow. Considerable snowfall may occur over high ground. Thunderstorms will occur here and there. It will be cold."* Notable was the lack of emphasis upon coastal flooding. The disastrous surge of 1953 was predicted by the Met Office and the Dutch Surge Warning Service; although systems for warning the public were not effective, and there was a lack of preparation. In contrast, before the 2013 event, a surge ensemble forecast was generated and disseminated as flood warnings. This forecast performed well, indicating a "low risk" of a high impact event 7 days in advance. By 5–6 days ahead of the event, a "significant risk" of an unusually dangerous period of surge activity (when combined with high tides) was forecast (Sibley et al., 2015). Subsequently, the Flood Forecasting Centre was able to pass briefings to the EA on 1 December, and on 5 December a COBRA (Cabinet Office Briefing Room A) meeting occurred reflecting the highest level of preparation in the UK for a potential regional or national disaster.

COMPARISON OF OBSERVED HIGH WATERS

The second objective was to compare the HW observations around the UK coast during both events, and contrast the relative tide, surge, and MSL contributions to the HWs and the respective return periods of these levels. A summary of HW values at sites around the UK is listed in **Table 2**. Due to the limited data for the 1953 event, the most accurate comparison of HWs is along the stretch of coastline from Aberdeen in Scotland to Newhaven in the English Channel. The HW levels listed in **Table 2** for different sites are plotted in **Figure 4A** against the distance along the coast from Aberdeen ("chainage"). The chainage values align with the Environment Agency's 2 km-spaced points each of which is associated with extreme sea level statistics (McMillan et al., 2011; Batstone et al., 2013), which are later used to discuss return periods of each event. A comparison of the HW return periods and the size of the skew surges are illustrated in **Figures 4**, **5** using line and dot plots, respectively.

Overview of High Water Elevations around the UK

A first key difference between the events, evident by considering the values listed in **Table 2** and plotted in **Figures 4**, **5**, was that the 1953 HWs were smaller on the northeast and south coasts, compared to December 2013. It can be inferred that the 5–6 December 2013 event also resulted in larger and more

extreme HWs in Wales and northwest England, although there is a lack of data on the west coast for the 1953 event. As noted in Section Comparison of Coastal Flooding and Impacts (and Appendix 2), there are no reports of flooding for areas other than the east coast during the 1953 event. The levels available in the Graff and Blackman (1978) database suggest that the 2013 event was larger on the west coast: the maximum HWs for the year 1953 at Liverpool and Dublin were smaller by 0.90 m and 0.37 m, respectively (than the HWs recorded at these sites on 5 December 2013). On the northeast coast of England, in Yorkshire to Lincolnshire, the 2013 HWs were, in places, more than half a meter larger than those of 1953. There were larger HWs during 31 January–1 February 1953 from Suffolk to Kent (**Figure 4B**), although in parts of Norfolk, Suffolk, and south Kent, HWs were similar between both events. In the Essex, Thames, and Kent region the 1953 HWs were, in places, more than half a meter higher than those of 2013. However, the 2013 HWs were larger from Dover (by approximately 0.2 m) and along the English Channel (in the order of half a meter beyond Dover to the far southwest) (**Figure 4A**).

High Water Timing and Extremes

Now, the timing of HW and the estimated return periods is considered, including a more detailed comparison of the HWs. The timing of HW is shown in **Figure 3**, and listed (where available) in **Table 2**. In December 2013, extreme HW events in UK coastal waters began at around 07:00 on 5 December, in northwest Scotland. This included 1 in 5 to 1 in 10 return period HWs at Tobermory and Ullapool. By early afternoon extreme HWs impacted Wales and Liverpool Bay. At Liverpool, the 2013 HW was approximately a 1 in 40 year return period. At 12:45 on 5 December 2013 at Wick in the North Sea, the HW was a 1 in 1 year return period, and reached Aberdeen by 15:00 as a 1 in 22 year return period. The 1953 HW at Aberdeen was 0.33 m smaller than 2013, although the 1953 record was not complete (**Figure 7A**) and Hickey (2001) suggested the possibility that the peak was underestimated. At Leith (north Edinburgh) 140 km further south, 2013's HW was up to 0.63 m larger than in 1953, but again there is doubt over the reliability of the 1953 level which Rossiter (1954) "*treated with some reserve*." An hour later, HW reached 200 km further south at North Shields (River Tees Entrance): the 2013 HW was 0.42 m larger than in 1953 and 100 km further south on the Yorkshire coast, the Whitby HW of 2013 was over 0.6 m higher than it had been in 1953. Further, south, the HW at Immingham in the Humber Estuary, occurred at approximately 19:00, with the 2013 HW exceeding the 1953 HW by as much as 0.7 m.

At the same time as water levels peaked in the Humber, HW was also occurring 100 km away in North Norfolk where Stoddard (2014) described that 2013 HWs were at least equal to and probably greater than the 1953 HWs. The HWs on this part of the coast were extreme in both events: at Wells almost a 1 in 700 year return period in 2013, and over 1 in 500 year return period in 1953. Following the 2013 event, Spencer et al. (2014) surveyed over 250 reference points (e.g., water marks on buildings, erosional notching, debris lines) in North Norfolk. This confirmed that along this 45 km coastline the peak water levels of 5–6 December 2013 were comparable to, and in places higher, than 1953 flood levels; although with complex inter-site variability (e.g., due to a combination of still water level, wave run-up, bathymetry and geomorphic setting). The 2013 HW return period is an outlier at Cromer (northeast Norfolk) at only 1 in 25 years (a 1953 comparative measurement is unavailable). Swell waves have been known to cause underestimation of HW at this location, due to drawdown of air in the pneumatic tubing (UKCMF, 2013), and wave action beneath Cromer Pier rendered the tide gauge readings unsuitable for analysis of the 2013 event (Spencer et al., 2015).

HW took 3 h to travel 70 km from Cromer to Lowestoft (north Suffolk), where the 1953 HW was larger by 0.18 m. At King's Lynn, in the southern Wash and 7 km inland on the River Ouse, the 2013 HW exceeded the 1953 HW by almost 0.3 m and also exceeded the previous largest event of this region, on 11 January 1978 (Steers et al., 1979; Spencer et al., 2015). Further east at Wells-next-the-Sea, the 2013 HW was 0.18 m larger than in 1953. Nearer the Norfolk-Suffolk county border at Great Yarmouth (<20 km north of Lowestoft), the 2013 HW was only a few centimeters larger (0.02–0.05 m) than the 1953 HW.

To the south of Great Yarmouth, the 1953 HW was in most locations higher than it had been in 2013 (**Figures 4B–D**); with the exception in southern Suffolk at enclosed tidal locations, such as the Deben frontage in Waldringfield (60 km south of Lowestoft and several km inland on the tidal Deben) for which Whiting (2014) noted that the 2013 HW exceeded the 1953 HW. However, on the Suffolk open coast the 1953 HWs considerably exceeded those of 2013, by 0.74 m at Southwold and by 0.61 m at Aldeburgh, which in 1953 respectively reached return periods of almost 1000 and 3000 years. The time of HW at these locations was around 23:00 (in 1953 and 2013). Extreme HWs were recorded around the coastlines of Essex, Thames Estuary and Kent after midnight. On the Suffolk side of the county border (with Essex to the south) lies Felixstowe, and <5 km further south (in Essex) is Harwich. The 1953 HW at Felixstowe was 0.6 m larger than the 2013 HW at Harwich (the nearest site for comparison in this area). The 2013 HW did not exceed 1 in 30 years at Harwich, Clacton, and Tilbury (on the Thames outer estuary), although it may have been higher at West Mersea Island on the outer Blackwater estuary as suggested by an upper measurement surveyed by Spencer et al. (2015). At Felixstowe the 1953 HW was 1 in 500 years, and at Southend almost 1 in 300 years, and in excess of 1 in 700 years at Tilbury. The HW at 03:00 on the 6 December 2013 was the highest at the mouth of the Thames Estuary since construction of the Thames Barrier was completed in 1982 (Reeder, 2013), but was not as large as the HW in 1953, as shown by the 0.6–0.7 m higher values (than of 2013) recorded at Sheerness and Tilbury. In 1953, the surge propagated upstream and came level with the Chelsea Embankment, nearly flooding central London (RMS, 2003). On the Thames, the December 2013 surge did not propagate beyond Greenwich, due to closure of the Thames Barrier, although caused a 2 m difference in water height between the front and back of the barrier, which remained closed for 2 days (Insurance Journal, 2013; The Actuary, 2013). At Herne Bay on the north side of the Kent peninsula, the 1953 HW was 0.69 m larger than

the 2013 HW (**Figure 7D**) and >1 in 1000 year return period. Further south at Dover, the 2013 HW exceeded the 1953 HW by over 0.2 m and was almost a 700 year return period—although the 1953 HW event was also extreme (a 1 in 350 year return period).

On the second day of each event (1 February 1953 and 6 December 2013) extreme HWs occurred in the eastern English Channel. At Rye Harbor, 45 km southwest of Dover, the 2013 HW was 1 in 1000 years and larger than the 1953 HW by 0.44 m. At Newhaven, Sussex, 50 km east-southeast of Rye, the 2013 HW was a 1 in 40 year return period, and 0.48 m larger than HW in 1953 (**Figure 7E**). By 02:00 the HW was occurring 90 km further east of Newhaven, in the Solent. At Portsmouth the 2013 HW was 0.36 m larger than in 1953. Note that at Portsmouth and Rye, the 1953 HW levels are based on the assumption that the annual maxima for 1953 in the Graff and Blackman (1978) database is attributable to the 1953 event. At Portsmouth the 2013 HW was the second highest (since the record starts in 1961), with a skew surge component of almost 0.7 m. The furthest west that an extreme HW occurred in 2013 (related to the propagation of the North Sea surge) was a 1 in 1 year event at West Bay in Dorset, comprising a 0.15 m skew surge at 08:45 on 6 December—almost 18 h after HW at Aberdeen and 8 h after HW at Dover.

Reasons for High Water and Extremes Variation between Events

The 5–6 December 2013 event has been referred to as the biggest North Sea surge for 60 years (e.g., BBC, 2013i), although for this assessment it is important to differentiate the terms "surge" and "high water"—the former refers to a meteorological component of sea level, the latter is the total observed sea level height. Both events comprised large storm surges: the largest observed in 1953 was 3.9 m at Harlingen (Netherlands) (Wolf and Flather, 2005), whilst satellite images during the 2013 event detected peak residuals of up to 3.4 m, as part of the surge spanned 200 km into the North Sea (Mills et al., 2013).

The skew surges of the 1953 and 2013 events were of similar height in Scotland (0.6–0.7 m at Aberdeen) and northeast England, although with different timings of surge peak in relation to time of tidal HW. For example, the 2013 peak surge at North Shields and Immingham occurred 1–2 h before high tide; whereas the 1953 peak surge followed after high tide (**Figures 7B,C**). However, it was in the southern North Sea that the 1953 HWs exceeded those of 2013, especially along the open coast between Norfolk and Kent. This was due to the amplification of the surge, from the more southerly track of the 1953 storm and extreme winds which can effectively generate a larger surge across the shallower southern North Sea waters. One of the largest observed 2013 skew surges was 2 m at Lowestoft, which was exceeded by the 2.4 m skew surge of 1953. There were even larger 1953 skew surges of approximately 2.7 m at Great Yarmouth and 3 m at Herne Bay (whereas the 2013 skew surge at Herne Bay was less than half this size). This suggests that the 1953 skew surge was probably larger along >750 km of coast (in the southern North Sea and also as it propagated into the English Channel). However, the 2013 event coincided with a period of higher astronomical tide. This meant that the 1953 HWs exceeded the 2013 HWs over a much smaller area (approximately 200 km), because the tide played a greater role in determining extreme sea level heights outside of the surge-dominated southern North Sea basin. The higher tide during the 2013 event is, for example, apparent from the data at Newlyn (**Table 1**) where a harmonic analysis was undertaken using the observed time series. The 6 December 2013 morning high tide was 0.49 m larger than the equivalent 1 February 1953 tide. Tidal predictions suggested a similar order of difference between the two events at Immingham and North Shields.

Large storm surges from the North Sea are known to propagate through the Straits of Dover (Rossiter, 1954) and as far west as the Solent (Henderson and Webber, 1977; Haigh et al., 2004, 2010). In the 2013 event this surge transmission into the English Channel can be tracked by 15 observations (inclusive of Dover to Newlyn): the skew surge amplitude remains quite large even as far as Swanage (Dorset) at 0.6 m, although is smaller at Weymouth (0.17 m), and in the far southwest 0.07 m at Newlyn (with a 0.12 m maximum non-tidal residual in the same tidal cycle). For the 1953 event, observations are unavailable between Portsmouth and Newlyn, although at each of these sites the surge was larger than in 2013. At Newlyn the skew surge and maximum non-tidal residual were 0.15 m and 0.32 m, respectively (0.08 m and 0.2 m larger than those that occurred in 2013), (**Table 1** and **Figure 7F**).

COMPARISON OF COASTAL FLOODING AND IMPACTS

The third and final objective was to compare the coastal flooding and impact of both events. We reiterate that this is not a comprehensive analysis, but gives a snapshot of impacts in each region.

A simplified summary of impacts is provided in **Figures 6A,B**, and Appendix 2 (Supplementary Materials) where the references provided contain more detail. An important difference between the events is highlighted by the fact that flood impacts in 1953 are primarily measured by loss of life (affecting Lincolnshire to the Thames), whilst in 2013 impacts are measured by property flooding (from Wales, clockwise around the coast to Hampshire). The 1953 floods affected over 1600 km of the east coast and inundated 647 km^2 of land (Steers, 1953; RMS, 2003). Flood defenses are known to have breached at about 1200 locations during the 1953 event (RMS, 2003), where breach refers to structural failures that generally cause the fastest rising water levels and most prolonged flooding (*c.f.* Muir Wood and Bateman, 2005). There were over 307 deaths, and 24,000 damaged houses (of which 500 were totally destroyed) and 200 industrial facilities damaged by floodwater (RMS, 2003). At a number of locations properties were subjected to the repeated entry of the tides for days to weeks as seawater continued to flow through breaches; although the huge repair and recovery operation meant that around 90% of the breaches in England were closed within a month (RMS, 2003).

The December 2013 event killed 15 people in northwest Europe (Zurich, 2014), with no reported fatalities from the coastal floods. In the UK, the 2013 event's total flood extent is

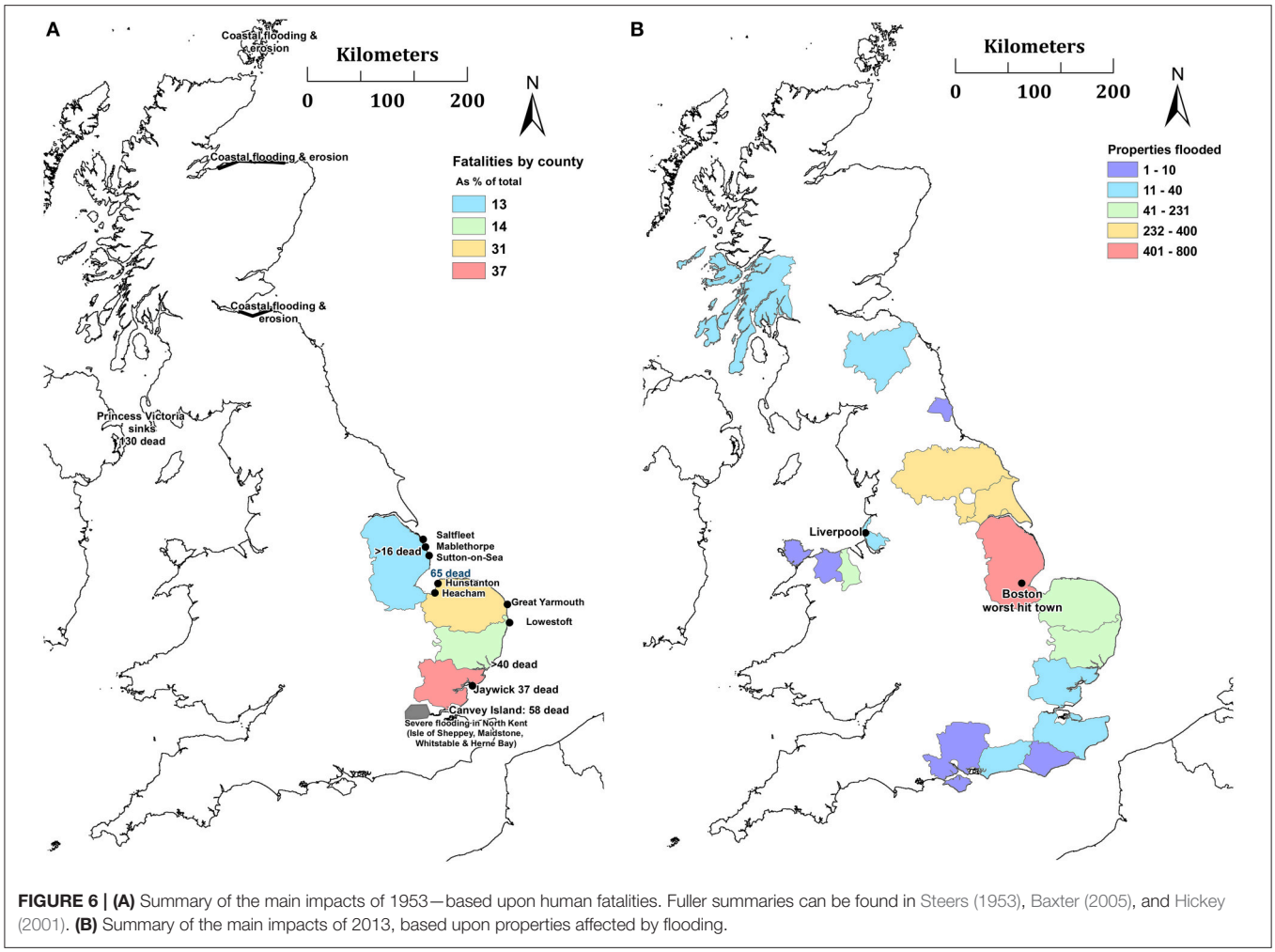

FIGURE 6 | (A) Summary of the main impacts of 1953—based upon human fatalities. Fuller summaries can be found in Steers (1953), Baxter (2005), and Hickey (2001). **(B)** Summary of the main impacts of 2013, based upon properties affected by flooding.

not quantified although the available estimates indicate this is dwarfed by 1953. It was generally acknowledged that defenses prevented much more serious losses (e.g., Zurich, 2014), although the total damage to the EA in December 2013 (for defense repairs and flood operations) was estimated to be in the range £44 million to £83 million (MetOffice, 2014b). Over 2800 properties were reported flooded (EA, 2014d), and an estimated 6800 ha [6.8 km^2] of agricultural land (EA, 2014b). Land flooded behind overtopped and breached earthen barriers amounted to 480 ha [4.8 km^2] in North Norfolk, and 660 ha [6.6 km^2] in Suffolk (Spencer et al., 2015); and there was 2.4 km^2 of flooding in East Riding, Yorkshire (ERYC, 2014).

In the 2013 event over 10,000 people were evacuated along the east coast, and 800,000 properties were protected by 2800 km of flood defenses (along the UK's coastline). Throughout Europe, insured losses were in the range of EUR 1.4–1.9 Billion, an aggregated figure for both wind damage and storm surge-related flooding (Zurich, 2014); and initial estimates for insured losses due to the floods in the UK were up to £100 million (Insurance Times, 2013), with some of the largest insurance claims attributable to business interruption, in addition to property damage claims (Artemis, 2013). Recent and comprehensive damage estimates are not publicly unavailable. We can generate a speculative approximation (for property damage cost) if assuming each of the 2800 properties flooded (**Table 3**) experienced somewhere between £10,000 and £30,000 damage (if flood depths are assumed as in the range 0.1–0.5 m, and values are taken from an average residential depth-damage curve by Penning-Rowsell et al., 2005). From this, 2013's coastal flooding property damage may have been in the range of £28–£84 million. The largest damages of the 2013 event occurred in northeast England and parts of Lincolnshire; whilst the hardest hit town was Boston, Lincolnshire (north of The Wash on the banks of the River Haven). This included flooding of 701 residential and 118 commercial properties, with almost £3 million damage to defenses, and £1 million damage to the Stump Church (EA, 2014a). The 1953 event in Boston did not cause severe damage or loss of life; whereas the 11–12 January 1978 event flooded 180 properties (due to a wall collapse, and had a larger HW than 1953 by 0.25 m) (Steers et al., 1979). The 2013 HW levels exceeded (by over half a meter) both the 1953 and 1978 events and caused more severe flooding.

In 2013, there were numerous reports of roads affected by coastal flooding, and railway damage (e.g., Conwy Valley line,

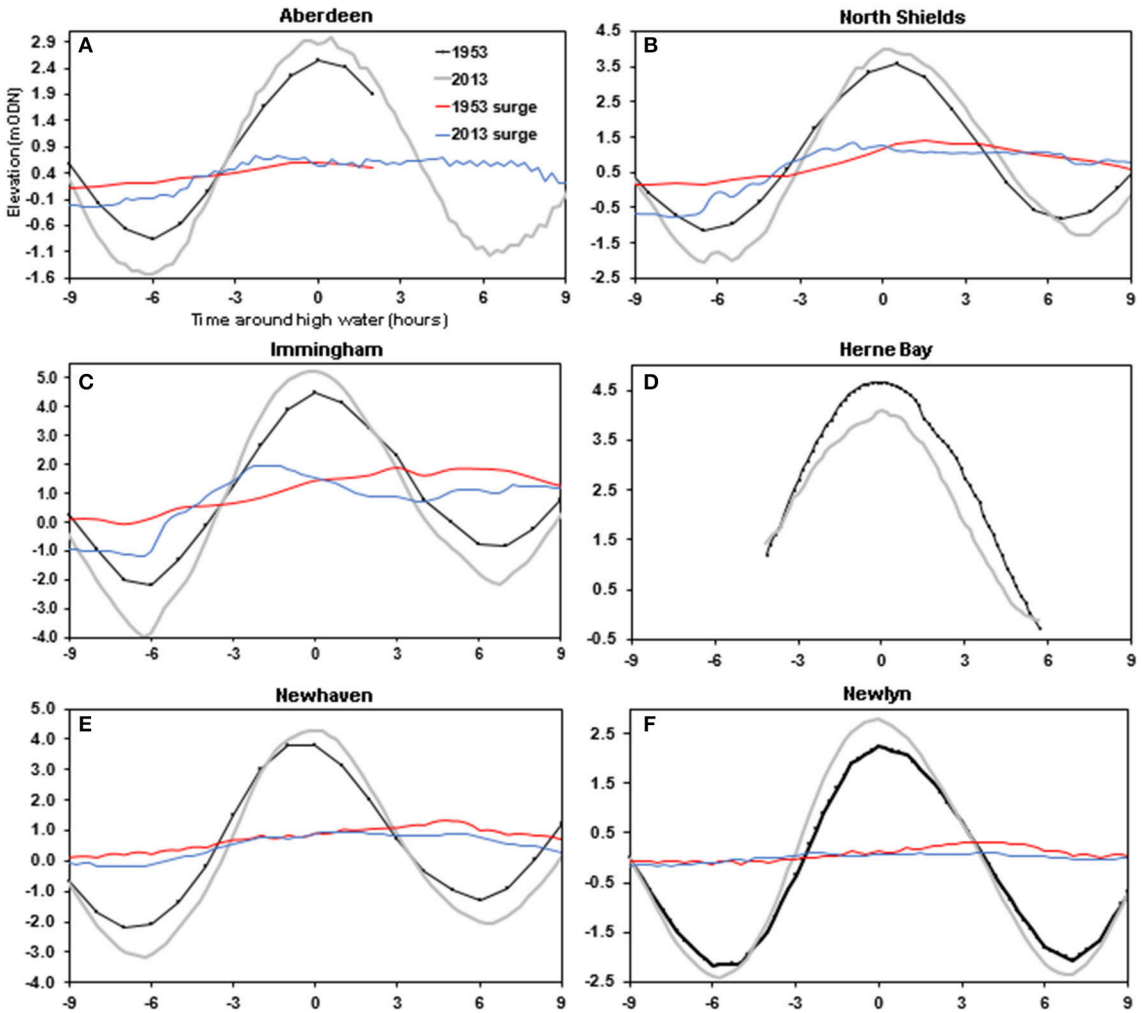

FIGURE 7 | Selection of 1953 and 2013 sea level time series recorded and corresponding surge values at: (A) Aberdeen, (B) North Shields, (C) Immingham, (D) Herne Bay, (E) Newhaven, and (F) Newlyn; with 1953 sea level and surge represented by the black and red lines, and the 2013 sea level and surge represented by the gray and blue lines.

Lowestoft-Norwich, Lowestoft-Ipswich, and Brighton-Seaford) which caused disruption—for example in Sussex flooding occurred during the morning of 6 December (at peak commute times). Some communities and habitats on the east coast are in the process of recovering more than a year on from the event (e.g., BBC, 2014c,d; National Trust, 2014). Both events caused substantial coastal erosion (an issue which is discussed less in this paper than flooding). This includes morphological changes that were both permanent (e.g., cliff collapse) and temporary (e.g., over-wash of barriers, breaches which have since re-sealed). The 1953 storm was a prominent morphological event along the Suffolk coastline (Pye and Blott, 2006, 2009)—and comparisons of barrier retreat (Grove, 1953; Spencer et al., 2015) for Covehithe (Suffolk) and Scolt Head (Norfolk) suggest 1953 was more severe (in erosion terms) than 2013. More recently there has been the increasing availability of data and methods which allow for a detailed spatial analysis: Spencer et al. (2015) determined that the December 2013 event resulted in "a pulse of shoreline translation landwards equivalent to about 10 years of normal shoreline retreat." In northeast, the higher 2013 HW (than 1953) caused greater coastal erosion and damage. For example, the 2013 event damage caused to Spurn Head (the iconic sand spit at the mouth of the Humber) was described as a site of "desolation" and for which a "new landscape" emerged (whilst Steers noted this area was not severely impacted in 1953) (Hull Daily Mail, 2013). In NW England, the 2013 impacts included dune frontage losses (4.5–12 m) along the Sefton shoreline in Liverpool Bay (Smith, 2014), and retreat of dunes in the order of 10 m in multiple locations in Wales (CNC/NRW, 2014b).

Off the west coast, storm conditions in the Irish Sea sank the Princess Victoria on the morning of 31 January 1953, killing 133 people (Jonkman and Kelman, 2005); although there are no reports of flooding in adjacent coastal areas. In contrast, during the better forecasted 2013 event there were no maritime

TABLE 3 | Summary of the impacts during the 1953 and 2013 events in the UK, primarily from data compiled by the Environment Agency.

Category	1953	2013
Deaths (flood related)	307	0
People evacuated	32,000	18,000
Properties flooded	24,000	2,800
Defense breach locations	1200	< 50
Land area inundated (Km^2)		
Agricultural	650	68
Total	834 (Steers, 1953)	N/A
Industrial sites inundated	200	N/A
Livestock killed	47,000 cattle 140,000 poultry	100 sheep/cattle 700,000 poultry
Energy supply impacts	2 power stations, 12 gas works	Electricity sub station flooded in Middlesbrough
Ports impacted	Tilbury, Felixstowe	Immingham
Transport impacts		
Roads	160 km	>160 km
Railways	320 km	200 km
Cost (for year 2014)	£1.2 Bn*	£0.25 Bn**
Worst hit county	Essex	Lincolnshire
County with most extreme sea levels	Suffolk	North Lincolnshire

**MetOffice (2014a).*

***An accurate figure for 2013 damage costs is unavailable—this is an approximation based upon estimates of defense and property damage (Section Comparison of Coastal Flooding and Impacts and Appendix 2 in Supplementary Materials).*

disasters, but flooding hit coastal communities during the early afternoon on 5 December, on the north coast of Wales and the west coast of England. The town of Rhyl (North Wales) was severely impacted and over 400 people evacuated. In northwest England sea walls were overtopped and there were instances of flooding around Liverpool Bay. Further north there were also floods across Lancashire, notably in Blackpool, and Cumbria.

The 1953 storm had major impacts in Scotland, exacerbated by the post-war disrepair of defenses (Lamb, 1991; Hickey, 2001). Nineteen people died in boating-related incidents caused by the rough seas and more than 41 locations were affected by coastal flooding (Hickey, 2001). Impacts were felt along almost the entire coastline of mainland Scotland and as far north as the Orkney Isles—and Hickey (2001) concluded: *"The storm of 31 January to 1 February 1953 is probably the most devastating to have affected Scotland over the last 500 years."* Coastal flooding mostly occurred in the Orkney Isles and NE Scotland. The 2013 storm also caused wind-related damages and coastal flooding—although most notably on the west coast for example in the town of Oban within Argyll and Bute.

In the northern regions of the English North Sea, coastal damage was reported in both 1953 and 2013, with flooding in Northumberland, Durham, and on the coasts of north-east Yorkshire. The 2013 event was here, in places, more severe than 1953. The Tyne catchment was affected by flooding in both events—although the effects are more pronounced in 2013 for the city of Newcastle, 15 km from the River Tyne Entrance where the HW was 1 in 400 years at North Shields. Further south at Sunderland on the River Wear there were incidences of flooding in 2013 (but no known flooding during 1953). In the Yorkshire town of Whitby the 2013 HW was half a meter higher than in 1953, and up to 200 properties were flooded in 2013 (whereas in 1953 there is only evidence of overtopping). In the Humber, following flood warnings throughout the day, water began to overtop defenses at Victoria Dock in Hull at 17:30, 5 December 2013 (Skinner, 2013). The city's flood barrier held, with 0.4 m to spare, although overtopping at other locations flooded 400 properties (HCC, 2014). The Port of Immingham flooded, with severe damage to the dock facilities (ABPmer, 2014). Locations along the tidal River Trent (connected to the Humber) were also flooded.

The county of Lincolnshire suffered 42 fatalities in 1953: towns from Cleethorpes and southwards were badly hit and it was reported that "the army took over" in what the press dubbed the "Lincolnshire Dunkirk." Situated approximately 18 km from the North Sea on the River Nene in the Fens of Cambridgeshire, the town of Wisbech experienced flooding in both events, although more severely during 1953. In Norfolk the 1953 event killed over 100 people (80 of these fatalities were in north Norfolk) (Kelman, 2009), and ruined 3500 homes (BBC, 2003). In just one coastal section (Heacham and Downham Market) 40 km^2 of land was flooded (Grove, 1953). The 2013 event inundated 150 properties and at least 4.8 km^2 of land in north Norfolk (Spencer et al., 2015). Erosion and environmental impacts in 2013 were severe although not as dramatic as in 1953. Steers (1953) noted that *"Along the coast of north Norfolk, from Old Hunstanton to Weybourne, the most obvious effect of the storm was the flooding of all the reclaimed marshes. The sea walls were overtopped, and breaches formed in most cases from the rear."* At King's Lynn, one-fifth of the town flooded in 1953, 1800 people were evacuated from their homes and there were 15 deaths—cars were picked up by the force of the floodwater and the streetlights of London Road *"exploded"* as the water rose, plunging the town into darkness as dead animals floated down the streets (Lynn Museum, n.d.). Along the cliffed coast of Norfolk, the 1953 event caused flooding and erosion, particularly the lower cliffs at Bacton and Walcott. Walcott was flooded in 2013, although more severely in 1953 when the town's main street was *"destroyed, and many buildings wrecked"* (Steers, 1953). Further south, at Great Yarmouth, 10 people were killed in 1953, and floods ruined 3500 homes (BBC, 2003); whereas in 2013 *"a few"* properties were flooded and 600 people were moved to an evacuation center (GYBC, 2014).

In Suffolk, as a result of the 1953 event there was *"not a single estuary or valley that was not affected by the flooding"* (Steers, 1953) and off the coast the Lowestoft trawler *Guava* sank, killing 11 men. On land 46 people were killed (drowned, shock, or exposure) and >20,000 acres of land were flooded (Suffolk Coastal, 2013). This included 41 deaths in Felixstowe due to the catastrophic collapse of flood walls on the Orwell Estuary. The resulting torrent of water flooded the south of the town, and at Langer (an estate of single story prefabricated houses), homes were washed away and occupants struggled to climb to safety on their roofs, and 30 died (Baxter, 2005). The 2013 event inundated 230 properties across the county, and the town of Lowestoft was flooded in both events (LL, 2014)—although more severely in

1953 (approximately 400 properties, compared to 100 in 2013). There were however no fatalities in Lowestoft from the 1953 flood (e.g., GNUK, 2013). In Essex the 1953 flood killed 120 people—impacts were much less in 2013 (40 properties flooded, no loss of life). Particularly high mortality rates occurred at Jaywick (36 of the 700 residents died) and Canvey Island (58 of 12,000 residents were killed), from a combination of drowning and exposure (including strokes, heart failure, and accidents) (Grieve, 1959; Baxter, 2005; Jonkman and Kelman, 2005). A further 889 flood casualties were admitted/treated at the local hospitals, and additional deaths of elderly (after the flood) are not recorded in the official figures (Baxter, 2005). In Harwich, seven people were killed as floodwater flowed into the town from three sides (HD, 2014), described as a "*two meter high wall of rolling water*" (ERO, 2013).

In the Thames region on 31 January-1 February 1953, flooding impacted Tilbury to London's docklands. Oil refineries, factories, cement works, gasworks, and electricity generating stations were flooded and brought to a standstill. In London's East End, 100 yards [91 m] of sea wall collapsed, causing more than 1130 houses to be flooded killing one person at Tidal Basin (Taylor, 2011) and 640,000 m^3 of Thames water to flow into the streets of West Ham (MetOffice, 2014b). Floods impacted the BP oil refinery on the Isle of Grain, and the Naval Dockyard at Sheerness. The 1953 HW did not quite overtop the Thames embankment and proceed to flood central London. In Kent, during 1953 more than 5000 acres [20 km^2] land was flooded, and thousands of livestock were drowned; whereas in 2013 the county did not experience as widespread flooding as was predicted (1000 homes in Sandwich, Seasalter, Faversham, and Medway were evacuated). There are no known incidences of the 1953 event causing flooding on English Channel coasts, which is in contrast to 2013. In Sussex homes, roads, railways, and Shoreham airport were inundated on the 6 December. Locations in West Sussex, Havant, Chichester, Isle of Wight, Hampshire, and the New Forest were flooded overnight, mainly those within the tidal reaches of rivers and harbors. Sea water covered roads and threatened properties as far along the English Channel as the city of Southampton (over 600 km along the coast from Lincolnshire, and 200 km west of Dover).

DISCUSSION

The first objective was to compare the meteorological characteristics of the 1953 and 2013 events. Both were storm types known to produce dangerous surges over the North Sea; although as highlighted the 2013 event also produced extreme sea level conditions on the west coast (especially Liverpool Bay). On the east coast, the 1953 storm moved more slowly as it tracked toward the southern North Sea. This caused a more extreme sea surface response and higher HWs in the Anglia, Thames, and North Kent regions; whereas the 2013 HW was more extreme to the north of Norfolk (and also outside of the North Sea). As noted by Flather (1984) the intensity, track, elongation, and slow speed, were all characteristics that made the 1953 storm capable of producing such severe wave and surge conditions in the southern North Sea.

The second objective, to compare high water levels, included a collation of sea levels at 100 observation locations around the UK. Both events generated extreme return period HWs—the 1953 HWs were larger than the 1 in 500 year return period at 23 locations, and the 2013 HWs were above this threshold at 18 locations. The extremity of some of the very large return periods (>1000 years) could be artifacts of the data length and analysis, although mostly are in locations where the meteorological conditions and local impacts are also documented as severe (e.g., North Norfolk in both events; Southwold, Aldeburgh, and Herne Bay in 1953; Spurn Head and Humber region in 2013). There was a difference in the spatial footprint of the events. The available data suggests that the 1953 extreme HWs began with a 1 in 2 year HW at Aberdeen, and moving south to a 1 in 1 year HW at Portsmouth. Muir Wood et al. (2005) remarked that the 1953 surge affected 1600 km of the coastline of eastern England. In addition to the east coast, the 2013 observations show that extreme HWs affected the west coast along two separate 350 km-long coastal segments: the four tide gauges from north Wales to Morecambe Bay (Holyhead, Llandudno, Liverpool, and Heysham) and four gauges in northwest Scotland (Tobermory, Ullapool, Stornoway, and Kinlochbervie). In-between these areas there were non-extreme HWs (at the Workington, Port Erin, Portpatrick, and Millport gauges on the coastline adjacent to the Isle of Man and Northern Island). The south coast footprint of 2013's extreme HWs was from Dover to West Bay, Dorset (a 1 in 1 year HW)—an almost 400 km coastal length. The larger spatial footprint of the 2013 extreme HWs highlights the significance of the astronomical tidal component. When it is a period of spring tides, then it will be spring tide mostly everywhere within the same cycle; whereas the extreme surge generation of 1953, as commented by Flather (1984), took place in a few areas of limited extent where the strongest winds and currents occurred in a favorable combination. In the southern North Sea, the 1953 surge was more than 1 m larger than the surge of 2013; whereas the tide of the 1953 event was in places approximately 0.5 m less than that of the 2013 event—due to the 2013 event occurring in the middle of the spring cycle, and being toward the peak of the 18.6 year lunar nodal cycle. Steers (1953) commented that (of the 1953 HW): *"the surge did not occur at the top of the tide and, did not occur on a high spring tide: the predicted tides for January 31 were 1–3 feet [0.3–0.9 m] less (according to locality) than can occur at other times of the year."*

There are many further factors that caused the different incidences of flooding between the events and locations. Waves superimposed upon extreme HWs are a particularly critical factor: damage and overtopping can occur from the impacts of individual waves, and also from increased still water level. Wave setup can contribute to an increase in nearshore sea level of more than 10% of the deep water significant wave height (WMO, 1998). Spencer et al. (2015) compared numerical modeling of the 1953 event (Wolf and Flather, 2005) to the 2013 offshore wave observations; which suggested that significant waves heights in North Norfolk at Scolt Head and Cley would have been 2.2 m and 2.7 m in 2013, compared to 4.4 m and 5.5 m, respectively in 1953. The North Kent coastline is also orientated to have

faced the persistent northerly winds that ensued at the time of the 1953 HW. Hence both surge and wave set-up could explain the extreme HW the return periods observed during the 1953 event at the exposed coasts of Suffolk (Southwold and Aldeburgh) and North Kent (Herne Bay). Furthermore, longer wave periods are also likely (during 1953's prolonged northerly gales) which would have further exacerbated run-up and flooding. Observers commented that the 2013 event would have been much worse in Norfolk and Suffolk given larger waves (e.g., Suffolk Coastal, 2013). As previously noted, localized effects (e.g., bathymetry combined with various nearshore storm-tide-wave processes) along this coastline can cause complex alongshore variations in HW (Lewis et al., 2013); as reflected in the surveys of Spencer et al. (2014, 2015).

In Liverpool Bay, the 2013 event comprised an ideal combination of conditions to cause coastal flooding, which included south-westerly winds that veered to the west, which also coincided with high tide (within the large tidal range of this region) (c.f. Brown et al., 2010). In other work, consideration of wave height and HW in a joint probability analysis at Liverpool vastly increased the event return period estimate (to >1 in 200 years), compared to considering water level alone; with the same analysis having the opposite effect in Suffolk (Wadey et al., 2015). The 2013 HWs were larger than 1953 HWs in several rivers and estuaries; for example, the Rivers Tyne and Humber, and also at Boston and King's Lynn. The tide and the storm track may be attributed to this; and in Suffolk there were some higher 2013 HWs along rivers (e.g., the Deben) which were in contrast to adjacent open coast areas (where 1953 HWs had been larger). Several aspects of these events warrant future work; for example the influence of (freshwater) river levels, since Steers (1953) commented how it was fortunate that the rivers (particularly those flowing through the fenlands—the marshy areas of eastern England) were not in flood, which would have resulted in extensive freshwater flooding. Given additional influences such as wave set-up and freshwater input, future joint-probability comparisons could consider additional variables to sea (tide-surge) level. It should also be noted that where there were hourly water level values (in the 1953 data) these are more likely to have underestimated maximum HW readings (whereas the tide gauges in 2013 provided readings of at least 15-minute resolution).

The linear MSL trend 1915–2014 at Newlyn suggests 0.11 m SLR from 1953 to 2013 (Wadey et al., 2014). The magnitude of the respective tide and surges of the events, and the effects of waves, make it awkward to infer what role that changes to MSL may have played in the 2013 flood event. However, in south coast areas where tidal range and surge heights are less extreme than on the west and east coasts, this may have important future implications. For example in the city of Southampton properties on low-lying, undefended areas of the River Itchen came with "several centimeters" of flooding (Taylor, 2013). As sea levels rise, future surges that propagate from the North Sea will be a growing threat, although the worst coastal impacts to the central and southwest English Channel coast result from south-westerly storms (since the accompanying extreme waves can overtop coastal defenses) (e.g., Wadey et al., 2013a,b; Palmer et al., 2014).

The starkest contrast between these events was the greater human impact of the 1953 floods, especially the large loss of life. Floods also inundated more land and were more prolonged, with the destruction of properties and damage (for many years) of large swathes of agricultural land. This is partly attributed to the complete lack of flood warnings, the poor state of coastal flood defenses, and vulnerable post-war (e.g., prefabricated) housing. The risk management responses to this event were pivotal in reduction of consequences in events since then, including in 2013.

CONCLUSIONS

This paper has described and compared the two most significant North Sea surge events to impact the UK over a 60-year period. This included descriptions of meteorological conditions, a collation of high water data at 100 locations, and an overview of flooding impacts.

The first objective, a comparison of the storms, utilized a wind and pressure field data set; and also revisited observations from previous studies. This highlights how both storms shared some similarities in the northern UK, but the 1953 storm tracked further south, in an unusually slow manner which caused extreme wave and surge setup in the southern North Sea. The nature of the 2013 storm's track over the west coast was also conducive to extreme sea levels in those regions, particularly in Liverpool Bay.

The second objective, the high water comparison, highlighted that both storms produced extreme sea levels, especially on the east coast. In 1953 these were dominated by the surge component, particularly in the southern North Sea. The 2013 event produced similar surge heights to 1953 in northeast England and towards Norfolk, but was also characterized by a large tidal component. In 2013 however, there was not such strong wind set-up in the southern North Sea. The 1953 data is too sparse for a definitive comparison with 2013 on the west coast and for much of the English Channel; although the available observations suggest that the 2013 event produced more extreme sea levels (than 1953) in northwest England and the English Channel. Both surges propagated eastwards at least as far as Newlyn, where 1953's surge was larger but the total HW was smaller (as a result of the larger tide in 2013). The assessment of floods also revealed complex spatial variations that we could not fully explain. For example the 1953 and 2013 floods were worse than one another for different areas in Scotland; whilst Spencer et al. (2014) observed detailed alongshore variability in Norfolk's coastal water levels. Localized effects (e.g., tide locking of rivers, high rainfall, local magnification of surge, wind direction, waves, resonant waves etc.) may be relevant for a more detailed comparison of events at some locations, and are areas for future research.

The third objective, to compare the consequences of each event, captured only a small but representative sample of the human (and other) impacts that occurred. Both events caused extensive flooding, with the worst impacts aligning quite closely with the locations of the most extreme HWs. The 31 January–1 February 1953 floods are well-known as the worst natural catastrophe to impact the UK in living memory. This was a

consequence of the extremity of the surge and wave conditions, the lack of warnings and preparation, and the pre-existing state of the defenses. Floods severely impacted Scotland and the east coast from Lincolnshire to Kent, with highest loss of life in Essex. The 2013 floods also occurred mainly along the east coast, although particularly affecting regions further north (e.g., Humber and North Lincolnshire). However, 2013 was not just an east coast flood, with floods also in northwest England, Wales and on the south coast as far as the Solent—areas outside of the North Sea accounted for up to 20% of the national total of flooded properties.

The analysis here illustrates the value of tide and wave data to characterize and understand extreme coastal flood events. However, hourly records from many tide gauges have been lost or are inaccessible for the 1953 event, only single HW values remain. This lack of sea level time series is unfortunate, and limits the detail within the HW comparison. Furthermore, many of these values are accompanied by some uncertainty. Given the sparse data available for the 1953 event, it would be interesting in future work to generate comparative numerical simulations of the 1953 and 2013 events to further explore their different behavior, such as the high sea levels on the west coast. This would build on the earlier work such as Wolf and Flather (2005). Field collection of HW marks (Steers, 1953; Spencer et al., 2014, 2015) complement (and can compensate for) a lack of digital data. In related work, Haigh et al. (2015) have developed a UK database called SurgeWatch (http://www.surgewatch.org). This paper's collation of data about the 1953 event allows a comparison with other events such as the 2013 event, and is an integral part of the database. Similar analyses are happening elsewhere (e.g., Needham et al., 2015). This shows that it is important that coastal flood events are systematically monitored and understood. Such documentation of flood event characteristics, mechanisms and impacts can provide useful data for future flood planning, and education.

ACKNOWLEDGMENTS

We thank the following for providing sea level data: the British Oceanographic Data Centre, National Tidal, and Sea Level Facility, Channel Coastal Observatory, Associated British Ports; and the Environment Agency (also for the sea level return periods). MW, IH, and JB's contributions to this paper were funded through the Engineering and Physical Science Research Council (EPSRC) Flood Memory Project (grant number EP/K013513/1).

SUPPLEMENTARY MATERIAL

The Supplementary Material for this article can be found online at: http://journal.frontiersin.org/article/10.3389/fmars.2015.00084

REFERENCES

ABI. (2006). *Coastal Flood Risk – Thinking for Tomorrow, Acting Today*. Summary report commissioned by the Association of British Insurers, caried out by by Entec in collaboration with Risk Management Solutions and Risk & Policy Analysts. Available online at: http://static1.1.sqspcdn.com/static/f/270724/1875611/1220367794127/abi_coastal_flooding_report.pdf?token=u6qVELwpoHYO6xSI99wr9agO0ww%3D (Accessed November 19, 2014).

ABPmer. (2014). *Ensuring Flood Resilience: An overview of 5/6 December 2013 UK storm surge*. Report: 1400/30. ABP Marine Environmental Research.

Artemis. (2013). *Flood Defences Keep Windstorm Xaver Insured Losses Down*. Available Online at: http://www.artemis.bm/blog/2013/12/11/flood-defences-keep-windstorm-xaver-insured-losses-down/ (Accessed July 14, 2015).

Baker, E. (2006). *A History of Firefighting*. Jeremy Mills Publishing.

Bates, P. D., Dawson, R. J., Hall, J. W., Horritt, M. S., Nicholls, R. J., Wicks, J., et al. (2005). Simplified two-dimensional numerical modelling of coastal flooding and example applications. *Coast. Eng.* 52, 793–810. doi: 10.1016/j.coastaleng.2005.06.001

Batstone, C., Lawless, M., Tawn, J., Horsburgh, K., Blackman, D., McMillan, A., et al. (2013). A UK best-practice approach for extreme sea-level analysis along complex topographic coastlines. *Ocean Eng.* 71, 28–39. doi: 10.1016/j.oceaneng.2013.02.003

Baxter, P. J. (2005). The east coast Big Flood, 31 January–1 February 1953: a summary of the human disaster. *Philos. Trans. R. Soc.* 363, 1293–1312. doi: 10.1098/rsta.2005.1569

BBC. (2003). *Norfolk Remembers the Floods of 1953 - 01 February 2003 1642 GMT*. Available Online at: http://www.bbc.co.uk/norfolk/senseofplace/floods1953.shtml (Accessed November 19, 2014).

BBC. (2013a). *400 People Leave Homes in Rhyl After Flooding. 5 December 2013 Last Updated at 19:20 GMT*. Available Online at: http://www.bbc.co.uk/news/uk-wales-25237781 (Accessed November 13, 2013).

BBC. (2013b). *Flooding in New Brighton leaves cars and shops under water 5 December 2013 Last updated at 16:19*. Available Online at: http://www.bbc.co.uk/news/uk-england-merseyside-25232665 (Accessed November 13, 2014).

BBC. (2013c). *Newcastle Storms: Court Evacuated Over River Flooding 5 December 2013 Last Updated at 18:25*. Available Online at: http://www.bbc.co.uk/news/uk-england-tyne-25231342 (Accessed November 13, 2014).

BBC. (2013d). *Shoreham Airport Under Water After Tidal Surge. 6 December 2013 Last Updated at 18:52 GMT*. Available Online at: http://www.bbc.co.uk/news/uk-england-sussex-25267611 (Accessed November 13, 2013).

BBC. (2013e). *Tidal Surge: Homes in Whitby flooded 6 December 2013 Last updated at 14:05 GMT*. Available Online at: http://www.bbc.co.uk/news/uk-25258150 (Accessed November 13, 2014).

BBC. (2013f). *Flood of 1953: Memories from Kent. 30 January 2013*. Available Online at: http://www.bbc.co.uk/news/uk-england-kent-21262231 (Accessed March 25, 2015).

BBC. (2013g). *Flood of 1953: Protecting Kent from Another Surge. 31 January 2013*. Available Online at: http://www.bbc.co.uk/news/uk-england-kent-21274713 (Accessed March, 2015).

BBC. (2013h). *Norfolk Floods: Seven Hemsby Homes Badly Damaged by Waves. 6 December 2013*. Available online at: http://www.bbc.co.uk/news/uk-england-norfolk-25254808 (Accessed April 22, 2015).

BBC. (2013i). *Lethal Storm and Tidal Surge Sees Thousands Out of Homes. 6 December 2013*. Available Online at: http://www.bbc.co.uk/news/uk-25220224 (Accessed April 22, 2015).

BBC. (2014a). *The Great 1928 Flood of London. BBC News Magazine*. Available Online at: http://www.bbc.co.uk/news/magazine-26153241 (Accessed February, 2014).

BBC. (2014b). *10 Key Moments of the UK Winter Storms, 17 February 2014. BBC News*. Available Online at: http://www.bbc.co.uk/news/uk-26170904 (Accessed April, 22 2015).

BBC. (2014c). *East Coast Storm Surge: What Happened Next? BBC News Norfolk. By Richard Haugh, 5 December 2014.* Available Online at: http://www.bbc.co.uk/news/uk-england-norfolk-30183045 (Accessed May, 14 2015).

BBC. (2014d). *Boston Floods: A Year on from the Tidal Surge. By Dave Wade BBC News, East Midlands.* Available Online at: http://www.bbc.co.uk/news/uk-england-lincolnshire-30225852 (Accessed May, 14 2015).

Berwickshire News. (2013). *VIDEO: Storm Hits Eyemouth Harbour, by Simon Duke.* Available Online at: http://www.berwickshirenews.co.uk/news/local-news/all-local-news/video-storm-hits-eyemouth-harbour-1-3222261 (Accessed November, 13 2014).

Blake, E. S., Kimberlain, T. B., Berg, R. J., Cangialosi, J., and Beven, II, J. L. (2013). Tropical cyclone report: hurricane sandy. *Nat. Hurric. Center* 12, 1–10. Available online at: http://www.nhc.noaa.gov/data/tcr/AL182012_Sandy.pdf

Bradley, S. L., Milne, G. A., Teferle, F. N., Bingley, R. M., and Orliac, E. J. (2009). Glacial isostatic adjustment of the British Isles: new constraints from GPS measurements of crustal motion. *Geophys. J. Int.* 178, 14–22. doi: 10.1111/j.1365-246X.2008.04033.x

Brown, J. M., Souza, A. J., and Wolf, J. (2010). An investigation of recent decadal-scale storm events in the eastern Irish Sea. *J. Geophys. Res.* 115, C05018. doi: 10.1029/2009JC005662

Chronicle Live. (2013). *Newcastle Quayside Flooded Following Tidal Surge Caused by Storm - 21:42, 5 December 2013. By Sarah Jeffery.* Avaialble Online at: http://www.chroniclelive.co.uk/news/north-east-news/newcastle-quayside-flooded-following-tidal-6377123 (Accessed March, 2015).

CNC/NRW. (2014a). *Wales Coastal Flooding Review Phase 1 Report – Assessment of Impacts. Cyfoeth Naturiol Cymru/Natural Resources Wales.* Available Online at: http://naturalresourceswales.gov.uk/content/docs/pdfs/flooding-and-alerts-pdfs/wales-coastal-flooding-review-phase-1.pdf?lang=en (Accessed November 13, 2014).

CNC/NRW. (2014b). "Welsh coastal storms, december 2013 & january 2014 – an assessment of environmental change," in *Natural Resources Wales Natural Resources Wales Evidence Report No. 33* eds C. Duigan, N. Rimington, and M. Howe. Available Online at: http://naturalresources.wales/media/1976/welsh-coastal-storms-december-2013-and-january-2014-an-assessment-of-environmental-change.pdf (Accessed May 13, 2015).

Collins, R. (2013). *The 1953 Lincolnshire Floods ∼ Disaster ! Lincolnshire thro' History, Life, Lens and Words. A Site About Everything and Nothing!* Available Online: http://www.rodcollins.com/wordpress/the-1953-lincolnshire-floods-disaster (Accessed November 4, 2014).

Compo, G. P., Whitaker, J. S., Sardeshmukh, P. D., Matsui, N., Allan, R., Yin, X., et al. (2011). The twentieth century reanalysis project. *Q. J. R. Meteorol. Soc.* 137, 1–28. doi: 10.1002/qj.776

Curran, J. (2014). *Agency board meeting 11 February 2014.* Chief Executive's Report, Board report Number: SEPA 09/14, Scottish Environment Protection Agency (SEPA). Available Online at: https://www.sepa.org.uk/media/41535/sepa-09-14-chief_executive_report_feb2014.pdf (Accessed November 9, 2014).

Davies, A. (2013). *Statement: Recent Flooding in North Wales - your Senedd.* Available Online at: http://www.yoursenedd.com/debates/2013-12-10-statement-recent-flooding-in-north-wales (Accessed November 13, 2014).

De Kraker, A. M. J. (2006). Flood events in the southwestern Netherlands and coastal Belgium, 1400–1953. *Hydrol. Sci. J.* 51, 913–929. doi: 10.1623/hysj.51.5.913

de Vries, H., Breton, M., de Mulder, T., Krestenitis, Y., Ozer, J., Proctor, R., et al. (1995). A comparison of 2D storm surge models applied to three shallow European seas. *Environ. Softw.* 10, 23–42. doi: 10.1016/0266-9838(95)00003-4

EA. (2011). *Somerset Floods - 30 Years On! 13-Dec-2011 Environment Agency.* Available online at: http://www.environment-agency.gov.uk/news/135721.aspx

EA. (2014a). *Appendix (b) Section 19 December 2013 East Coast Surge. Environment Agency.* Available Online at: http://lincolnshire.moderngov.co.uk/documents/s7054/Tidal%20Surge%20Event%20-%20Coastal%20Surge%20-%20Appendix%20A3.pdf (Accessed November 4, 2014).

EA. (2014b). *Managing Flood and Coastal Erosion Risks in England 1 April 2013 to 31 March 2014. Environment Agency.* Available Online at: https://www.gov.uk/government/uploads/system/uploads/attachment_data/file/356341/S18_report_2013_14_Final_v2.pdf (Accessed November, 19 2014).

EA. (2014c). *Tidal Surge Recovery Briefing, Environment Agency 28 March 2014.* Available Online at: http://www.norfolkcoastaonb.org.uk/mediaps/pdfuploads/pd003172.pdf (Accessed November 4, 2014).

EA. (2014d). *Properties Flooded Since the Start of December 2013. Figure Produced by the Environment Agency, Ref no: 100026380, 2014.* Available Online at: https://www.facebook.com/environmentagency/photos/a.10152005392033026.1073741829.169797688025/10152005392148026/ (Accessed April 22, 2015).

EA/GOVUK. (2014). *Work Begins on Boston Flood Bank - Press Release by the Environment Agency 1 October 2014.* Available Online at: https://www.gov.uk/government/news/work-begins-on-boston-flood-bank (Accessed April 22, 2015).

ERO. (2013). *The 1953 Floods in Essex - from the Blog of the Essex Record Office, the Storehouse of Essex History.* Available Online at: http://www.essexrecordofficeblog.co.uk/the-1953-floods-in-essex/ (Accessed October 31, 2014).

ERYC. (2014). *Flood Investigation Report - Tidal Surge on 5 December 2013. Report to The Cabinet, 24 June 2014 by East Riding of Yorkshire Council.* Available Online at: http://www.eastriding.gov.uk/public_reports/TheCabinet/24%20June%202014/Flood%20Investigation%20Report%20-%20Tidal%20Surge%20on%205%20December%202013.pdf (Accessed November, 13 2013).

Essex Life (2013). *Personal Memories of the Floods of 1953.* Available online at: http://www.essexlifemag.co.uk/people/personal_memories_of_the_floods_of_1953_1_1923995 (Accessed October 26, 2015).

Essex Record Office (2013). *The 1953 Floods in Essex. The Blog of the Essex Record Office, the Storehouse of Essex History.* Available online at: http://www.essexrecordofficeblog.co.uk/the-1953-floods-in-essex/ (Accessed October 26, 2013).

Fenland Citizen (2013). *Flooding in Wisbech.* Available online at: http://www.fenlandcitizen.co.uk/news/latest-news/flooding-in-wisbech-1-5731934 (Accessed March 25, 2015).

Flather, R. A. (1984). A numerical model investigation of the storm surge of 31 January and 1 February 1953 in the North Sea. *Q. J. R. Meteorol. Soc.* 110, 591–612. doi: 10.1002/qj.49711046503

Fritz, H. M., Blount, C. D., Thwin, S., Thu, M. K., and Chan, N. (2009). Cyclone Nargis storm surge in Myanmar. *Nat. Geosci.* 2, 448–449. doi: 10.1038/ngeo558

Gerritsen, H. (2005). What happened in 1953? The big flood in the Netherlands in retrospect. *Philos. Trans. R. Soc. A* 363, 1271–1291. doi: 10.1098/rsta.2005.1568

Gönnert, G., Dube, S. K., Murty, T. S., and Siefert, W. (2001). *Global Storm Surges: Theory Observation and Applications.* Heide in Holstein: Westholsteinische Verlagsanstalt Boyens & Co, 623.

GNUK. (2013). *UK: Memories of the Great Flood of 1953 – 310113 1310z - January 31, 2013 by Goaty's News.* Available Online at: https://goatysnews.wordpress.com/2013/01/31/uk-memories-of-the-great-flood-of-1953-310113-1310z/ (Accessed May 1, 2015).

Graff, J., and Blackman, D. L. (1978). Analysis of maximum sea levels in southern England. *Coast. Eng.* 53, 931–948. doi: 10.9753/icce.v16.%25p

Grieve, H. E. P. (1959). *The Great Tide: The Story of the 1953 Flood disaster in Essex.* Chelmsford: County Council of Essex.

GYBC. (2014). *Draft Report on the Council Response to the Tidal Surge 5/6th December 2013. Great Yarmouth Borough Council.* Available Online at: http://great-yarmouth.cmis.uk.com/Great-Yarmouth/Document.ashx? (Accessed November 19, 2014).

Grove, A.T. (1953). IV. The sea flood on the coasts of Norfolk and Suffolk. *Geography* 38, 164–170.

HCC. (2014). *Hull City Council Flood Investigation Report December 2013 City Centre Tidal Surge Flood Event. 4 February, 2014.* Available Online at: https://cmis.hullcc.gov.uk/ (Accessed November 13, 2014).

HD. (2014). *A Memorable Year: Harwich Flood Disaster 1953. Website published by Harwich & Dovercourt "a time gone by".* Available Online at: http://www.harwichanddovercourt.co.uk/a-memorable-year/ (Accessed October 28, 2014).

Haigh, I., Butcher, P., Harris, J. M., Cooper, N. J., and Trip, I. (2004). "Developing an improved understanding of storm surges in the Solent," in *39th DEFRA Flood and Coastal Management Conference, June 29 - July 1 2004,* (York).

Haigh, I., Nicholls, R., and Wells, N. (2010). Assessing changes in extreme sea levels: application to the English Channel, 1900–2006. *Continen. Shelf Res.* 30, 1042–1055. doi: 10.1016/j.csr.2010.02.002

Haigh, I. D., Wadey, M. P., Gallop, S. L., Loehr, H., Nicholls, R. J., Horsburgh, K., et al. (2015). A user-friendly database of coastal flooding in the United Kingdom from 1915–2014. *Sci. Data* 2:150021. doi: 10.1038/sdata.2015.21

Harwood. (2013). *Highest North Sea Surge for 60 Years. eSurge.* Available Online at: http://www.storm-surge.info/highest-north-sea-surge-60-years (Accessed May 28, 2015).

Heart. (2013). *Essex: Flooding Latest. 6th December 2013, 11:29.* Available Online at: http://www.heart.co.uk/essex/news/local/west-mersea-severe-flood-warning-issued/ (Accessed November 13, 2013).

Henderson, G., and Webber, N. B. (1977). Storm surges in the UK south coast. *Dock Harb. Authority* 57, 21–22.

Hickey, K. R. (2001). The storm of 31 January to 1 February 1953 and its impact on Scotland. *Scott. Geograph. Magaz.*117, 283–295. doi: 10.1080/00369220118737129

Horsburgh, K. J., Williams, J. A., Flowerdew, J., and Mylne, K. (2008). Aspects of operational forecast model skill during an extreme storm surge event. *J. Flood Risk Manage.* 1, 213–221. doi: 10.1111/j.1753-318X.2008.00020.x

Horsburgh, K. J., and Wilson, C. (2007). Tide-surge interaction and its role in the distribution of surge residuals in the North Sea. *J. Geophys. Res.* 112, 1–13. doi: 10.1029/2006jc004033

Hull Daily Mail. (2013). *What Next for Spurn Point, left desolate by North Sea tidal Surge?* Available Online at: http://www.hulldailymail.co.uk/Spurn-Point-left-desolate-North-Sea-tidal-surge/story-20374811-detail/story.html (Accessed May 14, 2015).

Insurance Journal. (2013). *AIR Estimates Windstorm Xaver Insured Losses: $963 Million to $1.92 Billion. December 13, 2013.* Available Online at: http://www.insurancejournal.com/news/international/2013/12/13/314377.htm (Accessed July 14, 2015).

Insurance Times. (2013). *PwC: Friday's Floods to Cost Insurers up to £100m. 10 December 2013 |By Newsdesk*. Available Online at: http://m.insurancetimes.co.uk/pwc-fridays-floods-to-cost-insurers-up-to-100m/1406182.article (Accessed August 20, 2015).

ITV. (2013). *North Blyth Hit by Floods - 5 December 2013 at 7:35pm*. Available Online at: http://www.itv.com/news/tyne-tees/update/2013-12-05/north-blyth-hit-by-floods/ (Accessed November 14, 2014).

IWCP. (2013). *Firefighters on Alert for Flooding; Article by Richard Wright, Friday, December 6, 2013, Isle of Wight County Press.* Available Online at: http://www.iwcp.co.uk/news/news/firefighters-on-alert-for-flooding-51989.aspx?mn=2 (Accessed November 13, 2014).

Johnson, M. (2014). *December 2013 Tidal Surge. Environment Agency Presentation by Mark Johnson – Area Coastal Manager, Essex Coastal Forum, 25 February 2014*. Available Online at: http://dnn.essex.gov.uk/coastalforum/AboutUs/Meetings.aspx (Accessed November 13, 2013).

Jonkman, S., and Kelman, I. (2005). "Deaths during the 1953 North Sea storm surge," in *Proceedings of the Solutions to Coastal Disasters Conference, American Society for Civil Engineers (ASCE)* (Charleston, SC). 8–11.

Jonkman, S. N., Maaskant, B., Boyd, E., and Levitan, M. L. (2009). Loss of life caused by the flooding of new orleans after hurricane Katrina: analysis of the relationship between flood characteristics and mortality. *Risk Anal.* 29, 676–698. doi: 10.1111/j.1539-6924.2008.01190.x

Kelman, I. (2009). *1953 Storm Surge Deaths: U.K. Version 5, 17 August 2009 (Version 1 was 30 November 2002)*. Available online at: http://www.ilankelman.org/disasterdeaths/1953DeathsUK.doc

Kent News (2013). *Remembering the Floods of 1953 - Devastation in North Kent*. Article by N. Ames. Available online at: http://www.kentnews.co.uk/news/remembering_the_floods_of_1953_1_1856346 (Accessed March 25, 2015).

Kent Online. (2013a). *Families Start to Return Home after Severe Flood Warnings for Kent and Hundreds of Homes Evacuated Amid Worst Tidal Storm Surge in Decades. 07 December 2013*. Available Online at: http://www.kentonline.co.uk/kent/news/kent-floods-9812/ (Accessed November 13, 2014).

Kent Online. (2013b). *Tidal Surge Brings Floods to Sandwich and Dover. 06 December 2013*. Available Online at: http://www.kentonline.co.uk/deal/news/tidal-surge-latest-residents-evacuated-9892/ (Accessed April 22, 2015).

Lamb, H. (1991). *Historic Storms of the North Sea, British Isles and Northwest Europe*. Cambridge: Cambridge University Press.

LeComte, D. (2014). International weather highlights 2013: super typhoon haiyan, super heat in Australia and China, a long winter in Europe. *Weatherwise* 67, 20–27. doi: 10.1080/00431672.2014.899800

Lennon, G.W. (1963). A frequency investigation of abnormally high tidal levels at certain west coast ports. *Proc. Inst. Civil Eng.* 25, 451–484. doi: 10.1680/iicep.1963.10543

Lewis, M., Schumann, G., Bates, P., and Horsburgh, K. (2013). Understanding the variability of an extreme storm tide along a coastline. *Estuar. Coast. Shelf Sci.* 123, 19–25. doi: 10.1016/j.ecss.2013.02.009

Lin, I. I., Chen, C. H., Pun, I. F., Liu, W. T., and Wu, C. C. (2009). Warm ocean anomaly, air sea fluxes, and the rapid intensification of tropical cyclone Nargis (2008). *Geophys. Res. Lett.* 36:L03817. doi: 10.1029/2008gl035815

LL. (2014). *Great Floods of Lowestoft 1953 & 2013. Posted on 29 April 2014 by 'Love Lowestoft'*. Available Online at: http://www.lovelowestoft.co.uk/tag/lowestoft-floods-1953/ (Accessed May 1, 2015).

Lumbroso, D. M., and Vinet, F. (2011). A comparison of the causes, effects and aftermaths of the coastal flooding of England in 1953 and France in 2010. *Nat. Hazards Earth Syst. Sci.* 11, 2321–2333. doi: 10.5194/nhess-11-2321-2011

Lynn Museum. (n.d.). *The 1953 Floods at King's Lynn*. Available online at: http://www.museums.norfolk.gov.uk/view/NCC095922 (Accessed March 2015).

May, V. (1980). *SPURN HEAD*. Available online at: http://jncc.defra.gov.uk/pdf/gcrdb/GCRsiteaccount2111.pdf (Accessed October 25, 2015).

McMillan, A., Batstone, C., Worth, D., Tawn, J. A., Horsburgh, K., and Lawless, M. (2011). *Coastal Flood Boundary Conditions for UK Mainland and Islands. Project: SC060064/TR2: Design Sea Levels*. Bristol: Environment Agency.

McRobie, A., Spencer, T., and Gerritsen, H. (2005). The big flood: north sea storm surge. *Philos. Trans. R. Soc. A* 363, 1263–1270. doi: 10.1098/rsta.2005.1567

MetOffice. (2014a). *1953 East Coast Flood - 60 Years On*. Available Online at: http://www.metoffice.gov.uk/news/in-depth/1953-east-coast-flood (Accessed February 2015).

MetOffice. (2014b). *The Devastation Floods Can Cause - Met Office Education*. Available Online at: http://www.metoffice.gov.uk/education/teens/case-studies/floods (Accessed November 19, 2014).

Mills, I., Scharroo, R., and Fenoglio, L. (2013). "Xaver affected much of northern Europe on 5 and 6 December and caused worst storm surge for decades in the North Sea," in *Report for EUMETSAT*. Available online at: http://www.eumetsat.int/website/home/Images/ImageLibrary/DAT_2087062.html (Accessed November 19, 2014).

Muir Wood, R., and Bateman, W. (2005). Uncertainties and constraints on breaching and their implications for flood loss estimation. *Philos. Trans. R. Soc. A* 363, 1423–1430. doi: 10.1098/rsta.2005.1576

Muir Wood, R., Drayton, M., Berger, A., Burgess, P., and Wright, T. (2005). Catastrophe loss modelling of storm-surge flood risk in eastern England. *Philos. Trans. R. Soc. A* 363, 1407–1422. doi: 10.1098/rsta.2005.1575

National Trust. (2014). *December 2013 Tidal Storm Surge, One Year On. Blakeney National Nature Reserve*. Available Online at: http://www.nationaltrust.org.uk/blakeney/visitor-information/article-1355872771719/ (Accessed May 14, 2015).

NCC. (2010). *Level 1 Strategic Flood Risk Assessment. Appendix A: Historical Flood Events. Northumberland County Council*. Available Online at: http://www.northumberland.gov.uk/idoc.ashx?docid=1f474bcd-b02e-46fd-bfb0-2faa7e12a41f&version=-1 (Accessed November 14, 2014).

NCC. (2015). *Northumberland County Council Flood Investigation Report - Investigation of the Tidal Surge 5th/6th December* 2013. Available online at: http://www.northumberland.gov.uk/WAMDocuments/9471BDBE-05BB-4730-8277-60F9ECC7D9E5_1_0.pdf?nccredirect=1 (Accessed November 13, 2014).

Needham, H., Keim, B. D., and Sathiaraj, D. (2015). A review of tropical cyclone−generated storm surges: global data sources, observations and impacts. *Rev. Geophys.* 53, 545–591. doi: 10.1002/2014RG000477

Neumann, B., Vafeidis, A. T., Zimmerman, J, and Nicholls, R. J. (2015). Future coastal population growth and exposure to sea-level rise and coastal flooding - a global assessment. *PLoS ONE* 10:e0118571. doi: 10.1371/journal.pone.0118571

News North Wales. (2014). *£11m Flood Plan for Denbighshire Set to be Approved- Published date: 23 July 2014 |Published by: Staff Reporter*. Available Online at: http://www.newsnorthwales.co.uk/news/135953/-11m-flood-plan-for-denbighshire-set-to-be-approved.aspx (Accessed November 13, 2014).

NRA Anglian. (n.d.). *Ipswich Flood Defences. National Rivers Authority Anglian Region., Monograph - Date Unknown (Before 1996).* Available Online at: http://ea-lit.freshwaterlife.org/archive/ealit:2828/OBJ/20001205.pdf (Accessed May 27, 2015).

NWRM. (2014). *North West Regional Monitoring Newsletter - Issue 3 - July 2014.*

Oban Times. (2013). *Winds Batter West Highlands and Islands - on December 5th,2013. The Oban & West Highland Times*. Available Online at: http://

www.obantimes.co.uk/2013/12/05/winds-batter-west-highlands-and-islands/ (Accessed November 13, 2014).

Palmer, T., Nicholls, R., Wells, N., Saulter, A., and Mason, T. (2014). Identification of 'energetic'swell waves in a tidal strait. *Cont. Shelf Res.* 88, 203–215. doi: 10.1016/j.csr.2014.08.004

Parker, S. (2014). *Flooding to properties in Rhyl - report by Steve Parker of Debignshire County Council*. Available online at: http://www.dailypost.co.uk/news/north-wales-news/magnitude-rhyl-floods-highlighted-shocking-8878726 (Accessed November 13, 2014).

Penning-Rowsell, E., Johnson, C., Tunstall, S., Tapsell, S., Morris, J., Chatterton, J., et al. (2005). *The Benefits of Flood and Coastal Risk Management: A Handbook of Assessment Techniques*. London: Middlesex University Press.

Plüß, A., Rudolph, E., and Schrödter, D. (2001). Characteristics of storm surges in German estuaries. *Clim. Res.* 18, 71–76. doi: 10.3354/cr018071

Pollard, M. (1978). *North Sea Surge: Story of the East Coast Floods of 1953*. Lavenham: Terence Dalton.

Posner, R. (2004). *Wyre Flood and Coastal Defence Strategy Plan, March 2004*. Report Produced by Wyre Borough Council.

Pratt, I. (1995). The storm surge of 21 February 1993. *Weather* 50, 42–48. doi: 10.1002/j.1477-8696.1995.tb06075.x

Pugh, D. T. (1987), *Tides, Surges and Mean Sea-Level: A Handbook For Engineers And Scientists*. Hoboken, NJ: John Wiley, 472.

Pye, K., and Blott, S. J. (2006). Coastal processes and morphological change in the Dunwich-Sizewell area, Suffolk, UK. *J. Coast. Res.* 22, 453–473. doi: 10.2112/05-0603.1

Pye, K., and Blott, S. J. (2009). Progressive breakdown of a gravel-dominated coastal barrier, Dunwich–Walberswick, Suffolk, U.K.: processes and implications. *J. Coast. Res.* 25, 589–602. doi: 10.2112/07-0982.1

Reeder, T. (2013). *The storm surge of 2013 – 6th December. London Climate Change Partnership*. Available online at: http://climatelondon.org.uk/articles/the-storm-surge-of-2013/ (Accessed October 31, 2014).

RMS. (2003). *1953 UK Floods: 50 Year Retrospective*. Risk Management Solutions.

Rossiter, J. R. (1954). The North Sea storm surge of 31 january and 1 february 1953. *Philos. Trans. R. Soc. Lond. Ser. A Math. Phys. Sci.* 246, 371–400. doi: 10.1098/rsta.1954.0002

Ruocco, A., Nicholls, R., Haigh, I., and Wadey, M. (2011). Reconstructing coastal flood occurrence combining sea level and media sources: a case study of the Solent, UK since 1935. *Nat. Hazards* 59, 1773–1796. doi: 10.1007/s11069-011-9868-7

SDC. (2014). *East Coast Tidal Surge - 5 & 6 December 2013. Suffolk District Council*. Available online at: http://www.suffolkcoastal.gov.uk/yourdistrict/planning/coastal-management/tidalsurge/ (Accessed October 28, 2014).

Shennan, I., and Horton, B. (2002). Holocene land- and sea-level changes in Great Britain. *J. Q. Sci.* 17, 511–526. doi: 10.1002/jqs.710

Sibley, A., Cox, D., and Titley, H. (2015). Coastal flooding in England and Wales from Atlantic and North Sea storms during the 2013/2014 winter. *Weather* 70, 62–70. doi: 10.1002/wea.2471

Skegness Today. (2013). *The Great Flood – 50th Anniversary Supplement, Issue 1-3*. Avaialble online at: http://www2.skegnesstoday.co.uk/sites/floods/floods2_8.html (Accessed April 22, 2015).

Skegness Standard. (2014). *FEATURE: December Storm Surge 2013 - Impact on Local Wildlife One Year on, by Lee Croft*. Available online at: http://www.skegnessstandard.co.uk/news/local/feature-december-storm-surge-2013-impact-on-local-wildlife-one-year-on-1-6449673 (Accessed May 14, 2015).

Skinner, C. (2013). *The Surge 2013. Posted on "GEES-ology: Geography, Environment and Earth Science in action" Webpage, Wednesday 11 December 2013*. Available online at: http://gees-talk.blogspot.co.uk/2013/12/the-surge-2013.html (Accessed March, 2015).

Smith, P. H. (2014). *Effects of Winter Storm Surges on the Sefton Coast, North Merseyside. Sand Dune and Shingle Network Eighteenth Newsletter, March 2014*. Linking Science and Management. Liverpool Hope University. Available online at: http://coast.hope.ac.uk/media/liverpoolhope/contentassets/images/coast/media,38794,en.pdf (Accessed Novermber 6, 2014).

Spencer, T., Brooks, S. M., Möller, I., and Evans, B. R. (2014). where local matters: impacts of a major north sea storm surge. *Eos Trans. Am. Geophys. Union* 95, 269–270. doi: 10.1002/2014EO300002

Spencer, T., Brooks, S. M., Evans, B. R., Tempest, J. A., and Möller, I. (2015). Southern North Sea storm surge event of 5 December 2013: water levels, waves and coastal impacts. *Earth Sci. Rev.* 146, 120–145. doi: 10.1016/j.earscirev.2015.04.002

Steers, J., Stoddart, D., Bayliss-Smith, T., Spencer, T., and Durbidge, P. (1979). The storm surge of 11 January 1978 on the east coast of England. *Geogr. J.* 145, 192–205. doi: 10.2307/634386

Steers, J. A. (1953). The East Coast floods, january 31 - february 1 1953. *Geogr. J.* 119, 280–295. doi: 10.2307/1790640

Stevens, A. J., Clarke, D., Nicholls, R. J., and Wadey, M. P. (2015). Estimating the long-term historic evolution of exposure to flooding of coastal populations. *Nat. Hazards Earth Syst. Sci. Discuss.* 3, 1681–1715. doi: 10.5194/nhessd-3-1681-2015

Stoddard, A. (2014). *The December 2013 Floods - a North Norfolk Perspective. Rare Bird Alert report by Andy Stoddard*. Available online at: http://www.rarebirdalert.co.uk/v2/Content/The_December_2013_Floods_a_north_Norfolk_perspective.aspx?s_id=990948523 (Accessed October 28, 2013).

STV News. (2013). *Nineteen Flood Warnings Issued as Storm Surge Hits East Coast. By Cara Sulieman 5 December 2013 15:01 GMT*. Available online at: http://news.stv.tv/east-central/251759-nineteen-flood-warnings-issued-as-storm-surge-forecast-for-east-coast/ (Accessed May 7, 2015).

Suffolk Coastal. (2013). *The Great Flood of 1953 in Suffolk - Report by the Coastal Management Team of Suffolk Coastal and Waveney District Councils, the Environment Agency and Red Cross*. Available online at: http://www.suffolkcoastal.gov.uk/yourdistrict/planning/coastal-management/intelligence-information/1953-floods/ (Accessed November 19, 2014).

Summers, D. H. (1978). *The East Coast Floods*. Newton Abbott: David and Charles.

Sunderland Echo. (2013). *Sunderland Counting Cost of Storm Damage. Published 11:30 Saturday 14 December 2013*. Available online at: http://www.sunderlandecho.com/news/sunderland-counting-cost-of-storm-damage-1-6315599 (Accessed March, 2015).

Suthons, C.T. (1963). Frequency of occurrence of abnormally high sea levels on the east and south coasts of England. *Proc. Inst. Civil Eng.* 25, 433–450. doi: 10.1680/iicep.1963.10542

Taylor, K. (2011). *The Great Flood of Canning Town. 1st February 1953. A Record of the Flood and the Aftermath taken from Archive Records and Personal Memories of Canning Town People*. Available online at: http://www.docklandsmemories.org.uk/Floods1953.pdf (Accessed November 19, 2014).

Taylor, P. (2013). *Southampton has a North Sea Storm Surge!* Report provided by Peter Taylor, resident of St Denys, Southampton.

The Actuary. (2013). *Insured Losses from Cyclone Xaver 'Could Reach €1.4bn'. 13 DEC 2013 |THE ACTUARY TEAM*. Available online at: http://www.theactuary.com/news/2013/12/insured-losses-from-cyclone-xaver-could-reach-14bn/ (Accessed July 24, 2015).

The Bay. (2013). *Lancashire & Cumbria Hit By Floods. Thursday, December 5th 2013 13:15*. Available online at: http://www.thebay.co.uk/news/local-news/lancashire-and-cumbria-hit-by-floods/ (Accessed November 13, 2014).

The Southwold Museum. (n.d.). *The Sea – Killer Floods. Story and Pictures*. Available online at: http://www.southwoldmuseum.org/thesea_1953Floods.htm (Accessed May 14, 2015).

UKCMF. (2013). *UK Coastal Monitoring and Forecasting Annual Report for 2013 for the UK National Tide Gauge Network*. Available online at: https://www.bodc.ac.uk/data/online_delivery/ntslf/reports/documents/2013annualreport.pdf (Accessed August 20, 2015).

Wadey, M. P., Brown, J. M., Haigh, I. D., Dolphin, T., and Wisse, P. (2015). Assessment and comparison of extreme sea levels and waves during the 2013/14 storm season in two UK coastal regions. *Nat. Hazards Earth Syst. Sci.* 15, 2209–2225. doi: 10.5194/nhess-15-2209-2015

Wadey, M. P., Haigh, I., and Brown, J. (2014). A century of sea level data and the UK's 2013/14 storm surges: an assessment of extremes and clustering using the Newlyn tide gauge record. *Ocean Sci. Discuss.* 11, 1995–2028. doi: 10.5194/osd-11-1995-2014

Wadey, M. P., Nicholls, R. J., and Haigh, I. (2013a). Understanding a coastal flood event: the 10th March 2008 storm surge event in the Solent, UK. *Nat. Hazards*, 67, 829–854. doi: 10.1007/s11069-013-0610-5

Wadey, M. P., Roberts, H., and Harris, J. (2013b). Impacts of climate change on built structures (onshore and coastal). *MCCIP Sci. Rev.* 4, 284–294. doi: 10.14465/2013.arc30.284-294

Wahl, T., Jensen, J., Frank, T., and Haigh, I. (2011). Improved estimates of mean sea level changes in the German Bight over the last 166 years. *Ocean Dyn.* 61, 701–715. doi: 10.1007/s10236-011-0383-x

Wells, N. C., Baldwin, D. J., Wang, J. Y., and Collins, M. B. (2001). Modelling of extreme storm surge events in the English Channel for the period 14–18 December 1989. *Glob. Atmos. Ocean Syst.* 7, 275–294.

Welsh Consumer Council. (1992). *In Deep Water: A Study of Consumer Problems in Towyn and Kinmell Bay after the 1990 Floods*. Welsh Consumer Council.

Whiting. (2014). *East Coast Tidal Surge Report, Essex Coastal Forum & Essex County Council (Author: Mark Whiting), 7 December 2013*. Available online at: http://dnn.essex.gov.uk/coastalforum/News/NewsReport/TabId/2353/ArtMID/5993/ArticleID/323/Default.aspx (Accessed October 28, 2014).

Wirral. (2014). *Flood Investigation Report for December 5th 2013, Wirral Council*. Available online at: http://www.wirral.gov.uk/my-services/advice-and-benefits/emergencies/floods/flood-monitoring-and-reports (Accessed November 13, 2014).

WMG. (2013). *UPDATE: Roads Reopen Across Cumbria after County Hit by Strong Winds*. The West Moorland Gazette. Available online at: http://www.thewestmorlandgazette.co.uk/news/10857068.UPDATE__Roads_reopen_across_Cumbria_after_county_hit_by_strong_winds/?ref=rss (Accessed April 22, 2015).

WMO. (1998). *World Meteorological Organization – Guide to Wave Analysis and Forecasting*, 2nd Edn., WMO Report No. 702. Available online at: https://www.int/pages/prog/amp/mmop/documents/WMO%20No%20702/WMO702.pdf (Accessed July 24, 2015).

Wolf, J., and Flather, R. A. (2005). Modelling waves and surges during the 1953 storm. *Philos. Trans. R. Soc. A Math. Phys. Eng. Sci.* 363, 1359–1375. doi: 10.1098/rsta.2005.1572

Yates, B. (2013). *Flood 6th December 2013*. Available Online at http://www.ryeharbour.net/picture/number364.asp (Accessed August 15, 2014).

YV. (1978). *Britain Battered By Storm - 13 January 1978*. Youngstown Vindicator. Available online at: https://news.google.com/newspapers?id=opNIAAAAIBAJ&sjid=vYMMAAAAIBAJ&dq=storm+1978+january+north+sea&pg=1444,4177071&hl=en (Accessed August 20, 2015).

Zurich. (*2014). After the storm: how the UK's flood defences performed during the surge following Xaver – Risk Nexus*. Zurich Insurance Group Limited, 32. Available online at: http://www.preventionweb.net/english/professional/publications/v.php?id=39185 (Accessed November 9, 2014).

Conflict of Interest Statement: The authors declare that the research was conducted in the absence of any commercial or financial relationships that could be construed as a potential conflict of interest.

frontiers in Marine Science

ORIGINAL RESEARCH
published: 21 March 2016
doi: 10.3389/fmars.2016.00029

Spatial and Temporal Variability and Long-Term Trends in Skew Surges Globally

Robert J. Mawdsley and Ivan D. Haigh*

Ocean and Earth Science, National Oceanography Centre Southampton, University of Southampton, Southampton, UK

Storm surges and the resulting extreme high sea levels are among the most dangerous natural disasters and are responsible for widespread social, economic and environmental consequences. Using a set of 220 tide gauges, this paper investigates the temporal variations in storm surges around the world and the spatial coherence of its variability. We compare results derived from two parameters used to represent storm surge: skew surge and the more traditional, non-tidal residual. We determine the extent of tide-surge interaction, at each study site, and find statistically significant (95% confidence) levels of tide-surge interaction at 59% of sites based on tidal level and 81% of sites based on tidal-phase. The tide-surge interaction was strongest in regions of shallow bathymetry such as the North Sea, north Australia and the Malay Peninsula. At most sites the trends in the skew surge time series were similar to those of non-tidal residuals, but where there were large differences in trends, the sites tended to have a large tidal range. Only 13% of sites had a statistically significant trend in skew surge, and of these approximately equal numbers were positive and negative. However, for trends in the non-tidal residual there were significantly more negative trends. We identified 8 regions where there were strong positive correlations in skew surge variability between sites, which meant that a regional index could be created to represent these groups of sites. Despite strong correlations between some regional skew surge indices, none were significant at the 95% level, however, at the 80% level there was significant positive correlation between the north-west Atlantic—south and the North Sea. Correlations between the regional skew surge indices and climate indices only became significant at the 80% level, where Niño 4 was positively correlated with the Gulf of Mexico skew surge index and negatively correlated with the east Australia skew surge index. The inclusion of autocorrelation in the calculation of correlation greatly reduced their significance, especially in the short time-series used for the regional skew surge indices. Skew surge improved the representation of storm surge magnitudes, and therefore allows a more accurate detection of changes on secular and inter-annual time scales.

Keywords: storm surge, extreme sea level, tide-surge interaction, regional climate, skew surge

OPEN ACCESS

Edited by:
Janine Nauw,
Royal Netherlands Institute for Sea Research, Netherlands

Reviewed by:
Thomas Wahl,
University of South Florida, USA
Andreas Sterl,
Koninklijk Nederlands Meteorologisch Instituut, Netherlands
Fernando Mendez,
Universidad de Cantabria, Spain

****Correspondence:***
Robert J. Mawdsley
robert.mawdsley@noc.soton.ac.uk

Specialty section:
This article was submitted to Coastal Ocean Processes, a section of the journal Frontiers in Marine Science

Received: *08 December 2015*
Accepted: *29 February 2016*
Published: *21 March 2016*

Citation:
Mawdsley RJ and Haigh ID (2016) Spatial and Temporal Variability and Long-Term Trends in Skew Surges Globally. Front. Mar. Sci. 3:29. doi: 10.3389/fmars.2016.00029

INTRODUCTION

Storm surges and the resulting extreme high sea levels are among the most dangerous events influencing the coastal zone (von Storch and Woth, 2008), and have been responsible for many devastating natural disasters, both in terms of loss of life (e.g., Typhoon Haiyan in November 2013) and economic losses (e.g., Hurricane Sandy in October 2012; Pugh and Woodworth, 2014). The widespread social, economic, and environmental impacts associated with such events have driven research to better understand their generating mechanisms and propagation into shallow coastal areas. However, the large number of stochastic processes that influence storm surges over a range of time and space scales, mean that they remain difficult to predict over periods longer than a few days. Understanding the risks associated with storm surges and how these might change in the future is therefore essential to aid coastal zone management and sustainable developmental planning in coastal regions (Wong et al., 2014). Using a set of 220 tide gauges, this paper builds on previous studies (e.g., Woodworth and Blackman, 2004; Menéndez and Woodworth, 2010) and assesses the regional spatial coherence of storm surges around the world and their temporal variations.

Storm surges are the response of the sea surface to forcing by the atmosphere. Several factors influence their generation and propagation into coastal waters, including: meteorological influences (i.e., wind speed, direction, persistence and spatial distribution, and sea level pressure); oceanographic effects (i.e., sea-surface temperature (SST), water density, and sea ice cover); and topographic features (i.e., water depth, width of continental shelf, as well as sand bars and reefs; Pugh and Woodworth, 2014). These characteristics are non-stationary, with variations occurring on scales from hourly to centennial, influenced by both internal natural variability and anthropogenic climate change.

Climate change could alter the frequency, intensity and tracks of storms thus influencing storm surges and extreme sea levels (Church et al., 2013). An increase in the ambient potential intensity, caused by high SST, that tropical cyclones move through should shift the distribution of intensities upwards (Seneviratne et al., 2012). However, this relationship is complicated by uncertainties concerning the response to warming (Vecchi and Soden, 2007), and the strength of counteracting mechanisms (Vecchi and Soden, 2007; Emanuel et al., 2008). As such, confidence remains low for centennial changes in tropical cyclone activity, even after accounting for past changes in observing capabilities (Hartmann et al., 2013). However, in the North Atlantic, it is virtually certain that the frequency and intensity of the strongest cyclones has increased since the 1970's (Kossin et al., 2007). Meanwhile, a net increase in frequency and intensity of extra-tropical storms, coupled with a poleward shift in storm tracks has been observed since the 1950s in both the North Atlantic and North Pacific (Trenberth et al., 2007).

The relatively short observational data set of meteorological conditions makes detecting long-term changes difficult, because of inter-annual variability (Hartmann et al., 2013). Therefore, sea level records have been often used as a proxy for storminess (e.g., Zhang et al., 2000; Araújo and Pugh, 2008; Haigh et al., 2010; Menéndez and Woodworth, 2010; Dangendorf et al., 2014), since some hourly sea level records extend back over 100 years. These studies have generally investigated changes in the non-tidal residual (NTR; the component that remains once the astronomical tidal component has been removed), or extreme sea levels (ESL; which includes changes in all components of sea level, namely, storm surges, mean sea level (MSL) and astronomical tide). The most comprehensive of these studies, by Woodworth and Blackman (2004) and Menéndez and Woodworth (2010), found that increases in ESL over the twentieth century were similar to the increases observed in MSL at most sites around the world. Further regional studies of the Mediterranean (Marcos et al., 2009), the English Channel (Araújo and Pugh, 2008; Haigh et al., 2010), the Caribbean (Torres and Tsimplis, 2013), the U.S. East Coast (Zhang et al., 2000; Thompson et al., 2013), the South China Sea (Feng and Tsimplis, 2014), had similar findings. This suggests that changes in storm surges, and therefore the meteorological conditions that drive them, were not significant over the twentieth Century and early part of the twenty-first Century, at most locations.

However, Menéndez and Woodworth (2010) did observe significant (at 95% confidence) secular trends in the NTR at a few sites. These included: increases in the Caribbean and the Gulf of Mexico; and decreases around most of Australia and parts of the east coast of the USA north of Cape Hatteras. Grinsted et al. (2012) also observed decreases in storm surge activity along the northeast US coast, but Talke et al. (2014) found evidence for an increase in annual maximum storm tide (which includes the tidal component) at New York. Significant differences between the trends in ESL and MSL have been observed for several other regions, including: the Mediterranean, at Camargue (Ullmann et al., 2007), Venice (Lionello et al., 2005), and Trieste (Raicich, 2003); the German Bight (Müdersbach et al., 2013); and sites along the western coastline of North America (Bromirski et al., 2003; Abeysirigunawardena and Walker, 2008; Cayan et al., 2008).

Many of the studies mentioned above assessed changes in ESL without separating out the tide and non-tidal components. Several recent studies have found significant trends in tidal levels and tidal constituents along the coasts of the USA or in the German Bight (e.g., Jay, 2009; Ray, 2009; Woodworth, 2010; Müdersbach et al., 2013; Mawdsley et al., 2015), and these changes in the tide may have contributed toward the observed changes in ESL at some sites. To determine changes in storm surge activity accurately any non-meteorological influence, such as non-meteorological MSL fluctuations, tidal variations and tide-surge interactions, should be removed.

Tide-surge interaction is an important component to consider and occurs for two main reasons (Horsburgh and Wilson, 2007). First, wind stress is more effective at generating storm surges at low tide, compared to high tide, because of the reduced water depth at low tide. Second, the greater water depth present during a positive surge increases the speed of tidal wave propagation, often resulting in the observed high water occurring before predicted high water (Wolf, 1981; Pugh and Woodworth, 2014). Tide-surge interaction has been most studied in the southern

North Sea, where the largest positive NTR are observed to occur on the rising tide (Horsburgh and Wilson, 2007). Tide-surge interactions have also been observed across other continental shelf regions and in shallow water areas, including: the English Channel (Haigh et al., 2009b; Idier et al., 2012); Canada (Bernier and Thompson, 2007); Australia (Haigh et al., 2014); the South China Sea (Feng and Tsimplis, 2014); the Bay of Bengal (Antony and Unnikrishnan, 2013); and was observed during Hurricane Sandy off the USA east coast (Valle-Levinson et al., 2013). However, the extent to which tide-surge interactions occur has not been assessed for large stretches of the world's coastline.

Recently, several studies have used the parameter "skew surge," rather than the traditional NTR, to assess ESL in north-west Europe (Batstone et al., 2013; Dangendorf et al., 2014), and in the USA (Wahl and Chambers, 2015). A skew surge is the difference between the maximum observed sea level and the maximum predicted tidal level regardless of their timing during the tidal cycle. There is one skew surge value per tidal cycle. A skew surge is thus an integrated and unambiguous measure of the storm surge that represents the true meteorological component of sea level (Haigh et al., 2015). For the UK, Batstone et al. (2013) found that variations in skew surge heights are independent of the tidal level, and therefore by using them, one does not have to consider the complications of non-linear tide-surge interactions.

Whatever parameter is used, understanding changes in storm surge requires analysis of low frequency variability, which can have a considerable effect on storm surge conditions. This is often done by comparing storm surge parameters to regional climatic variations, by the use of simple indices, typically based on sea level pressure (SLP) or SST and gives a simplified description of the regional climatic conditions.

The El Niño Southern Oscillation (ENSO) has one of the most widespread influences on climate variability, stretching across the Pacific and into the Atlantic. For example, the number of hurricanes in the Atlantic is known to reduce during strong El Niño events (Bell and Chelliah, 2006). However, Menéndez and Woodworth (2010) found a small positive correlation between the Niño 3 index and the magnitude of the NTR at sites between Cape Hatteras and Cape Cod. In the Caribbean, Torres and Tsimplis (2013) found that 2 out of the 5 sites they studied were anti-correlated with ENSO, but Menéndez and Woodworth (2010) found no significant relationship. Woodworth and Menéndez (2015) found that ESL largely followed the pattern of MSL response to ENSO. By contrast, the tropical west Pacific and the coast of Australia showed a negative correlation (Feng and Tsimplis, 2014). Positive correlation was observed between ENSO, the number of storms that make landfall (Feng and Tsimplis, 2014) and the magnitude of the NTR (Menéndez and Woodworth, 2010) in China, although Feng and Tsimplis (2014) found that neither ENSO nor the Pacific Decadal Oscillation (PDO) was an indicator of a change in magnitude of ESL. Elsewhere in the Pacific, increases in ESL at sites in British Columbia were attributed to a strong positive trend in the PDO (Abeysirigunawardena and Walker, 2008).

In the North Atlantic, the North Atlantic Oscillation (NAO) is the most dominant regional climate signal. Marcos et al. (2009) found that the median and higher percentiles of sea level were both strongly correlated with NAO. However, the correlation between NAO and the NTR was weaker. Haigh et al. (2010) showed that there was a weak negative correlation to the winter NAO throughout the English Channel and a stronger significant positive correlation at the boundary with the southern North Sea. This latter finding is supported by Menéndez and Woodworth (2010) who found a positive correlation of the Arctic Oscillation (AO) and NAO, for most sites around the UK (but not the English Channel) and Scandinavia. In the eastern Atlantic, Talke et al. (2014) and Ezer and Atkinson (2014) both observed anti-correlation between NAO and their different measures of ESL.

In summary, although much research has been conducted to determine the temporal variability of storm surge activity on decadal and longer time-scales, the majority of past studies have focused on the NTR. Skew surges can quantify the meteorological component of sea level better, by removing the impact of phase offsets and tide-surge interactions. However, until now (to our knowledge) they have only been used to assess changes in storm surge activity around north-west Europe and USA. Little research has been conducted into tide-surge interaction in many regions, and therefore it would be prudent to identify further regions where this may have an important impact on the magnitude of ESL. Furthermore, few studies have examined the spatial coherence in storm surge variability along stretches of coastlines and between regions. This is despite the fact that regional climatic variability can account for much of the inter-annual and multi-decadal variability in storm surges (Marcos et al., 2015; Wahl and Chambers, 2016).

Therefore, the overall aim of this paper is to assess the spatial and temporal variations in storm surge activity (and thus infer changes in storminess) over the twentieth century and early part of the twenty-first century at a quasi-global scale, addressing the issues highlighted above. We build on two comprehensive global studies undertaken by Woodworth and Blackman (2004) and Menéndez and Woodworth (2010) and utilize an updated version of their Global Extreme Sea Level Analysis (GESLA) tide gauge dataset (Mawdsley et al., 2015). We have four specific objectives. Our first objective is to determine the extent of tide-surge interaction, at each of our 220 study sites, as this determines the scale of the differences between skew surge and NTR values. Our second objective is to compare how the use of skew surge or NTR, effects the assessment of storm surge activity. Our third objective is to assess the extent to which there is spatial coherence in skew surge variability, both locally (i.e., between adjacent tide gauge sites) and regionally (i.e., across ocean basins). Our fourth and final objective is to compare inter-annual and multi-decadal variations in skew surge with fluctuations in regional climate.

The format of the paper is as follows. The data and methodology are described in Sections Data and Methodology, respectively. The results for each of the four objectives are presented in Section Results in turn. Key findings are discussed in Section Discussion and conclusions are given in Section Conclusions.

DATA

High-resolution (i.e., at least hourly) sea level data is required to analyse storm surge characteristics. The most comprehensive

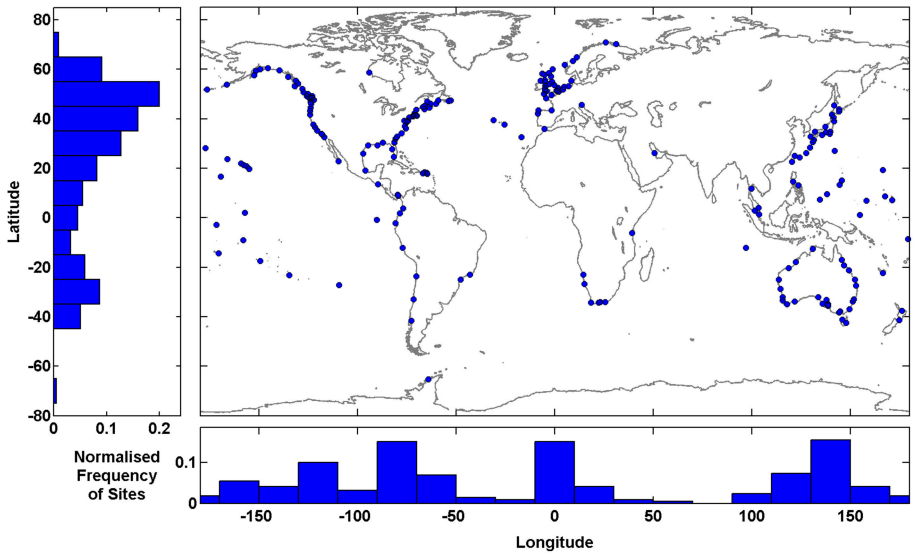

FIGURE 1 | Location map of 220 selected sites used in the analysis. Normalized frequency histograms are plotted along the x-axis for longitude and y-axis for latitude.

high frequency sea level dataset available is the GESLA database. This dataset was originally collated by staff from the National Oceanography Centre (NOC) in the UK and the Antarctic Climate and Ecosystems Cooperative Research Centre (ACECRC) in Australia. The GESLA dataset has primarily been used to assess changes in ESL (e.g., Woodworth and Blackman, 2004; Menéndez and Woodworth, 2010; Hunter, 2012; Hunter et al., 2013; Marcos et al., 2015) but has also been used to evaluate changes in the tides (Woodworth, 2010; Mawdsley et al., 2015).

We have extended the original GESLA dataset, to include additional sites and updated the records to the end of 2014 (see Mawdsley et al., 2015 for details). Many records in the GESLA dataset were excluded from this analysis by a number of criteria designed to ensure that data were of sufficient length and quality for robust analysis. These criteria are detailed in Mawdsley et al. (2015) and resulted in 220 eligible sites, the locations of which are shown in **Figure 1** (and documented in the Supplementary Material). The sites used in this study were determined by the needs of the previous study on change in tidal levels (Mawdsley et al., 2015) and hence sites in the Mediterranean and Baltic seas have not been used, because the tide was too small to be analyzed on an annual basis in these areas. We conducted further quality control on all records to ensure any remaining spikes, or datum and phase offsets were flagged and excluded from the analysis. Data clearly affected by tsunamis were also removed, since the occurrence of these non-climate related events are unpredictable and can affect results. Small tsunami signals are difficult to separate from the NTR, and therefore some events remain in the dataset. Tide gauge measurements are deemed acceptable if they have an accuracy of less than 1 cm, according to the Intergovernmental Oceanographic Commission (IOC; 2006). Many modern day instruments are accurate to approximately 3 mm, but all instruments used in this study will meet the minimum requirements of the IOC.

We used 8 climate indices: the Atlantic Multi-decadal Oscillation (AMO), AO, NAO, Niño 3, Niño 4, North Pacific (NP), PDO, Southern Oscillation Index (SOI). The NAO index was downloaded from the Climate Research Unit of the University of East Anglia (https://crudata.uea.ac.uk/cru/data/nao/nao.dat). The other indices were obtained from the National Oceanic and Atmospheric Administration (NOAA) (http://www.cpc.ncep.noaa.gov).

METHODOLOGY

At each of the 220 study sites, the observed sea level record was separated into its three main component parts for each year: MSL, tide and NTR (Pugh and Woodworth, 2014). We followed the same method as detailed in Mawdsley et al. (2015), and used their technique for extracting the time and magnitude of tidal high waters (HW), from here on described as predicted HW. For every predicted HW at each site, we calculated a skew surge value. Batstone et al. (2013) used a method that identified the maximum predicted and observed water levels between successive low waters. However, we found this approach was not appropriate in mixed tidal regimes, and given the global nature of this study we developed another method that works across all tidal regimes. We calculated skew surges by finding the largest local maxima in the observed sea level, within a ± 3 h window of the time of each predicted HW (**Figure 2**). Most observed HW occurred within this window, but if no observed HW were found during this window we extended it to ± 6 h. In a mixed tidal regime, the coupling of each observed HW to each predicted HW is more complicated. Therefore, we introduced two criteria to ensure

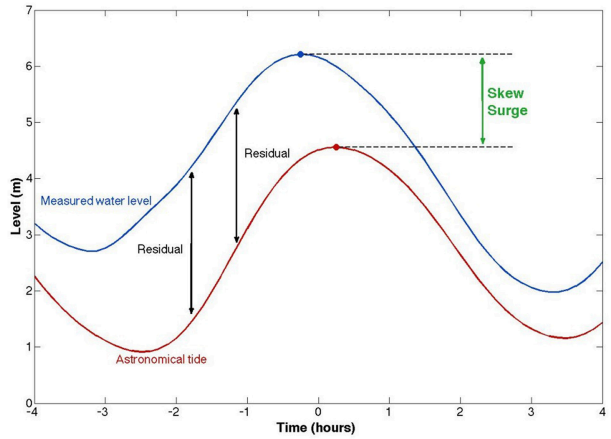

FIGURE 2 | Schematic example of a storm surge event and the different calculation methods for the NTR and skew surge.

that the observed HW is primarily caused by the predicted HW to which it is coupled. Firstly, if the predicted HW is between double low tides we do not assign an observed HW. Secondly, if a second predicted HW is closer in time to an observed HW than its coupled predicted HW, we remove the coupling between that predicted and observed HW. These caveats mean that some predicted HW did not have an associated observed HW, but this method captured a mean of 95% of observed HWs at all sites. Two sites (Bunbury and Hoek van Holland) had an observed HW assignment less than 80%, because many observed HWs occurred around double low tides and were removed.

We then examined the differences between the skew surge and NTR time series, at each of our 220 study sites, and determined the extent of tide-surge interaction. Initially we compared the maximum values of skew surge and NTR from the entire time series, where concurrent values in both time series occur for an event at each site. For example, the maximum NTR at Galveston, USA was generated by Hurricane Ike in September 2008, however, the tide gauge broke just before the predicted HW and no corresponding skew surge value for this particular tidal cycle could be calculated. We also compared the maximum skew surge value with the maximum NTR at high water (if tide-surge interaction is negligible you would expect these two values to be the same). We used the chi-squared (χ^2) test, which was first used for sea level studies by Dixon and Tawn (1994) but was modified by Haigh et al. (2010) to quantify the level of tide-surge interaction at each site. The χ^2 test calculates the probability that the observed dataset is different to an expected dataset. In this case, if the two are different then it demonstrates that tide-surge interaction is significant. Dixon and Tawn's (1994) approach, from here on called the tidal-level method, involved splitting the astronomical tidal range into five equi-probable bands. If the tide and NTR were independent processes, the number of NTR per tidal band would be equal, but if interaction is significant the number of NTR per tidal band would differ. As Haigh et al. (2010) pointed out, this method does not distinguish that interaction tends to be different on the ebb and flood phases of the tide (Horsburgh and Wilson, 2007). Haigh et al. (2010) therefore modified the method to compare the relative timing of the peak NTR to the predicted HW, and this method is from here on called the tidal-phase method. The tide was divided into 13 hourly bands between 6.5-h before and after high water. With no tide–surge interaction the expected number of occurrences in each of the 13 bands would be the same. See Haigh et al. (2010) for the mathematical details. We use the same 13 hourly bands to assess tide-surge interaction in the tidal-phase method, but use 6 equi-probable bands for the tidal-level. The results from both methods are based on the largest 200 NTR events, where an event is defined by a 72-h window centered on the peak NTR, to ensure that each NTR peak is independent. Statistical significance for the χ^2 test is given for a $p < 0.05$.

Next, we assessed the long-term trends in skew surge time-series, at each site and compared these to trends calculated from the NTR time-series. We used the percentiles method (e.g., Haigh et al., 2010; Menéndez and Woodworth, 2010), which ranks the parameter values for each year. The 50th percentile of the NTR time-series (the median) approximates to zero, while the 99.9th percentile is about the level of the 8th highest hourly sea level value. For skew surges, the tidal regime at each site affects the annual number of HWs. In semi-diurnal regimes there are approximately 705 skew surge values a year, whereas for a diurnal regime an average of 352 skew values would occur. Therefore, the 99th percentile represents a value between the 4th and 7th highest values in the skew surge time series. Trends were calculated for these percentiles, using linear regression, while standard errors were estimated using a Lag-1 autocorrelation function to allow for any serial autocorrelation in the time-series (Box et al., 1994). From here on, when we use the term "significant trends," this signifies that the trends are statistically (at 95% confidence level) different from zero.

We chose high percentiles because they represent the largest events at each site, but the inter-annual variability present in the higher percentile time-series can obscure the inter-decadal variability and secular trends. To assess the extent to which there is spatial coherence in skew surge variability, we calculated a correlation coefficient between the skew surge percentile time-series for each pair of sites. We identified groups of sites, along a stretch of coastline, where the correlation between them was high, and designated them as coherent regions. We created regional skew surge indices by calculating the mean of the de-trended and normalized time-series of the 99th percentile of skew surge for each site in that area. We only derived regional indices for the period from 1970 to 2010, when there was sufficient overlap of data among sites in each region, but increase the temporal comparison by comparing individual long-time series from each region. We filtered the regional skew surge indices using a locally regressed least squares (Loess) approach (Cleveland and Devlin, 1988), which through testing gave the lowest standard error. This non-parametric method combines a multiple regression model with a nearest-neighbor model. Each point of the loess curve was fitted using local regression, using a 2nd degree polynomial to the points within a 10-year window centered on that point. These filtered time-series are used to assess the temporal variations in the regional skew surge indices and the correlation of those

indices between each other and against the regional climate indices, listed in Section Data. The significance of the correlation between the different regional skew surge indices and between them and the climate indices, is determined by using the Lag-1 autocorrelation function (Box et al., 1994).

RESULTS

Tide-Surge Interactions

Our first objective was to identify any tide-surge interaction, at each of the 220 study sites, and we did this using the 4 methods detailed in Section Methodology. The difference between the maximum skew surge value and the maximum NTR over the whole time series, is shown for each site in **Figure 3A**. We expect small differences at sites where tide-surge interaction is negligible. Results shows that the difference is predominantly largest in regions surrounded by shallow bathymetry, such as the German Bight, Northern Australia, the Gulf of Panama and parts of the east coast of North America. However, there are other sites with large differences, including: sites in northern Australia (Port Hedland, Broome, Wyndham, Townsville and Bundaberg); Easter and Wake Islands in the Pacific Ocean; Funchal on Madeira, Portugal; and Yakutat in Alaska. At 120, 80, and 20 sites, the difference is larger than 10, 20, and 50 cm, respectively. When we calculate the difference between the maximum skew surge and the maximum NTR observed at the time of predicted HW we find that 137 sites have a value of zero, as shown in **Figure 3B**. However, sites in the North Sea, the US east coast, north-west Australia and a few other individual locations have non-zero values which suggests that in these regions the tide-surge interaction shifts the peak in NTR away from predicted HW.

Figures 3C,D present the magnitude of the χ^2 test statistic as a colored dot (where $p < 0.05$) and a black dot where no significant difference was found between the observed and expected datasets. The results for the tidal-level method are shown in **Figure 3C**, and show that tide-surge interaction is statistically significant (95% confidence) at 130 of the 220 sites (59%). These sites include those listed above, which are mainly in shallow regions, but also include sites on the Malay Peninsula and along the coast of Washington and Oregon, USA. The results for the tidal-phase method, are shown in **Figure 3D**, and show that tide-surge interaction is statistically significant at 175 of the 220 sites (81%). As mentioned earlier, Haigh et al. (2010) modified Dixon and Tawn's (1994) original χ^2 test statistic as it did not distinguish that interaction tends to be different on the ebb and flood phases of the tide. Interestingly, these results show the tidal-phase method identifies a greater number of sites at which tide-surge interaction is statistically significant.

At several sites the differences between the maximum skew surge and NTR values are large, but the χ^2 statistic values are small, and this is most often caused by the impact of one large storm. For example, at Wake Island, Pacific, it is Typhoon Ioke in 2006 (skew surge = 0.97 m, NTR = 1.45 m), at Broome, Australia it is Cyclone Rosito in 2000 (skew surge = 0.82 m, NTR = 2.24 m) and for Townsville, Australia it is Cyclone Yasi in 2011 (skew surge = 0.93 m, NTR = 2.10 m). At Easter Island, Chile the event in June 2006 is a high frequency signal, similar to seiching, but further research is needed to determine its cause (skew surge = 0.51 m, NTR = 1.18 m).

The difference between skew surges and NTRs at a site can vary considerably between individual events as a result of the timing of the peak in the NTR relative to the predicted HW. This is illustrated in **Figure 4**, for 8 selected sites. The scatter sub-plots show the magnitude of the 200 largest NTR events plotted against the magnitude of the associated skew surge. The histogram sub-plots show the time of the peak in NTR for 200 events relative to time of predicted HW. The colors on each plot display the maximum NTR (green), the top 10 NTRs (red), the top 25 NTRs (blue), and the remainder of the top 200 NTR's (black). At Atlantic City, USA (**Figure 4A**), Galveston, USA (**Figure 4D**) and Naze in Japan (**Figure 4F**), the largest skew surge and largest NTR occurred during the same event. However, at the other selected sites, the timing of the peak NTR relative to the HW means that the largest skew surge and largest NTR are not coincident. For example, at Immingham, UK, the maximum NTR occurred 6 h before predicted high water and because the mean tidal range (MTR; as defined by Mawdsley et al., 2015) is 4.8 m, the magnitude of the skew surge was only the 56th largest from the top 200 NTR events (**Figure 4E**). The timing relative to predicted HW is less important where MTR is small. At Galveston, USA (MTR = 0.24 m) for example, the largest NTR (with the values caused by Hurricane Ike removed) occurred during Hurricane Carla in 1961. The peak NTR occurred at the same time as predicted HW, and 7 of the 10 largest events occur within 3 h of predicted HW (**Figure 4D**).

As mentioned earlier, tide-surge interaction has been most studied in the southern North Sea, where the largest positive NTR tend to occur on the rising tide and not at high water. This pattern can be clearly observed in the results for Immingham shown on **Figure 4E**. However, these distributions vary around the world. For example, at Fremantle in Australia (**Figure 4C**) tide-surge interaction appears to lead to most peaks in NTR occurring near the time of predicted HW. For Charleston (**Figure 4B**) and Seattle (**Figure 4H**) in USA, the majority of peaks in NTR occur on the ebb tide.

Skew Surge and Non-Tidal Residual Comparison

Our second objective was to determine if using skew surge to assess changes in storm surge activity, gave different results compared to using the NTR. As we identified in the section above, tide-surge interaction is evident at a large proportion of the study sites, suggesting that trends in skew surges and NTR may also differ. The trends calculated for the 95th, 99th, and 99.9th percentiles of the NTR are plotted in **Figure 5**, against the trends in skew surge time-series for the same three percentiles. Given the differences in sampling of the two parameter, as summarized in Section Methodology, comparisons of trends in different percentiles gives an understanding of how to relate the percentiles of the two parameters to each other. If the trends were the same between skew surge and NTR, all points would lie along the 1:1 ratio line shown on each figure. Trend differences between the skew surge and the NTR are generally small, with trends of the same percentiles of skew surge and NTR showing

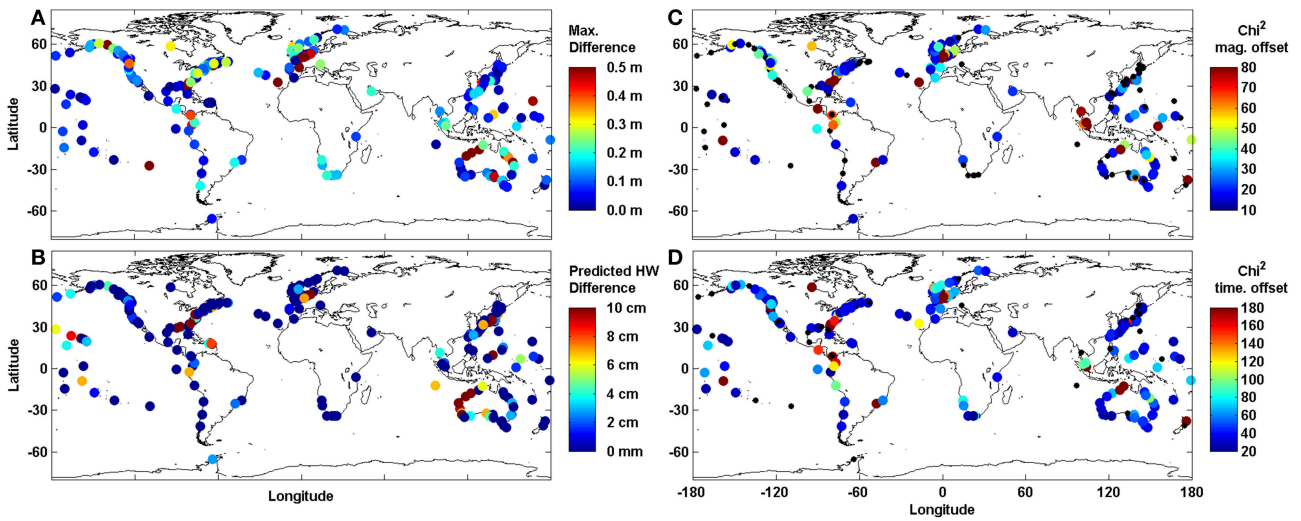

FIGURE 3 | Global maps of the 220 selected sites. (A) difference between the maximum NTR and the maximum skew surge value. **(B)** difference between the maximum skew surge value and the maximum NTR occurring at the same time as predicted HW **(C)** χ^2 values showing magnitude of tide at time of peak NTR for the 200 largest NTR. **(D)** χ^2 values showing time of peak NTR relative to predicted HW for the 200 largest NTR event. Black dots **(C,D)** show non-significant values in the chi-squared test (based on *p*-values larger than 0.05).

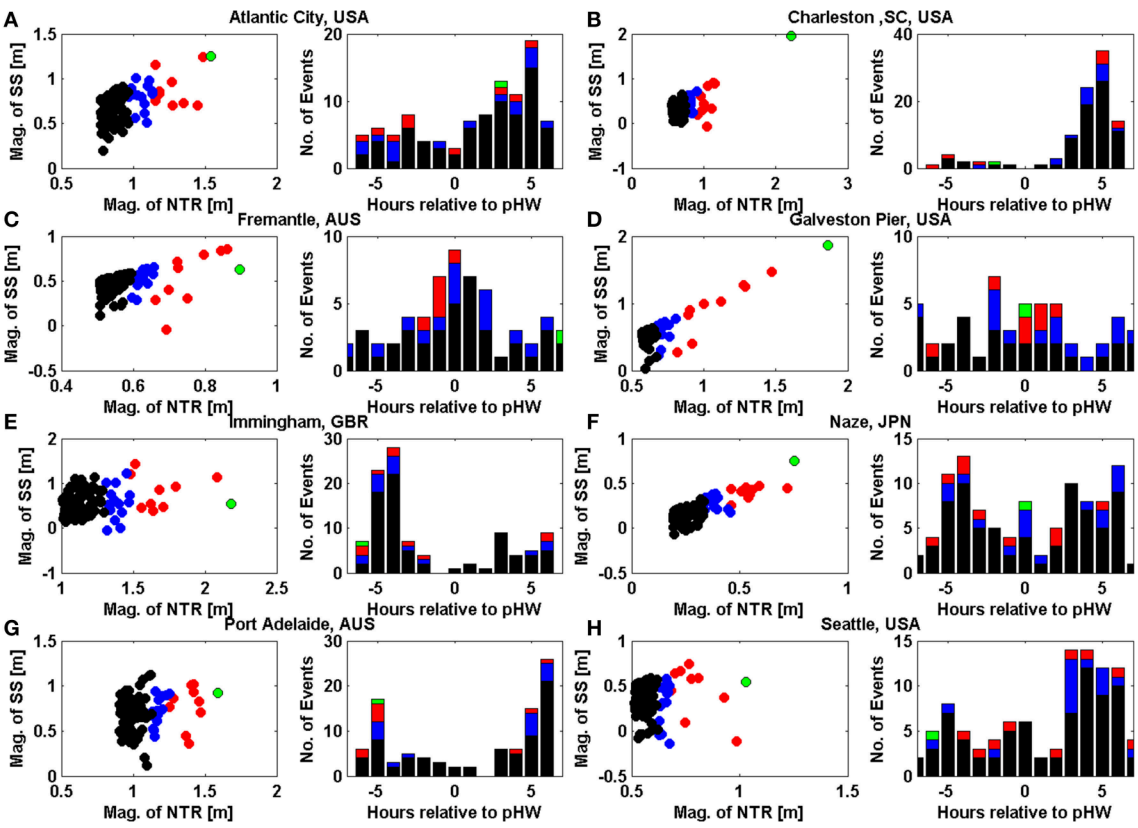

FIGURE 4 | For eight selected sites: (A) Atlantic City, USA; (B) Charleston, USA; (C) Fremantle, Australia; (D) Galveston, USA; (E) Immingham, UK; (F) Naze, Japan; (G) Port Adelaide, Australia; (H) Seattle, USA. Left, scatter plot of 200 largest NTR and the associated skew surge value, right histogram of the time of the peak NTR relative to predicted high water. Both plots are cultured according to magnitude with green showing the maximum NTR, red the top 10 NTR and blue the top 25 NTR, black are the remainder of the top 200 NTR.

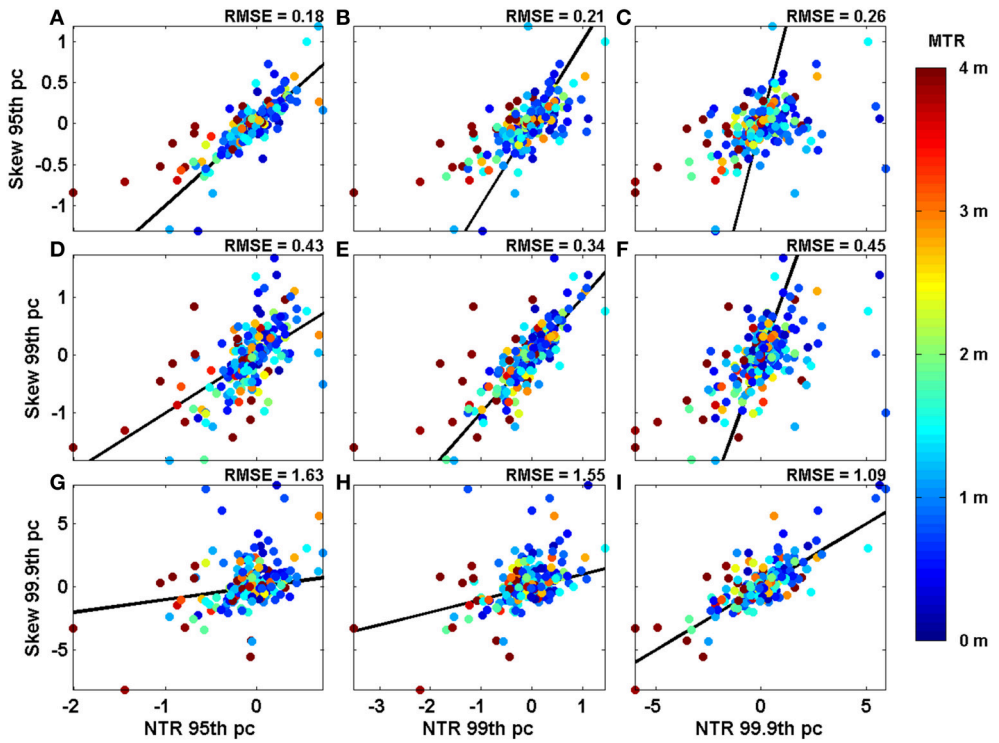

FIGURE 5 | Scatter plots comparing trends in the 95th, 99th and 99.9th percentiles and NTR (labeled along the x-axis), to the same percentiles of skew surge (labeled along the y-axis). Each point is shaded according to the average mean tidal range at each site. The black line shows 1:1 ratio. The root mean squared error value for each plot is the value for the best fit (red line).

the closest comparison (i.e., the closest 1:1 match occurs between the 99th percentile of NTR and the 99th percentile of skew surge). The color of each dot in **Figure 5** represents the height of MTR at that site. Sites with the largest difference between trends in skew surge and NTR typically have a large MTR. These sites include Broome, Australia, Ilfracombe, UK and Hoek van Holland, Netherlands, and these sites also have a large tide-surge interaction as quantified by the χ^2 test statistics (**Figures 3B,C**). At three further sites, Calais, France, Darwin, Australia and Eastport, USA, the trend in skew surge is significantly larger than the trend in NTR (i.e., the 95% confidence intervals of the two trends do not overlap). The trends at Calais and Eastport change from significant negative trends (at the 95% level) to positive trends that are significant at the 66% level. The root mean squared error (RMSE) between skew surge trends and NTR trends are listed for each plot on **Figure 5**. The RMSEs are largest for the 99.9th percentile, since trends in this percentile can be affected by individual large events.

The time-series of the 99th (blue) and 99.9th (red) percentiles of skew surges are presented in **Figure 6** for selected sites, along with the linear trends in these time-series and the corresponding 95% confidence intervals. The variability around the 99.9th percentile, which captures only the annual maximum of skew surge, is large relative to the magnitude of the linear trend and therefore very few significant trends can be detected. Therefore we use the 99th percentile of skew surge throughout the rest of the paper. Previous studies, including Menéndez and Woodworth (2010), used the 99th percentile of NTR, so our choice allows direct comparison with the results of that study.

Linear trends calculated for the 99th percentile of skew surge and NTR are shown for each site in **Figures 7A,B** respectively. Significant trends are shown with larger dots, with the color representing the magnitude of the trends. Overall there are few significant trends in skew surge time-series, with significant negative trends at 18 sites and significant positive trends at 11 sites. For the NTR there are significant negative trends at 33 sites and significant positive trends at only 5 sites. There are 15 sites with negative trends in both parameters, and 4 sites with positive trends in both. Trends were calculated at sites with enough years for the last 20, 40, 60, and 80 years, and compared to the trend of the entire time series. These results are presented in Supplementary Material and show that the number of positive and negative trends are roughly similar, and low in relation to the number of sites. Despite the low numbers of sites with significant trends there are some regions with consistent trends between neighboring stations, such as coherent decreases around north Australia and the Atlantic coast of southern Europe.

Spatial Variability of Skew Surge

Our third objective is to assess the extent to which there is spatial coherence in skew surge variability, both locally (i.e., between adjacent tide gauge sites) and regionally (i.e., across ocean basins). For each site in turn, correlation coefficients were calculated between the unfiltered 99th percentile time series at

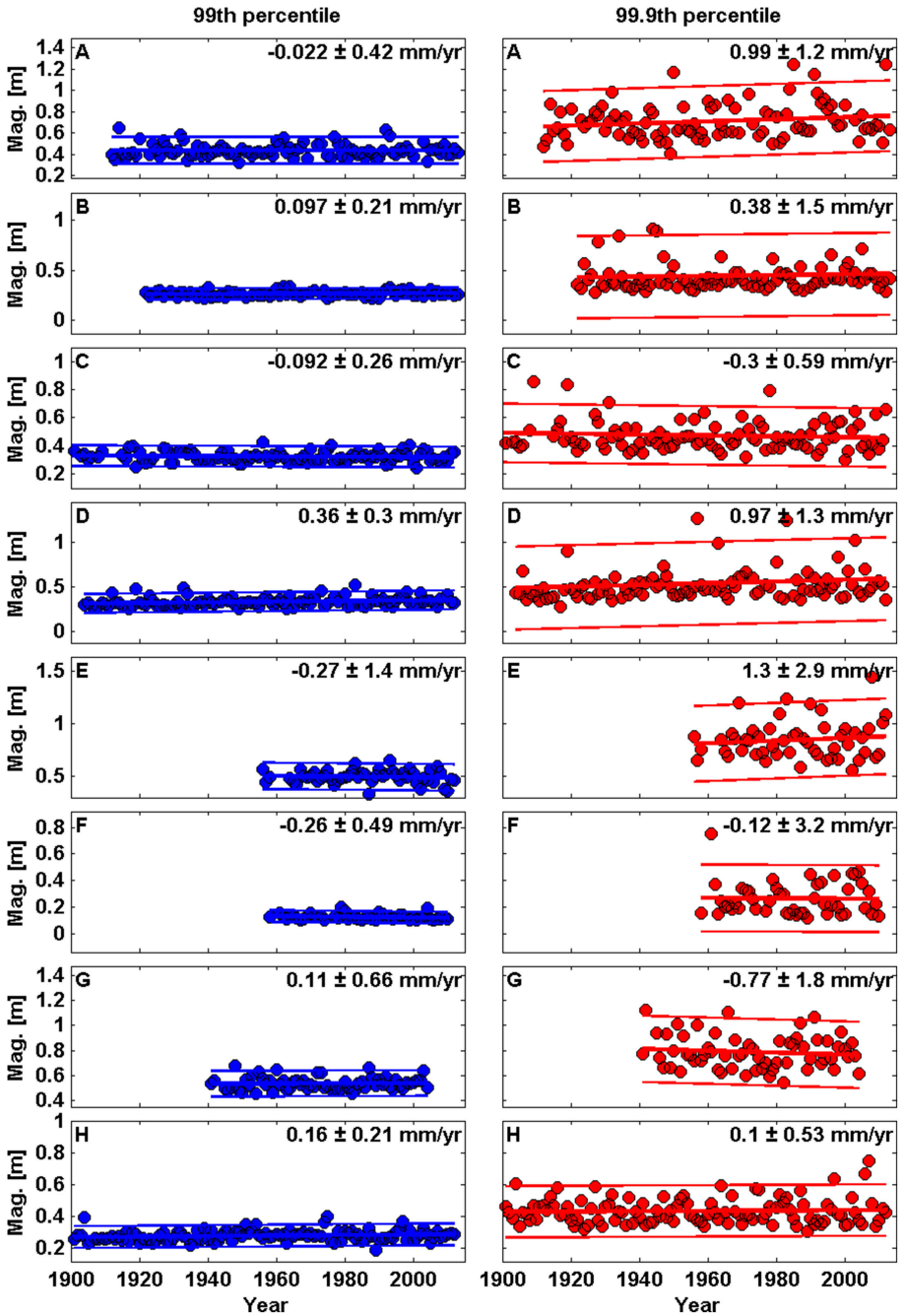

FIGURE 6 | Time series plots of annual values of the 99th (blue) and 99.9th (red) percentile for skew surge at 8 selected sites. (A) Atlantic City, USA; **(B)** Charleston, USA; **(C)** Fremantle, Australia; **(D)** Galveston, USA; **(E)** Immingham, UK; **(F)** Naze, Japan; **(G)** Port Adelaide, Australia; **(H)** Seattle, USA.

that site and each of the other 219 sites. The results are shown in **Figure 8**. There are distinct regions where strong positive correlations occur among neighboring sites. These include the north-east Pacific, north-west Atlantic and sites in northern Europe. Interestingly, sites on the west coast of the US are weakly anti-correlated (at the 66% level) with several sites in northern Europe.

The strong correlation between groups of sites implies that we can create regional skew surge indices that represent the average skew surge conditions for a particular region; similar to what other studies have done for MSL (e.g., Shennan and Woodworth, 1992; Woodworth et al., 1999, 2009; Haigh et al., 2009a; Wahl et al., 2013; Dangendorf et al., 2014; Thompson and Mitchum, 2014). We identified 8 regions, where a large density of sites meant that strong positive correlations existed between them. These regions, and the sites of which they are comprised, are detailed in **Table 1** and include the: north-east Pacific (NEP), Gulf of Mexico (GOM), north-west Atlantic South

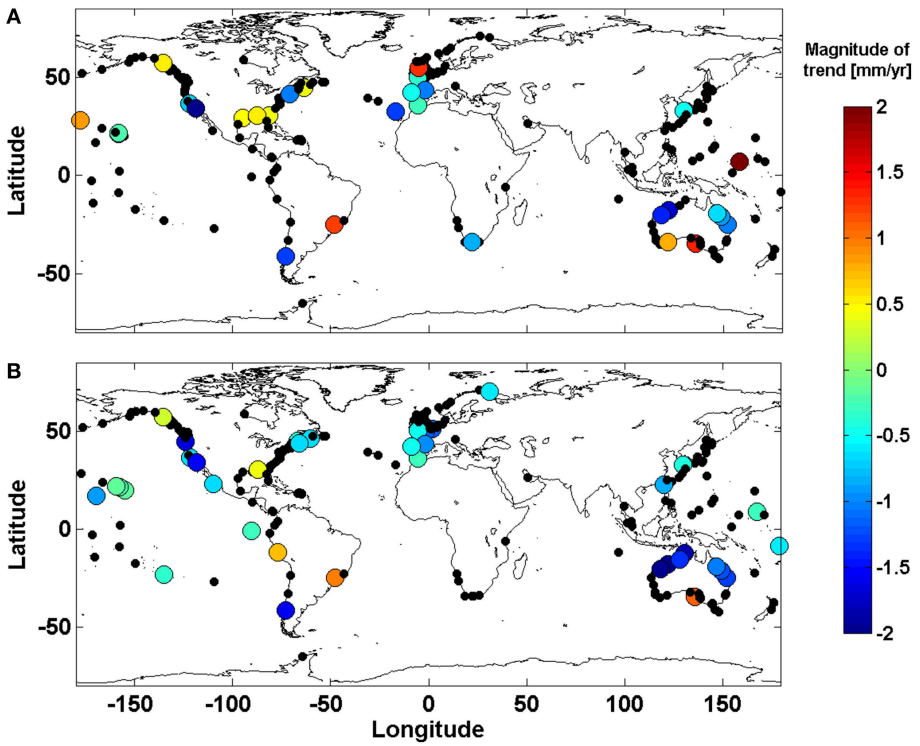

FIGURE 7 | Shows the magnitude of the trend in in the 99th percentile of (A) skew surge and (B) NTR, for the 220 sites analyzed. Large dots show that the trend is significant at the 95% level.

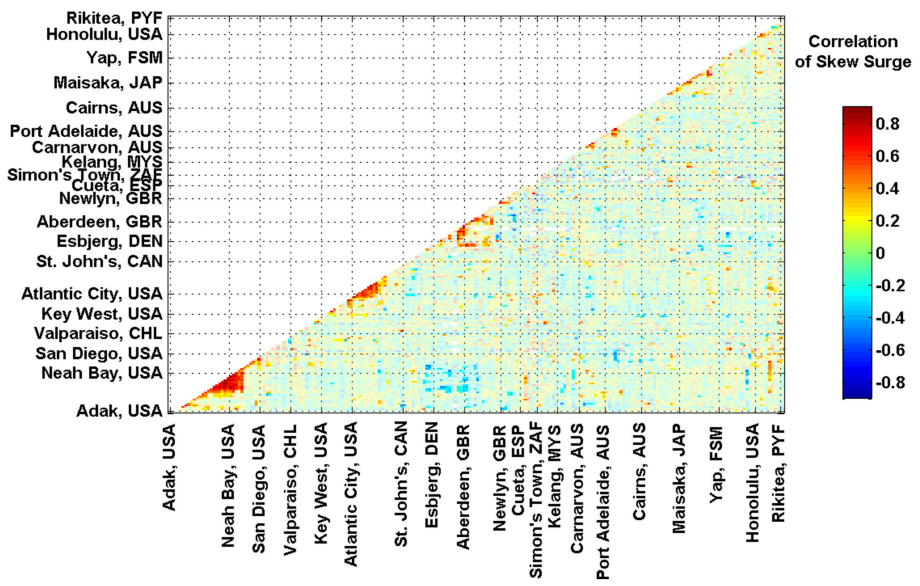

FIGURE 8 | Correlation between each site. Each site is plotted along an imaginary coastline running from Alaska down the west and up the east coast of the America, across to the Atlantic to Norway, down through Europe around Africa, around the Indian Ocean, up the western Pacific Ocean and then across the Pacific Islands to the east. Sites with correlations at the 66% level are shown as bold color.

TABLE 1 | Details of sites included in each of the regional indices.

Regional index name (and abbreviation)	Sites included in index
North East Pacific (NEP)	Canada: Bella Bella, Port Hardy, Tofino, Campbell River, Point Atkinson, Vancouver, Bamfield, Victoria, Patricia Bay.
	USA: Seattle, Neah Bay.
Gulf of Mexico (GOM)	USA: Port Isabel, Galveston, Grand Isle, Pensacola, St. Petersburg, Key West.
North-west Atlantic—South (NWA-S)	USA: Fernandina Beach, Mayport, Fort Pulaski, Charleston, Wilmington.
North-west Atlantic—North (NWA-N)	USA: Duck Pier, Chesapeake Bay, Baltimore, Lewes, Cape May, Atlantic City, New York (Battery), New London, Montauk, Newport, Boston, Woods Hole, Portland, Nantucket, Eastport.
North Sea (NS)	Denmark: Esbjerg.
	Netherlands: Delfzijl, Den Helder.
	France: Calais.
	UK: Dover, Sheerness, Lowestoft, Immingham, North Shields, Aberdeen, Wick.
Western Australia (WAUS)	Australia: Darwin, Broome, Port Hedland, Carnarvon, Geraldton, Fremantle, Bunbury, Albany, Esperance
Eastern Australia (EAUS)	Australia: Wyndham, Thevenard, Port Lincoln, Port Pirie, Port Adelaide, Port Lonsdale, Victor Harbor, Geelong, Williamstown, Burnie, Spring Bay, Fort Denison, Newcastle, Brisbane, Bundaberg, Mackay, Townsville, Cairns.
Japan (JAP)	Japan: Nishinoomote, Aburatsu, Kushimoto, Maisaka, Miyakejima, Mera, Ofunato, Hachinohe, Hakodate.

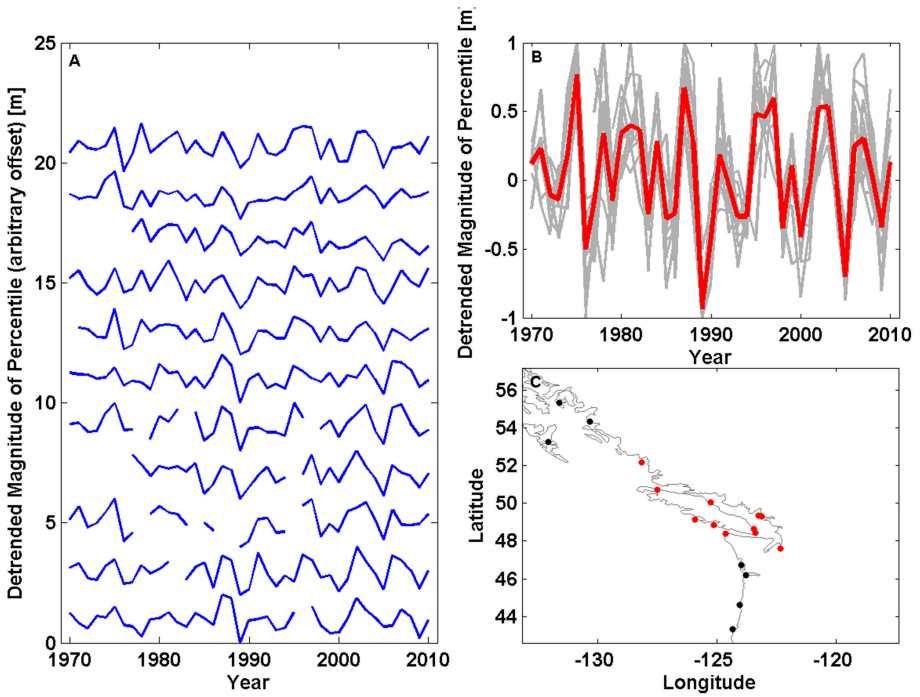

FIGURE 9 | Creation of regional skew surge index for the north-east Pacific. (A) The de-trended time series of the 99th percentile for each site from north to south (see **Table 1** for site ID), **(B)** All the time-series with the mean of all sites plotted in red, and **(C)** the sites that are in this region highlighted in red.

(NWA-S), north-west Atlantic North (NWA-N), North Sea (NS), west Australia (WAUS), east Australia (EAUS), and Japan (JAP).

An example of the creation of a regional index is shown in **Figure 9** for the north-east Pacific. The de-trended, normalized time-series from each of the 11 selected sites in the region are plotted in **Figure 9A**, with an arbitrary offset. These time series are overlaid in **Figure 9B**. The thicker red lines shows the regional time-series that has been created by averaging the de-trended, normalized time-series for each of the 11 sites. The locations of the 11 sites used to calculate the regional index are shown in **Figure 9C**, as red dots. Similar figures for the other 8 regions are shown in the Supplementary Material.

There is considerable year-to-year variability in the 8 regional indices. To better investigate the inter-decadal variability we applied a Loess filter to each of the 8 regional skew surge indices, and the filtered time series are shown in **Figure 10A**. Concurrent peaks in skew surge are observed in multiple regions, most notably in 1992–1993 in the north-west Atlantic (North and South indices) and the North Sea. Peaks in skew surge in the southern North Atlantic throughout the 1990s appear to lag

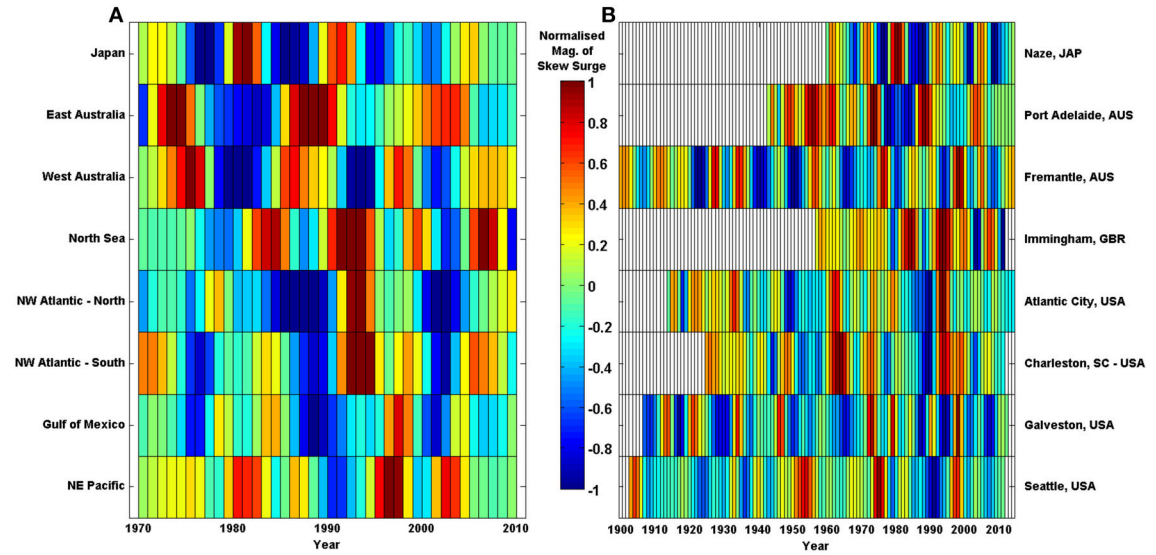

FIGURE 10 | Temporal variability of 8 selected regions as shown by the de-trended normalized and then filtered magnitude of skew surge for: (A) regional indices; (B) selected long site from each region, which has a strong correlation with the regional index.

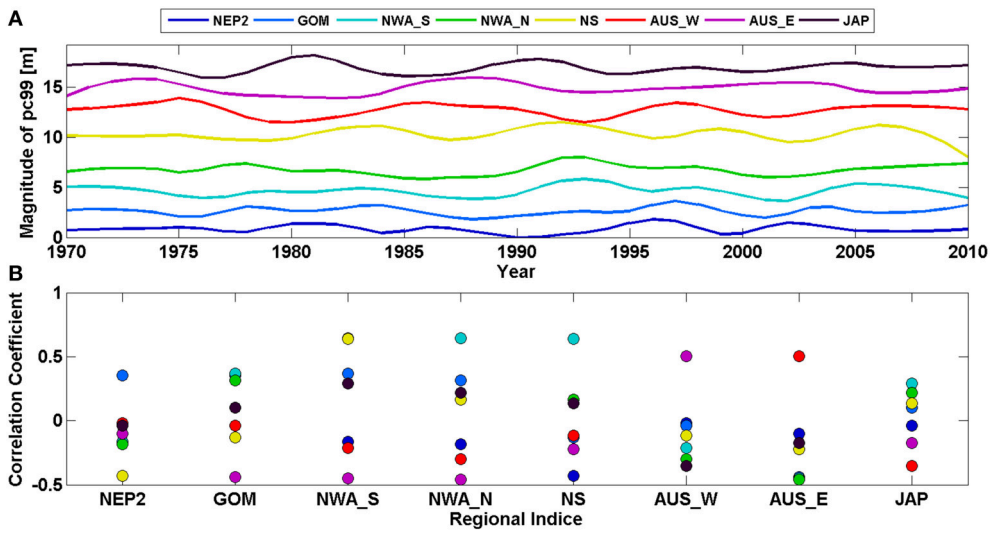

FIGURE 11 | (A) Stacked time series of filtered regional skew surge indices, with arbitrary offset applied, **(B)** Correlation of each filtered regional skew surge index against the others.

peaks in the Gulf of Mexico by approximately 1 year. Storm seasons for these regions are summer and winter respectively and the lag may be a result of this or a delay in the response to changes in regional scale climatology.

The 8 regional skew surge indices are plotted as stacked time series in **Figure 11A**, with the correlations between them shown in **Figure 11B**. Between many regions, there is a strong correlation ($r > 0.5$), but at the 95% level these are not significant, due largely to the reduction in the number of effective observations when autocorrelation is accounted for. Strong correlations exist between: the two north-west Atlantic indices ($r = 0.65$, p = 0.02), the Gulf of Mexico and both two north-west Atlantic indices (South: $r = 0.37$, $p = 0.33$; North: $r = 0.31$, $p = 0.4$), the North Sea and north-west Atlantic—South ($r = 0.65$, $p = 0.12$). Therefore, only this last correlation is significant at the 80% level.

The regional skew surge indices were only calculated for the period 1970–2010, because fewer sites with valid data outside of this period increases the variability in the indices. To allow longer temporal comparisons between regions, we selected individual sites within each region that were both long and highly correlated with the regional index. The 8 sites with long records, across the

8 regions, are shown in **Figure 10B**. Note, these time series have also be subjected to the same Loess filter, applied to the regional time series. The simultaneous peak in the 1990s, mentioned above, is also present in the individual sites. However, a peak in the signal in the filtered time series at Charleston and Atlantic City, USA in the 1960s is not clear at Immingham, UK. The reverse is true in the late 1980s, where an increase at Immingham is not present at Charleston or Atlantic City.

Comparison of Skew Surge to Climate Indices

Our fourth objective is to compare inter-annual and multi-decadal variations in skew surge with fluctuations in regional climate. Correlation coefficients were calculated between the 8 regional skew surge indices and each of the 8 regional climate indices. The results are shown in **Figure 12**.

There are no statistically significant correlations at the 95% level, again largely because of the large degree of autocorrelation in the filtered time-series. Strong positive correlations ($r > 0.5$) occur between: the North Sea and NAO ($r = 0.60$, $p = 0.28$), the Gulf of Mexico and Niño 4 ($r = 0.52$, $p = 0.19$) and western Australian and SOI ($r = 0.59$, $p = 0.31$). Strong negative correlations ($r < -0.5$) occur between the north-east Pacific and AO ($r = -0.57$, $p = 0.28$) and NAO ($r = -0.50$, $p = 0.40$), the Gulf of Mexico and AO ($r = -0.53$, $p = 0.32$), western Australia and NP ($r = -0.56$, $p = 0.28$), and eastern Australia and Niño 4 ($r = -0.52$, $p = 0.19$). The correlations detailed above that involve Niño 4 are the only correlations significant at the 80% level.

The peak observed in the north-east Pacific index in 1997–1998 (**Figure 10A**), corresponds to one of the strongest El Niño events in the time-series. The peak observed in both the Seattle record and the NEP index in 1982–1983 corresponds to another strong El Niño event, however, the El Niño event of 1972 is not evident in the skew surge time series. Also, the typically positive Niño 3 values observed through the early 1990s coincide with a trough in the north-east Pacific index. The presence of a peak in north-east Pacific index during only the strongest El Niño events suggest a complex relationship between skew surge and the magnitude of variability in regional climate.

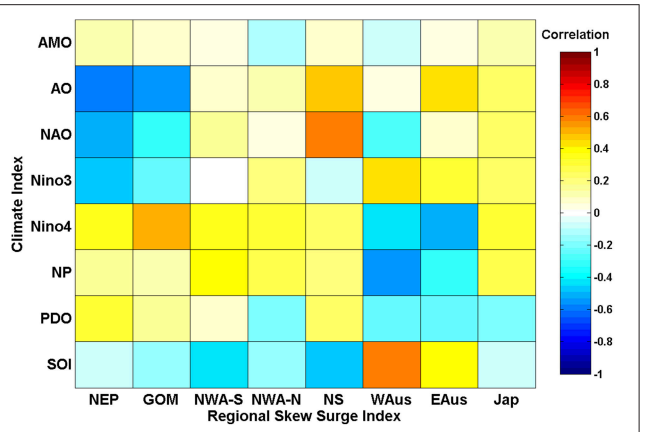

FIGURE 12 | Correlation of regional indices of skew surge against key climatic indices.

DISCUSSION

One of the key goals of this paper was to determine if different results are obtained when using skew surge to assess changes in storm surge activity, compared to the more traditional NTR. As Horsburgh and Wilson (2007) showed, while the NTR primarily contains the meteorological contribution termed the surge, it may also contain harmonic prediction errors or timing errors, and non-linear interactions, which can bias analysis of storm surges. It is for this reason that we wanted to assess the alternative use of skew surges. The advantage of using skew surge is that it is an integrated and unambiguous measure of the storm surge (Haigh et al., 2015). Changes in skew surges have only previously been assessed (to our knowledge) at sites around the north-west Europe (Batstone et al., 2013; Dangendorf et al., 2014) and the USA (Wahl and Chambers, 2015). Both of these regions generally display semi-diurnal tidal behavior, but our method works well in all tidal regimes.

We found that significant tide-surge interaction occurs at 130 of the 220 sites analyzed (59%) based on the tidal-level method, and 175 sites (81%) based on tidal-phase approach. These sites include those previously reported, as well as regions not previously identified in the literature, such as the Gulf of Panama and the Malay Peninsula. We also found that tide-surge interaction is not limited to locations with large adjacent areas of shallow bathymetry. Smaller but still statistically significant interactions occur along the Pacific coast of North America, on a number of Pacific Islands and around the Iberian Peninsula. The topography of these sites is highly variable. Some sites are in shallow water such as Willapa Bay, USA, which is in a large bay, and Astoria, USA, which is influenced by the Columbia River. Other sites are on volcanic islands rising steeply from the ocean floor, such as Papette, French Polynesia and Pohnpei, the Federated States of Micronesia. For both these island sites there is an increased frequency of peaks in NTR around the time of predicted HW, a pattern that is also observed at Galveston, USA (**Figure 4D**).

In some regions the timing of the peak NTR relative to tidal-phase, and therefore the level of tide-surge interaction is site specific. For example, around the UK, peak NTR usually occurs away from predicted HW (Horsburgh and Wilson, 2007; Haigh et al., 2010; Olbert et al., 2013), and in the North Sea Horsburgh and Wilson (2007) showed that the external surge component will always peak away from predicted HW. However, at Larne and Bangor in Northern Ireland, peak NTR most frequently occurred at predicted HW (Olbert et al., 2013). These sites have similar tidal conditions and are geographically close but highlight that small changes in bathymetry and tidal range can influence the extent of tide-surge interaction.

Individual storm characteristics vary from the average pattern, and where these deviations occur in the largest storm surges the difference in skew surge magnitude can be important. At Wake Island in the Pacific, Typhoon Ioke generated a NTR of 1.5 m

but a skew surge of only 1.0 m, because the peak NTR for this event occurred 5 h before predicted HW (see Figure A3.10 in Supplementary Material, Site 434). However, no significant tide-surge interaction is observed at this site and the peak NTR for an event like Typhoon Ioke could have occurred at predicted HW. Conversely, at Brest, France, where significant tide-surge interaction meant that peaks in NTR usually occurred away from predicted HW, the maximum NTR (caused by the so-called Great Storm in October 1987) occurs at the same time as predicted HW. Therefore, although the skew surge is a more reliable indicator of the average meteorological influence on sea level, individual storm surges may have different characteristics. Parameterization of any physical process aims to use one value to represent a complex system, and this must be considered when we use skew surge in ESL calculations. This is especially true in regions with small tidal ranges or those affected by tropical cyclones. The rapid peak in storm surge associated with tropical cyclones reduces the influence of storm surge on tidal propagation, and may lead to a more uniform distribution of peak NTR timing relative to predicted HW.

Although tide-surge interaction is evident at many sites, and there are differences between skew surge and NTR values, we found that at most sites, the trends in skew surge are very similar to those in NTR. The largest differences in trends are at sites along the north-coast of Australia or the French coast of the English Channel, and this results in the reversal of trends at Calais and Darwin. Both locations have macro-tidal regimes with significant tide-surge interaction. The general similarity in trends means we can compare our results to previous studies which used NTR. Menéndez and Woodworth (2010) found more negative trends in NTR than positive trends globally. We also find more negative trends in NTR, but no statistically significant difference between the number of positive and negative trends in skew surge time-series. Our findings are consistent with those of Wahl and Chambers (2015) for the US, who found a greater number of sites had significant trends in NTR compared to skew surge. The number of sites with significant trends in skew surge and NTR may be generated from chance, but a formal assessment has not been made here, because of the spatially non-homogenous dataset. Methods such as that of Livezey and Chen (1983) could be adapted to assess whether the number of trends is statistically significant. Even so, there are a greater number of negative trends in NTR than skew surge and this may be caused by timing errors or changes in the tide-surge interaction. Timing errors are particular evident in early records that have been digitized from paper charts and are often associated with issues with the older mechanical tide gauges (Pugh and Woodworth, 2014). Therefore, timing errors are more prevalent in the early part of the tide gauge records, and if they are included in the analysis they may introduce a negative bias into the NTR time-series. By definition, time-series of skew surges are not influenced by such timing errors. Another possible reason for the difference in trends is that the magnitude of the tide-surge interaction is changing through time, because of changes in the phase or magnitude of the tide (e.g., Mawdsley et al., 2015). Previous studies in the North Sea (Horsburgh and Wilson, 2007) and English Channel (Haigh et al., 2010) however, found no significant changes in tide-surge interaction over time. We have not investigated this, in this study.

We found little spatial coherence in the magnitude and sign of trends among sites, mainly because the trends are insignificant at most sites. However, in northern Australia a number of sites display significant negative trends in skew surge (**Figure 7**) and in NTR, which is consistent with Menéndez and Woodworth (2010), while our findings also support their research showing positive trends at sites in the Gulf of Mexico and along the Atlantic coast of Florida. However, most other findings vary from those of Menéndez and Woodworth (2010). We find a decrease at sites in southern Europe, and an increase at a number of sites in southern Australia. No coherent trend along the north-east coast of America is observed in this study, which agrees with Zhang et al. (2000) but contradicts the increase found in this region by both Menéndez and Woodworth (2010) and Grinsted et al. (2012). Differences between our findings and those of Menéndez and Woodworth (2010) may be the result of further quality control, or the inclusion of new data, which along the north-east coast of America included large storms surges in 2010 and 2012, generated by Hurricanes Irene and Sandy, respectively. Figures A3.1–3.4, in the Supplementary Material, show that trends over the last 20–80 years change depending on the period studied, and therefore extra data can change results. In other studies of ESL, changes may also be caused by the inclusion of tide, such as the increases in New York (Talke et al., 2014), western Northern America (Bromirski et al., 2003; Abeysirigunawardena and Walker, 2008; Cayan et al., 2008) and the German Bight (Müdersbach et al., 2013). Mawdsley et al. (2015) observed significant increases in tidal HW in all these regions, and we speculate that this has contributed toward the observed increase in ESL, in other studies, and the lack of trends in skew surges identified by this paper in these areas. With the growing literature regarding changes in tide (e.g., Jay, 2009; Woodworth, 2010; Pickering et al., 2012; Pelling et al., 2013; Mawdsley et al., 2015), it is essential that studies of storm surge use parameters that just relate to meteorological changes and identify other drivers of change, such as the tide or tide-surge interaction.

The number of statistically significant trends is low, in part, because of the large inter-annual variability in the high percentiles of skew surges. The creation of filtered regional skew surge indices removed the high frequency variability and helped to reveal underlying inter-decadal variability and the spatial coherence between regional signals. However, despite strong correlations between some regions around the North American coastline and across the Atlantic to the North Sea, none of the correlations are significant at the 95% level. Just prior to completing our study, we learnt of a similar investigation by Marcos et al. (2015). Using the GESLA dataset, they showed that the intensity and frequency of ESL unrelated to MSL display a regional coherence on decadal time-scales. Their finding points toward large-scale climate drivers of decadal changes in storminess (Marcos et al., 2015). The string correlations between neighboring sites show that these large scale climatic drivers are important, but there significance is difficult to assess in relatively short datasets have a high degree of temporal auto-correlation.

Comparisons of regional storm surge time-series and climate indices have been undertaken in numerous past studies.

Menéndez and Woodworth (2010) found the Niño 3 index had a positive correlation with the magnitude of NTR in the eastern Pacific and a negative correlation in the western equatorial Pacific. The magnitude of an El Niño appears to influence the north-east Pacific index, with peaks in the index associated with the largest El Niño events in 1982–1983 and 1997–1998, but a trough in the index during small but positive values of the Niño 3 index in the early 1990s. Also in the Pacific the PDO was previously shown to correlate positively with sites in the northeast Pacific (Abeysirigunawardena and Walker, 2008), however we do not find any significant correlation. The findings related to the North Sea index supports previous studies (e.g., Haigh et al., 2010) that find a positive correlation with the NAO, although our correlation is not significant. Studies by Ezer and Atkinson (2014) and Talke et al. (2014) found anti-correlation between the NAO and sites on the US east coast, but we find very weak (and non-significant) correlations. Our method of using filtered regional skew surge indices, means that although strong correlations ($r > 0.5$) are observed between some regional skew surge indices and climate indices, they are not deemed significant at the 95% level. The effect of autocorrelation in the calculation reduces the degrees of freedom (effective observations) from 40 to less than 8 for all correlation calculations, and therefore increases the size of the confidence intervals. The significance of correlations may improve with increased data length or reduced filter size, however, filters are a widely used and during the development of the methodology the 10 year Loess filter was found to give the lowest RMSE. In this study we have correlated skew surge time-series against climate indices, but it would be more appropriate to use wind and pressure datasets, as these are the parameters that directly cause storm surges. In the future, we hope to do this using meteorological re-analysis datasets, like Bromirski et al. (2003), Calafat et al. (2013) and Wahl and Chambers (2015) did to assess storm surge variability in their regional studies.

One of the main limitations of this study (and other studies) remains the relatively small number of sites and the limited length of the time-series available. Although the GESLA dataset is probably the most comprehensive collection of hourly sea level data, there are still many under-represented regions in the database. The 8 regional indices we derived all cover data dense regions since this is where the strongest correlations are, but even here the number of datasets longer than 40 years limited the length of the regional skew surge indices. The application of the filter, which is necessary to extract relationships between the datasets, meant that the confidence intervals increased and the significance of the correlations decreased. There is a need for either more sites or better access to data in under-represented areas, especially areas that are prone to large storm surges, such as the Caribbean, the Bay of Bengal and countries around the South China Sea. Conversely, the already global nature of the study does not allow for a detailed understanding of the findings presented here. Further work conducted on a local to regional scale, should be undertaken to assess the mechanisms that are driving the tide-surge interaction, and control its specific signature. Such assessment could consider differences in the tide-surge interaction for tropical and extra-tropical storms, the influence of slope angle or shelf width, or the effect of changes in bathymetry.

CONCLUSIONS

In this paper, we have used time series of skew surge to assess changes in storm surges on a quasi-global scale for the first time. Past studies that have assessed changes in storm surges have tended to focus on the NTR, which includes contributions from non-meteorological generated factors, which may bias results. This study also assessed the spatial and temporal variability in the skew surge, using regional indices.

First, we determined the extent of tide-surge interaction, at each of the 220 study sites, as this determines the scale of the differences between skew surge and NTR values. Using χ^2 test statistics we found statistically significant (95% confidence) levels of tide-surge interaction at 130 of the 220 sites (59%) based on tidal-level and 175 sites (81%) based on tidal-phase. The tide-surge interaction is strongest in regions of shallow bathymetry such as the North Sea, north Australia and the Malay Peninsula. However, non-standard distributions are also observed at sites on open ocean islands, although at these sites the peak in NTR often tended toward the time of predicted HW, rather than away from it as experienced in shallow water areas (such as the North Sea).

Second, we determined if different results are obtained when using skew surges to assess changes in storm surge activity, compared to the more traditional NTR. At most sites the trends in skew surge are similar to those of NTRs. Where the differences in trends were large, the sites tended to have a large tidal range, such as those in northern Australia and northern France. Although at most sites the trends in skew surges were not statistically significant, we observed approximately equal numbers of positive and negative trends. However, there were more negative trends in the NTR. This suggests that skew surge improves the calculation of trends, because phase offsets caused by time errors are not present in time series of skew surges.

Third, we examined the extent to which there is spatial coherence in skew surge variability, both locally (i.e., among adjacent tide gauge sites) and regionally (i.e., across ocean basins). We identified 8 regions, where there were strong positive correlations among neighboring sites, and hence derived a regional index for each region. We observed a number of strong ($r > 0.5$) correlations between regions, including: positive correlation between the two regions on North American Atlantic coast, positive correlation between the north-west Atlantic—south and the North Sea; and negative correlation between the North Sea and north-east Pacific. However, these trends were not significant at the 95% level, since the high degree of autocorrelation in the filtered dataset increased the size of the confidence intervals.

Finally, we compared multi-decadal variations in skew surge with fluctuations in regional climate. Again strong correlations were observed, but were not significant at the 95% level. Correlations significant at the 80% level included those between the Gulf of Mexico and eastern Australia and the Niño 4 index.

AUTHOR CONTRIBUTIONS

RM conducting the data quality control for all tide gauge sites, before developing and coding the method for extraction of the skew surge. Also was primarily involved in creation of Figures and writing of text. IH developed and coded some of the method for skew surge extraction, as well as the chi-squared test to assess tide-surge interaction. Also heavily involved with editing of text.

ACKNOWLEDGMENTS

This study was funded by the University of Southampton, School of Ocean and Earth Science and the National Environmental Research Council (NERC). Conversations and feedback from Phillip Woodworth, Neil Wells and Francisco Calafat at the National Oceanography Centre have been invaluable. We thank the reviewers of the paper, whose excellent comments have improved this paper. The GESLA data set was initially collated by staff from the National Oceanography Centre (NOC), Liverpool in the UK and the Antarctic Climate and Ecosystems Cooperative Research Centre (ACE CRC) in Australia. Extensions to the dataset were provided by: University of Hawaii Sea Level Center (UHSLC), National Oceanographic and Atmospheric Authority (NOAA), British Oceanographic Data Centre (BODC), Norwegian Mapping Authority (NMA), Marine Environmental Data Service (MEDS); Bureau of Meteorology (BOM); and Norwegian Mapping Authority (NMA). This paper contributes to the Engineering and Physical Science Research Council Flood Memory Project (grant number EP/K013513/1).

SUPPLEMENTARY MATERIAL

The Supplementary Material for this article can be found online at: http://journal.frontiersin.org/article/10.3389/fmars.2016.00029

REFERENCES

Abeysirigunawardena, D. S., and Walker, I. J. (2008). Sea level responses to climatic variability and change in Northern British Columbia. *Atmosp. Ocean* 46, 277–296. doi: 10.3137/ao.460301

Antony, C., and Unnikrishnan, A. S. (2013). Observed characteristics of tide-surge interaction along the east coast of India and the head of Bay of Bengal. *Estuarine Coast. Shelf Sci.* 131, 6–11. doi: 10.1016/j.ecss.2013.08.004

Araújo, I. B., and Pugh, D. T. (2008). Sea levels at Newlyn 1915–2005: analysis of trends for future flooding risks. *J. Coastal Res.* 24, 203–212. doi: 10.2112/06-0785.1

Batstone, C., Lawless, M., Tawn, J., Horsburgh, K., Blackman, D., McMillan, A., et al. (2013). A UK best-practice approach for extreme sea-level analysis along complex topographic coastlines. *Ocean Eng.* 71, 28–39. doi: 10.1016/j.oceaneng.2013.02.003

Bell, G. D., and Chelliah, M. (2006). Leading tropical modes associated with interannual and multidecadal fluctuations in North Atlantic hurricane activity. *J. Clim.* 19, 590–612. doi: 10.1175/JCLI3659.1

Bernier, N., and Thompson, K. (2007). Tide-surge interaction off the east coast of Canada and northeastern United States. *J. Geophys. Res.* 112, C06008. doi: 10.1029/2006jc003793

Box, G. E. P., Jenkins, G. M., and Reinsel, G. C. (1994). *Time Series Analysis: Forecasting and Control. 3rd Edn*. Upper Saddle River, NJ: Prentice-Hall.

Bromirski, P. D., Flick, R. E., and Cayan, D. R. (2003). Storminess variability along the California Coast: 1858–2000. *J. Clim.* 16, 982–993. doi: 10.1175/1520-0442(2003)016<0982:SVATCC>2.0.CO;2

Calafat, F. M., Chambers, D. P., and Tsimplis, M. N. (2013). Inter-annual to decadal sea-level variability in the coastal zones of the Norwegian and Siberian Seas: the role of atmospheric forcing. *J. Geophys. Res.* 118, 1287–1301. doi: 10.1002/jgrc.20106

Cayan, D. R., Bromirski, P. D., Hayhoe, K., Tyree, M., Dettinger, M. D., and Flick, R. E. (2008). Climate change projections of sea level extremes along the California coast. *Clim. Change* 87, S57–S73. doi: 10.1007/s10584-007-9376-7

Church, J. A., Clark, P. U., Cazenave, A., Gregory, J. M., Jevrejeva, S., Levermann, A., et al. (2013). "Sea level change," in *Climate Change 2013: The Physical Science Basis. Contribution of Working Group I to the Fifth Assessment Report of the Intergovernmental Panel on Climate Change*, eds T. F. Stocker, D. Qin, G.-K. Plattner, M. Tignor, S. K. Allen, J. Boschung, A. Nauels, Y. Xia, V. Bex, and P. M. Midgley (Cambridge, UK; New York, NY: Cambridge University Press), 1137–1216.

Cleveland, W. S., and Devlin, S. J. (1988). Locally weighted regression: an approach to regression analysis by local fitting. *J. Am. Stat. Assoc.* 83, 596–610. doi: 10.1080/01621459.1988.10478639

Dangendorf, S., Calafat, F. M., Arns, A., Wahl, T., Haigh, I. D., and Jensen, J. (2014). Mean sea level variability in the North Sea: processes and implications. *J. Geophys. Res.* 119, 6820–6841. doi: 10.1002/2014jc009901

Dixon, M. J., and Tawn, J. A. (1994). *Extreme Sea-Levels at the UK A-Class Sites: Site-by-Site Analyses*. Proudman Oceanographic Laboratory, Internal Document, No. 65, 229.

Emanuel, K. A., Sundararajan, R., and Williams, J. (2008). Hurricanes and global warming: results from downscaling IPCC AR4 simulations. *Bull. Am. Meteorol. Soc.* 89, 346–367. doi: 10.1175/bams-89-3-347

Ezer, T., and Atkinson, L. P. (2014). Accelerated flooding along the U.S. East Coast: on the impact of sea-level rise, tides, storms, the Gulf Stream, and the North Atlantic Oscillations. *Earth Fut.* 2, 362–382. doi: 10.1002/2014EF000252

Feng, X., and Tsimplis, M. N. (2014). Sea level extremes at the coasts of China. *J. Geophys. Res.* 119, 1593–1608. doi: 10.1002/2013jc009607

Grinsted, A., Moore, J. C., and Jevrejeva, S. (2012). Homogeneous record of Atlantic hurricane surge threat since 1923. *Proc. Natl. Acad. Sci. U.S.A.* 109, 19601–19605. doi: 10.1073/pnas.1209542109

Haigh, I., Nicholls, R., and Wells, N. (2009a). Mean sea level trends around the English Channel over the 20th century and their wider context. *Cont. Shelf Res.* 29, 2083–2098. doi: 10.1016/j.csr.2009.07.013

Haigh, I., Nicholls, R., and Wells, N. (2009b). Twentieth-Century changes in extreme still sea levels in the English channel. *Coast. Eng. 2008.* 1–5, 1199–1209. doi: 10.1142/9789814277426_0100

Haigh, I., Nicholls, R., and Wells, N. (2010). Assessing changes in extreme sea levels: Application to the English Channel, 1900–2006. *Cont. Shelf Res.* 30, 1042–1055. doi: 10.1016/j.csr.2010.02.002

Haigh, I., Wijeratne, E. M. S., MacPherson, L., Pattiaratchi, C., Mason, M., Crompton, R., et al. (2014). Estimating present day extreme water level exceedance probabilities around the coastline of Australia: tides, extra-tropical storm surges and mean sea level. *Clim. Dynam.* 42, 121–138. doi: 10.1007/s00382-012-1652-1

Haigh, I. D., Wadey, M. P., Gallop, S. L., Loehr, H., Nicholls, R. J., Horsburgh, K., et al. (2015). A user-friendly database of coastal flooding in the United Kingdom from 1915–2014. [Data Descriptor]. *Sci. Data* 2, 150021. doi: 10.1038/sdata.2015.21

Hartmann, D. L., Klein Tank, A., and Rusticucci, M. (2013). "Observations: ocean," in *Climate Chanage 2013: The Physical Scientific Basis. Working Group I Contribution to the Intergovernmental Panel on Climate Change 5th Assessment Report,* eds J. Hurrell, J. Marengo, F. Tangang, and P. Viterbo (Cambridge, UK; New York, NY: Cambridge University Press), 159–254.

Horsburgh, K. J., and Wilson, C. (2007). Tide-surge interaction and its role in the distribution of surge residuals in the North Sea. *J. Geophys. Res.* 112, C08003. doi: 10.1029/2006jc004033

Hunter, J. (2012). A simple technique for estimating an allowance for uncertain sea-level rise. *Clim. Change* 113, 239–252. doi: 10.1007/s10584-011-0332-1

Hunter, J. R., Church, J. A., White, N. J., and Zhang, X. (2013). Towards a global regionally varying allowance for sea-level rise. *Ocean Eng.* 71, 17–27. doi: 10.1016/j.oceaneng.2012.12.041

Idier, D., Dumas, F., and Muller, H. (2012). Tide-surge interaction in the English Channel. *Nat. Hazards Earth Syst. Sci.* 12, 3709–3718. doi: 10.5194/nhess-12-3709-2012

Jay, D. A. (2009). Evolution of tidal amplitudes in the eastern Pacific Ocean. *Geophys. Res. Lett.* 36, L04603. doi: 10.1029/2008gl036185

Kossin, J. P., Knapp, K. R., Vimont, D. J., Murnane, R. J., and Harper, B. A. (2007). A globally consistent reanalysis of hurricane variability and trends. *Geophys. Res. Lett.* 34:L04815. doi: 10.1029/2006gl028836

Lionello, P., Mufato, R., and Tomasin, A. (2005). Sensitivity of free and forced oscillations of the Adriatic Sea to sea level rise. *Clim. Res.* 29, 23–39. doi: 10.3354/cr029023

Livezey, R. E., and Chen, W. Y. (1983). Statistical field significance and its determination by monte carlo techniques. *Mon. Weather Rev.* 111, 46–59. doi: 10.1175/1520-0493(1983)111<0046:sfsaid>2.0.co;2

Marcos, M., Calafat, F. M., Berihuete, Á., and Dangendorf, S. (2015). Long-term variations in global sea level extremes. *J. Geophys. Res.* 120, 8115–8134. doi: 10.1002/2015jc011173

Marcos, M., Tsimplis, M. N., and Shaw, A. G. P. (2009). Sea level extremes in southern Europe. *J. Geophys. Res.* 114:C01007. doi: 10.1029/2008JC004912

Mawdsley, R. J., Haigh, I. D., and Wells, N. C. (2015). Global secular changes in different tidal high water, low water and range levels. *Earth Fut.* 3, 66–81. doi: 10.1002/2014EF000282

Menéndez, M., and Woodworth, P. L. (2010). Changes in extreme high water levels based on a quasi-global tide-gauge data set. *J. Geophys. Res.* 115, C10011. doi: 10.1029/2009JC005997

Müdersbach, C., Wahl, T., Haigh, I. D., and Jensen, J. (2013). Trends in high sea levels of German North Sea gauges compared to regional mean sea level changes. *Cont. Shelf Res.* 65, 111–120. doi: 10.1016/j.csr.2013.06.016

Olbert, A. I., Nash, S., Cunnane, C., and Hartnett, M. (2013). Tide–surge interactions and their effects on total sea levels in Irish coastal waters. [journal article]. *Ocean Dynam.* 63, 599–614. doi: 10.1007/s10236-013-0618-0

Pelling, H. E., Mattias Green, J. A., and Ward, S. L. (2013). Modelling tides and sea-level rise: to flood or not to flood. *Ocean Modell.* 63, 21–29. doi: 10.1016/j.ocemod.2012.12.004

Pickering, M. D., Wells, N. C., Horsburgh, K. J., and Green, J. A. M. (2012). The impact of future sea-level rise on the European Shelf tides. *Cont. Shelf Res.* 35, 1–15. doi: 10.1016/j.csr.2011.11.011

Pugh, D., and Woodworth, P. (2014). *Sea-level Science: Understanding Tides, Surges, Tsunamis and Mean Sea-level* Changes: Cambridge University Press.

Raicich, F. (2003). Recent evolution of sea-level extremes at Trieste (Northern Adriatic). *Cont. Shelf Res.* 23, 225–235. doi: 10.1016/S0278-4343(02)00224-8

Ray, R. D. (2009). Secular changes in the solar semidiurnal tide of the western North Atlantic Ocean. *Geophys. Res. Lett.,* 36, L19601. doi: 10.1029/2009gl040217

Seneviratne, S. I., Nicholls, N., Easterling, D., Goodess, C. M., Kanae, S., Kossin, J., et al. (2012). "Changes in climate extremes and their impacts on the natural physical environment," in *Managing the Risks of Extreme Events and Disasters to Advance Climate Change Adaptation*. A *Special Report of Working Groups I and II of the Intergovernmental Panel on Climate Change (IPCC)*, eds C. B. Field, V. Barros, T. F. Stocker, D. Qin, D. J. Dokken, K. L. Ebi, et al. (Cambridge; New York, NY: Cambridge University Press), 109–230.

Shennan, I., and Woodworth, P. L. (1992). A comparison of late Holocene and twentieth-century sea-level trends from the UK and North Sea region. *Geophys. J. Intern.* 109, 96–105. doi: 10.1111/j.1365-246X.1992.tb00081.x

Talke, S. A., Orton, P., and Jay, D. A. (2014). Increasing storm tides in New York Harbor, 1844–2013. *Geophys. Res. Lett.* 41, 3149–3155. doi: 10.1002/2014GL059574

Thompson, P. R., and Mitchum, G. T. (2014). Coherent sea level variability on the North Atlantic western boundary. *J. Geophys. Res.* 119, 5676–5689. doi: 10.1002/2014jc009999

Thompson, P. R., Mitchum, G. T., Vonesch, C., and Li, J. (2013). Variability of Winter Storminess in the Eastern United States during the Twentieth Century from Tide Gauges. *J. Clim.* 26, 9713–9726. doi: 10.1175/JCLI-D-12-00561.1

Torres, R. R., and Tsimplis, M. N. (2013). Sea-level trends and interannual variability in the Caribbean Sea. *J. Geophys. Res.* 118, 2934–2947. doi: 10.1002/jgrc.20229

Trenberth, K. E., Jones, P. D., Ambenje, P., Bojariu, R., Easterling, D., Klein Tank, A., et al. (2007). "Observations: surface and atmospheric climate change," in *Climate Change 2007: The Physical Science Basis. Contribution of Working Group I to the Fourth Assessment Report of the Intergovernmental Panel on Climate Change,* eds S. Solomon, D. Qin, M. Manning, Z. Chen, M. Marquis, K.B. Averyt, M. Tignor, and H. L. Miller (Cambridge; New York, NY: Cambridge University Press), 235–336.

Ullmann, A., Pirazzoli, P. A., and Tomasin, A. (2007). Sea surges in Camargue: trends over the 20th century. *Cont. Shelf Res.* 27, 922–934. doi: 10.1016/j.csr.2006.12.001

Valle-Levinson, A., Olabarrieta, M., and Valle, A. (2013). Semidiurnal perturbations to the surge of Hurricane Sandy. *Geophys. Res. Lett.* 40, 2211–2217. doi: 10.1002/grl.50461

Vecchi, G. A., and Soden, B. J. (2007). Increased tropical Atlantic wind shear in model projections of global warming. *Geophys. Res. Lett.* 34:L08702. doi: 10.1029/2006gl028905

von Storch, H., and Woth, K. (2008). Storm surges: perspectives and options. *Sustainab. Sci.* 3, 33–43. doi: 10.1007/s11625-008-0044-2

Wahl, T., and Chambers, D. P. (2015). Evidence for multidecadal variability in US extreme sea level records. *J. Geophys. Res.* 120, 1527–1544. doi: 10.1002/2014jc010443

Wahl, T., and Chambers, D. P. (2016). Climate controls multidecadal variability in U. S. extreme sea level records. *J. Geophys. Res.* 121. doi: 10.1002/2015JC011057

Wahl, T., Haigh, I. D., Woodworth, P. L., Albrecht, F., Dillingh, D., Jensen, J., et al. (2013). Observed mean sea level changes around the North Sea coastline from 1800 to present. *Earth Sci. Rev.* 124, 51–67. doi: 10.1016/j.earscirev.2013.05.003

Wolf, J. (1981). "Surge-tide interaction in the North Sea and River Thames," in *Floods Due to High Winds and Tides*, ed D. H. Peregrine (New York, NY: Elseiver), 75–94.

Wong, P. P., Losada, I. J., Gattuso, J. P., Hinkel, J., Khattabi, A., McInnes, K. L., et al. (2014). "Coastal systems and low-lying areas," in *Climate Change 2014: Impacts, Adaptation, and Vulnerability. Part A: Global and Sectoral Aspects. Contribution of Working Group II to the Fifth Assessment Report of the Intergovernmental Panel of Climate Change,* eds C. B. Field, V. R. Barros, D. J. Dokken, K. J. Mach, M. D. Mastrandrea, T. E. Bilir, et al. (Cambridge; New York, NY: Cambridge University Press), 361–409.

Woodworth, P. L. (2010). A survey of recent changes in the main components of the ocean tide. *Cont. Shelf Res.* 30, 1680–1691. doi: 10.1016/j.csr.2010.07.002

Woodworth, P. L., and Blackman, D. L. (2004). Evidence for systematic changes in extreme high waters since the mid-1970s. *J. Clim.* 17, 1190–1197. doi: 10.1175/1520-0442(2004)017<1190:EFSCIE>2.0.CO;2

Woodworth, P. L., and Menéndez, M. (2015). Changes in the mesoscale variability and in extreme sea levels over two decades as observed by satellite altimetry. *J. Geophys. Res.* 120, 64–77. doi: 10.1002/2014jc010363

Woodworth, P. L., Teferle, F. N., Bingley, R. M., Shennan, I., and Williams, S. D. P. (2009). Trends in UK mean sea level revisited. *Geophys. J. Intern.* 176, 19–30. doi: 10.1111/j.1365-246X.2008.03942.x

Woodworth, P. L., Tsimplis, M. N., Flather, R. A., and Shennan, I. (1999). A review of the trends observed in British Isles mean sea level data measured by tide gauges. *Geophys. J. Intern.* 136, 651–670. doi: 10.1046/j.1365-246x.1999.00751.x

Zhang, K. Q., Douglas, B. C., and Leatherman, S. P. (2000). Twentieth-century storm activity along the US east coast. *J. Clim.* 13, 1748–1761. doi: 10.1175/1520-0442(2000)013<1748:TCSAAT>2.0.CO;2

Conflict of Interest Statement: The authors declare that the research was conducted in the absence of any commercial or financial relationships that could be construed as a potential conflict of interest.

frontiers in Marine Science

ORIGINAL RESEARCH
published: 22 July 2016
doi: 10.3389/fmars.2016.00125

Statistical Analysis of the Acceleration of Baltic Mean Sea-Level Rise, 1900–2012

*Birgit Hünicke * and Eduardo Zorita*

Institute of Coastal Research, Helmholtz-Centre Geesthacht, Geesthacht, Germany

We analyse annual mean sea-level records from tide-gauges located in the Baltic and parts of the North Sea with the aim of detecting an acceleration of sea-level rise over the twentieth and twenty-first centuries. The acceleration is estimated as a (1) fit to a polynomial of order two in time, (2) a long-term linear increase in the rates computed over gliding overlapping decadal time segments, and (3) a long-term increase of the annual increments of sea level. The estimation methods (1) and (2) prove to be more powerful in detecting acceleration when tested with sea-level records produced in global climate model simulations. These methods applied to the Baltic-Sea tide-gauges are, however, not powerful enough to detect a significant acceleration in most of individual records, although most estimated accelerations are positive. This lack of detection of statistically significant acceleration at the individual tide-gauge level can be due to the high-level of local noise and not necessarily to the absence of acceleration. The estimated accelerations tend to be stronger in the north and east of the Baltic Sea. Two hypothesis to explain this spatial pattern have been explored. One is that this pattern reflects the slow-down of the Glacial Isostatic Adjustment. However, a simple estimation of this effect suggests that this slow-down cannot explain the estimated acceleration. The second hypothesis is related to the diminishing sea-ice cover over the twentieth century. The melting of less saline and colder sea-ice can lead to changes in sea-level. Also, the melting of sea-ice can reduce the number of missing values in the tide-gauge records in winter, potentially influencing the estimated trends and acceleration of seasonal mean sea-level. This hypothesis cannot be ascertained either since the spatial pattern of acceleration computed for winter and summer separately are very similar. The all-station-average-record displays an almost statistically significant acceleration. The very recent decadal rates of sea-level rise are high in the context of the twentieth and twenty-first centuries, but they are not the highest rates observed over this period.

Keywords: Baltic-Sea, North Sea, sea-level, acceleration, Glacial Isostatic Adjustment

OPEN ACCESS

Edited by:
Francisco Mir Calafat, Natural Environment Research Council, UK

Reviewed by:
Gabriel Jorda, Universitat Illes Balears, Spain
Hans Visser, Netherlands Environmental Assessment Agency, Netherlands

****Correspondence:***
Birgit Hünicke
birgit.huenicke@hzg.de

Specialty section:
This article was submitted to Coastal Ocean Processes, a section of the journal Frontiers in Marine Science

Received: *28 January 2016*
Accepted: *06 July 2016*
Published: *22 July 2016*

Citation:
Hünicke B and Zorita E (2016) Statistical Analysis of the Acceleration of Baltic Mean Sea-Level Rise, 1900–2012. Front. Mar. Sci. 3:125. doi: 10.3389/fmars.2016.00125

1. INTRODUCTION

Global mean sea-level has generally risen during the twentieth and twenty-first century due to the warming of the world oceans, melting of glaciers and polar ice-caps (Church and White, 2011; Church et al., 2011). The mean rate of global mean sea-level rise over this period has turned to be difficult to quantify exactly because the available sea-level data set in this period is not

homogeneous, comprising a few tide-gauges records in the nineteenth century and the beginning of the twentieth century, and satellite altimetry in the twenty-first century with almost global coverage (Jevrejeva et al., 2008). The mean rate of sea-level rise has been estimated within an approximate range of 1.2 mm year^{-1} (Hay et al., 2015) to 1.5–2.0 mm year^{-1} (Hamlington and Thompson, 2015), whereas the most recent rates estimated from satellite altimetry indicate higher rates of the order of 3.1 mm year^{-1} (Cazenave et al., 2014; Jevrejeva et al., 2014).

The projections of global sea-level rise by the end of the twenty-first century derived from the thermal expansion of the world ocean in global climate simulations, together with estimation of melting of land-locked ice indicate an upper range of sea-level rise close to 0.9 m relative to the mean sea-level of the twentieth century (Church et al., 2013; Clark et al., 2015). Therefore, the projections of global mean sea-level rise by 2100 imply an acceleration of its rate, since a linear extrapolation of the twentieth century rate, or even of the higher more recent rate derived from satellite altimetry, would yield a global mean sea-level rise of at least of the order of 30–40 cm by 2100.

In this study, we focus tide-gauge records of sea-level in the Baltic Sea with the goal of detecting an acceleration of the observed sea-level rise in this region. The Baltic Sea records offer the advantage of its unusual temporal and spatial coverage, many of them spanning the whole twentieth century and a few even longer, but unavoidably they can only provide information on regional sea-level. Global sea-level reconstructions offer a much wider coverage but they are constructed combining different sources of information, such as tide-gauges and satellite altimetry, and with a time varying level of spatial coverage. Thus, their use for detection of a still emerging and not totally clear signal in the observational period might be compromised by inhomogeneities (Church and White, 2011; Hamlington and Thompson, 2015).

An important question in the detection of acceleration in a climate record is precisely the definition of acceleration. Although velocity and acceleration in a kinematic context are precisely defined as the first and second second time derivative, respectively, the application of these definitions to discreet time series is not straight forward.

Similarly to the definition of linear trend in a stochastic process as a linear change trough time of its mean the acceleration could be defined as a non-linear increase through time of its mean. This non-linear increase can be quadratic or adopt a more complex functional form. Due to the generally limited length of sea-level time series and the high level of noise usually present in them, the detection of a distinctly non-linear increase of the mean of the underlying process is challenging unless the signal-to-noise ratio is high. In the context of sea-level records, several publications have reviewed some of the methods to estimate accelerations used in studies of sea-level rise (e.g., Visser et al., 2015).

Visser et al. (2015) discussed in detail and classifies 30 methods to estimate trends in time series, with some of them also applicable to estimate the acceleration. As stressed in that publication, there is no clear best method—as the different methods may display competing properties of estimation variance and bias, and the true value of the acceleration is not known. Here, we will apply three methods (augmented with some variants) to estimate the acceleration. These methods are intended to be physically motivated, as the estimate quantities that are very often computed to monitor the evolution of sea-level.

One estimation method (1) (Houston and Dean, 2011) computes the acceleration as the second order coefficient (multiplied by 2) of a second-order polynomial fit to a sea-level record. This estimation method is parametric, since it assumes a predetermined functional form for the acceleration. If the acceleration does not conform to this functional form, the detection of acceleration might be compromised (Haigh et al., 2014).

A second estimation method (2) of acceleration relies on the calculation of gliding linear trends over a multiyear period. These gliding trends represent the rate of sea-level rise over this limited period. An acceleration would be then detected if the rates of sea-level rise display long-term increase (or decrease) over time. This estimation method has been frequently used (Holgate, 2007; Visser et al., 2015), although the exact definition of "changes over time" varies in the different studies so far. Usually, acceleration is considered to be detected when the rate of rise compared in two different periods separated in time, for instance at the beginning and at the end of the record, are significantly different (Jevrejeva et al., 2008; Haigh et al., 2014). A slightly different variant of this method was applied by one meta-study (Spada et al., 2015), based on a collection of published analysis of sea-level rates covering different periods, established a regression between those estimated rates and the mean point in time that each study covers. The acceleration is then estimated as the tendency of the sea-level rate to increase over time, as found in that particular collection of analyses. We will also explore a similar definition in the present study.

A third estimation method (3) computes the annual increments of sea-level, i.e., the value of annual mean sea-level in a certain year minus the value of annual mean sea-level in the previous year, and estimate the acceleration as a the long-term tendency of those annual increments to become larger (or smaller) over time. This increase could be assumed to be linear in a first approximation, i.e., a long-term linear trend, and in theory can be estimated by ordinary linear regression on time.

Related to these estimation methods is the question of the attribution of any acceleration to external climate forcing, such as anthropogenic greenhouse gases (Slangen et al., 2016). We do not address this question in this study, but we note here that, for attribution purposes, the analysis of the decadal rates according to definition (2) would be the more adequate among these three definitions, since a detection and attribution study would be first focused on determining at which point in time the estimated rates of sea-level rise leave the range of fluctuations that may be considered "natural" within a stable climate (Haigh et al., 2014).

The computation of acceleration at the regional scale is also important beyond purely scientific reasons. A robust detection of acceleration and even an estimation of its value, can be used to provide a better range, based on available observations, of future sea-level rise in the next decades than the purely linear

extrapolation of the more recent rate of rise, which could result in an underestimation of future sea-level rise. This information can be then incorporated in scientific assessments provided to regional planning agencies, although this approach would not cover any uncertainties due to new dynamics of the ice-sheets that may be triggered by future warming and that is not encapsulated in the observations until present.

In this study, we aim at detecting an acceleration of Baltic Sea-level analysing long records of the Baltic-Sea tide gauges applying these estimation methods.

The Baltic Sea is a semi-enclosed basin located at mid-to-high-latitudes in the Northern Hemisphere and strongly exposed to the atmospheric weather originating in the North Atlantic. For this reason, long-term trends of Baltic Sea-level, and changes thereof, may be influenced by other factors than the purely global sea-level rise due to global warming. The warming of the ocean water column has not been uniform over the globe and climate simulations also indicate a large spatial heterogeneity in the ocean warming (Church et al., 2004; Stammer et al., 2013; Slangen et al., 2014; Carson et al., 2015). Baltic-Sea level is strongly influenced by the westerly winds over the North Atlantic that push water from the North Sea into the Baltic Sea (Jevrejeva et al., 2005; Hünicke and Zorita, 2006; Barbosa, 2008; Bastos et al., 2013; Hünicke et al., 2015) rising Baltic Sea level. Thus, any long-term trends in internal modes of climate variability, like the North Atlantic Oscillation (NAO), will be also reflected in trends of sea-level (Calafat and Chambers, 2013). However, the influence of the NAO on Baltic Sea level is not spatially uniform due to the complex coastline of the Baltic Sea, with this influence being stronger in the North and East than in the South (Hünicke and Zorita, 2006). Other meteorological forcings (precipitation, run-off, local temperature) may also locally affect trends in Baltic-Sea level (Hünicke and Zorita, 2006).

The tide-gauges located in the North may be also influenced by sea-ice cover in winter. The melting of floating sea-ice, in contrast to floating pure water ice, may affect sea-level due to its lower salinity and temperature being lower than those of surrounding water (Jenkins and Holland, 2007; Shepherd et al., 2010). Another effect of diminishing ice cover in winter is a reduction of the missing values reported by the tide-gauges affected by sea-ice cover. Since the Baltic sea-level displays a clear annual cycle, this effect can spuriously affect the computed trends of sea-level trends and sea-level acceleration in those tide-gauges. The Bothnian Bay in the North is covered by sea-ice permanently for at least 150 days per year and the frequency and extent of sea-ice cover is diminishing in this area due to rising temperatures (Haapala et al., 2015).

In addition, the melting of polar-ice caps and land-glaciers also has a spatially heterogeneous fingerprint on regional sea-level due to the self-gravitational effect between land-ice and the ocean water masses (Mitrovica et al., 2001). For the Baltic Sea, the most important contribution from melting of land-ice stems from the Antarctic Ice sheets, whereas the contribution from Greenland is almost negligible—disregarding here the possible effect of Greenland melting on the circulation of the North Atlantic, which may also influence Baltic Sea level (Landerer et al., 2007). The time evolution of the melting of the Antarctic ice cap is still quite uncertain, with estimations of recent mass balance over the last few decades suggesting either sign (Zwally et al., 2015). Although higher temperatures over Antarctica will stimulate melting, these may also produce higher solid precipitation, so that the change in mass balance is a delicate difference between two uncertain quantities, at least in the recent decades. Therefore, the effect of the Antarctic contribution to Baltic Sea acceleration is also uncertain.

Finally, it is well-known that relative sea-level in the Baltic, as recorded by tide-gauges is subject to a very strong trend due to the Glacial Isostatic Adjustment (GIA), with relative sea-level falling in the North of the Baltic-Sea by about 10 mm^{-1} and rising the South of the Baltic Sea by about 1 mm^{-1} e.g., (Richter et al., 2012). The computation of acceleration is in theory not affected by the GIA as long as it is assumed that the effect of the GIA is linear within the time-scales analyzed here of about 100 years. However, the depression of the Earth crust caused by the ice load in the Last Glacial Maximum was of the order of several hundred meters. The current rate of recovery from this deformation is of the order of a few mm $year^{-1}$ and the acceleration estimated from tide-gauge records, as indicated later, is of the order of magnitude of tenths of μm $year^{-2}$. Therefore, an estimation of the possible effect of the GIA on the acceleration of relative sea-level is *a priori* justified and we will estimate this effect by using a simple physical model.

The total rise of sea-level in the Baltic sea by year 2100 has been recently projected at about 1 meter under the strongest emissions scenario RCP8.5 (Grinsted et al., 2015), which implies a very strong acceleration relative to the present rate of sea-level rise of 3.1 mm^{-1} (Stramska and Chudziak, 2013). All in all, the detection of acceleration of Baltic Sea level over several decades would support the future projections of increasing rates of sea-level rise. However, a lack of detection of acceleration can be due to multiple regional causes and would not necessarily disprove these future projections.

2. DATA

We use Revised Local Reference tide-gauge data of long records of Baltic Sea level kindly provided by the Permanent Service for Mean Sea Level (PSMSL), 2016, "Tide Gauge Data," (Retrieved 1 Nov 2015 from http://www.psmsl.org/data/obtaining/). These data have been profusely screened to detect inhomogeneities. We consider here all Baltic tide-gauges with time coverage starting no later than 1900, when the number of missing values is considerably reduced. A further selection rule of tide-gauges sets the limit of missing months in the records to 25% in the period 1900–2002, with the exception of two tide-gauges that include 27% of missing months. For the sake of completeness we include in the analysis some tide-gauges located also in the North Sea. We use annual means of sea-level until year 2012. **Table 1** contains the list of PSMSL records included in this study and their starting and end years as used in this analysis.

To test the statistical methods to detect the acceleration, we use the sea-level projections obtained from the suite of global climate models participating in the Climate Model

TABLE 1 | List of stations from the Permanent Service for Mean Sea Level (PSMSL) used in this study together with their geographical location and start and end dates of the records used in this analysis (some stations provide longer records beyond this time range).

Station name	Degrees North	Degrees East	Start year	End year
GEDSER	54.57	11.92	1900	2012
KOBENHAVN	55.70	12.60	1900	2012
HORNBAEK	56.09	12.45	1900	2012
KORSOR	55.33	11.14	1900	2012
SLIPSHAVN	55.28	10.82	1900	2012
FREDERICIA	55.56	9.75	1900	2012
AARHUS	56.14	10.22	1900	2012
FREDERIKSHAVN	57.43	10.54	1900	2012
HIRTSHALS	57.59	9.96	1900	2012
ESBJERG	55.46	8.44	1900	2012
OULU	65.04	25.41	1900	2012
VAASA	63.08	21.57	1900	2012
HANKO	59.82	22.97	1900	2012
HELSINKI	60.15	24.95	1900	2012
WARNEMUNDE2	54.16	12.10	1900	2012
WISMAR2	53.89	11.45	1900	2012
TRAVEMUNDE	53.95	10.87	1900	2012
CUXHAVEN2	53.86	8.71	1900	2010
KLAIPEDA	55.70	21.13	1900	2011
DELFZIJL	53.32	6.93	1900	2012
HARLINGEN	53.17	5.40	1900	2012
SWINOUJSCIE	53.91	14.23	1900	1999
VARBERG	57.10	12.21	1900	1981
YSTAD	55.41	13.81	1900	1981
KUNGSHOLMSFORT	56.10	15.58	1900	2012
OLANDS NORRA UDDE	57.36	17.09	1900	2012
LANDSORT	58.74	17.86	1900	2005
STOCKHOLM	59.32	18.08	1900	2012
NEDRE GAVLE	60.68	17.16	1900	1986
RATAN	63.98	20.89	1900	2012

Intercomparison Project version 5 (CMIP5) used by the Intergovernmental Panel on Climate Change (IPCC). This projections take into account the expansion of the ocean water column as simulated by the CMIP5 models, augmented by more uncertain estimations of land-ice melting (Carson et al., 2015). We use projections based on three different scenarios of atmospheric greenhouse gas concentrations, the so called Representative Concentration Paths RCP2.6, RCP4.5, and RCP8.5, labeled after their implied external radiative forcing in w m^{-2} by year 2100.

We compute the globally averaged mean sea-level and the mean sea-level averaged over a geographical box in the North Atlantic (40W-0E; 30N-60N) of the mean of over all models (ensemble mean). The purpose of this choice is to test the power of the methods to detect the acceleration of sea-level rise under more controlled conditions, in a situation with low noise (ensemble mean) and high signal (future scenarios). These projections of sea-level intrinsically contain an acceleration of global sea-level rise, so that we can evaluate to what extent the statistical methods are able to detect this acceleration.

3. METHODS

The estimation method (1), denoted in this study as pol_2, is based on the fit of a sea-level record to a time polynomial of order two:

$$sl(t) = sl_0 + bt + at^2 + \epsilon(t) \quad (1)$$

where sl_0 is the initial sea level, b is the linear trend in sea level rise, ϵ is the sea level variability not explained by the polynomial, and $2a$ is the acceleration of sea level. The parameters sl_0, b, and a can be estimated by Ordinary Least Squares. The estimation uncertainties can also be directly derived from the theory of Ordinary Least Squares if ϵ is assumed to be gaussian white noise. If this condition is not fulfilled, more complex methods based on bootstrapping are required to obtain realistic estimation uncertainties.

In this study we will use a parametric bootstrap to estimate the uncertainties in the parameter a within the estimation method (1). After fitting the sea-level records to a second order polynomial in time, the residuals $\epsilon(t)$ are used to construct surrogate residual time series that display the same serial correlation properties. These surrogate residuals are added to the deterministic part of the statistical model $sl_0 + bt + at^2$ and a new set of parameters is computed. This processes is repeated 10,000 times to obtain an empirical distribution of parameters.

The estimation method (2) to detect the acceleration relies on the computation of gliding linear trends over segments of the record. This record is denoted in the following as $gt(t)$, where t is a year index, and the linear trend is computed over the interval $(t - m, t + m)$. Most of the time in this study, $gt(t)$ represents annual means, but part of the analysis was also conducted with seasonal (summer or winter) means. The choice of the length of the time window in years of these segments m is a compromise between the need of a stable estimation of the gliding linear trends and the number of independent segments allowed by the length of the total sea-level record. Since the second step in the computation of the acceleration is the estimation of the long-term trend of the gliding trends, the number of independent segments will also influence the stability of the estimation of the acceleration.

In this study, we have chosen to compute gliding linear trends of 11-year segments ($m = 5$). The results do not essentially change when varying this number within a reasonable range of 7 ($m = 3$) to 15 years ($m = 7$). Some studies have suggested a much longer length of the time window to compute the linear trends, as long as 40 years ($m = 20$), but this suggestion aims at estimating the acceleration as the mean difference between two periods, and establishing its statistical significance. Since here we estimate the acceleration as the long-term trend of the gliding trends, a larger number of independent degrees of freedom is desirable.

The third estimation method of the sea-level acceleration on computing the annual increments of an annual mean sea-level record $sl(t)$ as $inc(t) = sl(t) - sl(t - 1)$, where t is again a year

index. The acceleration is then estimated as a long-term trend in the record of increments $inc(t)$.

The estimation of the long-term trend in $gt(t)$ or $inc(t)$ can be carried out also another method different from Ordinary Linear Least Squares (OLS) regression. Here, we also computed the acceleration using as second non-parametric method, the Theil-Sen (TS) estimator (Schmith, 2008), to estimate the long-term trend . This estimator does not assume a linear functional dependency of the record over time, as ordinary linear regression does. It is based on the computation of the difference between all possible pairs in a record, say $inc(t) - inc(t')$, where t and t' are two different years, with t occurring later than t'. The Theil-Sen estimator of the long-term trend is the sample median of all quantities $\frac{inc(t)-inc(t')}{t-t'}$.

Therefore, the acceleration estimators(2) and (3) can be implemented with two estimators of the long-term trend of $gt(t)$ and $inc(t)$. This yields four methods to estimate a final value of the acceleration, which will be denoted here as gt_{ols}, gt_{ts}, inc_{ols}, and inc_{ts}, following the convection gt = gliding trends, inc = annual increments, ols = ordinary least squares, and ts = Theil-Sen estimator, respectively.

The estimation of the uncertainties of the acceleration in the methods (2) and (3) are also obtained by bootstrapping. The records of gliding trends $gt(t)$, and quite possibly also the record of increments $inc(t)$ contain strong serial correlations, i.e., the individual samples are not independent. In the case of $gt(t)$, this is particularly clear since the gliding trends are computed over overlapping time segments, so that in the computation of the value of $gt(t)$ and the value of $gt(t-1)$ with $m = 5$ only two values of the original record sl are different. This serial correlation strongly hinders the estimation of the uncertainties in the long-term trend of $gt(t)$ or $inc(t)$ if only Ordinary Linear Least Squares regression of these records on the variable time were applied (Bos et al., 2014). The uncertainty bounds computed in this way would be too optimistic, since in reality the serial correlation of the record over long de-correlation length can give rise to spurious long-term trends, thus introducing a larger uncertainty in the estimation of the true trend. To avoid this pitfall, we use here a method based on the Monte Carlo generation of surrogate time series (Ebisuzaki, 1997). Within this method surrogate replicas of one record are produced that have the same serial correlation but otherwise are uncorrelated in time, as explained below.

Once a linear long-term trend in $gt(t)$ or $inc(t)$ has been estimated by linear regression on the variable time, a record of the regression residuals is stored. Thousand replicas of this residual record are generated by phase randomization and added to the original, but linearly detrended $gt(t)$ or $inc(t)$ record, thus obtaining thousand replicas of a theoretically trend-less record that contains residuals with the same serial correlation as the original record. The linear trends of the surrogate records are then estimated, providing an empirical distribution of sample trends. If the estimated trend in $gt(t)$ or $inc(t)$ is larger than the 95% quantile of this empirical distribution, the estimated long-term trend (acceleration) is claimed to be statistically significant.

4. TESTING THE DETECTION METHODS USING FUTURE SEA-LEVEL PROJECTIONS

Figure 1A displays the records of the ensemble mean of the global annual mean sea-level simulated by the CMIP5 ensemble of models driven by three scenarios of greenhouse gases atmospheric concentrations. As it is very well-known, the mean projection for all scenarios indicate a rising sea-level but with different magnitudes. As illustration of the possible acceleration of the mean sea-level rise, **Figure 1B** displays the corresponding gliding trends computed over 11-year segments $gt(t)$, and **Figure 1C** displays the record of annual increments $inc(t)$. The rates of sea-level rise estimated by these two methods show an increase with time, more clearly in the more pessimistic scenario RCP8.5, but not so clearly in the other two scenarios. In the scenario with smaller increase in radiative forcing, the rates of sea-level rise would even decelerate or remain nearly constant after 2020–2030.

This visual impression is confirmed by the numerical estimation of the acceleration based on the $gt(t)$ and $inc(t)$ records, as summarized in **Table 2**.

The values of the acceleration computed by the different methods are quite similar, supporting a robust estimation of its value, at least in this synthetic example in which the signal-to-noise ratio is high and averaging the global annual records over many models. Also, the accelerations detected in the scenarios RCP4.5 and RCP8.5 are statistically significant, corroborating the visual impression gained from **Figure 1**.

A more challenging test is to detect the acceleration not of the global mean sea-level but of the projected regional sea-level in the North Atlantic, a quantity more relevant for the analysis of the Baltic Sea acceleration. **Figure 2** displays the simulated ensemble-mean annual sea-level (**Figure 2A**), its gliding trends (**Figure 2B**) and annual increments (**Figure 2C**) for the geographical region (40W-0E, 30N-60N) located in the North Atlantic. In this case, as expected, the records contain more regional noise, and the acceleration here, understood as a systematic increment in the rate of sea-level rise, is not visually detectable except for the more pessimistic scenario RCP8.5. Particularly noisy are the records of annual increments shown in **Figure 2C**. In this latter case, it becomes quite clear that any statistical method would struggle

TABLE 2 | Acceleration of global annual mean sea-level rise derived from the CMIP5 ensemble-mean driven by three Representative Concentration Paths scenarios, estimated in the period 2006–2099 using four estimation methods (see main text).

Scenario	pol_2	gt_{ols}	gt_{ts}	inc_{ols}	inc_{ts}
RCP2.6	0.44 ± 0.84	1.2	−1.3	2.7	1.9
RCP4.5	$28.5^* \pm 1.5$	28.6*	30.8*	28.8*	29.4*
RCP8.5	$97.6^* \pm 0.66$	96.4*	97.1*	95.7*	96.4*

*pol_2, fit to a second order time polynomial; gt_{ols}, gliding linear trends with ordinary linear regression; gt_{ts}, gliding linear trends with Theil-Sen trend estimator; inc_{ols}, annual increments and ordinary linear regression; and inc_{ts}, annual increments and Theil-Sen estimator. Units 10^{-3} mm year^{-2}. The sign * denotes a statistically significant trend at the 95% level ($p < 0.05$; see Section Methods).*

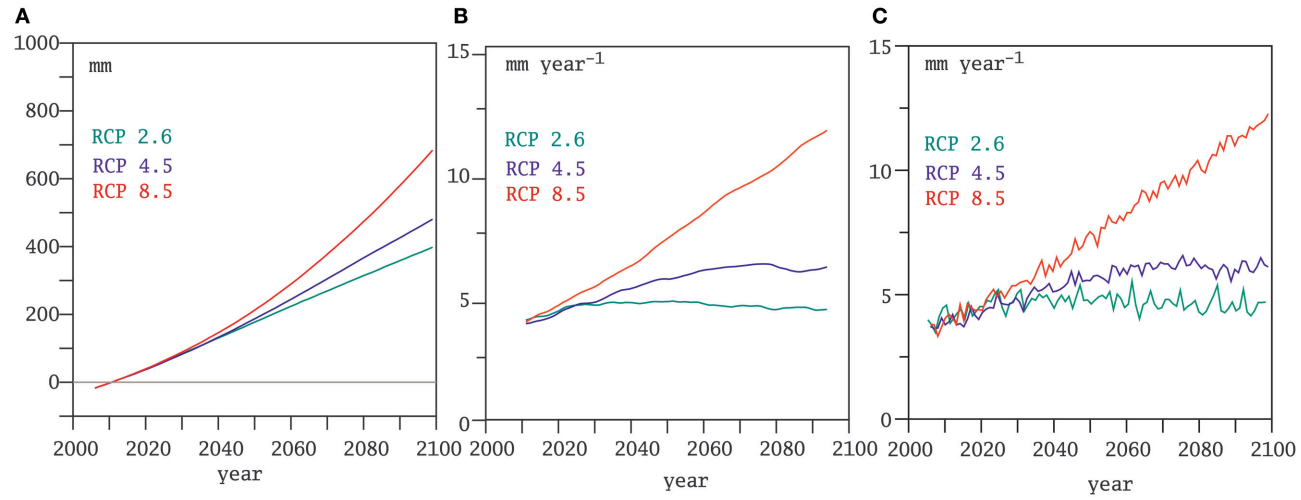

FIGURE 1 | Global annual mean sea level from the ensemble mean of the CMIP5 models driven by three RCP greenhouse gas scenarios. (A) deviations from the 2006–2015 mean; **(B)** gliding trends computed over 11-year overlapping periods; **(C)** annual increments of the global annual mean sea-level.

to detect a long term trend in the series of annual increments. This impression is supported by the numerical estimations of the acceleration contained in **Table 3**.

The simulated sea-level rise, its rates and the acceleration estimated for the North Atlantic are smaller than for the global mean, which could be physically justified considering the projected cooling in this region due to a possible slow-down of the meridional overturning circulation in the North Atlantic. The further discussion of this point lies, however, outside the scope of this study, although it has to be borne in mind when discussing the acceleration of the Baltic sea-level during the twentieth century. More relevant here is the conclusion that the statistical method based on the annual increments turns to be in this case less powerful to detect a significant acceleration. Whereas the pol_2 and both methods based on gliding trends gs_{ols} and gs_{ts} indicate that the acceleration in the North Atlantic for the scenario RCP85 is statistically significant—also supported by the visual inspection of the time series shown in **Figures 2A,B**—the methods based on the annual increments inc_{ols} and inc_{ts} are not able to detect a statistically significant trend, even in the more pessimistic scenario RCP8.5 .

We will, for the sake of brevity, show only the results obtained from the pol_2 and gt methods on the Baltic Sea tide-gauges records.

5. ACCELERATION OF BALTIC SEA LEVEL

Figure 3 shows the estimated sea-level acceleration of the annual mean sea-level in 30 tide-gauges from the PSMSL records, estimated with the pol_2 and the two gliding trends methods (gt_{osl} and gt_ts). The numerical values with their estimated uncertainties are included in **Table 4**. The spatial patterns are similar, with a range of spatial correlations between all three patterns ranging between r = 0.70 and r = 0.75. The value of the acceleration averaged over all stations is also similar in

TABLE 3 | Acceleration of North Atlantic annual mean sea-level rise derived from the CMIP5 ensemble-mean driven by three Representative Concentration Paths scenarios, estimated in the period 2006–2099 using four estimations methods (see main text).

Scenario	pol_2	gt_{ols}	gt_{ts}	inc_{ols}	inc_{ts}
RCP2.6	−14.2 ± 1.9	−14.1	−12.7	−1.0	−8.9
RCP4.5	7.2 ± 2.32	7.9	7.8	10.8	9.1
RCP8.5	68.8* ± 1.62	68.1*	68.4*	71.9	74.1

*pol_2, fit to a second order time polynomial; gt_{ols}, gliding linear trends with ordinary least squares- regression; gt_{ts}, gliding linear trends with Theil-Sen trend estimator; inc_{ols}, annual increments and ordinary least-square-regression; inc_{ts}, annual increments and Theil-Sen estimator. Units 10^{-3} mm year^{-2}. The sign * denotes a statistically significant trend at the 95% level ($p < 0.05$), negative trends are not considered significant (see Section Methods).*

the three cases, with 12.2 mm × 10^{-3} year^{-2} with the pol_2 method, 13.6 × 10^{-3} mm year^{-2} with the gt_{ols} method, and 17.7 × 10^{-3} mm year^{-2} obtained with the gt_{ts} method. Just as illustration of the consequences of an average acceleration of this magnitude, assuming that it is distributed uniformly over time and continues unchanged in the future, this value of the acceleration implies an additional sea-level rise relative to a simple linear extrapolation of the present rise of about 65 mm in 100 years for the all-stations-average. Very few of the individual accelerations computed for the individual tide-gauge records turns to be statistically significant applying any of the gliding trend methods.

The spatial patterns of accelerations do not show a very clear geographical structure. However, there is a tendency for larger accelerations to be found at the tide-gauges located toward the North and the East. This tendency is more clearly displayed in **Figure 4**. This figure shows the scatter plot of the annual (and also winter and summer for reasons discussed later) accelerations estimated with the gt_{ols} method as a function of geographical distance from the point 0W, 55N. The scatter plots also include the regression lines and their 95% uncertainty range. These

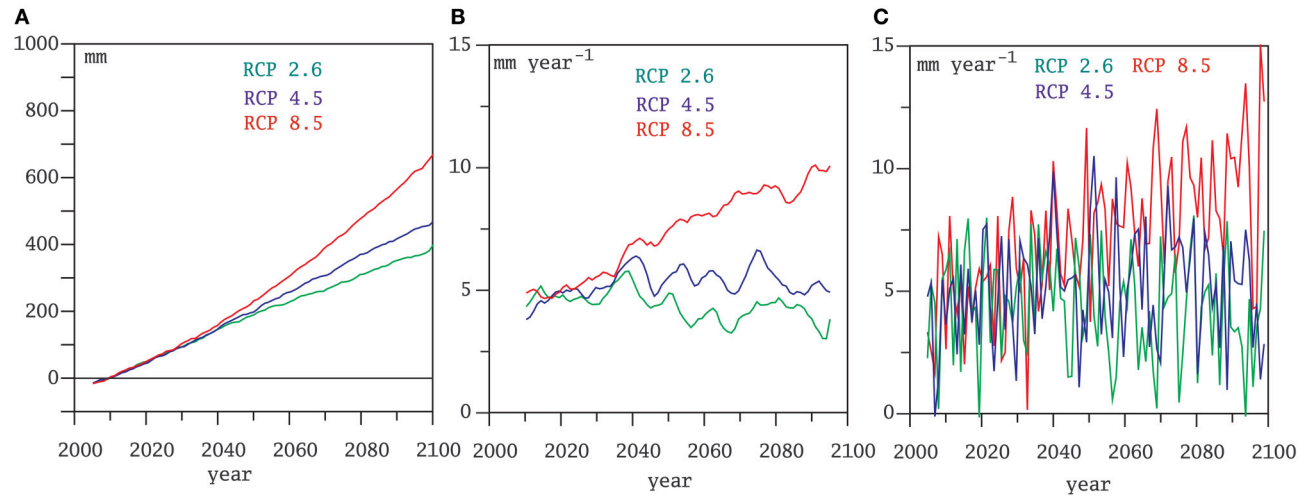

FIGURE 2 | Annual mean sea level averaged over the North Atlantic (40W-0E;30N-60N) from the ensemble mean of the CMIP5 models driven by three RCP greenhouse gas scenarios. (A) deviations from the 2006–2015 mean; **(B)** gliding trends computed over 11-year overlapping periods; **(C)** annual increments of the average annual mean sea-level.

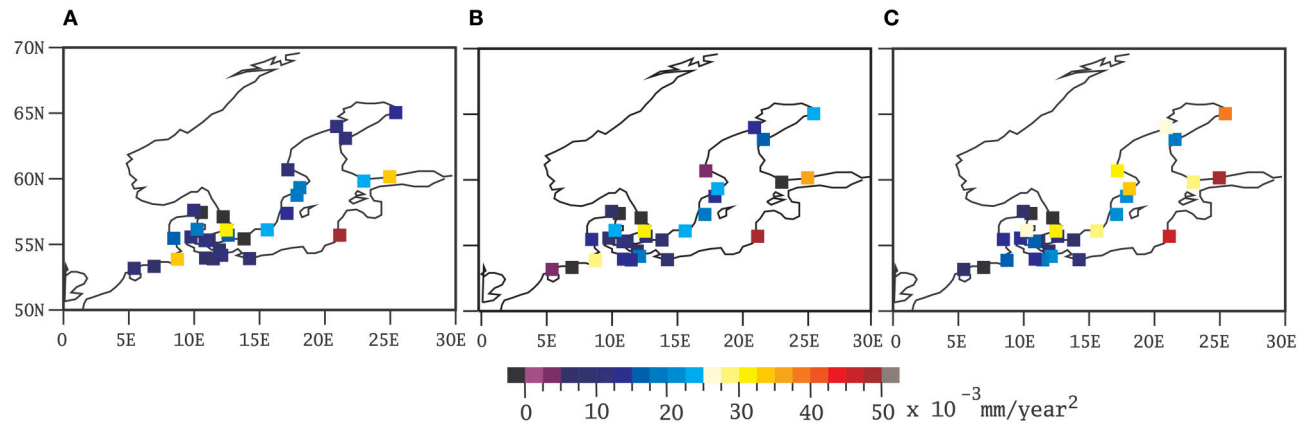

FIGURE 3 | Acceleration of the annual mean sea-level in the Baltic Sea tide-gauges estimated in the period 1900–2012 by the methods (A) pol_2, (B) gt_{ols}, and (C) gt_{ts}. See **Table 4**.

scatter plots indicate a large scatter around the regression lines, but all three confirm the visual impression from **Figure 3**.

As mentioned in the introduction, there are several spatially heterogeneous factors that affect Baltic Sea level and that could blur a spatially homogeneous patterns of acceleration. To check whether this local and regional noise can be filtered by computing an indicator of the spatial mean of Baltic Sea level, the all-stations-average time series has been computed and is displayed in **Figure 5A**, along with their record of decadal gliding trends in **Figure 5B**. Note that, since the magnitudes of the long-term trends caused by the GIA are spatially very heterogeneous, the individual tide-gauge records shown in **Figure 4A** have been previously linearly detrended and the deviations from their long-term mean also calculated, before computing the all-stations-average. This indicator of Baltic mean sea-level is not strictly well defined because the spatial coverage of the tide-gauges is not uniform: many stations in this set are clustered in the South - East of the Baltic Sea and the some in the basins connecting the North and the Baltic Seas. Also, the time correlation between the individual annual sea-level records is on average about 0.6, although there are pairs of tide-gauges that are correlated as low as 0.35. This means that it is difficult to compute a representative annual index of regional mean sea-level based on the available tide-gauges in this region.

Nevertheless, the all-stations-average record (**Figure 5A**) may be illustrative of the variations of Baltic Sea level through time in the twentieth and twenty-first centuries. The highest decadal gliding trends (**Figure 5B**) have been attained around 1945, in agreement with similar calculations based on the Warnemünde tide-gauge (Richter et al., 2012) The acceleration, estimated as the long-term ordinary-least-squares trend (method gt_{ols}) of the decadal gliding trends is positive

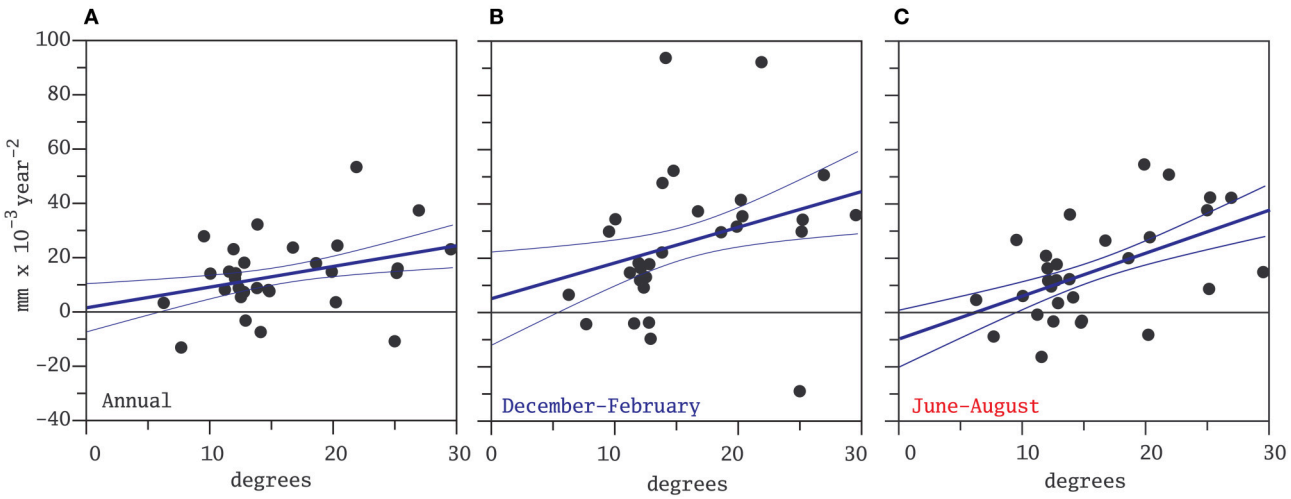

FIGURE 4 | Acceleration of the annual (A), winter (B), and summer (C) mean sea-level in the Baltic Sea tide-gauges estimated in the period 1900–2012 by the methods gt_{ols} as a function of their distance to the geographical point 0W, 55N. The plots include the regression lines estimated by Ordinary Least Squares and their 95% uncertainty range.

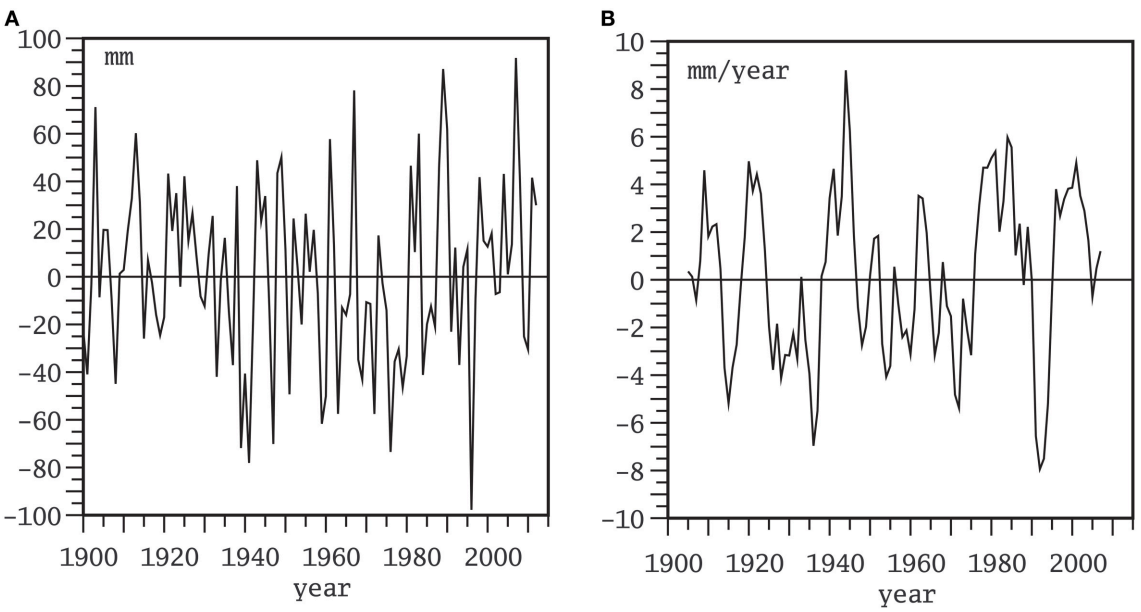

FIGURE 5 | (A) All-stations-average of annual mean sea-level derived from the PSMSL tide-gauge show in **Figure 3** in the period 1900–2012. **(B)** Its gliding trends computed over 11-year overlapping periods.

and attains a value of 14.5 $\times$ 10^{-3} mm year^{-2}. This value is close to the average of the individual accelerations computed for each tide-gauge (**Figure 5A**). This acceleration, though positive, is not statistically significant at the 95% level (p = 0.12). In contrast, most of the individual accelerations lie below the 95% significance level. Averaging over all stations, therefore, is able to filter out some noise, resulting in a marginally significant signal. This signal, however, remains weak, as illustrated in a barely discernible long-term trend in **Figure 5B**.

Very similar results are obtained with the gt_{ts} method to estimate the acceleration of the average record.

5.1. Influence of the Glacial Isostatic Adjustment

The spatial pattern of accelerations of relative sea-level in the Baltic Sea region suggests that tide-gauges located at higher latitudes may be experiencing stronger accelerations. The question arises as to whether this pattern could also be influenced by the GIA, as tide-gauges in the North are also subject to

TABLE 4 | Acceleration of the annual mean sea-level in the Baltic Sea tide-gauges and their estimated 95% uncertainty range derived by the methods pol_2, gt_{ols}, and gt_{ts} in 10^{-3} mm year^{-2} in the period 1900–2012.

Station name	pol_2	gt_{ols}	gt_{ts}
GEDSER	6 ± 11	7 ± 14	8 ± 13
KOBENHAVN	16 ± 14	9 ± 15	10 ± 15
HORNBAEK	30 ± 13	32 ± 33	31 ± 32
KORSOR	9 ± 11	9 ± 8	8 ± 8
SLIPSHAVN	11 ± 9	12 ± 14	17 ± 14
FREDERICIA	12 ± 9	8 ± 11	14 ± 11
AARHUS	19 ± 11	23 ± 22	26 ± 23
FREDERIKSHAVN	−6 ± 11	−3 ± 10	−9 ± 11
HIRTSHALS	11 ± 13	5 ± 24	7 ± 25
ESBJERG	16 ± 17	14 ± 20	14 ± 20
OULU/ULEABORG	13 ± 23	23 ± 92	40 ± 87
VAASA	11 ± 24	16 ± 91	19 ± 92
HANKO	22 ± 25	−11 ± 43	29 ± 42
HELSINKI	33 ± 21	37 ± 40	48 ± 43
WARNEMUNDE2	12 ± 11	18 ± 10	21 ± 10
WISMAR2	8 ± 10	14 ± 12	18 ± 14
TRAVEMUNDE	5 ± 9	15 ± 17	15 ± 15
CUXHAVEN2	33 ± 17	28 ± 25	17 ± 25
KLAIPEDA	50 ± 22	53 ± 40	45 ± 35
DELFZIJL	6 ± 13	−13 ± 23	−8 ± 22
HARLINGEN	8 ± 12	3 ± 13	6 ± 14
SWINOUJSCIE	9 ± 20	8 ± 18	11 ± 15
VARBERG	−40 ± 29	−7 ± 15	−25 ± 23
YSTAD	−25 ± 15	8 ± 12	7 ± 9
KUNGSHOLMSFORT	25 ± 15	24 ± 18	29 ± 18
OLANDS NORRA UDDE	15 ± 17	18 ± 27	22 ± 26
LANDSORT	18 ± 21	15 ± 46	20 ± 45
STOCKHOLM	20 ± 19	24 ± 60	34 ± 60
NEDRE GAVLE	8 ± 35	4 ± 30	32 ± 35
RATAN	10 ± 22	14 ± 90	26 ± 93

stronger relaxation velocities of the Earth's crust. In the following, we briefly estimate a possible order of magnitude of the effect of the GIA on acceleration.

The GIA is caused by the back-relaxation of the Earth's crust to the deformation caused by the load of land-ice during the last glacial period. The peak of the glacial period, the Last Glacial Maximum, was reached about 20,000 years ago and the de-glaciation in Fennoscandia was almost complete about 8000 years ago. The Earth's crust started rebounding after the ice load was released, pushed by the viscous rebalancing of the material in the Earth's mantle. It can be assumed that this GIA-related relaxation can be described by a simple exponential model:

$$A(t) = A_0(1 - e^{-t/\tau}) \tag{2}$$

where t is time, A_0 is the maximum depression caused by the load of the ice-sheets and τ is a the typical viscous relaxation time . A plausible value for τ in this simple model would be of the order of 5000 years (Wieczerkowski et al., 1999), although the exact value is not critical for this simple estimation.

The acceleration of the crust $\frac{d^2A}{dt^2}$ is then proportional to its velocity $\frac{dA}{dt}$:

$$\frac{d^2A(t)}{dt^2} = \frac{-1}{\tau}\frac{dA(t)}{dt} \tag{3}$$

The relative sea-level would experience the same magnitude of acceleration but with reversed sign, and thus present a pattern of acceleration reminiscent of the spatial pattern estimated here. In the North of the Baltic sea, where the GIA velocity is of the order of 10 mm year^{-1}, the GIA-related acceleration would amount to about 0.002 mm year^{-2}. This magnitude, therefore, seems to be small compared with the estimated accelerations displayed in **Figure 3** which are one order of magnitude larger than the GIA-related acceleration estimated with this simple model. Although the GIA may contribute to the acceleration, it is likely not the whole explanation according to this simple model.

5.2. Role of Ice Cover

The formation and melting of floating sea-ice cover may also influence sea-level (Jenkins and Holland, 2007; Shepherd et al., 2010). With warming proceeding through the last decades, the ice cover in the Baltic Sea has been systematically reduced (Haapala et al., 2015). Since ice cover in winter time is more relevant for those tide-gauges located at higher latitudes, the melting of sea-ice could in principle also influence the estimation of acceleration. Another reason by which sea-ice may influence the estimation of coastal sea-level is the annual cycle of Baltic sea level (Hünicke and Zorita, 2008) together with the number of reported missing values. Baltic Sea level generally displays a maximum during wintertime, more clearly so at its northern than at the southern coasts. If sea-ice cover at the coast hinders the tide-gauge measurement, a diminishing sea-ice cover in recent decades would increase the relative weight of wintertime measurements in the annual means, leading to an artificial increase in the reported annual mean sea-level and potentially to an apparent acceleration of annual mean sea level. To test this possibility, we have also computed the accelerations with the gt_{ols} method for the winter (December through February) and summer (June through August) seasons. The results are depicted in **Figure 6**.

The spatial pattern of acceleration derived from the winter and summer data still display a tendency for higher values at higher latitudes and longitudes although the summer pattern is now more tilted in the east-west direction. This tendency was also visible in **Figures 4B,C**. In addition, the two most northern tide-gauges display in summertime a rather small acceleration. It seems, therefore, that the influence of the diminishing ice coverage would not explain the spatial patterns of acceleration in the Baltic although it may have some influence.

6. CONCLUDING REMARKS

Within the caveats explained in the introduction, the statistical methods used here fail to detect a statistically significant acceleration in the Baltic Sea area since 1900, which can be due to the still small magnitude of he acceleration paired with a high random sea-level variability at the regional scale.

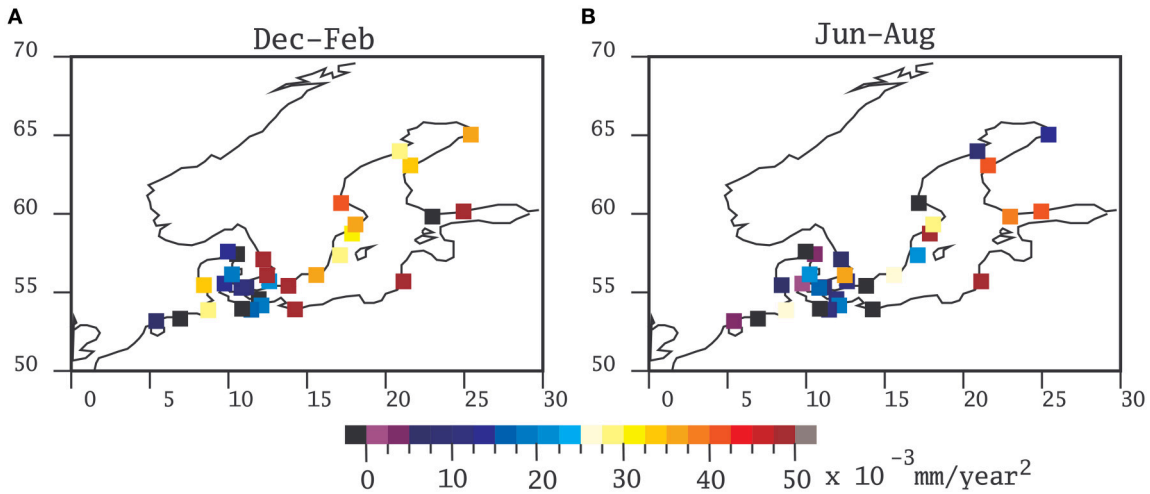

FIGURE 6 | Acceleration of the annual mean sea-level in the Baltic Sea tide-gauges estimated in the period 1900–2012 in wintertime (A) and summertime (B) by the method gt_{ols}.

Nevertheless, the computed individual accelerations in the Baltic Sea are mostly positive and the all-stations-mean almost attains the level of statistical significance. Its magnitude is nevertheless small. The implied increase by year 2100 over a purely linear extrapolation of the present rate would yield an additional increase of sea-level of few centimeters by year 2100.

We have adopted a definition of acceleration as a systematic increase of the rates of sea-level. This definition is not equivalent to other definitions of acceleration, more focused on the detection of "unusual" values, i.e., the comparison between recent rates and historical rates of sea-level rise. However, the adoption of this latter definition would also wrestle to claim an unusual rate of sea-level in the very last decades. The rates computed around year 2000 are indeed among the highest of the whole record, but they are not the absolute maximum (**Figure 5B**, see also Richter et al., 2012).

Unfortunately, global climate models lack the sufficient spatial resolution to realistically represent the Baltic Sea. Simulations with coupled regional climate models of the Baltic Sea would be very useful to ascertain if the acceleration of sea-level is also detectable in climate simulations, although it has to be borne in mind that all the subtle processes that may influence the long-term evolution of Baltic Sea level may not be realistically represented in these models, for instance, the connection to the North Sea or the dynamics related to sea-ice cover (Hordoir et al., 2015).

AUTHOR CONTRIBUTIONS

All authors listed, have made substantial, direct and intellectual contribution to the work, and approved it for publication.

ACKNOWLEDGMENTS

This study is part of the Cluster of Excellence Integrated System Analysis and Prediction (CLISAP), funded by the German Science Foundation, and of the Earth System Science Program for the Baltic Sea region (Baltic Earth). We thank Mark Carson of the Center für Erdsystemforschung und Nachhaltigkeit (CEN) of the University of Hamburg (Germany) for kindly providing the sea-level data of the CMIP5 simulation ensemble. We also thank the Permanent Service for Mean Sea Level (PSMSL) in Liverpool (UK) for proving an excellent data infrastructure. The manuscript benefited from very helpful comments from the reviewers.

REFERENCES

Barbosa, S. M. (2008). Quantile trends in Baltic sea level. *Geophys. Res. Lett.* 35, L22704. doi: 10.1029/2008GL035182

Bastos, A., Trigo, R., and Barbosa, S. (2013). Discrete wavelet analysis of the influence of the North Atlantic Oscillation on Baltic Sea level. *Tellus A* 65:20077. doi: 10.3402/tellusa.v65i0.20077

Bos, M., Williams, S., Araújo, I., and Bastos, L. (2014). The effect of temporal correlated noise on the sea level rate and acceleration uncertainty. *Geophys. J. Int.* 196, 1423–1430. doi: 10.1093/gji/ggt481

Calafat, F., and Chambers, D. (2013). Quantifying recent acceleration in sea level unrelated to internal climate variability. *Geophys. Res. Lett.* 40, 3661–3666. doi: 10.1002/grl.50731

Carson, M., Köhl, A., Stammer, D., A. Slangen, A. B., Katsman, C. A., van de Wal, R. S. W., et al. (2015). Coastal sea level changes, observed and projected during the 20th and 21st century. *Clim. Change* 134, 269–281. doi: 10.1007/s10584-015-1520-1

Cazenave, A., Dieng, H.-B., Meyssignac, B., von Schuckmann, K., Decharme, B., and Berthier, E. (2014). The rate of sea-level rise. *Nat. Clim. Change* 4, 358–361. doi: 10.1038/nclimate2159

Church, J. A., Clark, P. U., Cazenave, A., Gregory, J. M., Jevrejeva, S., Levermann, A., et al. (2013). Sea-level rise by 2100. *Science* 342, 1445–1445. doi: 10.1126/science.342.6165.1445-a

Church, J. A., Gregory, J. M., White, N. J., Platten, S. M., and Mitrovica, J. X. (2011). Understanding and projecting sea level change. *Oceanography* 24, 130–143. doi: 10.5670/oceanog.2011.33

Church, J. A., and White, N. J. (2011). Sea-level rise from the late 19th to the early 21st century. *Surv. Geophys.* 32, 585–602. doi: 10.1007/s10712-011-9119-1

Church, J. A., White, N. J., Coleman, R., Lambeck, K., and Mitrovica, J. X. (2004). Estimates of the regional distribution of sea level rise over the 1950-2000 period. *J. Clim.* 17, 2609–2625. doi: 10.1175/1520-0442(2004)017<2609:EOTRDO>2.0.CO;2

Clark, P. U., Church, J. A., Gregory, J. M., and Payne, A. J. (2015). Recent progress in understanding and projecting regional and global mean sea level change. *Curr. Clim. Change Rep.* 1, 224–246. doi: 10.1007/s40641-015-0024-4

Ebisuzaki, W. (1997). A method to estimate the statistical significance of a correlation when the data are serially correlated. *J. Clim.* 10, 2147–2153.

Grinsted, A., Jevrejeva, S., Riva, R. E. M., and Dahl-Jensen, D. (2015). Sea level rise projections for northern Europe under RCP8.5. *Clim. Res.* 64, 15–23. doi: 10.3354/cr01309

Haapala, J. J., Ronkainen, I., Schmelzer, N., and Sztobryn, M. (2015). "Recent change—sea ice," in *Second Assessment of Climate Change for the Baltic Sea Basin*, ed The BACC II Author Team (Cham: Springer International Publishing), 145–153.

Haigh, I. D., Wahl, T., Rohling, E. J., Price, R. M., Pattiaratchi, C. B., Calafat, F. M., et al. (2014). Timescales for detecting a significant acceleration in sea level rise. *Nat. Commun.* 5:3635. doi: 10.1038/ncomms4635

Hamlington, B. D., and Thompson, P. R. (2015). Considerations for estimating the 20th century trend in global mean sea level. *Geophys. Res. Lett.* 42, 4102–4109. doi: 10.1002/2015GL064177

Hay, C. C., Morrow, E., Kopp, R. E., and Mitrovica, J. X. (2015). Probabilistic reanalysis of twentieth-century sea-level rise. *Nature* 517, 481–484. doi: 10.1038/nature14093

Holgate, S. J. (2007). On the decadal rates of sea level change during the twentieth century. *Geophys. Res. Lett.* 34:L01602. doi: 10.1029/2006gl028492

Hordoir, R., Axell, L., Löptien, U., Dietze, H., and Kuznetsov, I. (2015). Influence of sea level rise on the dynamics of salt inflows in the Baltic Sea. *J. Geophys. Res. Oceans* 120, 6653–6668. doi: 10.1002/2014JC010642

Houston, J. R., and Dean, R. G. (2011). Sea-level acceleration based on US tide gauges and extensions of previous global-gauge analyses. *J. Coast. Res.* 27, 409–417. doi: 10.2112/JCOASTRES-D-10-00157.1

Hünicke, B., and Zorita, E. (2006). Influence of temperature and precipitation on decadal baltic sea level variations in the 20th century. *Tellus A* 58, 141–153. doi: 10.1111/j.1600-0870.2006.00157.x

Hünicke, B., and Zorita, E. (2008). Trends in the amplitude of Baltic Sea level annual cycle. *Tellus A* 60, 154–164. doi: 10.1111/j.1600-0870.2007.00277.x

Hünicke, B., Zorita, E., Soomere, T., Madsen, K. S., Johansson, M., and Suursaar, Ü. (2015). "Recent change—sea level and wind waves," in *Second Assessment of Climate Change for the Baltic Sea Basin*, ed The BACC II Author Team (Cham: Springer International Publishing), 155–185.

Jenkins, A., and Holland, D. (2007). Melting of floating ice and sea level rise. *Geophys. Res. Lett.* 34:L16609. doi: 10.1029/2007GL030784

Jevrejeva, S., Moore, J., Grinsted, A., Matthews, A., and Spada, G. (2014). Trends and acceleration in global and regional sea levels since 1807. *Glob. Planet. Change* 113, 11–22. doi: 10.1016/j.gloplacha.2013.12.004

Jevrejeva, S., Moore, J., Woodworth, P., and Grinsted, A. (2005). Influence of large-scale atmospheric circulation on European sea level: results based on the wavelet transform method. *Tellus A* 57, 183–193. doi: 10.1111/j.1600-0870.2005.00090.x

Jevrejeva, S., Moore, J. C., Grinsted, A., and Woodworth, P. L. (2008). Recent global sea level acceleration started over 200 years ago ? *Geophys. Res. Lett.* 35:L08715. doi: 10.1029/2008GL033611

Landerer, F. W., Jungclaus, J. H., and Marotzke, J. (2007). Regional dynamic and steric sea level change in response to the IPCC-A1B scenario. *J. Phys. Oceanogr.* 37, 296–312. doi: 10.1175/JPO3013.1

Mitrovica, J. X., Tamisiea, M. E., Davis, J. L., and Milne, G. A. (2001). Recent mass balance of polar ice sheets inferred from patterns of global sea-level change. *Nature* 409, 1026–1029. doi: 10.1038/35059054

Richter, A., Groh, A., and Dietrich, R. (2012). Geodetic observation of sea-level change and crustal deformation in the Baltic Sea region. *Phys. Chem. Earth* 53, 43–53. doi: 10.1016/j.pce.2011.04.011

Schmith, T. (2008). Stationarity of regression relationships: application to empirical downscaling. *J. Clim.* 21, 4529–4537. doi: 10.1175/2008JCLI1910.1

Shepherd, A., Wingham, D., Wallis, D., Giles, K., Laxon, S., and Sundal, A. V. (2010). Recent loss of floating ice and the consequent sea level contribution. *Geophys. Res. Lett.* 37:L13503. doi: 10.1029/2010GL042496

Slangen, A., Carson, M., Katsman, C., van de Wal, R., Köhl, A., Vermeersen, L., et al. (2014). Projecting twenty-first century regional sea-level changes. *Clim. Change* 124, 317–332. doi: 10.1007/s10584-014-1080-9

Slangen, A. B. A, Church, J. A., Agosta, C., Fettweis, X., Marzeion, B., and Richter, K. (2016). Anthropogenic forcing dominates global mean sea-level rise since 1970. *Nat. Clim. Change* 6, 701–705. doi: 10.1038/nclimate2991

Spada, G., Olivieri, M., and Galassi, G. (2015). A heuristic evaluation of long-term global sea level acceleration. *Geophys. Res. Lett.* 42, 4166–4172. doi: 10.1002/2015GL063837

Stammer, D., Cazenave, A., Ponte, R. M., and Tamisiea, M. E. (2013). Causes for contemporary regional sea level changes. *Annu. Rev. Mar. Sci.* 5, 21–46. doi: 10.1146/annurev-marine-121211-172406

Stramska, M., and Chudziak, N. (2013). Recent multiyear trends in the Baltic Sea level. *Oceanologia* 55, 319–337. doi: 10.5697/oc.55-2.319

Visser, H., Dangendorf, S., and Petersen, A. C. (2015). A review of trend models applied to sea level data with reference to the "acceleration-deceleration debate." *J. Geophys. Res. Oceans* 120, 3873–3895. doi: 10.1002/2015JC010716

Wieczerkowski, K., Mitrovica, J. X., and Wolf, D. (1999). A revised relaxation-time spectrum for Fennoscandia. *Geophys. J. Int.* 139, 69–86.

Zwally, H. J., Li, J., Robbins, J. W., Saba, J. L., Yi, D., and Brenner, A. C. (2015). Mass gains of the Antarctic ice sheet exceed losses. *J. Glaciol.* 61, 1019–1036. doi: 10.3189/2015JoG15J071

Conflict of Interest Statement: The authors declare that the research was conducted in the absence of any commercial or financial relationships that could be construed as a potential conflict of interest.

frontiers in Marine Science

ORIGINAL RESEARCH
published: 20 May 2016
doi: 10.3389/fmars.2016.00076

Recent Arctic Sea Level Variations from Satellites

*Ole B. Andersen * and Gaia Piccioni*

DTU Space, Technical University of Denmark, Lyngby, Denmark

Sea level monitoring in the Arctic region has always been an extreme challenge for remote sensing, and in particular for satellite altimetry. Despite more than two decades of observations, altimetry is still limited in the inner Arctic Ocean. We have developed an updated version of the Danish Technical University's (DTU) Arctic Ocean altimetric sea level timeseries starting in 1993 and now extended up to 2015 with CryoSat-2 data. The time-series covers a total of 23 years, which allows higher accuracy in sea level trend determination. The record shows a sea level trend of 2.2 ± 1.1 mm/y for the region between 66°N and 82°N. In particular, a local increase of 15 mm/y is found in correspondence to the Beaufort Gyre. An early estimate of the mean sea level trend budget closure in the Arctic for the period 2005–2015 was derived by using the Equivalent Water Heights obtained from GRACE Tellus Mascons data and the steric sea level from the NOAA Global Ocean Heat and Salt Content dataset. In this first attempt, we computed the budget based on seasonally averaged values, obtaining the closure with a difference of 0.4 mm/y. This closure is clearly inside the uncertainties of the various components in the sea level trend budget.

Keywords: Arctic, sea level, satellite altimetry, sea level budget, Arctic Ocean

OPEN ACCESS

Edited by:
Sönke Dangendorf, University of Siegen, Germany

Reviewed by:
Philip Thompson, University of Hawaii, USA
Alejandro Orfila, IMEDEA (CSIC-UIB), Spain

****Correspondence:***
Ole B. Andersen
oa@space.dtu.dk

Specialty section:
This article was submitted to Coastal Ocean Processes, a section of the journal Frontiers in Marine Science

Received: *29 January 2016*
Accepted: *02 May 2016*
Published: *20 May 2016*

Citation:
Andersen OB and Piccioni G (2016) Recent Arctic Sea Level Variations from Satellites. Front. Mar. Sci. 3:76. doi: 10.3389/fmars.2016.00076

INTRODUCTION

For the Arctic region, a reasonable number of tide gauge data is available along the Norwegian and Russian coasts since 1950, and most of published research on Arctic sea level extends cautiously from these areas (i.e., Pavlov, 2001; Proshutinsky et al., 2004; Henry et al., 2012). However, only a limited amount of data is available in the interior of the Arctic Ocean, and records with a length of several decades, are completely absent outside the Norwegian and Russian sectors.

Since the early 1990s, ERS-1, ERS-2, and ENVISAT satellites have been able to map the Arctic Ocean sea level up to the 82° parallel whenever the Ocean is not frozen. In 2010 CryoSat-2 satellite was launched, ensuring continuity to altimetric records until present, and extending the spatial coverage up to 88°N significantly improving our ability to retrieve sea level in ocean leads (Stenseng and Andersen, 2012).

Basin scale changes in sea level are primarily caused by two processes: variation in temperature and salinity and through the exchange of water masses between different basins and/or land reservoirs (Leuliette, 2014). The Arctic Ocean is classified as a Mediterranean sea because of its limited water exchange with other ocean basins and because its circulation is coupled with thermohaline differences (Tomczak and Godfrey, 2003). Internally in the Arctic Large Ocean mass variations can be found mainly driven by wind forcing (Volkov and Landerer, 2013; Volkov, 2014).

In this paper we present an updated version of the DTU Arctic Ocean altimetric sea level dataset (Cheng et al., 2015) called Version 3. This dataset has been updated and extended to 23 years in total (1993–2015). The main update consists of replacing the 2002–2003 period previously observed by ENVISAT with sea level from the older ERS-2, due to some unsolved issues with ENVISAT during its first years of operation. The extension of the Arctic Sea level record up to present is achieved by integrating the CryoSat-2 for the period 2010–2015.

Subsequently we present a new updated linear sea level trend map and time series for the Arctic Ocean from Satellite Altimetry for the region 66°N up to the 82°N and the period 1993–2015.

The increase of satellite observations during the last decades has led to a significant progress in sea level budget closure (Church et al., 2011). With the launch of GRACE in 2002 it has been possible to study quasi-global sea level trend budget of the last 12 years, by combining satellite altimetry with water mass variations and thermo- and halo-steric sea level variations from models.

Finally we present a first attempt to a regional sea level trend budget closure study for the Arctic Ocean for the 2005–2015 time-series in which we use satellite gravity observations of water mass changes from the GRACE Tellus Mascons dataset and the global steric sea level anomaly data. Sea level changes caused by thermo- and halo-steric contributions are taken from NOAA Ocean Heat and Salt content dataset.

DATASET

Updated DTU Arctic Sea Level Dataset

The DTU Arctic altimetric Sea level record has been derived to maximize the spatial and temporal extent of the altimetric data. Version 3 of the Arctic record was implemented by merging ERS-1, ERS-2, ENVISAT, and CryoSat-2 missions within the region 66°N–82°N in order to extend the time-series until 2015. These data were tailored, edited and processed according to Cheng et al. (2015), and are referenced to the DTU13 Mean Sea Surface (Andersen et al., 2015).

The raw DTU Arctic dataset is based on the Radar Altimetry Database System (RADS). RADS contains 1-Hz data for 9 missions, and it has the advantage to ensure consistency among the different missions in terms of reference (Scharroo et al., 2013) and corrections (Andersen and Scharroo, 2011).

In order to include Cryosat-2 data we had to account for the fact that Cryosat-2 operates in three different modes (LRM, SAR and SARin) as seen in **Figure 1**, and that only data from LRM and SAR are available through RADS. Furthermore, the standard editing in RADS does not allow for retrieval of sea level in leads (Stenseng and Andersen, 2012) which requires analysis of the 20 Hz data. For this reason SAR and SARIn data are acquired from DTU's in-house Lars Altimetry Retracking System (LARS) (Stenseng, 2011). LARS dataset contains data processed with eight different empirical retrackers, tailored to perform over highly specular surfaces, i.e., leads where SAR and SARIn data are retracked at 20-Hz with a simple threshold retracker. The subsequent processing of data closely followed the method described by Cheng et al. (2015).

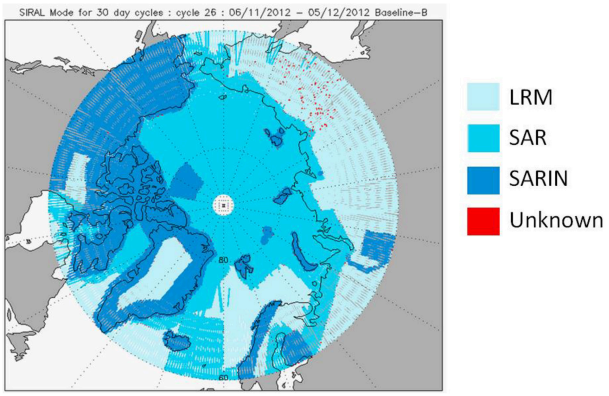

FIGURE 1 | An example of the mode mask of Cryosat-2 for the Arctic Ocean for November 2012. The mask is dynamically changing with time. Faint blue regions means that data in LRM mode. Light blue is data in SAR and dark blue is data in SAR-in. Picture is from Cryosat-2 mission quality monitoring center (http://cryosat.mssl.ucl.ac.uk/qa/mode.php).

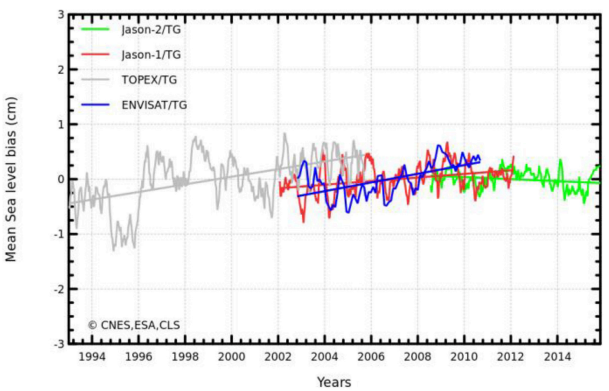

FIGURE 2 | Difference between altimetry sea surface heights and tide gauges *in situ* measurements for four altimetry missions. Ambiguous values are observed for Envisat for 2002 and 2005 (Ablain et al., 2009).

The previous version of DTU Arctic sea level dataset shows a questionable peak over the years 2002–2003, which corresponds to the first 2 years of ENVISAT, where particularly high sea level values are registered. A similar height anomaly is measured on global scale for the same period (Ablain et al., 2009; **Figure 2**). Currently this anomaly is still under investigation (ESA-CCI Sea level initiative, personal communication), and until it is understood we decided to update the version 3 of the Arctic time-series where we have replaced ENVISAT data with ERS-2 values along the period November 2002–July 2003. The comparison of the Arctic monthly averaged sea level over 66°N–82°N between version 2 and version 3 is displayed in **Figure 3**. The black curve represents the updated record. It can be noticed that a mean difference of 7.5 mm can be found between ERS-2 and ENVISAT (red curve) during the overlapping period.

Figure 4 shows the percentage of weekly observations available on the total amount of DTU Arctic sea level dataset. It is shown that within 20 years the largest number of observations

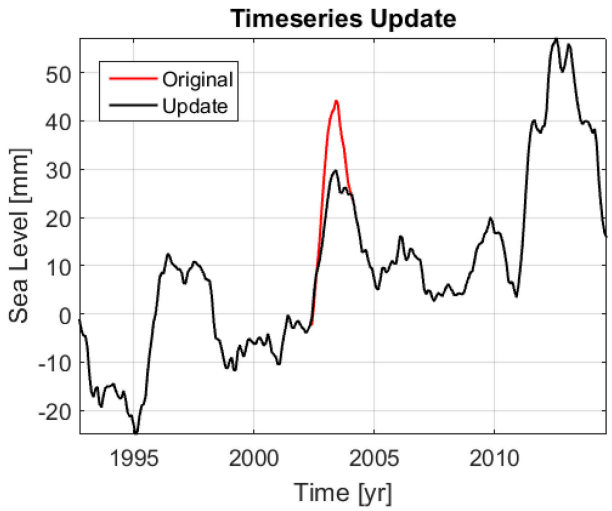

FIGURE 3 | Version 3 of the Sea level record (black) based on ERS-2 compared with Version 2 containing Envisat (red) between 2002 and 2004.

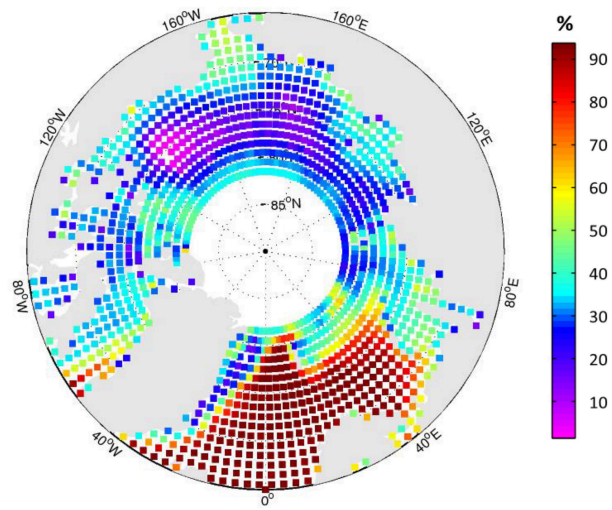

FIGURE 4 | Percentage of weekly altimetric observations (b).

is registered in the North Atlantic, while the availability of weekly data is down to around 20% between 120E and 120W (Cheng et al., 2015). This situation is related to the seasonal presence of ice in the interior of the Arctic Ocean. The irregular distribution of data both in space and time will impact on the interpretation and the subsequent computation of sea level trend budget closure. However, this result is still a huge improvement compared with standard edited datasets.

Grace Water Mass

For the subsequent regional Arctic sea level trend budget closure, monthly global Mascons products from GRCTellus JPL are used. The ocean data, also defined as Equivalent Water Thickness (EWT) are delivered as sampled on a one-by-one

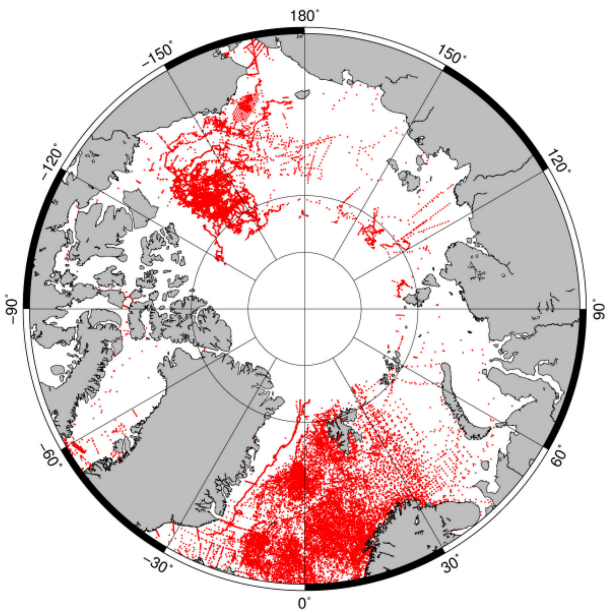

FIGURE 5 | Distribution of steric values available for period 2005–2015.

degree grids and covering the time period from 2003 to 2015 (Watkins et al., 2015). GRACE data are provided with associated errors.

Halo- and Thermo-steric Sea Level Data

Global gridded steric sea level anomalies with resolution one-by-one degree are provided by NOAA Ocean Heat and Salt content dataset. NOAA supplies separately thermo- and halo-steric values from https://www.nodc.noaa.gov/OC5/3M_HEAT_CONTENT/index.html. Both thermosteric and halosteric solutions are delivered every 3 months. Halosteric data at this temporal resolution are available for 2005 to present period, while thermosteric data cover the period 1955-present.

In **Figure 5** the distribution of steric data used for NOAA grids are plotted for the common time span 2005–2015. High density is observed in the North Atlantic area and in the Beaufort Sea, while sparse data are available over Russia and Canadian Islands. It is expected that this irregular distribution varies also in time, meaning that for certain periods few or no data are available. The small number of direct observations will impact the estimation of steric sea level. Unfortunately, NOAA does not provide access to the model and associated spatial distribution of errors. Fortunately, the steric contribution over the analyzed period is relatively small and is not a dominating signal.

ARCTIC LINEAR SEA LEVEL CHANGE (1993–2015)

To investigate the Arctic sea level trend in the region between 66°N and 82°N, the DTU Version 3 sea level dataset was used to compute the monthly mean sea level over the last

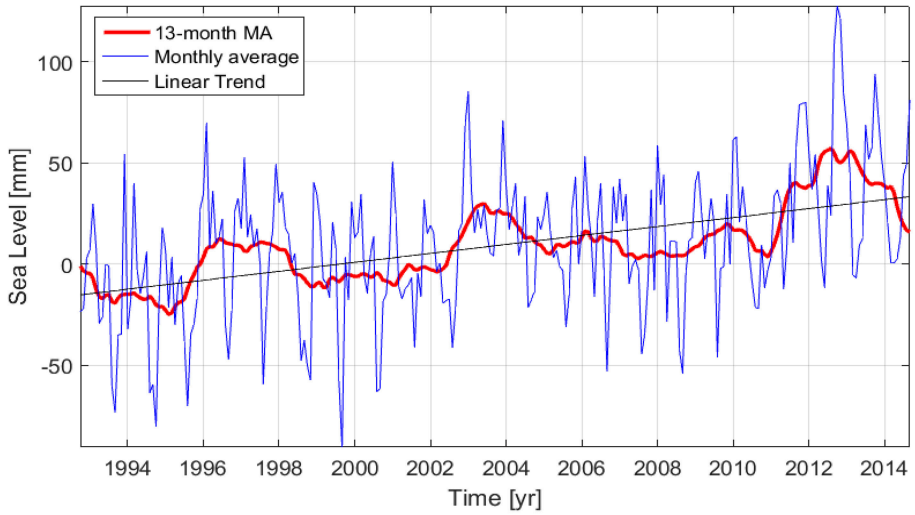

FIGURE 6 | Regional sea level variations over 1993–2015. Monthly averaged values are shown in blue and 13-month averaged values are shown in red.

23 years as shown in **Figure 6**. From 2011 the monthly measurements (blue curve) register slightly higher annual fluctuations, which correspond to the fact that CRYOSAT-2 has more observations during leads in the winter period compared with conventional altimetry from ERS-1/ERS-2 and ENVISAT.

The regional sea level trend computed over the period 1993–2015 indicates an increase of 2.2 ± 1.1 mm/y, which is relatively consistent with the results obtained by Svendsen (2015) for the Arctic Ocean. The red curve represents the 1-year filtered sea level computed through a 13 term moving average (Hyndman, 2011). This highlights inter-annual variation in sea level which is as large as the sea level trend. Consequently estimation of linear sea level trend over shorter period is highly dependent on the chosen period.

A detailed view of spatial pattern of the linear sea level trend for period 1993–2015 is presented in **Figure 7** with a resolution of $0.5^\circ \times 0.5^\circ$.

The trend pattern is dominated by a significant positive trend in the area of the Beaufort Sea, where an increase of almost 15 mm/y is registered. This is due to the Beaufort Gyre, a wind driven phenomenon that leads to freshwater accumulation (Rabe et al., 2011; Giles et al., 2012). In the northern part of the North Atlantic we observe regional sea level trend of 3–5 mm/years, which is comparable to what is seen by i.e., Nerem et al. (2010). Very close to the coast of Greenland the high sea level trend is questionable and can be attributed to the fact that few data exist during the ERS-1/ERS-2/ENVISAT period due to heavy sea ice coverage whereas in the same area Cryosat-2 provides a very narrow strip of SAR-in data.

Throughout most parts of the Russian Sector of the Arctic Ocean we only observe a relative small sea level trend of the order of 0–5 mm/year. This has to be further confirmed using tide gauges data in the region.

REGIONAL ARCTIC SEA LEVEL TREND BUDGET CLOSURE

The sea level budget equation in its simplest form reads:

$$\Delta S_{sl} = \Delta S_{mass} + \Delta S_{steric}$$

Where ΔS_{sl} is the observed sea level, ΔS_{mass} is the ocean mass variation and ΔS_{steric} is the steric component. Both sea level and ocean mass variations are corrected for GIA. Smaller contributions due to inflow and outflow from the Arctic Ocean as well as sea level pressure variations with time should be accounted in the overall sea level trend budget.

Here a first attempt on regional basin scale for the Arctic Ocean is evaluated by comparing the updated sea level record with GRACE EWT values combined with the NOAA steric heights during the overlapping period 2005–2015. GRACE ocean mass variations are processed without accounting for the atmospheric pressure component. This correction is therefore applied using the ECMWF ERA-Interim model, and integrated according to Wunsch and Stammer (1997).

It is important to notice that in this first approach on sea level trend budget closure several crude assumptions are made as the prime purpose of the study is to perform a validation of the observed change in altimetry sea level over the period 2005–2015. First, it must be considered that there is a spatial limitation due to satellite coverage, and the central part of the Arctic Ocean (above 82°N) is not included. The same limitation can be found in steric observations, as mentioned in Section Halo- and Thermosteric Sea Level Data. Secondly, the budget contains data from the Northern area of the Atlantic Ocean, which exchanges water with other parts of the Atlantic Ocean. This effect along with possible variations in the sea level pressure is not accounted for in this investigation. Finally, since NOAA steric data for 2005–2015 are provided with an interval of 3 months, both GRACE

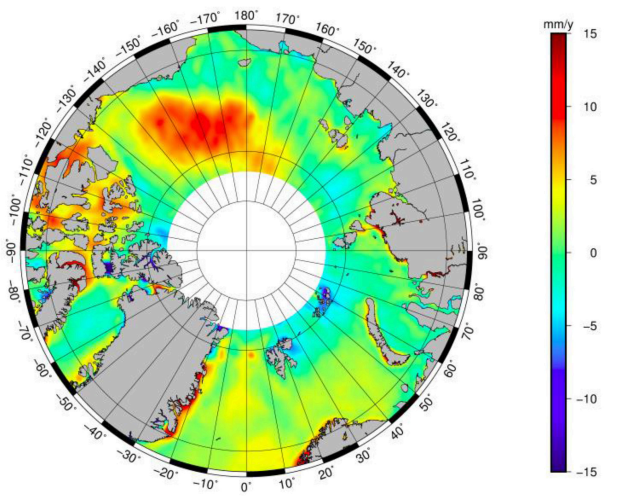

FIGURE 7 | Spatial distribution of linear sea level trend for the period 1993–2015. An increase of 15 mm/y is observed in the Beaufort Sea. In the North Atlantic values corresponding to global sea level rise (Nerem et al., 2010) are found.

TABLE 1 | Linear trend of sea level trend budget elements.

Components	Linear trend (2005–2015) [mm/y]
Sea level (Altimetry)	4.34 ± 2.44
Mass (GRACE)	3.85 ± 0.87
Total steric (NOAA)	0.09 ± 0.36
Thermosteric	0.33 ± 0.32
Halosteric	−0.24 ± 0.14
GRACE + steric	3.94 ± 0.94

and altimetry time-series are also averaged according to the same temporal resolution before comparing these.

Table 1 shows the linear trend of the different components obtained from a least squares fit. The uncertainties are estimated from the least squares fit, as suggested in Leuliette (2014). For period 2005–2015 the altimetric record measures a sea level rise of 4.34 ± 2.44 mm/y, while GRACE EWT registers an increase of 3.85 ± 0.87 mm/y. The large error associated with the altimetry trend is most likely due to great standard deviation in sea level values along the time-series which again stems from large seasonal variation. The same consideration can be done for the steric components: large variation of data through time leads to high errors in slope, in particular for the thermosteric values.

The sum of water mass and steric variations shows an increase in sea level of 3.94 ± 0.94 mm/y. This value falls within the error of altimetry trend, showing consistency between the results. The sea level trend budget based on seasonal values is closed with a difference of 0.4 ± 2.61 mm/y. This is believed to be an acceptable result from this first investigation considering the limitations described above.

In **Figure 8** the 3-month averaged sea level budget contributions for the 2005-2015 period are shown. Large differences are observed between the single values of mass + steric and sea level, showing that on short timescales the budget is not closed. This is likely due to the poor and seasonal spatial sampling from altimetry and steric contribution of intra-annual signals.

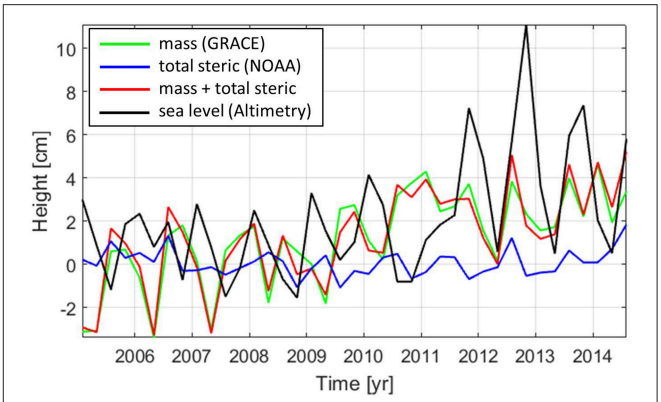

FIGURE 8 | Three-month sea level variation from Altimetry (black) and EWT from GRACE (green), steric contribution (blue), and the sum of ocean mass (GRACE) with steric height (red). All values are in centimeters.

Larger values registered in sea level from 2010 and continuing into 2013 can be observed also with smaller fluctuations in GRACE (green curve), and its combination with the steric components (red curve). The larger fluctuations starting in 2010 can be subscribed to the fact that Cryosat-2 SAR altimetry provides far more data in the interior of the Arctic Ocean due to its improved ability to detect sea level in smaller leads in the ice. The sea level event during 2012–2013, could likely be associated with the recording melting in the Arctic Region as also seen on Greenland (Khan et al., 2015), but more research is needed.

SUMMARY

In this study we have presented an improved version of the Arctic Ocean sea level record for the region 66°N–82°N covering the period 1993–2015. The dataset was modified to account for an unknown error in the ENVISAT data for the years 2002 and 2003, and it was updated with CRYOSAT-2 data until 2015. The record shows a total sea level rise of 2.2 ± 1.1 mm/y. The regional trend highlights a significant increase of 15 mm/y in the Beaufort Sea, corresponding to changes in the Beaufort Gyre. In the northern part of the North Atlantic we observe regional sea level trend of 3–5 mm/years, which is similar to what is seen by i.e., Nerem et al. (2010) for the global ocean.

With GRACE EWT products and NOAA steric models we have derived a first Arctic sea level trend budget closure for the period 2005–2015. Sea level trend of 4.4 mm/years were largely explained by similar trend in water mass derived from GRACE with a minor contribution from steric variations. This results in an acceptable sea level closure of 0.4 mm/y far within the errorbar of the altimetric sea level trend estimate. General agreement is found in the seasonal estimates between the altimetric records and the GRACE+steric combination, where a common increase is observed after 2010.

AUTHOR CONTRIBUTIONS

All authors listed, have made substantial, direct, and intellectual contribution to the work, and approved it for publication.

DATA

The various DTU Arctic sea level data can be found as along track data and as monthly gridded SLA anomalies for the Arctic Ocean through the DTU Space public portal: ftp://ftp.space.dtu.dk/pub/ARCTIC_SEALEVEL.

ACKNOWLEDGMENTS

We would like to acknowledge different agencies for providing the datasets. Altimetry measurements are obtained from RADS at: http://rads.tudelft.nl/rads/rads.shtml. GRACE ocean data available at http://grace.jpl.nasa.gov. More information can be found in Chambers and Bonin (2012). The steric dataset is found in NOAA Global Ocean Heat and Salt Content section, on: https://www.nodc.noaa.gov/OC5/3M_HEAT_CONTENT/index.html, and ECMWF model for atmospheric pressure at sea level, retrieved from: http://www.ecmwf.int/en/research/climate-reanalysis/browse-reanalysis-datasets.

REFERENCES

Ablain, M., Cazenave, A., Valladeau, G., and Guinehut, S. (2009). A new assessment of the error budget of global mean sea level rate estimated by satellite altimetry over 1993–2008. *Ocean Sci.* 5, 193–201. doi: 10.5194/os-5-193-2009

Andersen, O. B., Knudsen, P., and Stenseng, L. (2015). "The DTU13 MSS (Mean Sea Surface) and MDT (Mean Dynamic Topography) from 20 years of satellite altimetry," in *International Association of Geodesy Symposia* (Berlin; Heidelberg: Springer), 1–10. doi: 10.1007/1345_2015_182

Andersen, O. B., and Scharroo, R. (2011). "Range and geophysical corrections in coastal regions: and implications for mean sea surface determination," in *Coastal Altimetry*, eds S. Vignudelli, A. G. Kostianoy, P. Cipollini, and J. Benveniste (Berlin; Heidelberg: Springer), 103–145. doi: 10.1007/978-3-642-12796-0_5

Chambers, D. P., and Bonin, J. A. (2012). Evaluation of Release-05 GRACE time-variable gravity coefficients over the ocean. *Ocean Sci.* 8, 859–868. doi: 10.5194/os-8-859-2012

Cheng, Y., Andersen, O. B., and Knudsen, P. (2015). An improved 20-year Arctic Ocean altimetric sea level data record. *Mar. Geod.* 38, 146–162. doi: 10.1080/01490419.2014.954087

Church, J. A., White, N. J., Konikow, L. F., Domingues, C. M., Cogley, J. G., Rignot, E., et al. (2011). Revisiting the Earth's sea-level and energy budgets from 1961 to 2008. *Geophys. Res. Lett.* 38:L18601. doi: 10.1029/2011GL048794

Giles, K. A., Laxon, S. W., Ridout, A. L., Wingham, D. J., and Bacon, S. (2012). Western Arctic Ocean freshwater storage increased by wind-driven spin-up of the Beaufort Gyre. *Nat. Geosci.* 5, 194–197. doi: 10.1038/ngeo1379

Henry, O., Prandi, P., Llovel, W., Cazenave, A., Jevrejeva, S., and Stammer, D. (2012). Tide gauge-based sea level variations since 1950 along the Norwegian and Russian coasts of the Arctic Ocean: contribution of the steric and mass components. *J. Geophys. Res.* 117, C06023. doi: 10.1029/2011JC007706

Hyndman, R. J. (2011). "Moving averages," in *International Encyclopedia of Statistical Science*, ed M. Lovric (Berlin; Heidelberg: Springer), 866–869. doi: 10.1007/978-3-642-04898-2_380

Khan, S. A., Aschwanden, A., Bjørk, A. A., Wahr, J., Kjeldsen, K. K., and Kjær, K. H. (2015). Greenland ice sheet mass balance: a review. *Rep. Prog. Phys.* 78:046801. doi: 10.1088/0034-4885/78/4/046801

Leuliette, E. (2014). *Report on The Budget of Recent Global Sea Level Rise 2005-2013*. Available online at: http://www.star.nesdis.noaa.gov/sod/lsa/SeaLevelRise/documents/NOAA_NESDIS_Sea_Level_Rise_Budget_Report_2014.pdf

Nerem, R. S., Chambers, D. P., Choe, C., and Mitchum, G. T. (2010). Estimating mean sea level change from the TOPEX and Jason altimeter missions. *Mar. Geod.* 33(Suppl. 1), 435–446. doi: 10.1080/01490419.2010.491031

Pavlov, V. K. (2001). Seasonal and long-term sea level variability in the marginal seas of the Arctic Ocean. *Polar Res.* 20, 153–160. doi: 10.1111/j.1751-8369.2001.tb00051.x

Proshutinsky, A., Ashik, I. M., Dvorkin, E. N., Häkkinen, S., Krishfield, R. A., and Peltier, W. R. (2004). Secular sea level change in the Russian sector of the Arctic Ocean. *J. Geophys. Res.* 109, C03042. doi: 10.1029/2003JC002007

Rabe, B., Karcher, M., Schauer, U., Toole, J. M., Krishfield, R. A., Pisarev, S., et al. (2011). An assessment of Arctic Ocean freshwater content changes from the 1990s to the 2006–2008 period. *Deep Sea Res. Part I Oceanogr. Res. Papers* 58, 173–185. doi: 10.1016/j.dsr.2010.12.002

Scharroo, R., Leuliette, E. W., Lillibridge, J. L., Byrne, D., Naeije, M. C., and Mitchum, G. T. (2013). "RADS: Consistent multi-mission products," in *Proceedings of the Symposium on 20 Years of Progress in Radar Altimetry*, (Venice: Eur. Space Agency Spec. Publ., ESA SP-710), 4.

Stenseng, L. (2011). *Polar Remote Sensing by CryoSat-type Radar Altimetry*. Ph.D. thesis. National Space Institute, Technical University of Denmark.

Stenseng, L., and Andersen, O. B. (2012). Preliminary gravity recovery from CryoSat-2 data in the Baffin bay. *Adv. Space Res.* 50, 1158–1163. doi: 10.1016/j.asr.2012.02.029

Svendsen, P. L. (2015). *Arctic Sea Level Reconstruction*. Ph.D. diss., Technical University of Denmark.

Tomczak, M., and Godfrey, J. S. (2003). *Regional Oceanography: An Introduction, 2nd Edn*. Delhi: Daya Publication.

Volkov, D. L. (2014). Do the North Atlantic winds drive the nonseasonal variability of the Arctic Ocean sea level? *Geophys. Res. Lett.* 41, 2041–2047. doi: 10.1002/2013GL059065

Volkov, D. L., and Landerer, F. W. (2013). Nonseasonal fluctuations of the Arctic Ocean mass observed by the GRACE satellites. *J. Geophys. Res. Oceans* 118, 6451–6460. doi: 10.1002/2013JC009341

Watkins, M. M., Wiese, D. N., Yuan, D.-N., Boening, C., and Landerer, F. W. (2015). Improved methods for observing Earth's time variable mass distribution with GRACE using spherical cap mascons. *J. Geophys. Res. Solid Earth* 120, 2648–2671. doi: 10.1002/2014JB011547

Wunsch, C., and Stammer, D. (1997). Atmospheric loading and the oceanic inverted barometer effect. *Rev. Geophys.* 35, 79–107.

Conflict of Interest Statement: The authors declare that the research was conducted in the absence of any commercial or financial relationships that could be construed as a potential conflict of interest.

frontiers in Marine Science

ORIGINAL RESEARCH
published: 30 March 2016
doi: 10.3389/fmars.2016.00037

On the Decadal Trend of Global Mean Sea Level and Its Implication on Ocean Heat Content Change

Lee-Lueng Fu *

Jet Propulsion Laboratory, California Institute of Technology, Pasadena, CA, USA

The variability of the trend of the global mean sea level (GMSL) on decadal scales is of great importance to understanding the long-term evolution of the GMSL. Trend determination is affected by the temporally correlated processes in the record, which have often not been properly accounted for in previous studies. The problem is treated here as one of optimal estimation weighted by the auto-covariance of the time series, which takes into account the various underlying time scales affecting trend estimation. On decadal scales, the estimated standard error of the trend determined from the GMSL record from radar altimetry is about 0.3 mm/yr, which is comparable to the widely quoted 0.4 mm/yr systematic error and cannot be neglected in the error budget. The time scale of the systematic errors is assumed to be much longer than decadal scale, over which the formal error of the trend estimate becomes dominant. The approach is also applied to determining steric sea level from altimeter-measured sea level and ocean mass estimated from the GRACE observations. The estimated trend error of steric sea level, 0.12 mm/yr, suggests that the change of the global ocean heat content over decadal scales can be estimated from space observations to an accuracy on the order of 0.1 W/m^2. The difference between the steric sea level, estimated from Argo plus the estimated contribution from the deep ocean, and that from altimeter and GRACE, 0.18 ± 0.25 mm/yr, provides an estimate of the combined systematic errors of altimetry minus GRACE observations over the 10 year time span of overlapping Argo and GRACE data.

Keywords: sea level rise, Ocean heat content, radar altimetry, space gravimetry, argo float

OPEN ACCESS

Edited by:
Marta Marcos,
University of the Balearic Islands, Spain

Reviewed by:
Christopher Stephen Watson,
University of Tasmania, Australia
John Church,
CSIRO, Australia

***Correspondence:**
Lee-Lueng Fu
llf@jpl.nasa.gov

Specialty section:
This article was submitted to Coastal Ocean Processes, a section of the journal Frontiers in Marine Science

Received: *04 November 2015*
Accepted: *11 March 2016*
Published: *30 March 2016*

Citation:
Fu L-L (2016) On the Decadal Trend of Global Mean Sea Level and Its Implication on Ocean Heat Content Change. Front. Mar. Sci. 3:37. doi: 10.3389/fmars.2016.00037

INTRODUCTION

The decadal variability of the trend of the global mean sea level (GMSL) is of great importance to studying its long-term evolution as well as the associated change of the heat content of the ocean. Most climate time series such as the sea level record are characterized by a red noise process (e.g., Wunsch, 1999). The temporal correlation of the residuals from a linear trend fit has often been neglected in estimating the uncertainly of the fit, leading to underestimate of its errors. In this study the problem is treated as optimal estimation to minimize the residuals weighted by the autocovariance of the time series. The approach takes into account the variability of the time series over various time scales, and the subsequent effects on the estimate of a trend and its uncertainty.

Satellite radar altimetry has been applied to the measurement of the GMSL since the launch of the TOPEX/Poseidon Mission in 1992 (Nerem et al., 2010; Masters, 2012; Henry, 2014; Ablain et al., 2015; Dieng et al., 2015b). The systematic error in the altimetric sea level trend, a bias drift, has

been estimated from comparison to tide gauge observations, which have long-term (multi-decade scales) errors from land motions (Mitchum, 2000; Watson, 2015), which include the errors in the terrestrial reference frame (Collilieux and Woppelmann, 2011; Haines et al., 2015). After the bias drift correction, the remaining errors are primarily caused by the uncertainty in the knowledge of the vertical land motions at the tide gauge locations. The time scale of the vertical land motions is tectonic and generally much longer than a decade. These errors essentially cause a bias in the estimate of a trend over decadal scales. Such bias would be canceled for evaluating the change of decadal trends, of which the errors are dominated by the uncertainty in the estimation error.

As the contribution to sea level change from the change in ocean mass can be estimated from space gravimetry missions like GRACE (Johnson and Chambers, 2013). The variation of the global mean steric sea level can be estimated from the combination of altimetry and GRACE observations (Willis et al., 2008; von Schuckmann, 2014; Dieng et al., 2015a). The results have been compared to the observations made by Argo in the upper ocean. Although the results have substantial uncertainty, it is interesting to examine the decadal trend error of the global mean steric sea level for making inference on the rate of the change of the ocean heat content. This is an important indicator for the heat balance of the globe as more than 90% of the heat accumulated on Earth over the past century has been stored in the ocean (Levitus, 2012).

METHODOLOGY

The problem of fitting to a time series by a polynomial can be readily formulated as an optimal estimation problem (e.g., Wunsch, 1996). For the sake of clarity, the methodology described in Wunsch (1996) is briefly summarized here. The linear trend, denoted by b, can be solved for in the following equation:

$$a + bt + n(t) = y(t) \tag{1}$$

where a represents a constant, $n(t)$ random noise, and $y(t)$ the time series of observations at time t. Equation (1) can be written the following form:

$$\boldsymbol{D}\,\boldsymbol{a} + \boldsymbol{n} = \boldsymbol{y} \tag{2}$$

Where

$$\boldsymbol{D} = \begin{Bmatrix} 1 & t_1 \\ 1 & t_2 \\ . & \\ . & \\ 1 & t_m \end{Bmatrix}, \quad \boldsymbol{a} = \begin{bmatrix} \boldsymbol{a} \\ \boldsymbol{b} \end{bmatrix}, \quad \boldsymbol{y} = \begin{bmatrix} y(t_1) \\ y(t_2) \\ . \\ . \\ y(t_m) \end{bmatrix}, \tag{3}$$

and $\boldsymbol{n}(t)$ is the noise vector. Let the $m \times m$ autocovariance matrix of $\boldsymbol{y}$ be noted by $\boldsymbol{R}$, then the optimal solution for $\boldsymbol{a}$ is expressed as follows (Wunsch, 1996, p. 121):

$$\tilde{\boldsymbol{a}} = \begin{bmatrix} \tilde{a} \\ \tilde{b} \end{bmatrix} = \left[\boldsymbol{D}^T \boldsymbol{R}^{-1} \boldsymbol{D}\right]^{-1} \boldsymbol{D}^T \boldsymbol{R}^{-1} \boldsymbol{y} \tag{4}$$

The variance of the uncertainty of the estimate $\tilde{\boldsymbol{a}}$ about its mean is

$$\boldsymbol{P} = <(\tilde{\boldsymbol{a}} - \boldsymbol{a})^2> = \left[\boldsymbol{D}^T \boldsymbol{R}^{-1} \boldsymbol{D}\right]^{-1} \tag{5}$$

The autocovariance matrix $\boldsymbol{R}$ is given below:

$$\begin{bmatrix} R(0) & R(\Delta t) & R(2\Delta t) & . & R((m-1)\Delta t) \\ R(\Delta t) & R(0) & R(\Delta t) & . & R((m-2)\Delta t) \\ . & . & . & . & . \\ R((m-1)\Delta t) & & . & . & R(0) \end{bmatrix} \tag{6}$$

Where Δt is the interval of the time series $\boldsymbol{y}$ and the matrix elements are the autocovariance of $\boldsymbol{y}$ after a linear trend is removed. $\boldsymbol{R}$ thus represents the covariance of the error of estimating a linear fit to the time series $\boldsymbol{y}$. The solution for $\tilde{\boldsymbol{a}}$ from Equation (4) has minimum variance of uncertainty via a weighted least-squares approach. For the relatively short record of satellite altimetry measurement, the estimation error of $\boldsymbol{R}$ increases with time scales. The validity of the results on the decadal scales has been examined by comparison to the standard linear regressions analysis with the degrees of freedom determined by $\boldsymbol{R}$.

RESULTS

Sea Level

Displayed in **Figure 1** is the GMSL time series obtained from satellite altimeter measurements by TOPEX/Poseidon and its successors Jason-1 and Jason-2 (Nerem et al., 2010). The data were processed by the Sea Level Research Group of the University of Colorado (CU) with the seasonal cycle removed. The estimates of the sea level trend are somewhat different among the results from various groups, owing to the differences in treating the time-variable biases in the radiometer corrections, the sea-state bias models, the inter- and intra-mission biases, and the differing orbits (Dieng et al., 2015b). However, the result of the CU has the least residual trend (−0.03 mm/yr) after subtracting ocean mass from GRACE and steric sea level from Argo. This near closure of the sea level budget indicates the consistency of the CU record with other types of observation to the extent of their uncertainties.

In this study, it is assumed that the uncertainty in the sea level trend from the CU record consists in a systematic measurement error and the trend estimation error. With the seasonal cycle removed, the trend of sea level rise was estimated by the CU group to be 3.3 ± 0.4 mm/yr. The uncertainty was estimated from comparison to the observations from a global tide gauge network. As discussed in Mitchum (2000) and Watson (2015), the uncertainty is a systematic error dominated by that of the tide gauge observations caused by the land motions at the sites of the gauges. The errors in the terrestrial reference frame are imbedded in the land motion errors as well as manifested in orbit errors which have been estimated to be ∼0.3 mm/yr (Beckley et al.,

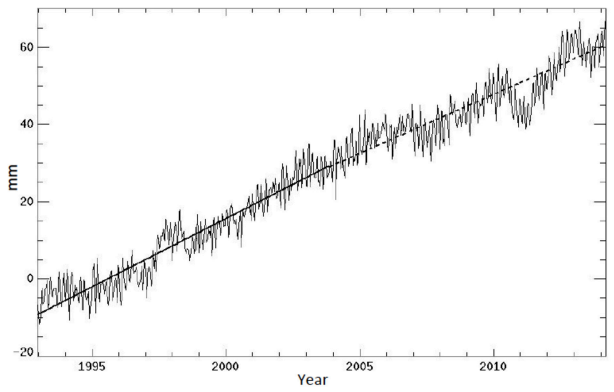

FIGURE 1 | GMSL (in mm) time series in 10-day intervals from 1993–2013, obtained from the altimeter measurements from the TOPEX/Poseidon, Jason-1, and Jason-2 missions (Nerem et al., 2010). The heavy solid and dashed lines represent linear fits of the first and second half of the record, respectively. The standard deviation of the random errors is 4.1 mm.

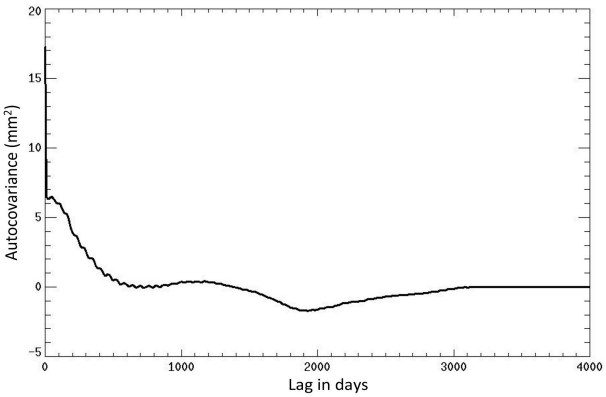

FIGURE 2 | The auto covariance of the time series shown in Figure 1.

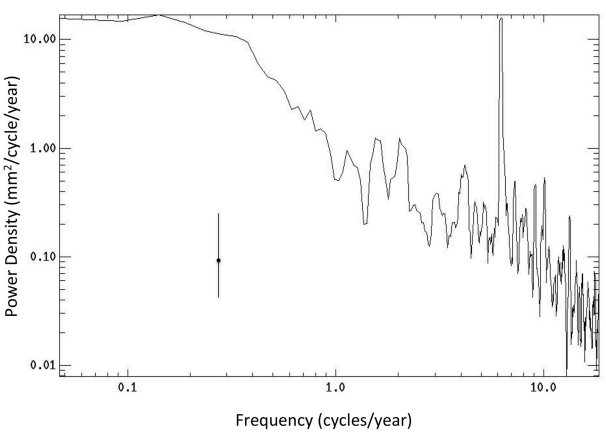

FIGURE 3 | The frequency spectrum of the time series shown in Figure 1 with a linear trend removed. The error bar represents the 95% confidence interval.

2007) for the period of 1993–2007. The trend estimation error was considered to be <0.1 mm/yr and ignored in the total error estimate of Nerem et al. (2010). The underlying causes for the systematic error from the slowly evolving land motions and the terrestrial reference frame have time scales much longer than a decade after the seasonal cycle is removed from the record. The systematic error is thus negligible in the determination of a trend on decadal scales.

With the increasing length of the record, we are often faced with questions like "How has the rate of sea level rise changed over the recent past? Is the change significant from decade to decade?" To answer such questions with quantified degree of certainty requires a rigorous estimate of the uncertainty in the estimate of a trend. To address possible change of the trend on decadal scales and its statistical significance, also shown in **Figure 1** are the linear fits to the first and the second half of the record computed using Equation (4), exhibiting slightly different rates: 3.54 ± 0.29 mm/yr for the first decade; 3.06 ± 0.31 mm/yr for the second decade. The purpose of this study is not about the reason for the apparent change of the trend, but the statistical uncertainty arising from the correlated signals. The error bars are estimated by taking the square root of the values obtained from Equation (5), with the auto-covariance of the sea level time series shown in **Figure 2**. The peak, $\sim$17 mm^2, at zero lag corresponds to the variance of the random error after averaging the altimeter data over the 10–day repeat cycles. It corresponds to an error bar (standard deviation) of 4.1 mm for each 10-day data point in the time series.

In practice, the autocovariance was obtained by applying the inverse Fourier Transform to the power spectrum of the GMSL time series after a linear trend is removed (**Figure 3**). The low-frequency plateau indicates the "red" nature of the time series dominated by the long time scales. There is a peak around 60 days associated with residual tidal and orbital errors. This peak is overwhelmed by the wide-band low-frequency signals that dominate the autocovariance. The correlation time scale of the time series, τ, can be estimated by Kendall and Stuart (1976)

$$\tau = 2\sum_{i=0}^{m-1} \frac{R^2(i\Delta t)}{R^2(0)}\Delta t \tag{7}$$

The evaluation of Equation (7) leads to $\tau = 480$ days. The correlated error of this time scale is accounted for in the minimum variance solution from Equation (4). Without accounting for the correlated error and assuming that each data point is independent, the standard error of the trend estimate of a 10-year record would be about 0.07 mm/yr, a severe underestimate compared to $\sim$0.3 mm/yr. Using Equation (4) the trend of the whole 22-year record is 3.28 ± 0.10 mm/yr. Note that the trend error without accounting for the correlated error would be 0.025 mm/yr.

To test the validity of the estimate of the correlation time scale from Equation (7), the time series shown in **Figure 1** was smoothed over 480 days and resampled at the same

interval. Then each of the resampled 16 data points should be independent. The linear trend was estimated with 16 degrees of freedom resulting in 3.20 ± 0.09 mm/yr. Note that the uncertainty is close to 0.10 mm/yr derived from the optimal estimation. This provides a consistency test of the accuracy of the autocovariance function and its role in Equations (4) and (7).

The fact that the two trend estimates are separate by more than one standard deviation suggests that the rate of sea level rise in the second decade is significantly less than in the first decade. Assuming the error statistics are Gaussian, the probability for the above statement being true is estimated 87% based on the trend values and respected standard deviations. The quantification of the uncertainty in the decadal change of the rate of sea level rise is important for determining the long-term evolution of the GMSL in terms of acceleration or deceleration.

Although there have been studies on the interannual variability of the GMSL in terms of the global hydrological cycle (e.g., Cazenave, 2014), there have been no explanations for the apparent deceleration on decadal scales until the study by Watson (2015). They used an improved tide gauge database for making altimeter bias drift correction. After the correction, the GMSL rose at a much slower rate over the first 6 years of the TOPEX/Poseidon record, which suffered from instrument degradation until the altimeter switched to a redundant side in 1999. As noted earlier, the present study does not address the physical mechanism of the variability of the decadal trend nor the altimeter bias drift correction, but only focus on the effects of correlated signals on the uncertainty in the decadal trend.

Ocean Heat Content

Another important piece of information from the decadal change of the rate of sea level rise is the change of the ocean heat content reflected by the steric component of sea level. As noted in the Introduction, steric sea level can be determined from the difference between altimeter-measured GMSL and GRACE-measured mass component. The GRACE data processed by the Center for Space Research of the University of Texas at Austin and analyzed by Llovel et al. (2014) were used for the present study. The data products from other groups have shown small differences (±0.08 mm/yr; Dieng et al., 2015b). The altimeter-determined GMSL (**Figure 1**) was smoothed over 60 days and subsampled at monthly intervals to match the GRACE data in the period of 2003–2013 as in Llovel et al. (2014). Shown in **Figure 4** is the steric sea level computed by subtracting the mass component from the GMSL. The rate of the rise estimated from Equation (4) is 0.88 ± 0.12 mm/yr. Not included in the error estimate are the long-term systematic errors of both altimetry and GRACE. The long-term 0.4 mm/yr error in the altimetry measurement is discussed previously. The dominant systematic error in the GRACE measurement is caused by the uncertainty in the correction for the Glacial Isostatic Adjustment. It is also estimated to be 0.4 mm/yr (Chambers et al., 2010) with a time scale longer than decadal and can be ignored in decadal trend error.

Compared to the estimate of Llovel et al. (2014), 0.77 ± 0.28 mm/yr, the new estimate is a larger trend with less error. The differences are partly caused by the effect of the correlated signals accounted for in the present study. The larger uncertainty of Llovel et al. (2014) was probably caused by the fact that their uncertainty estimate was a combination of the formal fit error (without accounting for the correlated signals) and the random observational error as described in their paper. The present approach has taken into account both the observational error and correlated signals by the use of the autocovariance function. In any case, the two estimates are within the quoted statistical uncertainties of each.

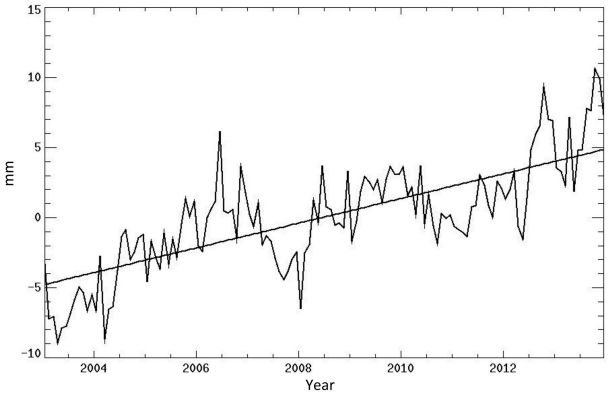

FIGURE 4 | The steric sea level obtained from the altimeter and GRACE data. The straight line shows a linear fit of the curve.

Based on global ocean climatologic conditions, Wunsch and Heimbach (2014) estimated the equivalence between the rate of sea level rise and the rate of ocean warming: 1 mm/yr corresponds to 0.75 W/m^2. This implies that the 1-sigma uncertainly in the rate of ocean warming on decadal scales determined from that of the steric sea level, 0.12 mm/yr, is close to 0.1 W/m^2. This is consistent with the estimate of Wunsch and Heimbach (2014) from model-based ocean state estimation. Given the estimated global ocean warming rate of 0.5–1 W/m^2 (Hansen, 2005; Roemmich and, 2015), the 0.1 W/ m^2 error provides an order of magnitude guide for determining if there is significant change in the ocean warming rate on decadal scales. The result suggests that the temporally correlated signals in the altimeter and GRACE observations have an effect comparable to the uncertainty of the Argo observations in the determination of the decadal trend of the ocean heat content. The contribution of the deep ocean is much less than the uncertainty of the heat budget on decadal scales.

Systematic Errors

Llovel et al. (2014) used the Argo data from 2005 to 2013 to estimate the steric sea level from the temperature and salinity observations of the upper 2000 m of the ocean. They obtained a linear trend of 0.90 ± 0.15 mm/yr, which is the average of 5 data products from Argo. The steric sea level derived from the altimeter and GRACE data over the same period is 0.82 ± 0.17 mm/yr. The two estimates are not distinguishable to the extent of the estimated uncertainty, consistent with the findings of Llovel et al. (2014). Note that the steric sea level from the water

below 2000 m is about 0.1 ± 0.1 mm/yr from direct observations (Purkey and Johnson, 2010), which is less than the uncertainties of both the Argo and satellite observations. The close agreement given above is a mutual validation of the Argo and satellite observations (Willis et al., 2010). Dieng et al. (2015b) presented the range of results from various Argo data products, showing small differences on the order of ± 0.08 mm/yr, which is smaller than the formal uncertainty of ± 0.15 mm/yr. However, we must keep this uncertainty in mind when interpreting the result of the present study, which is focused on the statistical uncertainty of the trend estimation.

The comparison of the steric sea level determined from Argo to the space observations from altimetry and GRACE provides an opportunity to assess the systematic errors of the space observations during the period when the three observations coexist. If we add the contribution from the deep ocean noted above, 0.1 ± 0.1 mm/yr, to the contribution from the upper ocean, 0.90 ± 0.15 mm/yr, we obtain 1.0 ± 0.18 mm/yr (the uncertainty is the root-sum-squares of the two) for the total steric sea level. Its difference from the space observation, 0.82 ± 0.17 mm/yr, yields 0.18 ± 0.25 mm/yr. Given the various assumptions noted earlier, this provides an estimate of the combined systematic errors of altimetry minus GRACE measurements during the period of coexistence of the three measurements, 2005–2013. The systematic errors of the measurement systems are likely to change with time, as indicated for example by the relatively large altimeter bias drift in the early part of the altimetry record of TOPEX/Poseidon (Watson, 2015)

CONCLUSIONS

The formal error in estimating a linear trend in the GMSL record is treated as a problem of optimal estimation. The temporally correlated variability of the record is accounted for by its autocovariance. For the 22-year record from the TOPEX/Poseidon, Jason-1, and Jason-2 missions, a linear trend of 3.28 ± 0.10 mm/yr is obtained. The overall error in estimating a bias drift from comparison to a network of globally distributed tide gauges is estimated to be 0.4 mm/yr (Mitchum, 2000). This error is primarily caused by the uncertainty in the vertical land motions at the tide gauge locations. The time scale of the variability of the uncertainty is associated with the long-term change of the solid earth and is much longer than a decade. On decadal time scales, the uncertainty in detecting a change of the trend of sea level has significant contribution from the formal error of the trend estimate, which is about 0.3 mm/yr for a 10-year record.

The mass component of the variation of the GMSL during 2003–2013 is determined from the gravity measurement from the GRACE mission. Subtraction of the mass component from the altimeter-determined sea level leads to an estimate of the global mean steric sea level, which exhibits a trend of 0.88 ± 0.12 mm/yr over the 10 year period. This corresponds to oceanic heat absorption at a rate of 0.66 ± 0.09 W/m^2. Although the absolute value is subject to an unknown bias on time scales longer than a decade, the error estimate applies to the uncertainty on a decadal scale. It is considered that the uncertainty in detecting a decadal change in the rate of oceanic heat uptake based on satellite altimetry and gravimetry measurement is on the order of 0.1 W/m^2. However, the contributions from the regions not covered by the satellite observations have been neglected (the ocean below 2000 m, the Arctic Ocean and other marginal seas).

The estimate of the steric sea level from altimetry and GRACE is subject to long-term systematic errors: approximately 0.4 mm/yr error in both the altimetry measurement and the GRACE measurement. The difference between of the steric sea level, estimated from Argo plus the estimated deep ocean contribution, and that from altimeter and GRACE, 0.18 ± 0.25 mm/yr, provides an estimate of the combined systematic errors of altimetry minus GRACE observations during 2005–2013. Longer records of altimetry, gravity, and Argo will shed light on the long-term stability of the systematic errors and the utility of spaceborne observations to determining the steric sea level and associated change in ocean heat content.

AUTHOR CONTRIBUTIONS

The author confirms being the sole contributor of this work and approved it for publication.

ACKNOWLEDGMENTS

The data used in the study is available at (1) Altimeter data: The University of Colorado Sea Level Research Group, URL: http://sealevel.colorado.edu/; (2) GRACE data were processed by the Center for Space Research of the University of Texas at Austin (release-5) and available at: NASA Physical Oceanography Distributed Active-Archive Center, URL: ftp://podaac-ftp.jpl.nasa.gov/allData/grace/L2/CSR/RL05. The research presented in the paper was carried out at the Jet Propulsion Laboratory, California Institute of Technology, under contract with the National Aeronautic and Space Administration. Discussions with Carl Wunsch of Harvard University, as well as with Felix Landerer and Josh Willis of JPL are gratefully acknowledged.

REFERENCES

Ablain, M., Cazenave, A., Larnicol, G., Balmaseda, M., Cipollini, P., Faugère, Y., et al. (2015). Improved sea level record over the satellite altimetry era (1993-2010) from the climate change initiative project. *Ocean Sci.* 11, 67–82. doi: 10.5194/os-11-67-2015

Beckley, B. D., Lemoine, F. G., Luthcke, S. B., Ray, R. D., and Zelensky, N. P. (2007). A reassessment of global and regional mean sea level trends from TOPEX and Jason-1 altimetry based on revised reference frame and orbits. *Geophys. Res. Lett.* 34, L14608. doi: 10.1029/2007GL030002

Cazenave, A., et al. (2014). The rate of sea-level rise. *Nat. Clim. Change* 4, 358–361. doi: 10.1038/nclimate2159

Chambers, D. P., Wahr, J., Tamisiea, M. E., and Nerem, R. S. (2010). Ocean mass from GRACE and glacial isostatic adjustment. *J. Geophys. Res.* 115, B11415. doi: 10.1029/2010JB007530

Collilieux, X., and Woppelmann, G. (2011). Global sea-level rise and its relation to the terrestrial reference frame. *Geod. J.* 85, 9–22. doi: 10.1007/s00190-010-0412-4

Dieng, H. B., Cazenave, A., von Schuckmann, K., Ablain, M., and Meyssignaac, B. (2015b). Sea level budget over 2005-2013: missing contributions and data errors. *Ocean Sci. Discuss.* 12, 701–734. doi: 10.5194/os-11-789-2015

Dieng, H. B., Palanisamy, H., Cazenave, A., Meyssignac, B., and von Schuckmann, K. (2015a). The sea level budget since 2003: inference on the deep ocean heat content. *Surd. Geophys*. 36, 209–229. doi: 10.1007/s10712-015-9314-6

Haines, B. J., Bar-Sever, Y. E., Bertiger, W. I., Desai, S. D., Harvey, N., Sibois, A. E., et al. (2015). Realizing a terrestrial reference frame using the global positioning system. *J. Geophys. Res. Solid Earth* 120, 5911–5939. doi: 10.1002/2015JB012225

Hansen, J., et al. (2005). Earth's energy imbalance: confirmation and implications. *Science* 308, 1431–1435. doi: 10.1126/science.1110252

Henry, O. et al. (2014). Effect of the processing methodology on satellite altimetry-based GMSL rise over the Jason-1 operating period. *Geod. J.* 88, 351–361. doi: 10.1007/s00190-013-0687-3

Johnson, G. C., and Chambers, D. P. (2013). Ocean bottom pressure seasonal cycles and decadal trends from GRACE Release-05: Ocean circulation implications. *J. Geophys. Res. Oceans* 118, 4228–4240. doi: 10.1002/jgrc.20307

Kendall, M., and Stuart, A. (1976). *The Advanced Theory of Statistics*, Vol. 3, *3rd Edn*. London: Griffin.

Levitus, S., et al. (2012). World ocean heat content and thermosteric sea level change (0–2000 m), 1955–2010. *Geophys. Res. Lett.* 39, L10603. doi: 10.1029/2012GL051106

Llovel, W., Willis, J. K., Lander, F. W., and Fukumori, I. (2014). Deep-ocean contribution to sea level and energy budget not detectable over the past decade. *Nat. Clim. Change* 4, 1031–1035. doi: 10.1038/nclimate2387

Masters, D., et al. (2012). Comparison of GMSL time series from TOPEX/Poseidon, Jason-1, and Jason-2, Marine Geodesy. *35(Suppl.* 1), 20–41. doi: 10.1080/01490419.2012.717862

Mitchum, G. T. (2000). An improved calibration of satellite altimetric heights using tide gauge sea levels with adjustment for land motion. *Mar. Geod.* 23, 145–166. doi: 10.1080/01490410050128591

Nerem, R. S., Chambers, D., Choe, C., and Mitchum, G. (2010). Estimating mean sea level change from the TOPEX and Jason altimeter missions. *Mar. Geod. 33(Suppl.* 1), 435–446. doi: 10.1080/01490419.2010.491031

Purkey, S. G., and Johnson, G. C. (2010). Warming of global abyssal and deep Southern Ocean waters between the 1990s and 2000s: contributions to global heat and sea level rise budgets. *Clim. J.* 23, 6336–6351. doi: 10.1175/2010JCLI3682.1

Roemmich, D., etal. (2015). Unabated planetary warming and its ocean structure since 2006. *Nat. Clim. Change* 5, 240–245. doi: 10.1038/nclimate2513

von Schuckmann, K., et al. (2014). Consistency of the current global ocean observing systems from an Argo perspective. *Ocean Sci.* 10, 547–557. doi: 10.5194/os-10-547-2014

Watson, C. S., et al. (2015). Unabated global mean sea-level rise over the satellite altimter era. *Nat. Clim. Change* 5, 565–568. doi: 10.1038/nclimate2635

Willis, J. K., Chambers, D. P., Kuo, C.-Y., and Shum, C. K. (2010). Global sea level rise: recent progress and challenges for the decades to come. *Oceanography* 23, 26–35. doi: 10.5670/oceanog.2010.03

Willis, J. K., Chambers, D. P., and Nerem, R. S. (2008). Assessing the globally averaged sea level budget on seasonal to interannual timescales. *J. Geophys. Res.* 113, C06015. doi: 10.1029/2007jc004517

Wunsch, C. (1996). *The Ocean Circulation Inverse Problem. Cambridge*: Cambridge University Press.

Wunsch, C. (1999). The interpretation of short climate records, with comments on the North Atlantic and Southern Oscillations. *Bull. Amer. Met. Soc. 80,* 245–255.

Wunsch, C., and Heimbach, P. (2014). Bidecadal thermal changes in the abyssal ocean. *J. Phys. Oceanogr.* 44, 2013–2030. doi: 10.1175/JPO-D-13-096.1

Conflict of Interest Statement: The author declares that the research was conducted in the absence of any commercial or financial relationships that could be construed as a potential conflict of interest.

frontiers in Marine Science

ORIGINAL RESEARCH
published: 29 April 2016
doi: 10.3389/fmars.2016.00056

The Impact of a Barrier Island Loss on Extreme Events in the Tampa Bay

Marius Ulm[1]*, *Arne Arns*[1], *Thomas Wahl*[1,2], *Steven D. Meyers*[2], *Mark E. Luther*[2] and *Jürgen Jensen*[1]

[1] Department of Civil Engineering, Research Institute for Water and Environment, University of Siegen, Siegen, Germany, [2] Ocean Monitoring and Prediction Laboratory, College of Marine Science, University of South Florida, St. Petersburg, FL, USA

Barrier islands characterize up to an eighth of the global coastlines. They buffer the mainland coastal areas from storm surge and wave energy from the open ocean. Changes in their shape or disappearance due to erosion may lead to an increased impact of sea level extremes on the mainland. A barrier island threatened by erosion is Egmont Key which is located in the mouth of the Tampa Bay estuary at the west-central coast of Florida. In this sensitivity study we investigate the impact a loss of Egmont Key would have on storm surge water levels and wind waves along the coastline of Tampa Bay. We first simulate still water levels in a control run over the years 1948–2010 using present-day bathymetry and then in a scenario run covering the same period with identical boundary conditions but with Egmont Key removed from the bathymetry. Return water levels are assessed for the control and the scenario runs using the Peak-over-threshold method along the entire Tampa Bay coastline. Egmont Key is found to have a significant influence on the return water levels in the Bay, especially in the northern, furthest inland parts where water levels associated with the 100-year return period increase between 5 and 15 cm. Additionally, wind wave simulations considering all 99.5th percentile threshold exceedances in the years 1980–2013 were conducted with the same control and scenario bathymetries. Assessing changes in return levels of significant wave heights due to the loss of Egmont Key revealed an increase of significant wave heights around today's location of the island.

Keywords: barrier islands, beach erosion, numerical modeling, extreme value statistics, extreme water levels, extreme wave heights, estuary, Tampa Bay

OPEN ACCESS

Edited by:
Ivan David Haigh,
University of Southampton, UK

Reviewed by:
Matthew John Eliot,
Damara WA Pty Ltd., Australia
Pushpa Dissanayake,
University of Konstanz, Germany

***Correspondence:**
Marius Ulm
marius.ulm@uni-siegen.de

Specialty section:
This article was submitted to Coastal Ocean Processes, a section of the journal Frontiers in Marine Science

Received: *16 December 2015*
Accepted: *11 April 2016*
Published: *29 April 2016*

Citation:
Ulm M, Arns A, Wahl T, Meyers SD, Luther ME and Jensen J (2016) The Impact of a Barrier Island Loss on Extreme Events in the Tampa Bay. Front. Mar. Sci. 3:56. doi: 10.3389/fmars.2016.00056

1. INTRODUCTION

Barrier islands are located near the mainland coast, often forming lagoons which are connected to the ocean by small tidal inlets. Oertel (1985) describes that coastal areas around and behind a barrier island are not merely independent from each other but rather part of an interrelated barrier island system with regard to hydrodynamic, hydrological, and geological processes. Globally, barrier islands can be found along 6.5% (Stutz and Pilkey, 2001) to 13% (Cromwell, 1973) of the coastlines. Examples in Europe are the Frisian Islands protecting the Wadden Sea (North Sea) or the barrier island system forming the Venice Lagoon (Mediterranean Sea). In the United States barrier island systems span large coastal areas along the Atlantic Ocean and Gulf of Mexico. Due to marked interdependency between barrier islands, the mainland coast, and adjacent waters, changes in individual parts may have an effect on the entire system (Oertel, 1985).

Changes in the barrier island system can also directly affect the mainland coastline behind the island. For instance, a reduction of storm surge and wave energy was described by Stone and McBride (1998), who found wave heights in some bays along the coast of Louisiana to be seven times larger in case of an erosion of the Isles Dernières barrier island chain. Furthermore, Stone et al. (2005) showed that decreased energy dissipation due to dredging may also lead to an increase in erosion of the mainland marshes.

A recent study by Passeri et al. (2015b) highlighted how changes of barrier islands over the last 150 years affected harmonic tidal constituents and led to extensive erosion along the coast of the Grand Bay estuary in the Mississippi Sound. In another study covering the same area Passeri et al. (2015a) showed that modeling the effects of sea level rise and extremes to barrier island systems should also include shoreline change predictions in order to consider the interdependencies between morphologic and hydrodynamic changes.

In numerical model experiments List and Hansen (1992) showed that wind speed as well as the depth and width of a bay behind a barrier island have a strong influence on wind waves. However, due to several simplifying model assumptions, concerning e.g., topography and wind conditions, the authors hesitantly concluded that narrow and deep bays benefit more from a barrier island than wide and shallow waters; the latter significantly influence wave energy due to the depth limited characteristic of waves. Nevertheless, the protective nature of barrier island systems becomes apparent from those examples.

The Florida west-central coast is located behind a large barrier island system spanning approximately 315 km from the Anclote Keys in northern Pinellas County to Marco Island in southern Collier County. Egmont Key is part of this barrier island system but situated in a very exposed position where the string of barrier islands is separated by the Tampa Bay inlet. The adjacent mainland is low-lying and therefore vulnerable to extreme water levels and waves. For instance, Weisberg and Zheng (2006) showed that a water level rise of 6 m, which is within the range of physically possible events during a hurricane storm surge, has the potential to cause widespread inundation at the Bay's barrier islands and the surrounding counties. A rigorous assessment of possible extreme water levels, induced by tropical cyclones or strong winter storms (e.g., nor'easters), and how they are influenced by natural and artificial coastal structures is needed to provide reliable protection strategies.

Egmont Key underwent extensive erosion in the last decades as shown by Stott and Davis (2003). Based on the findings of List and Hansen (1992), Stone and McBride (1998), Stone et al. (2005), Passeri et al. (2015b), and Passeri et al. (2015a) a disappearance of Egmont Key would probably impact extreme water levels, extreme wave heights, and may also affect estuarine circulation in the larger Tampa Bay area. However, a detailed assessment that quantifies the potential effects is currently missing. In this paper we estimate the hydrodynamic impacts of the loss of Egmont Key, primarily along the mainland shoreline, using a Delft3D (Lesser et al. (2004), http://oss.deltares.nl/web/delft3d) hydrodynamic-numerical model of Tampa Bay and the adjacent Gulf of Mexico. The Delft3D wave module (based on the SWAN wave model) is then used to assess changes in maximum significant wave heights within Tampa Bay. We note that complete erosion of Egmont Key is unlikely to occur in the near future and therefore our simulations represent a worst-case sensitivity study that helps bracket impacts of a future loss.

2. STUDY AREA

Tampa Bay is an estuary located at Florida's west-central coast at the Gulf of Mexico. It is surrounded by the counties Pinellas, Hillsborough, and Manatee containing large and densely populated cities such as St. Petersburg, Clearwater, and Tampa as shown in **Figure 1**. Several smaller cities are also located close to the Bay. The cities are heavily developed along the shoreline with residential, commercial, and industrial infrastructure. Overall the three counties are home of 2.6 million people (2014 estimates from the United States Census Bureau; http://quickfacts.census.gov).

The entire Tampa Bay has a surface of around 1033 km^2 (Kunneke and Palik, 1984) and is commonly divided into four major bay segments, also pictured in **Figure 1**. Old Tampa Bay and Hillsborough Bay are located in the north. Middle Tampa Bay forms the central region and Lower Tampa Bay connects with the Gulf of Mexico. Terra Ceia Bay and the tidal reach of the Manatee River are two segments in the south. Boca Ciega Bay creates the western coast of St. Petersburg and is protected by the islands Long Key, Treasure Island, and Sand Key. Egmont Key is located south of Mullet Key at the mouth of Tampa Bay, the connection between Lower Tampa Bay and the Gulf of Mexico. The alongshore profile of Egmont Key blocks more than a third of the Bay's mouth with a length of 3 km perpendicular to the outlet direction. Egmont Key arose from sediments provided by the Tampa Bay which were partially deposited in the ebb-tidal delta of the estuary due to the common action of tides and waves. The entire sediment complex below the barrier island extents 10 km into the Gulf of Mexico (Stott and Davis, 2003). The first detailed survey of Egmont Key dates back to 1877 and changes in shape and size were already documented at that time (see Figure 5 in Stott and Davis, 2003). Today the U.S. Army Corps of Engineers (USACE) tries to hinder the erosion of Egmont Key with beach nourishment measures which currently help maintaining the shape of the island.

Tampa Bay's connection to the Gulf of Mexico is narrowed by Egmont Key. A 30 m deep passage north of the island is used as the entrance to the main shipping channel. Overall Tampa Bay is characterized by shallow waters with an average depth of 3.5 m. Exceptions are, beside the mentioned outlet, the harbors and dredged shipping lanes to the ports of St. Petersburg, Tampa, and Port Manatee (Goodwin and Michaelis, 1984). The tidal regime is mixed semi-diurnal.

Like the entire Gulf region, the Tampa Bay area is threatened by tropical storms originating from the Atlantic Ocean or Caribbean Sea. In the past decades some severe tropical cyclones occurred in the eastern Gulf of Mexico but none directly

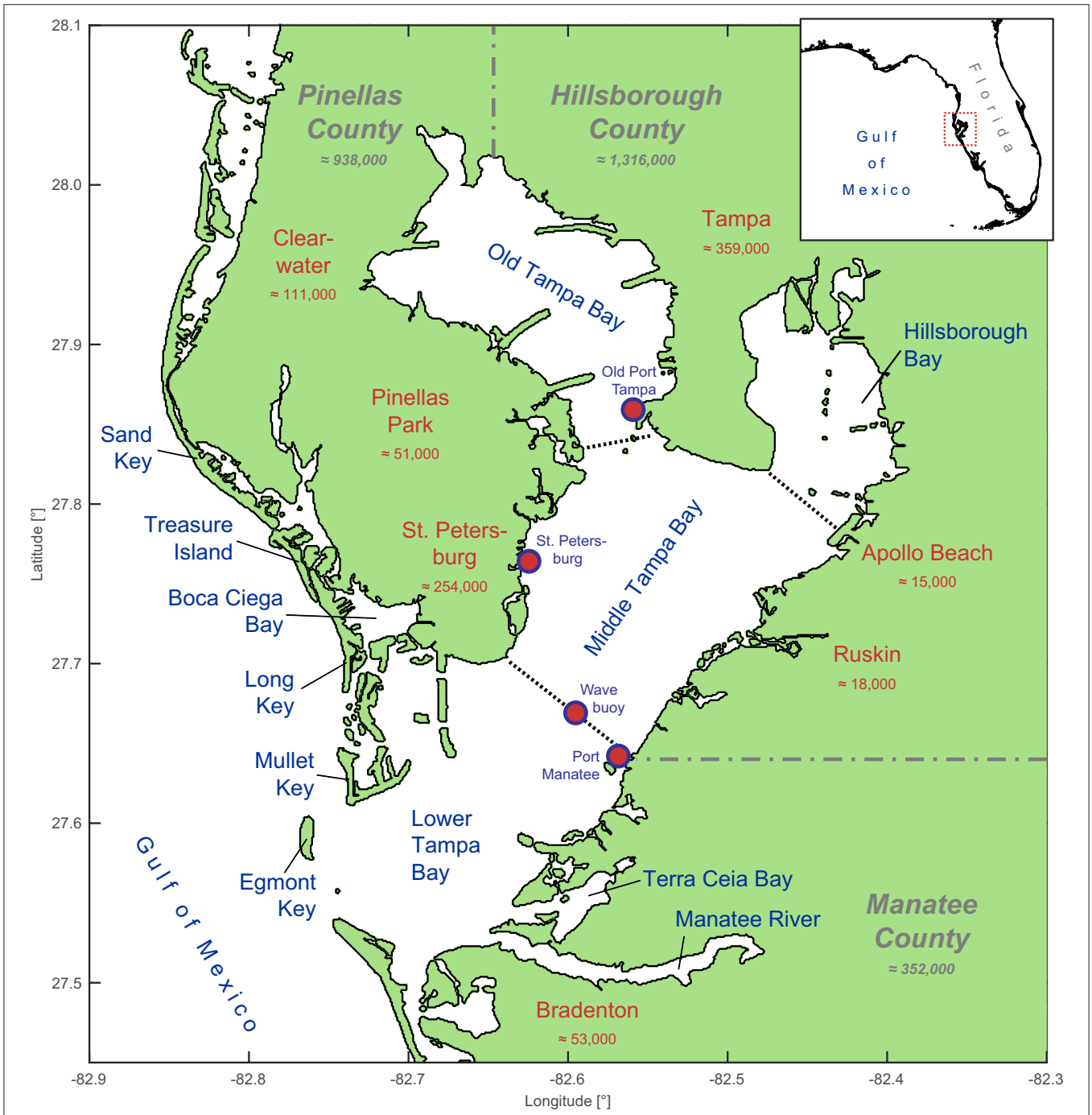

FIGURE 1 | Map of Tampa Bay with its bay sections as well as adjacent cities and counties with 2014 population estimates (from United States Census Bureau); tide and wave gauges are marked as red dots.

passed through or close by the Tampa Bay area. The last direct hit of a major hurricane dates back to 1921 (Doehring et al., 1994; Weisberg and Zheng, 2006). Furthermore, strong winter storms and nor'easters also have the potential to cause storm surges in Tampa Bay with water levels comparable to those induced by tropical events (e.g., event in January 1987).

3. METHODS

This study aims at investigating the effect of a barrier island loss on extreme still water levels and wind waves in the Tampa Bay. Therefore, we calibrate and validate a hydrodynamic numerical model, use control and scenario runs, and an extreme value analysis to quantify changes in extreme events. Results are

presented as changes in return levels (of still water and significant wave height) due to the modeled barrier island loss.

3.1. Numerical Model Setup

The investigations are based on numerical model experiments requiring hydrodynamic forces at the open boundaries as input. The tides and waves within Tampa Bay are primarily from the Gulf of Mexico but there is no continuous water level hindcast available covering the period under investigation or the investigated area. This is why we set up a two-dimensional, depth-averaged, barotropic tide surge model covering the entire Gulf of Mexico, hereafter referred to as Gulf Model. This large-scale model is intended to provide water level boundary conditions for a higher resolution model of the main study area covering the entire Tampa Bay, hereafter referred to as Bay Model. This setup enables us to fully describe all relevant hydrodynamic processes adjacent to and within Tampa Bay. Detailed information and references for all data sets described below are summarized in **Table 1**. The numerical model setup is briefly summed up in **Table 2**.

The models are set up and computed using the open source modeling suite Delft3D, provided by Deltares (Lesser et al., 2004). The spatial discretization is achieved using curvilinear grids, shown in **Figure 2**. In the Gulf Model, cell sizes between 30 and 3 km are used. The grid resolution increases from west to east in order to provide the most accurate results in front of Tampa Bay without spending too much computation time. In the Bay Model, cell sizes range from 400 to 150 m, depending on location and grid curvature. Both models are configured within a coastline provided by the Gulf of Mexico Coastal Ocean Observing System (GCOOS) with a spatially consistent resolution of 60 m.

As bathymetric input, the SRTM30 PLUS V6 data set based on the Shuttle Radar Topography Mission (SRTM) is used. It covers the entire Gulf of Mexico including Tampa Bay on a 1′ grid which is equivalent to a grid cell size of approximately 1.85 km at Gulf-latitudes. Furthermore, the Tampa Bay "Topobathy" bathymetric dataset with a resolution of approximately 30 m on an equidistant grid provided by the National Oceanic and Atmospheric Administration (NOAA) is used to increase the accuracy of spatial information in the main area of interest. To estimate the impact that a loss of Egmont Key would have on Tampa Bay the bathymetry of the Bay Model is altered around today's location of the barrier island. The assumed disappearance is modeled by lowering the bathymetry of Egmont Key. The present day bathymetry is shown in **Figure 3A**. The new bed level is interpolated between today's depth around the island. Complete erosion is the worst-case scenario but plausible since Egmont Key is a sand accumulation and not sitting on a bed rock raise (Stott and Davis, 2003). The result from removing Egmont Key from the bathymetry is a wide, slightly inclined channel connecting the Gulf of Mexico with Tampa Bay (**Figure 3B**).

The open boundaries of the Gulf Model are in the Florida Strait between the Everglades National Park (FL, USA) and Varadero (Cuba), and in the Yucatán Channel between Sandino (Cuba) and Cancún (Mexico) (see **Figure 2A**). Both boundaries are driven by astronomical tidal levels. As input we use phases

TABLE 1 | Data sets and data sources used for the study.

Data set	Source	Description
COMPS wave data	Coastal Ocean Monitoring and Prediction System, provided by University of South Florida, College of Marine Science	Five month of wave data near Port Manatee
ERA-20C	European Centre for Medium-Range Weather Forecasts (http://www.ecmwf.int/en/research/climate-reanalysis/era-20c)	Three-hourly wind and air pressure fields for the Gulf of Mexico and Tampa Bay
GSHHS Gulf of Mexico	Texas A&M University, Gulf of Mexico Coastal Ocean Observing System (http://gcoos.tamu.edu/products/topography/Shoreline.html)	Shoreline of the Gulf of Mexico including Tampa Bay
PSMSL time series	Natural Environment Research Council, Permanent Service for Mean Sea Level (http://www.psmsl.org)	Yearly mean sea level time series for St. Petersburg
SRTM30 PLUS V6	Texas A&M University, Gulf of Mexico Coastal Ocean Observing System (http://gcoos.tamu.edu/products/topography/SRTM30PLUS.html)	Bathymetry of the Gulf of Mexico including Tampa Bay
Tampa Bay Topobathy	National Oceanic and Atmospheric Administration, provided by University of South Florida, College of Marine Science	Topobathymetric data of the Tampa Bay area
TPXO 7.2	Oregon State University, College of Earth, Ocean, and Atmospheric Sciences (http://volkov.oce.orst.edu/tides/global.html)	Harmonic constituents for tidal boundaries of the Gulf Model
USACE WIS	United States Army Corps of Engineers (http://wis.usace.army.mil)	Wind and wave hindcast data for the Gulf of Mexico
Water level time series	National Oceanic and Atmospheric Administration, provided by University of Hawaii Sea Level Center (http://uhslc.soest.hawaii.edu/data/download/rq)	Hourly water level time series for several locations at the coast of the Gulf of Mexico and Tampa Bay

TABLE 2 | Overview: set up numerical models, used input, boundary conditions (BC), and conducted computations.

Model	Meteo.	Open BC	Bathymetry	Time	Computations
Gulf Model	ERA-20C	TPXO 7.2	SRTM	1948–2010	Water level BC for Bay Model (water levels)
Bay Model (water levels)	ERA-20C	Gulf Model water levels	Topobathy & SRTM	1948–2010	Hourly water level time series at coastal grid points
Bay Model (wave heights)	USACE WIS	WIS wave parameters	Topobathy & SRTM	1980–2013	Extreme wave events at the entire grid

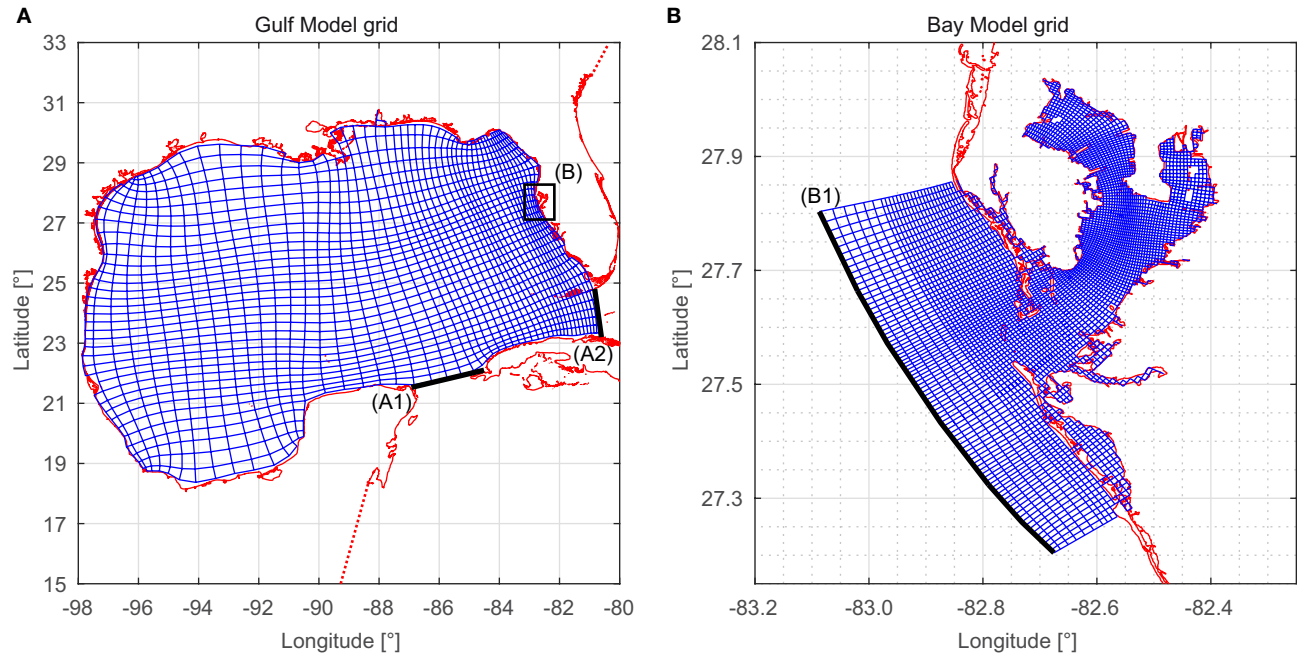

FIGURE 2 | Curvilinear grids (blue) and shoreline (red) used for the Gulf Model (A) and for the Bay Model (B). For clearness, the grids in this figure appear with a coarser resolution than used for the simulation. The Gulf Model grid **(A)** is actually two times higher resolved, the Bay Model grid **(B)** three times higher. Black lines indicate the model boundaries of the Gulf Model in the Yucatán Channel (A1), in the Florida Strait (A2) as well as the boundary toward the Gulf of Mexico in the Bay Model (B1).

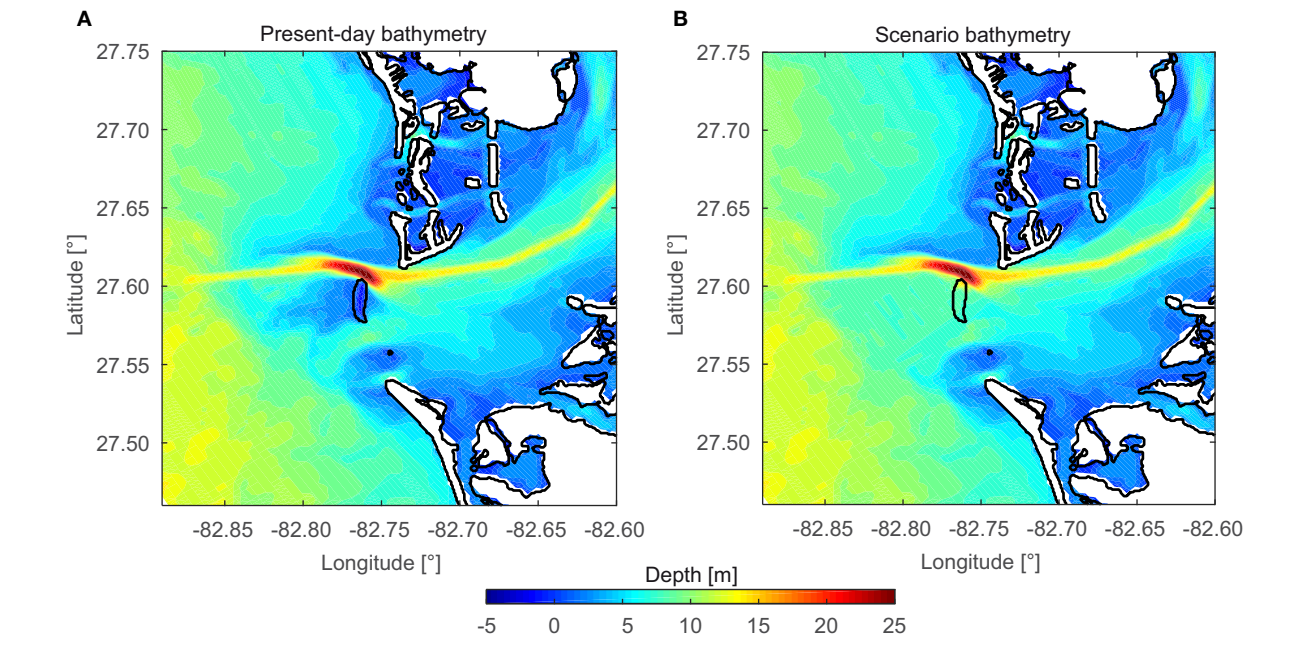

FIGURE 3 | Unchanged control run bathymetry (A) and scenario bathymetry without Egmont Key (B).

and amplitudes of the main tidal constituents obtained from the global ocean tides model TPXO 7.2, provided by the College of Earth, Ocean, and Atmospheric Sciences at the Oregon State University. The Gulf Model is used to model the transition of the tidal components from the Atlantic into the Gulf of Mexico ocean basin. TPXO 7.2 contains 13 harmonic constituents (M2,

S2, N2, K2, K1, O1, P1, Q1, MF, MM, M4, MS4, MN4) for each point on a global grid with a 0.25° resolution. Tidal boundary conditions are derived by interpolating the nearest TPXO 7.2 gridded information on the models open boundaries. Within both models, tidal forces acting on the entire body of water are also considered including eleven semi-diurnal, diurnal, and long period tidal constituents (M2, S2, N2, K2, K1, O1, P1, Q1, MF, MM, SSA). The water levels from the Gulf Model force the Bay Model at the boundary indicated in **Figure 2B**.

The models are additionally forced with spatially varying meteorological data (i.e., wind and atmospheric pressure fields) covering the entire model domain. We use data from the ERA-20C reanalysis provided by the European Centre for Medium-Range Weather Forecasts (ECMWF). The reanalysis data covers the period 1900–2010 and has a temporal resolution of 3 h and a spatial resolution of 1° on a global grid. For water level computations the years 1948–2010 have been chosen since observations at the gauge St. Petersburg (providing the longest record for the region) are limited to this period. The used reanalysis data are limited to the description of meteorological conditions at a supra-regional level due to the temporal and spatial resolution. Local and regional anomalies, e.g., in the proximity of tropical cyclones, are represented with little detail, but at the same time no major hurricane passed directly over Tampa Bay within the model time frame making the application of ERA-20C wind and pressure fields more suitable for the investigation area. The availability of the wave input from the USACE Wave Information Studies (WIS) project is restricted to the period 1980–2013. Therefore, wind data are also taken from this data base for the wave simulation as well as wave height, direction, amplitude, and spread information. The WIS hindcast is available at grid points along the entire U.S. coast. Three points close to the mouth of Tampa Bay are used to force the Bay Model. Between these points the boundary conditions are interpolated linearly.

In the Bay Model, mean sea level (MSL) changes are also considered using the Permanent Service for Mean Sea Level (PSMSL) time series of St. Petersburg obtained from the British Natural Environment Research Council. Since the computations for each year of the simulation time are run separately to handle the large output data, the MSL is adjusted according to the annual change in the PSMSL time series.

3.2. Numerical Model Calibration and Validation

The overall aim of this paper is to assess changes in both extreme still water levels along the coastline and wave heights as consequence of the loss of Egmont Key. Simplified, simulations of water level and wave height variables are conducted separately enabling to evaluate the contribution of each component to a total water level independently. Tides and wind set up off the mouth of Tampa Bay are extracted from three grid points of the Gulf Model. Bay Model water level time series are extracted at about 800 grid points along the coastline in intervals of approximately 1 km and wave parameters are extracted from the entire grid since we expect major changes off the coastline, with potential effects on navigation during extreme events.

In hydrological modeling various efficiency criteria are used to describe the goodness of model calibration (Krause et al., 2005). Here we use the coefficient of determination (r^2) and the root mean squared error (RMSE). The coefficient of determination is defined as the squared value of the coefficient of correlation (Krause et al., 2005). The coefficient is calculated with observed (x_o) and simulated (x_s) water level time series, each with k corresponding values:

$$r^2 = \left[\frac{\sum_{i=1}^{k} (x_{si} - \bar{x}_s)(x_{oi} - \bar{x}_o)}{\sqrt{\sum_{i=1}^{k} (x_{oi} - \bar{x}_o)^2} \sqrt{\sum_{i=1}^{k} (x_{si} - \bar{x}_s)^2}} \right]^2 \quad (1)$$

A value of $r^2 = 1$ [-] denotes that both time series, observed and simulated, are identical. A value of $r^2 = 0$ [-] indicates that there is no correlation (Krause et al., 2005). The root mean squared error is calculated using the time series mentioned above with k values:

$$\mathrm{RMSE} = \sqrt{\frac{1}{k} \sum_{i=1}^{k} (x_{oi} - x_{si})^2} \quad (2)$$

The calibration of the models is done stepwise by adjusting the modeled water levels to recorded data at specific locations using the introduced efficiency criteria. The Gulf Model is calibrated first since this model provides the input of the Bay Model. The tide gauge of Clearwater, located approximately 45 km north of the mouth of Tampa Bay is used as reference for the calibration. Furthermore, three tide gauges at the U.S. Gulf coast are used to check the model performance including Apalachicola (Florida), Grand Isle (Louisiana), and Galveston Pier (Texas). All time series are obtained from the NOAA tide gauge data base.

The Gulf Model's parameters and boundary conditions are adjusted in two steps. In the first step a calibration is done by varying the Manning's roughness coefficients (n values). In the second step the harmonic constituents at the open boundaries of the Gulf Model are adjusted. At the beginning of the calibration exercise, the n values are very uncertain. The Gulf Model is calibrated by iteratively computing the model with varying Manning's n values in the range $0.02 \leq n \leq 0.04$ s/m$^{1/3}$ and comparing the computation results (using the test statistics described above) with the tidal predictions from the tide gauge Clearwater provided by NOAA. The calibration consists of multiple simulations over 1 month periods, in each case with a spin-up time of 2 weeks.

A Manning's roughness of $n = 0.035$ s/m$^{1/3}$ shows the smallest achievable error with unmodified harmonic constituents. Using this roughness significantly increases the accuracy of the model results but deviations of up to 10 cm are still present. To reduce the remaining differences between simulated and observed data the second calibration step is conducted. The input of amplitudes and phases for each boundary point at the Florida Strait and the Yucatán Channel is corrected by adjusting the input amplitudes and phases in order to minimize the error. Similar to the roughness calibration this is done iteratively.

Tidal predictions provided by NOAA are separated into their underlying constituents and individually compared to the corresponding constituents from the simulation results. The tidal analyses are performed with the T_TIDE tool by Pawlowicz et al. (2002). The component breakdown shows which tidal components have the largest influence on the errors. Errors are reduced by the adjustment of corresponding constituents (amplitudes and phases) at the boundaries. A linear dependence between constituents at the gauge site and at the boundaries is assumed for the iterative calibration process. This approach disregards that tidal oscillations at the gauge are a combination of tidal oscillations at the boundaries and tides originating from the Gulf of Mexico but yet leads to a fast convergence of observed and simulated constituents. After calibration the correction factors for the amplitude f_{amp} are in a range of $0.9 \leq f_{amp} \leq 1.4$ [-] and the addends for the phase f_{pha} in the range of $-60° \leq f_{pha} \leq 15°$ respectively. All correction factors and addends are presented in **Table 3**.

After calibration the comparison of full time series at gauge Clearwater results in a coefficient of determination of $r^2 = 0.96$ [-], showing that the model reliably reproduces observed water levels at this site, close to the mouth of Tampa Bay. The RMSE calculation shows errors of 5.1 cm for tidal high water levels and 5.7 cm for tidal low water levels. The observed mean tidal range at gauge Clearwater is 58 cm. Overall the model tends to overestimate the minor high and low waters of the mixed semi-diurnal tide cycle, whereas higher high waters are computed more reliably enabling to simulate extremes properly.

The Bay Model is forced with the Gulf Model water levels and also calibrated. The calibration of the Bay Model is limited to the adjustment of the Manning's roughness coefficient n. The input boundary condition has been computed by the calibrated Gulf Model and therefore should not be changed. Tampa Bay is monitored by several hydrological and meteorological measuring stations. Three of four active tide gauges within the estuary are unaffected by inflowing rivers and are used here for calibration, validation, and bias correction of the Bay Model. These stations are located at the port of St. Petersburg in the west of the bay, at Port Manatee in the south-east, and at Old Port Tampa in the north (see **Figure 1**). The official tide predictions for these gauges, provided by NOAA, are used as reference. The roughness calibration is conducted in the same way the Gulf Model has been calibrated. The iterative test considers values in the range of $0.02 \leq n \leq 0.036$ s/m$^{1/3}$. The best fit of simulated time series against observed time series, regarding RMSE and coefficient of determination, is achieved by using a Manning's roughness coefficient of $n = 0.022$ s/m$^{1/3}$. The smaller coefficient, compared to the Gulf Model's roughness, is attributable to the significantly higher resolution of the seafloor topography in the Bay. The rather coarse resolution of the Gulf bathymetry only allows a smoothed seafloor in the Gulf Model. Geometric features smaller than the bathymetry resolution have to be added artificially by increasing the roughness. The Bay Model's bathymetry already depicts most of these features. Therefore, the calibration leads to a smaller roughness coefficient. The efficiency criteria after Krause et al. (2005) described above are also calculated for the Bay Model calibration results. RMSE and r^2 differ from gauge to gauge within Tampa Bay. Regarding tidal high water levels the RMSE does not exceed 4 cm; the coefficient of determination spans $0.92 \leq r^2 \leq 0.95$ [-]. The comparison of full time series also shows an RMSE of approximately 4 cm and $r^2 \geq 0.95$ [-] for all three gauges.

The wave simulations are conducted using the calibrated water level model of the Bay. A validation run (focusing on the significant wave height) has been performed indicating that the model reproduces large wave events well for the simulated period using one available buoy data set of the Coastal Ocean Monitoring and Prediction System (COMPS). The buoy data was recorded at the border of Middle and Lower Tampa Bay (see **Figure 1**) covering 5 months (April through August 2012) with hourly wave parameters. Several events from this period have been simulated. The model tends to underestimate small wave heights. With focus on the three largest events a comparison between simulated and observed significant wave heights gives an RMSE of 12 cm and $r^2 = 0.83$ [-] where absolute values range from 86 to 91 cm. The largest event shows a deviation of 3 cm in significant wave height. Based on the USACE WIS data only events larger than the tested wave heights are simulated for the comparison between control and scenario run. Therefore, the model can be used for the simulations disregarding the deficiencies in estimating small wave heights. Regarding wave periods the model shows peak periods of approximately 3 s for the highest events at the location of the wave buoy. Due to large gaps in the wave period record a validation of this parameter could not be conducted.

3.3. Statistical model setup

3.3.1. Pre-processing

The numerical model is used to simulate multi-decadal water level and wind wave time series which are required for reliable extreme value analysis (EVA) of both variables. Extreme water levels are assessed at individual grid points along the entire Tampa Bay coastline. The wave simulations are used to estimate return wave heights for the entire grid. In both cases, simulations are performed using (A) a current state bathymetry (control run) and (B) a bathymetry where Egmont Key is removed (scenario run; see **Figure 3**). Both water level simulations consider the same time period of 63 years (1948–2010) and the same hydrodynamic and meteorological boundary conditions. The wave simulations are only conducted for extreme events, since a continuous

TABLE 3 | Factors f_{amp} and addends f_{pha} used to correct the Gulf Model input amplitudes and phases.

TPXO constituents	M2	S2	N2	K2	K1	O1	P1	Q1	MF	MM	M4	MS4	MN4
f_{amp}	1.4	1.0	1.0	0.9	1.05	1.05	1.1	1.0	1.0	1.0	1.0	1.0	1.0
f_{pha}	−15	15	0	0	0	0	0	0	0	0	−60	0	0

simulation of several consecutive years would be computationally much more expensive without adding new relevant information on extremes. Furthermore, the available wave data used as input at the open boundaries is event based (not continuous) and covers the period 1980–2013. The results from the different model runs are used for the EVA.

A fundamental assumption for EVA is that time series are stationary and that events are independent (Coles, 2001; Arns et al., 2013). This is why linear detrending has been applied to all time series (simulated and observed) in order to account for the first criterion. To comply with the second criterion a declustering procedure has been applied to the data ensuring that the sample consists of independent events. The declustering procedure is conducted as follows: at first all peaks within the simulated and detrended hourly water level time series are selected and matched with the corresponding peaks in the detrended observation time series. Clusters are detected by identifying peaks that occurred within 6 h. A simple comparison of two neighboring peaks that fulfill the 6-h-criterion allows discarding the smaller one since this peak is assumed to be not independent of the larger one. Finally, only the largest peak of a tidal high water period is used for the EVA (Zachary et al., 1998).

3.3.2. Bias Correction

The model calibration successfully reduced the error between simulated and observed water levels but significant differences still remained due to model imperfections. This bias can be visualized by plotting observed water levels against the corresponding simulated water levels, as shown in **Figure 4A**. The regression (red) indicates the best linear fit against the scatter diagram in a least squares sense using the orthogonal distance of each point from the fit (orthogonal fit). The bias is the difference between the regression and the angle bisector (black, target regression), expressed as location and slope deviation. A parametric bias correction of the extreme water levels, as described in the following, has been conducted prior to the EVA in order to eliminate these deviations.

In case of a parametric bias correction the difference function between orthogonal fit and angle bisector is used to adjust the simulated values. A non-parametric or empirical bias correction adjusts each simulation value based on the absolute deviation from the observed value (Mudelsee et al., 2010). The empirical approach results in exactly corrected simulation values while the parametric correction shifts the values according to the correction function but does not eliminate the spreading. An advantage of the parametric approach, however, is that the correction function describes a systematic model error, e.g., a model tending to generally simulate too high or too low water levels as shown in **Figure 4A**. Therefore, the function determined for a site can be used to correct the same systematic error at all other locations even if the absolute values differ between the sites. Furthermore, the parametric approach can be used to adjust scenario data where systematic model errors are assumed to be consistent throughout all model runs.

In this study, the correction is applied to the largest Tampa Bay model results using observational data from St. Petersburg tide gauge covering the entire simulation period (1948–2010). We focus on the 99.8th percentile of threshold exceedances since only these data are used in the following EVA. Observations from the tide gauges at Port Manatee and Old Port Tampa are additionally used between 1999 and 2010. Simulated peaks in Tampa Bay are adjusted according to the differences between target data and orthogonal regression fit at each individual tide gauge. Results of this correction are shown exemplarily in **Figure 4B**. Following

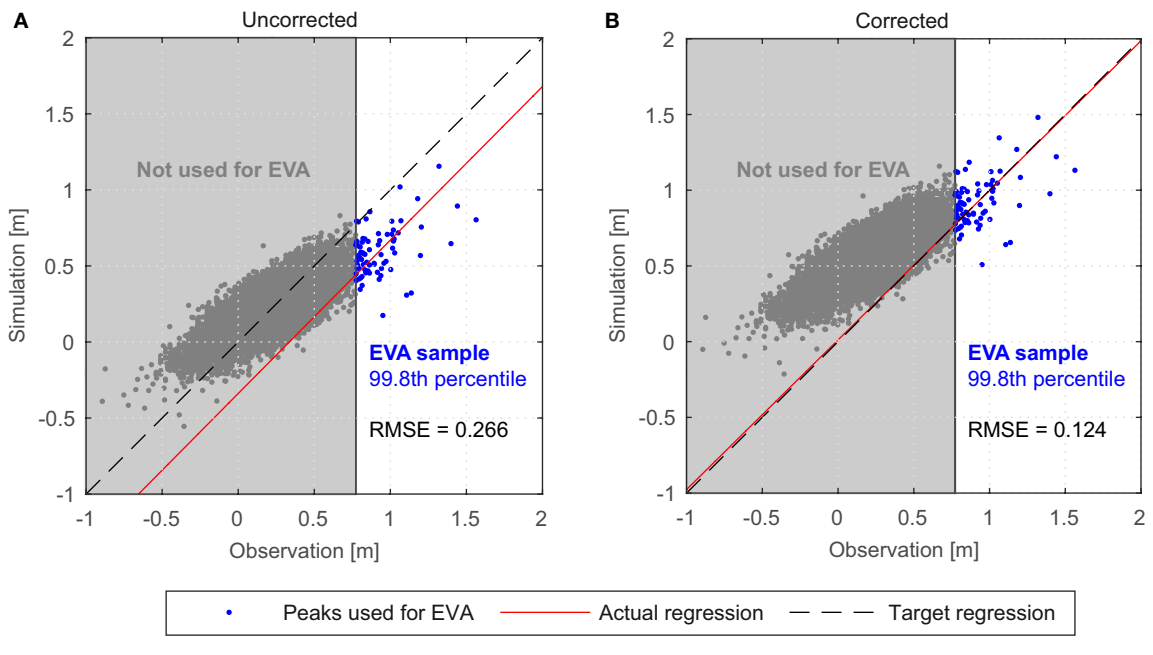

FIGURE 4 | Uncorrected water levels (A) and corrected water levels after the parametric bias correction (B).

this procedure, data sets at all ungauged grid points of the Bay Model are corrected using the correction factors estimated at the gauged sites. For the years 1999–2010, in which factors for all three gauges are available, an inverse distance weighting approach is used to interpolate the factors to ungauged locations along the entire Tampa Bay coastline. It is assumed that the bias mainly originates from model limitations, like the discretization of wind data or seafloor topography approximations. Therefore, the correction is also applied to the scenario run. Corrected scenario water levels are obtained by calculating the differences between uncorrected control and scenario run water levels and then adding them to the corrected control run water levels.

The wave control run has not been adjusted as the available wave data required as input for developing a bias correction only covers 5 months with only one extreme event on record. Thus, a reliable correction cannot be derived. In our numerical sensitivity study, we focus on changes in wave heights as consequence of a potential loss of Egmont Key. The overall aim of this assessment is to estimate relative changes in wave heights. Based on our validation we assume that the model is able to capture these changes reliably.

3.3.3. Return Level Assessment

The return level assessment is conducted with both control run and scenario run water level data at individual grid points along the Tampa Bay coastline and with the corresponding wave simulations with the intention to estimate the impact of the disappearing of Egmont Key. Two extreme value analysis approaches are tested prior to the final assessment, i.e., the Bock Maxima (BM) method using the Generalized Extreme Value Distribution (GEV) and the Peak-over-threshold (POT) method with the Generalized Pareto Distribution (GPD).

The BM sampling approach considers the r largest events within a specific time frame, e.g., the three highest water levels of each year. This yields a sample of events which allows an estimation of return water levels by fitting the GEV to the sample. The GEV unifies three fundamental extreme value distributions namely the Gumbel, Fréchet, and Weibull and is defined in Equation 3 with the location parameter $-\infty < \mu < \infty$, the scale parameter $\sigma > 0$, the shape parameter $-\infty < \xi < \infty$, and the BM values z (Coles, 2001):

$$GEV = \exp\left\{-\left[1+\xi\left(\frac{z-\mu}{\sigma}\right)\right]^{-1/\xi}\right\} \tag{3}$$

The POT sampling approach considers all values that exceed a defined threshold u, e.g., the 0.5% largest values of a record also referred to as the 99.5th percentile. The GPD is related to this sampling method and also couples various extreme value distributions. It is defined as

$$GPD = 1-\left(1+\frac{\xi\cdot z}{\sigma+\xi\cdot(u-\mu)}\right)^{-1/\xi} \tag{4}$$

where μ, σ, ξ, and z denote parameters and values as above (Coles, 2001).

The BM method has been tested with $r \in \{1, 2, 3\}$ values per year and the POT approach with the 99.6, 99.7, and 99.8th percentile of threshold exceedances. Both methods have been applied to subsets of observed and simulated time series of the tide gauge of St. Petersburg. The 100-year return water level has been estimated with both methods and different extreme value model setups using varying time series lengths. The results are shown in **Figure 5** indicating that the POT approach with the 99.8th percentile yields the most robust results. Compared to other approaches, these estimates are among the smallest variances of all return levels considering different time series lengths (within a range of 10 cm). The gray shade in **Figure 5** denotes time series lengths that are too short for a reliable 100-year return level estimation. Therefore, the results within and close to the shade vary heavily. With longer time series (especially starting between 1948 and 1964) the results are more robust, even when very large events (often associated with tropical cyclones) are excluded from the return level assessment (e.g., Hurricane Easy, 1950). Furthermore, this method with the 99.8th percentile subset only causes small differences of approximately 10 cm between return levels estimated from the observed and from the simulated time series using the longest period available. Other EVA model setups yield differences of up to 40 cm. Remaining small deviations are assumed to be negligible as we aim at investigating the changes induced by the vanishing of Egmont Key and deviations are caused by consistent model deficiencies that affect control and scenario runs alike.

Frequencies and magnitudes of extreme wave heights are estimated using the same approach as described above. However, in that case we use the 99.5th percentile of all events of the USACE WIS database. These selected extreme events are simulated individually using the control run and scenario bathymetries.

4. RESULTS

4.1. Return Water Levels

Extreme water levels are assessed for different return periods including the 5-, 25-, 50-, 100-, and 200-year events. Thus, the return period estimation does not exceed 3 to 4 times the length of the underlying time series. The latter limit is recommended e.g., by Pugh (2004). The differences in return water levels are visualized in **Figures 6**, **7** for the 25- and 100-year events, respectively. The return water levels are only used for estimating the differences a loss of Egmont Key would cause.

A comparison of **Figures 6**, **7** indicates the overall development of the results. Changes in water levels with return periods shorter than 100 years appear to have a spatially different characteristic compared to those with return periods greater than or equal to 100 years. At shorter return periods, increases can be found along the entire Tampa Bay coastline with significant changes in Hillsborough Bay and Old Tampa Bay. For a return period of 25 years, increases between 3 and 5 cm are found. At the tidal reach of the Manatee River and the coastline of Lower Tampa Bay, close to the mouth of the estuary, increases are in the order of 2 to 3 cm. Middle Tampa Bay is not affected. Regarding return periods of 100 years or more, largest return water level increases are found along Hillsborough Bay. Water levels increase by up to 15 cm. There are also changes

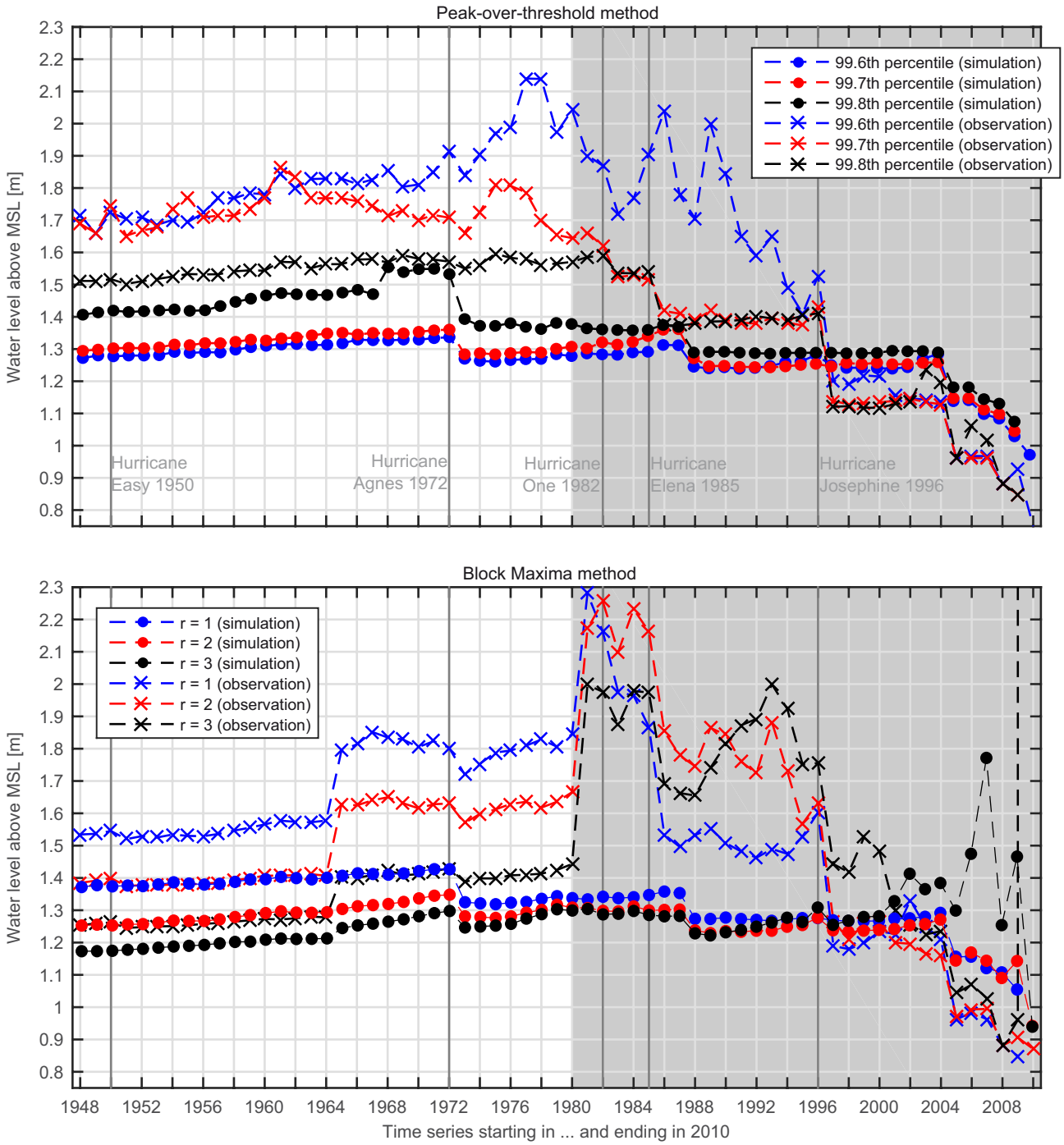

FIGURE 5 | Testing statistical approaches: 100-year return water level, estimated with different samples (colors) and with decreasing time series lengths (x-axis); the gray background denotes time series lengths which are too short for a reliable return level estimation (<30 years).

in Old Tampa Bay reaching 5 to 7 cm. The coastlines along the Manatee River and at Lower Tampa Bay would undergo changes in the 100-year event of only a few centimeters if Egmont Key disappeared. Parts of Middle Tampa Bay would even experience a small decrease. The development of extreme water levels in the Tampa Bay in case of a loss of Egmont Key is affirmed regarding the change in the 200-year return water levels (not shown). In Hillsborough Bay the return water levels would increase up to 30 cm whereas at the coast of Middle Tampa Bay they would decrease up to 20 cm.

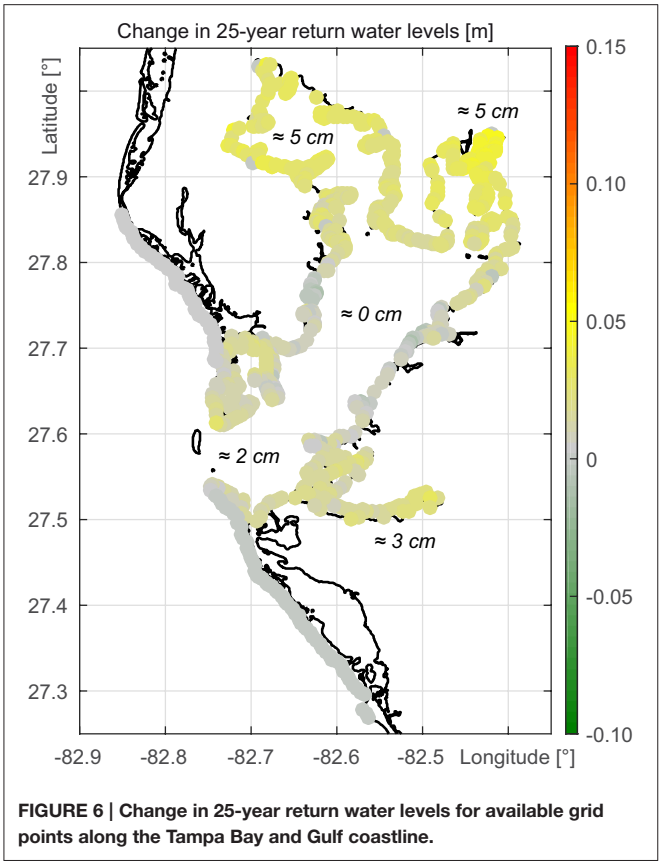

FIGURE 6 | Change in 25-year return water levels for available grid points along the Tampa Bay and Gulf coastline.

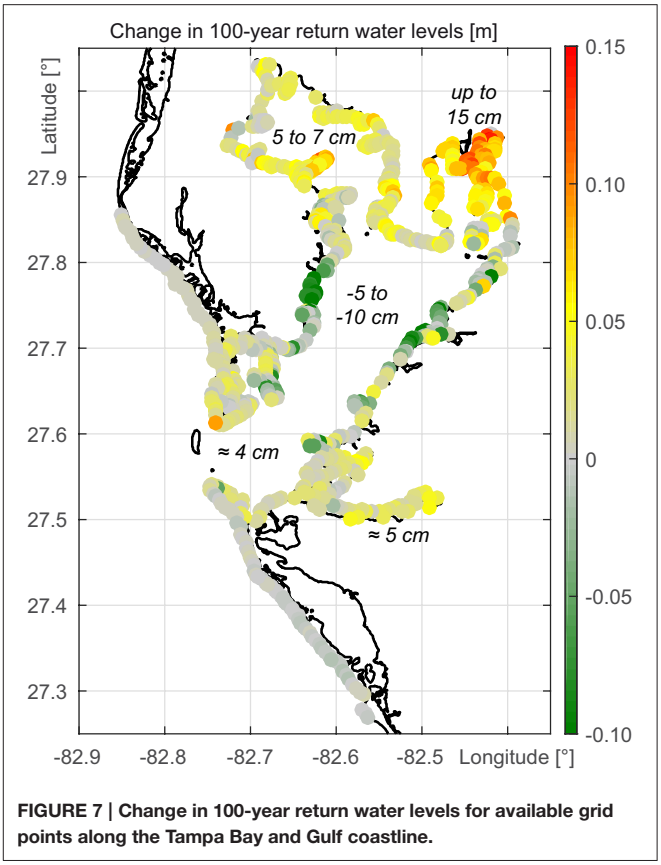

FIGURE 7 | Change in 100-year return water levels for available grid points along the Tampa Bay and Gulf coastline.

The return level assessment reveals that Egmont Key has a significant reducing influence on extreme water levels in the Tampa Bay. The northern parts of the estuary are protected by the barrier island and would be affected negatively by a loss of the barrier island. Even the smaller but more frequent storm surge events would increase along large parts of the Tampa Bay coastline.

In addition to the EVA results, differences in maximum water levels (scenario to control run) along the coast as well as relative increases have been calculated (**Figures 8A,B**). A loss of Egmont Key leads to water level increases of more than 4 cm in the entire Tampa Bay. Manatee River, Lower Tampa Bay, and northern Hillsborough Bay water levels increase up to 12 cm which is a change of up to 10%.

4.2. Return Wave Heights

Extreme wave heights are estimated at each grid point including areas of particular interest like shipping lanes and coastal zones. Overall the wave heights show strong increases around the location of today's Egmont Key in the Gulf of Mexico as well as in Lower Tampa Bay. The estimated wave heights for a return period of 25 years are shown in **Figure 9**. Entire Lower Tampa Bay would be affected with increases of mostly 0.4 to 1.0 m in areas without bathymetric changes. Close to today's location of Egmont Key, where the bathymetry has been changed, increases range from 1.3 to 1.7 m. In contrast, Middle Tampa Bay only shows increases of a few centimeters along the center line of the estuary and the northern parts of Tampa Bay are not affected at all.

Besides the EVA results, the maximum differences between the control and the scenario run and also the relative increases of wave heights have been calculated for each grid point (see **Figures 10A,B** respectively). Both plots confirm that changes in wave heights are only found in the Lower Tampa Bay area. Maximum differences between 1.5 and 2.0 m around the location of the barrier island could have a significant impact on the navigability since these increases are a doubling of the today's wave heights in this area. The eastern coast of Lower Tampa Bay would also see significant increases in wave heights (up to 300%). For the city Anna Maria, located on the barrier island south of Egmont Key, wave height increases of up to 13 cm are found.

Regarding the change in wave period increases are limited to the area described above. The loss of sheltering and the increased depth directly behind today's location of Egmont Key result in periods of 9 to 12 s in Lower Tampa Bay under scenario conditions where control runs show periods of 3 to 5 s. Wave directions are affected by the removal of Egmont Key as well, but only in close vicinity to the barrier island.

5. DISCUSSION AND CONCLUSIONS

The simulation of water levels and waves in the Tampa Bay with and without the barrier island Egmont Key shows that the island provides significant natural coastal protection. For extreme still

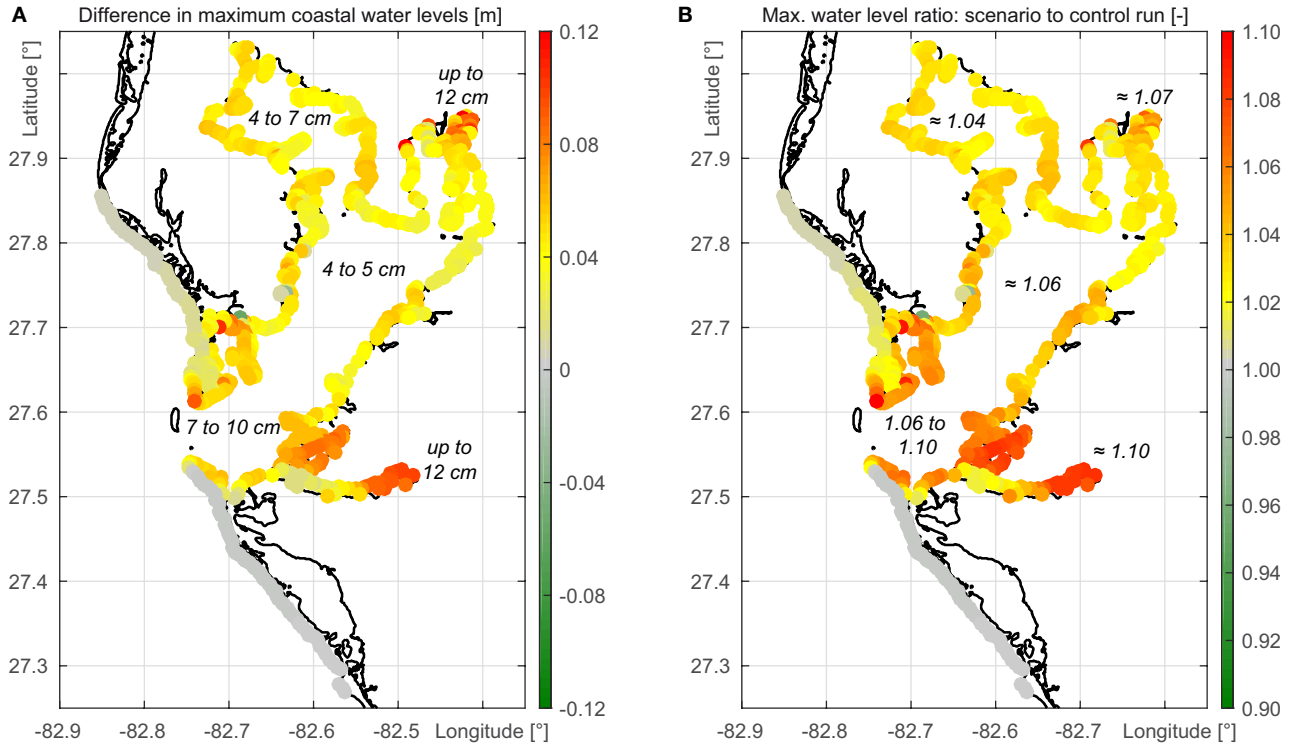

FIGURE 8 | Difference in maximum water levels along the coastline (A) and the difference expressed as ratio between scenario and control run simulation (B).

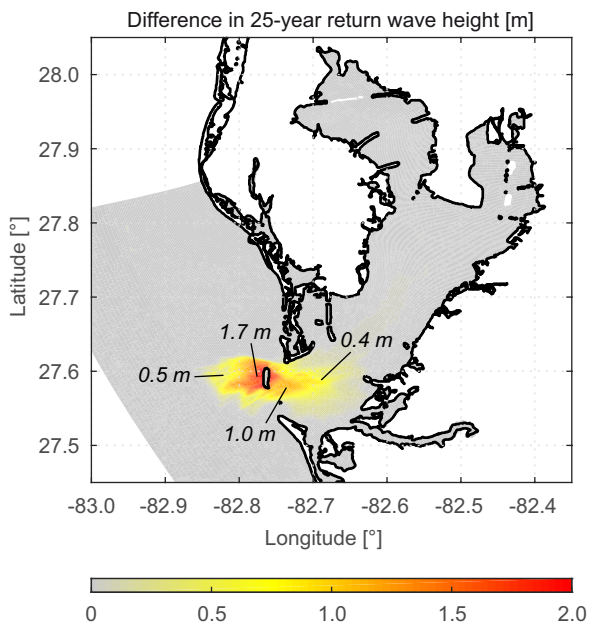

FIGURE 9 | Change in 25-year return wave height for all grid points.

water levels the removal of Egmont Key from the model's bathymetry yielded higher return water levels in the northern parts of the estuary. The absence of the barrier that blocks about a third of the mouth of Tampa Bay allows westerly winds to generate more wind set-up in the estuary. The northern bay sections as well as the Manatee River are affected most due to the very shallow waters and narrow connections to Middle Tampa Bay that only allow a limited near-ground back flow. The extreme water level increases in the northern bay sections are expected to be larger than a decimeter in case of a 100-year event which is a change of about 10%. The affected areas are densely populated and developed with residential, commercial, and industrial infrastructure close to the waterfront. Smaller events that occur more frequently (e.g., 25-year return period) are also expected to increase when Egmont Key disappears. From a coastal protection perspective, it is thus reasonable to put effort in the maintenance of Egmont Key since large parts of the adjacent mainland is low-lying and therefore already vulnerable to extreme water levels and waves. An increase in extreme events, adding up on the existing level, would increase the ecological and economical risk.

Middle Tampa Bay shows only small increases in 25-year return levels and even a decrease in the 100-year water level. This can primarily be attributed to a change of the shape parameter of the extreme value distribution. In this area, under scenario conditions, relative increases of smaller events are larger than those of the most extreme events. Therefore, the EVA leads to smaller return levels, especially for longer return periods. We speculate that the most extreme events do not increase as much as the smaller events due to an increased back flow since the

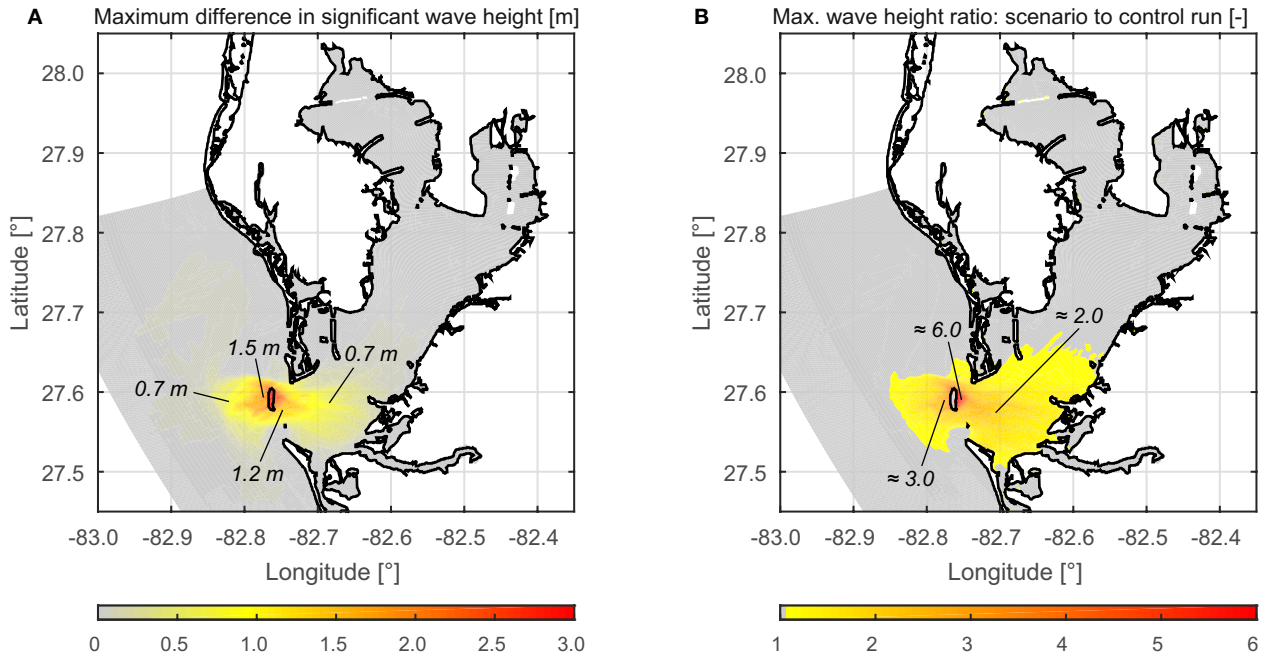

FIGURE 10 | Maximum difference in significant wave height considering all simulated events (A) and the difference expressed as ratio between scenario and control run simulation (B).

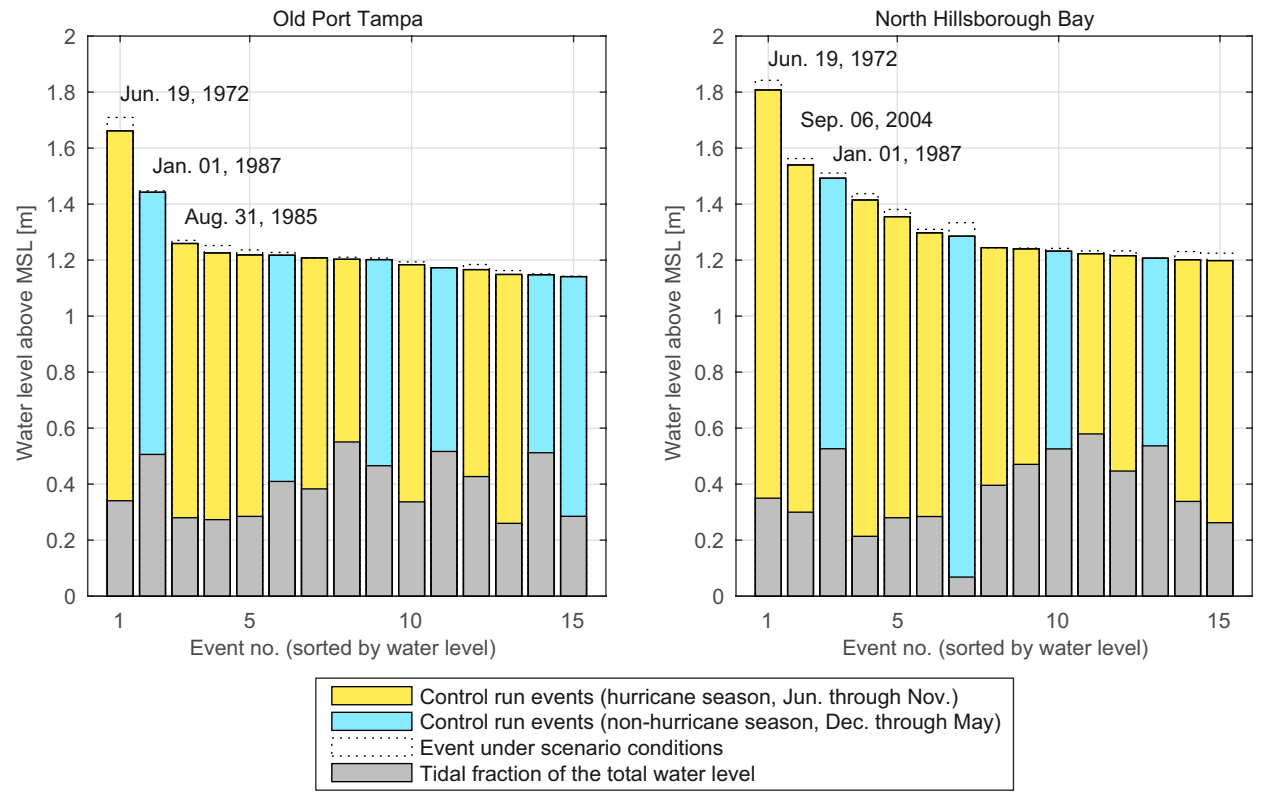

FIGURE 11 | Comparison of the 15 largest events (by total still water level under control run conditions) in northern Tampa Bay. Yellow bars indicate storm surges during the tropical season (June through November), blue bars indicate all other events (e.g., winter storms). The tidal contribution to the water level is depicted as gray overlay. The total water level under scenario conditions is shown as dotted bar edges.

removal of the barrier island also enlarges the outflow cross-section.

The wave height assessment shows that the potential loss of Egmont Key has a significant impact on the waves in Lower Tampa Bay but overall the influence occurs locally. The effect of Egmont Key is limited to an area which extends approximately 10 km into the Bay, measured from today's location of the island. Increasing wave heights in this area can be attributed to the missing barrier which today shelters Lower Tampa Bay directly, and to the increased depth around the location of Egmont Key. Areas in the northern Tampa Bay are protected by the shallow waters of the estuary, which would dissipate most wave energy in case that Egmont Key completely disappears. The very local change in wave directions is also attributable to the increased depth. With the loss of Egmont Key and the increase in water depth local shallow water effects like refraction and diffraction do not appear anymore. Waves from the Gulf of Mexico enter Tampa Bay unchanged until the depth limitation decreases wave heights significantly.

The EVA has been conducted without distinguishing between event types. Tampa Bay is located in an area where tropical cyclones occur during summer and fall months. Therefore, separate analyses of tropical and extra-tropical events would be a reasonable approach, as described e.g., by Haigh et al. (2014). Furthermore, this would be necessary in case that the study aims at estimating absolute heights for return periods. The simplified method used in this study is feasible since no major tropical cyclone directly hit Tampa Bay within the time period of interest. **Figure 11** shows that tropical and extra-tropical events in Tampa Bay led to similar total still water levels. Possible changes from other extreme events that occured beyond the period of observation are not considered in this particular study but could also have an effect on the shape of the underlying extreme value distribution. Additionally the return levels are only used for the A-B-comparison and therefore the chosen simplified method leads to suitable results.

Figure 11 also shows the tide-surge-ratio of the top events in Tampa Bay. Haigh et al. (2010) detected an underestimation for large return periods when using direct methods (i.e., conducting an EVA with the total water level signal instead of modeling and examining tide and surge components separately) in case that the tidal component is larger than twice the size of the non-tidal component. In this context, the large contribution of the surge component to the total still water levels in Tampa Bay confirms the applicability of the direct approach.

Regarding the analyzed processes, this study focuses on water levels and waves. Changes in estuarine circulations have been neglected but may also be significantly affected by a loss of Egmont Key. In particular, changes in the tidal prism, tidal currents, exchange circulation and flushing could occur. These changes are associated with alterations in the entire ecosystem and should be investigated in further studies.

Overall the complete removal of Egmont Key is a simplified approach and disregards other morphologic changes in the barrier island system which would probably occur simultaneously with an erosion of the island extending over several decades. Examples are coastline changes in Tampa Bay or at the Gulf coast near the mouth of the estuary, changes in depth due to sediment displacement, and the impact of sea level rise. Albeit using a worst-case scenario, the presented results show that Egmont Key significantly alters extreme events in Tampa Bay and that a detailed investigation of realistic scenarios is needed. Further studies could include the above-mentioned morphologic and hydrodynamic changes to improve the results. Furthermore, inundation of the low-lying islands and of the mainland during storm surges should be considered. Authorities and coastal managers could benefit from the results and use the findings to develop appropriate protection strategies for the Tampa Bay area.

AUTHOR CONTRIBUTIONS

AA, TW, and MU developed the concept. MU set up and ran the models, analyzed output data, and drafted the paper with the guidance of AA. SM provided fundamental model data. All authors revised and finalized the draft. ML and JJ supervised the research project and finally approved the paper.

ACKNOWLEDGMENTS

All analyses presented in this paper were part of the project *The effect of eroding barrier islands on coastal flood risk and estuarine health* (project ID 57052194), supported by the German Academic Exchange Service (DAAD) with funds of the German Federal Ministry of Education and Research (BMBF).

REFERENCES

Arns, A., Wahl, T., Haigh, I. D., Jensen, J., and Pattiaratchi, C. (2013). Estimating extreme water level probabilities: a comparison of the direct methods and recommendations for best practise. *Coast. Eng.* 81, 51–66. doi: 10.1016/j.coastaleng.2013.07.003

Coles, S. (2001). *An Introduction to Statistical Modeling of Extreme Values*. London: Springer.

Cromwell, J. E. (1973). "Barrier coast distribution: a world survey," in *Barrier Islands. Benchmark Papers in Geology*,Vol. 9, ed M. L. Schwartz, (Stroudsburg, PA: Douden, Hutchinson, and Ross), 407–408.

Doehring, F., Duedall, I. W., and Williams, J. M. (1994). *Florida Hurricanes and Tropical Storms: 1871-1993: An Historical Survey*, Vol. 71 of *Technical Paper*. Gainesville, FL: Florida Sea Grant College Program, University of Florida.

Goodwin, C. R., and Michaelis, D. M. (1984). *Appearance and Water Quality of Turbidity Plumes Produced by Dredging in Tampa Bay, Florida*, Vol. 2192 of *United States Geological Survey Water-Supply Paper*. Washington: G.P.O.

Haigh, I. D., MacPherson, L. R., Mason, M. S., Wijeratne, E. M. S., Pattiaratchi, C. B., Crompton, R. P., et al. (2014). Estimating present day extreme water level exceedance probabilities around the coastline of australia: tropical cyclone-induced storm surges. *Clim. Dyn.* 42, 139–157. doi: 10.1007/s00382-012-1653-0

Haigh, I. D., Nicholls, R., and Wells, N. (2010). A comparison of the main methods for estimating probabilities of extreme still water levels. *Coast. Eng.* 57, 838–849. doi: 10.1016/j.coastaleng.2010.04.002

Krause, P., Boyle, D. P., and Bäse, F. (2005). Comparison of different efficiency criteria for hydrological model assessment. *Adv. Geosci.* 5, 89–97. doi: 10.5194/adgeo-5-89-2005

Kunneke, J. T., and Palik, T. F. (1984). *Tampa Bay Environmental Atlas*, Vol. 85 (15) of *Biological Report / Fish and Wildlife Service*. Washington, DC: Fish and Wildlife Service, U.S. Dept. of the Interior.

Lesser, G. R., Roelvink, J. A., van Kester, J. A. T. M., and Stelling, G. S. (2004). Development and validation of a three-dimensional morphological model. *Coast. Eng.* 51, 883–915. doi: 10.1016/j.coastaleng.2004.07.014

List, J. H., and Hansen, M. E. (1992). "The value of barrier islands: 1. Mitigation of locally-generated wind-wave attack on the mainland," in *Open-File Report* (St. Petersburg, FL: United States Geological Survey), 92–722.

Mudelsee, M., Chirila, D., Deutschländer, T., Döring, C., Haerter, J., Hagemann, S., et al. (2010). Climate Model Bias Correction und die Deutsche Anpassungsstrategie. *DMG Mitteilungen* 03/2010, 2–7. doi: 10013/epic.37089

Oertel, G. F. (1985). The barrier island system. *Marine Geol.* 63, 1–18. doi: 10.1016/0025-3227(85)90077-5

Passeri, D. L., Hagen, S. C., Bilskie, M. V., and Medeiros, S. C. (2015a). On the significance of incorporating shoreline changes for evaluating coastal hydrodynamics under sea level rise scenarios. *Nat. Hazards* 75, 1599–1617. doi: 10.1007/s11069-014-1386-y

Passeri, D. L., Hagen, S. C., Medeiros, S. C., and Bilskie, M. V. (2015b). Impacts of historic morphology and sea level rise on tidal hydrodynamics in a microtidal estuary (Grand Bay, Mississippi). *Continent. Shelf Res.* 111, 150–158. doi: 10.1016/j.csr.2015.08.001

Pawlowicz, R., Beardsley, B., and Lentz, S. (2002). Classical tidal harmonic analysis including error estimates in MATLAB using T_TIDE. *Comput. Geosci.* 28, 929–937. doi: 10.1016/S0098-3004(02)00013-4

Pugh, D. (2004). *Changing Sea Levels: Effects of Tides, Weather and Climate*. Cambridge: Cambridge University Press.

Stone, G. W., and McBride, R. A. (1998). Louisiana barrier islands and their importance in wetland protection: forecasting shoreline change and subsequent response of wave climate. *J. Coast. Res.* 14, 900–915.

Stone, G. W., Zhang, X., and Sheremet, A. (2005). The role of Barrier Islands, muddy shelf and reefs in mitigating the wave field along coastal Louisiana. *J. Coast. Res.* 44, 40–55. Available online at: http://www.jstor.org/stable/25737048

Stott, J. K., and Davis, R. A. (2003). Geologic development and morphodynamics of Egmont Key, Florida. *Marine Geol.* 200, 61–76. doi: 10.1016/S0025-3227(03)00177-4

Stutz, M. L., and Pilkey, O. H. (2001). A review of global barrier island distribution. *J. Coast. Res.* 34, 15–22. Available online at: http://www.jstor.org/stable/25736270

Weisberg, R. H., and Zheng, L. (2006). Hurricane storm surge simulations for Tampa Bay. *Estuar. Coast* 29, 899–913. doi: 10.1007/BF02798649

Zachary, S., Feld, G., Ward, G., and Wolfram, J. (1998). Multivariate extrapolation in the offshore environment. *Appl. Ocean Res.* 20, 273–295. doi: 10.1016/S0141-1187(98)00027-3

Conflict of Interest Statement: The authors declare that the research was conducted in the absence of any commercial or financial relationships that could be construed as a potential conflict of interest.

frontiers in Marine Science

ORIGINAL RESEARCH
published: 19 April 2016
doi: 10.3389/fmars.2016.00049

Uncertainties in Sandy Shorelines Evolution under the Bruun Rule Assumption

Gonéri Le Cozannet[1,2], Carlos Oliveros[1], Bruno Castelle[3], Manuel Garcin[1], Déborah Idier[1], Rodrigo Pedreros[1] and Jeremy Rohmer[1]*

[1] Coastal Risks and Climate Change Unit, Risk and Prevention Department, BRGM (French Geological Survey), Orléans, France, [2] Laboratoire de Géographie Physique, Meudon, France, [3] Université de Bordeaux, CNRS, UMR EPOC, Pessac, France

In the current practice of sandy shoreline change assessments, the local sedimentary budget is evaluated using the sediment balance equation, that is, by summing the contributions of longshore and cross-shore processes. The contribution of future sea-level rise induced by climate change is usually obtained using the Bruun rule, which assumes that the shoreline retreat is equal to the change of sea-level divided by the slope of the upper shoreface. However, it remains unsure that this approach is appropriate to account for the impacts of future sea-level rise. This is due to the lack of relevant observations to validate the Bruun rule under the expected sea-level rise rates. To address this issue, this article estimates the coastal settings and period of time under which the use of the Bruun rule could be (in)validated, in the case of wave-exposed gently-sloping sandy beaches. Using the sedimentary budgets of Stive (2004) and probabilistic sea-level rise scenarios based on IPCC, we provide shoreline change projections that account for all uncertain hydrosedimentary processes affecting idealized low- and high-energy coasts. Hence, we incorporate uncertainties regarding the impacts of longshore processes, sea-level rise, storms, aeolian, and other cross-shore processes. We evaluate the relative importance of each source of uncertainties in the sediment balance equation using a global sensitivity analysis. For scenario RCP 6.0 and 8.5 and in the absence of coastal defenses, the model predicts a perceivable shift toward generalized beach erosion by the middle of the 21st century. In contrast, the model predictions are unlikely to differ from the current situation in case of scenario RCP 2.6. Finally, the contribution of sea-level rise and climate change scenarios to sandy shoreline change projections uncertainties increases with time during the 21st century. Our results have three primary implications for coastal settings similar to those provided described in Stive (2004) : first, the validation of the Bruun rule will not necessarily be possible under scenario RCP 2.6. Second, even if the Bruun rule is assumed valid, the uncertainties around average values are large. Finally, despite these uncertainties, the Bruun rule predicts rapid shoreline retreat of sandy coasts during the second half of the 21st century, if greenhouse gas concentration in the atmosphere are not drastically reduced (scenarios RCP 4.5, 6.0, and 8.5).

Keywords: sea-level, shoreline, erosion, Bruun, uncertainties

OPEN ACCESS

Edited by:
Sönke Dangendorf, University of Siegen, Germany

Reviewed by:
Athanasios Thomas Vafeidis, Christian-Albrechts-Universität zu Kiel, Germany
João Miguel Dias, University of Aveiro, Portugal

****Correspondence:***
Gonéri Le Cozannet
g.lecozannet@brgm.fr

Specialty section:
This article was submitted to Coastal Ocean Processes, a section of the journal Frontiers in Marine Science

Received: *08 December 2015*
Accepted: *30 March 2016*
Published: *19 April 2016*

Citation:
Le Cozannet G, Oliveros C, Castelle B, Garcin M, Idier D, Pedreros R and Rohmer J (2016) Uncertainties in Sandy Shorelines Evolution under the Bruun Rule Assumption. Front. Mar. Sci. 3:49. doi: 10.3389/fmars.2016.00049

1. INTRODUCTION

One of the most important challenge for coastal adaptation is the rise of sea-level caused by anthropogenic climate change (Slangen et al., 2014b; Dangendorf et al., 2015). At present, there are already evidences that extreme water levels are becoming higher and more frequent (Marcos et al., 2009; Menéndez and Woodworth, 2010; Woodworth et al., 2011; Woodworth and Menéndez, 2015). At longer timescales, contributions from polar ice-sheets largely exceeding one meter are now recognized possible (Golledge et al., 2015; Hansen et al., 2015; Winkelmann et al., 2015). Meanwhile, increased rates of shoreline retreat — and particularly of sandy beaches — are expected to take place (Nicholls and Cazenave, 2010).

A common approach to address sub- to multi-decadal shoreline variability on wave-exposed sandy coast with infinite sand availability is to use the sediment balance equation, which can be written as follows (e.g., Cowell et al., 2003b; Stive, 2004; Yates et al., 2011; Aagaard and Sørensen, 2013; Anderson et al., 2015):

$$\Delta S = \Delta\xi / tan(\beta) + f_{cross-shore} + f_{longshore} \quad (1)$$

where:

- ΔS is the cross-shore shoreline displacement over a given period of time (typically a few decades),
- $\Delta\xi$ is the change of mean sea-level over the same period of time,
- $tan(\beta)$ is the average slope between the top of the beach and the closure depth, also refered to as active profile or upper shoreface,
- $f_{cross-shore}$ and $f_{longshore}$ are the contributions of other processes causing losses or gains of sediments in the active beach profile.

Equation (1) applies to the upper shoreface of the coastal tract (Cowell et al., 2003a). It assumes that the upper shoreface keeps the same profile and translates seaward or landward depending on the sediment budget. In particular, the term $\Delta\xi / tan(\beta)$ represents the impacts of sea-level change and corresponds to the Bruun rule (Bruun, 1962). While this term has been subject of debate over the last decades (Cooper and Pilkey, 2004; Ranasinghe and Stive, 2009; Woodroffe and Murray-Wallace, 2012; Passeri et al., 2015), there is no clear recommendation to leave it out. Recent results regarding the global impact of sea-level rise on shoreline change are largely based on the Bruun rule (Hinkel et al., 2013). Alternative approaches exist, but they are more complex and they require more data (Ranasinghe et al., 2012; Wainwright et al., 2015). Finally, even if the concepts of the Bruun rule are abandoned, the formula $\Delta S_{sea-level-rise} = \Delta\xi / tan(\beta)$ will remain. Indeed, other conceptual models have been developed and finally came up with the same formula (Davidson-Arnott, 2005). In this paper, we leave aside the key question of the relevance of Equation (1) as a modeling tool to evaluate future shoreline change. Instead, considering that the Bruun rule will continue to be widely used in the future, we evaluate the type of results and the uncertainties that can be expected by using it.

To evaluate the expected impacts of present day and future sea-level rise to sandy beaches erosion, Stive (2004) considered typical values for each term in Equation (1). These values are shown in **Tables 1**, **2**. They are based on observations in the Netherlands and Australia. Stive (2004) showed that under present sea-level rise rates, the contribution of the Bruun effect to sediment losses and shoreline changes is of the same order of magnitude or lower than other effects. Because of the lack of long-term [O (10 years)] coastal data, firmly (in)validating the Bruun rule is difficult (e.g., Leatherman et al., 2000a,b; Sallenger et al., 2000), with the impacts of present-day sea-level rise on shoreline changes being challenging to observe (Stive, 2004; Le Cozannet et al., 2014). However, Stive (2004) showed that for higher rates of sea-level rise, the Bruun effect will not be neglectable any more, as it will significantly impact shoreline change. Hence, Stive (2004) not only helps understanding the behavior of Equation (1) in most general cases, but also provides a general background consistent with present-day observations.

The periods of time by which one will be able to (in)validate the use of Bruun rule in Equation (1) is a critical unknown. The question is complex, because all terms in Equation (1) are uncertain, and because the duration by which sea-level-rise-induced erosion is decipherable likely depends on climate change scenario and regional coastal settings. Ultimately, this effect might never be observed in some regions, if the impacts of sea-level rise remain smaller than those of other sedimentary processes causing shoreline change. To investigate this question, we consider the case of idealized wave-exposed sandy beaches with infinite sand availability, and we adapt an approach developed to quantify uncertainties in future flooding occurrence (Le Cozannet et al., 2015): we first define realistic probability density function for each uncertain parameter in Equation (1), using values from Stive (2004) and the IPCC (Church et al., 2013) (Section 2). In Section 3, we propagate these uncertainties through Equation (1) to provide shoreline change projections for different idealized coastal settings and climate change scenarios. Using a global sensitivity analysis (Sobol', 2001; Saltelli et al., 2008), we evaluate the contribution of each uncertain parameter to the variance of future shoreline changes. We use these results to assess where and when the Bruun effect should become observable. Finally, in Section 4, we discuss the results with respect to previous work and question the representativeness of the idealized sandy shorelines considered.

TABLE 1 | Order of magnitude for cross-shore sedimentary processes contributing to shoreline change for typical coastal settings in the Netherlands and Australia and for a closure depth of 10 m (data from Stive, 2004).

Processes	Impacts to shoreline changes
Bruun effect	Retreat 500 to 1000 times greater than sea-level rise depending on the beach slope
Aeolian processes	Retreat of 0.5 to 1 m/year
Other cross-shore effects (e.g., wave-nonlinearity-driven onshore sediment transport)	Seaward shoreline advance of 1, 5 to 4 m/year
Storm waves	Retreat of up to about 20 m per storm

TABLE 2 | Order of magnitude for the annual longshore sedimentary processes contributions to shoreline changes for typical coastal settings in the Netherlands and Australia and for a closure depth of 10 m (data from Stive, 2004).

Coastal site settings	Absence of groins	Presence of groins
High energy beaches	about ±1 m/year	about ±10 m/year
Low energy beaches	about ±0.1 m/year	about ±1 m/year

2. MATERIALS AND METHODS

The method proceeds in three steps, which are detailed below.

2.1. Modeling Uncertainties of Input Parameters

We model the uncertainties of each input variable in Equation (1) using the probability density functions indicated in **Table 3** and the values shown in **Tables 1**, **2**. These tables consider different types of idealized coastal sites, based on the values provided by Stive (2004) for representative beaches in Australia and the Netherlands. For example, **Table 2** indicates that if a groin extending far offshore is implemented on a high energy beach, it will act as a trap for the large longshore sediment transport and will contribute to shoreline change at a rate soundly exceeding 10 m/year. These orders of magnitudes can have a large site to site variability. This point is further discussed in the Section 5. Overall, in the absence of any other contribution similar to that of Stive (2004), we rely on the large uncertainties related to the contribution of each driving process shown in **Tables 1**, **2** to argue that they are applicable for a large number of sandy coasts.

When defining probability distributions representing the uncertainties of input parameters (**Table 3**), the information available is often limited. As a general guidance, it should be avoided to introduce arbitrary constraints besides what is known already. In other words, the statistical entropy of the selected probability distribution functions should be maximized (Mishra, 2002). For example, a uniform probability density function should be selected when only boundaries are known. This case is met for most of the parameters given in **Table 3**, including the beach slopes and the contributions of cross-shore and longshore processes to the sedimentary budget. This choice reflects the fact that the data provided by Stive (2004) define boundary values for each uncertain input parameter (see **Table 1**).

More complex distribution can be elaborated when sufficient information is available. This is the case here for future sea-level rise. This source of uncertainties increases with time, and several components must be distinguished: (1) the selection of a climate change scenario, (2) the uncertainties of future sea-level rise for each climate change scenario, and (3) the regional variability of sea-level rise.

The IPCC provides likely range and median values for four climate change scenarios (RCP 2.6, 4.5, 6.0, and 8.5), corresponding to different trajectories of greenhouse gas emissions. To select one of these sets of value, we use a uniform discrete probability distribution, that is, a random application with a probability of 1/4 to select each climate change scenario. This choice assumes that we do not know what will be future greenhouse gas emissions.

Even if the true climate change scenario was known, future sea-level rise would still remain uncertain, in particular because of insufficient knowledge on future ice-sheets melting and the Earth energy imbalance (Church et al., 2013; Kopp et al., 2014; von Schuckmann et al., 2016). Modeling results combined with expert judgements have suggested that this source of uncertainties can be adequately modeled by a skewed distribution with a finite support (Ben Abdallah et al., 2014; Jevrejeva et al., 2014). As in our previous article (Le Cozannet et al., 2015), we use a Beta distribution to represent this source of uncertainties. While many scientists estimate that the actual rates sea-level rise over the 21st century could exceed those anticipated by the IPCC (Horton et al., 2014), we strongly rely on their likely range and median values to elaborate our sea-level rise scenarios (Church et al., 2013). The upper bound of the distribution is a critical unknown, due to uncertainties in the dynamics of polar ice-sheets melting, which is currently accelerating (Rignot et al., 2011). Referring to recent modeling results of the Antarctic ice-sheet instability (Ritz et al., 2015), we use a conservative estimate of 1.5 m for the upper bound of sea-level rise by 2100. To our knowledge, there is presently no evidence that the low-probability and high impact event of an ice-sheet instability can be avoided, even for the climate change scenario RCP 2.6. Therefore, we use the same upper bound of 1.5m by 2100 for all climate change scenarii. This results in probabilistic sea-level rise scenarios as indicated in **Figure 1**.

Due to spatially non-uniform warming of the ocean and the response of the Earth to ice-sheets melting, sea-level rise will display regional variability (Slangen et al., 2014a; Carson et al., 2016). This introduces an additional source of uncertainties. We assume that it includes a large part of natural randomness, which we evaluate using Church et al. (2013) and Carson et al. (2016). These references suggest that in addition to the boundaries of the distribution, its most likely value is known. Hence, the principle of maximum entropy leads to the choice of a triangular distribution (Mishra, 2002).

Extreme events are generated here assuming their occurrence follows a Poisson distribution. While this assumption is commonly used (Ranasinghe et al., 2012; Wainwright et al., 2015), it is challenged by some storm sequences, such as the winter 2013–2014 events in western Europe (Masselink et al., 2016). Moreover, as we use a Poisson distribution with fixed parameters, only the interannual variability of storms is captured, and the natural randomness is assumed unaffected by climate change (Plant et al., 2014). This hypothesis could be justified, as it is still difficult to assess where and to which extent climate change will affect extreme winds and waves (Planton et al., 2008; Mori et al., 2010; Hemer et al., 2013). However, we consider here that the return periods of storms are uncertain as well. The range of values considered for this uncertain input parameter is sufficiently large to exceed any plausible change of storminess due to climate change and any other limitation related to the Poisson assumption (see **Table 1**). Finally, we assume that the shoreline retreats after each extreme event ranges from 0 to 20 m. The first value can correspond to a storm occurring at

TABLE 3 | Modeling of the different sources of uncertainties.

Variable of interest	Modeling	Values, references
Climate change scenario	Uniform discrete distribution	RCP 2.6, 4.5, 6.0, and 8.5 scenarios
Global sea-level rise	Beta distribution	Same as in Le Cozannet et al. (2015), considering 1.5 m as a upper bound for sea-level rise by 2100
Regional deviation to the global mean	Triangular distribution	Growing contribution from 0 to up to ±0.2 m by 2060 and beyond
Beach slopes	Uniform distribution	Same as in Stive (2004); see **Table 1**
Aeolian processes	Uniform distribution	Same as in Stive (2004); see **Table 1**
Other cross-shore effects	Uniform distribution	Same as in Stive (2004); see **Table 1**
Longshore processes	Uniform distribution	Same as in Stive (2004); see **Table 2**
Exposure to marine forcing	Uniform discrete distribution	Low or high energy beaches
Human impacts	Uniform discrete distribution	Presence or absence of groins
Extreme events occurence	Poisson law	See text
Shoreline retreat after a storm	Uniform distribution	Between 0 and 20 m
Return period of extreme events	Uniform distribution	Between 10 and 1000 year

Note that human impacts refer here to the presence of groins, which are coastal engineering structures acting as a trap for the longshore sediment transport to locally accrete beaches.

low tide. Field surveys shows that the second value can result from a collision regime after exceptional storms, and can even be exceeded in case of overwash or breaching, which are not considered in this study. **Figure 2** shows examples of shoreline retreats observed in western France after the storm Xynthia in February 2010 (Pedreros et al., 2010; Garcin et al., 2011). The return period of water levels for this storm is estimated to be approximately 200 year in the harbor of La Rochelle (Bulteau et al., 2015). Such return periods are consistent with our working hypothesis, and we note that shoreline retreat ranged from a few meters to 20 m, except where breach occurred. Similar values can be found in many other studies (e.g., Forbes et al., 2004; Mendoza and Jiménez, 2006; Roelvink et al., 2009; Loureiro et al., 2014).

As a summary, our approach relies on two major assumptions: (1) sea-level rise scenarios are based on IPCC; (2) we consider sites with gently sloping upper shorefaces, i.e., which are the most impacted by the Bruun effect. Other assumptions can be mentioned: some input parameters here are assumed independent, although they are not in practice. For example, for the same sediment size, beach slopes are expected to be steeper for low-energy beaches (Wright and Short, 1984). However, given the range of uncertainties provided in **Table 3**, such limitations can be left aside in a first attempt to propagate uncertainties through Equation (1).

2.2. Propagation of Uncertainties Through the Sediment Balance Equation

The second step of the approach consists in propagating these uncertainties through Equation (1).

The computational approach starts with defining auxiliary variables with uniform values in the interval [0,1]. Then we apply inverse cumulative distribution functions to these auxiliary variables, in order to generate distributions with the desired shapes (e.g., Beta distribution for sea-level rise). This computational approach ensures the independence of the different input parameters considered in **Table 3**, so that the Sobol' parameters (see next section) can be computed using a classical procedure. To reduce the computation time, we use a quasi-Monte-Carlo approach, where we assign values following a quasi-random Sobol' sequence (Sobol', 1967) to the auxiliary variables with values in [0,1]. We empirically determine the number of computations required to converge, by comparing purely random against quasi-random simulations in a test case corresponding to a situation of the end of the 21st century.

This procedure allows to produce generic probabilistic shoreline change projections based on the coastal tract assumptions. Importantly, all input parameters vary simultaneously during these simulations. Therefore, the probability density function of future shoreline change projections integrates the complete variability.

2.3. Quantifying and Ranking the Sources of Uncertainties in Shoreline Change Projections

Once uncertainties of all input parameters have been propagated through Equation (1), we obtain a distribution for future shoreline change as a function of time. To understand what this distribution means, we analyse the contribution of each uncertain input parameter to the variance of the model outcome using a global sensitivity analysis (Sobol', 2001; Saltelli et al., 2008).

The principle of variance-based global sensitivity analysis is to decompose the variance of the model outcome Y into several terms that relate to each uncertain input parameter X_i. These terms are called the Sobol' indices. Two subsets of terms are of particular interest for the evaluation of uncertainties: the first-oder and total order Sobol' indices.

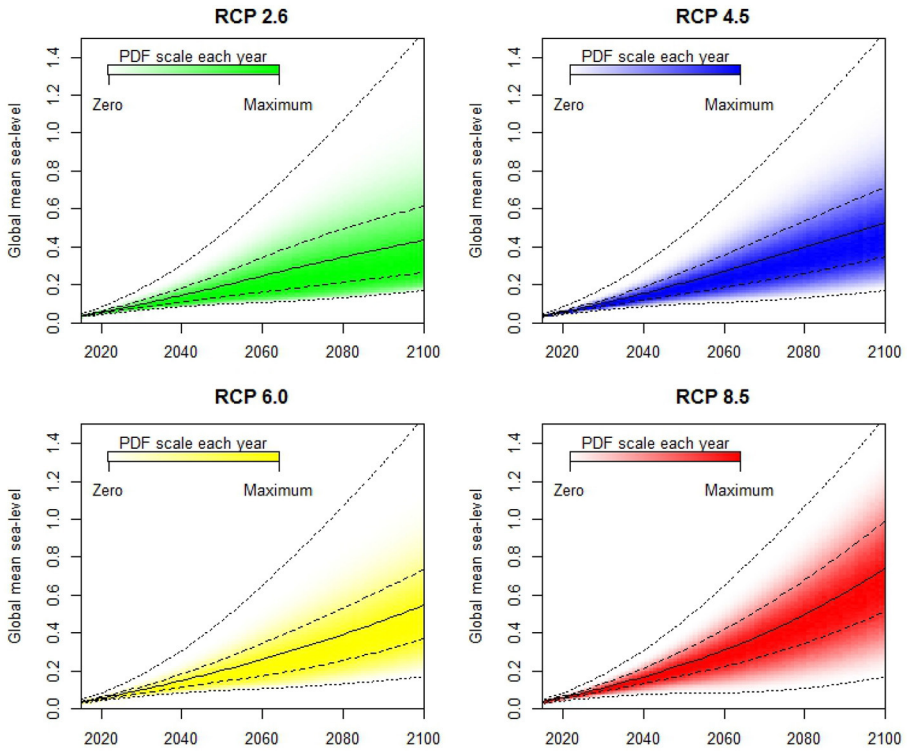

FIGURE 1 | Probabilistic global sea-level rise projections used in this study. For each date, the intensity of the color represents the probability density function (PDF), and the solid and dashed black lines represent the median and likely ranges. The dotted lines represent the minimum and maximum values.

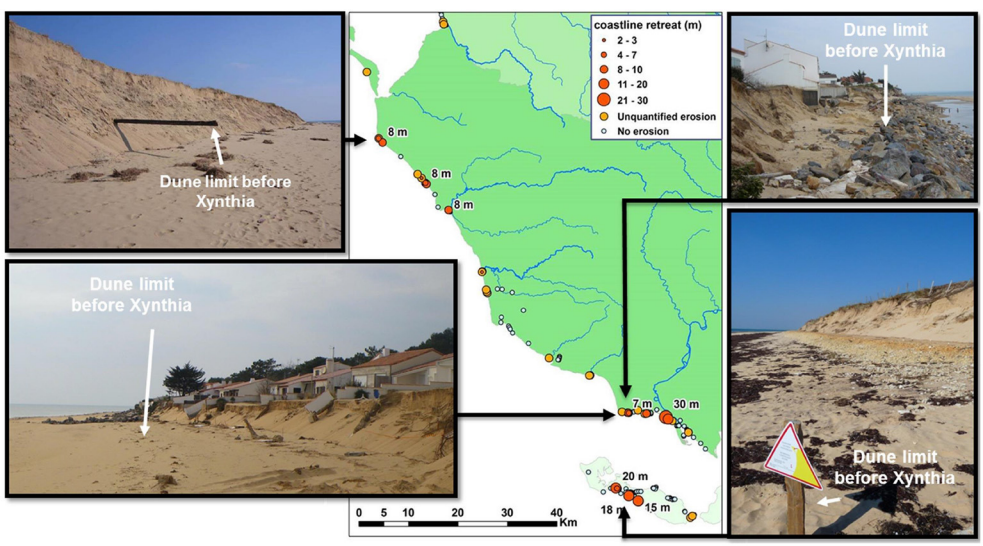

FIGURE 2 | Field evidences of sandy beaches retreats of up to 20 m after the storm Xynthia in 2010 (Data: Pedreros et al., 2010; Garcin et al., 2011). The photographs present examples of indicators that allow to quantify the dune retreats. After this storm, the only retreat exceeding 20 m corresponds to a breaching event. Note that the return period of water levels in the harbor of La Rochelle is estimated at about 200 year for Xynthia (Bulteau et al., 2015), and is therefore compatible with the random sample of storms considered in this study.

The first-order Sobol' indices (S_i) correspond to the contribution of a given input parameter alone to the variance of the model outcome:

$$S_i = \frac{Var(E(Y|X_i))}{Var(Y)} \quad (2)$$

They represent the expected proportion of the variance of the model outcome that would be removed if X_i was known.

The total order Sobol' index (S_{Ti}) represents the contribution of a given input parameter and all its interactions with other parameters to the variance of the model outcome. It is defined as:

$$S_{Ti} = 1 - \frac{Var(E(Y|X_{-i}))}{Var(Y)} \quad (3)$$

with X_{-i} the set of all X_j except X_i. This index is used to identify which parameters can be set to any possible value without much impact to the variance of Y.

All computations are done using R (R Core Team, 2014), using the same quasi Monte-Carlo approach as in the previous section. The values of the Sobol' indices are very similar for two consecutive years. Therefore, to reduce the computing time, we calculate these indices each 5 year and interpolate them over the 21st century. We use the codes developped by the Joint Research Center of the European Commission to compute the first and total order Sobol' indices (see Jansen, 1999; Saltelli et al., 2010, for the related algorithms and formulations).

3. RESULTS: WHEN WILL WE BE ABLE TO (IN)VALIDATE THE BRUUN RULE?

Figure 3 shows the probabilistic shoreline change projections $\Delta S(t)$ at year t, once uncertainties from the input parameters (**Table 3**) have been propagated through Equation (1). This represents $\Delta S(t)$ if no prior information is available, besides values in **Tables 1–3**. **Figures 4–6** show $\Delta S(t)$ for high and low energy beaches, with and without groins, and considering the different climate change scenarios separately.

As expected, a slight shift toward erosion is observed over the 21st century (**Figure 3**). However, in practice, the response is very different depending on the climate change scenario and the type of coast considered. In case of RCP 2.6, we can not identify any clear separation between present and future probability density functions of shoreline change rates. Conversely, for other climate change scenarios and for beaches without groins, the likely range of future shoreline change rates separates or nearly separates (case of RCP 4.5) from present days values (**Figures 4**, **5**). For example, in case of RCP 8.5 and coasts without groins, it is more than likely that observations will separate from their present values by the end of the 2060s for low-energy beaches, and in the early 2070s for high-energy beaches. Hence, using **Figures 4**, **5**, it becomes possible to identify times of emergence for a more than likely observable shift toward erosion of sandy beaches under the assumptions listed above. As a practical implication, it should be possible to assess the Bruun rule validity by the mid-21st century on beaches without groins with gently sloping shoreface, if efforts to reduce greenhouse gas concentrations in the atmosphere fail.

If groins are present on the beach, the longshore processes have a larger impact on the sedimentary budget (**Table 2**): on the one hand, large volumes of sediments can be trapped in protected areas, but on the other hand, these sediments are missing in adjacent locations. This does not prevent from observing a shift toward erosion in case of low-energy beaches and climate change scenarios RCP 4.5, 6.0, and 8.5 (**Figure 4**). In these cases, not enough sediments can be trapped to compensate the losses induced by sea-level rise. Conversely, if groins are built on high-energy beaches, the transport of sediment is severely altered. This results in high variability of shoreline advance and retreat, reaching ±10 m/year (see Stive, 2004, and **Table 2**), which may compensate the impacts of sea-level rise theoretically (**Figure 6**). However, it is widely acknowledged that groins are not a sustainable solution because they typically fix the erosion issue, but shift it nearby. Hence, it should not be concluded that groins are an efficient adaptation strategy for high-energy sandy coasts.

Drawing on these results, present day and future rates of shoreline change could remain indistinguishable if greenhouse gas emissions are reduced importantly (RCP 2.6 scenario). In addition, for coastal sites similar to those presented by Stive (2004), the times of emergence of a shift toward erosion induced

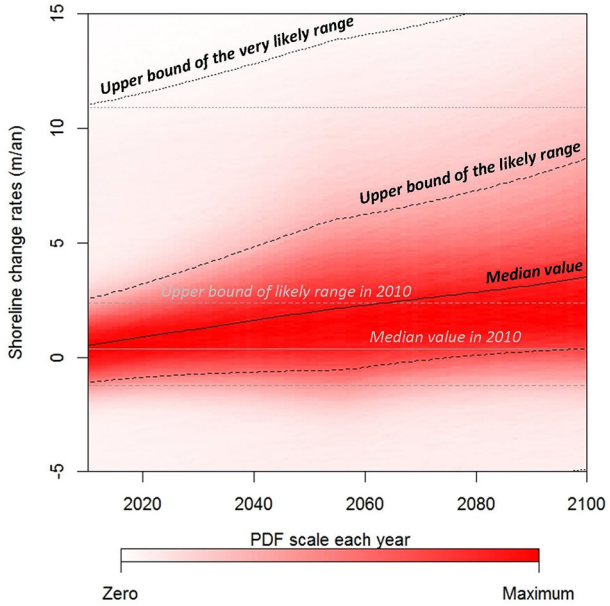

FIGURE 3 | Shoreline retreat rate projections for the 21st century, with no prior information regarding the type of sandy coast considered, the impacts of man-made infrastructures and the climate change scenario. Positive values corresponds to shoreline retreat. For each date, the intensity of the color represents the probability density function, and the solid, dashed and dotted black lines represent the median, likely, and very likely ranges. The gray lines represent present days rates: they are extended toward the whole 21st century for comparison. They represent a virtual case in which sea-level remains at its present level, whereas the black lines take into account uncertain sea-level rise scenarios of **Figure 1** using the Bruun rule.

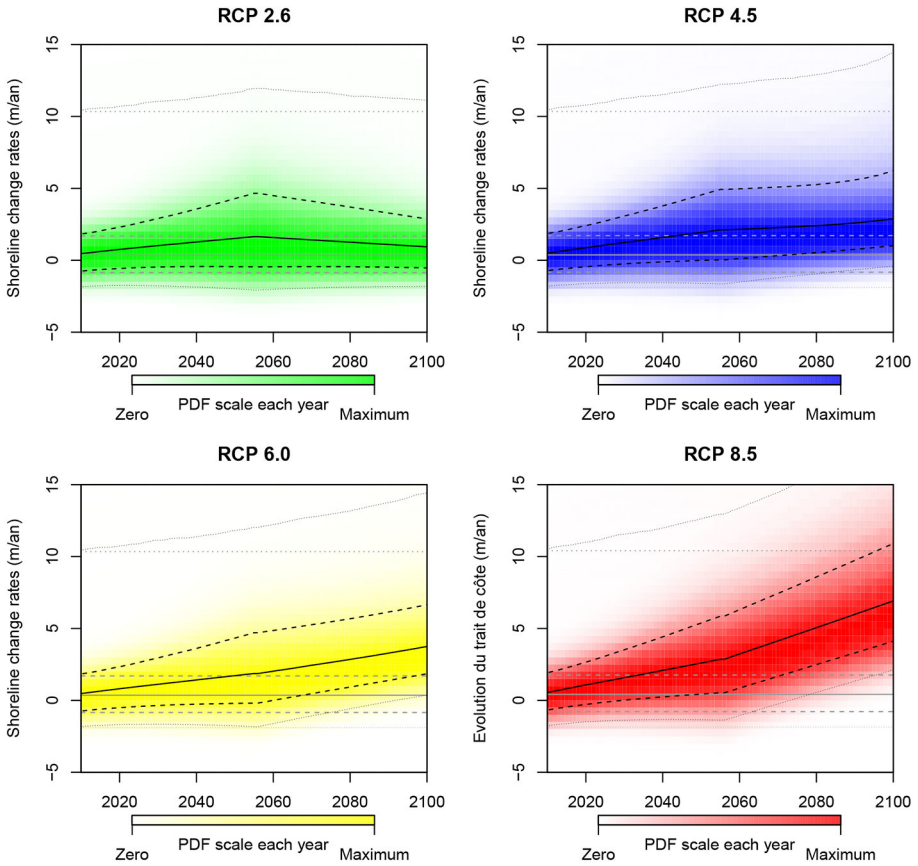

FIGURE 4 | Shoreline change rate projections for the 21st century for high-energy sandy coasts with no impacts of man-made infrastructures and for different IPCC climate change scenarios. The same results are obtained for low-energy beaches with groins (see values of the contributions of longshore processes to the sedimentary budget in **Table 2**). The meaning of gray and black lines is the same as in **Figure 3**.

by sea-level rise should occur during the second half of the 21st century, if sea-level rise follows the IPCC projections.

4. FURTHER INSIGHTS FROM THE GLOBAL SENSITIVITY ANALYSIS

Figure 3 reflects a situation where nothing is known regarding local coastal settings, future climate change and sea-level rise, except their probability density functions. To obtain this figure, 12 uncertain parameters were propagated in Equation (1), resulting in shoreline change projections with very large uncertainties. Indeed, the standard deviation of shoreline change projections rises from about 4 m/year now, to 4.5 m/year by 2050 and 5 m/year by 2100. These values are large, and the true values might be closer to 1 m/year (Bird, 1985). This suggests that the uncertainties in shoreline change projections can be reduced importantly with more knowledge regarding local coastal processes. Hence, the ensuing question is to understand what drives the variability of shoreline change projections in **Figure 3**. In this section, we investigate this issue using the results of the global sensitivity analysis. In other words, we separate the variance of $\Delta S(t)$ into several components corresponding to the contribution of the 12 uncertain input parameters, in order to gain further insight into the understanding of the upper shoreface sediment balance equation outcome under **Table 3** constraints.

Figures 7, **8** show the first and total order Sobol' indices obtained by the global sensitivity analysis. Using these figures, it becomes possible to classify input parameters according to their contribution to the variability of shoreline change rates: the first order Sobol' indices are used to rank input parameters, whereas the variability of parameters with total order Sobol' indices close to zero can be neglected without much impacts to the variability of the final results (Saltelli, 2004). In the following subsections, the uncertain input parameters of Equation (1) are classified according to their first and total order Sobol' indices, which reveal research priorities to better anticipate future shoreline change under the Bruun rule assumption.

4.1. Critical Unknowns for the Present Days

The random variables used to model the interannual variability of storms and the impacts of longshore sedimentary processes display large first and total order indices: **Figure 7** shows that

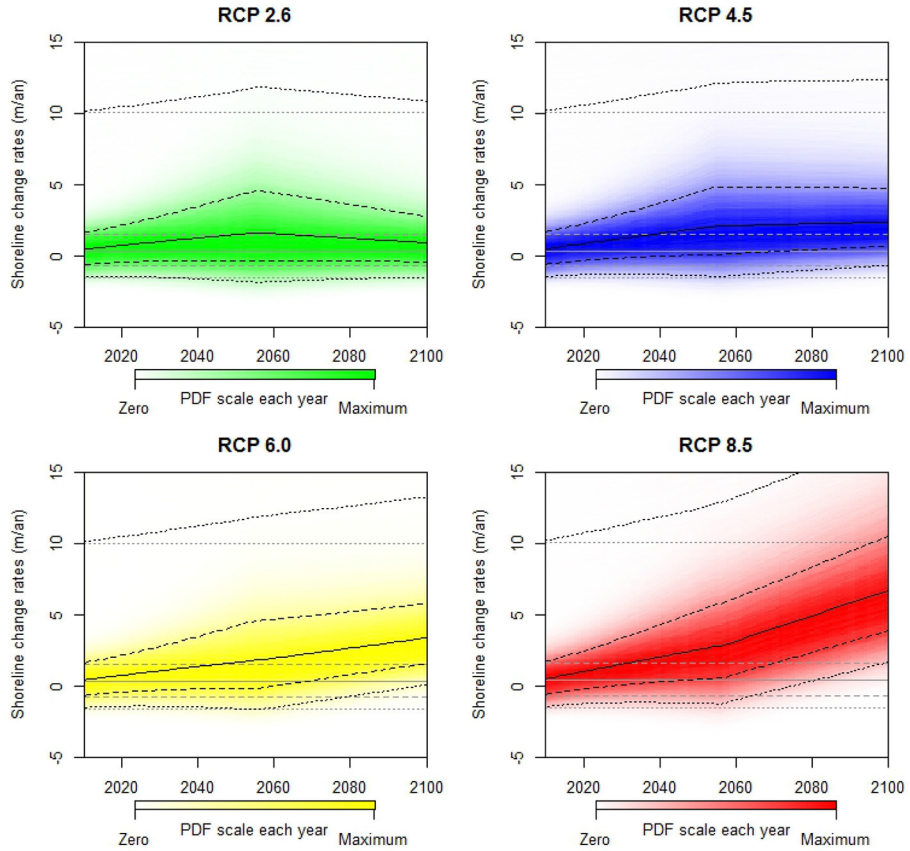

FIGURE 5 | Shoreline change rate projections for the 21st century for low-energy sandy coasts with no impacts of man-made infrastructures and for different IPCC climate change scenarios. The meaning of gray and black lines is the same as in **Figure 3**.

the value of the first order indices is of about 0.2. **Figure 7** indicates that the total order indices decreases from about 0.6–0.3 for longshore processes (0.4–0.3 for the interannual variability of storms). Therefore, these parameters account for a large part of the uncertainties in shoreline change projections. As a consequence, knowing more about these processes should be a priority for reducing the uncertainties resulting from the application of the sediment balance equation for sandy upper shorefaces with gentle slopes. For example, our results implies that a perfect knowledge of longshore processes would reduce the variance of shoreline change projections by a factor of nearly 20%. Many studies in the field of coastal research have studied these sources of uncertainties (Allen, 1981; Inman and Dolan, 1989; Slott et al., 2006; Roelvink et al., 2009; Castelle et al., 2015). However, it remains difficult to quantify precisely all the phenomena involved (see Section 5). Here, the results of the global sensitivity analysis just highlight that sandy shoreline change projections are more accurate if the impacts of storms and longshore sedimentary processes are taken into account. While integrating these processes at regional to global scales is a challenge, it is increasingly addressed in recent assessments of climate change impacts (e.g., Anderson et al., 2015).

4.2. Uncertain Parameters with Minor Impacts

At the opposite, the Sobol' first and total order indices representing the aeolian processes, other cross-shore effects (e.g., due to waves asymmetry) and the regional variability of sea-level rise are small. Therefore, the variability of these parameters can be neglected without any large impact to the variability of shoreline change projections. This result can seem surprising. In fact, several studies have highlighted the importance of cross-shore sedimentary processes in explaining seasonal and interannual shoreline changes (e.g., Yates et al., 2009; Splinter et al., 2014). To understand how our results can be related to these findings, we need to point out that Stive (2004) distinguishes the rapid erosive impacts of highly energetic events from the slow accretion due to the net onshore contributions from mild waves (**Table 1**).

The regional variability of sea-level rise also plays a minor role, whereas it can be much more important for strongly non-linear impact models. For example, urban coastal flooding generally becomes most damaging once a critical threshold has been exceeded (Hallegatte et al., 2013; Idier et al., 2013b; Miller et al., 2014). In this case, knowing more about the regional variability of sea-level rise would be one of the priorities for coastal managers

interested in understanding how risk will evolve over the coming decades (Le Cozannet et al., 2015).

According to **Table 1**, aeolian processes taking place on coastal beaches and dunes are expected to induce net sediment losses and shoreline retreat. However, these processes do not appear as a critical unknown either, in spite of their complexity (Arens, 1996; Hesp et al., 2013; Bauer et al., 2015). Again, our results highlight that when few data are available regarding other coastal processes, the values provided in **Table 1** are sufficiently narrow to anticipate the impacts of the slow recovery of beaches satisfactorily. Finally, as this result comes directly from the order of magnitude provided in **Tables 1**–**3**, it can be invalidated if new observations demonstrate that these processes have much larger impacts. This question of the representativeness of the values of **Tables 1**, **2** is addressed in details in the discussion section.

4.3. Interactions between Processes: Why is a Global Sensitivity Analysis Recommended?

Figures 7, **8** also reveal that for two random variables, the Sobol' first order indices are close to zero, whereas the total order indices are large. This is the case for example for the random variables indicating if groins are built on the beach, or if the beach is exposed to low- or high- energetic conditions: their total order Sobol' indices ranges from 0.1 to 0.2 (**Figure 8**). In this case, the principles of the global sensitivity analysis implies that the variability of the input parameters cannot be neglected, because it interacts with other random variables (Saltelli, 2004). In other words, this result indicates that, for instance, groins will have little impacts on shoreline change if longshore drift is weak.

Figure 7 shows that the sum of the first order Sobol' indices ranges from 0.45 to 0.6 depending on the period of time considered. This means that the interaction term is large. Hence, to a significant extent, the overall variability is driven by the combined variation of the parameters (joint effect). A very common way to perform a sensitivity analysis consists in evaluating the model response to each uncertain input factor independently. Our results show that despite the apparent simplicity of Equation (1), such an approach could fail to rank the impact of each uncertainty source: the total uncertainty on shoreline change can not be considered as the sum related to each uncertainty sources taken alone. On the contrary, the combined effect among them should be accounted for: here the interaction terms represent about the half of the total variance of shoreline change projections.

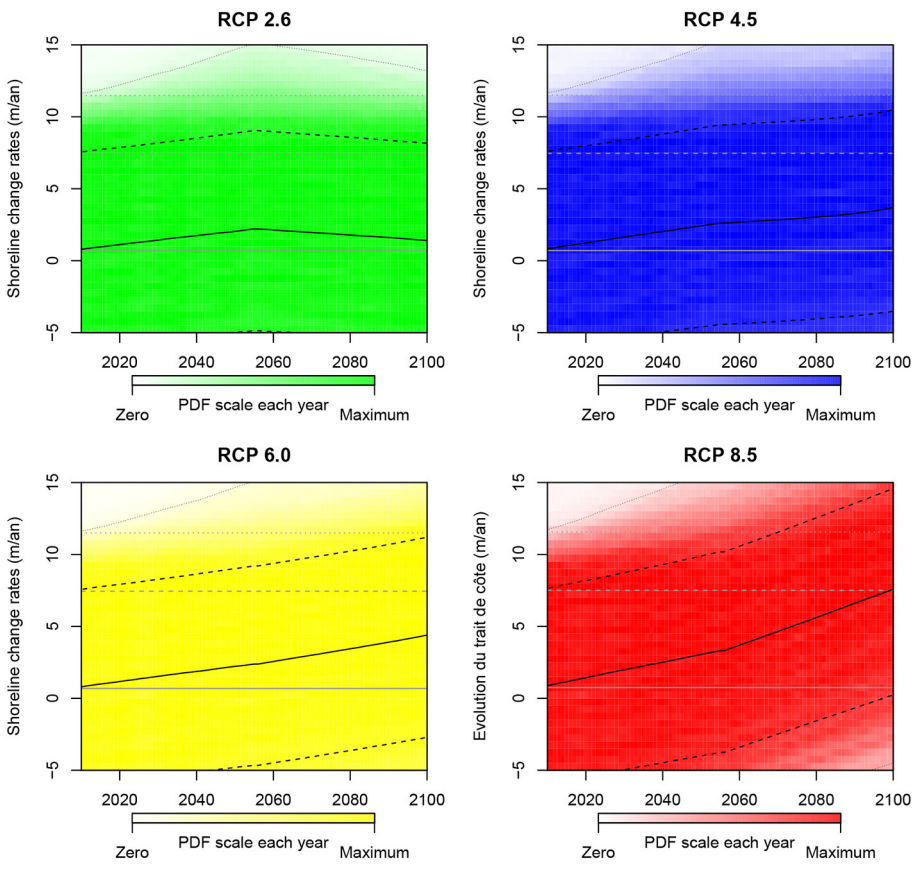

FIGURE 6 | Shoreline change rate projections for the 21st century for high-energy sandy coasts with groins and for different IPCC climate change scenarios. The meaning of gray and black lines is the same as in **Figure 3**.

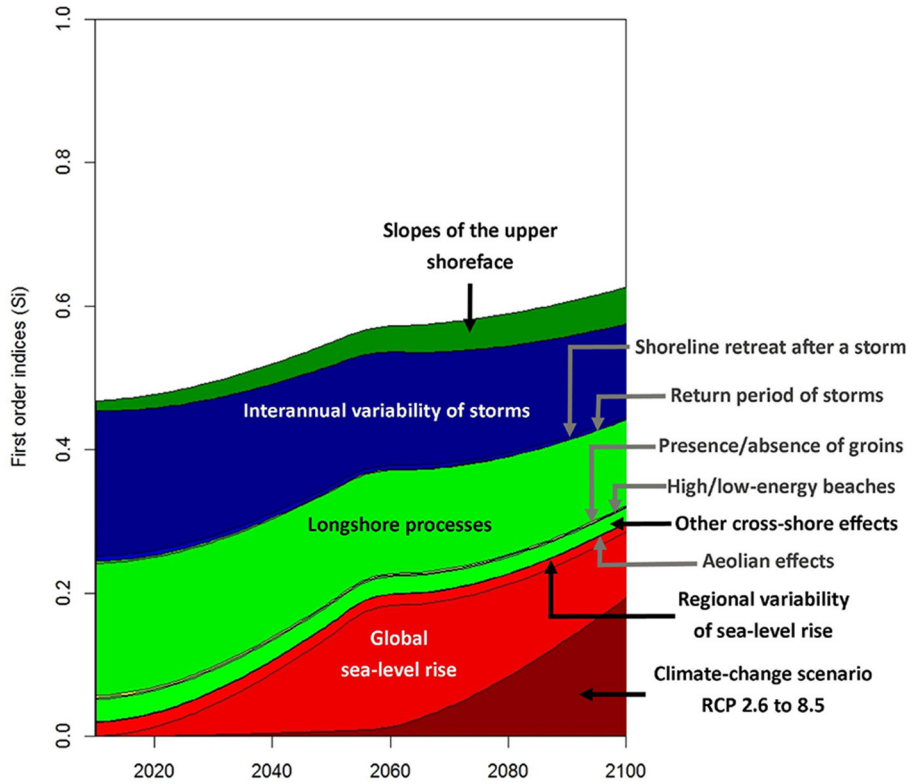

FIGURE 7 | Evolution of the first order Sobol' indices over the time, indicating the contribution of each varying parameter alone to the final uncertainty. Parameters indicated in gray have the smallest 1st order Sobol' indices. The inflexion of the curves after 2060 is due to two phenomena: first, the different climate change scenarios (RCP 2.6–8.5) induce different sea-level rise projections by that time (see **Figure 1**); second, shoreline change projections uncertainties by 2100 is much larger by 2100 than now (see text). The colors (red, green, blue, and yellow) indicate uncertainties related to (1) climate change and sea-level rise, (2) local site characteristics, (3) impacts of storms, and (4) of coastal defenses (groins).

4.4. Critical Unknowns for the Next Decades

Figures 7, **8** shows two distinct periods, during which the relative importance of sea-level rise, climate change scenarios, and beach slopes increase successively. This result primarily comes from the propagation of uncertain sea-level rise scenarios (**Figure 1**) in the Bruun term of Equation (1).

First, the climate change scenarios have small Sobol' indices during the 1st part of the 21st century. Therefore, as expected, the next decades do not appear as a relevant period of time to differentiate future shoreline change according to the future climate change scenarios. However, sea-level will be rising, and Equation (1) implies that this will induce a slight shift toward erosion. By 2050, uncertainties on global sea-level rise account for 20% of the variance of future shoreline change projections.

Conversely, there are large differences between e.g., RCP 2.6 and RCP 8.5 during the second part of the 21st century. **Figure 7** shows that if a decision is taken to follow a given climate change scenario, the variance of shoreline change projections is reduced by 20%. This is almost twice the maximum reduction of variance that we could expect, if we were able to predict accurately future sea-level rise given greenhouse gas emissions by 2100. Hence, even if nothing is known regarding coastal processes besides **Table 1**, the benefits of climate change mitigation and greenhouse gaz emissions reductions appear significant, as suggested by Nicholls and Lowe (2004) and Pardaens et al. (2011). Here, **Figures 7**, **8** constitute an other way to communicate this result, which was already identified in Section 3 and **Figure 3**.

4.5. Appropriate Coastal Settings for Validating the Use of the Bruun Rule in the Sediment Budget Equation

Figures 3–6 have indicated that if a large number of coastal sites are considered, (in)validating the use of the Bruun rule in Equation (1) will be straightforward by the end of the 21st century for RCP 6.0 and 8.5 scenarios (see Section 3). In a more general case, the results of the global sensitivity analysis (**Figures 7**, **8**) enable to identify which types of coastal sites are potential candidates for testing the use of the Bruun term in Equation (1): beaches without human impacts, little exposed to storms and where longshore drift can be quantified are among such sites. This result is not a surprise: previous studies that tried to validate the Bruun rule and detect an observable impact of sea-level rise on shoreline change actually focused precisely on this type of coasts (Leatherman et al., 2000b; Zhang et al., 2004). In practice however, the selection of such sites is not straightforward, and

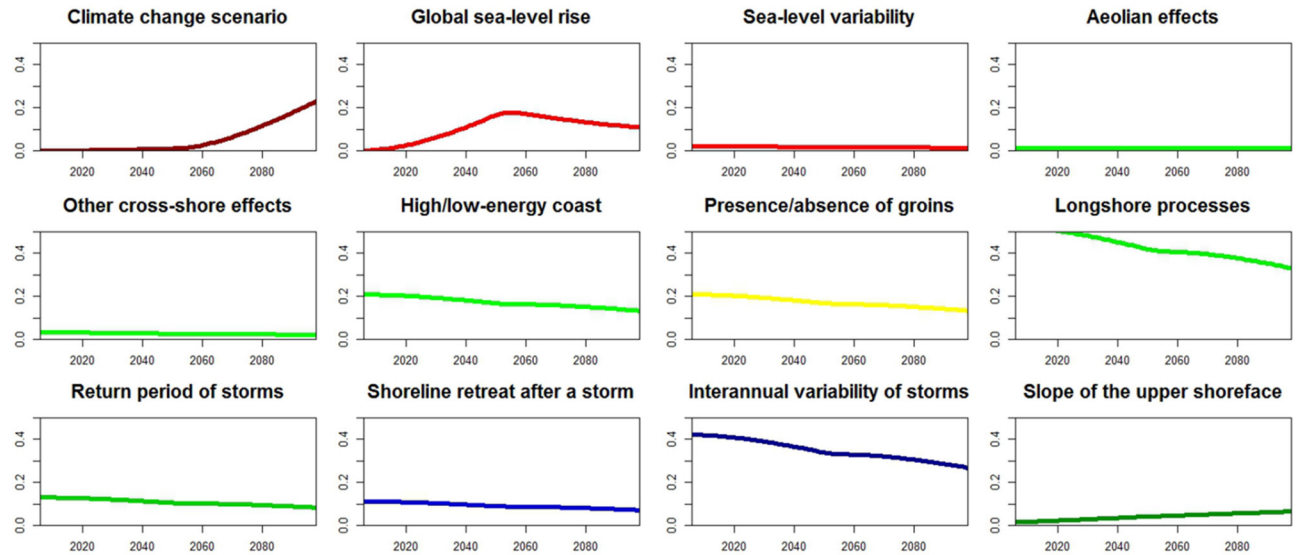

FIGURE 8 | Evolution of the total order Sobol' indices over the time, indicating which parameter can be fixed to any possible values without much impact to the variance of the model outcome. Please refer also to the legend of **Figure 7** for explanations on the colors and inflexions of the curves.

there remains question regarding the possibility to remove the impacts of longshore drift in the analysis (Leatherman et al., 2000a; Sallenger et al., 2000). Nevertheless, these results provide a perspective for coastal observatories currently collecting coastal evolution observations with the aim of better understanding coastal impacts of climate change.

5. DISCUSSION: REPRESENTATIVENESS OF THE SELECTED IDEALIZED COASTAL SITES

Our study relies on the orders of magnitudes provided by Stive (2004) for typical coastal settings in the Netherlands and Australia. Though there is no study providing orders of magnitude at other representative sites, it is hypothesized that the respective contribution of each process in **Tables 1**, **2** vary considerably for other coastal settings. For instance, on open and straight sandy beaches exposed to high-energy oblique ocean waves, longshore sediment transport rate can be high [e.g., $O(10^6$ m^3/year)] but without any alongshore gradients. In such a situation, longshore sedimentary processes do not contribute to shoreline change. This is the case of the southern Gironde Coast, SW France, where gradients in longshore sediment transport are negligible (Idier et al., 2013a) and where the observed shoreline variability on the timescales from hours to years can be explained by cross-shore processes only (Castelle et al., 2014). Yet, even in this simplified coastal setting, there is to date no detailed quantification of the contribution of aeolian processes and other cross-shore processes to the overall shoreline change. As far as extreme storms are concerned, it is impossible to quantify maximum storm wave erosion for given return period exceeding a few decades simply because there is no such long time series of storm-driven erosion. At the same beach, the cumulative impact of a series of outstanding storms during the winter 2013/2014 only drove a 15 m dune retreat over 3 months (Castelle et al., 2015). The same outstanding severe storms drove highly variable erosion patterns along Western Europe (Masselink et al., 2016), revealing the complexity of quantifying the erosion driven by multi-decadal or multi-centennial return period storms.

While providing numbers for this simple case of open beaches with no alongshore sediment transport gradients is arguably challenging, this is even worst for embayed beaches. Embayed beaches are ubiquitous worldwide given that nearly half of the world's coast consists of hilly or mountainous coastline. In addition, beaches artificially bounded by groins or jetty can behave as embayed beaches. Shoreline variability along embayed beaches is dominated by rotation signal (Ranasinghe et al., 2004). However, the respective contributions of cross-shore and longshore processes to the embayed beach rotation signal is still a subject of debate (Ranasinghe et al., 2004; Harley et al., 2011, 2015).

Overall, although we do not pretend to address all sandy coasts worldwide, we advocate that the values given by Stive (2004) are sufficiently large to be representative of many coastal settings. It is obvious that further work is required (1) to decipher the respective contributions of the different driving processes to shoreline change in different coastal settings and (2) to develop alternative model framework in which the different processes can be accounted for explicitly. In this framework, reduced-complexity modeling approaches (e.g., Splinter et al., 2014; Reeve et al., 2015) appear as a relevant avenue.

Noteworthy, Stive (2004) refers to coastal sites with gentle slopes, ranging from 0.001 to 0.002, which corresponds to very gentle slopes actually (Hinton and Nicholls, 1998; Marsh et al., 1998). Shoreface slopes are often larger. For instance

in SW France, high-energy beaches display coastal slopes of about 0.015 (Castelle et al., 2014), whereas they reach about 0.012 for low-energy Mediterranean beaches in Languedoc (Yates et al., 2011). In practice, however, the use of the Bruun rule in Equation (1) is more questionable for steep coasts. Other models would be required in such coastal sites, for example considering the sediment losses and gains during and after each storm (Larson et al., 2004; Ranasinghe et al., 2012). Nevertheless, we acknowledge that beach slopes values that can be calculated from **Table 3** correspond to coastal sites where the Bruun effect will have the strongest impacts.

The approach presented here could be applied to other medium-complexity geomorphic evolution modeling approaches (French et al., 2015), in order to finally identify research priorities. However, in the case of complex coastal settings with limited sand availability, the constraints imposed by the geology, the continental sedimentary supply or the role of coastal lagoons should be considered as well.

6. CONCLUSION

In this article, we examined where and by which period of time the Bruun effect should become observable on wave-exposed sandy coasts. To do this, we refered to Stive (2004) to evaluate the order of magnitude of each physical process contributing to shoreline change in the case of coastal upper-shoreface with gentle slopes. We also considered probabilistic sea-level rise scenarios based on the IPCC (Church et al., 2013). We propagated these uncertainties through the sediment balance equation, that sums the Bruun effect with other drivers such as longshore and cross-shore processes. This allowed to identify a time of emergence of an observable Bruun effect by the middle of the 21st century in the case of beaches with gentle slopes without groins, and for climate change scenarios RCP 4.5, 6.0, and 8.5 only. Under the assumptions above, the absence of generalized sea-level-rise-driven beach erosion by the end of the 21st century is only achieved for RCP 2.6 climate change scenario.

Rather than predictions of future shoreline changes, our results can be viewed as an attempt to better understand where and when the Bruun rule can be (in)validated. Using a global sensitivity analysis, our results confirm that low-energy gently sloping beaches with little human impacts and small gradients in longshore drift and sheltered from storms are the most relevant to assess the validity of the Bruun rule in the sediment balance equation. These results could be further improved through a better integration of the primary driving processes of shoreline change in the sediment balance equation, and refined probability distribution functions. This also implies collecting site-specific and more accurate values than those listed in **Tables 1**, **2**. Whatever the amount of data collected, part of the uncertainties in future shoreline change projections will remain. In addition, it should be noted that new knowledge may also illuminate some "not-yet envisaged" complex processes, of which our understanding may still be poor, and would require new research efforts in the future. Overall, and regardless the shortcomings discussed above, our approach is a relevant modeling framework to further improve communication to stakeholders and general public on uncertainties in sea-level rise impact assessments.

AUTHOR CONTRIBUTIONS

Overall design of the study: GC. Detailed design and implementation of the study: GC, CO, BC, MG, DI, RP, JR. Interpretation and discussion: All. Writing and correcting the paper: All.

ACKNOWLEDGMENTS

This project has been funded by BRGM through the "Adaptation to Climate Change Risks" project. BC was funded by the CHIPO project (ANR-14-ASTR-0004-01), financially supported by the Agence Nationale de la Recherche (ANR). The field mission following Xynthia (**Figure 2**) was funded by BRGM, and conducted by MG and RP, Daniel Monfort, Julie Mugica, Yann Krien, and Benjamin Francois. We thank Thomas Bulteau, Anny Cazenave, Franck Desmazes, Franck Lavigne, Cesca Ribas, and Marcel Stive for useful discussions and comments that finally resulted in this study. Finally, we thank the two reviewers for their very useful comments.

REFERENCES

Aagaard, T., and Sørensen, P. (2013). Sea level rise and the sediment budget of an eroding barrier on the danish North sea coast. *J. Coast. Res.* SI65, 434–439. doi: 10.2112/SI65-074.1

Allen, J. R. (1981). Beach erosion as a function of variations in the sediment budget, Sandy-Hook, New-Jersey, USA. *Earth Surf. Process. Land.* 6, 139–150.

Anderson, T. R., Fletcher, C. H., Barbee, M. M., Frazer, L. N., and Romine, B. M. (2015). Doubling of coastal erosion under rising sea level by mid-century in Hawaii. *Nat. Hazards* 78, 75–103. doi: 10.1007/s11069-015-1698-6

Arens, S. (1996). Patterns of sand transport on vegetated foredunes. *Geomorphology* 17, 339–350.

Bauer, B. O., Hesp, P. A., Walker, I. J., and Davidson-Arnott, R. G. (2015). Sediment transport (dis)continuity across a beach–dune profile during an offshore wind event. *Geomorphology* 245, 135–148. doi: 10.1016/j.geomorph.2015.05.004

Ben Abdallah, N., Mouhous-Voyneau, N., and Denoeux, T. (2014). Combining statistical and expert evidence using belief functions: application to centennial sea level estimation taking into account climate change. *Int. J. Approx. Reason.* 55, 341–354. doi: 10.1016/j.ijar.2013.03.008

Bird, E. (1985). *Coastal Changes: A Global Review*. New York, NY: Wiley.

Bruun, P. (1962). Sea-level rise as a cause of shore erosion. *J. Waterway. Harbour. Div.* 88, 117–130.

Bulteau, T., Idier, D., Lambert, J., and Garcin, M. (2015). How historical information can improve estimation and prediction of extreme coastal water levels: application to the Xynthia event at La Rochelle (france). *Nat. Hazards Earth Syst. Sci.* 15, 1135–1147. doi: 10.5194/nhess-15-1135-2015

Carson, M., Köhl, A., Stammer, D., Slangen, A., Katsman, C., van de Wal, R., et al. (2016). Coastal sea level changes: observed and projected during the 20th and 21st century. *Clim. Change* 134, 269–281. doi: 10.1007/s10584-015-1520-1

Castelle, B., Marieu, V., Bujan, S., Ferreira, S., Parisot, J.-P., Capo, S., et al. (2014). Equilibrium shoreline modelling of a high-energy meso-macrotidal multiple-barred beach. *Mar. Geol.* 347, 85–94. doi: 10.1016/j.margeo.2013.11.003

Castelle, B., Marieu, V., Bujan, S., Splinter, K. D., Robinet, A., Sénéchal, N., et al. (2015). Impact of the winter 2013–2014 series of severe western europe storms on a double-barred sandy coast: beach and dune erosion and megacusp embayments. *Geomorphology* 238, 135–148. doi: 10.1016/j.geomorph.2015.03.006

Church, J., Clark, P., Cazenave, A., Gregory, J., Jevrejeva, S., Merrifield, M., et al. (2013). *Sea Level Change*. Climate Change 2013: The Physical Science Basis. Contribution of Working Group I to the Fifth Assessment Report of the Intergovernmental Panel on Climate Change. (Cambridge, UK; New York, NY: Cambridge University Press), 1137–1216.

Cooper, J. A. G., and Pilkey, O. H. (2004). Longshore drift: trapped in an expected universe. *J. Sediment. Res.* 74, 599–606. doi: 10.1306/022204740599

Cowell, P. J., Stive, M. J., Niedoroda, A. W., de Vriend, H. J., Swift, D. J., Kaminsky, G. M., et al. (2003a). The coastal-tract (part 1): a conceptual approach to aggregated modeling of low-order coastal change. *J. Coast. Res.* 19, 812–827.

Cowell, P. J., Stive, M. J., Niedoroda, A. W., Swift, D. J., de Vriend, H. J., Buijsman, M. C., et al. (2003b). The coastal-tract (part 2): applications of aggregated modeling of lower-order coastal change. *J. Coast. Res.* 19, 828–848.

Dangendorf, S., Marcos, M., Müller, A., Zorita, E., Riva, R., Berk, K., et al. (2015). Detecting anthropogenic footprints in sea level rise. *Nat. Commun.* 6:7849. doi: 10.1038/ncomms8849

Davidson-Arnott, R. G. (2005). Conceptual model of the effects of sea level rise on sandy coasts. *J. Coast. Res.* 21, 1166–1172. doi: 10.2112/03-0051.1

Forbes, D. L., Parkes, G. S., Manson, G. K., and Ketch, L. A. (2004). Storms and shoreline retreat in the southern gulf of St. Lawrence. *Mar. Geol.* 210, 169–204. doi: 10.1016/j.margeo.2004.05.009

French, J., Payo, A., Murray, B., Orford, J., Eliot, M., and Cowell, P. (2015). Appropriate complexity for the prediction of coastal and estuarine geomorphic behaviour at decadal to centennial scales. *Geomorphology* 256, 3–16. doi: 10.1016/j.geomorph.2015.10.005

Garcin, M., Pedreros, R., Krien, Y., Monfort, D., Mujica, J., and Francois, B. (2011). *Base de données d'observations de la Tempete Xynthia Sur le Littoral*. Technical Report, BRGM. rapport BRGM/RP-59395-FR.

Golledge, N., Kowalewski, D., Naish, T., Levy, R., Fogwill, C., and Gasson, E. (2015). The multi-millennial Antarctic commitment to future sea-level rise. *Nature* 526, 421–425. doi: 10.1038/nature15706

Hallegatte, S., Green, C., Nicholls, R. J., and Corfee-Morlot, J. (2013). Future flood losses in major coastal cities. *Nat. Clim. Change* 3, 802–806. doi: 10.1038/nclimate1979

Hansen, J., Sato, M., Hearty, P., Ruedy, R., Kelley, M., Masson-Delmotte, V., et al. (2015). Ice melt, sea level rise and superstorms: evidence from paleoclimate data, climate modeling, and modern observations that 2°C global warming is highly dangerous. *Atmos. Chem. Phys. Discus.* 15, 20059–20179. doi: 10.5194/acpd-15-20059-2015

Harley, M., Turner, I., and Short, A. (2015). New insights into embayed beach rotation: the importance of wave exposure and cross-shore processes. *J. Geophys. Res. Earth Surf.* 120, 1470–1484. doi: 10.1002/2014JF003390

Harley, M., Turner, I., Short, A., and Ranasinghe, R. (2011). A reevaluation of coastal embayment rotation: the dominance of cross-shore versus alongshore sediment transport processes, Collaroy-Narrabeen beach, southeast Australia. *J. Geophys. Res. Earth Surf.* 116:F04033. doi: 10.1029/2011JF001989

Hemer, M. A., Fan, Y., Mori, N., Semedo, A., and Wang, X. L. (2013). Projected changes in wave climate from a multi-model ensemble. *Nat. Clim. Change* 3, 471–476. doi: 10.1038/nclimate1791

Hesp, P. A., Walker, I. J., Chapman, C., Davidson-Arnott, R., and Bauer, B. O. (2013). Aeolian dynamics over a coastal foredune, Prince Edward island, Canada. *Earth Surf. Process. Land.* 38, 1566–1575. doi: 10.1002/esp.3444

Hinkel, J., Nicholls, R. J., Tol, R. S., Wang, Z. B., Hamilton, J. M., Boot, G., et al. (2013). A global analysis of erosion of sandy beaches and sea-level rise: an application of DIVA. *Glob. Planet. Change* 111, 150–158. doi: 10.1016/j.gloplacha.2013.09.002

Hinton, C., and Nicholls, R. J. (1998). Spatial and temportal behavior of depth of closure along the Holland coast. *Coast. Eng. Proc.* 1, 2913–2925. doi: 10.1061/9780784404119.221

Horton, B. P., Rahmstorf, S., Engelhart, S. E., and Kemp, A. C. (2014). Expert assessment of sea-level rise by ad 2100 and ad 2300. *Q. Sci. Rev.* 84, 1–6. doi: 10.1016/j.quascirev.2013.11.002

Idier, D., Castelle, B., Charles, E., and Mallet, C. (2013a). Longshore sediment flux hindcast: spatio-temporal variability along the sw atlantic coast of France. *J. Coast. Res.* 2, 1785. doi: 10.2112/SI65-302.1

Idier, D., Rohmer, J., Bulteau, T., and Delvallée, E. (2013b). Development of an inverse method for coastal risk management. *Nat. Hazards Earth Syst. Sci.* 13, 999–1013. doi: 10.5194/nhess-13-999-2013

Inman, D. L., and Dolan, R. (1989). The outer banks of North-Carolina - budget of sediment and inlet dynamics along a migrating barrier system. *J. Coast. Res.* 5, 193–237.

Jansen, M. J. (1999). Analysis of variance designs for model output. *Comput. Phys. Commun.* 117, 35–43.

Jevrejeva, S., Grinsted, A., and Moore, J. C. (2014). Upper limit for sea level projections by 2100. *Environ. Res. Lett.* 9:104008. doi: 10.1088/1748-9326/9/10/104008

Kopp, R. E., Horton, R. M., Little, C. M., Mitrovica, J. X., Oppenheimer, M., Rasmussen, D. J., et al. (2014). Probabilistic 21st and 22nd century sea-level projections at a global network of tide-gauge sites. *Earth Future* 2, 383–406. doi: 10.1002/2014EF000239

Larson, M., Erikson, L., and Hanson, H. (2004). An analytical model to predict dune erosion due to wave impact. *Coast. Eng.* 51, 675–696. doi: 10.1016/j.coastaleng.2004.07.003

Le Cozannet, G., Garcin, M., Yates, M., Idier, D., and Meyssignac, B. (2014). Approaches to evaluate the recent impacts of sea-level rise on shoreline changes. *Earth Sci. Rev.* 138, 47–60. doi: 10.1016/j.earscirev.2014.08.005

Le Cozannet, G., Rohmer, J., Cazenave, A., Idier, D., Van de Wal, R., De Winter, R., et al. (2015). Evaluating uncertainties of future marine flooding occurrence as sea-level rises. *Environ. Model. Softw.* 73, 44–56. doi: 10.1016/j.envsoft.2015.07.021

Leatherman, S. P., Zhang, K., and Douglas, B. C. (2000a). Reply to comment on sea level rise shown to drive coastal erosion. *Eos Trans. Am. Geophys. Union* 81, 437–441. doi: 10.1029/00EO00330

Leatherman, S. P., Zhang, K., and Douglas, B. C. (2000b). Sea level rise shown to drive coastal erosion. *Eos Trans. Am. Geophys. Union* 81, 55–57. doi: 10.1029/00EO00034

Loureiro, C., Ferreira, Ó., and Cooper, J. A. G. (2014). Non-uniformity of storm impacts on three high-energy embayed beaches. *J. Coast. Res.* 70, 326–331. doi: 10.2112/SI70-055.1

Marcos, M., Tsimplis, M. N., and Shaw, A. G. (2009). Sea level extremes in southern Europe. *J. Geophys. Res. Oceans* 114:C01007. doi: 10.1029/2008jc004912

Marsh, S., Nicholls, R., Kroon, A., and Hoekstra, P. (1998). Assessment of depth of closure on a nourished beach: Terschelling, the Netherlands. *Coast. Eng. Proc.* 1, 3110–3123. doi: 10.1061/9780784404119.236

Masselink, G., Castelle, B., Scott, T., Dodet, G., Suanez, S., Jackson, D., et al. (2016). Extreme wave activity during winter 2013/2014 and morphological impacts along the atlantic coast of Europe. *Geophys. Res. Lett.* 45, 2135–2143. doi: 10.1002/2015GL067492

Mendoza, E. T., and Jiménez, J. A. (2006). "Storm-induced beach erosion potential on the catalonian coast," in *Journal of Coastal Research, Proceedings of the 3rd Spanish Conference on Coastal Geomorphology* (Las Palmas de Gran Canaria: Coastal Education & Research Foundation, Inc.), 81–88.

Menéndez, M., and Woodworth, P. L. (2010). Changes in extreme high water levels based on a quasi-global tide-gauge data set. *J. Geophys. Res. Oceans* 115:C10011. doi: 10.1029/2009jc005997

Miller, A., Jonkman, S. N., and Van Ledden, M. (2014). Risk to life due to flooding in post-Katrina New-Orleans. *Nat. Hazards Earth Syst. Sci. Discus.* 2, 825–864. doi: 10.5194/nhessd-2-825-2014

Mishra, S. (2002). *Assigning Probability Distributions to Input Parameters of Performance Assessment Models*. Stockholm: SKB.

Mori, N., Yasuda, T., Mase, H., Tom, T., and Oku, Y. (2010). Projection of extreme wave climate change under global warming. *Hydrol. Res. Lett.* 4, 15–19. doi: 10.3178/hrl.4.15

Nicholls, R. J., and Cazenave, A. (2010). Sea-level rise and its impact on coastal zones. *Science* 328, 1517–1520. doi: 10.1126/science.1185782

Nicholls, R. J., and Lowe, J. A. (2004). Benefits of mitigation of climate change for coastal areas. *Glob. Environ. Change* 14, 229–244. doi: 10.1016/j.gloenvcha.2004.04.005

Pardaens, A., Lowe, J., Brown, S., Nicholls, R., and De Gusmâo, D. (2011). Sea-level rise and impacts projections under a future scenario with large greenhouse gas emission reductions. *Geophys. Res. Lett.* 38:L12604. doi: 10.1029/2011gl047678

Passeri, D. L., Hagen, S. C., Medeiros, S. C., Bilskie, M. V., Alizad, K., and Wang, D. (2015). The dynamic effects of sea level rise on low gradient coastal landscapes: a review. *Earth Future* 3, 159–181. doi: 10.1002/2015EF000298

Pedreros, R., Garcin, M., Monfort, D., and Krien, Y. (2010). *Tempete Xynthia: Compte Rendu de Mission Préliminaire*. Technical Report, BRGM. rapport BRGM/RP-58261-FR.

Plant, N. G., Flocks, J., Stockdon, H. F., Long, J. W., Guy, K., Thompson, D. M., et al. (2014). Predictions of barrier island berm evolution in a time-varying storm climatology. *J. Geophys. Res. Earth Surf.* 119, 300–316. doi: 10.1002/2013JF002871

Planton, S., Déqué, M., Chauvin, F., and Terray, L. (2008). Expected impacts of climate change on extreme climate events. *Comptes Rendus Geosci.* 340, 564–574. doi: 10.1016/j.crte.2008.07.009

R Core Team (2014). *R: A Language and Environment for Statistical Computing*. Vienna: R Foundation for Statistical Computing.

Ranasinghe, R., Callaghan, D., and Stive, M. J. F. (2012). Estimating coastal recession due to sea level rise: beyond the bruun rule. *Clim. Change* 110, 561–574. doi: 10.1007/s10584-011-0107-8

Ranasinghe, R., McLoughlin, R., Short, A., and Symonds, G. (2004). The southern oscillation index, wave climate, and beach rotation. *Mar. Geol.* 204, 273–287. doi: 10.1016/S0025-3227(04)00002-7

Ranasinghe, R., and Stive, M. J. F. (2009). Rising seas and retreating coastlines. *Clim. Change* 97, 465–468. doi: 10.1007/s10584-009-9593-3

Reeve, D. E., Karunarathna, H., Pan, S., Horrillo-Caraballo, J. M., Różyński, G., and Ranasinghe, R. (2015). Data-driven and hybrid coastal morphological prediction methods for mesoscale forecasting. *Geomorphology* 256, 49–67. doi: 10.1016/j.geomorph.2015.10.016

Rignot, E., Velicogna, I., Van den Broeke, M., Monaghan, A., and Lenaerts, J. (2011). Acceleration of the contribution of the Greenland and Antarctic ice sheets to sea level rise. *Geophys. Res. Lett.* 38:L05503. doi: 10.1029/2011gl046583

Ritz, C., Edwards, T. L., Durand, G., Payne, A. J., Peyaud, V., and Hindmarsh, R. C. A. (2015). Potential sea-level rise from Antarctic ice-sheet instability constrained by observations. *Nature* 528, 115–118. doi: 10.1038/nature16147

Roelvink, D., Reniers, A., van Dongeren, A., de Vries, J. v. T., McCall, R., and Lescinski, J. (2009). Modelling storm impacts on beaches, dunes and barrier islands. *Coast. Eng.* 56, 1133–1152. doi: 10.1016/j.coastaleng.2009.08.006

Sallenger, A. H., Morton, R., Fletcher, C., Thieler, E. R., and Howd, P. (2000). Comment on sea level rise shown to drive coastal erosion. *Eos Trans. Am. Geophys. Union* 81, 436–436. doi: 10.1029/EO081i038p00436-02

Saltelli, A. (2004). "Global sensitivity analysis: an introduction," in *Proceedings of the 4th International Conference on Sensitivity Analysis of Model Output (SAMO'04)* (Los Alamos, NM), 27–43.

Saltelli, A., Annoni, P., Azzini, I., Francesca Campolongo, Ratto, M., and Tarantola, S. (2010). Variance based sensitivity analysis of model output. design and estimator for the total sensitivity index. *Comput. Phys. Commun.* 181, 259–270. doi: 10.1016/j.cpc.2009.09.018

Saltelli, A., Ratto, M., Andres, T., Campolongo, F., Cariboni, J., Gatelli, D., et al. (2008). *Global Sensitivity Analysis: The Primer*. Chichester, UK: John Wiley & Sons.

Slangen, A., Carson, M., Katsman, C., van de Wal, R., Köhl, A., Vermeersen, L., and Stammer, D. (2014a). Projecting twenty-first century regional sea-level changes. *Clim. Change* 124, 317–332. doi: 10.1007/s10584-014-1080-9

Slangen, A., Church, J. A., Zhang, X., and Monselesan, D. (2014b). Detection and attribution of global mean thermosteric sea level change. *Geophys. Res. Lett.* 41, 5951–5959. doi: 10.1002/2014GL061356

Slott, J. M., Murray, A. B., Ashton, A. D., and Crowley, T. J. (2006). Coastline responses to changing storm patterns. *Geophys. Res. Lett.* 33:L18404. doi: 10.1029/2006gl027445

Sobol', I. M. (1967). On the distribution of points in a cube and the approximate evaluation of integrals. *USSR Comput. Math. Math. Phys.* 7, 86–112. doi: 10.1016/0041-5553(67)90144-9

Sobol', I. M. (2001). Global sensitivity indices for nonlinear mathematical models and their Monte Carlo estimates. *Math. Comput. Simul.* 55, 271–280. doi: 10.1016/S0378-4754(00)00270-6

Splinter, K. D., Turner, I. L., Davidson, M. A., Barnard, P., Castelle, B., and Oltman-Shay, J. (2014). A generalized equilibrium model for predicting daily to interannual shoreline response. *J. Geophys. Res. Earth Surf.* 119, 1936–1958. doi: 10.1002/2014JF003106

Stive, M. J. F. (2004). How important is global warming for coastal erosion? an editorial comment. *Clim. Change* 64, 27–39. doi: 10.1023/B:CLIM.0000024785.91858.1d

von Schuckmann, K., Palmer, M., Trenberth, K., Cazenave, A., Chambers, D., Champollion, N., et al. (2016). An imperative to monitor Earth's energy imbalance. *Nat. Clim. Change* 6, 138–144. doi: 10.1038/nclimate2876

Wainwright, D. J., Ranasinghe, R., Callaghan, D. P., Woodroffe, C. D., Jongejan, R., Dougherty, A. J., et al. (2015). Moving from deterministic towards probabilistic coastal hazard and risk assessment: development of a modelling framework and application to Narrabeen beach, New South Wales, Australia. *Coast. Eng.* 96, 92–99. doi: 10.1016/j.coastaleng.2014.11.009

Winkelmann, R., Levermann, A., Ridgwell, A., and Caldeira, K. (2015). Combustion of available fossil fuel resources sufficient to eliminate the Antarctic ice sheet. *Sci. Adv.* 1:e1500589. doi: 10.1126/sciadv.1500589

Woodroffe, C. D., and Murray-Wallace, C. V. (2012). Sea-level rise and coastal change: the past as a guide to the future. *Q. Sci. Rev.* 54, 4–11. doi: 10.1016/j.quascirev.2012.05.009

Woodworth, P. L., and Menéndez, M. (2015). Changes in the mesoscale variability and in extreme sea levels over two decades as observed by satellite altimetry. *J. Geophys. Res. Oceans* 120, 64–77. doi: 10.1002/2014jc010363

Woodworth, P. L., Menendez, M., and Gehrels, W. R. (2011). Evidence for century-timescale acceleration in mean sea levels and for recent changes in extreme sea levels. *Surv. Geophys.* 32, 603–618. doi: 10.1007/s10712-011-9112-8

Wright, L., and Short, A. D. (1984). Morphodynamic variability of surf zones and beaches: a synthesis. *Mar. Geol.* 56, 93–118.

Yates, M., Guza, R., and O'Reilly, W. (2009). Equilibrium shoreline response: Observations and modeling. *J. Geophys. Res. Oceans* 114:C09014. doi: 10.1029/2009JC005359

Yates, M. L., Le Cozannet, G., and Lenotre, N. (2011). "Quantifying errors in long-term coastal erosion and inundation hazard assessments," in *Journal of Coastal Research, Proceedings of the 11th International Coastal Symposium* (Szczecin), 260–264.

Zhang, K. Q., Douglas, B. C., and Leatherman, S. P. (2004). Global warming and coastal erosion. *Clim. Change* 64, 41–58. doi: 10.1023/B:CLIM.0000024690.32682.48

Conflict of Interest Statement: The authors declare that the research was conducted in the absence of any commercial or financial relationships that could be construed as a potential conflict of interest.

frontiers in Marine Science

ORIGINAL RESEARCH
published: 11 May 2016
doi: 10.3389/fmars.2016.00069

Assessing Future Flood Hazards for Adaptation Planning in a Northern European Coastal Community

Carlo Sorensen[1,2]*, *Niels H. Broge*[3], *Mads R. Molgaard*[4], *Charlotte S. Schow*[5], *Peter Thomsen*[5], *Karsten Vognsen*[3] and *Per Knudsen*[1]

[1] DTU Space, Department of Geodesy, Technical University of Denmark, Kongens Lyngby, Denmark, [2] Coast and Climate, Danish Coastal Authority, Lemvig, Denmark, [3] Danish Geodata Agency, Copenhagen, Denmark, [4] Geo, Kongens Lyngby, Denmark, [5] Ramboll, Viborg, Denmark

From a transdisciplinary approach in the town of Thyboron, Denmark, we investigate couplings between sea state (i.e., mean and extreme) and flooding hazards today and ahead. This includes analyses of change and variability in the groundwater table, precipitation, land motion, geotechnical ground properties, sewerage systems and other infrastructure to outline a more complete platform for the integration of knowledge into climate adaptation schemes at this highly vulnerable coastal location. It involves the engagement of the main stakeholders who, although having different responsibilities, interests, needs of knowledge and data, and different timeframes for investment and planning, must join in a common appraisal of the challenges faced ahead to provide for better adaptation measures. Apart from obvious adverse effects from future storm surge events, knowledge about the coupled effects of the abovementioned parameters needs to be taken into account to reach optimal mitigation and adaptation measures. Through stakeholder interviews it becomes clear that an enhanced focus on transdisciplinary research is a viable way forward to develop such measures: it will bring in more knowledge, a broader scope, and it will provide for more holistic solutions that both serve to protect the town and allow for business development and better municipal planning ahead.

Keywords: sea level rise, local impact, extremes, land motion, geotechnical properties, integrating tools, stakeholder collaboration

OPEN ACCESS

Edited by:
Marta Marcos, University of the Balearic Islands, Spain

Reviewed by:
Goneri Le Cozannet, Bureau de Recherches Géologiques et Minières (BRGM), France
Ivica Vilibic, Institute of Oceanography and Fisheries, Croatia

***Correspondence:**
Carlo Sorensen
carlos@space.dtu.dk

Specialty section:
This article was submitted to Coastal Ocean Processes, a section of the journal Frontiers in Marine Science

Received: *11 December 2015*
Accepted: *22 April 2016*
Published: *11 May 2016*

Citation:
Sorensen C, Broge NH, Molgaard MR, Schow CS, Thomsen P, Vognsen K and Knudsen P (2016) Assessing Future Flood Hazards for Adaptation Planning in a Northern European Coastal Community. Front. Mar. Sci. 3:69. doi: 10.3389/fmars.2016.00069

INTRODUCTION

The future impact of climate change to people and the environment in coastal regions due to floods, inundation and erosion is substantial (Nicholls et al., 2007; IPCC, 2012). Furthermore, the groundwater table may be affected on varying time scales as may ground stability and the overall morphodynamics off the coastal locations. Climate research has advanced our knowledge of current and potential future sea level changes at global and regional scales (IPCC, 2013; Grinsted et al., 2015), of extreme water levels (Arns et al., 2015), natural variability and the anthropogenic footprint in sea level (Dangendorf et al., 2015), and of methods to evaluate sea level change from satellite (Nerem et al., 2010) and tide gauge data (Wahl et al., 2013; Visser et al., 2015; Watson, 2015).

Knowledge of climate change effects on society is in many ways still fragmented regarding approaches to adaptation, however. Updates on sea level rise projections and real-time monitoring

of change need better integration in planning tools, and consequences should be looked at in a more holistic way. For several reasons gaps exist between scientific knowledge and societal measures to mitigate climate change effects: First, the translation of climate change evidence to concrete impact measures is difficult. Second, the dissemination of uncertainty in projections and climate scenarios is certainly not a "one size fits all." Depending on the user, the information on uncertainty must be transformed to concrete impact variables used for e.g., adaptation and mitigation. Third, different and shifting agendas and opinions across levels of governance challenge the ways we address, perceive, and act on climate change issues in society. In order to bridge gaps, we thus need to address the translation of climate change parameters like sea level rise (SLR) and extreme events to actual effect measures; we must evaluate other contributors affecting climate change impact in time and space, and we must consider the stakeholders that may be affected as well as the actual assets that become threatened.

Many studies deal with current and future coastal hazards, exposure and vulnerability, risk and risk reduction on global (e.g., Nicholls, 1995; Hallegatte et al., 2013), regional (e.g., Du et al., 2013; Gibbs, 2015; Kuklicke and Demeritt, 2016) or local scales (e.g., Hallegatte et al., 2011; Kortenhaus and Oumeraci, 2014) that use different methodologies and modeling practices (Bosello and De Cian, 2014; Gallina et al., 2016; Nguyen et al., 2016). Often the research shows that a comparison between locations (or methodologies) is difficult as "the impacts of climate change on the coastal zone are expected to be largely site specific, due to the influence of local factors" (Linham and Nicholls, 2010). In relation to climate change adaptation the conclusion may even be that "coastal communities are unique and defy generalization" (Lane et al., 2015).

The quantification of potential hazards from climate change is governed by uncertainty and simplified assumptions about the impacts, and this affects the calculated exposure, vulnerability and risk of the area of investigation. Through independent and interdependent natural processes and potential interactions from multiple hazards—that may act differently through space and time, climate change impact studies gain complexity. In Denmark, for instance, flood risk mapping of the EU Flood Directive (EU, 2007; DCA, 2013a) uses a source-pathway-receptor approach with simplified assumptions made regarding the hazards and pathway of potential flooding. Also, a multitude of local national flood studies, typically carried out by consulting companies, tend to be "off the shelf" work that only look into one source of flooding (i.e., either sea floods, precipitation and runoff, or, the sewerage system) depending on the contracting entity. This often causes the decision-making process regarding mitigation measures to be uncoordinated between sectors and local governance administrations which lead to suboptimal solutions.

The starting point of the present study is to investigate couplings between sea state (mean and extremes) and flooding hazards today and ahead for a small coastal community in Denmark. We seek to include land motion, precipitation, geology, geotechnical properties, the sewerage system, and changes in groundwater level to reveal a more detailed picture of the climate impact. Through interviews with main stakeholders we investigate their roles, responsibilities and incitements to act. From this we discuss the added value of using existing data together with ongoing and future data provision for climate adaptation, and we address the diversified needs for knowledge and tools among the stakeholders. In doing so, we move from a cross-disciplinary scientific platform to a transdisciplinary research approach (using the definition by Jahn et al., 2012, pp. 8–9) to address local future practice-oriented adaptation collaboration where "transdisciplinarity is a gradual process of conceptual and methodological articulation" (Visser, 2001).

As such, we present ongoing research and also include data and preliminary results that may become focal points of collaboration between stakeholders. Not all scientific aspects are treated in detail and the paper rather addresses general links between disciplines, and it provides an overview of locally coupled climate change impact factors that may prove useful to advance climate change research and adaptation. The main research focus is thus on the identified coastal hazards to provide managers and decision-makers with a more complete common platform for the integration of knowledge in climate adaptation and planning.

DATA AND METHODS

History is an important but often neglected factor to the understanding of current and future hazards. As such, potentially important knowledge about an area may not be included in adaptation planning. We start by providing a fairly detailed historical overview of the area of interest, thereby also identifying hazards not included in the present study and factors that affect the future impact from climate change—apart from climate change itself. We then proceed to present the legislative framework and main stakeholders, and the methods applied dealing with land motion, sea state, groundwater, geological and geotechnical modeling, and hydrological modeling in relation to coastal hazards.

The Study Area

The town of Thyboron (population 2015: 2104), **Figure 1**; belongs to the Lemvig Municipality. A breach of the sandy barrier during a storm surge in 1862 led to the formation of Thyboron Channel. Since 1900 the channel has been maintained by groins along the channel banks and on the North Sea coast north and south of the channel, respectively (Sorensen et al., 1996; Knudsen et al., 2011). The coastal protection works and opening of a harbor in 1914 led to population growth. From the 1930s the ongoing coastal erosion, and doubts about whether it was possible protect the town, led the Danish Parliament to pass an act to close the Thyboron Channel with large dams and a sluice (MPW, 1942; DP, 1946). Dams were built on the fjord side of the barriers both north and south of the channel, but the decision to close the channel and the scientific reasoning for doing so was soon disputed (Bruun, 1954; MPW, 1968) and in 1970 a decision

FIGURE 1 | Study area. The Danish town of Thyboron is located on the eastern North Sea coast and hosts a large harbor by the Thyboron Channel that connects the North Sea and the Limfjord. The town has experienced several minor floods like in 1981 (Photo: Thyboron-Harboore-Engbjerg Local Archive).

was made to maintain an open channel and let the Danish Coastal Authority monitor the evolution (DP, 1970; DCA, 1975).

The "Thyboron question" is still controversial, however (e.g., Larsen and Beck, 2009; Norgaard et al., 2014). An expanding channel cross section (Bruun and Gerritsen, 1960; Knudsen et al., 2011) leads to increased water transport into and higher surge levels in the fjord during storms. Between 1958 and 2005 a statistical 100-year extreme water level in the town of Lemvig has increased from 1.73 to 1.99 m DVR90, and it is expected to increase further to 2.38 m DVR90 by 2060 excluding effects of sea level rise, if the channel is allowed to develop naturally (Christensen, 2011a,b; Knudsen et al., 2012; Sorensen et al., 2013). All heights refer to the Danish Datum DVR90 which corresponds to Danish mean sea level around 1990 (Schmidt, 2000) unless otherwise stated. The Danish Coastal Authority has sketched several possible solutions to mitigate future storm surge levels inside the fjord (Ingvardsen et al., 2012) but no efforts have been made toward reaching a solution. The decision (or lack of such) on how to handle Thyboron Channel is a large, unknown factor in flood protection and adaptation planning in Thyboron and other communities located at the shores of the Limfjord.

A large sea dike and a transverse dike toward south protect Thyboron against flooding from the North Sea for a 1000 year storm surge event according to the Danish Coastal Authority, who is in charge of the coastal protection along the 110 km central part of the Danish North Sea coast (DCA, 2013b). Lemvig Municipality is in charge of protection against floods from the channel and fjord. Coastal erosion challenges (Jensen and Sorensen, 2008; DCA, 2013b) and dike strength assessments are not within the scope of this paper but are, of course, important in relation to the future safety of Thyboron. Today, sand nourishments on the North Sea coast are used for protection.

A small part of Thyboron, locally known as "old town," in the south-west dates back to the nineteenth century and is the remnant of the pre-1862 settlement not lost to coastal erosion (see Sorensen, 2015a). Aerial photography provides a visual impression of town growth, **Figure 2**. The road and railway track to Thyboron are both toward west in 1945—just east of the "dike trenches" seen as dark patches in the lower left of the photo. Most houses are situated between the main road and the North Sea, and houses and infrastructure have been built in connection with the port. In the 1950s, the large dam/dike is being finalized in conjunction with a new road and railway along the fjord to the east. In Thyboron, an area between the railway and the road shows marshlands to the west and shallow water with deeper parts draining under the road to the fjord. The very light-colored appearance of the town is indicative of a very sandy environment. In 1965 the harbor is expanding and the north-east part of the town has developed. In addition, a new development is forming on sandy landfill on the aforementioned marshland (middle of photo). Gradually, between 1965 and 1992 the town development continues in this area in 4–5 major stages and with the local heating plant in the south-eastern most part opening in late 1992. Since 1992 the development has slowed down and the largest changes are witnessed in the north-west corner of the town and in connection with the harbor. A harbor expansion is currently being developed on new landfill areas southeast of the area shown.

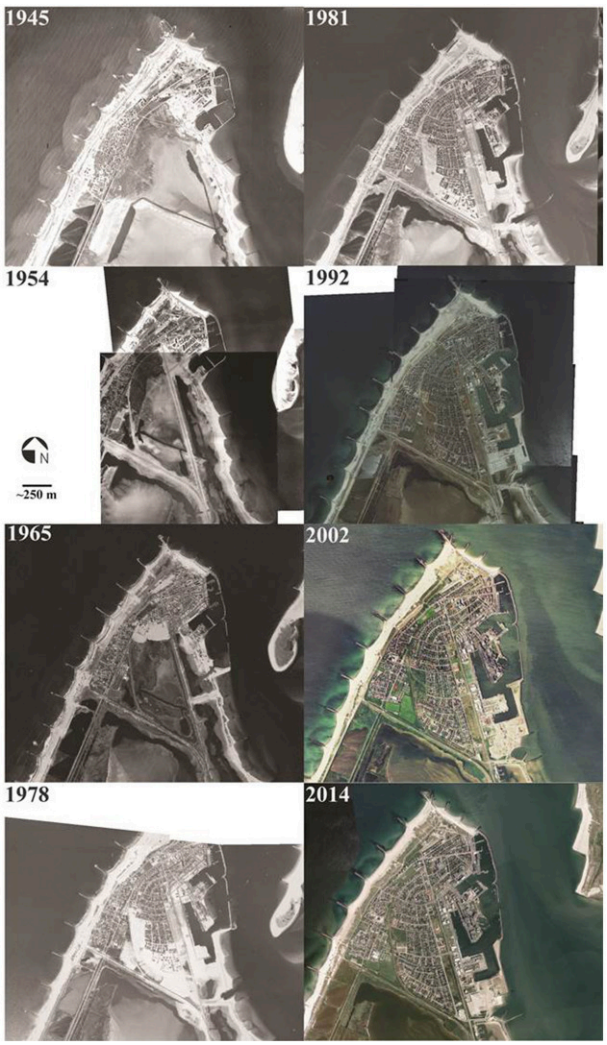

FIGURE 2 | Aerial photography of Thyboron covering the period 1945–2014. Sources: arealinformation.miljoeportal.dk (I-GIS 1945; DDO®, © COWI 1954, 2002, 2014), flyfotoarkivet.dk (© Geomidt/Lemvig Municipality 1965, 1978, 1981, 1992).

Governance and Main Stakeholder Interviews

Denmark has three levels of governance: national, regional (5 regions) and local (98 municipalities). Regions have a small role in facilitating climate adaptation and mitigation processes. The European Union plays a role at the coast e.g., through the implementation of the Floods Directive in member states (EU, 2007). The Danish Coastal Protection Act (MT, 2009) is one of several laws regulating the coastal zone (see Figure 15 in Sorensen, 2015b). Through national legislation passed (DP, 2012a,b) the Danish municipalities have made climate adaptation plans and are in the process of preparing measures to mitigate future events. The plans only focus on water related issues and with a strong emphasis on flash floods, however. The Lemvig Municipality adaptation plan points out Thyboron as a focus area (Lemvig Municipality, 2014) and, although initially unrelated to the municipal work, the present research relates to the challenges faced by the municipality and other stakeholders to address coastal hazards in their adaptation planning.

The Port of Thyboron, Lemvig Municipality, Lemvig Water and Wastewater, and the Danish Coastal Authority (DCA) are identified as the four main stakeholders in relation to climate change adaptation in Thyboron. The local population is not considered in the present study. The institutions have formal responsibilities and are all a part of a political system governed by legislation and rules. Although, the Port of Thyboron and Lemvig Water and Wastewater (LWW) both operate as independent corporations, they are either owned entirely or partly by and have board members from Lemvig Municipality. The municipality itself follows strict rules regarding their expenditure, and the Danish Coastal Authority needs to act according to national legislation with reference to the Minister for the Environment and Food. As mentioned the Danish Coastal Authority is responsible for the flood protection toward the North Sea. Lemvig Municipality is responsible for the flood protection toward the Thyboron Channel and the fjord, or, at least the Danish Coastal Authority is not.

Semi-structured interviews were held in September 2015 with Port of Thyboron Director, Mr. Jesper Holt Jensen, and Technical Director, Mr. Christian Vrist; the Director at Lemvig Water & Wastewater Inc., Mr. Lars Noergaard Holmegaard; the Head of Nature and Environment Department at Lemvig Municipality, Mr. Thomas Damgaard, and Danish Coastal Authority Director Ms. Merete Loevschall. Interviews were held in Danish and an English translation of the interview summaries enters the research.

The scope of the interviews was to bring out opinions and reflections on the current level of preparedness in relation to coastal floods (from all sources); positions in relation to current legislation; potential future or already planned actions in relation to climate change adaptation; collaboration issues, and the need of information regarding climate change and e.g., data and tools for adaptation. Previous to the interviews the stakeholders were consulted in late 2014 for the provision of data relevant to the study presented. In the course of research Lemvig Municipality has provided spatial data from house registers etc. and local knowledge, and Lemvig Water and Wastewater has financed the groundwater monitoring setup.

Although, potentially biased from knowledge of and varying interests in the ongoing research by the stakeholders, the information provided and main learnings from the interviews are included to discuss the concrete use and integration of research and data in adaptation planning.

Ethics Statement

The scientific data use fulfills the Danish Ethical legislation as authorized in writing by the responsible institution Legal Affairs at the Technical University of Denmark (DTU), 15 April 2016, regarding the legal and ethical handling of personal data. The Data Protection Act implementing Directive 95/46 was passed on in Law no. 429 of 31/05/2000. The Act faithfully transposes the provisions of the EC Directive into Danish law. The University

(DTU) follows the Danish Statutory Order on Security on Data processing of Personal data, no. 528 of 15/06/2000 when processing Personal Data. According to § 10.2 in The Danish Statutory Order on Security on Data processing of Personal data, public universities may handle personal data without the permission from the subject (person) where the processing takes place for the sole purpose of carrying out statistical or scientific studies of significant public importance and where such processing is necessary to carry out these studies.

Ground Deformation and Topography

The NE part of Denmark experiences larger absolute national scale glacio-isostatic uplift rates than SW (Mertz, 1924; Duun-Christensen, 1990). Several studies deal with surface deformation on regional and local scale in Denmark due to sedimentary processes and tectonics (Andersen et al., 1996; Lykke-Andersen and Borre, 2000; Hanssen and Perski, 2007; Gregersen and Voss, 2010, 2015; Pedersen et al., 2011; Hansen et al., 2012; Jakobsen et al., 2013). In European collaboration projects (PanGeoProject.eu; SubCoast.eu; Terrafirma.eu.com, and Absrate, Knudsen et al., 2009) Danish issues of coastal hazards from land subsidence have been addressed. Here, we investigate the local pattern of vertical ground movement from a combination of methods to relate it to climate change impact.

Glacio-Isostatic Uplift

The glacio-isostatic land uplift rates within the study area, and for Denmark in general, are found from uplift model calculations (Knudsen et al., Supplementary Material 1 [S1]) related to the Milne et al. (2004) uplift model, three national leveling campaigns over the past century, long tide gauge series (Holgate et al., 2013; Permanent Service for Mean Sea Level, 2015), and to vertical deformation rates from permanent GPS station data in Denmark (Khan, 2014). The model is used to evaluate the overall rates of land uplift currently experienced.

Precision Leveling

Repeated motorized, geometric precision leveling (Vognsen et al., 2013a,b) to a few existing and +60 newly established height benchmarks, typically bolts, along the Limfjord Barriers and in Thyboron was carried out in 2006, 2009, 2012, and 2015, respectively, **Figure 3**. Across the Thyboron Channel, the height determination is carried out in relation to the geometric leveling by simultaneous-reciprocal trigonometric leveling under favorable weather conditions. All campaigns were carried out in late summer/early autumn of the corresponding year. Leveling was performed between two assumedly stable benchmarks north and south of the barriers, respectively, and with the northern benchmark kept at a fixed height (Id. 72-12-9021; determined in 1995). Differences in the calculated heights at the southern benchmark (Id. 125-06-9026; determined 2006) between individual leveling campaigns, which is ascribed to small differences in general glacio-isostatic land uplift between the two points, are small and within the allowed uncertainty for the individual leveling campaigns. Therefore, no subsequent corrections of individual benchmarks are made, and the uncertainty in their height determination over this 9 year period is evaluated at ±0.003 m (Vognsen et al., 2013b). Ahead, however, a recalculation of the benchmark heights covering the area should be performed when either point is connected to the national leveling network again. Older leveling data were digitized, recalculated, transformed from the former Danish Ordnance Datum (DNN) to DVR90, and quality assessed for calculations of vertical velocities extending back in time.

Elevation of Sewers

In 2012, elevations of the bottom of the sewers were measured beneath man-hole covers at 57 accessible locations to compare these with elevations measured between 1980 and 1990 (in parts of Thyboron this was not possible due to floating manhole covers that could not readily be removed). So far, it has not been possible to date the older measurements more precisely. The uncertainty in the 2012 height determination is evaluated to be better than ± 0.013 m; refer to Vognsen et al. (2013b) for more information on methods. The 1980–1990 measurements are believed to represent the bottom level of sewers well although the uncertainty is unknown and probably somewhat larger.

Land Motion from Satellite Interferometry

Imagery from the ERS radar satellite has been used as an alternative method to reveal land deformation at Thyboron. The methodology is based on analysis of time series of co-registered radar satellite images known as persistent scatterer interferometry, PSI (Ferretti et al., 2007). The method has been applied to monitor land deformation from a number of geo-hazards like landslides, earthquakes, volcanism, and coastal flooding.

In the present study time series of ERS radar images from 1995 to 2001 [ERS SAR: Track 108, frame 2457: 48 scenes (period: 1995–2001)] were collected by courtesy of the European Space Agency (Levinsen et al., 2015). The images were acquired and processed by the Geological Survey of Norway. After a detailed quality assessment of the results, a threshold measure of 0.55 is set on the "coherence" parameter, which is a measure of reliability of each PSI point with a calculated vertical velocity. Although, newer satellite imagery is desirable, this has not been possible due to lack of coverage, data series not being sufficiently available for calculations, or, due to inhibitive costs for inclusion in the present study. No subdivision of the PSI data set has been attempted and the data thus provides information about the averaged relative rates of vertical land deformation 1995–2001 in Thyboron relative to a point near the northern benchmark mentioned above for the leveling. Thus, the PSI calculated vertical velocities do not include the contribution from the glacial isostatic adjustment.

Digital Terrain Model

The Digital Terrain Model (DTM) from the Danish 2007 Digital Elevation Model (DK-DEM) used throughout this study has a 1.6 * 1.6 m resolution, a horizontal accuracy of 0.67 m RMSE and an averaged vertical accuracy of 0.059 m RMSE (Hawa et al., 2011; Rosenkranz and Frederiksen, 2011). Data are available free of charge through the Danish "basic data program" (eng.gst.dk). In addition to the DTM (DK-DEM), a hydrological adaptation layer

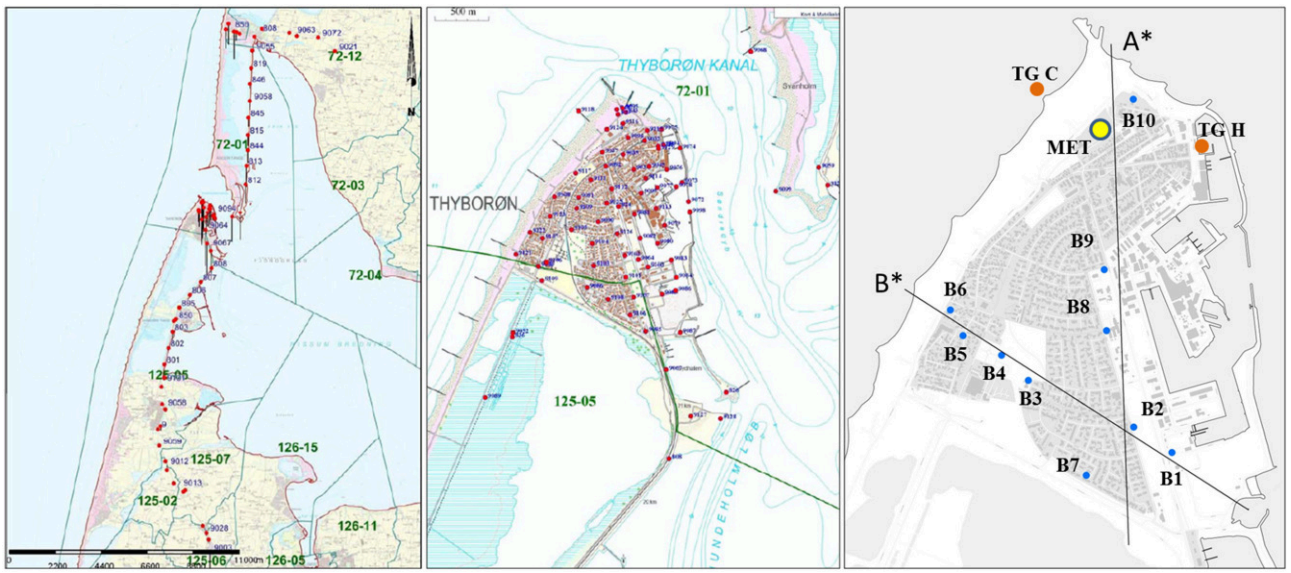

FIGURE 3 | Benchmarks along the Limfjord barrier (left) between Vestervig Church (NE) and Hove Church (S) and a zoom-in on Thyboron (middle). Groundwater monitoring (B1–B10), tide gauge (TG C & TG H) and meteorological (MET) station positions are plotted (right) together with lines (A*, B*) along which groundwater stations are approximately aligned.

has been produced and is also available for download. A stretch of quay that has been heightened by 0.5 m since the acquisition of the DEM is not included but is unlikely to affect the overall results. According to Thyboron Port Authorities and confirmed in our own investigations, the new quay height corresponds well to the initial height when the original quay was constructed approximately 50 years ago indicating land subsidence rates in the order of 10 mm/year.

Tide Gauge Data and Sea State

Two continuous tide gauge (TG) digital data series exist for Thyboron and are operated by the Danish Coastal Authority. Thyboron Harbor TG (Id: 4201; from 1974) is in the northern part of the harbor, and Thyboron Coast TG (Id: 4203; from 1975) is placed in a groin on the open coast, **Figure 3**. In addition, analog data exist back to c. 1935 for the harbor TG but still await digitization. Historical extreme water levels and storm events have been digitized in the past. No systematic metadata have been collected and kept for the central Danish North Sea West Coast TGs and data series (service & maintenance, benchmark and water level corrections etc.) and no concise manual for their operation exists. Correction of data, services, and benchmark leveling has been performed in the past, however, and can be traced in the data series (e.g., linear corrections in time and datum shifts). From a close manual scrutiny of the data, the TG series (1975–2012) have been corrected and validated as far as possible, e.g., by recalculating of the TG benchmarks and omitting erroneous data. Furthermore, tide gauge data from the Limfjord are available from a number of stations. 2015 TG measurements are used in relation to the groundwater level observations. Regarding extreme water levels and statistics, numbers are adopted from Sorensen et al. (2013).

Groundwater and Precipitation Data

Ten stations measuring the groundwater level in Thyboron were established in august 2015, **Figure 3**. Their current spatial distribution reflects a plan to monitor variations N-S and W-E, interests in certain areas in the town, and that the deployment should be on municipal land. Although covering a mere 3 months only, the data logging in 5 min intervals are included to, at least, discuss their potential value ahead in assessing climate impacts in Thyboron. The measured groundwater levels are related to DVR90 from GPS measurements at time of deployment and validated in the DTM. Precipitation is measured in Thyboron (10 min intervals) and is cumulated on a daily basis. Wind is also recorded but these data are not used in the present study (Id: 4200).

Geological Modeling and Geotechnical Data

A geological model is a spatial representation of the local subsurface conditions and its quality depends on the accuracy and availability of geological information. A geological model rarely accounts for the entire geology of an area but it can focus on specific layers such as the shallow geology or the pre-Quaternary conditions (Binzer and Stockmarr, 1994; Nielsen et al., 2007). We use standard methods (Jorgensen et al., 2008; Sandersen, 2008) to define layers which potentially play a role for land subsidence in Thyboron, and to preliminarily discuss issues related to the groundwater level and coastal hazards. These layers are generated in GeoScene3D (I-GIS, 2015) accordingly and appear as continuous near-surface layers (0–30 m depth) in the resultant geological model.

Incorporation of Data

Various subsurface information from public and private archives, such as geological (Geo, 2015; GEUS, 2015a), geophysical (GEUS, 2015b), hydrological (GEUS, 2015c,d), and geotechnical data (Geo, 2015) are integrated into the model. A combination of these data can considerably increase the model's accuracy. The local geological knowledge primarily results from public and private well data as well as from a soil map of the upper 1 m (GEUS, 2015e), where according to Jakobsen et al. (2015) the Thyboron area is among the 10% of the country which is still not included in the map. Geophysical information for the area exists in the form of DUALEM-421s data collected in the framework of this study. No additional geophysical data have been located except for a single geophysical log in well no. 44.571 located SE of Thyboron (Petersen et al., 2008). Hydrologic data are from groundwater level measurements, hydraulic tests in wells and from a groundwater mapping campaign previously conducted in the area.

Digitization of Borehole Logs

A review of the Geo (2015) geotechnical archive located +200 geotechnical boreholes, all of which are geo-referenced based on the old site plans and digitized based on the old borehole reports to enter the GeoGIS database. The boreholes were mainly conducted in relation to construction works and, unlike most of the publicly available drilling from Thyboron (GEUS, 2015a), contain a high level of detail that describes the geological and geotechnical parameters such as water content and strength; e.g., Geoteknisk Institut (1978) and Geoteknisk Institut (1983), Figure S1. Groundwater levels are often registered, too, if established below the groundwater level. The Geo (2015) geotechnical boreholes are mainly concentrated in the eastern and southern part of the town facing the harbor and are not evenly distributed. At the same time, the exact location of the boreholes from the old site plans is uncertain. By combining this data set with boreholes from the GEUS (2015a) database, although in less detail, it seems possible to achieve a fairly good coverage in major areas of the town, **Figure 4**. The model of the geological conditions is expected to be more accurate around the harbor, however.

Geophysical Data (DUALEM-421s)

Geophysical data were collected in Thyboron during May 2015. The ground conductivity meter DUALEM-421s was applied for detailed mapping of the electrical resistivity of the upper 6 meters of the ground. Data have been collected at all available green areas, parking lots and on some roads with the DUALEM-421s deployed to an ATV (max. speed 30 km/h) with simultaneous video and GPS recordings. Data is inverted using a constrained multi-layer model (Vignoli et al., 2015). **Figure 4** shows the inverted resistivity in depth interval 1–1.5 m. Green colors indicate clay, whereas red and purple colors indicate the presence of more coarse sediments like sand and gravel. The results from the DUALEM-421s survey will together with borehole information represent data input for the geology of the upper few meters of the soil.

Hydrologic Flow Modeling

To gain insights about hydrological conditions in Thyboron today as well as in the future modeling is performed using the MIKE software (dhigroup.com). MIKE FLOOD couples the models MIKE URBAN and MIKE 21. MIKE URBAN is a hydraulic 1D-model used to simulate the flow and thereby stowage levels in the sewers. The calculation in MIKE URBAN is divided into two parts: first the runoff on terrain and thereby hydrography (flow over time) which runs into the individual wells in the sewer system is calculated. Secondly, the flow and backflow into sewers, wells, sump pumps, water outlet drains, basins etc. are calculated. A detailed digital mapping of the sewer system was kindly provided by the Lemvig Water and Wastewater Company and used in the model. Connecting this 1D calculation with 2D calculations in MIKE 21 via MIKE FLOOD water stowage from the sewers can propagate across the terrain indicated to the model by the aforementioned DTM including the hydrological adaptation layer. Thereby MIKE FLOOD calculates dynamic flood levels at any given precipitation event. Similarly, storm surge events are modeled. The results indicate a potential flood from various scenarios, sources, and durations by showing the maximum water depth in each cell (1.6 * 1.6 m) of the DTM/DK-DEM. This may not necessarily occur simultaneously, however, and results thus show maximum potential flooding.

Hydrological conditions are calculated for the following precipitation events:

- 5 year rain event including climate factor; corresponding to the Danish operation practice precipitation for storm water sewers (IDA, 2005),
- 10 year rain event including climate factor; corresponding to the Danish operation practice precipitation for combined household and storm water sewers (IDA, 2005), and
- 100 year rain event including climate factor.

Values of rain intensity including a climate factor are adopted from Gregersen et al. (2014).

The combined effects of precipitation, land subsidence (projected from 2006 to 2012 leveling results and general uplift in the DEM) and sea level rise/extreme water levels have been calculated for various future scenarios, **Table 1**.

Subsidence rates are assumed constant in time in the calculations. The sea level rise scenario is adopted from Grinsted (2015) and Olesen et al. (2014) and modified to 2065 and 2115, respectively. Extreme water levels are adopted from Sorensen et al. (2013) using the Thyboron Harbor statistics. Linearity in 100 year event extreme water levels with SLR is assumed and e.g., changes in climate conditions (storm frequency and intensity), tides, morphodynamic conditions, construction works etc. are not considered. The effect of wave overtopping on flooding is not considered in the present study. The 2015 mean water level (0.05 m) accounts for the relative SLR since determination of the DVR90 datum around 1990. The Thyboron tide gauge statistics are assumed to be representative of extreme water levels in the channel and fjord thus disregarding potential gradients in the extreme water levels along the coastline. Furthermore,

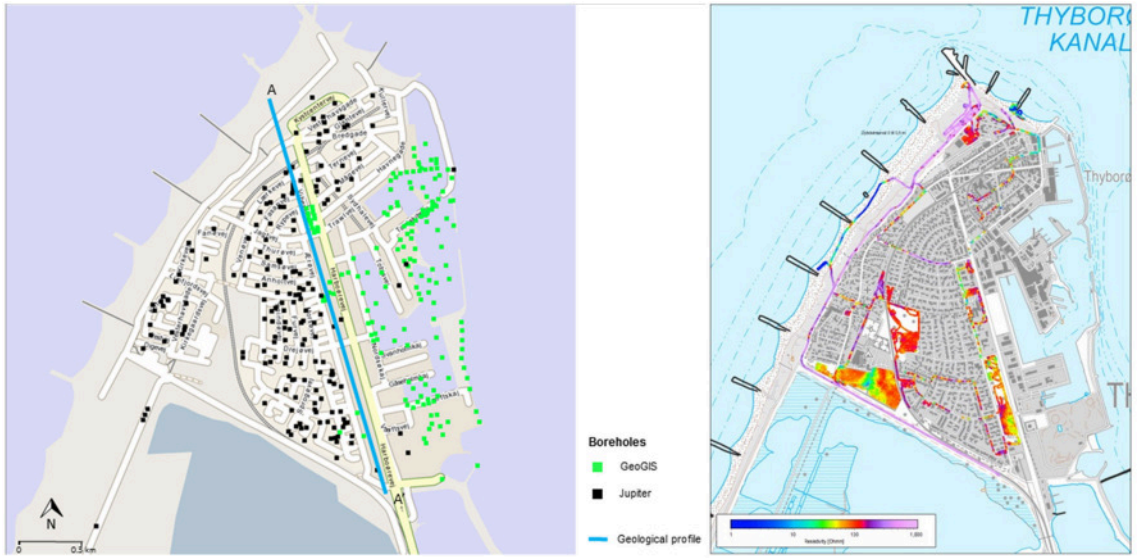

FIGURE 4 | Available subsurface data for Thyboron. The green dots indicate wells from Geo's well database and black dots show wells available from the public Jupiter database. The blue line indicates the position of the geological profile A-A′. DUALEM-421s data coverage is exemplified by resistivity measurements at 1–1.5 m depth (right).

TABLE 1 | Scenarios modeled in MIKE for a range of combinations of precipitation, sea level rise, and extreme water levels with and without land movement, and looking 50 and 100 years ahead.

Scenario	Explanation	Year	SLR (m)	MWL (m DVR90)	100 year extreme storm surge level (m DVR90)
Status	No subsidence, no sea level rise	2015	0	0.05	(1.93)
Future 1	Subsidence in 50 years, no sea level rise	(2065)	0	0.05	–
Future 2-A	No subsidence, sea level rise in 50 years	2065	0.30	0.35	–
Future 2-B	No subsidence, sea level rise in 100 years	2115	0.70	0.75	–
Future 3-A	Subsidence in 50 years, Sea level rise in 50 years	2065	0.30	0.35	–
Future 3-B	Subsidence in 50 years, 100 year extreme event in 50 years (duration 3 h).	2065	(0.30)	(0.35)	2.23
Extreme 4	Subsidence in 50 years, 100 year extreme event in 100 years (duration 3 h).	(2115)	(0.70)	(0.75)	2.63

considerably higher extreme storm surge levels on the North Sea coast, which may potentially lead to breaches of the sea dike, are not considered.

RESULTS

Results from *in situ* and satellite measurements are presented and joined in modeling results. Main stakeholder interview results are briefly presented.

Water Levels

The central Danish North Sea coast TGs' data are of a varying quality, **Figure 5**, Figure S2. The Thyboron Coast TG data are not as complete as the Harbor TG and data quality is lower mainly due to the harsher physical environment and more difficult access. From around 1990 the Thyboron series show a good correlation to the long tide gauge series in Esbjerg and Hanstholm (from Hansen, 2013) in annual mean water levels, Figure S3. Calculated rates of change in mean water levels from linear regression, used only here to evaluate datum/benchmark corrections of the TG's, seem reasonable and within the expected range for Thyboron, Table S1. Results imply that the Thyboron TG's can be useful to regional sea level studies and, on the other hand, that the data represent well the overall measured annual mean sea level variations in the eastern North Sea over the past decades. Results from relevant regional sea level studies may thus be representative for consideration at Thyboron at the current stage of research. Especially in the Hvide Sande TG data apparent local land subsidence effects still need to be accounted for in a more thorough TG benchmark and leveling reanalysis, if possible. Considering the usefulness of the DK North Sea TGs, an effort should be made, in general, to upgrade TG maintenance, benchmarking, and data collection to international standards.

Storm water levels can get significantly higher on the coast than in the harbor and Thyboron Channel and often with a strong gradient in water levels. In the vane of storms or after prolonged periods of windy conditions, the water level inside the fjord may be significantly higher than on the coast with a

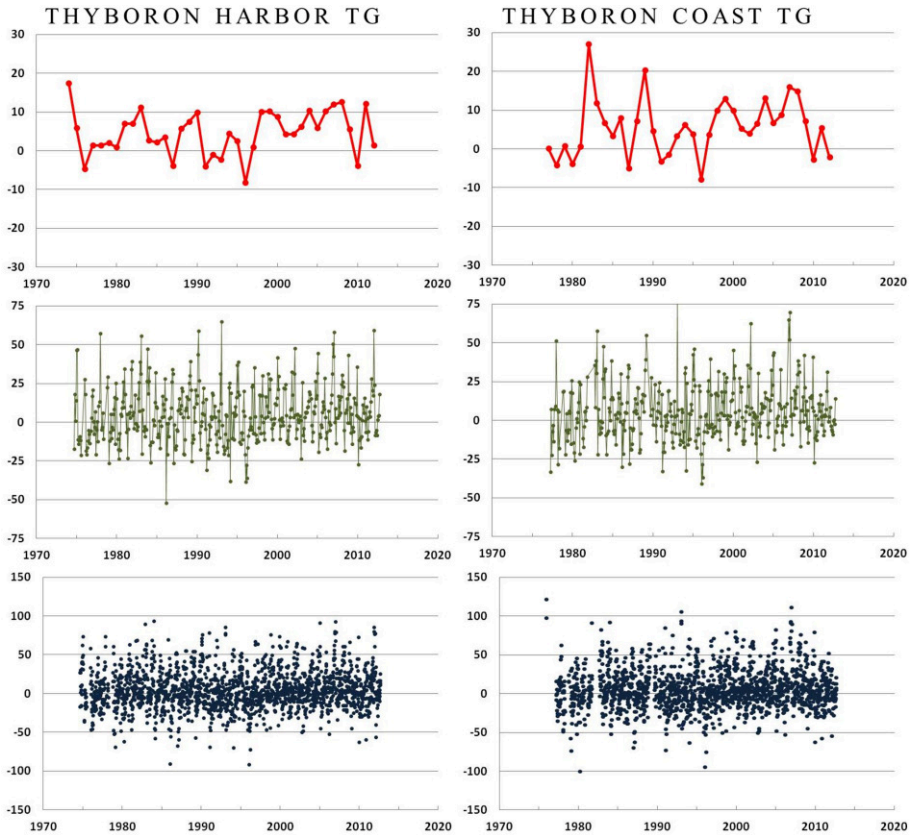

FIGURE 5 | Yearly, monthly, and weekly means (top to bottom) water levels (in cm) at the two Thyboron tide gauges. Discrepancies between the series are mainly due to data quality issues and to local wave setup effects during storms at the coastal TG (Adopted from Sorensen et al., 2015).

general water level in the fjord of c. 0.6–1.0 m DVR90, Figure S4. Regarding extreme water levels, a 100-year event at Thyboron Harbor is 1.93 m DVR90 (Thyboron Coast, 2.64 m) according to Sorensen et al. (2013) who also provide a list of the 40 highest water levels recorded. These show some variability in numbers and intensity over time at Thyboron Harbor, Figure S5.

Vertical Ground Motion

Observations of land deformation investigated from repeated benchmark leveling in 2006, 2009, 2012, and 2015 relative to an assumed stable point; from leveling the bottom of sewers in 1980/1900 and 2012, and from persistent scatterer interferometry (data from 1995 to 2001) all reveal the same pattern of subsidence, **Figure 6**, Figure S6. The subsidence rates of the bottom of sewers are up to 10 mm/year, from PSI up to 9 mm/year, and from leveling up to 7 mm/year, respectively, and results are thus consistent. Especially the independent results from PSI serve to validate the calculated leveling benchmark subsidence rates and vice versa. The two methods represent data acquired at different time periods points for the calculation of subsidence rates. Regarding PSI the measured rates of individual points are relative to the movement of a stable point that is only influenced by glacial uplift.

The PSI uncertainty is somewhat larger than from the leveling, but the spatial coverage (number of points measured) is larger and the risk of human error influencing calculations and thus the results is smaller. The separation in time points to the fact that subsidence is not a new phenomenon, and the subsidence does not seem to be restricted to individual buildings but is more widespread throughout the area (although differences may exist between building and ground subsidence rates). The apparent subsidence of the sewer system substantiates this. Also, there is a close connection between the year of construction of houses and infrastructure and rates of subsidence. This is, of course, not surprising considering the history of Thyboron (e.g., **Figure 2**). The area in SW which shows no/little sign of subsidence holds the oldest housing in town. Furthermore, the older parts of the harbor has probably been constructed on what was then believed to be the most stable location along the Thyboron Channel. Unfortunately, the digitization and investigation of historic leveling yielded little information that could be connected directly to the present study through "surviving" benchmarks. A few benchmarks have reliable results dating back to 1954, Figure S7, showing large subsidence rates on the then new-build dam north of Thyboron Channel, small but consistent subsidence rates of 1–2 mm/year in the more stable areas of Thyboron and on the Limfjord barrier, and stability north and south of the barrier, respectively.

The relative subsidence measured from leveling and PSI does not take into account the overall land movement from glacial

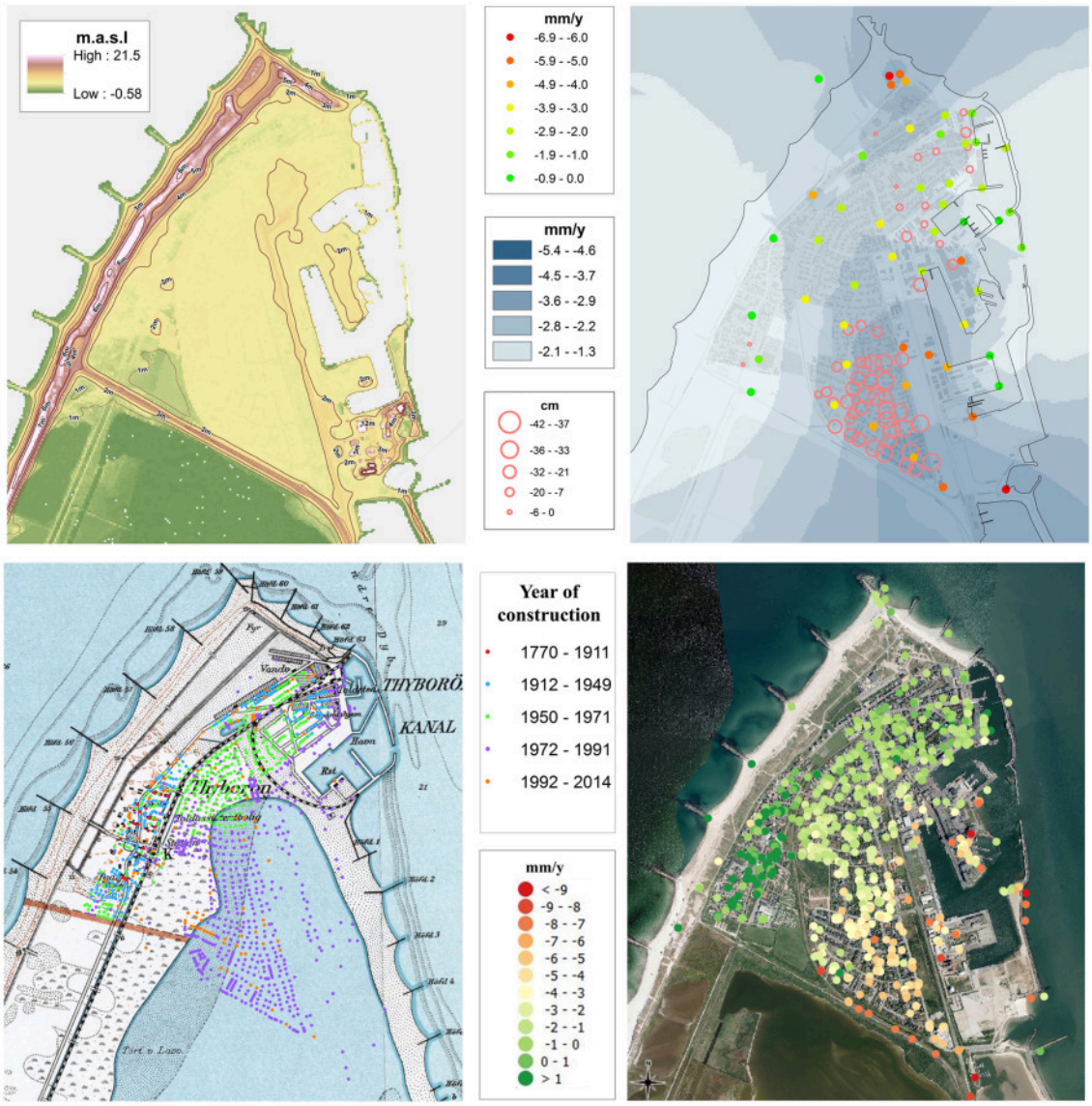

FIGURE 6 | The DTM of Thyboron shows the high dikes and dunes toward the North Sea. Also, the road into Thyboron is elevated above the general land surface of the town at or below 2.0 m (top left). Repeated leveling of benchmarks (colored dots) show subsidence rates of 1–7 mm/year (2006–2015) and from ordinary kriging a small area toward N and a large area toward S experience large subsidence rates, whereas areas toward SW and N are relatively more stable. Also, the total change (1980/1990–2012) of the bottom of sewers (circles) shown a pattern that seems to closely resemble that from leveling (top right). A spatial-temporal analysis of constructions years (bottom left) shows that most houses built after 1971 (blue dots) are located on a former part of the fjord (map from c. 1930). PSI-results show the same pattern of subsidence where the SW part of town is stable and rates of subsidence are increasing from N toward SE with rates of up to 9 mm/year (1995–2001).

effects. From the modeling an uplift value of $+0.6 \pm 0.2$ mm/year is found for Thyboron and slightly more for the stable benchmark at Vestervig, **Figure 7**. Here, +0.8 mm/year is used and added in the hydrologic modeling to the subsidence rates measured from leveling at individual points (to yield slightly smaller subsidence rates than from leveling alone).

Geological Modeling

The geologic and geotechnical information are combined in the geological model. Results of the preliminary work to render all available geo-information are presented at an N-S profile (position is shown in **Figure 4**) in the eastern part of Thyboron, **Figure 8**. The surface is generally at an elevation of 1.6–2.0 m DVR90 and the upper three meters (+2 – −1 m) consist of landfill (incl. reworked marine sand). The marine sand fill may include layers or lenses of varying thickness of organic material that contains plant remains and root and wood fragments.

Beneath the fill, a gyttja layer of a varying thickness (0.5–3.0 m) is found. Gyttja layers can be highly compressible. Below the gyttja is marine sand to −7 m, where marine clay is found. The model suggests that the surface of the marine sand and clay forms ridges, which may be interpreted as several former

marsh areas; some shallower than others. Along parts of the profile results are enhanced by inclusion of the DUALEM-421s results for the upper 1–2 m, Figure S8 (as **Figure 8** but showing DUALEM-421s results as well). The DUALEM-421s data, Figure S9, are difficult to interpret in most places due to the shallow groundwater level. The geophysical logging in well no. 44.571 SE of Thyboron (Petersen et al., 2008) indicates a high salinity in the groundwater. The DUALEM-421s resistivity measurements corroborate these findings but need verification from additional salinity measurements to e.g., map the salinity profile of the groundwater.

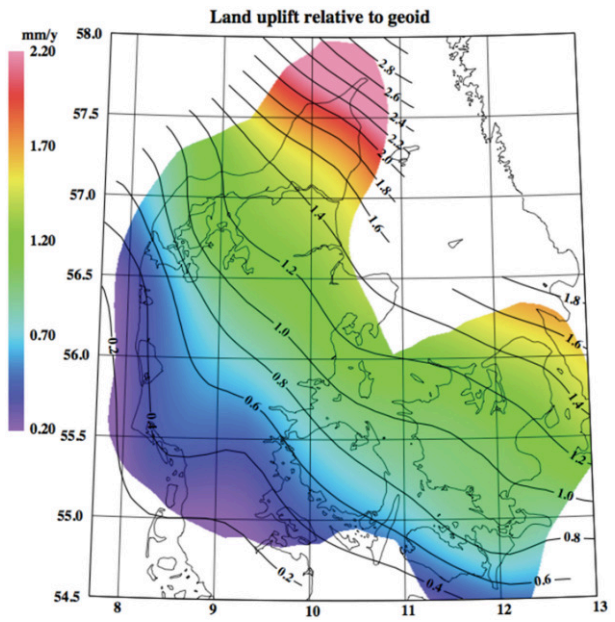

FIGURE 7 | The calculated land uplift rates for Denmark relative to the geoid .

Hydrological Modeling and Groundwater

Although, covering less than 4 months (Aug 15–Nov 15), initial results from the 10 groundwater monitoring stations are included but do not offer sufficient data for a thorough analysis of the spatial-temporal variations in the groundwater level due to individual factors like ocean water level and waves, precipitation, temperature and saturation, infrastructure etc. Still, observations are worthy of an inspection following a dry period in October and a wet in November, **Figure 9**, including a minor storm event in late November with water levels of 1.5 m DVR90 in Thyboron Harbor. To separate effects from high (or low) water levels and wave run-up at the North Sea coast, and very high/low water level in the fjord, and in the sluice regulated lagoon south of Thyboron, more data is needed. Results show, however, that groundwater levels vary by at least up to 0.5 m in a few months, **Figure 10**, Figure S10. Also, at some locations along the profile lines and elsewhere the groundwater is likely to be present just below the ground surface. Whereas the average groundwater level is lowering toward south in profile A*, the picture is more unclear in profile B* and needs further investigation including effects from roads/railroad, sewers and drains etc. Some attenuation of the signal is apparent in B7. This may be due to the proximity to the sluice regulated lagoon experiencing smaller variations in water level. When longer coincident time series become available from the groundwater monitoring stations, from the Thyboron TGs, and from newly established gauges on either side of the sluice, groundwater level variations will be investigated further and the profiles integrated in the geological model as well as the hydrological model.

In the MIKE modeling it is demonstrated that future subsidence will lead to an increased risk of flooding for both a 5 year and a 100 year precipitation event, **Figure 11**. As a result of the subsidence the sewer system will, and to some extent already does, experience stagnant water, sludge deposits, reversed slopes, and broken pipes leading to a dysfunctional sewer system accompanied with more frequent floods. Rainwater is pumped from the sewer and drainage system to the sea

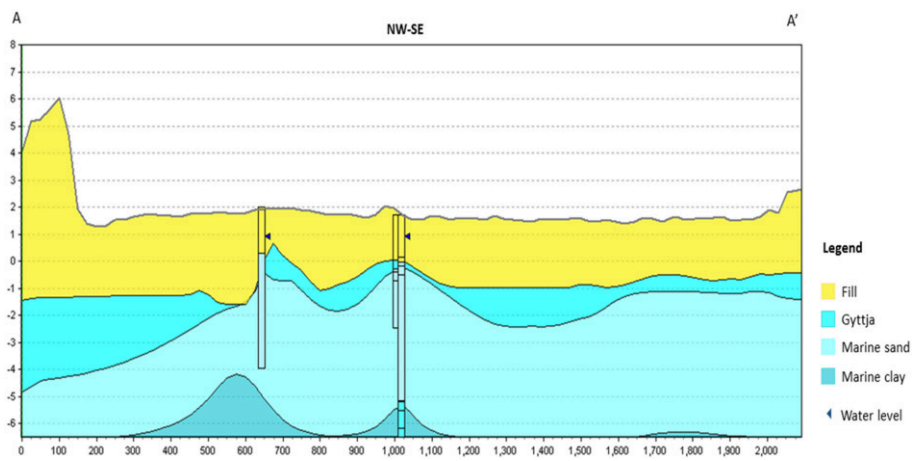

FIGURE 8 | Geological profile A-A′ of the upper 7 m stretching from NW to SE (unit m on both axes). The geological profile includes wells from Geo's well database with a projection distance of less than 10 m. The blue triangle represents the water level observed in the wells.

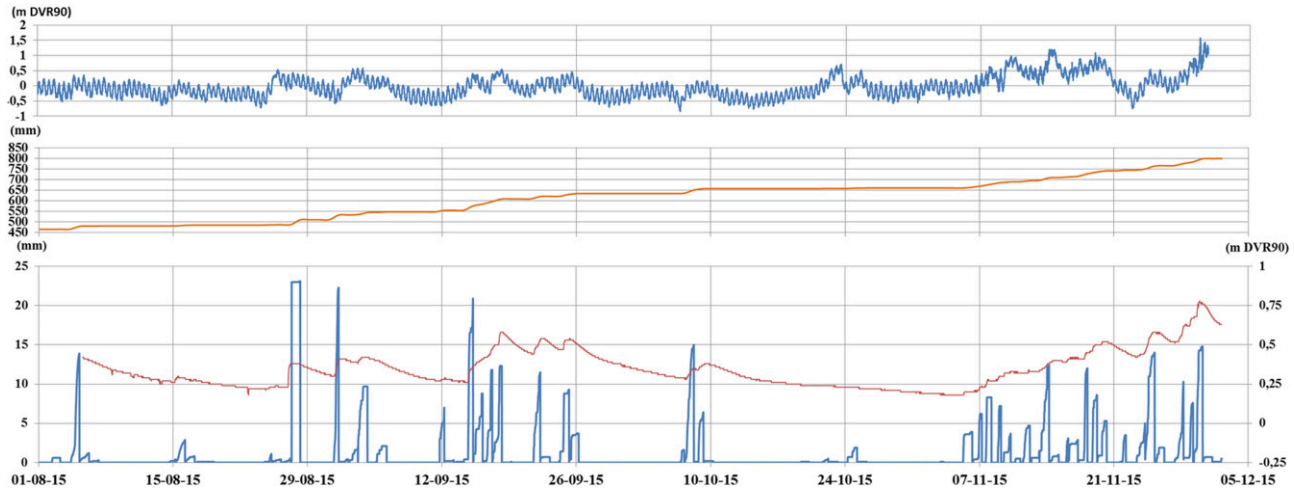

FIGURE 9 | Water levels at Thyboron Harbor tide gauge (top), cumulated precipitation for 2015 at Thyboron (middle), and daily precipitation (bottom) showed together with groundwater levels in borehole B7 for the period 5 Aug–30 Nov 2015 .

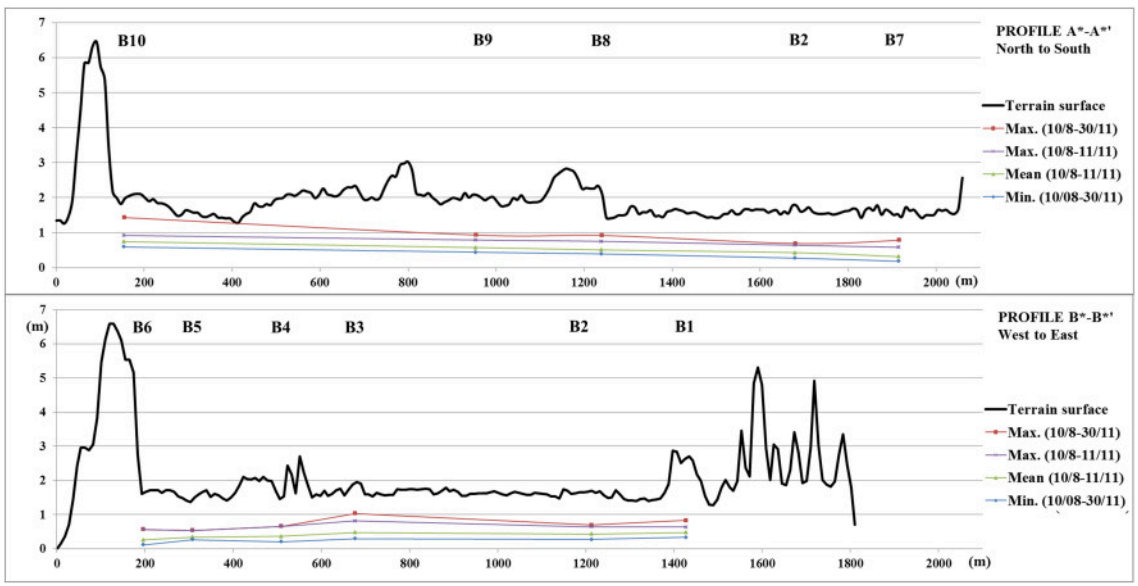

FIGURE 10 | Groundwater level. Terrain profiles A*-A*′ (N-S) and B*-B*′ (W-E) with measured maximum, mean and minimum groundwater levels from the station data series plotted. Total measuring period 5 Aug–30 Nov 2015 but due to the lack of from B4 to B6 in November, the mean and maximum have been calculated for the period 10/8–11/11. Lines between the stations are only indicative of the groundwater levels between stations. To the left (N and W, respectively) in both profiles the c. 6 m high dike is seen. The "spikes" in profile A* toward E are mounds of sand and gravel.

and a general rise in sea level has a minimal impact on the sewer ability to divert to recipients, whereas problems may occur during storm surges. As Thyboron is at the coast there is a clear relationship between groundwater and sea levels. Increased sea levels will lead to increased groundwater levels. This will increase the risk of seepage to leaking parts of the sewer system.

Rising groundwater stocks due to climate change (rising sea level and increased rainfall) can lead to a high water table where seepage is not possible all year round, especially during extreme water levels in the sea. At the same time an increased water table leads to the drainage system being filled with groundwater. This will significantly increase the risk of flooding in these areas as the existing drainage system is not working and a new sewage system must be constructed. A range of combinations of the modeled future scenarios may cause flooding at Thyboron, and many of the processes are coupled to enhance their effects on the hydrological system. As such, the hydrological modeling suggests that it is not the sea level rise itself that yields the largest impact but derived effects of prolonged periods of high ocean water

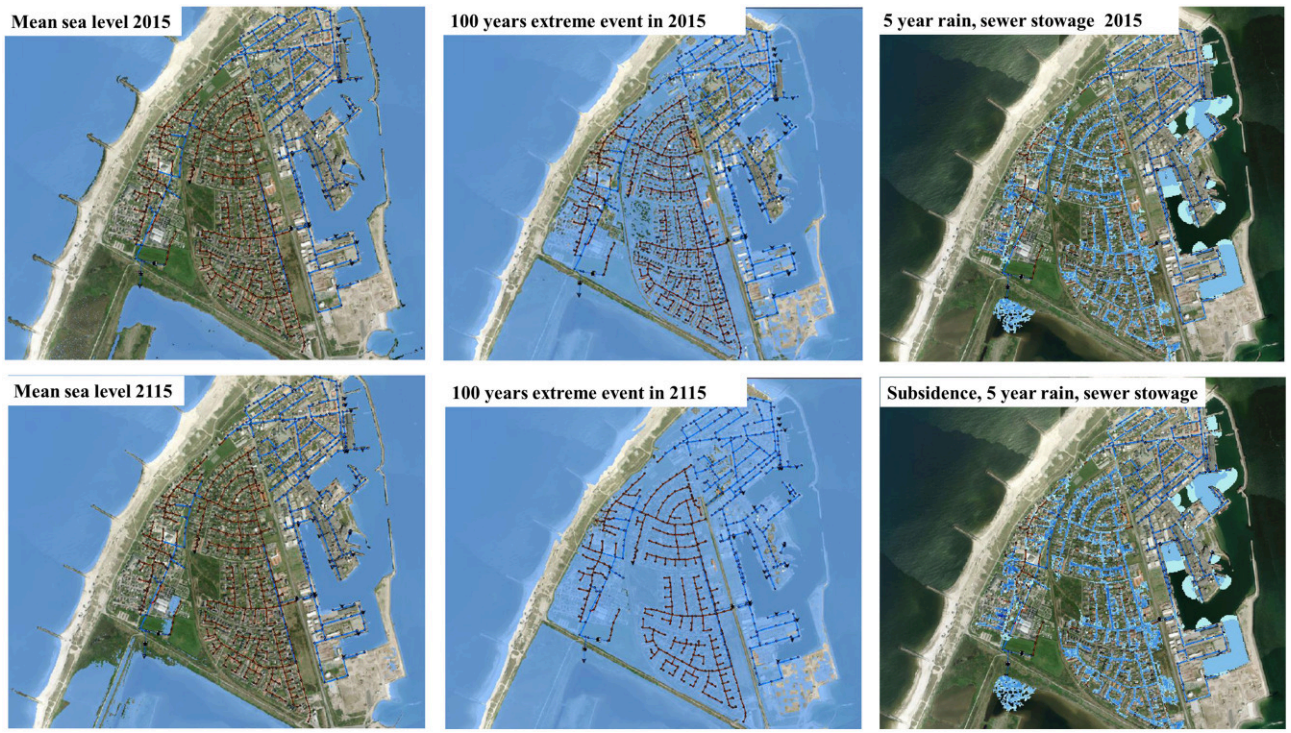

FIGURE 11 | Examples from the MIKE modeling. A rise in mean water level will in itself not have a significant impact on flooding in 2115 compared with today, even if the groundwater level is raised **(left)**. Today Thyboron is potentially at risk of getting flooded from a 100 year event. A similar event in 2115 including sea level rise and land subsidence will "drown" the town (a similar scenario potentially can occur in 2065) **(middle)**. The sewer system will experience increased stow up from precipitation with a raised groundwater level, or, due to subsidence **(right)**.

levels, extreme events, changing groundwater levels, and with subsidence being an important factor to increase flooding in both time and space e.g., through the degradation of the sewer system.

Stakeholder Approaches to Climate Change and Adaptation

The four main stakeholders identified and interviewed in relation to this study are each playing an important role in relation to climate change adaptation in Thyboron, **Table 2**. The Port of Thyboron feels a responsibility toward to their customers (e.g., ships berthing and companies residing on port property) but as stated: "This is Thyboron, and this is a harbor. We occasionally get flooded and then we clean up." Whereas most other business infrastructure and private housing in Denmark is partly covered by the "Danish national storm surge relief fund" for floods exceeding a 20 year water level event, this is not the case for harbor areas (DP, under revision). Individual business insurances may cover some losses but, in general, e.g., damages to buildings and production time losses are not covered. The Port of Thyboron does take actions to make buildings flood resilient to optimize their business, however, but does not perceive storm surges and climate change related floods as any immediate threat to their business and future development. The harbor accounts for a projected sea level rise related to an average life expectancy of 50–100 years for new quay areas, however. In recent years the harbor areas has experienced flooding on a couple of occasions but only in the case of much more frequent and severe storm surge events will the Thyboron Harbor act. The Thyboron Harbor is aware that the "underground is difficult" and is interested in more dynamic representations of the subsurface conditions. Finally, the harbor relies on a functioning sewerage system and, of course, is aware that sea water is most likely to pass harbor areas in order to flood the town.

LWW seeks to keep a service level to avoid flooding exceeding 10 cm on street level due to heavy precipitation up to a 10 year event, and through their large investments in the water and wastewater pipe systems and costs for maintenance; they have a strong economic interest in the future. House owners and other businesses (otherwise not considered here) are responsible for their own protection against flooding.

The Lemvig Municipality, of course, has an interest in keeping their citizens happy and to develop the community for the benefit of all. To a large extent this is done through the municipal planning act. Also, the abovementioned municipal climate adaptation plan, which is to be integrated in the municipal plan, serves as an instrument for mitigation efforts in relation to climate change and in the development of the community. Climate change adaptation is ranked fairly high on the municipal agenda—at least in the future, and is something that the municipality will have to deal with. But, as pointed out, there are many other and more immediate challenges that the

TABLE 2 | Tabulated summary of information provided from semi-structured interviews held with main stakeholders in September 2015.

		Danish Coastal Authority	Lemvig Municipality	Lemvig Water And Wastewater	Port of Thyboron
General	**Level**	**National**	**Municipal**	**Municipal**	**Local**
	Position/Role	State authority in the coastal area, including coastal protection, climate change and sea level rise. App. 70 employees.	Municipality (516 km^2; Pop. C. 20,000). App. 2000 employees, 200 in central administration, and 15 in Department of Nature and Environment.	An independent holding company under Lemvig Utility with all the shares owned by Lemvig Municipality. Actives for 600 million €.	Infrastructure and areal business which provides land and infrastructure for rent (900.000 m^2; 19 Employees; 4.5 mio. € turnover in 2014). A main fisheries port in Denmark.
	Main tasks	Adviser to the Minister; specific operational tasks, and permitting coastal protection in Denmark.	"Running" the municipality, planning, carry out council decisions. Climate a recent task of Nature and Environment.	Ensure clean drinking water to all citizens. Operation and maintenance of 600 km water pipes and 600 km wastewater pipes. Two wastewater treatment plants.	Costumers pay for berthing–everything that goes over the berth. 1200 people are employed in relation to port activities. Gross turnover 200 Million €.
	Main challenges	Working in a field with large time scale; here-and-now events create solution needs but also a need for long-term solutions when it comes to climate issues. Size for task performance.	People are moving away—diminishing finances. How to attract people? Size. Lack of professionalism as small municipality. Keeping sufficient specialized knowledge skills.	Our largest challenge currently is new rules and legislation in general. Tax is a potential problem due to large assets (pipes). Life expectancy of the pipe system.	EU fishing quotas. Growth limiting factor is a lack of skilled labor. Consolidation in the harbor sector—a need for new facilities. Water depth is important for growth (+10 m). Geography, a long way by land to get to/from Thyboron.
	Challenge: Climate Change (rank 1–10)	High in long-term (8–9)	Locally connected to the wind turbine industry. No major businesses working on climate action and solutions (2–3).	If you are prepared, you are able to control the consequences but if unprepared the "hazard" will be at 10.	Low (2–3) but addressed in new expansion projects.
	Challenge: Floods (rank 1–10)	High, as the costs are high to the affected people (8–9), in both short and long term.	(5) We can handle challenges. It costs a bit of money but we believe there are a number of solutions to mitigate flooding. Politically somewhat lower.	Floods are in the higher numbers (7–10).	(3–4) Short term; (8–9) Long term. Harbors are used to flooding. The height of the quays corresponds to the ships. We cannot heighten the quays and the areas behind.
	Responsibility in relation to floods	Contribution to EU Floods Directive's hazard, vulnerability and risk mapping; advice e.g., to dike associations and written guidelines for coastal planning in relation to floods.	Local preparedness and emergency staff. Climate plans. Preparation of contingency plans. Responsible planning and development. Assisting citizens with advice.	Participate in emergency events and have a clear strategy to prevent unwanted incidents.	Possible external emergency service. Port Control is ready and we are in contact with the skippers during storms concerning their ships, however.
Thyboron today	Experience with floods?	Many historic accounts nationwide and past national engagement mainly in the Wadden Sea and on the North Sea coast.	Yes, several in Lemvig latest in 2013 and 2015. Minor floods in Thyboron in 1981 and 2015.	In 2015 in Lemvig. The consequences were minor as we were well-prepared and know exactly at which level the water can reach without causing trouble. Some basements and houses were flooded, but no panic.	We have previously experienced floods—storm surges. By Consumption Centre and docks it can be handled but in the city and in business area it is a problem. In Jan. 2015 some flooding occurred.
	Current level of preparedness toward floods?	Low to medium, but the recent events have increased political focus. Know that a 1000 year event may occur. Can provide tools for municipalities.	No definite preparedness plan. A function in the Roads and Parks Department who know what needs to be done and when. Work is underway to develop true emergency preparedness plans.	Yes. We are prepared. But we are also aware that we currently do not have a preparedness level that can mitigate severe flood events. We do not have a clear goal in Thyboron like in Lemvig.	Fairly well prepared. The "Material Yard" has an action plan; the water enters, retreats, and then we clean up. This is how we see it. People are aware that floods occur, but you are from Thyboron and live with it. It is not something you discuss with people. It may change in the future.

(Continued)

TABLE 2 | Continued

		Danish Coastal Authority	Lemvig Municipality	Lemvig Water And Wastewater	Port of Thyboron
General	**Level**	**National**	**Municipal**	**Municipal**	**Local**
	Evaluation of Economic consequences	Partly through the Danish Storm Surge Relief funding scheme.	Only partly, cost for a jetty due for a replacement anyway. Insured losses in Lemvig.	No 2015 account in Thyboron, but very detailed for LWW costs in Lemvig.	Statements of the Dec. 2013 and Jan 2015 event cost for clean-up and repair. Some businesses also experienced economic loss but we do not have an account of this.
	Responsibility locally	DCA guarantees dike protection from a 1000 year event from the North Sea. Common agreement covers only the sea.	When making contingency plans for Lemvig this is also performed for Thyboron. Analyses for climate adaptation action ongoing.	We have a plan for severe precipitation events and must, in collaboration with Lemvig Municipality work on a common plan for sea floods also.	The port does not have a current plan to involve customers, since it requires that you can show the way. We do continuously work on making our assets more resilient.
	Actions taken	Maintenance of sea dikes and erosion protection (sand nourishments). Evaluation of the Thyboron Channel effect on water levels.	Few so far. From the head of emergency staff there is knowledge of that storm surge water levels may reach the streets of the town, but not violently.	For LWW the requirement is that people do not experience the sewers overflow and we have made a large effort to avoid this.	We now add 20 cm to allow for sea level rise. In maintenance work we have heightened a quay by 50 cm corresponding to the subsidence experienced at that location in the past 50 years. We have strengthened the outer breakwaters.
	Sufficient capacity to act?	Depends on level of action and the political agenda.	Yes. Floods gain little attention and only in the days following an event. In relation to comparable municipalities I feel we have made quite a large effort at a fairly early stage.	Yes, there is in the preparedness plan. We did however concentrate our effort in Lemvig in January 2015 where threats were more immediate.	The port can handle existing situations.
	Level of co-ordination/ collaboration between stakeholders	Systematic dialogue between stakeholders in conjunction with the Floods Directive and municipal climate adaptation plans. The insurance industry shows interest. No plan for flood management coordinated but a need for this in the future!	Good collaboration with e.g. emergency squad, Lemvig Water and Wastewater, DCA and other municipalities. Flooding linked to Thyboron Channel is a central issue. The regional body acts as a process facilitor. Dialogue with the Port of Thyboron in its initial phase.	During the Jan. 2015 event DCA delivered numbers and information. DANVA [Danish Water and Wastewater Association] may play a future role. Climate and climate change will become a point of discussion about whether DANVA should assist in this area.	Discussed with the municipality in connection with rainwater and groundwater. Good dialogue but there is no preparation.
	Strategy toward citizens/businesses	We inform. In general, a tendency toward that people do not accept floods—but also cultural/geographical differences.	In Thyboron they are aware of flooding hazards but not conscious of the overall challenges. We want substantial knowledge before orienting the citizens. This is a balance between "sufficient knowledge" and timely information.	Regarding business grounds this is contained in our collaborative agenda with the municipality. It describes that LWW must be involved and we have been 100% engaged in that. We also do provide individual advice to house owners.	Business approach—other players—coordination: We have addressed and discussed it informally—what to do in the town.
	Incorporation of CC in "business development"?	Working in the field of climate change/CCA is a core task to the DCA.	We would really like to. The current business support initiatives are not sufficient. We seek to create good stories/solutions that also yield added value e.g. to recreation and that are nice.	Yes, this is included to a high extent e.g., in relation to seepage. We will not accept overflow of treatment plants. And we build basins to contain water. The environment is also in the top-3 list. We cannot pollute at all.	We are not prepared when we get a sea level rise or higher storm surge levels and have not incorporated it in plans. A resilience plan could become a future task.

(Continued)

TABLE 2 | Continued

		Danish Coastal Authority	Lemvig Municipality	Lemvig Water And Wastewater	Port of Thyboron
General	**Level**	**National**	**Municipal**	**Municipal**	**Local**
Future and Solutions	Knowledge about climate change?	We know what we can expect based on international and national climate reports, but it is a field to be explored.	Resolved along with other tasks but lacks some professionalism to be sharp on solutions. We have the right networks and people to handle the job currently.	The more I get to know the more I feel I lack. If it affects our pipelines and treatment plants, we need to do something about it. We have already 100% separation between household and storm water sewers.	Future is left with the challenge of sea levels rise. Background is predictions from the DCA. The port can only look at existing buildings and increase their resilience. Dimensioning of storm water drain by new construction. CC is in our minds as something we are going to relate to.
	Knowledge about future flooding hazards?	We collect data and make tools but we rely on research and colleagues nationally and internationally working with these issues.	We keep track of storm surge levels. Cloudbursts are not a challenge at the same level. There are related issues with groundwater level and rising water levels where water cannot escape.	Land subsidence in some areas and sea level rise. Erroneously coupled pipes are a problem. Groundwater seepage into the pipes may occur e.g., during high-intensity precipitation. Local Drainage Solutions are in place, but in Thyboron there is no potential.	Large societal perspective, Municipality and State responsibility. The port sees itself as a business - not a public company. We are aware that we potentially will observe more frequent storm surges.
	Sufficient knowledge about CC to act?	Yes. The premise is that we must have a spread and not a real scenario or prediction. Because you can act in a span and not in a real climate adaptation scenario. This approach is typical Danish way to manage from.	We were instructed to make a climate change adaptation plan. It is a good idea putting together the problems. In this context, we feel quite safe, and we have started acting.	We have a good overview of all of our system and can determine where the risks are and act accordingly and prioritize our efforts to our economy. Our preparedness level is closely related to valid prognoses for the future.	We can act relatively quickly. We see the state government as unusually passive in relation to CCA and e.g., in relation to Thyboron Channel. The port would like to push, in favor of increasing the depth. But it is hard to be pioneers.
	Contribute to risk awareness among citizens?	More citizen-centered efforts; apps, early warning systems, alarms, etc. Communication is important and citizens must be involved in the risk management approach.	We plan for this. However, as long as the municipality does not inform about problems at public meetings, citizens probably think that what we do is ok!	To the individual citizen, they themselves still have a responsibility. We can provide counseling and advice if needed to minimize consequences of floods ahead.	In relation to customers, neither the Jan. 2015 nor Dec. 2013 made it topical. In relation to the Thyboron Channel debate, we will raise a voice as it concerns the entire town.
	Concrete measures and solutions planned?	Depends on the DCA role. The executive role are citizens or municipalities so that DCA should support this by including tools for their planning.	Private initiatives. Pump and dike associations were made to come together to work on common solutions and levels of protection and we seek more projects along this line.	We must still reduce seepage; and we need maintenance and renewal of sewers. For this we need numbers about climate change effects.	The culture out here is to be prepared, follow. You live close to it. Future measures are related mainly to the channel solution.
	Which meas., methods and tools best support CCA and DRM?	Value concepts needs to be unfolded to solve more problems simultaneously and look at the different values as well as intangible assets. Is it growth, socio-economic, etc. These values must be highlighted and promoted in the debate.	We would like to have some dynamic models. How does it look today and in the future? Clear future scenario(s). Models that can be linked to future scenarios; derived and being useful on an intuitive level.	Create data that can be translated into how climate, erosion, and land subsidence affect LWW pipe system and focus on the problems. Use tools and results, e.g., drawn on maps that project the land movement 10–20 or 50 years forward and 90, 50, and 10% probability. Similarly for groundwater level the median but include also deviations and extremes.	We would like realistic scenario in timescale of decades. Method development and methods to work with that include our infrastructure etc., and are simple and credible.

(Continued)

TABLE 2 | Continued

		Danish Coastal Authority	Lemvig Municipality	Lemvig Water And Wastewater	Port of Thyboron
General	**Level**	**National**	**Municipal**	**Municipal**	**Local**
	How can methods developed create value?	Increased focus on groundwater. The dynamics must be understood in order to illustrate the different conditions at a single decision basis. It must come from independent data to the "total" decisions. Complex issues need to be resolved complex! You risk losing important points if you oversimplify it too much.	Continuous and real-time monitoring of the land subsidence. Also, to be able to follow the level of the groundwater. Dynamic measurements instead of static. A little extra knowledge about the areas in and around Thyboron that can provide increased safety.	Then we need to combine the results. Useful models for how it looks and then put some consequences to it. The maps can lead to better understanding of the dimensioning of pipes in the future and be used by the Board in relation to our implementation. Data must be transferable to other systems.	Operating and investment terms: What should be solved/ issues, setting priorities, the economy in it etc.
	Does current legislation support desired path?	Need for a more pure authority processing and planning tools for municipalities. Need for new legislation that can support a holistic coastal protection focus, and not just individual casework!	The process has been good and democratic in relation to the dike associations. Like that, when we have challenges, we can handle them. But I am not quite sure what to do, when many other adaptation and mitigation efforts are dependent upon whether and when solutions are applied in relation to the Thyboron Channel.	The basis is how the economy is linked. Today we have economy and climate pools to use. AEP 2 (Aquatic Environment Plan from EU) should take fundamental account of CC. If there are gaps it may be difficult to handle through regulations and acts. We have different challenges than in larger cities. Each exposure is weighed very high and may reduce the degrees of freedom for further work.	Adapting to climate change takes place in terms of whether it is man-made—you relate to that it is a problem—but not how to approach the problem. Danish Ports: Where is the debate—It's not there. The industry currently focuses elsewhere and therefore climate in the background. Climate and adaptation issues are not a part of Ports Legislation and should not be. Still, the state must take a more prominent role.

municipality has to tackle and climate change adaptation has hitherto not been the most prominent. That said the municipality still feels that it is ahead of many other Danish municipalities regarding hazard mapping and addressing future challenges, e.g., by initiating investigative work in relation to Thyboron. The citizens of Thyboron have a reputation of coping and not complaining, an impression shared with the DCA and Thyboron Harbor, and the municipality has so far not invited the citizens to participate in the broader adaptation work. The reason for this is that the municipality wants a more elaborate scientific background and ideas about where they are heading before engaging the community. The municipality does, however, inform the citizens individually when needed and takes interest in local water related challenges. The Lemvig Municipality sees the continuous expansion of the Thyboron Channel and its effect on current and future storm surge water levels as the overarching future adaptation challenge to Thyboron. The town's mitigation and adaptation measures will very much depend on whether and which solution to decrease the amount of water entering the fjord is implemented. Besides looking into local actions, the municipality is therefore active both politically and in a cross-municipal project funding search with other municipalities bordering the Limfjord to reach a future solution regarding Thyboron Channel.

The DCA is in charge of the implementation of the EU Flood Directive and is responsible for preliminary national flood hazard assessments and for the hazard, vulnerability, and risk assessment and mapping for areas appointed under the Directive. As mentioned before, DCA also is responsible for the erosion and flooding protection of Thyboron from the sea, currently in 5 year plans with economic contributions from Lemvig and other municipalities along the central Danish North Sea coast. DCA thus has a strong focus on the protection level toward the sea in Thyboron and, more general, a focus on tools for risk reduction and decision-making to e.g., municipalities.

Common to the stakeholders is the acknowledgment that coastal floods and climate change are factors that must be addressed and taken into account in future planning. Although, the perception of the timescale needed for action differs between the stakeholders according to their core business areas (and depending on potential future flooding experiences!), they all agree that collaboration is important to achieve the best solutions. Except for some co-work between the LWW and the municipality, no such collaboration is operational yet when it comes to coastal hazards and climate change adaptation. The stakeholders have quite varied needs for data, information, knowledge and tools. Whereas the Danish Coastal Authority sees itself as a provider of tools etc., as experts on coast protection and coastal climate adaptation and does give legal and coastal engineering advice, the LWW and Lemvig Municipality have fairly detailed but different demands for updated information and "dynamic results." Port of Thyboron basically wants "a number to plan from."

Although, direct questions about economy and funding were deliberately omitted—this will soon enough become a matter

of attention, the interviews still provide some information on stakeholders' positions and ability to engage in collaborative efforts for climate change adaptation. The LWW essentially only has its customers to pay for adaptive measures, but they are forced to safeguard their investments in water supply and sewerage in relation to future conditions. The municipality is financed by the tax-payers and has to prioritize their initiatives very strictly in a time of budget-cuts due to a decreasing population, and the Port of Thyboron basically sees itself as a private enterprise with no formal responsibility toward climate adaptation and mitigation of the town of Thyboron. The three stakeholders to some extent all point to the national government to take a lead in adaptation and to assist economically. Opposed to this, DCA takes the economic responsibility given by the legislation and lets politicians make decisions regarding the national economic engagement at Thyboron and elsewhere in Denmark. However, through its scientific work DCA continuously aims at providing knowledge and better tools for decision support.

DISCUSSION

The investigated coastal climate hazards from sea level rise and associated effects from storm surges, prolonged periods of a raised water level, and a general rise in the groundwater level will in combination with precipitation and land subsidence adversely impact the local community of Thyboron, Denmark. The future coastal erosion, erosion protection, and the effect of morphodynamic changes on storm surge levels in Thyboron due to an ongoing expansion of the cross-sectional area of the Thyboron Channel are additional challenges not considered in the present study. They, too, are significant in the evaluation of future options for adaptation and planning. Some results are preliminary and need further work. They are included to exemplify potential links between processes and impacts to the different sectors and main municipal stakeholders with interests and responsibilities in relation to adaptation in Thyboron. As such both scientific and societal aspects of hazards and impacts are parts of ongoing investigations into how coastal climate change issues are addressed to stakeholders to reveal their motivation, ideas, and needs in relation to knowledge and tools for adaptation management in each of their areas, and to create a local platform for transdisciplinary collaboration for mitigation and adaptation.

Toward Transdisciplinary Research and Collaboration

The development of a common language and to move from consulting to participatory transdisciplinary research (Mobjörk, 2010) and management may prove viable in Thyboron in relation to climate change adaptation. Serrao-Neumann et al. (2015) reviewed transdisciplinary literature and approaches, and provided learnings about sectorial and cross-sectorial climate change research and management of climate change impacts in SE Queensland, Australia. Particularly relevant to this study are the authors' reflections and conclusions regarding the concept of learning-by-doing and doing-by-learning concerning the development of theoretical knowledge from practice, and the development of practical knowledge from theory, respectively, proposed by Loorbach and Rotmans (2011, cf. Serrao-Neumann et al., 2015): learning-by-doing was pursued by engaging stakeholders representing all sectors and various scales (local, regional and state), and, the research team was able to integrate the practice/corporate/agency knowledge across sectors when formulating and refining adaptation options. In parallel, doing-by-learning was carried out by reframing adaptation options proposed in the literature to improve their capacity of being adopted and implemented in a pragmatic way based on stakeholders' feedback. In addition, a solution-oriented transdisciplinary research collaboration (opposed to a problem-oriented) was an advantage; and a selected sector can successfully be used as a platform to (re)integrate and apply created knowledge according to Serrao-Neumann et al. (2015).

At our local study location, the implementation of concrete adaptation measures is a matter of (preliminiary) discussion but cross-sector and transdisciplinary co-work is only slowly forming. Still, inasmuch as learnings are transferrable across scales, our work corroborates the findings of Serrao-Neumann et al. (2015) that transdisciplinary research is conducive to climate adaptation research. The research and cross-sector collaboration presented here has gradually evolved from a scientific interest in flooding hazards, data provision from leveling by national authorities, and an interest in these results by the local municipality. In relation to the work ahead several factors may prove advantageous: The currently involved stakeholders represent both public and private actors across levels of governance and legislation, and a common understanding of the legislative frameworks is already established. To some extent the political and/or economic standpoints of the individual actors have been clarified, and an initial platform for collaboration is "under construction" based on the research presented with positive (and realistic??) expectations from the stakeholders. Still, methods for the integration of knowledge need to be defined (e.g., Hinkel, 2008).

The research thus grows from a combined natural science and science-governance perspective. As the Thyboron Harbor, DCA and LWW mainly are technically founded, a technology/science base may well serve as the platform for transdisciplinary work and integration—gradually bringing in more social science oriented work. Although, there is a political agenda for adaptation actions, the "slow and small start" with no imminent need for actions may become a great advantage toward transdisciplinary work to decide upon optimal adaptation and mitigation measures. One major threat may be impatience among actors, including academia, to reach results, and another is a lack of focus on the process by the involved actors.

As climate change impact manifests itself in ways that do not consider administrative borders the identified main stakeholders must, although working in different areas and on different timescales for e.g., investment and maintenance, work together in a common appraisal of the challenges faced. By somehow deflecting scenarios of sea level rise, which can be difficult to relate to and address, into very concrete results on the natural

processes this provides an alternative way of addressing climate change impact. For instance, the ongoing land subsidence is very concrete and easy to relate to for all stakeholders although the subsidence rates ahead may be governed by the same level of uncertainty as sea level rise. The measured land subsidence will almost certainly increase the vulnerability toward flooding, however. Here, the transformation of scientific knowledge into applicable measures can optimally provide a platform for this common work. In addition, the research presented seeks to explore how existing and new data can be utilized for this purpose. As such the work mainly addresses the transformation of current scientific knowledge for use in decision-making to create a joint platform for data, knowledge (sharing), and planning that satisfies the individual needs of the stakeholders, and at the same time optimizes the decision-making process to provide better common solutions for adaptation and planning—in Thyboron and elsewhere.

The presented research implicitly intends to address the added-value of cross-sectoral collaboration in climate change adaptation from private consulting and local companies, municipal and national government levels agencies, and academia. As these entities have different scopes of work that all must be satisfied within such a framework, a large effort must be made to clarify scopes, agendas, and perspectives of engagement to reach a consensus for collaboration. Equally, the research and development work must bear implications of advancement in a wider sense (e.g., economically through the transferability of results and methods developed, added value of data, business and research advancement, and optimal local solutions). This is no easy task as such co-work necessitates excursions into the unknown and at the same time it requires continuous attention to provide concrete results to the local politicians and decision-makers. Also, all material must be shared in a clear and concise way to be comprehendible to all actors. The research and local adaptation work has not yet addressed and engaged the local inhabitants. This is one of the forthcoming challenges that also call for enhanced inclusion of social sciences as well as someone to take responsibility of the process work ahead. So far, addressing common challenges between stakeholders seems a good starting point for collaboration.

The Probability of Sea Floods

Quality reassessment and analysis of two digital tide gauge series (late 1970s–2012/2015) from Thyboron have provided reliable results of the water level variations. Especially the harbor TG series (with additional data extending back to 1935 still in an analog form, and some daily recordings dating back to 1874) seems robust. A comparison of the harbor TG with the long TG series from the Danish North Sea coast at Esbjerg and Hanstholm shows a good correlation in the annual means. This potentially provides sea level research with additional data from the North Sea coast, and at this stage of investigation justifies that regional projections of water levels can be used for Thyboron, too. In addition, extreme water levels at Thyboron show a marked decadal variability. This variability is to be investigated further e.g., in a comparison with other TG series in Denmark and from the countries bordering the North Sea. The extremity of events in the Danish North Sea TG data has to be evaluated very carefully due to local effects in both open coast and harbor locations. For Thyboron Harbor a 100 year event has previously been calculated to 1.93 m DVR90 which is used in this study. This level is according to the digital elevation model just above the threshold where sea water may potentially flood large parts of Thyboron. As the three most extreme recordings at Thyboron Harbor TG are between 1.85 and 1.90 m DVR90, and the harbor area is flooded at c. 1.80 m DVR90, special attention to the most extreme events must be given ahead in relation both to the statistics, and to the actual probability of flooding. So far, the town has only experienced minor floods except on harbor areas. The 100 year event has been used in the hydrologic flow modeling, and scenarios of future extremes are based on Grinsted et al. (2015) adding SLR only to current statistical extreme water levels.

Land Deformation and Perspectives

Thyboron is subsiding. As the surface elevation generally is between 1.4 and 2.5 m DVR90 subsidence is relevant to consider in relation to the current and future vulnerability to flooding. Repeated precise leveling campaigns in 2006, 2009, 2012, and 2105 provide a detailed and quite unique dataset, at least in a Danish context, to show subsidence rates of 2–7 mm/year and with the largest rates toward SE. A recalculation of the leveling and corrections of the height benchmarks should be performed the next time the assumed stable points are connected to the national network. This will not change the overall results substantially but will connect the local, relative measurements to regional and national scale vertical land motion.

Considering the historic development of Thyboron over the past 100 years, subsidence may not come as a surprise as large parts of the town rests on landfill on the former fjord bottom. Only the oldest part of the town—residing on a previous fjord holm, does not experience any substantial subsidence, except perhaps c. 1 mm/year as witnessed on the barrier N and S of Thyboron, respectively. The leveling results are consistent and rates are, to a first approximation, considered linear between the measurements (9 years). As witnessed from aerial photographs and house registers there is a strong correlation between subsidence rates and time of landfill, and it is assumed that the thickness of fill material is larger toward SE. As the bottom of sewer wells show a similar pattern of subsidence (up to 10 mm/year) it is also assumed that the entire area is subsiding. The differentiated subsidence between N and S has led to broken pipes and to reverse sloping of the pipes at a considerable cost to the Lemvig Water and Wastewater Company over the past years.

Although, local land subsidence is a well-known phenomenon, data from Denmark are scarce. Detailed leveling is costly and densification and/or renovation of the Danish height system have not been carried out in many areas. Benchmarks were established by the Danish Geodata Agency in assumedly stable positions to avoid e.g., organic soils susceptible to land movement. However, local land subsidence issues have gained attention recently due to their adverse effect on flooding vulnerability, and other local areas of subsidence are currently being identified (Broge et al., 2013). In a Danish perspective a geographic focus of investigation may be related to coastal towns

where low-lying former meadows have been urbanized in recent decades. Like in Thyboron, a screening that combines historical landscape information, house registers, and satellite imagery may be a viable way to proceed.

The PSI Insar mapping of Thyboron from 1995 to 2001 ERS satellite data provides results that are consistent with the leveling in terms of both subsidence rates and spatial variation. Although, separated in time, the leveling and PSI methods and results compliment and validate each other. Despite the low-resolution imagery compared to newer satellites' coverage, the PSI results appear to reflect the differentiated subsidence pattern in Thyboron very well. The difference in subsidence rates within the small area of Thyboron is a main reason for the good results. A combination of the two methods, e.g., by normalizing the PSI rates to the benchmark rates from leveling can be attempted ahead to enhance the spatial resolution and provide a more rightful map of subsidence than applying an ordinary kriging method from leveling as performed here.

PSI methods are used in many studies for detection of land subsidence in relation to coastal flooding hazard mapping. However, it is the first time convincing results are presented and validated by detailed leveling in Denmark. Knudsen et al. (2011) did not reach univocal conclusions regarding the method's applicability in a coastal setting (Esbjerg). Pedersen et al. (2011) initially set out to relate to coastal flooding in their work but the quality of mapping was not sufficient to address this further. Here PSI methods are applied directly in relation to the investigation and evaluation of coastal climate impact. When sufficient Sentinel-1 satellite data are available for subsidence mapping in mid-2016 (expectedly), this will provide access to near real-time (repeat cycle 12 days) subsidence mapping in Thyboron and the rest of Denmark. This will potentially become a strong tool to the local stakeholders provided that a service is set up to monitor the changes and deliver the results. With the launch of the twin Sentinel-1 satellite in April 2016, data acquisition frequency will double to the benefit of future updates of satellite based subsidence maps.

The rates in Thyboron are liable to decrease over time depending on the causes of subsidence. This is to be investigated further. However, we assume linearity (until 2065) in the rates from leveling in a first appraisal of the combined effect on flooding from land movement and sea level rise. This allows a dynamic modeling of the cumulated elevation changes in the DTM. As both the leveling and PSI methods show relative values, 0.8 mm/year uplift from GIA in the Danish uplift model [S1] is added to the rates and used in the hydrological model (using the ordinary kriging interpolation). The results show that the relative change in sea level also bears implications on sea flooding inland and not solely at the coast/at tide gauges.

GIA rates are small ($\approx 0 - +2$ mm/year) as Denmark lies at the margin of the last glaciation and thus also at the edge of most Fennoscandian GIA and uplift models. With the increased accessibility to land movement information ahead, this will allow for improvement of both the uplift model on a national scale (better fit to data) and yield a more detailed picture of regional (e.g., due to tectonics and basin compaction) and local deviations from the overall pattern. As the results from Thyboron show, land subsidence is, indeed, a factor that must be accounted for locally in Denmark.

Subsurface Interactions

Consideration must be given to sea level—groundwater interactions. Permanent or temporary changes in the groundwater level may affect the coastal flooding risk. Also, the geology plays a role. Although, the short data series (Aug–Nov 2015) from the 10 stations are too short for a detailed interpretation, variations in the groundwater level exceeding 0.5–0.8 m are witnessed, and by the end of the investigated period the groundwater levels is less than 0.6 m below terrain at low-lying stations, and likely less at some unmonitored locations. Groundwater is already a challenge in Thyboron. The groundwater information will enter the ongoing 3D geological model setup to couple to the geologic and geophysical mapping of the upper layers, which is expected to provide a more solid basis to interpret causes and magnitudes of subsidence and provide information that can be rendered useful for the hydrologic flow modeling and interpretation. With the increased repeat cycle of e.g., the Sentinel 1 satellites' imagery, seasonal variation in subsidence rates and the potential relation to the groundwater level can be resolved.

The coupling in a model of engineering geological and geotechnical analyzes and satellite borne subsidence mapping opens up a range of options, too. In and around Thyboron a large amount of geological and geotechnical parameters have been collected from decades of experience in construction works. By comparing these data with other available data in a 3D model, spatial analyzes of the underground conditions in relation to subsidence mapping can be performed. This allows for a comparison of cumulated layers of filling and observed compressible layers with actually recorded subsidence rates. Analyzes may also include geotechnical strength parameters, water content of sediments, and historic hydrological observations of water levels. Since the data coverage of the geotechnical information in Thyboron area is not evenly distributed spatially, the possible relation between subsidence rates and thickness of filling layers etc. from areas of good coverage may be used to predict thicknesses expected in areas which are not covered by geotechnical information. Satellite based subsidence mapping will then become a very useful source of data to support the establishment of engineering geological models for the area to be used by the individual stakeholders with a spatial interest in the area. The models can then be used in conditional assessments and climate proofing of existing facilities and infrastructure, in future design and planning, as well as for economic risk analysis of future investment conditions. This also means that subsidence attenuation better can be estimated and used in planning.

The DUALEM-421s geophysical results were not very successful due to the shallow and saline groundwater table (and limited spatial coverage). In other areas the method will contribute to detailing the 3D model (up to 10 m depth), however. Typically, geophysical surveys are constrained by existing infrastructure, land-use, access, noise sources in the area (metal fences, wires in land, buildings, etc.). The geophysical

mapping can only be expected to cover certain areas of an urban environment, and should always be correlated against existing or new geotechnical wells to support the interpretation of the measured resistivity in the ground. Opposed to this, existing geotechnical data are typically located in or at the footprint of buildings. In this study it has therefore only so far been possible to correlate the geophysical data with the geological and geotechnical observations in a relatively small area in the SE part of Thyboron.

Insights gained about the subsurface geology will nevertheless be useful to the stakeholders. Based on the interviews the interest in the subsurface conditions may become a pivotal point of collaboration, and further research into the relations between geophysical subsurface properties, land subsidence, and future coastal climate change impact may reveal hitherto unrecognized connections for which existing geotechnical data may be utilized.

Flooding Thyboron

Through the hydrologic flow modeling in MIKE an initial assessment of the impact from sea state, precipitation, and land subsidence on the sewer system and flooding extent and depths has been made for a range of future scenarios based on the research results from land movement in this study and climate change scenarios for precipitation and sea level rise. At the current stage the modeling serves to gain insight to the relative importance of the various contributors; individually and in combination. Results are not interpreted into detail, and the model will subsequently be refined e.g., by use of the updated version of DK-DEM that is expected for release in 2016. The updated DK-DEM samples aircraft Lidar data with a much higher point density (4–5 points per m^2) to allow for a better resolution of surface features to lead to an improved modeling of surface water flow and accumulation. This is accomplished by updating hydrologically important features such as sluices, aqueducts etc. to produce a hydrologically conditioned elevation model.

Whereas sea level rise in itself is unproblematic according to the model results, a generally rising groundwater level in combination with subsidence is a flooding challenge. In addition, this will severely affect the entire sewer system. Interestingly, precipitation will also increase the probability of flooding and is locally a focus of attention today. Ahead the surface flow and surface-sewerage interactions will be investigated in further detail based on the abovementioned updated DK-DEM, as well as the model will incorporate the joint probability of heavy precipitation and storm surges.

The low elevation threshold means that a large part of the town already today potentially may get flooded from a 100-year storm surge event. In 2115, flooding depths may potentially exceed 1 m on a regular basis. Measures to increase the threshold level for flooding are being planned by the municipality based on the modeling results and include heightening of the lowermost areas toward the northern part of the harbor. Here, an old and small dike has been neglected for decades and can fairly easy be restored to increase the current protection level from storm surges. This measure will probably satisfy the local politicians' call for action for a while. It will not deal with long term challenges nor will it address future adaptation and planning needs, however. Ahead, further work is needed on the modeling to yield more detailed results that also take into account e.g., dike strength, wave overtopping, morphodynamic changes, and to improve the relation between subsurface processes and potential flooding.

Work and Research Ahead

The stakeholders do state very different needs for knowledge and models about climate change at the current state. Although, the Port of Thyboron states that climate change adaptation is not a part of their business foundation, an enhanced knowledge about e.g., subsurface processes, geology etc. definitely will provide them with a useful platform for development. The point is that challenges related to climate change can also be addressed as something else and carry the knowledge and capacity-building forward. It is the shared opinion by the main stakeholders that people from Thyboron do not panic or complain. It is a part of their culture. A couple of severe flooding events can change this, of course, but ideally this provides a less hectic environment and provides time and room for the stakeholders to reach a common appraisal of the future challenges.

The presented research from Thyboron can be seen as the first step toward creating a common platform for integration of knowledge and data for climate adaptation and planning. However, the main stakeholders show a strong interest to build this platform together. It is also indicated that existing data can be revitalized and, especially in combination with in situ and satellite data, become very useful in creating tools to monitor and project climate change and impact in Thyboron and to allow for dynamic updates, as the scientific knowledge about what to expect advances.

Although, the presented transdisciplinary approach is very valuable, it also requires a high degree of coordination between the various professions and scientific disciplines. In a long term an optimization of the framework is essential, e.g., by providing free data through the Danish "basic data program" with standardized data formats. This will moreover strongly increase the popularity of data amongst the private sector and in this way support the advancement of perspectives for the concept provided.

CONCLUSIONS

Low-lying coastal towns may face severe challenges in relation to a changing climate. From a transdisciplinary approach in the community of Thyboron on the Danish North Sea coast, climate change impact on future flooding vulnerability has been investigated and related to the main stakeholders. Results from repeated precise leveling and satellite methods consistently show that Thyboron is subsiding by 2–7 mm/year which will adversely affect the flooding probability and extent ahead. Preliminary results presented in relation to the coupling between sea state, groundwater level, subsurface geology, the sewer system, and the observed land motion show increasing challenges ahead. The results have been addressed in relation to the responsibilities of the main stakeholders and their needs of knowledge, tools and models for planning and adaptation. By addressing potential

water-related impact from climate change in a very concrete form, the stakeholders can more easily relate to the complexity and uncertainty in climate scenarios and projections. The combination of a revitalization and use of existing data, and in situ and satellite data collection is promising and may provide for better adaptation and planning measures, not only in Thyboron but also in other communities in Denmark and elsewhere.

AUTHOR CONTRIBUTIONS

CS constructed the research framework and set-up, participated in all areas of the work including the conduction of interviews, field studies, data analysis and interpretation (except the hydrological model setup), and wrote the initial version of the manuscript. KV planned and led the calculations of the precise leveling campaigns. NB led the PSI data interpretation and collaborated on the precise leveling. MM led the geological and geotechnical data collection, interpretation and geological model setup. PT led geophysical data collection and interpretation, CSS led the data collection and the model setup for hydrological modeling, and PK did the main work on land uplift model setup and calculations and participated in the quality assessment of benchmark calculations. All authors have contributed with input, discussions, and critical comments to the final manuscript.

ACKNOWLEDGMENTS

The authors wish to acknowledge and thank Bo Hviid Nielsen, Albert Jensen, and Jan Nielsen (Lemvig Water and Wastewater) for implementing the groundwater monitoring campaign and for sharing their "subsurface" stories; Pieter Mogree, Kirsten Harbo, and Martin Ronn Hansen (Lemvig Municipality) for providing local information and data; Britta Bockhorn (Geo) for assisting in preparing the geological model; and Roar Engell, Danish Geodata Agency, for assisting in preparing leveling data and graphic work. Christian Vrist and Jesper Holt Jensen (Port of Thyboron), Lars Norgaard Holmegaard (Lemvig Water and Wasterwater), Merete Lovschall (Danish Coastal Authority), and Thomas Damgaard (Lemvig Municipality) shared their views, ideas and visions for the future of Thyboron in relation to coastal climate adaptation and planning. For this we are grateful. Co-funding for an Industrial PhD scholarship (Grant no. 1355-00193) is provided by Innovation Fund Denmark.

SUPPLEMENTARY MATERIAL

The Supplementary Material for this article can be found online at: http://journal.frontiersin.org/article/10.3389/fmars.2016.00069

REFERENCES

Andersen, H. L., Thorsen, G., and Hauerbach, P. (1996). "Geotechnical and geological aspects of differential subsidence in the Skaw Spit, Denmark," in *Proceedings of the XII Nordic Geotechnical Conference: NGM-96, Vol. 1,* eds S. Erlingsson and H. Sigursteinsson (Reykjavik: Icelandic Geotechnical Society), 339–346.

Arns, A., Wahl, T., and Jensen, J. (2015). The impact of sea level rise on storm surge water levels in the northern part of the German Bight. *Coast. Eng.* 96, 118–131. doi: 10.1016/j.coastaleng.2014.12.002

Binzer, K., and Stockmarr, J. (1994). *Geological Map of Denmark, 1:500 000. Pre-Quaternary surface topography of Denmark.* Copenhagen: Geological Survey of Denmark.

Bosello, F., and De Cian, E. (2014). Climate change, sea level rise, and coastal disasters. a review of modeling practices. *Energy Economics* 46, 593–605. doi: 10.1016/j.eneco.2013.09.002

Broge, N. H., Vognsen, K., Steffensen, F., Sonne, I. B., Sørensen, C., Knudsen, P., et al. (2013). *Kortlaegning af Omraader Med Foroeget Sandsynlighed for Landsaenkning, Vol. 17.* Technical Report Series, Danish Geodata Agency, Copenhagen.

Bruun, P. (1954). *Coast Stability*. Copenhagen: Danish Technical Press.

Bruun, P., and Gerritsen, F. (1960). *Stability of Coastal Inlets*. Amsterdam: North Holland Publishing Company.

Christensen, B. B. (2011a). *Stormflodsundersoegelse i Limfjorden. Modelgrundlag, Kalibrering og Foelsomhedsanalyse.* Technical Report, DHI for the Danish Coastal Authority, Horsholm.

Christensen, B. B. (2011b). *Stormflodsmodellering Vestlig Limfjord*. Technical Report, DHI for the Danish Coastal Authority, Horsholm.

Dangendorf, S., Marcos, M., Müller, A., Zorita, E., Riva, R., Berk, K., et al. (2015). Detecting anthropogenic footprints in sea level rise. *Nat. Commun.* 6, 7849. doi: 10.1038/ncomms8849

DCA (1975). *Limfjordstangerne, 1975*. Lemvig: Danish Coastal Authority.

DCA (2013a). *Kortlægning af Fare og Risiko for Oversvømmelse*. Metoderapport. EU's Oversvømmelsesdirektiv (2007/60/EF), Plantrin 2. Lemvig: Danish Coastal Authority, the Ministry of Transportation.

DCA (2013b). *Straekningen Lodbjerg - Nymindegab. Bilag til Faellesaftale om Kystbeskyttelsen for Perioden 2014-18*. Lemvig: Danish Coastal Authority.

DP (1946). *Lov om Foranstaltninger til Sikring af Limfjordstangerne, Thyboron Havn og Thyboron Kanal.* Act no. 454 of 14 Aug. 1946. Copenhagen: Danish Parliament.

DP (1970). *Lov om Ophævelse af Lov om Foranstaltninger til Sikring af Limfjordstangerne, Thyborøn Havn og Thyborøn kanal.* Act no. 477 of 9 Dec 1970. Copenhagen: Danish Parliament.

DP (2012a). *Lov om Ændring af Lov om Planlægning (L148, 29 May 2012)*. Copenhagen: Danish Parliament.

DP (2012b). *Lov om Ændring af Lov om Vandsektorens Organisering og Økonomiske forhold (L149, 29 May 2012)*. Copenhagen: Danish Parliament.

Du, Y.-D., Cheng, X.-H., Wang, X.-W., Ai, H., Duan, H.-L., He, J., et al. (2013). A review of assessment and adaptation strategy to climate change impacts on the Coastal Areas in South China. *Adv. Clim. Change Res.* 4, 201–207. doi: 10.3724/SP.J.1248.2013.201

Duun-Christensen, I. (1990). "Long-term variations in sea level at the Danish coast during the recent 200 years," in *Proceedings of the 1st International Coastal Symposium* (Skagen).

EU (2007). *Directive 2007/60/EC of the European Parliament and of the Council of 23 October 2007 on the Assessment and Management of Flood Risks*. Luxembourg: Official Journal of the European Union, L 288/27 (6/11/2007).

Ferretti, A., Monti-Guarnieri, A., Prati, C., Rocca, F., and Massonnet, D. (2007). *InSAR Principles: Guidelines for SAR Interferometry Processing and Interpretation (TM-19, February 2007),* ed. K. Flethcher. Noordwijk: European Space Agency, ESA Publications/ESTEC.

Gallina, V., Torresan, S., Critto, A., Sperotto, A., Glade, T., and Marcomini, A. (2016). A review of multi-risk methodologies for natural hazards: Consequences and challenges for a climate change impact assessment. *J. Environ. Manag.* 168, 123–132. doi: 10.1016/j.jenvman.2015.11.011

Geo (2015). "Database of geotechnical surves in Denmark (Geo-GIS)," in *Private Geotechnical Database* (Copenhagen: Geo). Available online at: http://www.geo.dk

Geoteknisk Institut (1978). *Ny Administrationsbygning Thyboron/Harboore, Case no. 78117*. Geotechnical Report. Geotechnical Institute (now Geo), Copenhagen.

Geoteknisk Institut (1983). *Thyboron, Nordsokaj, Case no. 140 02987*. Geotechnical Report. Geotechnical Institute (now Geo), Copenhagen.

GEUS (2015a). *Jupiter - Denmark's Geological and Hydrological Database*. Denmark and Greenland Geological Survey. Available online at: http://www.geus.dk/DK/data-maps/jupiter/Sider/default.aspx

GEUS (2015b). *GERDA - Danish National Database on Shallow Geophysical Data*. Denmark and Greenland Geological Survey. Available online at: http://www.geus.dk/gerda/gerda-uk.htm

GEUS (2015c). *GEUS' Model Base*. Denmark and Greenland Geological Survey. Available online at: http://www.geus.dk/DK/data-maps/Sider/default.aspx

GEUS (2015d). *Groundwater Reports Database*. Denmark and Greenland Geological Survey. Available online at: http://www.geus.dk/DK/data-maps/Sider/default.aspx

GEUS (2015e). *Digital Soil Map of Denamrk 1:25.000*. Denmark and Greenland Geological Survey. 1:25 000. Available online at: http://www.geus.dk/DK/data-maps/Sider/j25-dk.aspx

Gibbs, M. T. (2015). Coastal climate risk and adaptation studies: The importance of understanding different classes of problem. *Ocean Coast. Manag.* 103, 9–13. doi: 10.1016/j.ocecoaman.2014.10.018

Gregersen, I. B., Madsen, H., Linde, J. J., Krüger, and Arnbjerg-Nielsen, K. (2014). *Opdaterede Klimafaktorer og Dimensionsgivende Regnintensiteter*. Copenhagen: Ingeniorforeningen i Danmark - IDA Spildevandskomiteen, Skrift nr. 30.

Gregersen, S., and Voss, P. (2010). Irregularities in Scandinavian postglacial uplift/subsidence in time scales tens, hundreds, thousands of years. *J. Geodyn.* 50, 27–31. doi:10.1016/j.jog.2009.11.004

Gregersen, S., and Voss, P. (2015). Consistency of postglacial geodynamics for the Kattegat region, southern Scandinavia, based on seismological, geological and geodetic data. *Geol. Surv. Den. Greenl.* 33, 21–24.

Grinsted, A. (2015). "Projected change – Sea level, 2015," in *Second Assessment of Climate Change for the Baltic Sea Basin,* eds The BACC II Author Team (Regional Climate Studies, Springer Open), 252–263.

Grinsted, A., Jevrejeva, S., Riva, R. E., and Dahl-Jensen, D. (2015). Sea level rise projections for northern Europe under RCP8.5. *Clim. Res.* 64, 15–23. doi: 10.3354/cr01309

Hallegatte, S., Green, C., Nicholls, R. J., and Corfee-Morlot, J. (2013). Future flood losses in major coastal cities. *Nat. Clim. Change* 3, 802–806. doi: 10.1038/nclimate1979

Hallegatte, S., Ranger, N., Mestre, O., Dumas, P., Corfee-Morlot, J., Herweijer, C., et al. (2011). Assessing climate change impacts, sea level rise and storm surge risk in port cities: a case study on Copenhagen. *Clim. Change* 104, 113–137. doi: 10.1007/s10584-010-9978-3

Hansen, J. M., Aagaard, T., and Binderup, M. (2012). Absolute sea levels and isostatic changes of the eastern North Sea to central Baltic region during the last 900 years. *Boreas* 41, 180–208. doi: 10.1111/j.1502-3885.2011.00229.x

Hansen, L. (2013). *Sea Level Data 1889-2012 From 14 Stations in Denmark. Mean, Maximum and Minimum Values Calculated on Monthly and Yearly Basis Including Plots of Mean Values*. Technical Report 13-15, Danish Meteorological Institute, Copenhagen.

Hanssen, R., and Perski, Z. (2007). *Reconnaissance Skagen, Denmark. Status Overview 22 Jan 2007*. TUDelft. Available online at: http://cct.gfy.ku.dk/skagen/skagen.htm

Hawa, M. N., Knudsen, T., Kokkendorff, S. L., Olsen, B. P., and Rosenkranz, B. C. (2011). *Horizontal Accuracy of Digital Elevation Models, Vol. 10*. Technical Report Series, National Survey and Cadastre, Copenhagen.

Hinkel, J. (2008). *Transdisciplinary Knowledge Integration. Cases from Integrated Assessment and Vulnerability Assessment*. Ph.D. thesis, Wageningen University, Wageningen.

Holgate, S. J., Matthews, A., Woodworth, P. L., Rickards, L. J., Tamisiea, M. E., Bradshaw, E., et al. (2013). New data systems and products at the Permanent Service for Mean Sea Level. *J. Coast. Res.* 29, 493–504. doi:10.2112/jcoastres-D-12-00175.1

I-GIS (2015). *GeoScene3D - Geological Modelling and Visualization Software*. Available online at: http://www.i-gis.dk/GeoScene3D/tabid/62/language/en-GB/Default.aspx

IDA (2005). *Funktionspraksis for Afloebssystemer Under Regn*. Copenhagen: Ingeniorforeningen i Danmark - IDA Spildevandskomiteen, Skrift nr,. 27.

Ingvardsen, S. M., Knudsen, S. B., Madsen, H. T., Sørensen, C., and Bisgaard, C. (2012). *Thyboron Kanal og Vestlige Limfjord*. Technical Report, Danish Coastal Authority, Lemvig.

IPCC (2012). *Managing the Risks of Extreme Events and Disasters to Advance Climate Change Adaptation. A Special Report of Working Groups I and II of the Intergovernmental Panel on Climate Change*, eds C. B. Field, V. Barros, T. F. Stocker, D. Qin, D. J. Dokken, K. L. Ebi, M. D. Mastrandrea, K. J. Mach, G. -K. Plattner, S. K. Allen, M. Tignor, and P. M. Midgley (Cambridge, UK; New York, NY: Cambridge University Press), 582.

IPCC (2013). *Climate Change 2013: The Physical Science Basis. Contribution of Working Group I to the Fifth Assessment Report of the Intergovernmental Panel on Climate Change*, eds T. F. Stocker, D. Qin, G. -K. Plattner, M. Tignor, S. K. Allen, J. Boschung, A. Nauels, Y. Xia, V. Bex, and P. M. Midgley (Cambridge, UK; New York, NY: Cambridge University Press), 1535.

Jahn, T., Bergmann, M., and Keil, F. (2012). Transdisciplinarity: Between mainstreaming and marginalization. *Ecol. Econ.* 79, 1–10. doi: 10.1016/j.ecolecon.2012.04.017

Jakobsen, P. R., Hermansen, B., and Tougaard, L. (2015). *Danmarks Digitale Jordartskort 1:25000 Version 4.0*. Geological Survey of Denmark and Greenland, Report 2015/30.

Jakobsen, P. R., Wegmuller, U., Capes, R., and Pedersen, S. A. S. (2013). Terrain subsidence detected by satellite radar scanning of the Copenhagen area, Denmark, and its relation to the tectonic framework. *Geol. Surv. Den. Greenl.* 28, 25–28.

Jensen, J., and Sorensen, C. (2008). *Fremskrivning af Fodringsindsatsen paa Vestkysten*. Lemvig: Danish Coastal Authority.

Jorgensen, F., Kristensen, M., Hojberg, A. L., Klint, K. E. S., Hansen, C., Jordt, B. E., et al. (2008). *Opstilling af Geologiske Modeller til Grundvandsmodellering*. Copenhagen: Geo-Vejledning 3, Geological Survey of Denmark and Greenland.

Khan, S. A. (2014). *Report: GPS Time Series for Permanent GPS Stations in Denmark*. DTU Space, Lyngby.

Knudsen, S. B., Ingvardsen, S. M., Madsen, H. T., Sorensen, C., and Christensen, B. B. (2012). *Increased Water Levels Due to Morphodynamic Changes; the Limfjord, Denmark*. Santander: Coastal Engineering Proceedings.

Knudsen, S. B., Sorensen, C., Madsen, H. T., and Ingvardsen, S. M. (2011). *Thyboron Kanal 2009*. Technical Report, Danish Coastal Authority, Lemvig.

Knudsen, T., Dalaa, N. S., Knudsen, P., and Jakobsen, P. R. (2009). *ABSRATE – Absolute Subsidence Rates from Persistent Scatterer Interferometry Data*. Final report. Technical Report No. 5, National Survey and Cadastre (KMS), Copenhagen.

Kortenhaus, A., and Oumeraci, H. (2014). "Flood risk assessments - results, applications and future requirements," in *Proceedings of 34th Conference on Coastal Engineering* (Seoul). doi: 10.9753/icce.v34.management.15

Kuklicke, C., and Demeritt, D. (2016). Adaptive and risk-based approaches to climate change and the management of uncertainty and institutional risk: the case of future flooding in England. *Global Environ. Change* 37, 56–68. doi: 10.1016/j.gloenvcha.2016.01.007

Lane, D. E., Clarke, C. M., Clarke, J. D., Mycoo, M., and Gobin, J. (2015). "Managing adaptation to changing climate in Coastal Zones," in *Coastal Zones, Solutions for the 21st Century*, eds J. Baztan, O. Chouinard, B. Jorgensen, P. Tett, J.-P. Vanderlinden, and L. Vasseur (Amsterdam: Elsevier), 141–160. doi: 10.1016/B978-0-12-802748-6.00009-7

Larsen, T., and Beck, J. B. (2009). Stormflodsvandstande i Limfjorden ved lukning af Thyborøn Kanal. *Teknik Miljoe* 2009, 54–57.

Lemvig Municipality (2014). *Klimatilpasningsplan 2014-2017*. Lemvig: Lemvig Municipality.

Levinsen, J., Dall, J., Skriver, H., Kusk, A., Broge, N. H., and Sorensen, C. (2015). *Derivation of Land Deformation Over Three Locations in Denmark*. Copenhagen: ESA Project, Id. 30907.

Linham, M. M., and Nicholls, R. J. (2010). "Technologies for climate change adaptation – Coastal Erosion and flooding," in *TNA Guidebook Series,* ed X. Zhu (New Delhi: UNEP Risø Centre. Magnum Custom Publishing), 152.

Loorbach, D., and Rotmans, J. (2011). The practice of transition management: examples and lessons from four distinct cases. *Futures* 42, 237–246. doi: 10.1016/j.futures.2009.11.009

Lykke-Andersen, H., and Borre, K. (2000). Aktiv tektonik i Danmark: der er liv i Sorgenfrei-Tornquist Zonen. *Geol. Nyt*. 6, 12–13.

Mertz, E. L. (1924). *Oversigt Over de Sen- og Postglaciale Niveauforandringer i Danmark*. Copenhagen: Danmarks Geologiske Undersøgelse, II Rk., Nr.41.

Milne, G. A., Mitrovica, J. X., Scherneck, H.-G., Davis, J. L., Johansson, J. M., Koivula, H., et al. (2004). Continuous GPS measurements of postglacial adjustment in Fennoscandia: 2. Modeling results. *J. Geophys. Res.* 109, B02412. doi: 10.1029/2003JB002619

Mobjörk, M. (2010). Consulting versus participatory transdisciplinarity: a refined classification of transdisciplinary research. *Futures* 42, 866–873. doi: 10.1016/j.futures.2010.03.003

MPW (1942). *Betaenkning Vedrorende Foranstaltninger til Sikring af Limfjordstangerne og Thyboron havn. By Commission of 16 Apr 1937*. Copenhagen: Ministry of Public Works.

MPW (1968). *Betaenkning Vedrorende Thyboron Kanal. No. 472.* ed S. L. Moellers Bogtrykkeri. Copenhagen: Ministry of Public Works.

MT (2009). *Bekendtgørelse af Lov om Kystbeskyttelse, 2009.* LBK nr 267 af 11/03/2009. Copenhagen: Danish Ministry of Transportation.

Nerem, R. S., Chambers, D., Choe, C., and Mitchum, G. T. (2010). Estimating Mean Sea Level Change from the TOPEX and Jason Altimeter Missions. *Marine Geod.* 33 (Suppl. 1), 435–446. doi: 10.1080/01490419.2010.491031

Nguyen, T. T. X., Bonetti, J., Rogers, K., and Woodroffe, C. D. (2016). Indicator-based assessment of climate-change impacts on coasts: a review of concepts, methodological approaches and vulnerability indices. *Ocean Coast. Manag.* 123, 18–43. doi: 10.1016/j.ocecoaman.2015.11.022

Nicholls, R. J. (1995). Coastal megacities and climate change. *Geo J.* 37, 369–379.

Nicholls, R. J., Wong, P. P., Burkett, V. R., Codignotto, J. O., Hay, J. E., McLean, R. F., et al. (2007). "Coastal systems and low-lying areas," in *Climate Change 2007: Impacts, Adaptation and Vulnerability. Contribution of Working Group II to the Fourth Assessment Report of the Intergovernmental Panel on Climate Change,* eds M. L. Parry, O. F. Canziani, J. P. Palutikof, P. J. van der Linden, and C. E. Hanson (Cambridge: Cambridge University Press), 315–356.

Nielsen, T., Mathiesen, A., and Bryde-Auken, M. (2007). Base Quaternary in the Danish parts of the North Sea and Skagerrak. *Geol. Surv. Den. Greenl. Bull.* 15, 37–40.

Norgaard, J. Q. H., Bentzen, T. R., Larsen, T., Andersen, T. L., and Kvejborg, S. (2014). Influence of closing storm surge barrier on extreme water levels and water exchange; Limfjord, Denmark. *Coast. Eng. J.* 56, 1–16. doi: 10.1142/S0578563414500053

Olesen, M., Madsen, K. S., Ludwigsen, C. A., Boberg, F., Christensen, T., Cappelen, J., et al. (2014). *Fremtidige Klimaforandringer i Danmark, 2014*. Copenhagen: Danmarks Klimacenter, Rapport 6 (Summary in English).

Pedersen, S. A. S., Gaset, M., Cooksley, G., and Jakobsen, P. R. (2011). Detection of terrain changes in southern Denmark using persistent scatterer interferometry. *Geol. Surv. Den. Greenl.* 23, 41–44.

Permanent Service for Mean Sea Level (2015). "(PSMSL) Tide Gauge Data," Available online: http://www.psmsl.org/data/obtaining/

Petersen, A., Andersen, H., and Thomsen, O. (2008). *Borehulslogging Thyboron Sydhavn*. DGU no. 44.571 (Feb. 2008). Copenhagen: Orbicon Inc.

Rosenkranz, B. C., and Frederiksen, P. (2011). *Quality Assessment of the Danish Elevation Model (DK-DEM), Vol. 12*. Technical Report Series, National Survey and Cadastre, Copenhagen.

Sandersen, P. B. E. (2008). "Uncertainty assessment of geological models – a qualitative approach," in *Calibration and Reliability* in *Groundwater Modelling: Credibility Of Modelling,* eds J. C. Refsgaard, K. Kovar, E. Haarder, and E. Nygaard (International Association of Hydrological Sciences (IAHS) Publication 320), 345–349.

Schmidt, K. E. (2000). *The Danish Height System DVR90*. Skrifter 4. Rk., bd. 8. Copenhagen: Kort and Matrikelstyrelsen.

Serrao-Neumann, S., Schuch, G., Harman, B., Crick, F., Sano, M., Sahin, O., et al. (2015). One human settlement: a transdisciplinary approach to climate change adaptation research. *Futures* 65, 97–109. doi: 10.1016/j.futures.2014.08.011

Sorensen, C. (2015a). Elskede, forhadte Vesterhav - Livgivende forkaetrede kanal. *Geogr. Orientering* 45, 6–13.

Sorensen, C. (2015b). "Water NOT wanted - Coastal Floods and Flooding Protection in Denmark," in *Sicherung von Dämmen, Deichen und Stauanlagen. Handbuch für Theorie und Praxis, Vol. V,* eds. R. A. Herrmann and J. Jensen (Siegen: Universität Siegen), 3–21.

Sorensen, C., Broge, N., Knudsen, P., and Andersen, O. B. (2015). "Combining sea state and land subsidence rates in an assessment of flooding hazards at the Danish North Sea Coast," in *Workshop on Global and Regional Sea Level Variability and Change, 10-12 June 2015* (Mallorca: University of the Balearic Islands), 62.

Sorensen, C., Madsen, H. T., and Knudsen, S. B. (2013). *Hojvandsstatistikker 2012*. Lemvig: Danish Coastal Authority.

Sorensen, T., Fredsoe, J., and Jakobsen, P. R. (1996). "History of coastal engineering in Denmark," in *History and Heritage of Coastal Engineering*, ed N. Kraus (New York, NY: ASCE), 103–141.

Vignoli, G., Fiandaca, G., Christensen, A. V., Kirkegaard, C., and Auken, E. (2015). Sharp spatially constrained inversion with applications to transient electromagnetic data. *Geophys. Prospect.* 63, 243–255. doi: 10.1111/1365-2478.12185

Visser, H., Dangendorf, S., and Petersen, A. C. (2015). A review of trend models applied to sea level data with reference to the "acceleration-deceleration debate." *J. Geophys. Res. Oceans* 120, 3873–3895. doi: 10.1002/2015JC010716

Visser, L. E. (2001). "Reflections on transdisciplinarity, integrated coastal development, and governance," in *Challenging Coasts - Transdisciplinary Excursions into Integrated Coastal Zone Development*, ed L. E. Visser (Amsterdam: MARE Publication Series No. I, Amsterdam University Press), 23–47.

Vognsen, K., Jepsen, C., and Kokkendorff, S. L. (2013a). *Guidelines for Motoriseret Geometrisk Praecisionsnivellement*. Copenhagen: Danish Geodata Agency.

Vognsen, K., Sonne, I. B., Broge, N. H., Sorensen, C., and Knudsen, P. (2013b). *Metode til Fremskrivning af Oversvoemmelsesomfang Ved Stormflod, Vol. 16.* Technical Report Series, Danish Geodata Agency, Copenhagen.

Wahl, T., Haigh, I. D., Woodworth, P. L., Albrecht, F., Dillingh, D., Jensen, J., et al. (2013). Observed mean sea level changes around the North Sea coastline from 1800 to present. *Earth Sci. Rev.* 124, 51–67. doi: 10.1016/j.earscirev.2013.05.003

Watson, P. J. (2015). Development of a unique synthetic data set to improve sea-level research and understanding. *J. Coastal Res.* 31, 758–770. doi: 10.2112/jcoastres-D-14-00143.1

Conflict of Interest Statement: The authors declare that the research was conducted in the absence of any commercial or financial relationships that could be construed as a potential conflict of interest.

frontiers in Marine Science

ORIGINAL RESEARCH
published: 05 April 2016
doi: 10.3389/fmars.2016.00041

Effects of Scale and Input Data on Assessing the Future Impacts of Coastal Flooding: An Application of DIVA for the Emilia-Romagna Coast

Claudia Wolff[1]*, *Athanasios T. Vafeidis*[1], *Daniel Lincke*[2], *Christian Marasmi*[3] and *Jochen Hinkel*[2, 4]

[1] Coastal Risks and Sea-Level Rise Research Group, Department of Geography, Christian-Albrechts-University Kiel, Kiel, Germany, [2] Global Climate Forum, Berlin, Germany, [3] Directorate General Environment, Soil and Coast Protection, Bologna, Italy, [4] Berlin Workshop in Institutional Analysis of Social-Ecological Systems, Humboldt-University, Berlin, Germany

This paper assesses sea-level rise related coastal flood impacts for Emilia-Romagna (Italy) using the Dynamic Interactive Vulnerability Assessment (DIVA) modeling framework and investigate the sensitivity of the model to four uncertainty dimensions, namely (1) elevation, (2) population, (3) vertical land movement, (4) scale and resolution of assessment. A one-driver-at-a-time sensitivity approach is used in order to explore and quantify the effects of uncertainties in input data and assessment scale on model outputs. Of particular interest is the sensitivity of flood risk estimates when using datasets of different resolution. The change in assessment scale is implemented through the use of a more detailed digital coastline and input data for the coastline segmentation process. This change leads to a 35-fold increase in the number of coastal segments and in a more realistic spatial representation of coastal flood impacts for the Emilia-Romagna coast. Furthermore, the coastline length increases by 43%, considerably influencing adaptation costs (construction of dikes). With respect to input data our results show that by the end of the century coastal flood impacts are more sensitive to variations in elevation and vertical land movement data than to variations in population data in the study area. The inclusion of local information on human induced subsidence rates increases the relative sea-level by 60 cm in 2100, resulting in coastal flood impacts that are up to 25% higher compared to those generated with the global DIVA values, which mainly account for natural processes. The choice of one elevation model over another can result in differences of ∼45% of the coastal floodplain extent and up to 50% in flood damages by 2100. Our results emphasize that the scale of assessment and resolution of the input data can have significant implications for the results of coastal flood impact assessments. Understanding and communicating these implications is essential for effectively supporting decision makers in developing long-term robust and flexible adaptation plans for future changes of highly uncertain scale and direction.

Keywords: coastal flooding, impact assessment, sensitivity analysis, scale and resolution, sea-level rise

OPEN ACCESS

Edited by:
Ivan David Haigh,
University of Southampton, UK

Reviewed by:
Goneri Le Cozannet,
BRGM, France
Matthew Lewis,
Bangor University, UK

***Correspondence:**
Claudia Wolff
wolff@geographie.uni-kiel.de

Specialty section:
This article was submitted to Coastal Ocean Processes, a section of the journal Frontiers in Marine Science

Received: *02 December 2015*
Accepted: *15 March 2016*
Published: *05 April 2016*

Citation:
Wolff C, Vafeidis AT, Lincke D, Marasmi C and Hinkel J (2016) Effects of Scale and Input Data on Assessing the Future Impacts of Coastal Flooding: An Application of DIVA for the Emilia-Romagna Coast. Front. Mar. Sci. 3:41. doi: 10.3389/fmars.2016.00041

INTRODUCTION

Coastal flooding constitutes a major risk for coastal regions throughout the world and this risk is expected to worsen considerably during the twenty-first century with rising sea-levels and as future societal development increases the number of people and value of assets in the coastal floodplain (Hinkel et al., 2014). Therefore, there is a growing need of coastal communities and decision makers to access information on current and future risks as well as on strategies for managing and reducing risks. For instance, national and regional Mediterranean Coastal Administrations have expressed needs for improved methods to evaluate flood risk in Mediterranean coastal areas and to identify comprehensive plans to reduce these risks in recent years (Lupino et al., 2014).

Evaluating and managing coastal flood risk under climate change, as well as climate risk in general, requires to consider uncertainty about present and future risks as comprehensively as possible, because not considering uncertainty may only partially lead to maladaptation (Jones et al., 2014; Hinkel et al., 2015). For coastal flooding, uncertainty relates not only to the amount or rate of sea-level rise (SLR) and socio-economic development, but also to the input data used in the analysis. While scenario uncertainty is generally explored in coastal impact assessments, data uncertainty has not received as much attention in the literature (Le Cozannet et al., 2015). Initial work carried out (Lichter et al., 2011; Mondal and Tatem, 2012) has shown that variations in estimates of area and population exposure are highly dependent on the input datasets. Hinkel et al. (2014) found that coastal flood impacts are much more sensitive to elevation data uncertainty than to, e.g., sea-level rise uncertainty stemming from the choice of climate model. Generally, a significant limitation of flood impact analysis on all scales is the unavailability of free high-accuracy datasets (Gesch, 2009; Mondal and Tatem, 2012; Neumann et al., 2015).

To our knowledge, there is, however, no study that has explored the uncertainty of coastal flood risk assessment with regard to the spatial scale of analysis and spatial resolution of input data. Scale is bound to be an essential parameter in flood risk analysis (de Moel et al., 2015) because different kinds of population, elevation and vertical land movement input data sets are available at different scales. Of particular interest thereby is the sensitivity of flood risk when switching from data sets with global coverage to local, high resolution ones, because the latter are more accurate but only available for few regions. Comparing flood risk attained between global and local datasets thus helps to understand how accurate flood risk assessments are in regions where local high resolution data are not available.

This paper contributes to improve our understanding of the above uncertainties in the context of global coastal flood risk assessment. We do this by taking the Dynamic Interactive Vulnerability Assessment (DIVA) flood risk module from Hinkel et al. (2014) and applying it to the Emilia-Romagna region in Italy using two scales of analysis: (i) a low resolution one based on the global coastline segmentation of Vafeidis et al. (2008) also used by Hinkel et al. (2014); and (ii) a newly developed high-resolution segmentation of the Emilia-Romagna region. The exercise is directly related to a policy process taking place within the EU-funded "Coastal Governance and Adaptation Policies in the Mediterranean" (COASTGAP) project aiming at providing policy-relevant guidance on local coastal flood impacts of climate change.

Specifically, our research objectives are the following:

(1) Explore the sensitivity of coastal flood risk estimates to the effects of different coastlines and segmentations
(2) Explore the sensitivity of coastal flood risk estimates to different population and higher resolution elevation and vertical land movement input datasets

The remainder of this paper is structured as follows. Section Study Area, Methods, and Data provides an overview of the study area, the coastal flood impact model, the segmentation process as well as the sensitivity analysis approach used in this paper. Furthermore, the underlying datasets as well as future climate and socio-economic scenarios will be described. Section Results presents the sensitivity analysis from a selected number of simulation outputs of impacts due to different input datasets and segmentations. Finally, key findings are evaluated and discussed in the Discussion Section.

STUDY AREA, METHODS, AND DATA

Overview

The determination of the effects of scale and sensitivity of impacts to different segmentations and input data follows a multi-level step procedure. The first step was the downscaling process of the assessment units using a more detailed coastline and segmentation process in order to create a data structure that enables the model to run and to be able to quantify the improvements of a more detailed coastline and segmentation. The second step was the calculation of exposure using different vertical land movement, elevation and population datasets, leading to the six datasets of various combinations of four uncertainty dimensions shown in **Table 1**. In a final step, the DIVA coastal flood module was used to assess potential flood impacts in terms of the following three parameters:

(1) Potential floodplain extent of the 1-in-100-year extreme water level [in km^2]
(2) The average number of people flooded annually through extreme water level events [people/year]
(3) The average annual damage caused by coastal flooding [in million US$]

These model outputs are used in order to determine the sensitivity of the model.

Study Area

Emilia-Romagna is situated in the southern part of the Po basin in northern Italy (see **Figure 1**). It is inhabited by 4.4 million people and covers an area of 22,124 km^2. The gross domestic product (GDP) per capita in Emilia-Romagna is 24,396 Euro (Istat, 2009), which is higher than the national average (20,043 Euro). The coastal strip is often higher in elevation than the hinterland, of which more than 100,000 ha are below

TABLE 1 | Datasets used to investigate the sensitivity of coastal impacts to the four uncertainty dimensions (coastline segmentation, elevation, population, and vertical land movement).

Coastline segmentation	Digital elevation model	Population	Vertical land movement
High-resolution segmentation	LiDAR	LandScan	Peltier (2000) + 2 mm/year delta subsidence
	LiDAR	GRUMP	Peltier (2000) + 2 mm/year delta subsidence
	SRTM	LandScan	Peltier (2000) + 2 mm/year delta subsidence
	SRTM	GRUMP	Peltier (2000) + 2 mm/year delta subsidence
	LiDAR	LandScan	PInSAR
Global segmentation	SRTM	GRUMP	Peltier (2000) + 2 mm/year delta subsidence

sea-level (Preti et al., 2009). The low-lying coastal strip is characterized by different levels of human modification and development. The level of modification is ranging from natural to urbanized areas (93 km of the coast or 71% are urbanized). The coastline of urbanized regions has remained relatively stable due to human intervention such as hard shoreline protections or beach nourishment (Armaroli et al., 2012). Hard shore protection, mainly offshore breakwaters, protects 60% of the coastline from flooding and erosion (Nordstrom et al., 2015). The entire region is currently experiencing a sediment deficit which is a result of decreasing fluvial sediment transport caused by stabilization of slopes and hydraulic works along the river bed. Furthermore, there is a current interruption of long-shore sediment transport due to shore protection structures. More than 10 million m^3 of sediment was replenished to the beach of Emilia-Romagna between 1983 and 2012 (Montanari and Marasmi, 2014). The dominant coastal type is considered to be sandy beach with an average width of 70 m (emerged beach). Wave energies are normally low in Emilia-Romagna. The wave height is generally below 1.25 m (91%), but storms from the south/southeast (Scirocco) and northeast (Bora) result in high waves and storm surge levels. According to Houtenbos et al. (2005), the relative sea-level rise is higher in Emilia-Romagna than the global eustatic component due to subsidence. Along the Emilia-Romagna coastal area, the degree of subsidence due to natural causes entails a few millimeters per year, while the anthropogenic subsidence has reached high speeds of 50 mm/year in the 80's. Main drivers to cause anthropogenic subsidence include underground extraction of water and natural gas. The Integrated Coastal Zone Management (ICZM) effort in the Emilia-Romagna region started in 2002 and ended with the emanation of ICZM Guidelines approved by the Regional council in the beginning of 2005. They represent the tool to address all coastal activities toward economic, social and environmental sustainability, in compliance with EU Recommendation of the 30th May 2002. According to Preti et al. (2009), the touristic use dominates nearly 85 km of the coast. With more than 36 million overnight stays per year, Emilia-Romagna is one of Italy's most attractive tourist destinations.

Methods

Calculating Flood Risk

We used the DIVA (Dynamic Interactive Vulnerability Assessment) coastal flood module (Version 5.0.0) as presented in Hinkel et al. (2014) in order to calculate coastal flood impacts over the next century. The DIVA model operates on data attributed to coastline segments. Global applications of DIVA used a segmented coastline of the world, which comprises 12,148 units of variable length (average of 70 km) based on Vafeidis et al. (2008). Every segment represents a uniform response to SLR within the coastal system. More than 80 physical, ecological and socioeconomic parameters (e.g., uplift/subsidence in mm/year or coastal population) of the world's coastal zone (excluding Antarctica) are spatially referenced to these units. DIVA is driven by climatic and socioeconomic scenarios which will be described in chapter Sea-Level Rise Scenarios and Socio-Economic Scenarios. One important innovation introduced by DIVA is the explicit incorporation of a range of adaptation options, as impacts do not only depend on the selected climatic and socio-economic scenarios but also on the selected adaptation strategy. Possible adaptation strategies in the DIVA modeling framework in order to reduce coastal flood risk are the construction of dikes.

DIVA's flooding module uses a cumulative people and asset exposure function in order to estimate the potential socio-economic impacts of coastal flooding. In order to get the potential number of people living below a certain elevation level and therefore prone to flooding, a digital elevation model (DEM) was combined with a spatial population dataset (a more detailed description of the calculation can be found in Section Exposure Data). Based on extreme water levels given for different return periods in the DIVA database (Vafeidis et al., 2008) the potential exposed area and number of people living in these areas is calculated using a bathtub approach. The extreme water levels within the DIVA database were calculated based on the methodology described in Hoozemans et al. (1993). Relative sea-level rise is then added to the current extreme water level probability distribution, leading to shorter average return periods of flood levels. Hinkel et al. (2014) compute the number of people flooded by only making the binary distinction between flooded and not flooded. The estimation of the value of assets on a given elevation is done by multiplying the number of people with the GDP per capita times an empirically estimated GDP-to-assets ratio of 2.8 taken from Hallegatte et al. (2013). The amount of damage depends on the depth by which the asset is flooded. Hinkel et al. (2014) uses a depth-damage function in order to calculate the fraction of assets that will be damaged when flooded by a certain depth. The depth-damage function reflects the fact that the damage rate decreases with increasing water levels. It is assumed that a flood depth of 1 m destroys 50% of the assets. According to Hinkel et al. (2014), this assumption is a good indication based on the information available to date. If dikes are present, a damage of 0 is assumed for floods lower than the actual dike height. By default, a dike is constructed if at least 1 person per km^2 lives on the coast. The dike height is calculated based on a demand for safety function, which depends on the GDP per capita and population density. Following this function, dikes are built and upgraded for each coastline segment in each time

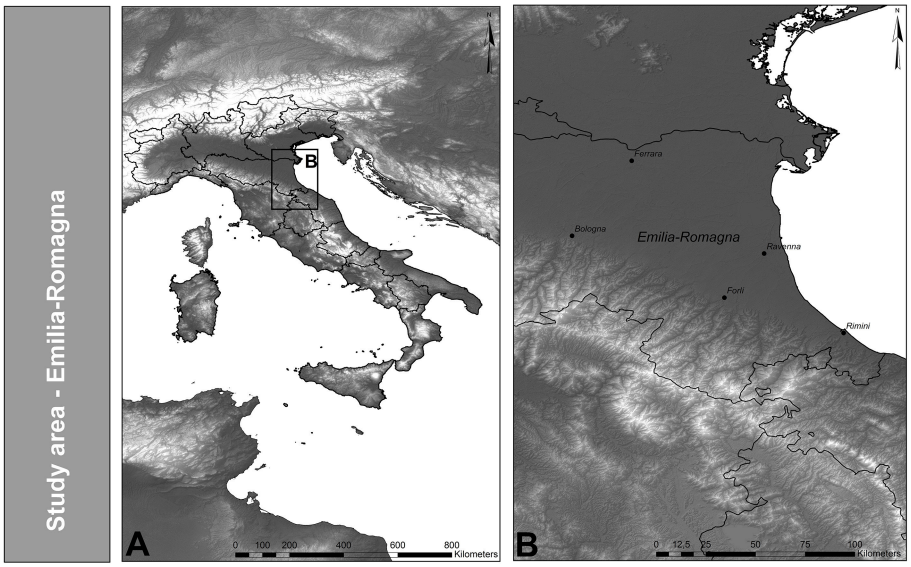

FIGURE 1 | Study area—Emilia-Romagna. (A) Italy **(B)** Emilia-Romagna.

step (5 years) until 2100. Future exposure is attained by applying national population and GDP growth rates of the socio-economic scenarios (Hinkel et al., 2014). A more detailed description of the coastal flood module used in this study can be found in Hinkel et al. (2014).

Coastline Segmentation

In order to downscale the assessment scale of DIVA it was necessary to refine the existing coastline and segmentation. The segmentation is an essential step in order to generate a data structure that enables the model to run, and it defines the scale of assessment. The original DIVA segmentation was based on a digital global coastline data set (ESRI, 2002), with a cartographic scale of 1: 3,000,000. As this level of scale is too general for the purpose of a sub-national study due to the loss of important coastal features, a more detailed digital coastline was employed (see Section Coastline Segmentation Data). This coastline was then segmented into units, based on the original concept of McFadden et al. (2007) and using the following parameters relevant for coastal-flood risk assessment and management (1) administrative boundaries, (2) the geomorphic structure of the coastal environment, (3) the expected morphological development of the coast given sea-level rise, and (4) population density. We extended those parameter to also include (5) river mouths as these often have a much greater RSLR due to subsidence than other areas.

Sensitivity Analysis

A sensitivity analysis aims at exploring how much model outputs are affected by changes in input data (Saltelli et al., 2000). We used a simple One-Driver-At-a-Time (OAT) approach. This single factor approach is undertaken by modifying one input variable, e.g., the elevation data, while keeping all remaining inputs consistent. This enables us to explore and to systematically quantify the impacts of different assumptions on the calculated flood impacts. Sensitivity is calculated as the difference between the impacts in 2100. It is a useful method in order to identify key drivers which strengthen the understanding and interpretation of the DIVA modeling framework. In this study we do not quantify how interactions between input factors affect the variability of the model results, as the generation of input data for each point in the uncertainty space considered is computation and labor intensive. For each data point a large number of processing steps is required as the coastline needs to be segmented and the database needs to be populated with e.g., population, vertical land movement, and elevation data. Therefore, deriving more data points for conducting a general sensitivity analysis was not possible within the scope of this study.

Data

Sea-Level Rise Scenarios

We uses regional SLR scenarios of Hinkel et al. (2014), which are based on the Representative Concentration Pathways (RCP) 2.6, 4.5, and 8.5 and comprise the following two main components:

(1) The steric contribution, produced by the Hadley Global Environment Model2—Earth System (HadGEM2-ES; Collins et al., 2008).
(2) Land ice contribution consisting in the mass contribution of glaciers and ice caps, based on Marzeion et al. (2012). The mass contribution of the Greenland ice sheet and peripheral ice caps taken from Fettweis et al. (2013) and the mass contribution from the Antarctic based on Levermann et al. (2012). By combing the three mass contributions a low (5th percentile), medium (50th percentile), and high (95th percentile) land-ice scenario was created (see **Table 2**). These scenarios also consider gravitational, rotational, and local land

TABLE 2 | Global mean sea-level rise in 2100 with respect to 1985–2005.

Scenario	Model	Steric [cm]	Mass [cm]				Total [cm]
			Glacier	Antarctica	Greenland	Sum	
RCP2.6	HadGEM2-ES	14	14 (14, 15)	7 (2, 23)	0 (0, 0)	21 (16, 39)	35 (29, 52)
RCP4.5	HadGEM2-ES	18	17 (16, 19)	8 (2, 29)	7 (5, 8)	32 (23, 56)	50 (41, 75)
RCP8.5	HadGEM2-ES	29	22 (20, 26)	10 (2, 41)	12 (10, 14)	44 (31, 81)	72 (60, 110)

The median and, in parentheses, the 5 and 95% percentiles are provided (Hinkel et al., 2014).

uplift effects that results from changes in ice masses and ocean circulations. To implement these effects, the model of Bamber and Riva (2010) was used which considers a uniform mass reduction over the ice sheets.

For this study, we use three SLR scenarios that sample the full uncertainty space covered by Hinkel et al. (2014). A lower bound scenario (RCP2.6 combined with the 5% quantile of ice-melting projections), hereafter referred to as low SLR, a medium scenario (RCP 4.5 combined with the median), referred to as medium SLR, and an upper bound scenario (RCP8.5 combined with the 95% quantile), referred to as high SLR. The sea-level scenarios for Italy vary between 31 (low SLR scenario) and 122 cm (high SLR scenario) by the end of the twenty-first century (see **Figure 2**). For every coastline segment, the relative sea-level rise is generated by linking the regional sea-level rise values with the vertical land movement.

Socio-Economic Scenarios

Three socio-economic scenarios have been used, based on the IPCC Shared Socio–economic Pathways (SSP) storylines (O'Neill et al., 2014), to present a range of potential future development directions in the Emilia-Romagna region. The SSP3 storyline assumes a high population growth and a slow economic development and represents a fragmented world. In this storyline the world is separated into extreme poverty, moderate wealth and a bulk of regions that struggle to maintain living standards for a rapid growing population. The SSP5 represents a conventional development which is oriented toward economic growth. The population growth is generally low. SSP2 assumes medium growth in socio-economic development worldwide.

The amount of assets and people that will be located in the coastal zone determines the future exposure to coastal flooding. In DIVA the two variables population growth and GDP growth are the main drivers to determine future socio-economic development. The total population of Italy ranges between 22.8 and 75.4 million (see **Figure 3**) and the GDP per capita between 27,716 and 160,602 US dollar by 2100 (see **Figure 4**) following the SSP storylines. Those growth rates are applied to the exposure data in order to estimate future coastal flood impacts. According to the global flood risk assessment conducted by Hinkel et al. (2014), the flood costs are highest for SSP5 (economic growth) and lowest for SSP3 (security), reflecting the socio-economic growth rates developed by Kc and Lutz (2014). In order to cover the full range of uncertainty and future pathways, SSP3 and SSP5 have been chosen as well as SSP2 which reflects a world with medium assumptions.

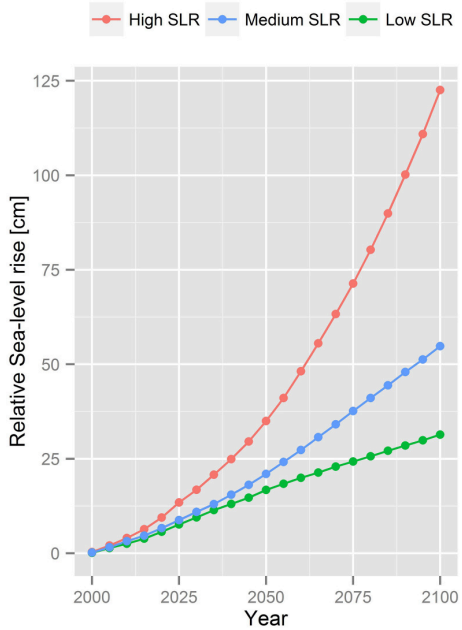

FIGURE 2 | The average relative sea-level rise for Emilia-Romagna under all sea-level rise scenarios.

Coastline Segmentation Data

For this study the coast has been resegmented using a more detailed digital coastline (see Supplementary Figure 1 for a comparison between the global and detailed coastline) and data. We selected the Global Administrative Areas (GADM, http://www.gadm.org/) level 01 coastline and corrected artifacts related to the format (e.g., "pixelization" of coastline) using a smoothing algorithm (polynomial approximation) and a tolerance of 100 m.

The availability of consistent datasets on coastal morphology and characteristics is a common limitation for global-, regional-, and national-scale impact assessments. Due to the lack of consistent coastal morphologies and geological characteristics data for the Emilia-Romagna region, an independent consistent data set was generated with Google earth. Google earth provides free satellite images and aerial pictures (Chang et al., 2009) for the whole study area. Based on the concept described in Scheffers et al. (2012), seven different classes [(i) sandy, (ii) unerodible, (iii) pebble, (iv) rocky with pocket beaches, (v) sandy with wave-breakers, (vi) muddy, and (vii) fortified coast—see **Figure 5**] have

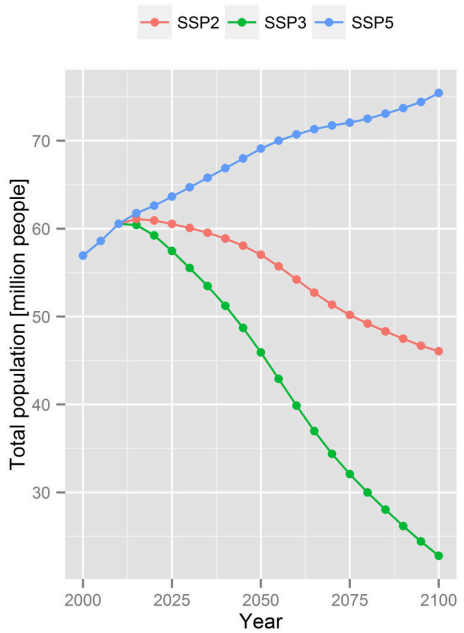

FIGURE 3 | Total population of Italy for each storyline used in this study.

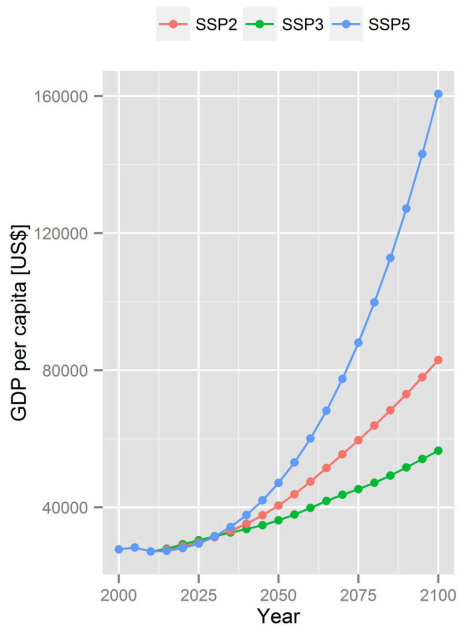

FIGURE 4 | GDP per capita in Italy for each storyline used in this study.

been classified based on visual interpretations of Google Earth imagery and location-tagged photographs from the web-service Panoramio which offers geographically tagged photographs from users. The coastline was split every time the type of coast changed. The coastal plain characteristics were segmented with the help of the geomorphic structure data developed by McGill (1958). The parameter provides information about the geomorphology and elevation of the coast. The third biophysical parameter is the river mouth layer. This layer was created with the help of Google earth as well. The population density information splits the coast into two classes, (i) urban/human settlements and (ii) rural (see **Figure 5**). This indicates variations in the population distribution of the Emilia-Romagna coast which is essential for the assessment of vulnerability to SLR, as e.g., dikes are only build where people are actually living. This spatial dataset was derived with the help of satellite image from Google earth. Furthermore, according to McFadden et al. (2007), institutional and governmental arrangements play an important role in defining the response of coastal systems to an accelerated sea-level. The inclusion of the political system (GADM level 03) is therefore important as different political and administrative controls react differently to SLR in terms of adaptation strategies. Finally, the created layers, described before, were overlaid in order to create segments that represent a uniform response to sea-level forcing.

Exposure Data

The segmentation creates units for the analysis (data structure) to which information (e.g., elevation or population data) is attached. Hence, after the segmentation the DIVA database was populated and updated with the help of the data provided from the COASTGAP partners or with the DIVA data. Topography or elevation is one of the main parameters that determine the vulnerability of coastal zones to sea-level rise. In order to assess areas exposed to inundation, two different digital elevation models were used. First, the freely available (1) Shuttle Radar Terrain Mission (SRTM) digital elevation model (Jarvis et al., 2008). It has a vertical resolution of 1 m and spatial resolution of 03 arc seconds (~90 m at the equator). The SRTM (datum wgs84) employs an imaging radar system. It is important to note that the elevation represents the height of the first reflective surface. In open terrain, the SRTM elevation will represent the ground elevation, but in vegetated or urban areas the ground-elevation might be overestimated. According to Gesch (2009), this mix of ground elevation and non-bare ground elevation in SRTM data could be a source of error in inundation mapping in vegetated and urban areas (Baugh et al., 2013; Lewis et al., 2013; Griffin et al., 2015). The second data set used is the (2) Light detection and ranging (LiDAR) digital elevation model (datum wgs84) with a spatial resolution of 5 m and a vertical accuracy of (±)20 cm which was provided by the Emilia-Romagna region. LiDAR employs the airborne laser scanning technique which can resolve a point density of 2 points per m^2. Both the 90 and 5 m-resolution data have been used in order to calculate the exposure of areas. A simple "bathtub approach" in which a grid cell becomes flooded if it is below a certain elevation has been used. In order to reflect surface flow connections, an eight-side-rule has been used, where the grid cell becomes a flooded grid cell if the cardinal and diagonal directions are connected. Following this approach, a mask that represents areas hydrologically connected to the sea was created. Afterwards, buffer zones per coastline segment have been produced in order to calculate the number of pixel flooded per segment. The zones also extend seaward, in order

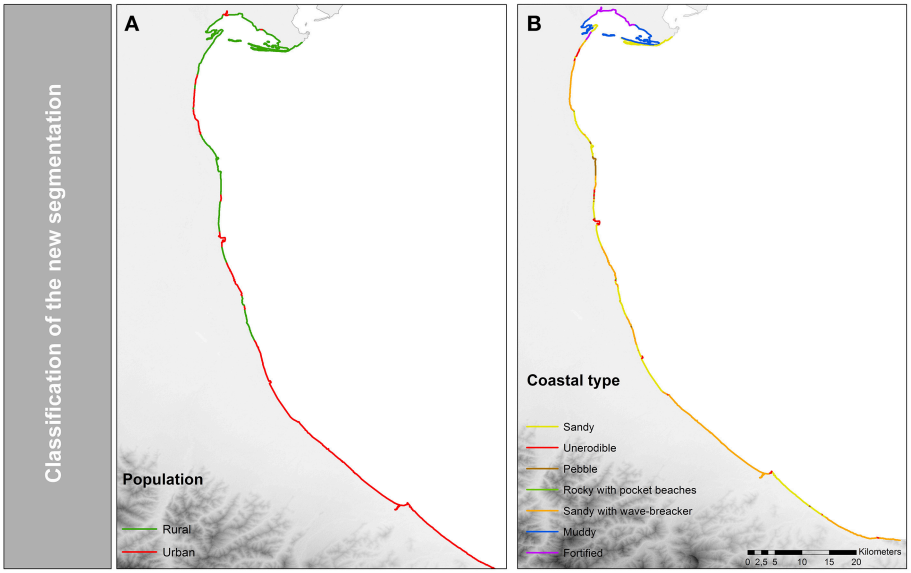

FIGURE 5 | Results of the high-resolution segmentation model. (A) Coastal settlements. **(B)** Coastal typology classification.

to ensure the inclusion of population mismatching which is important in order to calculate exposure of people. As local population data was unavailable, two different global population data sets have been used in order to calculate the exposure of people. The population count datasets of LandScan (2006) (Bright et al., 2007) and the Global Rural Urban Mapping Project (GRUMP 2000) (Center for International Earth Science Information Network - Ciesin - Columbia University et al., 2011) were obtained. Both have a spatial resolution of 30 arc seconds and are based on census population counts. The main differences are the base year, administrative levels of input data and the modeling approach used to allocate and disaggregate these data (Mondal and Tatem, 2012). The total global population between those two population datasets varies by around 8% (Lichter et al., 2011), mainly due to the different base years. In this study, this deviation has been recalculated afterwards to the common base year 1995, using the growth rates of the SSP scenarios. The LandScan global population project allocated annual midyear population estimates, usually at province level, based on weightings derived from land cover, roads, slope, urban areas, and high resolution imagery analysis. It represents an "ambient" population distribution and hence, presents a highly modeled population distribution. In contrast to that, GRUMP was produced by population census data from administrative units and was originally developed in order to reallocate census population counts to urban and rural areas. People were not only redistributed based on areal weighting, but urban populations were also reallocated based on night-time light as GRUMP defines population distribution according to where people actually live (Mondal and Tatem, 2012). Exposure was calculated by combining the information on elevation data with the population distribution data. The number of people at risk was calculated by summarizing population per elevation per increment, per coastline segment. Those values were stored as attributes to the coastline segment.

Vertical Land Movement Data

Vertical land movement is a downward (subsidence) or upward movement (uplift) of the land relative to sea level. Subsidence often occurs in regions associated with alluvial sediments, such as deltas (Ericson et al., 2006) as in the case of the study area, Emilia-Romagna. In this study we compare the vertical land movement of global modeled datasets, which are often used in flood risk assessment, with higher resolution local datasets, which are often not available for flood risk assessments because they are expensive to generate. In particular we consider a global model of glacial isostatic adjustment of Peltier (2000) together with an estimated 2 mm/year subsidence for delta regions as used by Hinkel et al. (2014). Human-induced subsidence rates were not considered. However, it is an important parameter for regions such as Emilia-Romagna where human-induced subsidence due to extraction of water, oil, and gas (Armaroli et al., 2012) is an issue. Data that include both natural and human-induced subsidence were available for this study through the COASTGAP partners. The data were generated from the Permanent Scatter Interferometric Synthetic Aperture Radar (PSInSAR). According to Ferretti et al. (2001), the PSInSAR is a surface displacement observation technique based on conventional radar interferometry. The data was provided by the Emilia-Romagna region in a raster format with a spatial resolution of 100 m. The coastal vertical land movement was calculated by combining the area below 3 m with the PSInSAR data. The coastal vertical land movement was calculated by averaging the rates per zone. Afterwards, the values were joined to the coastline segment. **Table 3** shows the Peltier (2000) + 2 mm/year delta subsidence and PSInSAR values used in this study.

TABLE 3 | Comparison between mean, maximum and minimum values of the globally modeled and locally measured vertical land movement data for the study area.

mm/year	Mean	Min	Max
Peltier (2000) + 2 mm/year delta subsidence	0.14	0.15	0.14
PSInSARs	4.88	0.59	19.62

Positive values indicate subsidence while negative values indicate uplift.

RESULTS

Segmentation

For the Emilia-Romagna coastline the global segmentation produced three segments with an average segment length of 40 km (minimum length 5.5 km, maximum length 98.8 km, total: 121.5 km). In comparison, the high-resolution segmentation generated 113 segments with an average length of 1.5 km (minimum length is 0.03 km, maximum length is 11.2 km, total: 174.6 km). Thus, the coastline length increased by 43% (53.1 km). The high-resolution segmentation has a 28-fold increase compared to the global DIVA assessment scale referring to the average length of segments. In the global DIVA database the entire coast of Emilia-Romagna was characterized by a sandy coastal morphology and urban settlements while in the new version a more detailed distinction (e.g., 57 segments or 86 km represents coastal settlements, 55 km are classified as sandy plus 59 km as sandy with wave breaker—see **Figure 5**) was made. The comparison of the different segmentation models indicates that the new segmentation approach increased not only the length of the coast but also the spatial representation of impacts in the Emilia-Romagna region (see **Figure 7**).

Sensitivity to Segmentation

Using the high-resolution segmentation, the 100-year floodplain has an extent of 3309 km^2 (using the SRTM elevation model), assuming a high SLR, in 2100. That covers 15% of the entire area of Emilia-Romagna. The potential flood area extent differs by 789 km^2 depending on the scale and resolution of assessment in 2100 (see **Table 4**). This situation shows that even if the underlying data (SRTM) remains the same, the total local values deviate due to the different scale of analysis. The main reason for that is the creation of buffer zones (see Supplementary Figure 2) which were used in order to calculate the exposure statistics per increment. The average number of people potentially flooded annually through extreme water level events is presented in **Figure 6** and in Supplementary Table 1. The results depend on the coastal topography, population, and adaptation strategy, as well as sea-level rise and socio-economic developments. Assuming that there are no protection measures in place, the number of people flooded varies between 90,909 and 511,198 people in 2100, using different assessment scales.

In the worst case, the choice of one particular assessment scale over another can result in an additional difference of 2.6% concerning the total population of Emilia-Romagna at risk. The spatial distribution of the people at risk per coastline segment for both assessments scales is presented in **Figure 7**. The detailed coastline represents the spatial distribution of people at risk more realistically, due to the more refined assessment scale and the increase of units.

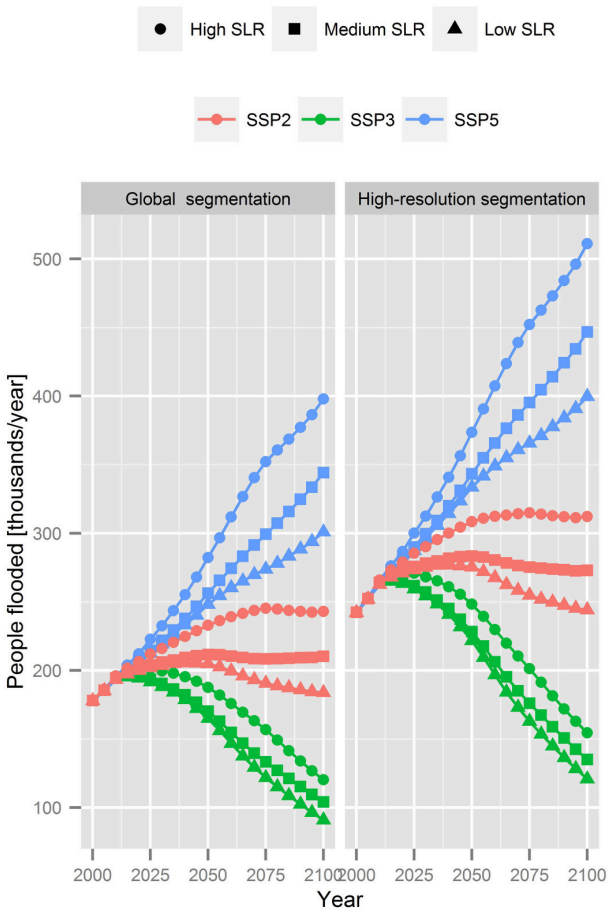

FIGURE 6 | Average annual people flooded from 2000 to 2100 under all SLR scenarios.

TABLE 4 | Sensitivity of coastal flood impacts to the four uncertainty parameters in 2100 (SSP5, high SLR).

Uncertainty dimension	Area of the 100-year floodplain *[km^2]*	Number of people flooded annually	Flood cost *[million/US$]*
Elevation	1049 (46%)	119,839 (33%)	37,368 (49%)
Vertical land movement	93 (4%)	91,458 (18%)	19,826 (26%)
Population	–	26,476 (08%)	576 (0.8%)
Segmentation	789 (31%)	113,349 (28%)	279 (0.2%)

The impacts represent an average difference while only one of the listed parameters is modified at a time.

Impacts are also very sensitive to population density threshold that determines when dike building starts. Setting this threshold is a normative decision depending on the risk preferences of coastal societies. If this threshold is set to 1 person per km^2, the entire coastline of the Emilia-Romagna is protected by dikes for both assessment scales (see **Table 5**). Considering a dike

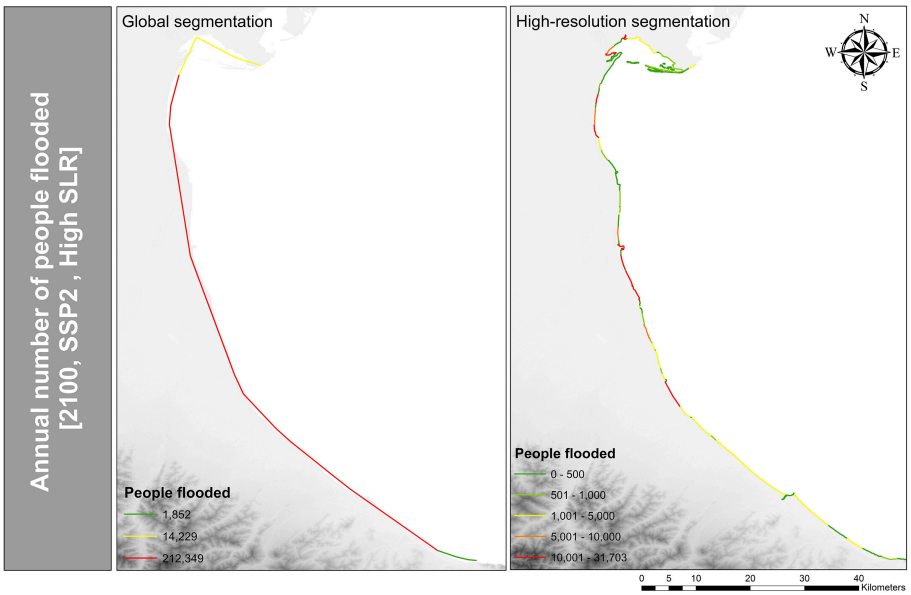

FIGURE 7 | Comparison of the spatial distribution of the expected number of people flooded annually using the global and high-resolution segmentation in 2100 (SSP2, High SLR).

TABLE 5 | Protected coastline length and cost of dikes for different dike construction thresholds using two different assessment scales in 2100 (medium SLR).

Dike building threshold		1 People/ km^2	10 People/ km^2	100 People/ km^2
High-resolution segmentation	Dike [km] (%)	174 (100%)	164 (94%)	112 (64%)
	Dikecost [millions US$/year]	2.4	2.3	1.5
Global segmentation	Dike	121 (100%)	121 (100%)	104 (86%)
	Dikecost [millions US$/year]	1.7	1.7	1.4

construction threshold of 10 people per km^2, 94% of the coast will be protected via dikes using the high-resolution segmentation assuming a medium SLR in 2100. In contrast, no change in the protection length was observed in the study area using the global assessment units. A threshold of 100 people per km^2 decreased the dike length by 36% using the detailed coastline and by 14% using the global coastline segmentation. The flood cost varies up to 279 million US dollar due to the change in the assessment scales. To conclude, the change in assessment scale, namely the increase of segments and length, showed a high sensitivity in this study (see **Table 4** and Supplementary Table 2).

Sensitivity to Elevation Data

The coastal flood impact calculation showed the highest sensitivity to the change in the elevation data in this study (see **Table 4** and Supplementary Table 3). The estimated areas exposed to coastal flooding are smaller with LiDAR DEM than those calculated with the SRTM DEM. This leads to an increase in the exposed area and potential coastal flood impacts. The choice of one particular elevation model over another can translate to a difference of more than 1049 km^2 of the current potential 100-year floodplain (see **Table 6**). The floodplain increases by 4–26% in 2100 (referring to 2015), depending on the elevation model and sea-level rise scenario chosen (see Supplementary Table 4). The differences of potential impacts using different digital elevation models decrease toward the end of the century when using a higher SLR scenario. This situation occurs due to the large differences between two elevation models in the area below 5 m. Those low-lying areas mainly influence the extent of the 100-year floodplain. Hence, the influence of the data sets used is higher under a low sea-level rise due to the fact that the elevation data differs the most at low elevations, as illustrated in **Figure 8**.

The potential of people exposed to annual coastal flooding and the average of annual damage caused by coastal flooding showed a high sensitivity to the change in elevation data (see **Table 4**). The potential impacts of coastal flooding are higher using the SRTM elevation model due to increasing areas at risk of coastal flooding (as shown in **Table 6**). The difference of 33% in the potential flood area leads to an increase of 49% in flood costs and to a 46% higher amount of people at risk compared to the impacts calculated with the LiDAR elevation model.

Sensitivity to Vertical Land Movement Data

The inclusion of measured data on human induced subsidence rates in the vertical land movement data led to an increase of relative sea-level rise (see **Table 7**). In 2100, an additional relative sea-level rise of 60 cm is reached, using the PSInSAR data which has a higher influence than the low and medium sea-level rise scenarios used in this study. This leads to a significant increase in

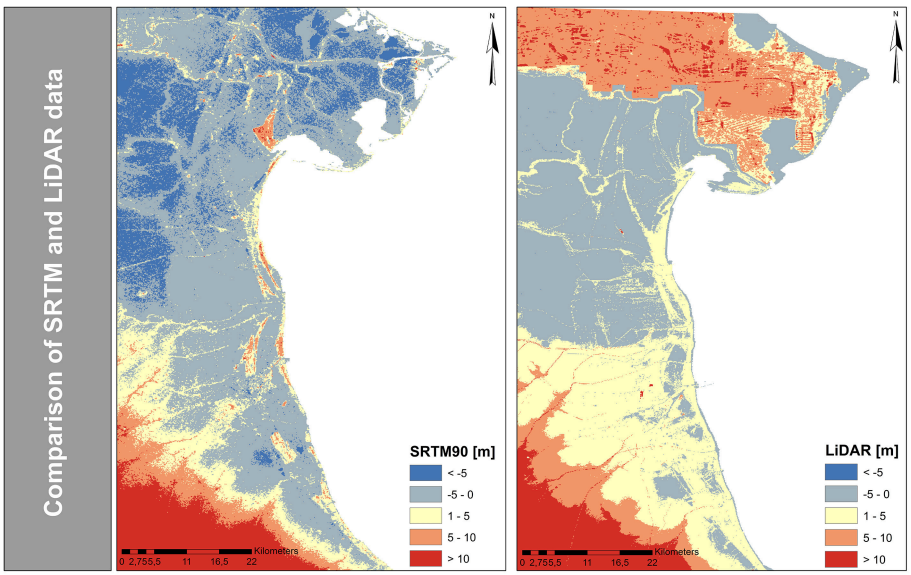

FIGURE 8 | Comparison of the SRTM90 and LiDAR digital elevation data for the Emilia-Romagna region.

TABLE 6 | 100-year floodplain under three different SLR scenarios using LiDAR and SRTM (today and in 2100).

Potential flood area (km^2)	2015	2100		
		Low SLR	Medium SLR	High SLR
LiDAR	1783	1958	2033	2260
SRTM	2819	3060	3126	3309
Sensitivity	1036 (58%)	1102 (56%)	1093 (53%)	1049 (46%)

The sensitivity is calculated based on the difference between various potential flood areas.

the potential impacts as it increases the exposure of people and area to coastal flooding due to the landward displacement of the flood extent.

The expected annual number of people flooded is highest using the PSInSAR vertical land movement data under SSP5, reflecting the highest population numbers, and a high SLR. The influence of the change in data is highest under the low SLR scenario and lowest under the high SLR scenario in 2100. Impacts intensify throughout the century under all socio-economic scenarios. Using the PSInSAR vertical land movement data, including human induced subsidence, impacts are up to 25% higher (e.g., flood cost) than those estimated using the DIVA values, which only account for natural processes.

Sensitivity to Population Data

Model outputs were least sensitive to variations of population data (see **Table 4**). The estimated number of exposed people using GRUMP is smaller than those calculated with LandScan. The total amount of population for Emilia-Romagna using the LandScan dataset is 0.7% higher than using the GRUMP (total population of Emilia-Romagna using GRUMP: 4016951 and LandScan: 4046404). Due to the different reallocation methods and administrative levels of input data (explained in Section Coastline Segmentation Data) the number of estimated people exposed to coastal flooding differs with respect to the two datasets. In an area of around 15%, which represents the potential 100-year flood plain of Emilia-Romagna using the SRTM elevation model, ∼10% of the total population of Emilia-Romagna is living in the flood plain and therefore is potentially at risk to the 100 year surge. The expected number of people annually flooded due to the switch in datasets differs by 26,476 people (8%) in 2100. The potential coastal flood cost differs by 576 million US dollar (0.8%; see **Table 4**).

DISCUSSION

Effects of Different Coastlines and Segmentations to Coastal Flood Impact Assessment

Within the framework of the COASTGAP project and for the purpose of the current analysis, the DIVA assessment scale has been downscaled to be applicable at a sub-national scale. The distribution of features along the coast, the scale of the coastline and the defined classes for each parameter as well as available data used in order to segment the coast, determines the number of segments that were produced. The main effect due to the change in scale of the coastline was the increase in coastal length which influences adaptation cost (construction of dikes) considerably. The change in assessment units (segmentation), namely the increase of segments and the decrease of segment average length led to a high sensitivity of model outputs in this study. The main difference results from the creation of buffer zones which depend on the shape of the coast and segment

TABLE 7 | Comparison of relative sea-level rise values using the old DIVA and the PSInSAR values.

RSLR [m]	Peltier, 2000			PSInSAR		
	Low SLR	Medium SLR	High SLR	Low SLR	Medium SLR	High SLR
2000	0.00	0.00	0.00	0.03	0.03	0.03
2050	0.16	0.21	0.34	0.48	0.52	0.66
2100	0.31	0.54	1.22	0.91	1.15	1.82

(see Section Coastline Segmentation Data and Supplementary Figure 2) that was used in order to calculate the exposure per segment. Using the global segmentation model and buffer zones, parts of the flood extent are potentially added to the neighboring administrative unit as the segments are quite large. Hence, one main improvement of the refined segmentation is the increased spatial accuracy of impacts on a sub-national scale as the number of segments and zones increase (see **Figure 7**). Thus, impacts are more concentrated and spatially accurate than before. This improves the assessment by making future predictions more realistic than before and suggests that the refined segmentation is more appropriate to be used when more detailed data (e.g., population) become available or underlying normative assumptions, such as dike building computation, are adopted for more detailed application. Thus, even if the underlying data improve, model algorithms/assumptions may also need to be adjusted to represent sub-national to local processes more realistically.

The aim of the COASTGAP project was to develop adaptation policies to reduce risk along the coast and to create new common tools and opportunities for coastal zone development in the Mediterranean. The developed approach can be used to support this development as it would enable consistent and comparable coastal flood impact assessments for local policy makers with limited data availability. The approach can also be useful for the implementation of the provisions of EC Directive 2007/60 in the assessment and management of flood risks which entered into force in 2007 (2007/60/EC). In particular, the Directive now requires Member States to assess if all water courses and coastlines are at risk from flooding, to map the flood extent, assets, humans at risk in these areas and to take adequate and coordinated measures to reduce this flood risk. These requirements can be realized by applying the DIVA modeling framework for the respective calculations. On a more refined scale it is more realistic to identify hot spots, for instance where people are at risk of coastal flooding (see comparison **Figure 7**) or calculate adaptation needs. This simplifies the identification of priority regions that are highly vulnerable to SLR and need further research effort. Future work could be a scoping study in the Mediterranean using a downscaled version of the DIVA model in order to serve the need for basic information to politicians and decision-makers on the overall risk situation in the coastal zone and pinpoint hot spots. Finding the appropriate spatial scale which is most relevant for the objective of the research question or decision makers is highly important as vulnerability to SLR in the coastal zone is scale-dependent (Sterr, 2008; Fekete et al., 2010). It is important to keep in mind that a more detailed method to calculate coastal flood impacts requires more effort per unit of an area. The developed approach could be a starting point to close the gap and assess impacts and risk at an intermediate scale using a global coastal flood impact model. Furthermore, the link between different spatial scales could be a promising future research area as it would enable rapid coastal flood impact assessments with limited data and enable consistent and comparable coastal flood impact assessments worldwide (de Moel et al., 2015).

Model Sensitivity to Input Data

Results of the study showed a high sensitivity to the change in elevation input data, which is consistent with previous studies (e.g., Poulter and Halpin, 2008; Lichter et al., 2011; Hinkel et al., 2014). Nevertheless, it is difficult to compare those studies as the estimates of area and population exposure in the coastal zone vary depending on the scale (global to local), input datasets (e.g., SRTM, Globe, Aster, LiDAR), methods (e.g., hydrological connectivity rule) and objectives of the study. According to Gesch (2009), the identification of areas exposed to a certain sea-level rise scenario improves considerably when higher-resolution and -accuracy data, such as LiDAR data, are used. He found the inundation area to be two times higher when the vertical accuracy of coarser elevation datasets, such as GTOPO30, is considered in the calculation of area exposure. In contrast to that, the LiDAR-based exposure calculation increases by only 14% when the accuracy of the elevation model is considered. Previous coastal impact studies have primarily used SRTM data due to the fact that these cover nearly the entire world and are freely available. The results of the present study showed a significant difference between the LiDAR (high resolution data) and SRTM digital elevation model. The SRTM data produced a much larger potential coastal floodplain than the LiDAR DEM, contrary to what was initially anticipated as the SRTM digital elevation model is a surface model and the elevation represents the height of the first reflective surface. In contrast to that van De Sande et al. (2012) reported a four times smaller coastal floodplain using STRM data instead of LiDAR in a delta region in Nigeria (Lagos State and Lagos City). Therefore, it is important to evaluate and quantify data differences in order to improve our understanding of global digital elevation datasets and how these influence flood risk assessments.

If one compares the SRTM with land use data, such as the CORINE land use cover (see **Figure 9**), it becomes obvious that low elevation values occur over agricultural and low-vegetation areas, while high-elevation values occur in forests and cities. This effect can be accounted for in local studies by, for example,

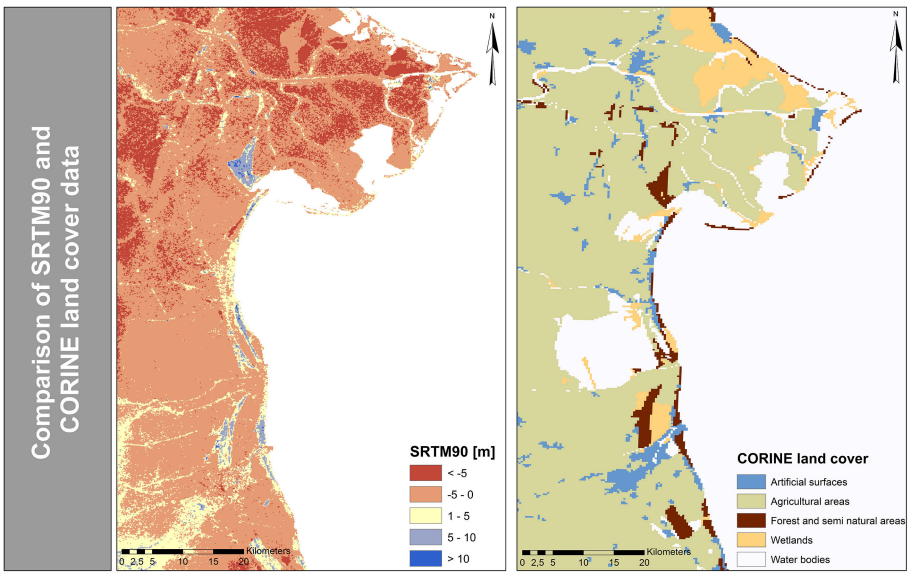

FIGURE 9 | Comparison of the SRTM90 digital elevation data and CORINE land cover data in Emilia-Romagna.

reducing the elevation values of SRTM by the average height of vegetation derived on the basis of field measurements (Kaiser et al., 2011) or other sources of spatially distributed vegetation height data (Baugh et al., 2013). However, additional factors may also influence the elevation values of the model. Although the overestimation of elevation values, for instance in urban areas or vegetated terrain, is well documented in the literature (e.g., Hofton et al., 2006; Rodríguez et al., 2006), some studies have found SRTM to underestimate elevation values (Jarvis et al., 2004). For example, in a study conducted in two vegetation-free areas in Iowa and North Dakota (USA) Kellndorfer et al. (2004) reported absolute errors of −4.0 and −1.1 m, respectively. Notably, most studies express the vertical accuracy in absolute values (e.g., Gorokhovich and Voustianiouk, 2006; Berry et al., 2007) and do not specify an over- or under-estimation of SRTM values. In this study, an overestimation of the potential coastal floodplain is observed using the SRTM elevation data, suggesting a negative bias in the data, which leads to much higher potential impacts. Understanding the effects of the use of elevation models of different resolution and accuracy would be of high value for coastal flood impact assessments as the choice of the digital elevation model can significantly influence the assessment of coastal flood impacts, as shown in this study. Importantly, high-resolution and -accuracy data cannot be employed for global or regional studies due to computational constraints and lack of such data.

Human-induced subsidence which leads to higher relative sea-level rates is a major source of uncertainty in coastal flood impact assessment as data is hardly available. The results indicate that the flood risk estimates for the region considered here have a moderate sensitivity to vertical land movement input data, as these can significantly influence the relative sea-level rise. In our study relative sea-level rise increased on average by 5 mm/year using data that include human-induced subsidence (PSInSAR data). This is in line with the study conducted by Syvitski et al. (2009), who estimated a relative sea-level rise of 4–60 mm/year, for the Po delta (the Po delta is the northern boundary of the study area). Furthermore, Taramelli et al. (2015) estimated coastal subsidence of 7–9 mm/year in the Ravenna coastal area and Bevano River. This study was undertaken in regions where there is intensive mining activity (freshwater or hydrocarbon) and the subsidence rates can be higher than a meter per century. This increase in relative sea-level rise leads to a significant increase in exposure of people and areas to coastal flooding due to the landward displacement of the flood extent, and thus in the exacerbation of potential impacts. This study indicates that the global results of Hinkel et al. (2014) using global vertical land movement data underestimates impacts due to the non-consideration of human induced subsidence even in non-delta regions like Emilia-Romagna.

In order to calculate potential coastal flood impacts a further uncertainty source is the distribution of people (and assets) along the coastline. Flood risk estimates showed a relevant but small sensitivity to changes in population input data. A similar trend was observed at global scale by Hinkel et al. (2014). Nevertheless, relative flood impact can differ substantially per segment, administrative unit or country, even if the total numbers do not differ significantly. The GRUMP model distributes people much more uniformly than the Landscan model. **Figure 10** shows the comparison between the GRUMP and LandScan difference grid in comparison with the urban areas of the MODIS land cover data. Here, it can be seen that LandScan allocates higher population values in urban areas and human settlements. This explains why LandScan distributes more people to the coast than GRUMP in this study as popular tourist resorts, such as Ravenna and Rimini, are part of the floodplain. Thus, in order

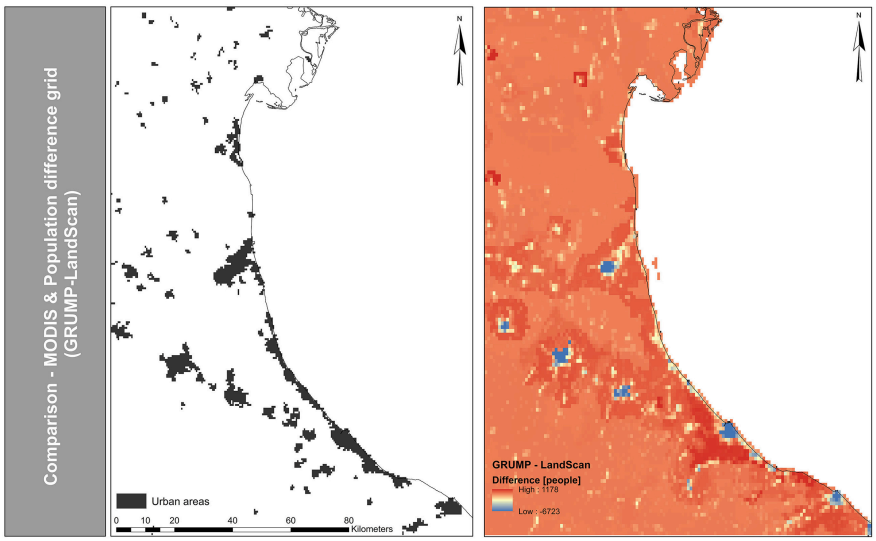

FIGURE 10 | Comparison of the GRUMP-LandScan difference grid to the urban areas of the MODIS land cover data.

to interpret the flood risk estimates correctly it is important to keep the different representations/ assumptions of population distributions in mind. However, both population models seem to be useful in order to calculate coastal flood impact trends. For a more robust evaluation of the global datasets high-resolution data would be necessary.

Overall, the largest uncertainty when looking at the present day situation is the elevation data, as shown in previous work (Lichter et al., 2011; Hinkel et al., 2014). Different elevation datasets can have substantial effects, increasing or decreasing the floodplain area by factor 2–3. Our analysis confirms these findings. In our case study the DEM is the most important factor for assessing current exposure and risk. For assessing the future impacts of coastal flooding, sea-level rise is the most important factor, which is also in accordance with Hinkel et al. (2014). Nevertheless, in our case study sea-level rise is strongly influenced by human induced subsidence, which, as shown by previous work (Nicholls, 1995), is usually a local phenomenon often occurring in megacities. Thus, a further insight from our study is that exposure and risk are increasing in the heavily subsiding broader Emilia-Romagna region, although no major city is located in this region.

CONCLUSION

This study presented an assessment of sea-level rise impacts on the coastal region of Emilia-Romagna using different input datasets and assessment scales. The first objective of the study was to explore the potential benefits of the use of a more refined coastline and segmentation. The high-resolution segmentation improves the potential coastal flood impact representation as future predictions are more concentrated and spatially explicit. This study is a first approach to downscale the DIVA assessment scale and data for sub-national applications and refines the existing segmentation model and database; and a first step to downscale global coastal flood impact assessments for specific areas. Downscaling global coastal flood impact models could be a promising future research area as it would enable rapid coastal flood impact assessments for local policy makers with limited data and resource availability. Furthermore, identifying links between spatial scales can enable consistent and comparable coastal flood impact assessments and would constitute a useful tool for global actors (e.g., Re-insurers, European flood directive, World Bank).

The second objective of the study was to explore the model sensitivity to different input data on elevation, population, and vertical land movement when assessing coastal flood impacts. This study indicates that the lack of high-accuracy elevation and vertical land movement data remains a significant constraint in global coastal flood impact analysis. We must also note that coastal flood impact assessment also includes other sources of uncertainties that should be investigated in future work, such as the spatial (Lewis et al., 2013) and temporal variability (Quinn et al., 2014) of extreme water levels and their implications in coastal flood impact assessment. Understanding the whole range of uncertainties and communicating their implications is essential for the development of long-term robust and flexible adaptation plans for future changes of highly uncertain scale and direction. Further work aims to assess the sensitivity of different input datasets and scale of analysis in different regions, in order to gain a more complete understanding of the use of global datasets in flood-impact modeling and the sensitivity of the DIVA flooding module to input data and scale.

AUTHOR CONTRIBUTIONS

CW, AV, JH, DL designed research. CW and DL set up the model. CW and CM collected the data. CW, AV, DL, CM, and JH analyzed the results. CW wrote the paper with contributions

from AV, DL, CM, and JH. All authors read and approved the final manuscript.

ACKNOWLEDGMENTS

CW, AV, and CM were supported by the COASTGAP project (1CAP-MED012-08) which was co-financed by the European Regional Development Fund (ERDF). DL and JH have been supported by the EU-funded projects, RISES-AM (Grant Nr: 603396) and GREEN-WIN (Grant Nr: 642018). The authors would also like to thank Dr. Eva Papaioannou who assisted in the implementation of the coastline segmentation.

SUPPLEMENTARY MATERIAL

The Supplementary Material for this article can be found online at: http://journal.frontiersin.org/article/10.3389/fmars.2016.00041

REFERENCES

Armaroli, C., Ciavola, P., Perini, L., Calabrese, L., Lorito, S., Valentini, A., et al. (2012). Critical storm thresholds for significant morphological changes and damage along the Emilia-Romagna coastline, Italy. *Geomorphology* 143–144, 34–51. doi: 10.1016/j.geomorph.2011.09.006

Bamber, J., and Riva, R. (2010). The sea level fingerprint of recent ice mass fluxes. *Cryosphere* 4, 621–627. doi: 10.5194/tc-4-621-2010

Baugh, C. A., Bates, P. D., Schumann, G., and Trigg, M. A. (2013). SRTM vegetation removal and hydrodynamic modeling accuracy. *Water Resour. Res.* 49, 5276–5289. doi: 10.1002/wrcr.20412

Berry, P. A. M., Garlick, J. D., and Smith, R. G. (2007). Near-global validation of the SRTM DEM using satellite radar altimetry. *Remote Sensing Environ.* 106, 17–27. doi: 10.1016/j.rse.2006.07.011

Bright, E. A., Coleman, P. R., and King, A. L. (2007). *LandScan 2006*. Oak Ridge, TN: Oak Ridge National Laboratory.

Center for International Earth Science Information Network - Ciesin - Columbia University, International Food Policy Research Institute - Ifpri, The World Bank, and Centro Internacional De Agricultura Tropical - Ciat (2011). *Global Rural-Urban Mapping Project, Version 1 (GRUMPv1): Population Density Grid*. Palisades, NY: NASA Socioeconomic Data and Applications Center (SEDAC).

Chang, A. Y., Parrales, M. E., Jimenez, J., Sobieszczyk, M. E., Hammer, S. M., Copenhaver, D. J., et al. (2009). Combining Google earth and GIS mapping technologies in a dengue surveillance system for developing countries. *Int. J. Health Geogr.* 8, 49. doi: 10.1186/1476-072X-8-49

Collins, W. J., Bellouin, N., Doutriaux-Boucher, M., Gedney, N., Hinton, T., Jones, C. D., et al. (2008). *Evaluation of the HadGEM2 Model*. Met Office Hadley Centre Technical Note no. *HCTN* 74.

de Moel, H., Jongman, B., Kreibich, H., Merz, B., Penning-Rowsell, E., and Ward, P. J. (2015). Flood risk assessments at different spatial scales. *Mitigation Adapt. Strateg. Glob. Chang.* 20, 865–890. doi: 10.1007/s11027-015-9654-z

Ericson, J. P., Vorosmarty, C. J., Dingman, S. L., Ward, L. G., and Meybeck, M. (2006). Effective sea-level rise and deltas: causes of change and human dimension implications. *Glob. Planet. Change* 50, 63–82. doi: 10.1016/j.gloplacha.2005.07.004

ESRI (2002). *Digital Chart of the World*. Redlands, CA: Environmental Systems Research Institute.

Fekete, A., Damm, M., and Birkmann, J. (2010). Scales as a challenge for vulnerability assessment. *Nat. Hazards* 55, 729–747. doi: 10.1007/s11069-009-9445-5

Ferretti, A., Prati, C., and Rocca, F. (2001). Permanent scatterers in SAR interferometry. *IEEE Trans. Geosci. Remote Sens.* 39, 8–20. doi: 10.1109/36.898661

Fettweis, X., Franco, B., Tedesco, M., Van Angelen, J. H., Lenaerts, J. T. M., Van Den Broeke, M. R., et al. (2013). Estimating the Greenland ice sheet surface mass balance contribution to future sea level rise using the regional atmospheric climate model MAR. *Cryosphere* 7, 469–489. doi: 10.5194/tc-7-469-2013

Gesch, D. B. (2009). Analysis of lidar elevation data for improved identification and delineation of lands vulnerable to sea-level rise. *J. Coas. Res.* 10053, 49–58. doi: 10.2112/SI53-006.1

Gorokhovich, Y., and Voustianiouk, A. (2006). Accuracy assessment of the processed SRTM-based elevation data by CGIAR using field data from USA and Thailand and its relation to the terrain characteristics. *Remote Sensing Environ.* 104, 409–415. doi: 10.1016/j.rse.2006.05.012

Griffin, J., Latief, H., Kongko, W., Harig, S., Horspool, N., Hanung, R., et al. (2015). An evaluation of onshore digital elevation models for modelling tsunami inundation zones. *Front. Earth Sci.* 3:32. doi: 10.3389/feart.2015.00032

Hallegatte, S., Green, C., Nicholls, R. J., and Corfee-Morlot, J. (2013). Future flood losses in major coastal cities. *Nat. Clim. Change* 3, 802–806. doi: 10.1038/nclimate1979

Hinkel, J., Jaeger, C., Nicholls, R. J., Lowe, J., Renn, O., and Peijun, S. (2015). Sea-level rise scenarios and coastal risk management. *Nat. Clim. Change* 5, 188–190. doi: 10.1038/nclimate2505

Hinkel, J., Lincke, D., Vafeidis, A. T., Perrette, M., Nicholls, R. J., Tol, R. S. J., et al. (2014). Coastal flood damage and adaptation costs under 21st century sea-level rise. *Proc. Natl. Acad. Sci. U.S.A.* 111, 3292–3297. doi: 10.1073/pnas.1222469111

Hofton, M., Dubayah, R., Blair, B., and Rabine, D. (2006). Validation of SRTM elevations over vegetated and non-vegetated terrain using medium footprint lidar. *Photogram. Eng. Remote Sens.* 2006, 279–285. doi: 10.14358/PERS.72.3.279

Hoozemans, F. M. J., Marchand, M., and Pennekamp, H. A. (1993). *Sea Level Rise: A Global Vulnerability Assessment Vulnerability Assessments for Population, Coastal Wetlands and Rice Production on a Global Scale*. Delft: Delft Hydraulics.

Houtenbos, A. P. E. M., Hounjet, M. W. A., and Barends, B. J. (2005). "Subsidence from geodetic measurements in the Ravenna area," in *Proceedings of the 7th International Symposium on Land Subsidence* (Shanghai: Deltares (WL)), 79–99.

Istat (2009). *Pil Pro Capite Per Regione*. Available online at: http://noi-italia2012.istat.it/fileadmin/user_upload/allegati/91.pdf

Jarvis, A., Reuter, H. I., Nelson, A., and Guevara, E. (2008). *Hole-Filled SRTM for the Globe Version 4.* Available online at: http://srtm.csi.cgiar.org/

Jarvis, A., Rubiano, J., Nelson, A., Farrow, A., and Mulligan, M. (2004). *Practical Use of SRTM Data in the Tropics: Comparisons with Digital Elevation Models Generated from Cartographic Data*. Working Document No. 198. Cali: International Center for Tropical Agriculture (CIAT) and the International Plant Genetic Resources Institute (IPGRI).

Jones, N., Koukoulas, S., Clark, J. R. A., Evangelinos, K. I., Dimitrakopoulos, P. G., Eftihidou, M. O., et al. (2014). Social capital and citizen perceptions of coastal management for tackling climate change impacts in Greece. *Reg. Environ. Change* 14, 1083–1093. doi: 10.1007/s10113-013-0540-5

Kaiser, G., Scheele, L., Kortenhaus, A., Løvholt, F., Römer, H., and Leschka, S. (2011). The influence of land cover roughness on the results of high resolution tsunami inundation modeling. *Nat. Hazards Earth Syst. Sci.* 11, 2521–2540. doi: 10.5194/nhess-11-2521-2011

Kc, S., and Lutz, W. (2014). The human core of the shared socioeconomic pathways: population scenarios by age, sex and level of education for all countries to 2100. *Glob. Environ. Change*. doi: 10.1016/j.gloenvcha.2014.06.004. Available online at: http://www.sciencedirect.com/science/article/pii/S0959378014001095#FCANote

Kellndorfer, J., Walker, W., Pierce, L., Dobson, C., Fites, J. A., Hunsaker, C., et al. (2004). Vegetation height estimation from shuttle radar topography mission and national elevation datasets. *Remote Sens. Environ.* 93, 339–358. doi: 10.1016/j.rse.2004.07.017

Le Cozannet, G., Rohmer, J., Cazenave, A., Idier, D., Van De Wal, R., De Winter, R., et al. (2015). Evaluating uncertainties of future marine flooding occurrence as sea-level rises. *Environ. Modell. Softw.* 73, 44–56. doi: 10.1016/j.envsoft.2015.07.021

Levermann, A., Albrecht, T., Winkelmann, R., Martin, M. A., Haseloff, M., and Joughin, I. (2012). Kinematic first-order calving law implies potential for abrupt ice-shelf retreat. *Cryosphere* 6, 273–286. doi: 10.5194/tc-6-273-2012

Lewis, M., Bates, P., Horsburgh, K., Neal, J., and Schumann, G. (2013). A storm surge inundation model of the northern Bay of Bengal using publicly available data. *Q. J. R. Meteorol. Soc.* 139, 358–369. doi: 10.1002/qj.2040

Lichter, M., Vafeidis, A. T., Nicholls, R. J., and Kaiser, G. (2011). Exploring data-related uncertainties in analyses of land area and population in the "low-elevation coastal zone" (LECZ). *J. Coast. Res.* 274, 757–768. doi: 10.2112/JCOASTRES-D-10-00072.1

Lupino, P., Bellacicco, S., Di Cosimo, M., Scaloni, P., Pedetta Peccia, S., Montanari, R., et al. (2014). *Practical Guide to COASTGAP MED Capitalisation Initiative*. Rome: Regione Lazio.

Marzeion, B., Jarosch, A. H., and Hofer, M. (2012). Past and future sea-level change from the surface mass balance of glaciers. *Cryosphere* 6, 1295–1322. doi: 10.5194/tc-6-1295-2012

McFadden, L., Nicholls, R. J., Vafeidis, A., and Tol, R. S. J. (2007). A Methodology for modeling coastal space for global assessment. *J. Coast. Res.* 234, 911–920. doi: 10.2112/04-0365.1

McGill, J. T. (1958). Map of coastal landforms of the world. *Geogr. Rev.* 48, 402–405. doi: 10.2307/212259

Mondal, P., and Tatem, A. J. (2012). Uncertainties in measuring populations potentially impacted by sea level rise and coastal flooding. *PLoS ONE* 7:e48191. doi: 10.1371/journal.pone.0048191

Montanari, R., and Marasmi, C. (2014). *Il Sistema Gestionale Delle Celle Litoranee SICELL in Aggiornamento 2006-2012*. Regione Emilia-Romagna. Servizio Difesa del Suolo, della Costa e Bonifica.

Neumann, B., Vafeidis, A. T., Zimmermann, J., and Nicholls, R. J. (2015). Future coastal population growth and exposure to sea-level rise and coastal flooding-a global assessment (vol 10, e0118571, 2015). *PLoS ONE* 10:e0118571. doi: 10.1371/journal.pone.0118571

Nicholls, R. J. (1995). Coastal megacities and climate change. *GeoJournal* 37, 369–379. doi: 10.1007/BF00814018

Nordstrom, K. F., Armaroli, C., Jackson, N. L., and Ciavola, P. (2015). Opportunities and constraints for managed retreat on exposed sandy shores: examples from Emilia-Romagna, Italy. *Ocean Coast. Manag.* 104, 11–21. doi: 10.1016/j.ocecoaman.2014.11.010

O'Neill, B. C., Kriegler, E., Riahi, K., Ebi, K. L., Hallegatte, S., Carter, T. R., et al. (2014). A new scenario framework for climate change research: the concept of shared socioeconomic pathways. *Clim. Change* 122, 387–400. doi: 10.1007/s10584-013-0905-2

Peltier, W. (2000). *ICE4g (VM2) Glacial Isostatic Adjustment Correction on Sea Level Rise, History and Consequences*. San Diego, CA: Academic Press. International Geophysics Series 75.

Poulter, B., and Halpin, P. N. (2008). Raster modelling of coastal flooding from sea-level rise. *Int. J. Geogr. Inf. Sci.* 22, 167–182. doi: 10.1080/13658810701371858

Preti, M., De Nigris, N., Morelli, M., Monti, M., Bonsignore, F., and Aguzzi, M. (2009). *Stato del Litorale Emiliano-Romagnolo ALL'ANNO 2007 e Piano Decennale di Gestione*. Ravenna: Regione Emilia-Romagna.

Quinn, N., Lewis, M., Wadey, M. P., and Haigh, I. D. (2014). Assessing the temporal variability in extreme storm-tide time series for coastal flood risk assessment. *J. Geophys. Res. Oceans* 119, 4983–4998. doi: 10.1002/2014JC010197

Rodríguez, E., Morris, C. S., and Belz, J. E. (2006). A global assessment of the SRTM performance. *Photogrammetric Eng. Remote Sensing* 72, 249–260. doi: 10.14358/PERS.72.3.249

Saltelli, A., Tarantola, S., and Campolongo, F. (2000). Sensitivity analysis as an ingredient of modeling. *Stat. Sci.* 15, 377–395. doi: 10.1214/ss/1009213004

Scheffers, A. M., Scheffers, S. R., and Kelletat, D. H. (2012). *The Coastlines of the World with Google Earth*. Dordrecht: Springer.

Sterr, H. (2008). Assessment of vulnerability and adaptation to sea-level rise for the coastal zone of Germany. *J. Coast. Res.* 242, 380–393. doi: 10.2112/07A-0011.1

Syvitski, J. P. M., Kettner, A. J., Overeem, I., Hutton, E. W. H., Hannon, M. T., Brakenridge, G. R., et al. (2009). Sinking deltas due to human activities. *Nat. Geosci.* 2, 681–686. doi: 10.1038/ngeo629

Taramelli, A., Di Matteo, L., Ciavola, P., Guadagnano, F., and Tolomei, C. (2015). Temporal evolution of patterns and processes related to subsidence of the coastal area surrounding the Bevano River mouth (Northern Adriatic) – Italy. *Ocean Coast. Manage.* 108, 74–88. doi: 10.1016/j.ocecoaman.2014.06.021

Vafeidis, A. T., Nicholls, R. J., McFadden, L., Tol, R. S. J., Hinkel, J., Spencer, T., et al. (2008). A new global coastal database for impact and vulnerability analysis to sea-level rise. *J. Coast. Res.* 244, 917–924. doi: 10.2112/06-0725.1

van De Sande, B., Lansen, J., and Hoyng, C. (2012). Sensitivity of coastal flood risk assessments to digital elevation models. *Water* 4, 568–579. doi: 10.3390/w4030568

Conflict of Interest Statement: The authors declare that the research was conducted in the absence of any commercial or financial relationships that could be construed as a potential conflict of interest.

Advantages of publishing in Frontiers

OPEN ACCESS
Articles are free to read, for greatest visibility

COLLABORATIVE PEER-REVIEW
Designed to be rigorous – yet also collaborative, fair and constructive

FAST PUBLICATION
Average 85 days from submission to publication (across all journals)

COPYRIGHT TO AUTHORS
No limit to article distribution and re-use

TRANSPARENT
Editors and reviewers acknowledged by name on published articles

SUPPORT
By our Swiss-based editorial team

IMPACT METRICS
Advanced metrics track your article's impact

GLOBAL SPREAD
5'100'000+ monthly article views and downloads

LOOP RESEARCH NETWORK
Our network increases readership for your article

Frontiers
EPFL Innovation Park, Building I • 1015 Lausanne • Switzerland
Tel +41 21 510 17 00 • Fax +41 21 510 17 01 • info@frontiersin.org
www.frontiersin.org

Find us on